# RESOLUTION IMPROVEMENT IN ACOUSTIC HOLOGRAPHY USING APERTURE EXPANSION TECHNIQUES

Volume 2

by

RADWAN E. S. ABDEL-AAL

THESIS

Presented to the University of Strathclyde

Department of Electronic and Electrical Engineering

for the degree of

Doctor of Philosophy

June 1983

CONTENTS


| | Page No |
|---|---|
| Figures for Chapter 2 | 1 |
| Figures for Chapter 3 | 15 |
| Figures for Chapter 4 | 19 |
| Figures for Chapter 5 | 53 |
| Figures for Chapter 6 | 80 |
| Figures for Chapter 7 | 103 |
| Appendix A : Listing of a BASIC Routine for Hologram Simulation and Expansion | 141 |
| Appendix B : Description of the Basic Phase Measuring Circuit | 145 |
| Appendix C : Listing of the TMS 9900 Microprocessor Software for the FFT Algorithm | 148 |
| Appendix D : Publications | 160 |

# Figures for Chapter 2

a. Hologram recording

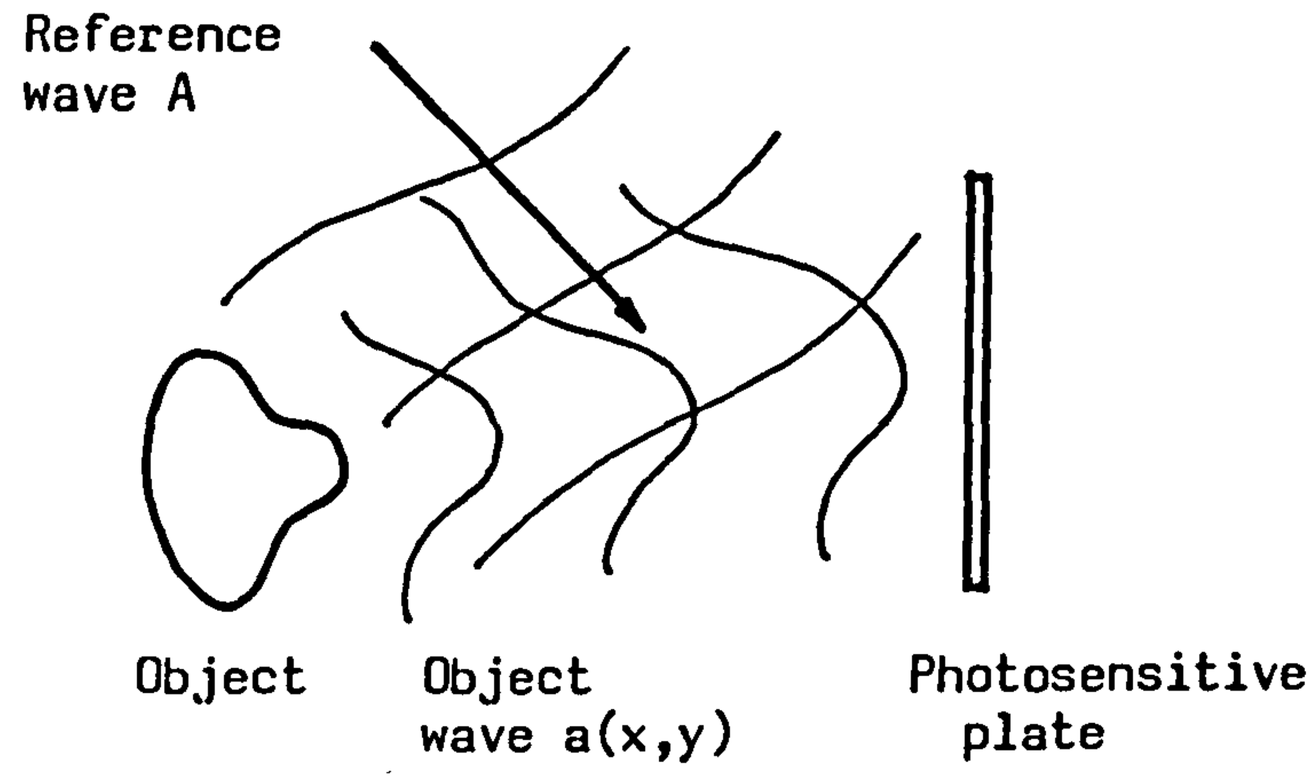


b. Hologram reconstruction with the reconstruction wave equal to the original reference

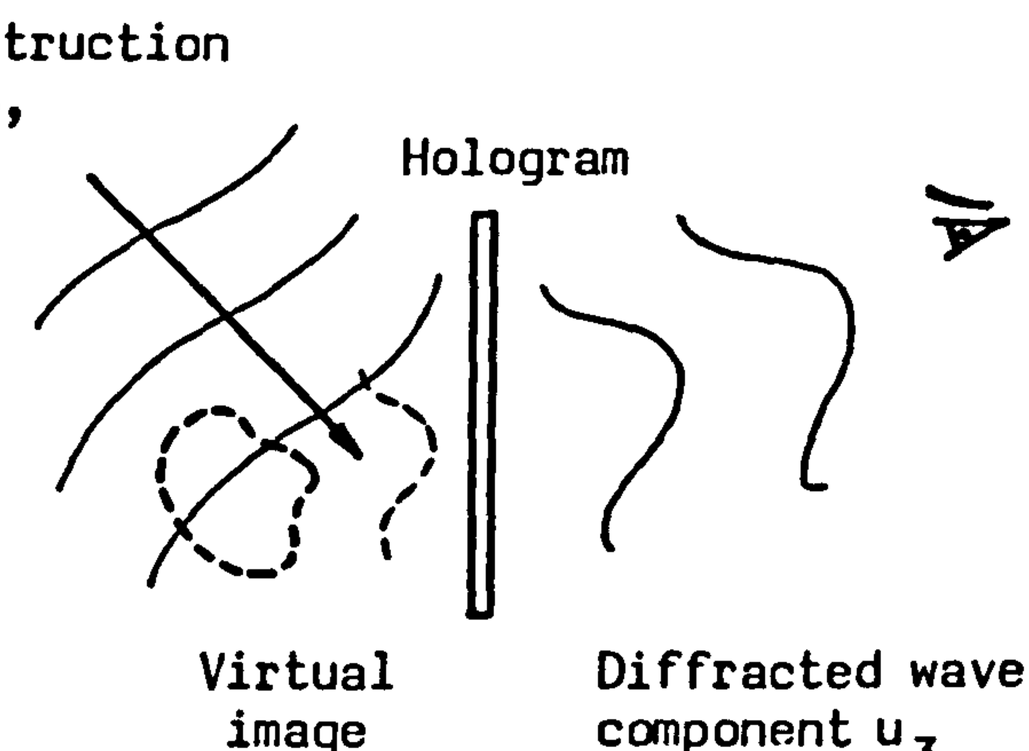


c. Hologram reconstruction with the reconstructed wave equal to the conjugate of the original reference

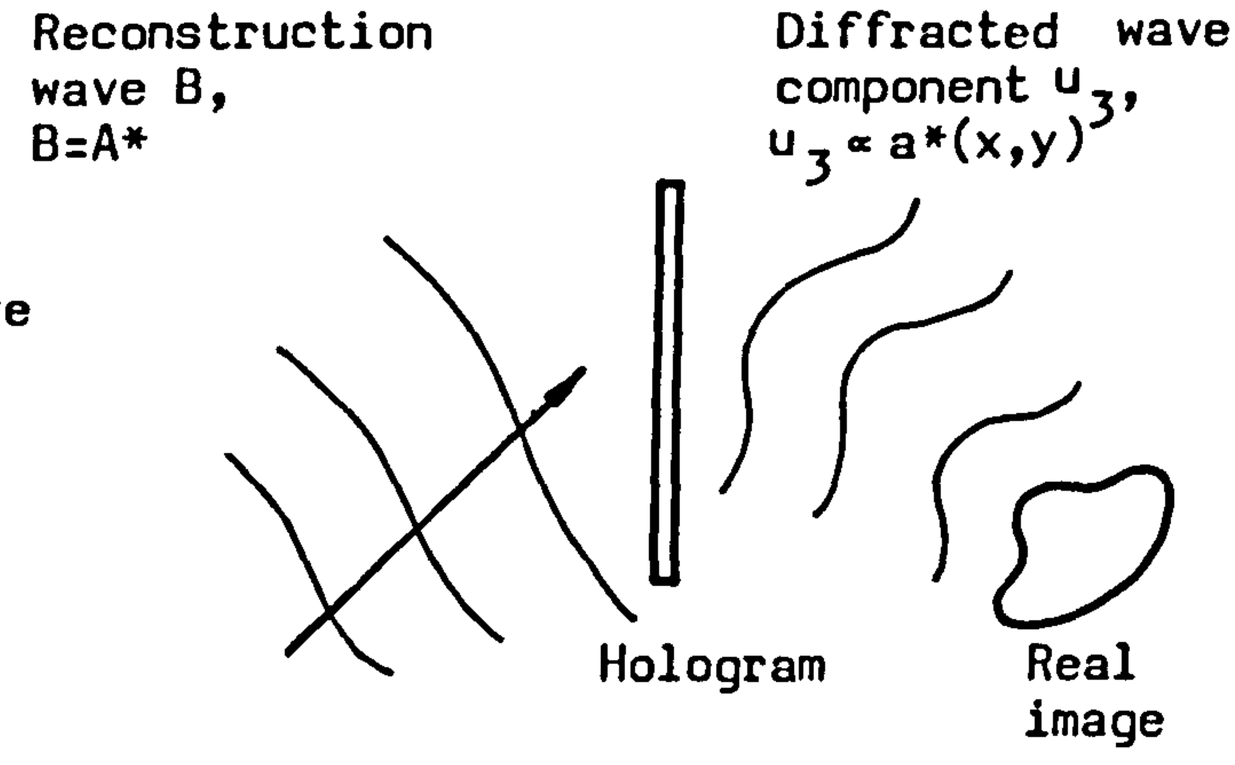


Fig. 2.1 : Imaging with Wavefront Reconstruction

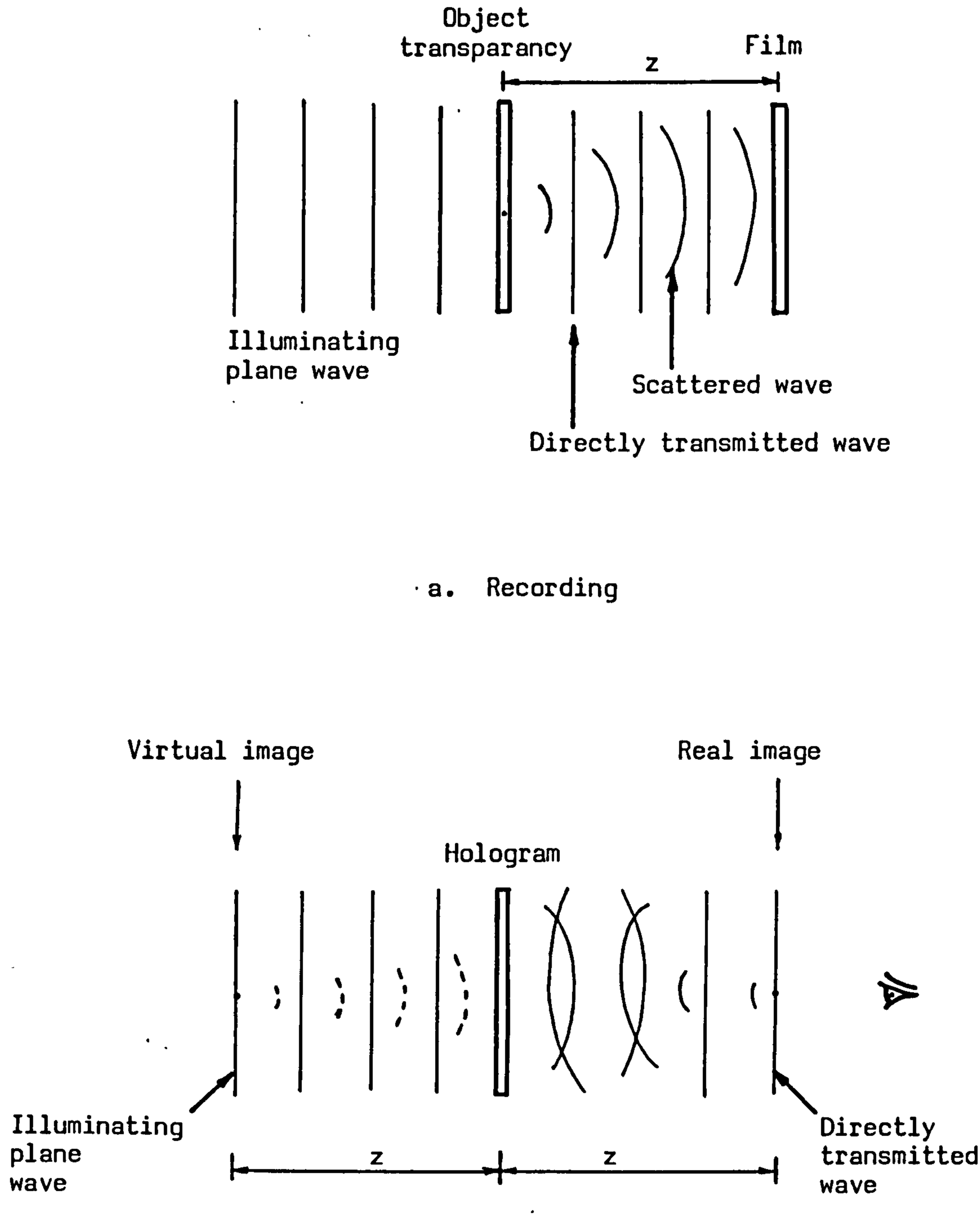


Fig. 2.2 : Recording and Reconstruction of an On-axis Hologram

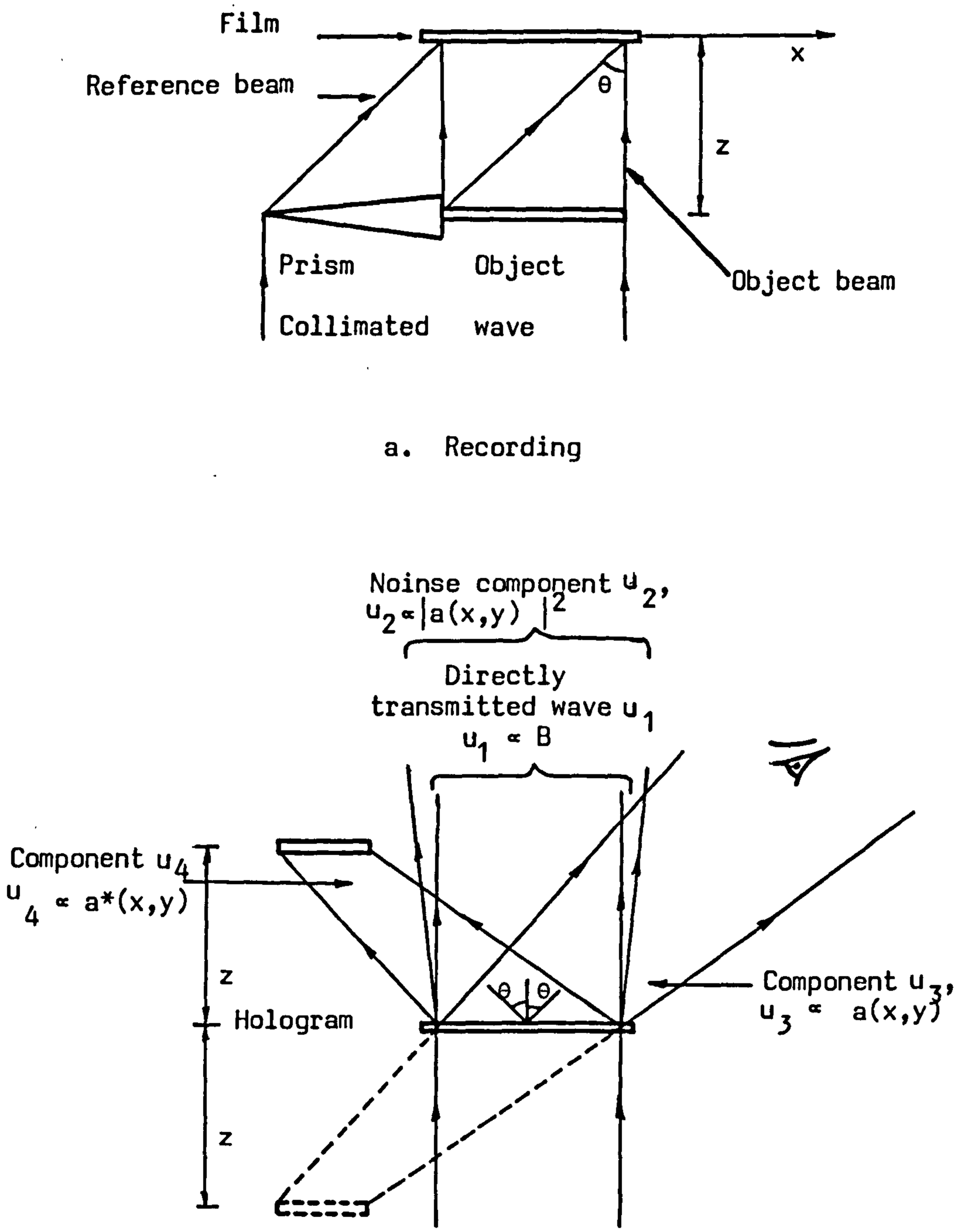


a. Recording

b. Reconstruction

Fig. 2.3 : Recording and Reconstruction of an Off-axis Hologram

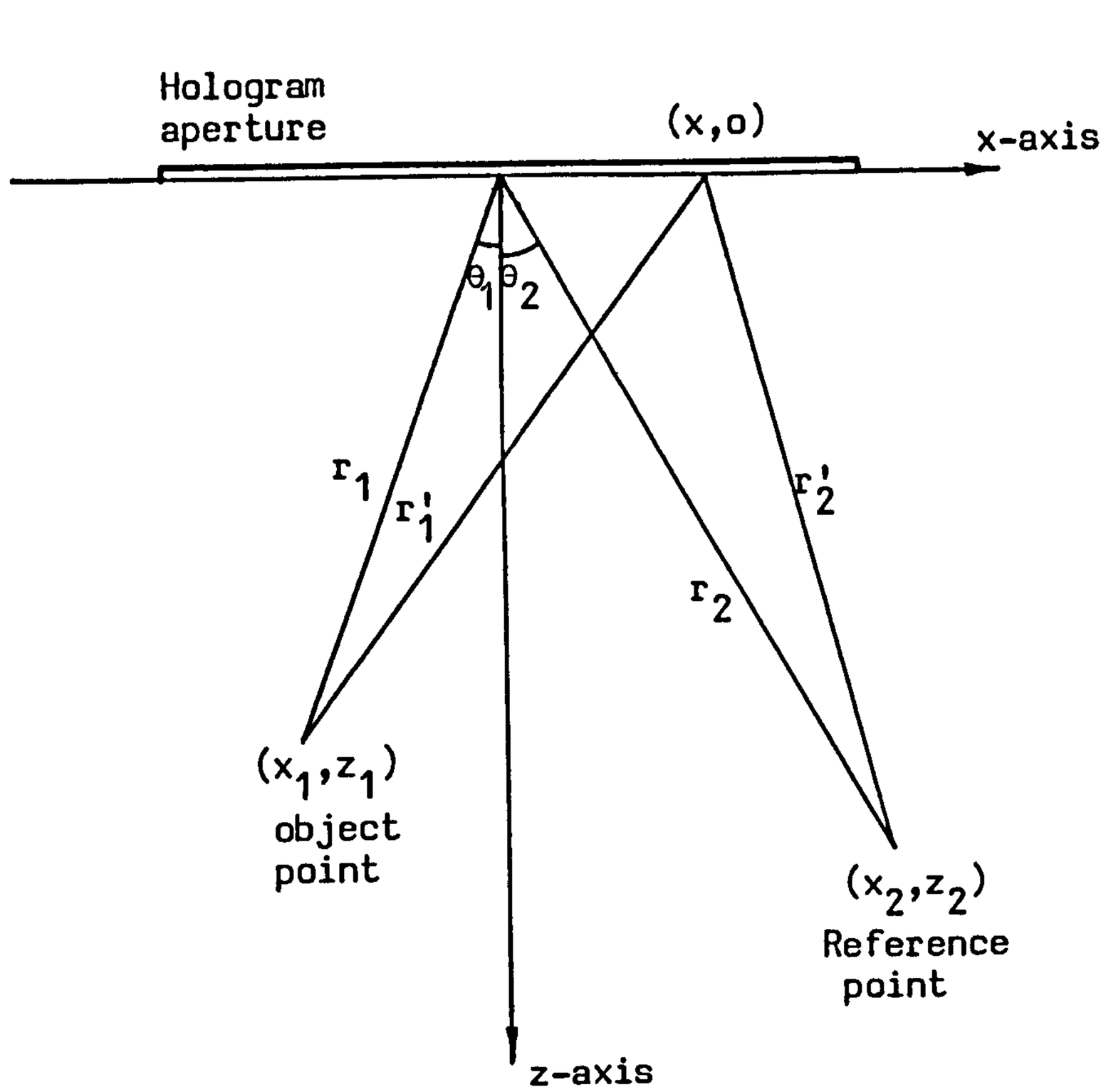


Fig. 2.4 : Geometry for Determining the Maximum Spatial Frequency on the Hologram

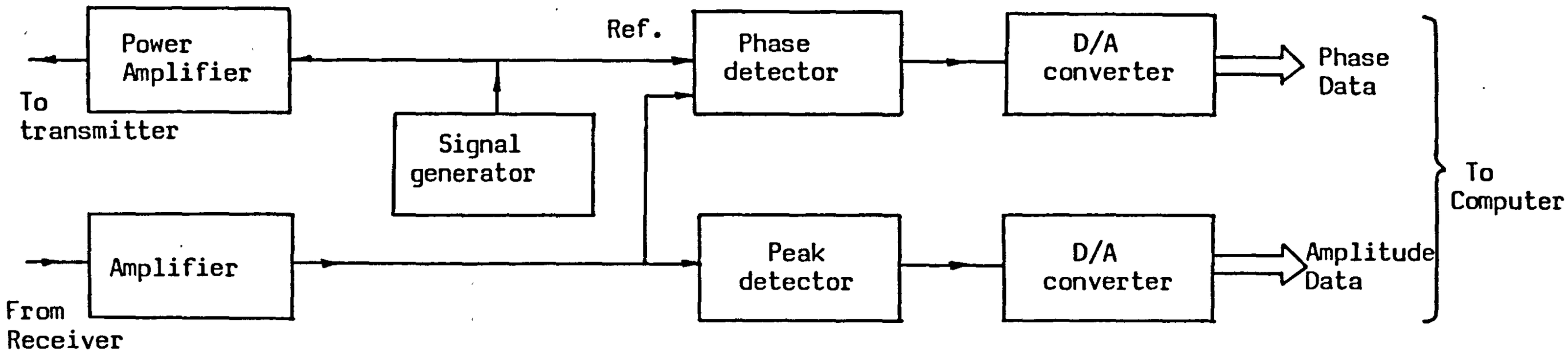


a. Measurement of the amplitude and phase

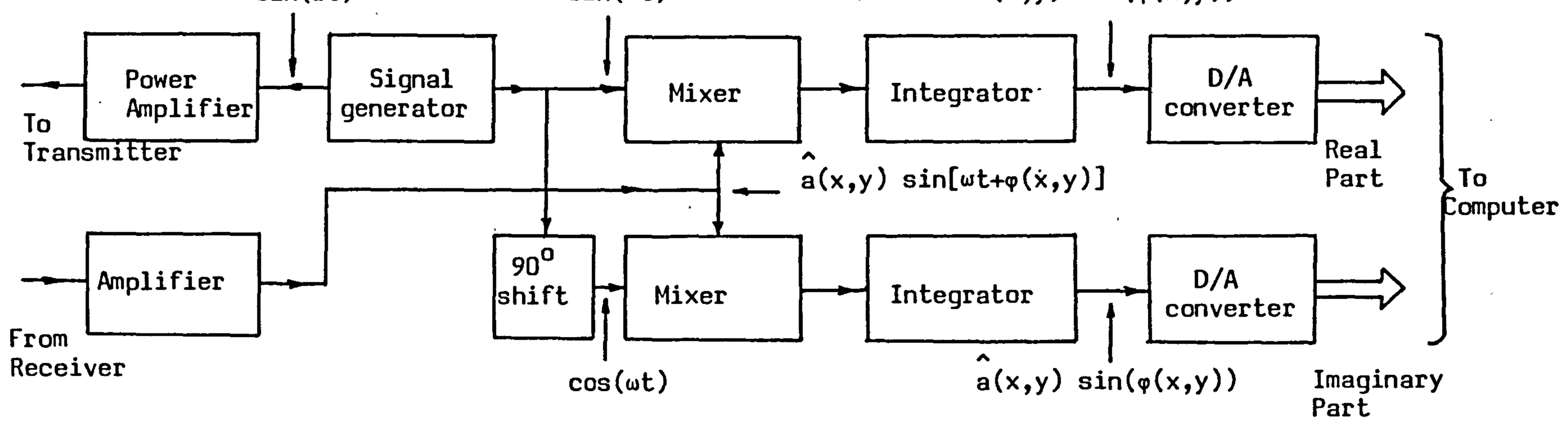


b. Measurement of the real and imaginary parts

Fig. 2.5 : Methods of complex Hologram Acquisition

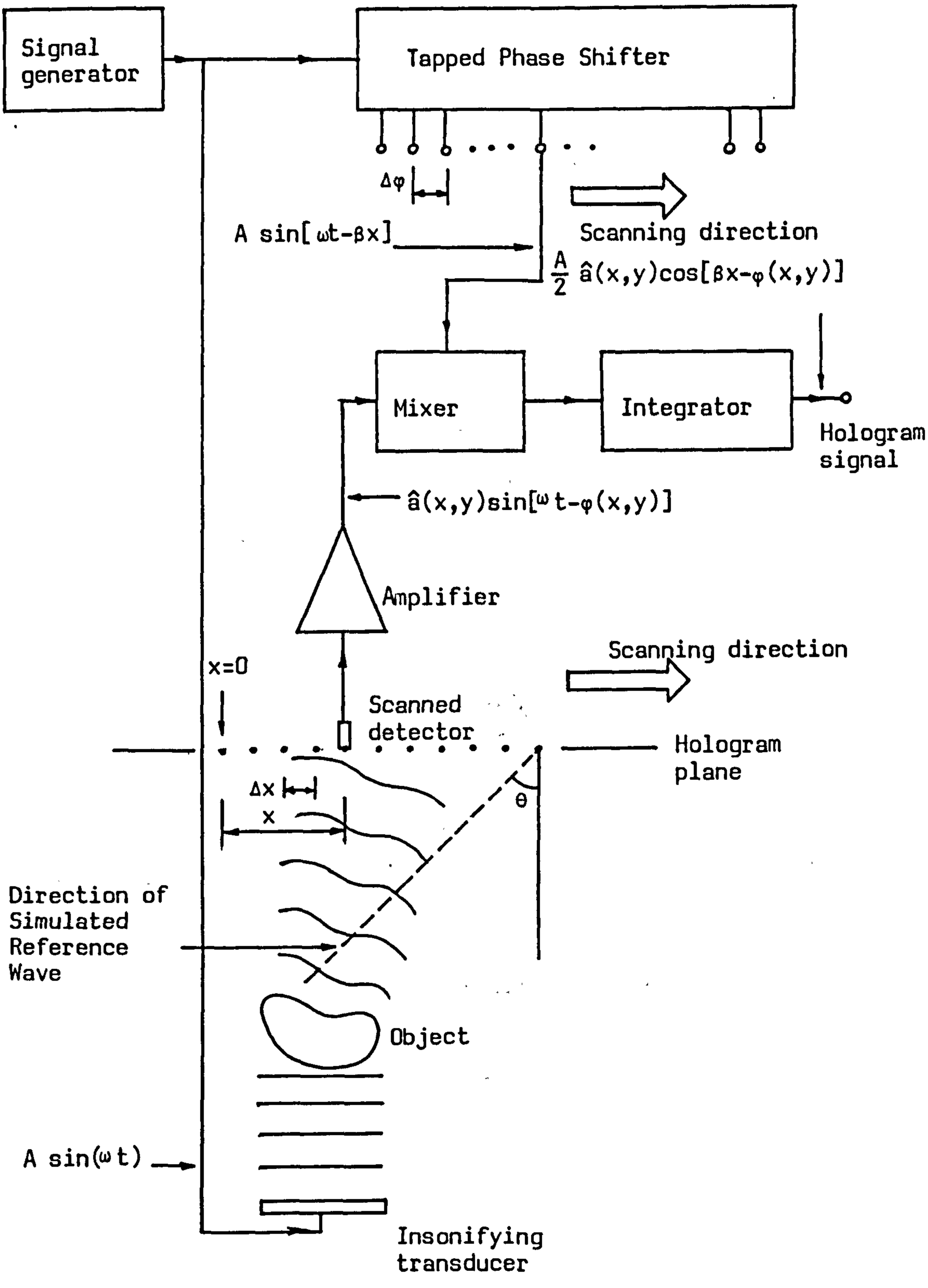


Fig. 2.6 : Simulation of an Off-axis plane wave reference

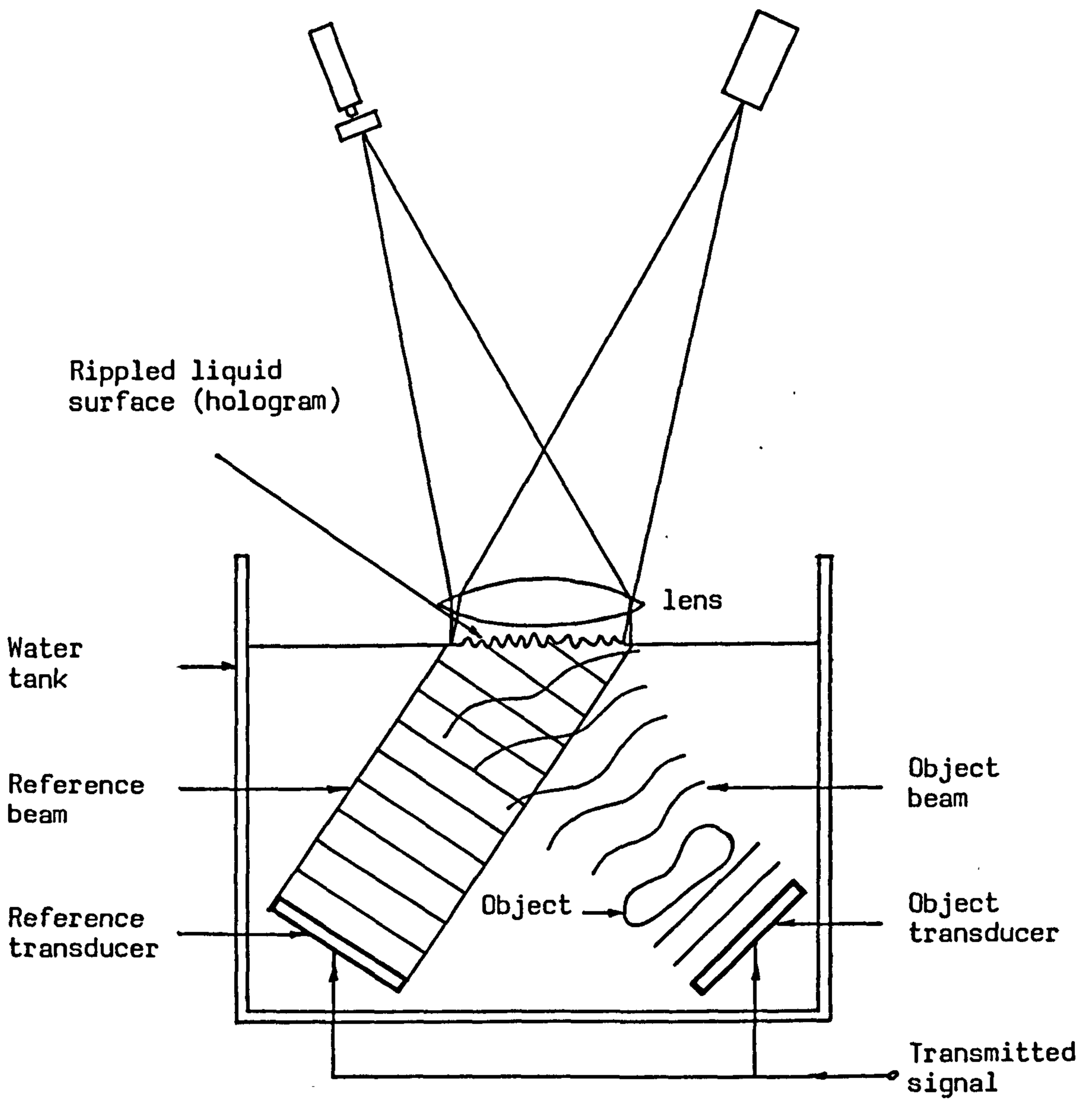


Fig. 2.7 : Liquid-Surface Holographic Imaging with Real-time Reconstruction

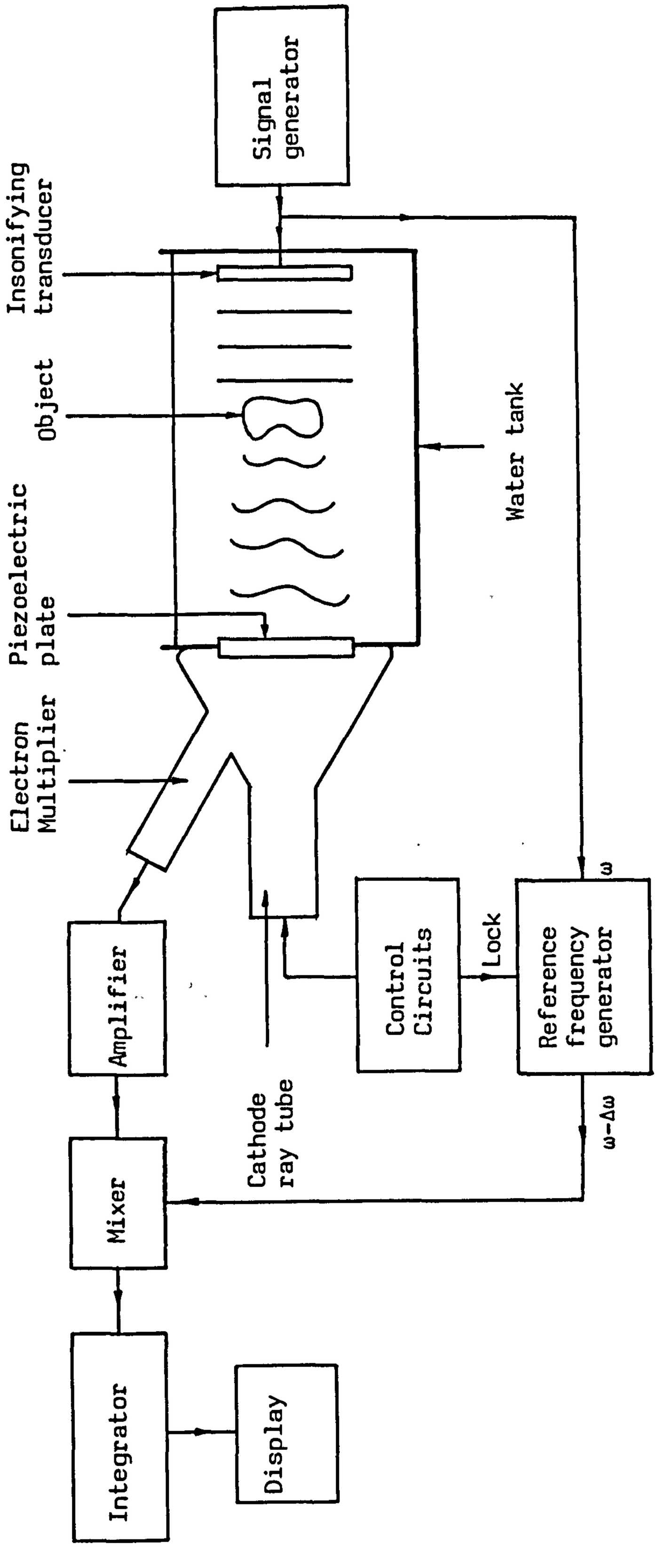


Fig. 2.8 : Schematic Diagram for Hologram Recording with the Ultrasonic Camera Using Electronic Reference

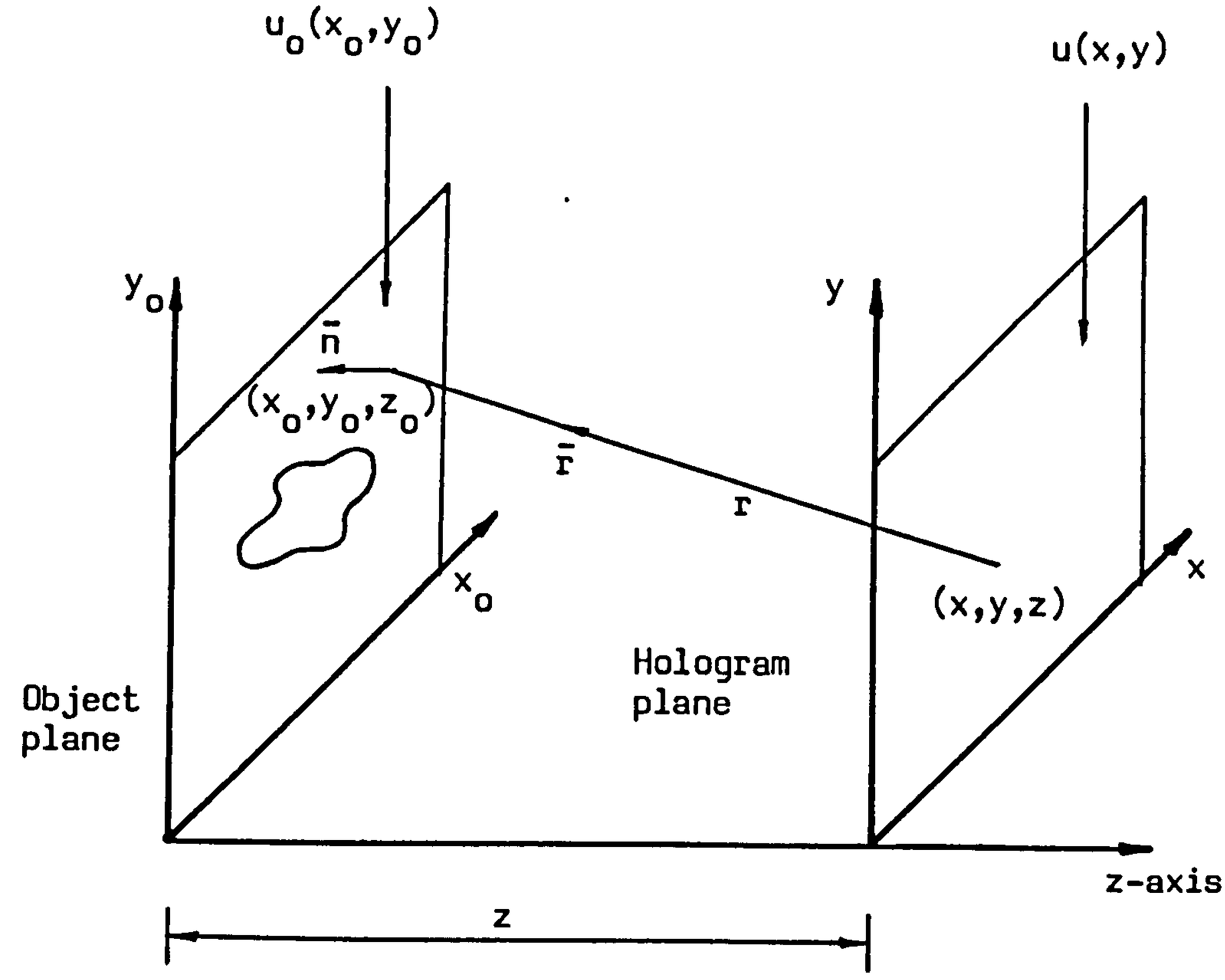


Fig. 2.9 : Geometry for Object Scattering and Hologram Sensing

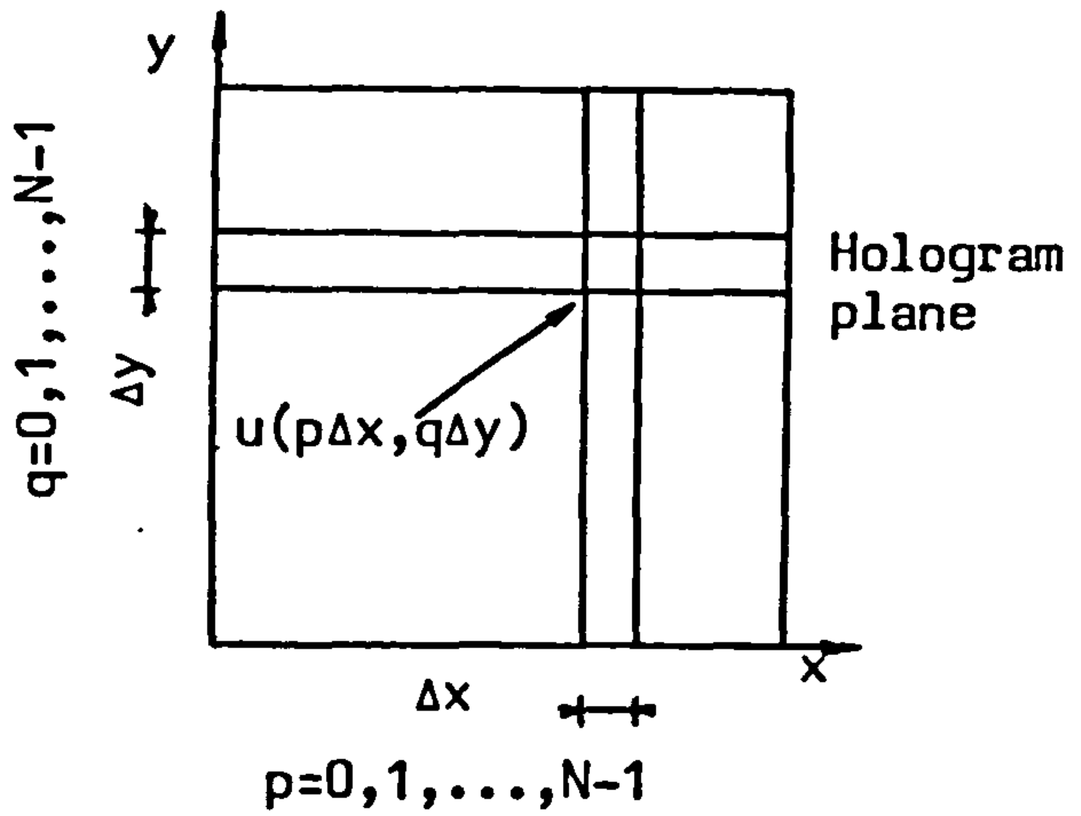


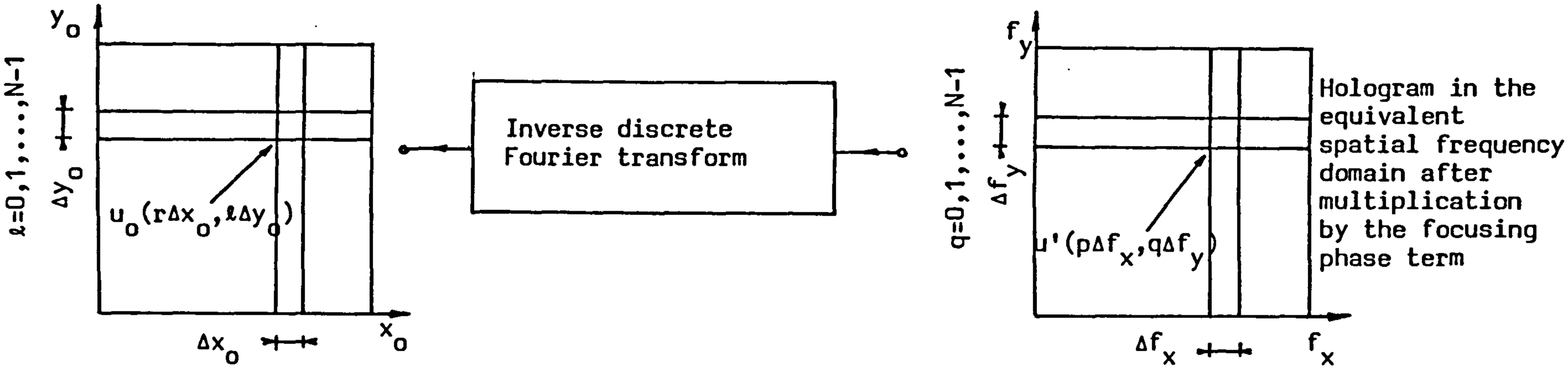


$$u'(p\Delta f_x, q\Delta f_y) = u(p\Delta x, q\Delta y)\exp\{-j\frac{k}{2z}[(p\Delta x)^2+q\Delta y)^2]\}$$

Fig. 2.10 : Configuration for Image Reconstruction Using the Fresnel Integral Algorithm in the Discrete Form

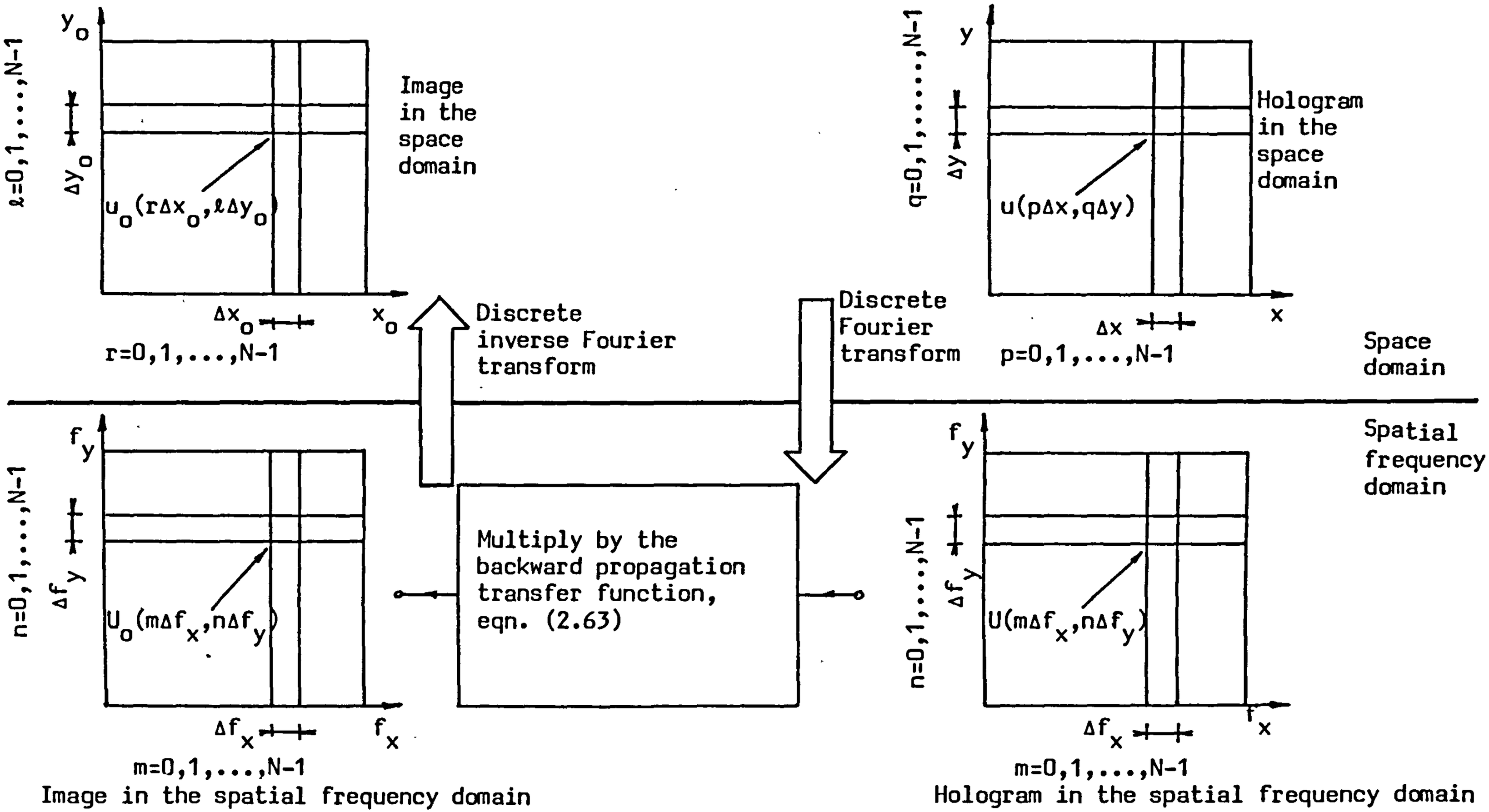


Image in the spatial frequency domain

Hologram in the spatial frequency domain

Fig. 2.11 : Configuration for Image Reconstruction Using the Backward Propagation (Frequency Domain) Algorithm in the Discrete Form

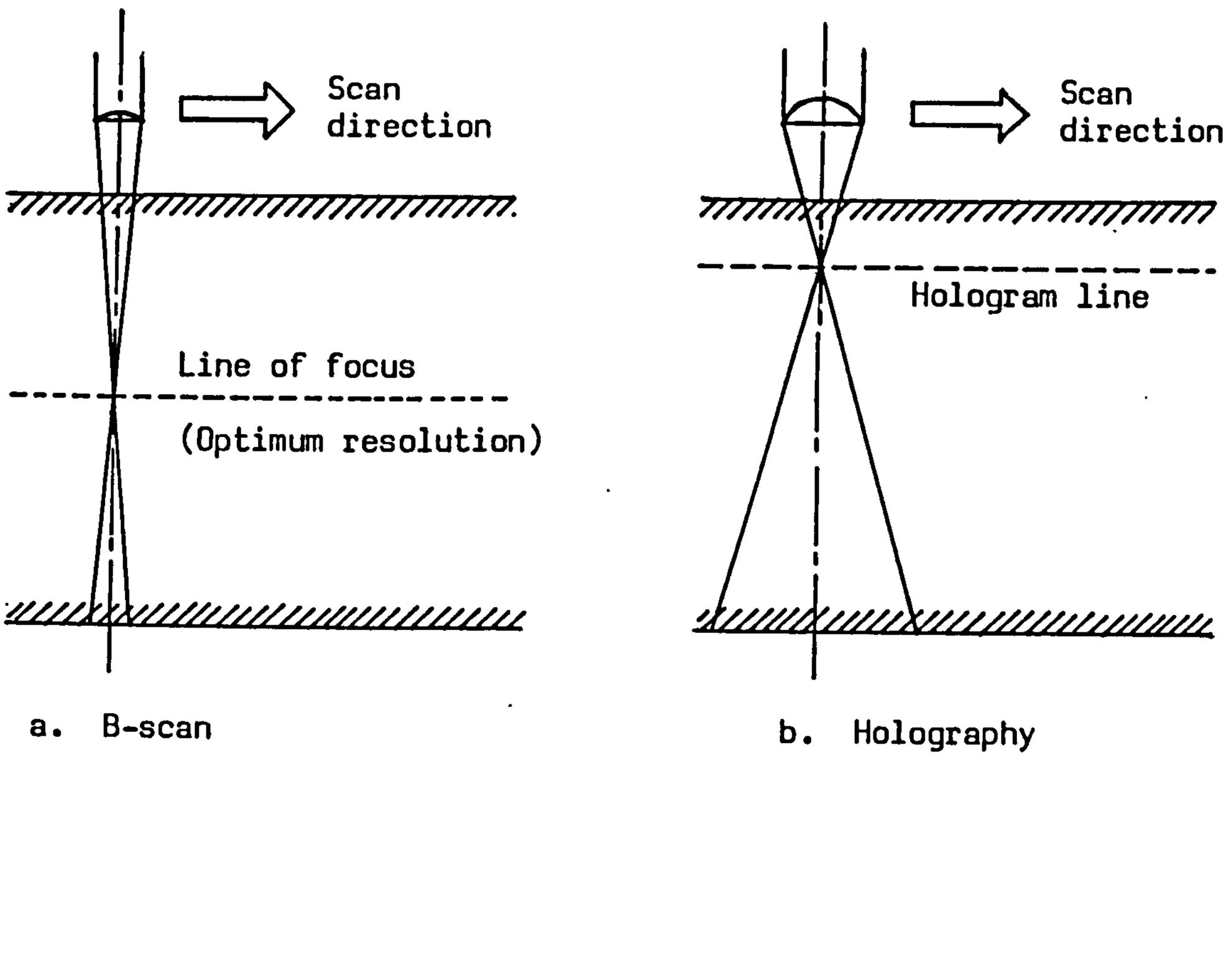


Fig. 2.12 : Comparison Between the Transducer focusing requirements for Both B-scan and Holography

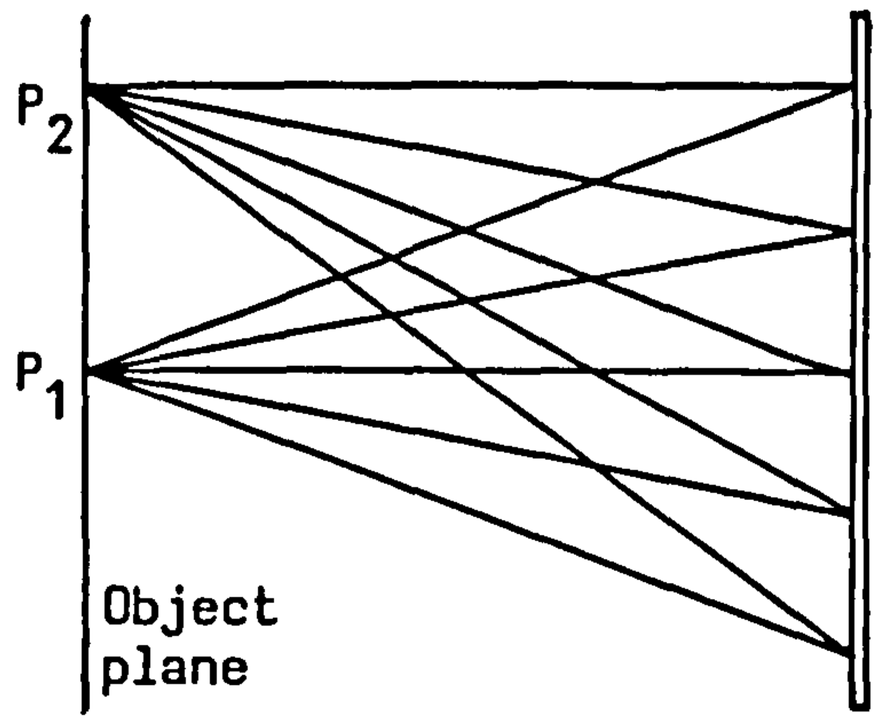


a. Basic problem in orthoscopic imaging

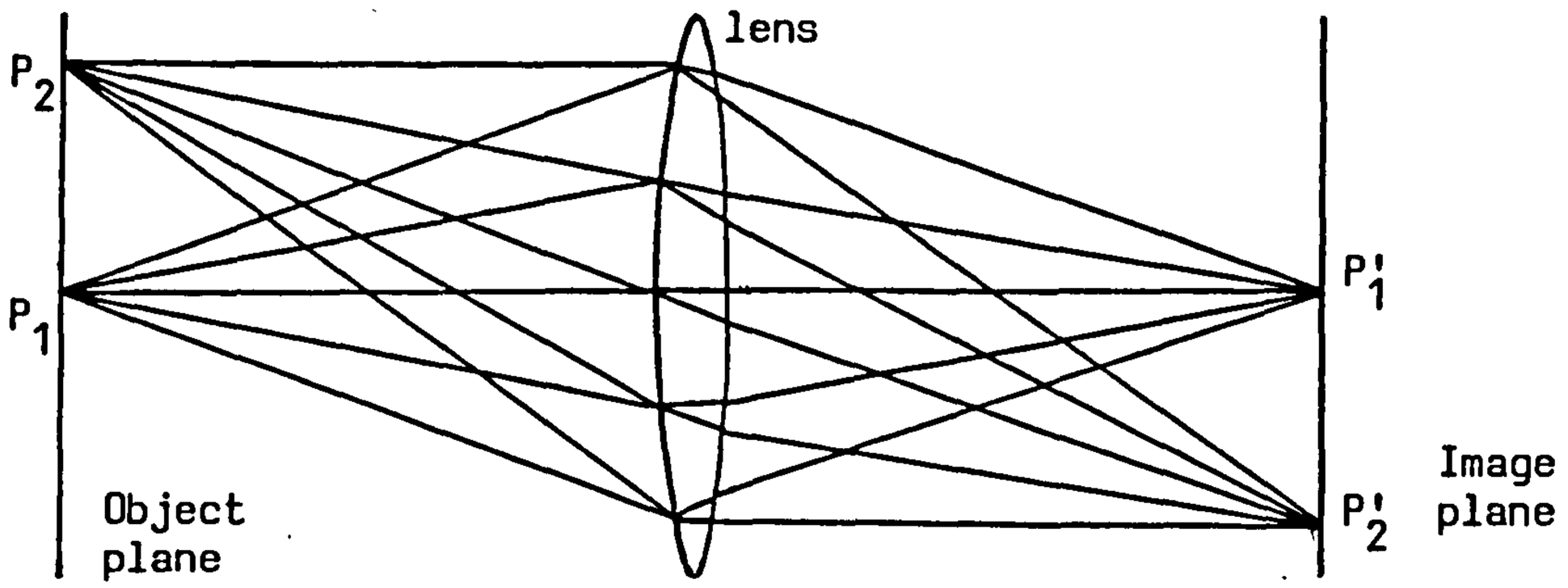


b. Principle of image generation in lens systems

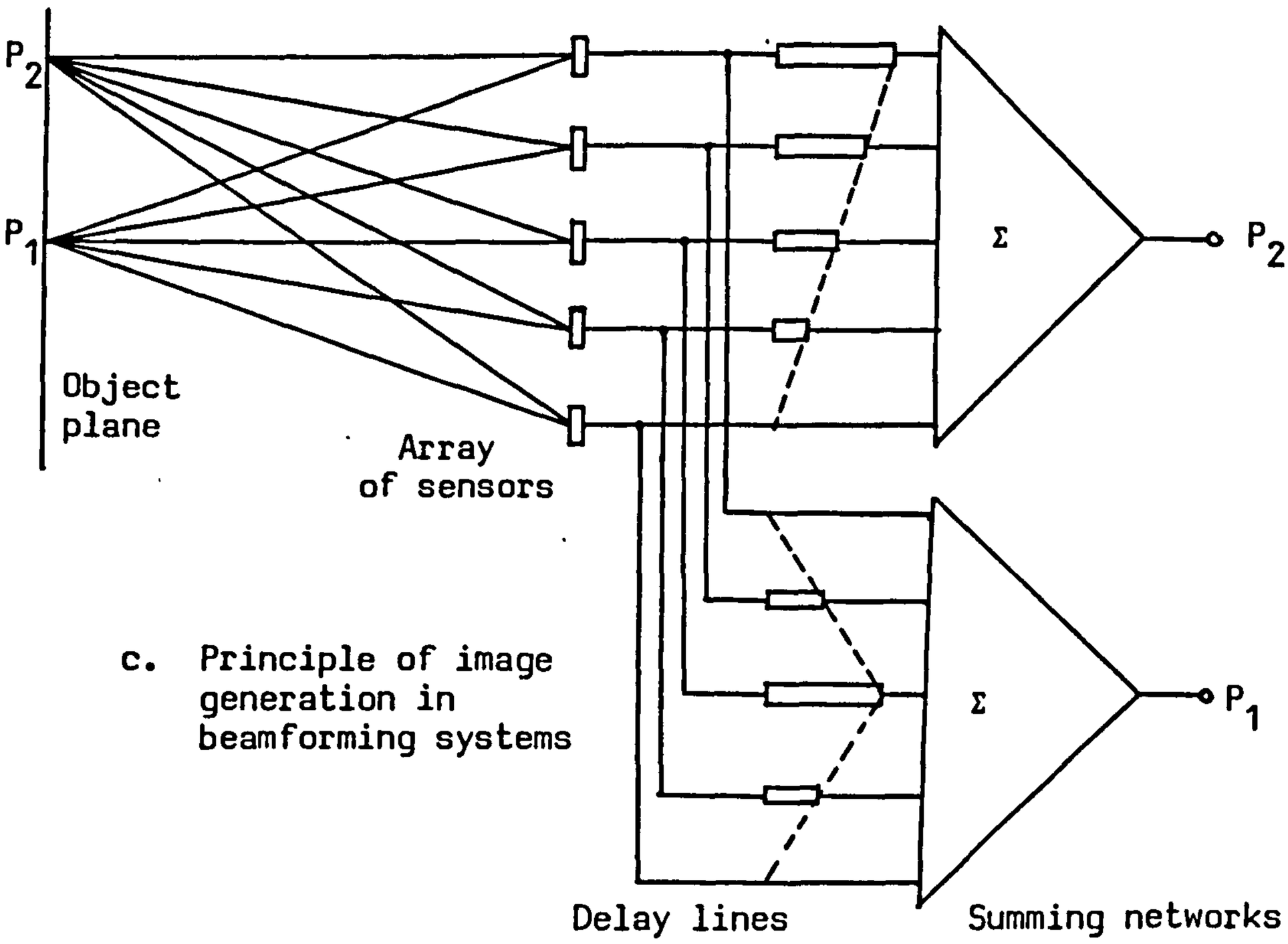


c. Principle of image generation in beamforming systems

Fig. 2.13 : Principles of Orthoscopic Acoustic Imaging

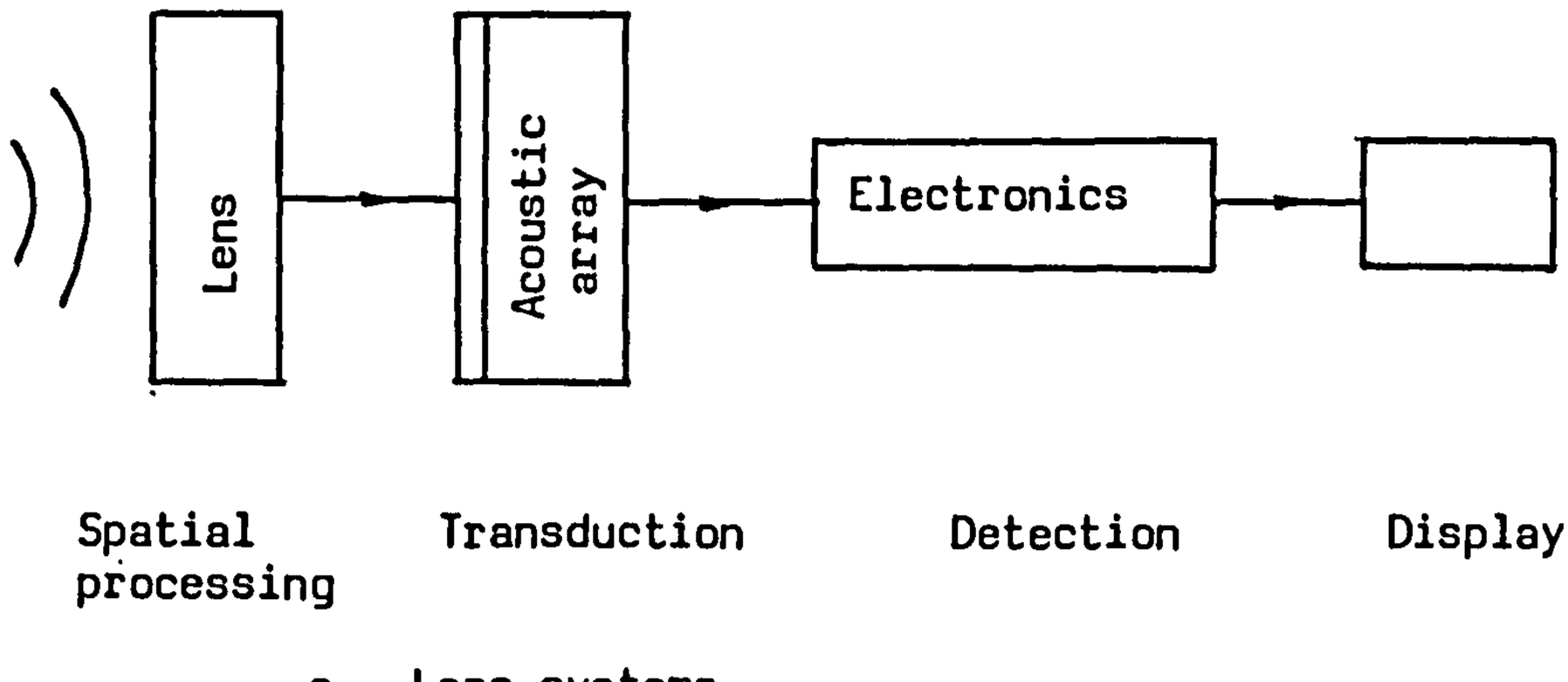


a. Lens systems

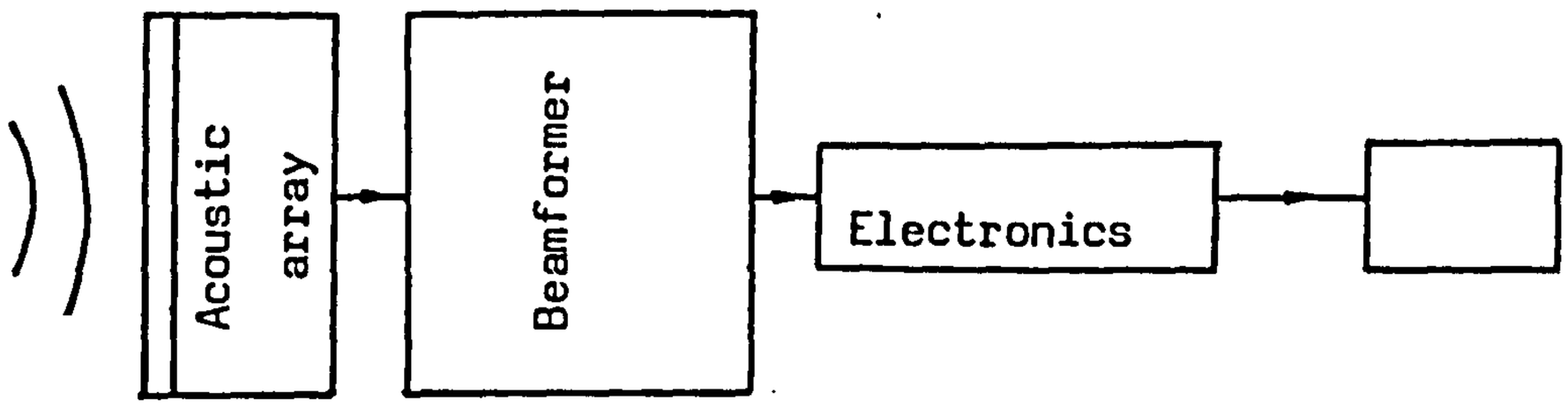


b. Beamforming systems

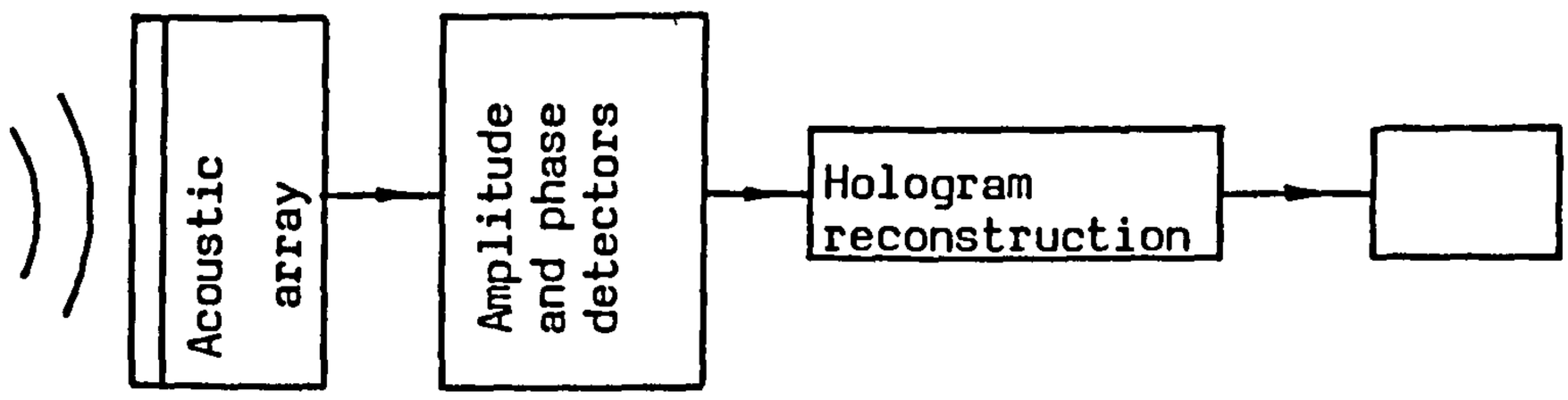


c. Holographic systems

Fig. 2.14 : Basic Operations in Orthoscopic Acoustic Imaging Systems

# Figures for Chapter 3

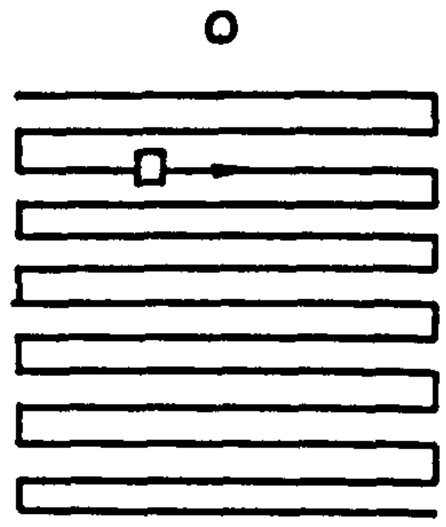

a. Raster scan of a single receiver



b. Linear scan of a linear RX array

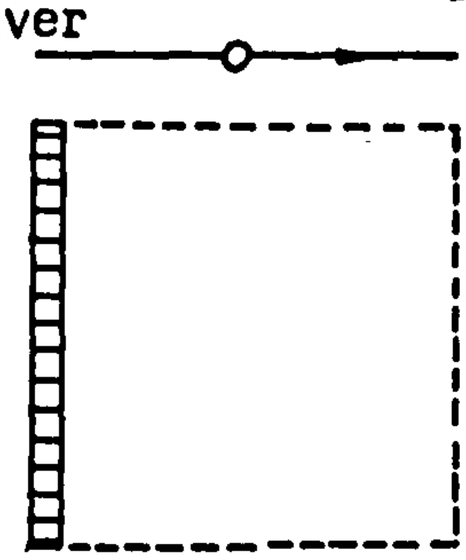


c. Fixed linear RX array and a scanned single transmitter

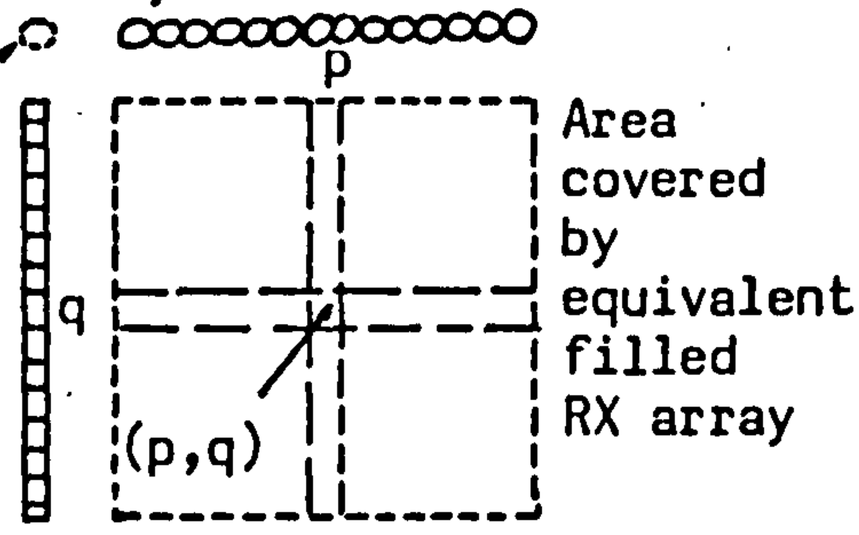


d. Fixed linear RX array and a switched linear TX array (Well's cross)

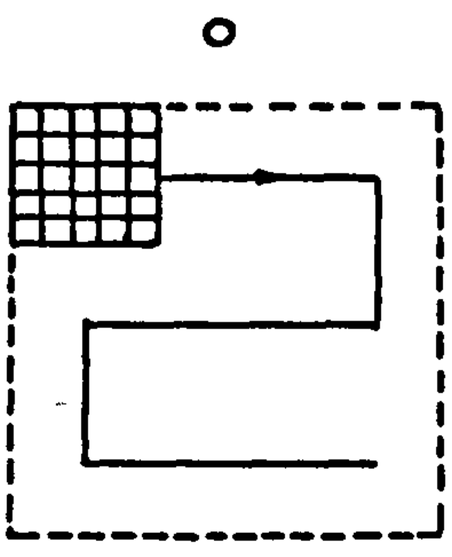

e. Raster scan of a small filled RX array

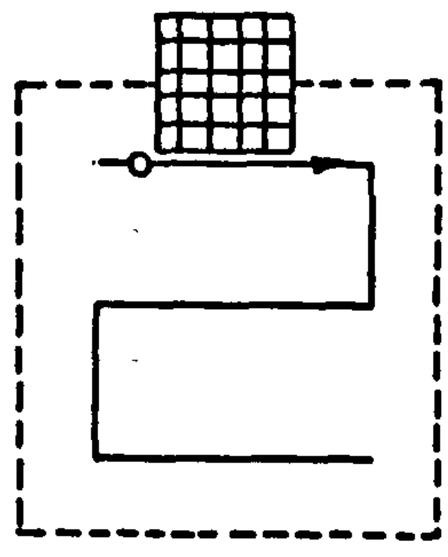

f. Raster scan of a single transmitter, with a fixed,small, filled RX array

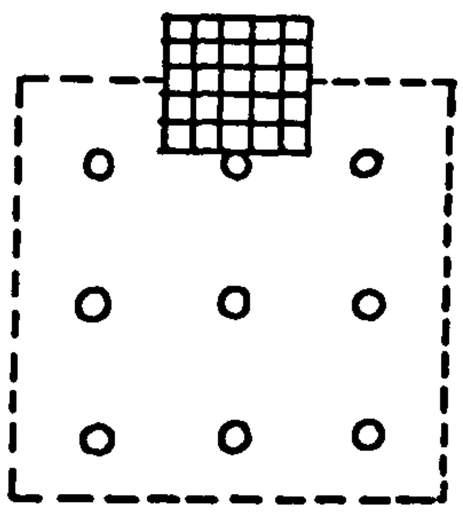

g. A sparse TX array with a small filled RX array

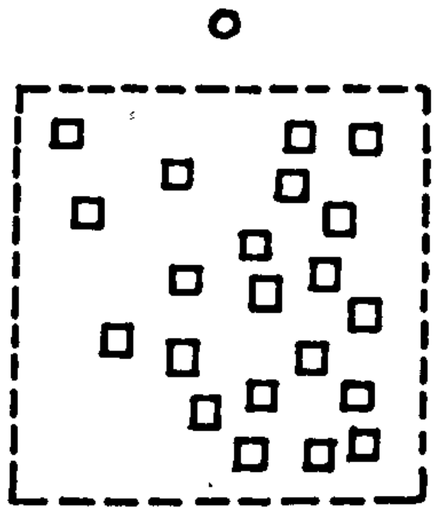

h. Thinning of a filled RX array using nonuniform sampling

o: Transmitter(TX), □: Receiver (RX)

Fig. 3.1 : Synthetic Aperture Techniques

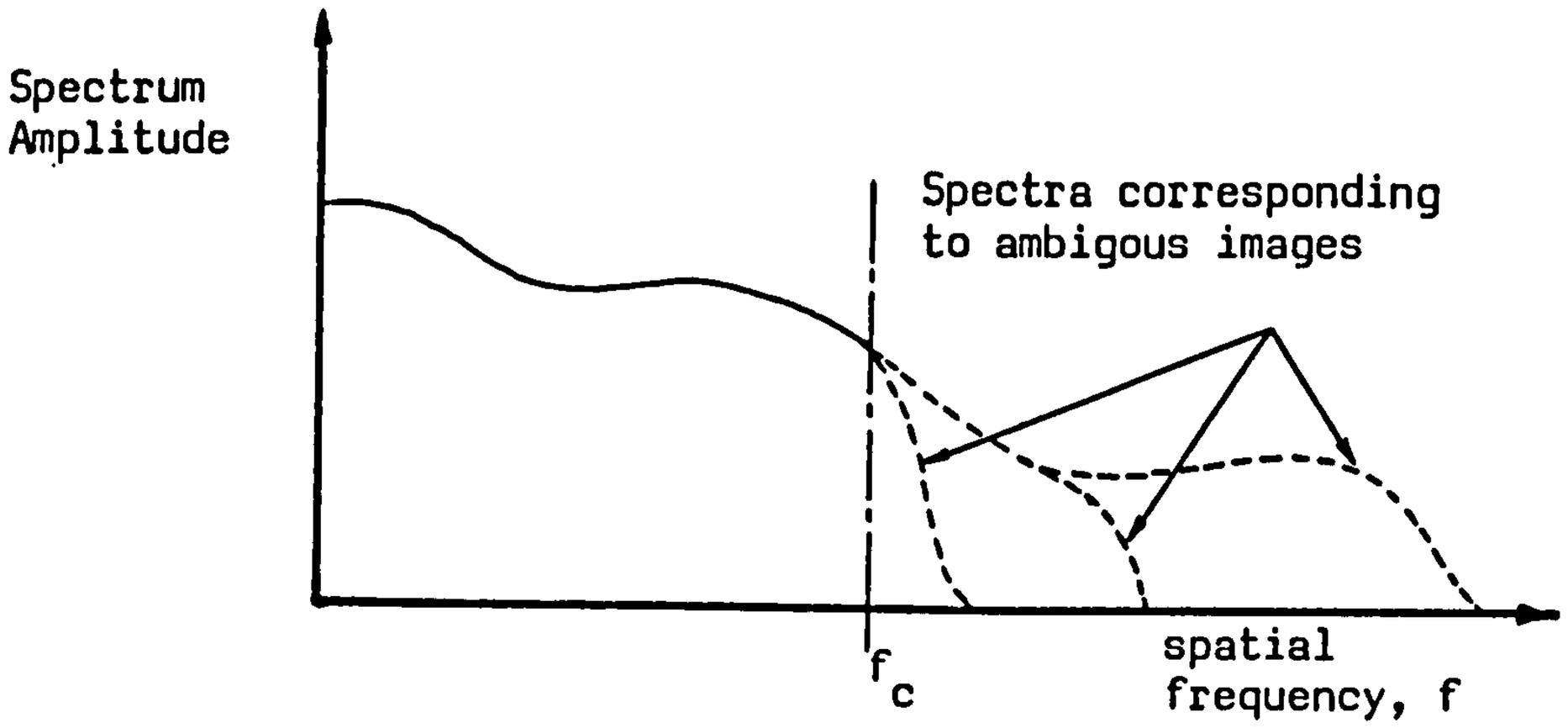


Fig. 3.2 : The concept of ambigous images in the spatial frequency domain

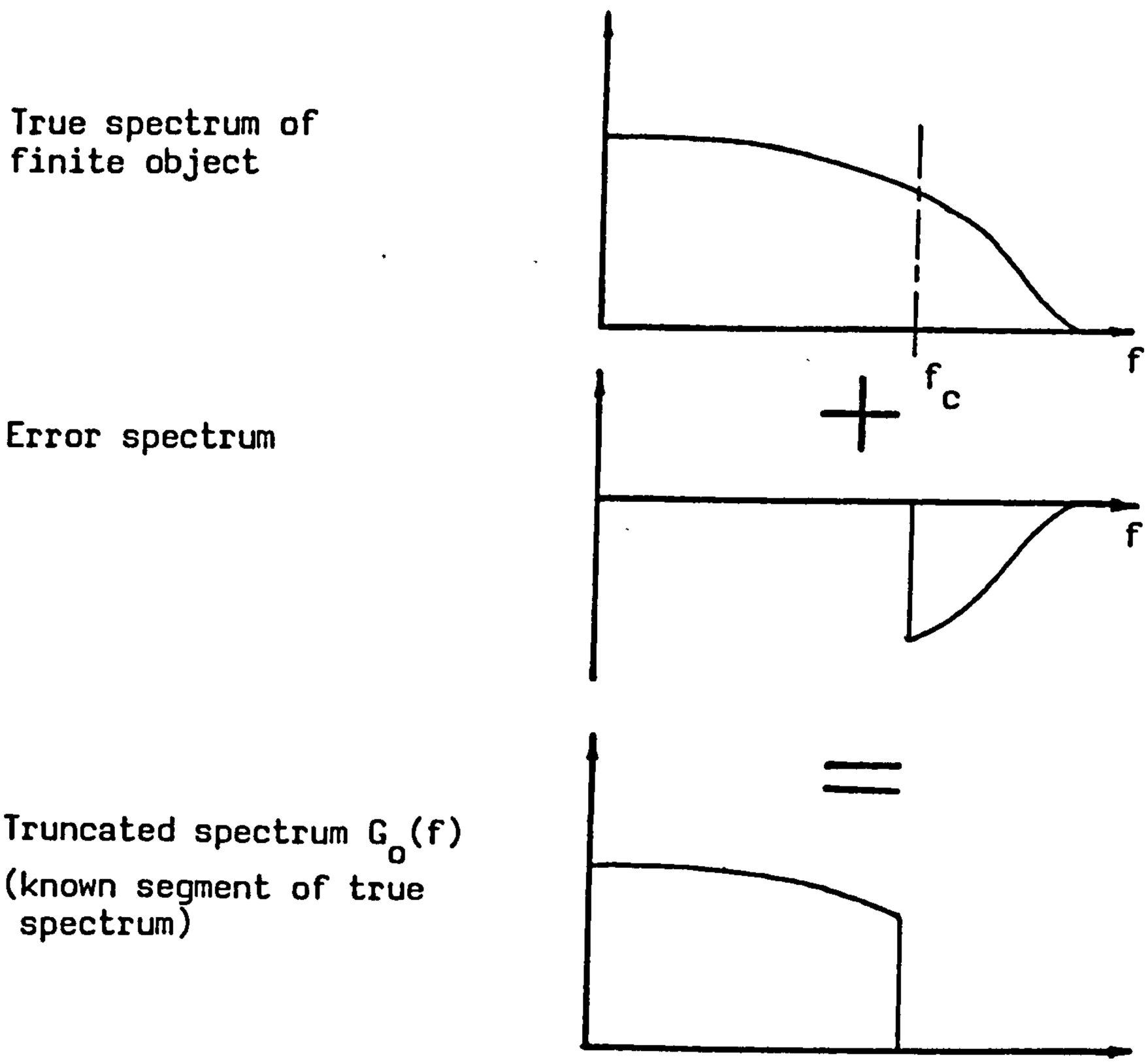


Fig. 3.3 : The concept of error spectrum in Gerchberg's method for object restoration

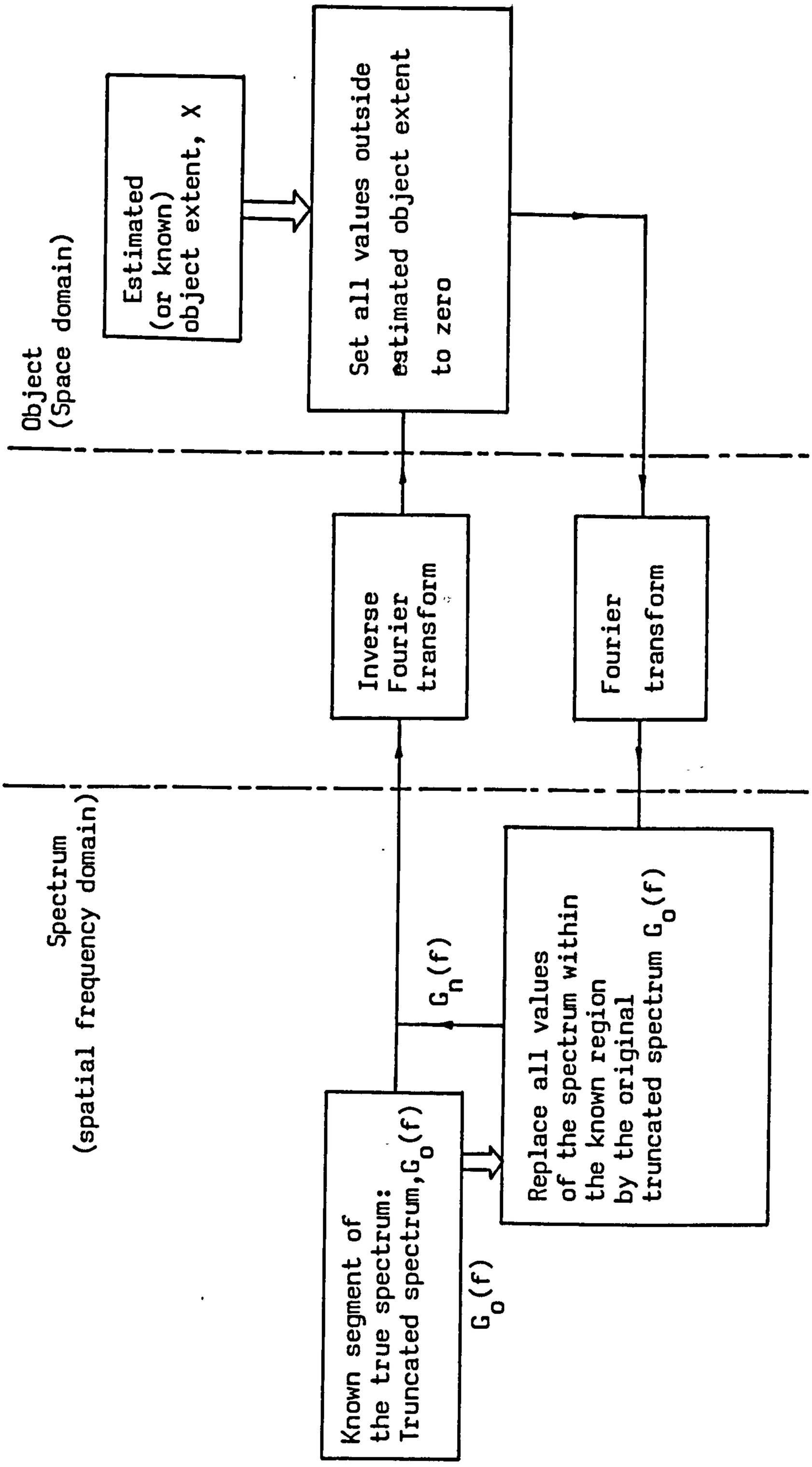


Fig. 3.4 : Schematic diagram of Gerchberg's method for object restoration

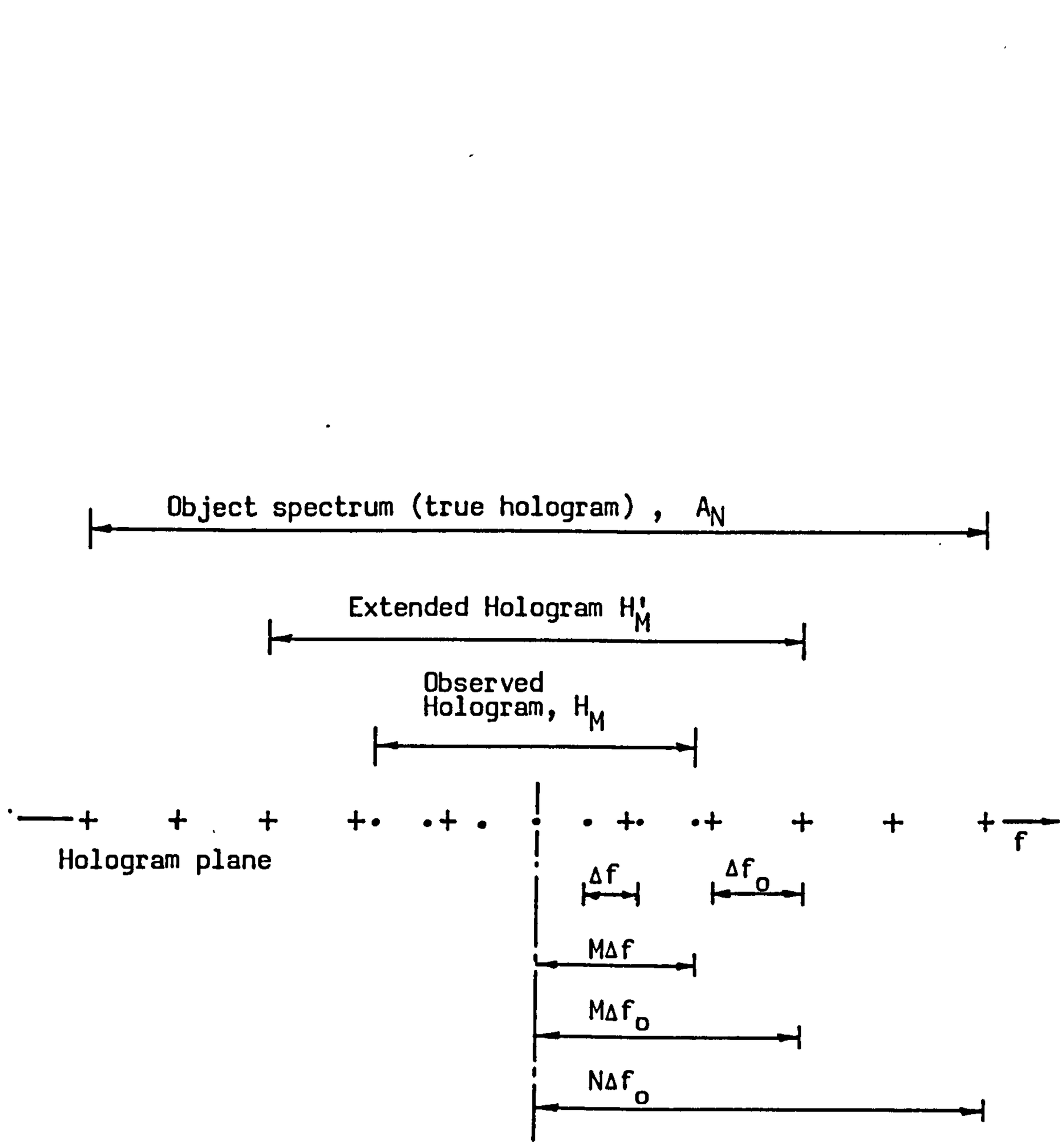


• Observed samples

+ Samples to be estimated

Fig. 3.5 : Schematic construction to show the relationship between the observed, estimated, and true holograms in Sato's technique for aperture expansion

# Figures for Chapter 4

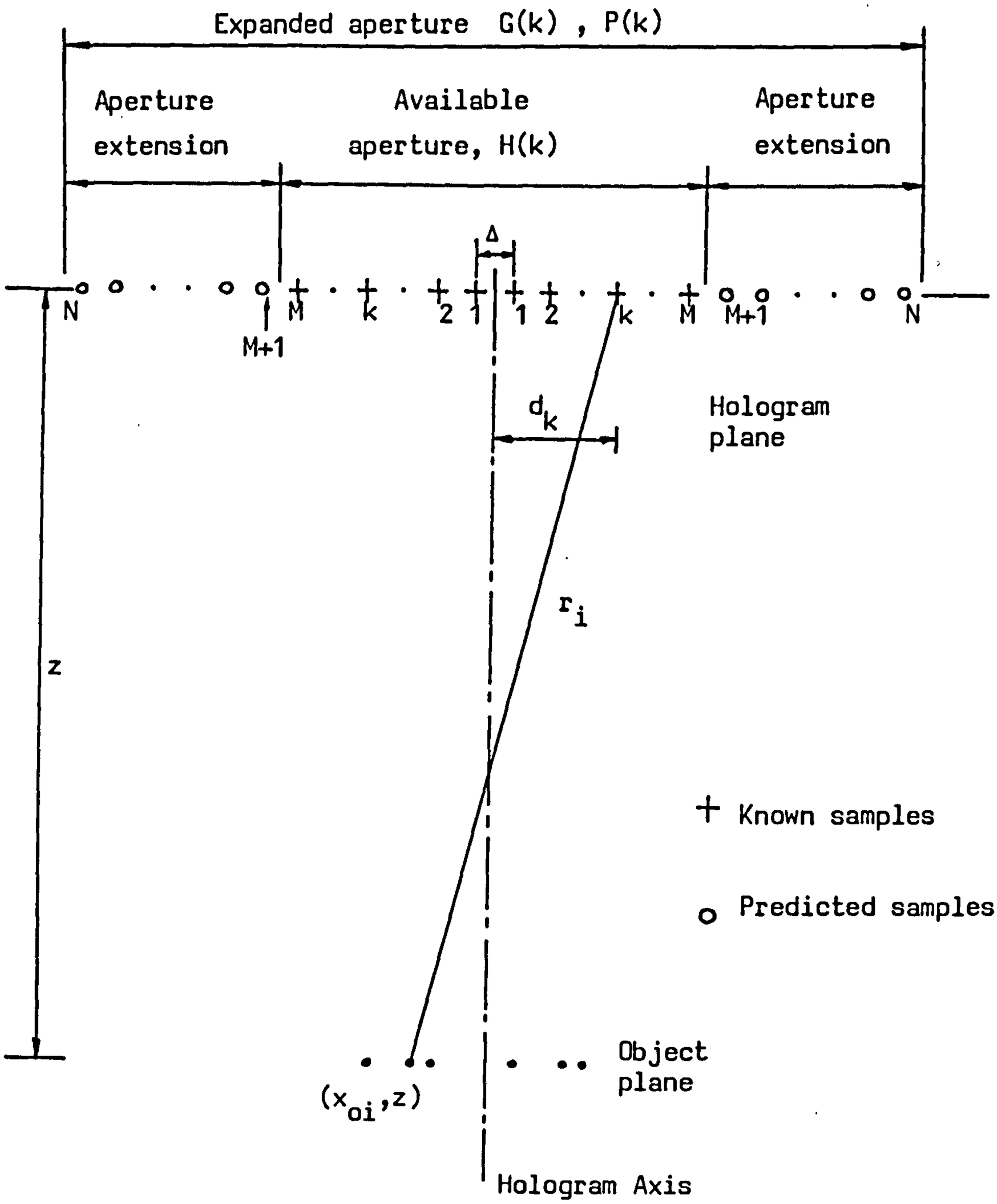


Fig. 4.1 : Geometry for aperture expansion in a holographic imaging system

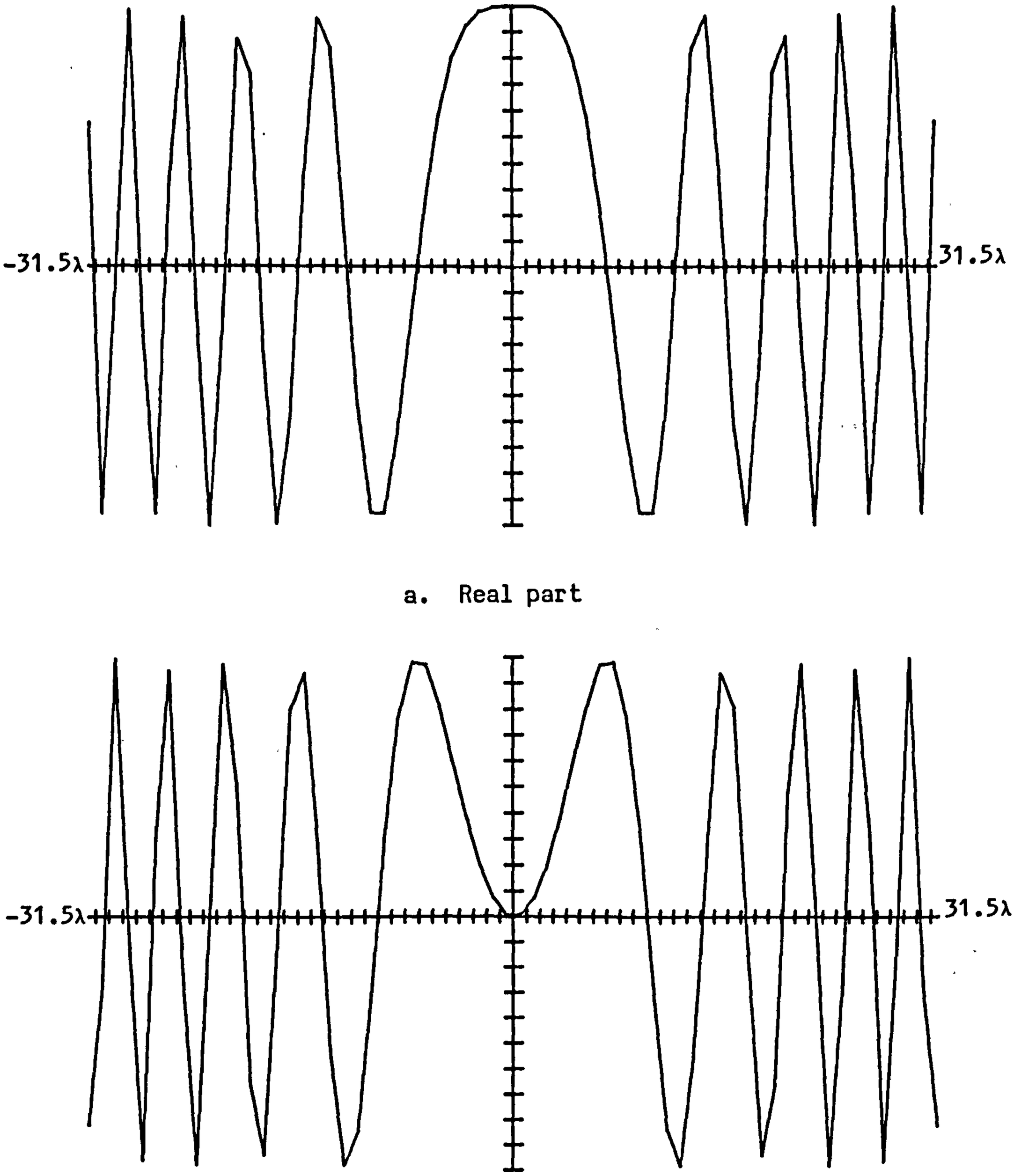


a. Real part

b. Imaginery part

Hologram : N=64 ,Δ =1

Object : 1-point ; $x_o$ = 0, z = 100λ

Fig. 4.2 : Hologram function for a 1-point object

a. Prediction error over the aperture

<u>Hologram</u>:

$\Delta = 1\lambda$
$M = 8$
$N = 32$

<u>Object</u>:

$x_o = 0$
$z^o = 100\lambda$

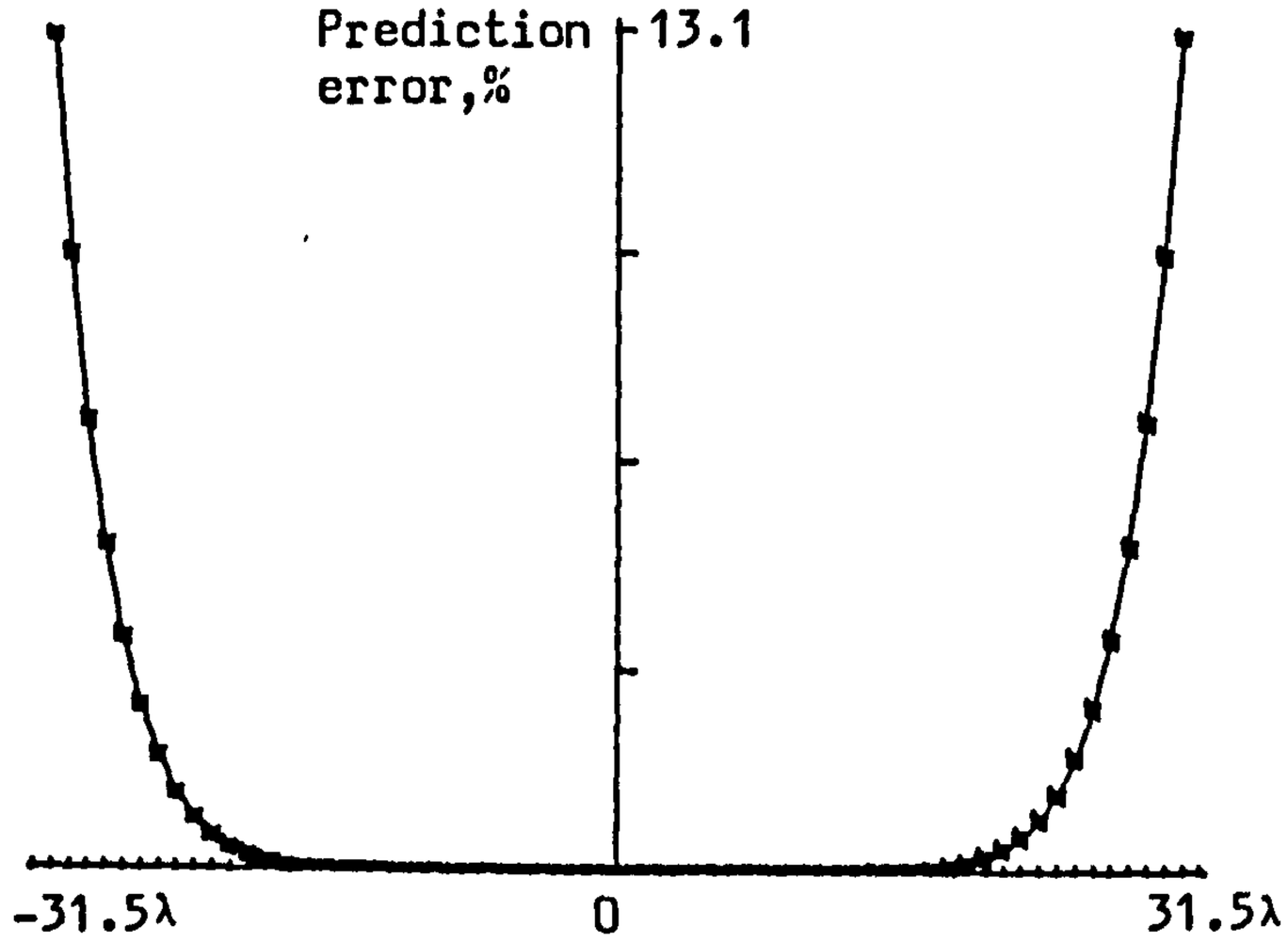


b. Intensity of reconstructed images from the small, true, and predicted apertures

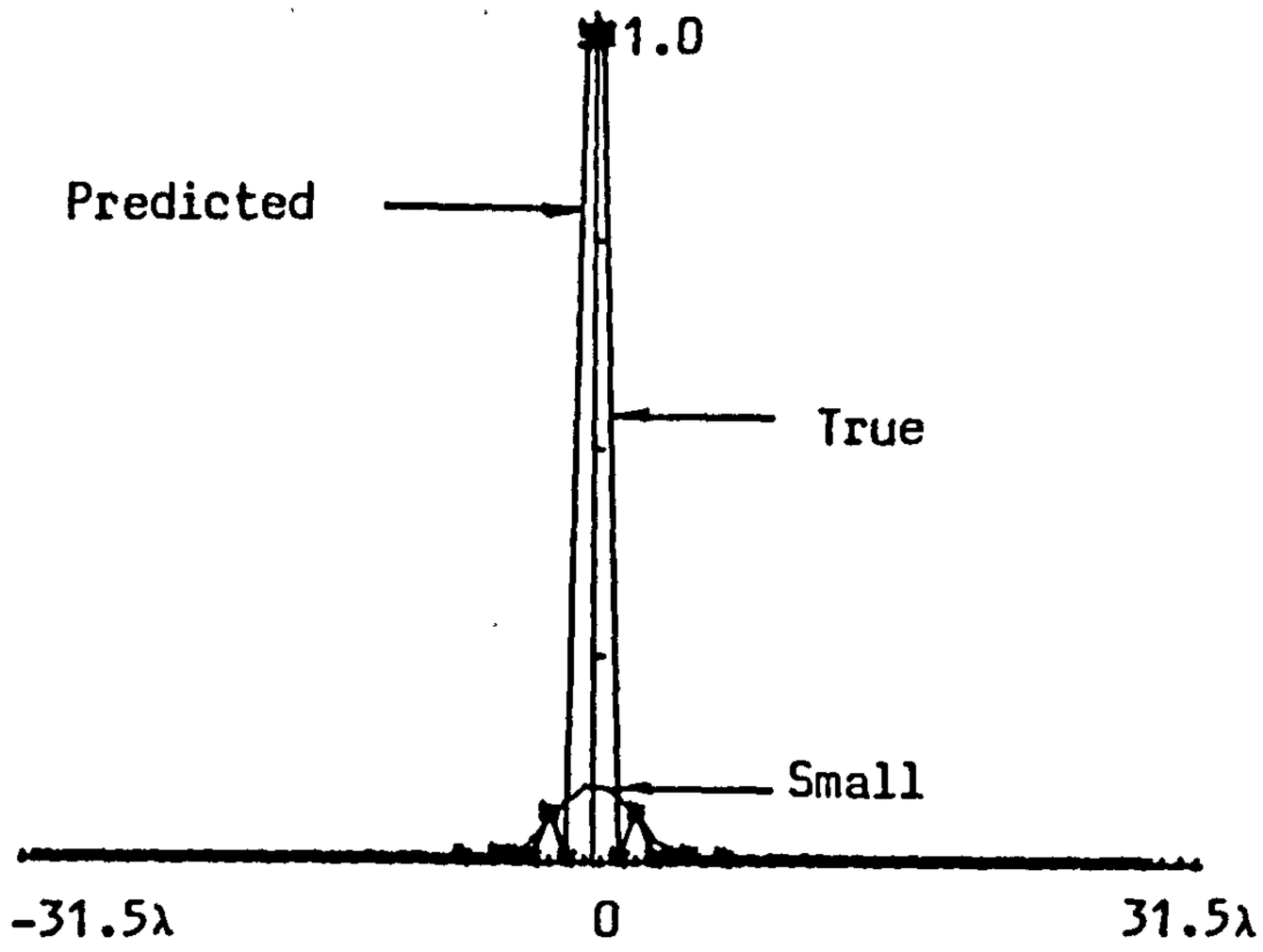


c. Intensity of reconstructed images normalized to the same peak value

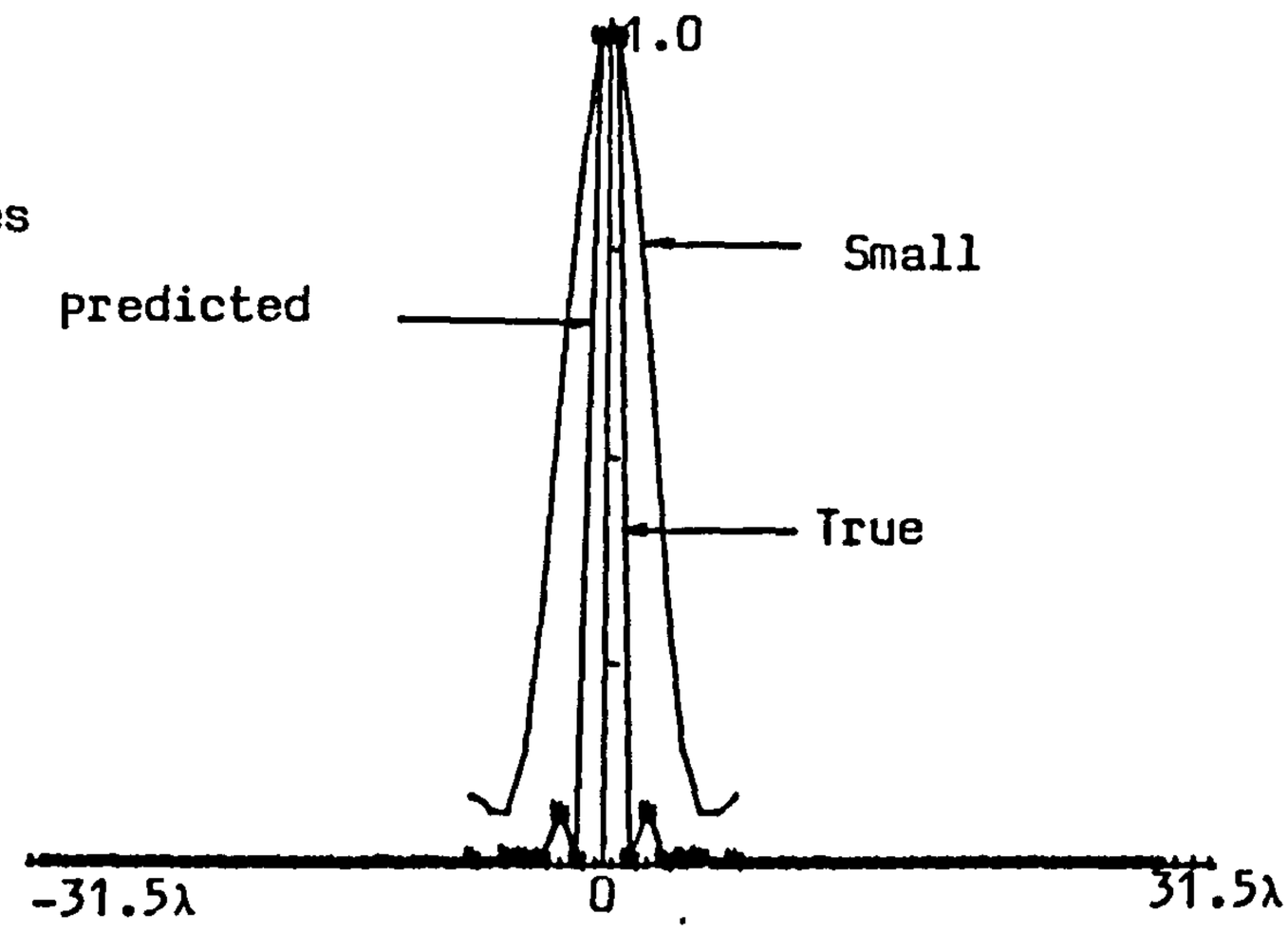


Fig. 4.3 : Expanding a 16-point aperture four times using a power series polynomial predictive model.

Object : 1-point

a. Prediction error over the aperture

<u>Hologram:</u>

$\Delta = 1\lambda$
M = 8
N = 32

<u>Object:</u>

$x_o = 5\lambda$
$z^o = 100\lambda$

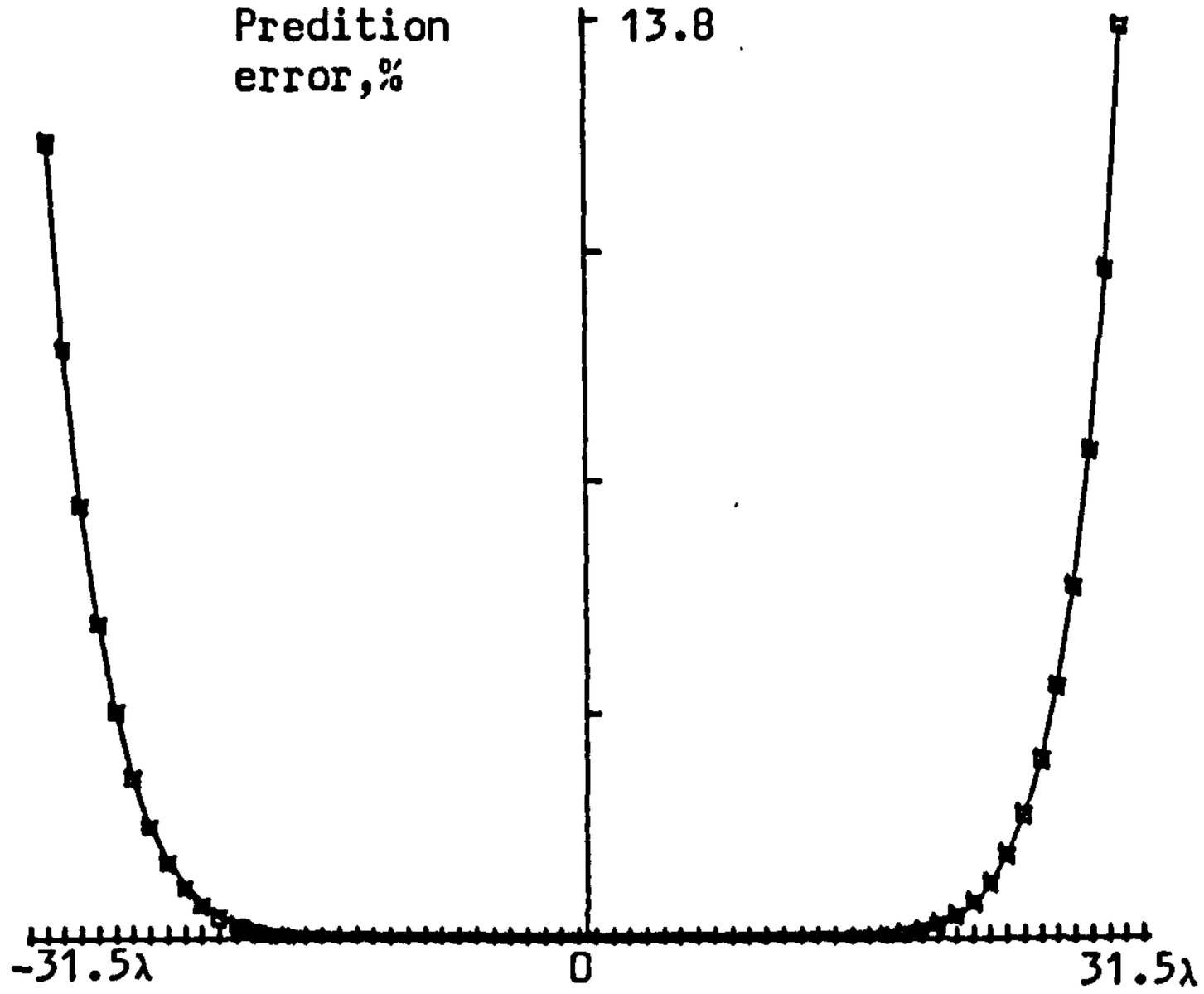


b. Intensity of reconstructed images normalized to the same peak value

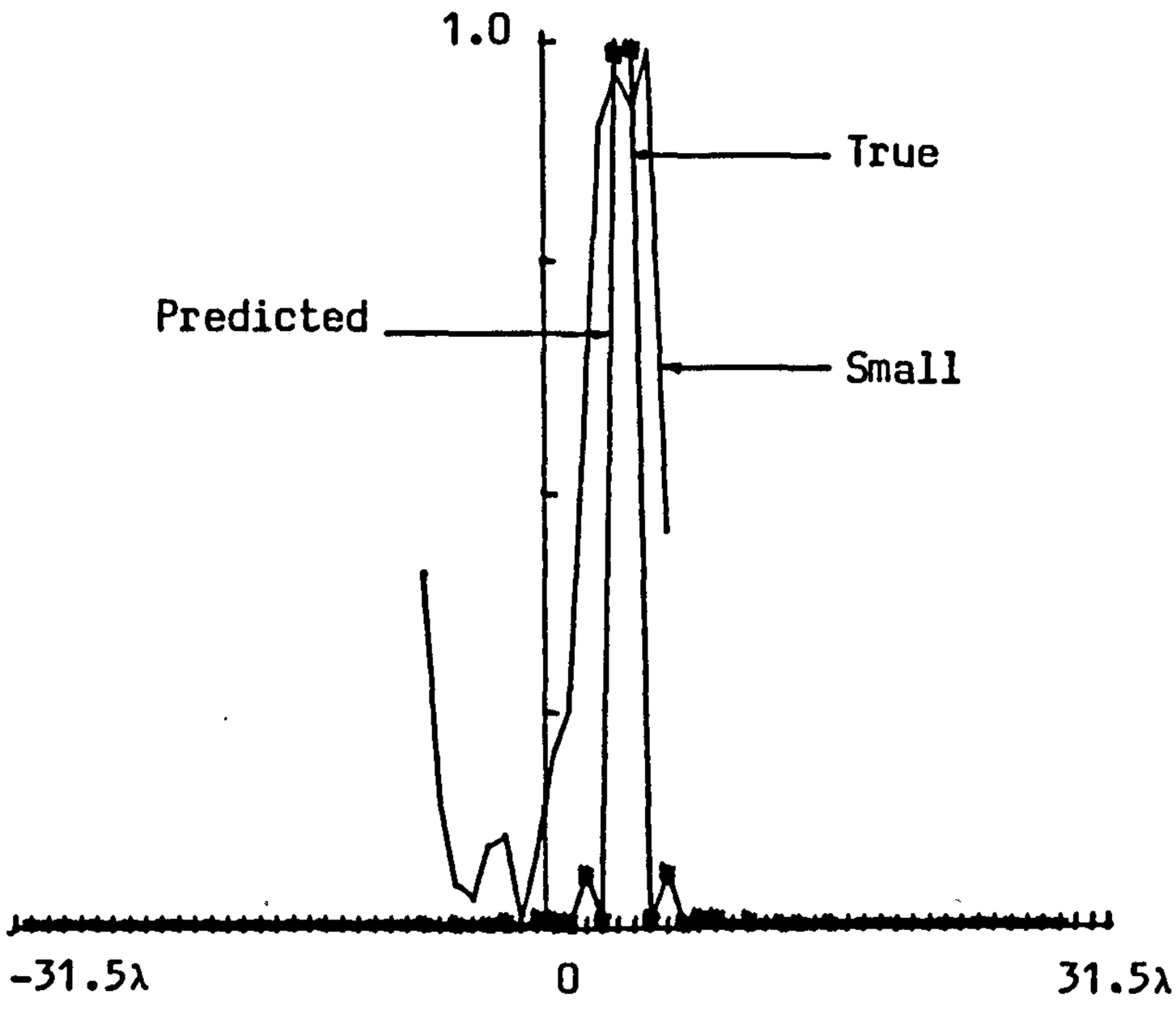


Fig. 4.4 : Prediction errors and reconstructed images obtained when the hologram of an offset point object is expanded four times using a power series polynomial predictive model.

a. Prediction error over the aperture

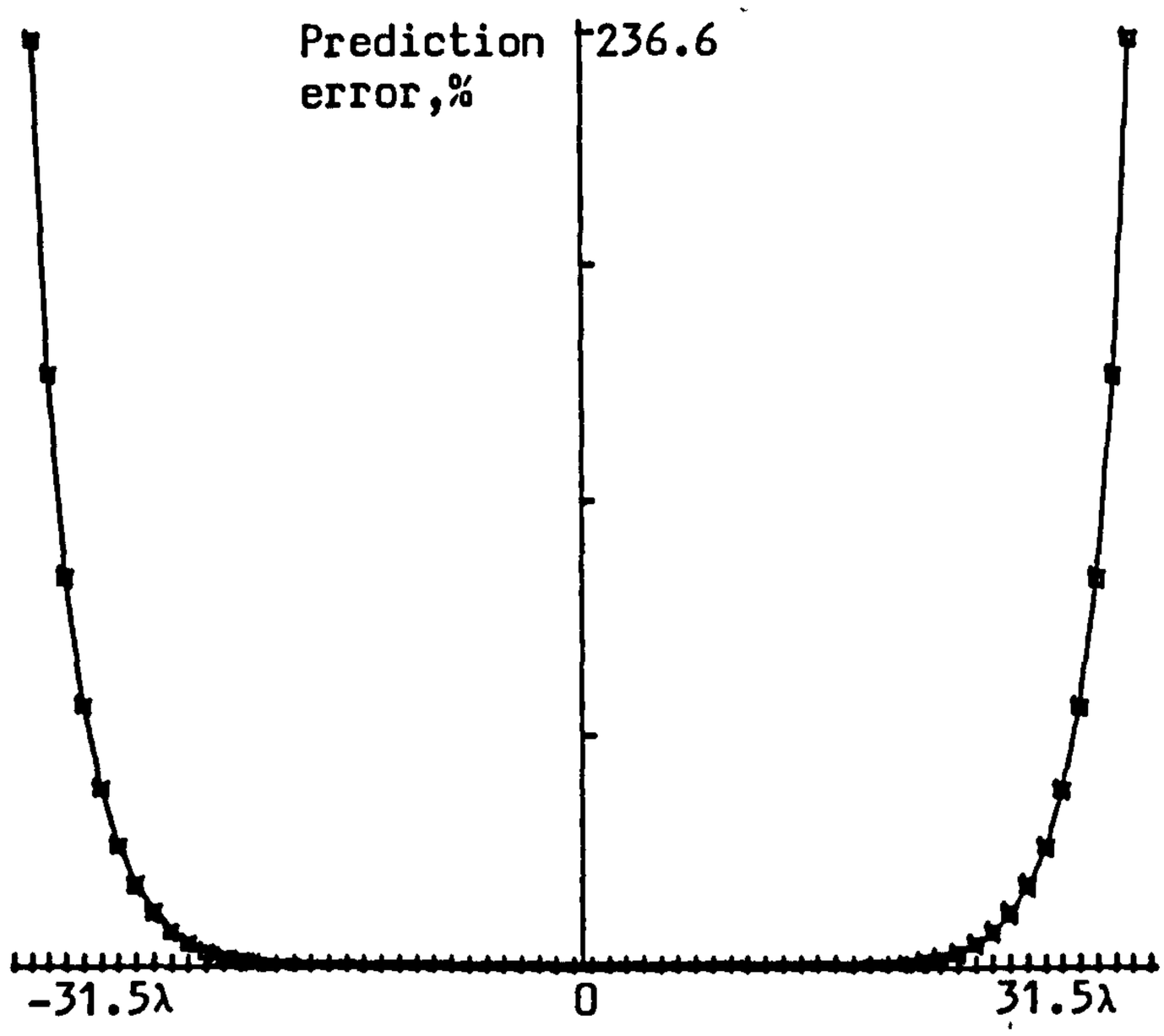


Hologram:

Δ = 1λ
M = 8
N = 32

Object:

$x_o$ = 0
$z_o$ = 70λ

b. Intensity of reconstructed images normalized to the same peak value

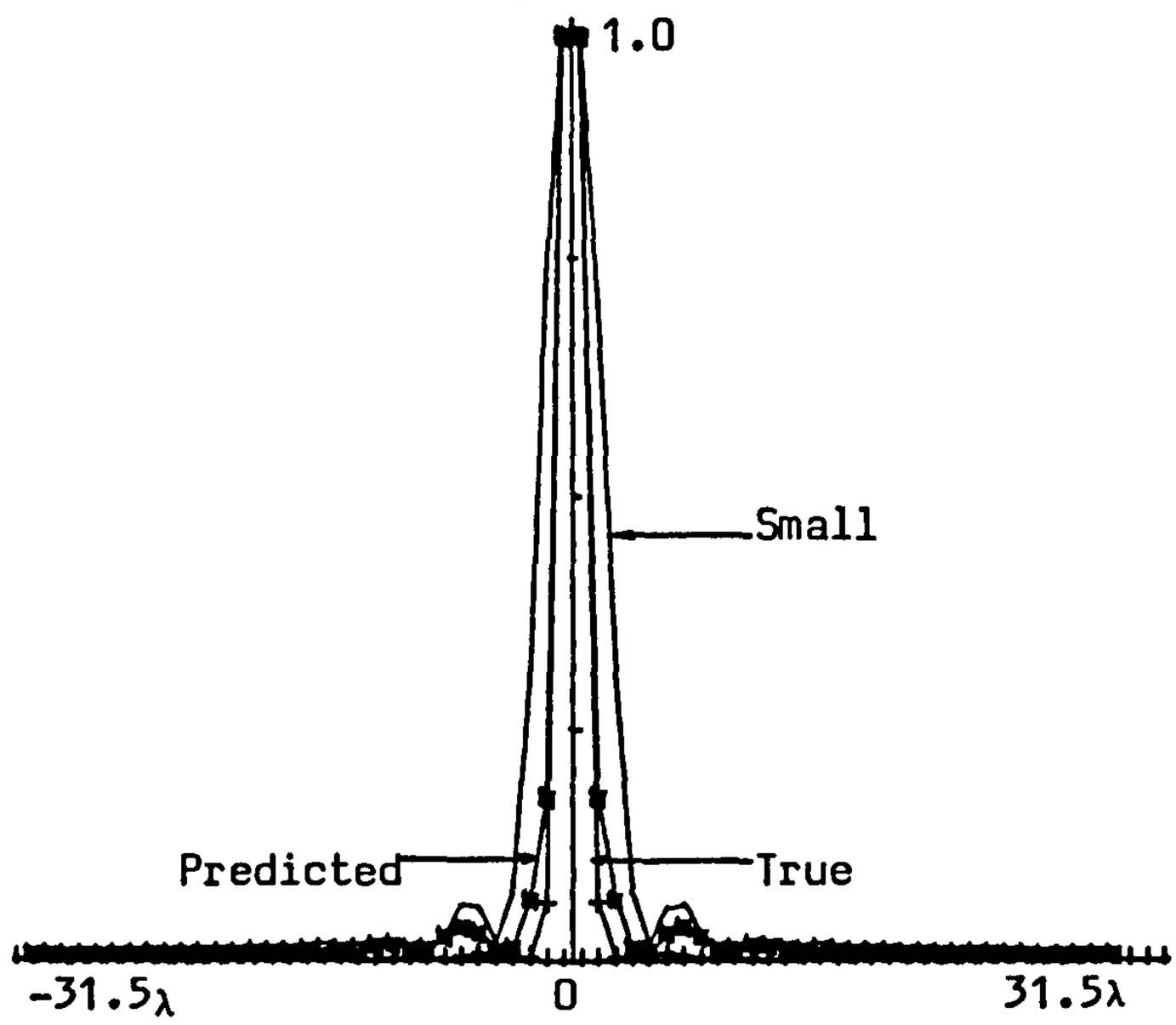


Fig. 4.5 : Effect of reducing the range on the prediction errors and the reconstructed image when expanding the aperture of a point object four times using a power series polynomial model.

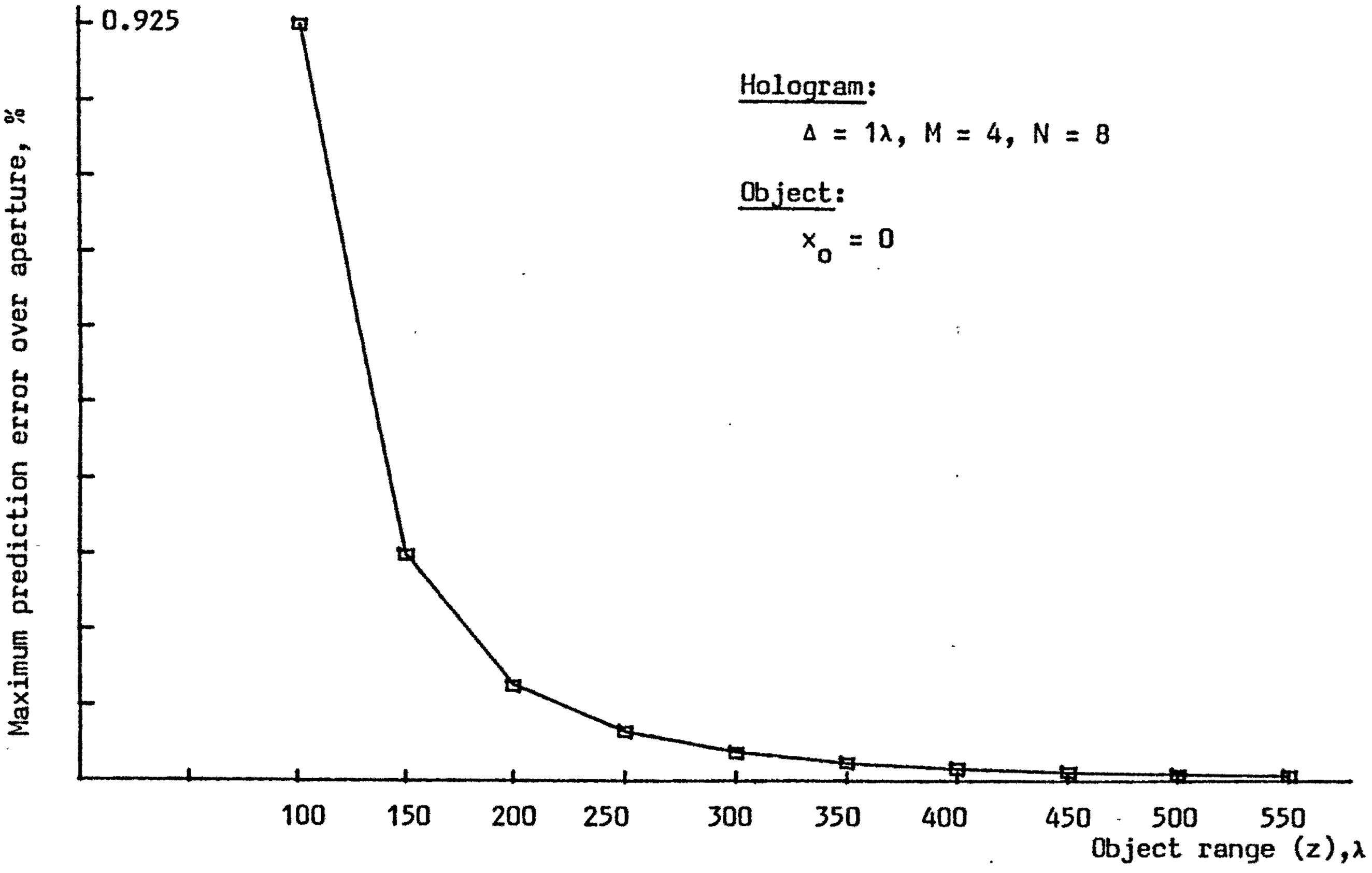


Hologram:

$\Delta = 1\lambda$, M = 4, N = 8

Object:

$x_o = 0$

Fig. 4.6 : Maximum prediction error over expanded aperture versus the range of a 1-point object. Predictive model : Power series polynomial

a. Object on the hologram axis

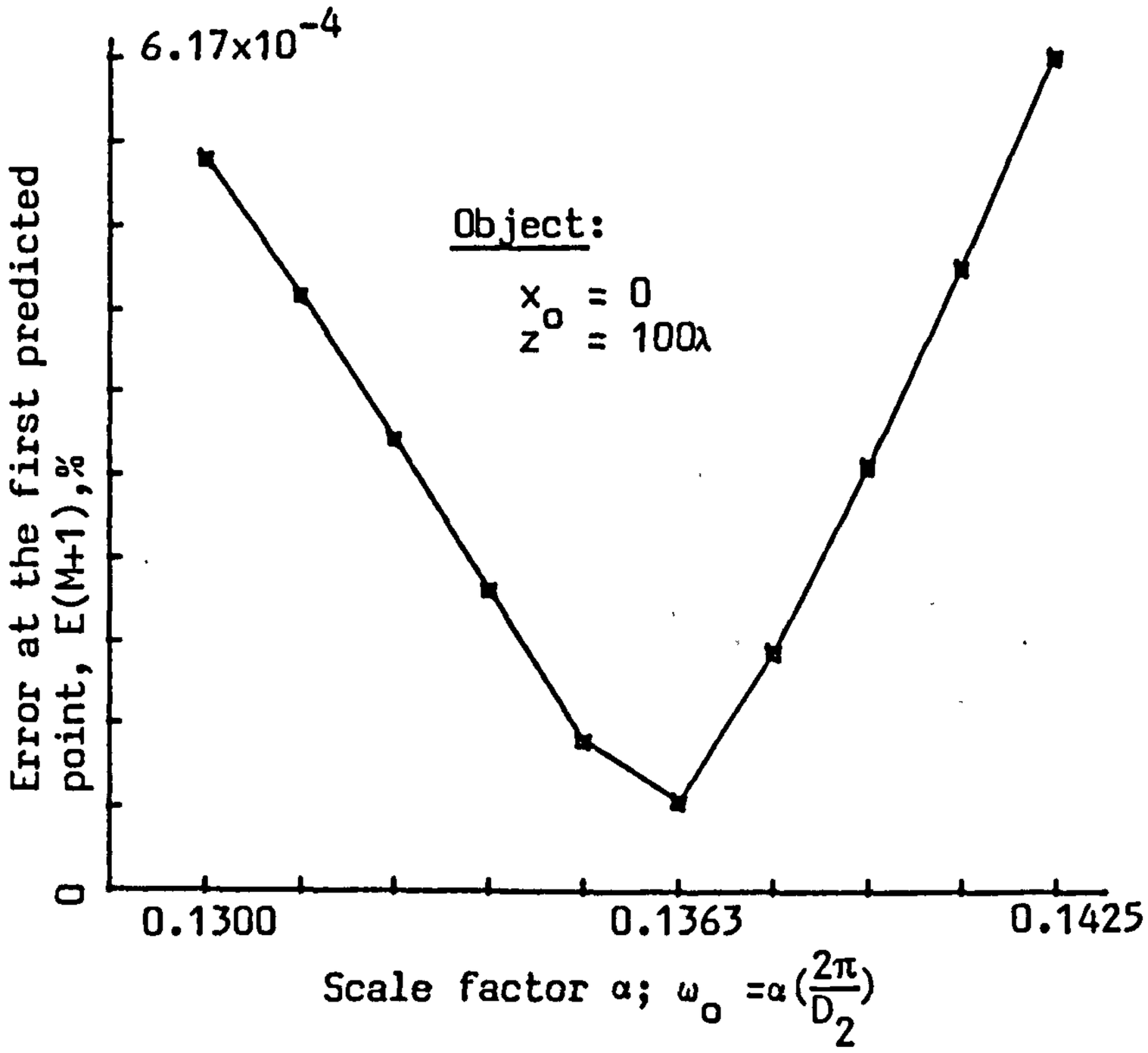


b. Object offset in the direction of the line hologram

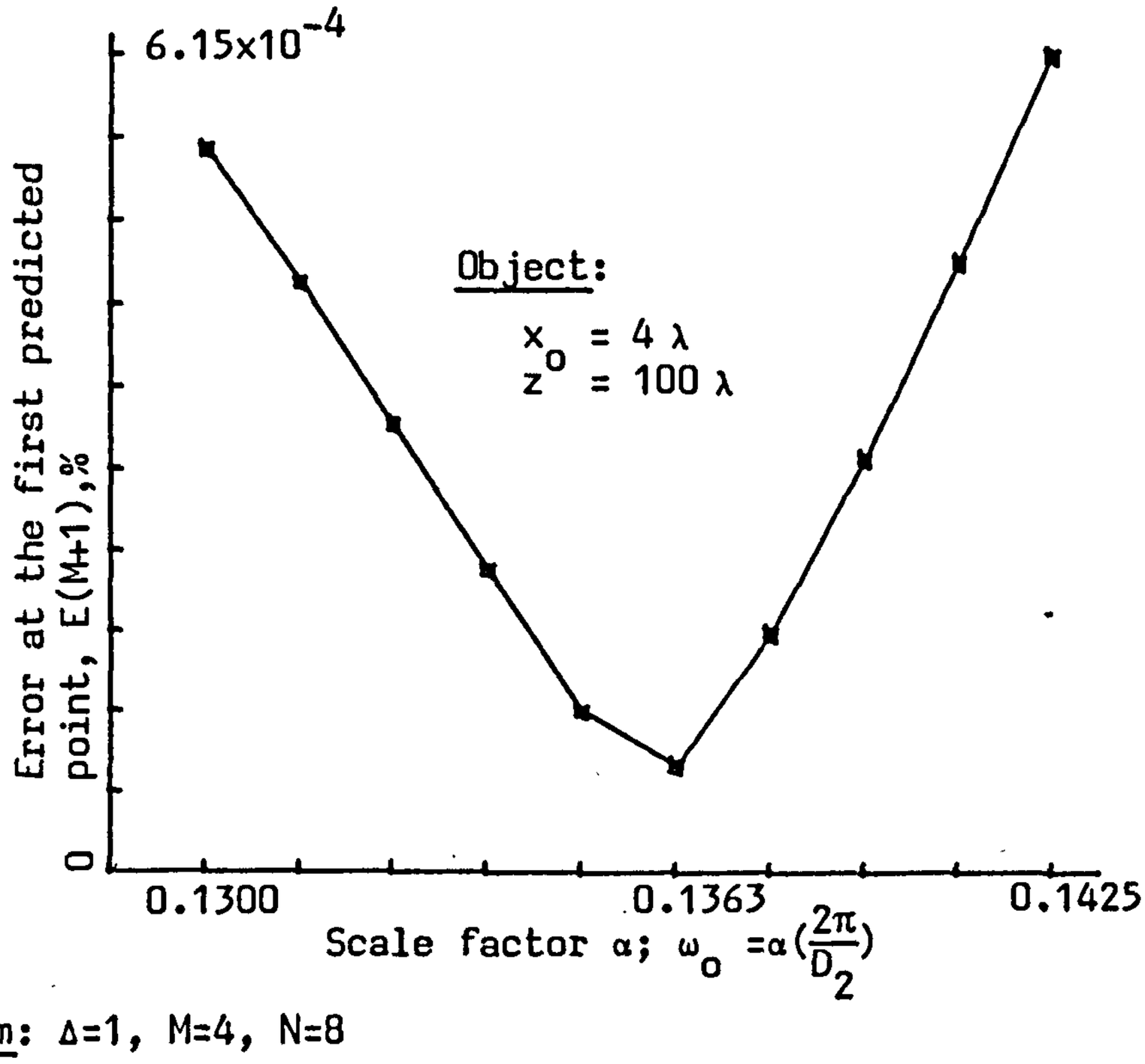


Hologram: Δ=1, M=4, N=8

Fig. 4.7 : Optimum fundamental frequency $\omega_o$ for the Fourier series predictive model when expanding the hologram of a 1-point object

a. Optimum fundamental frequency $\omega_o$ versus object range

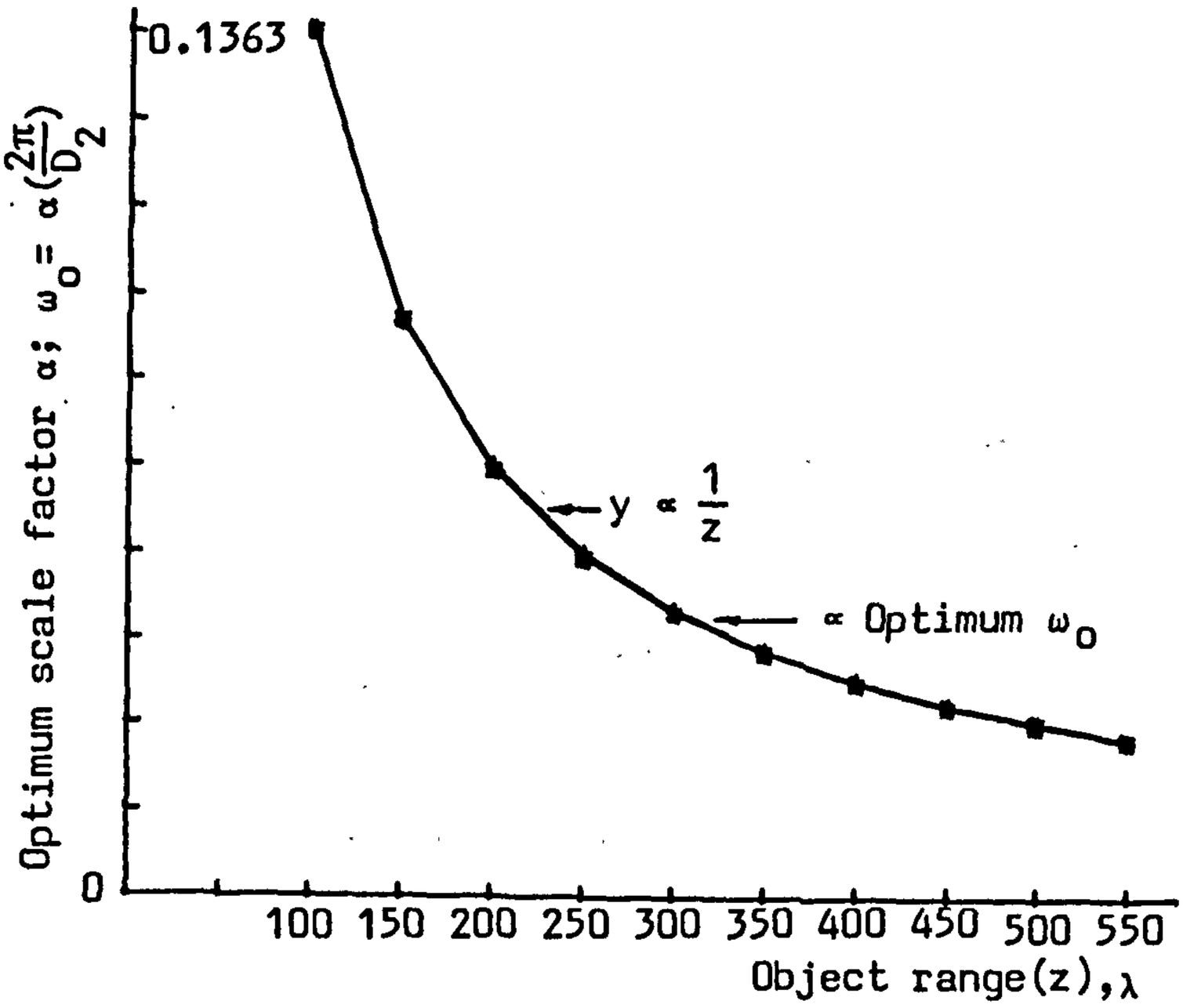


b. Error at optimum $\omega_o$ versus object range

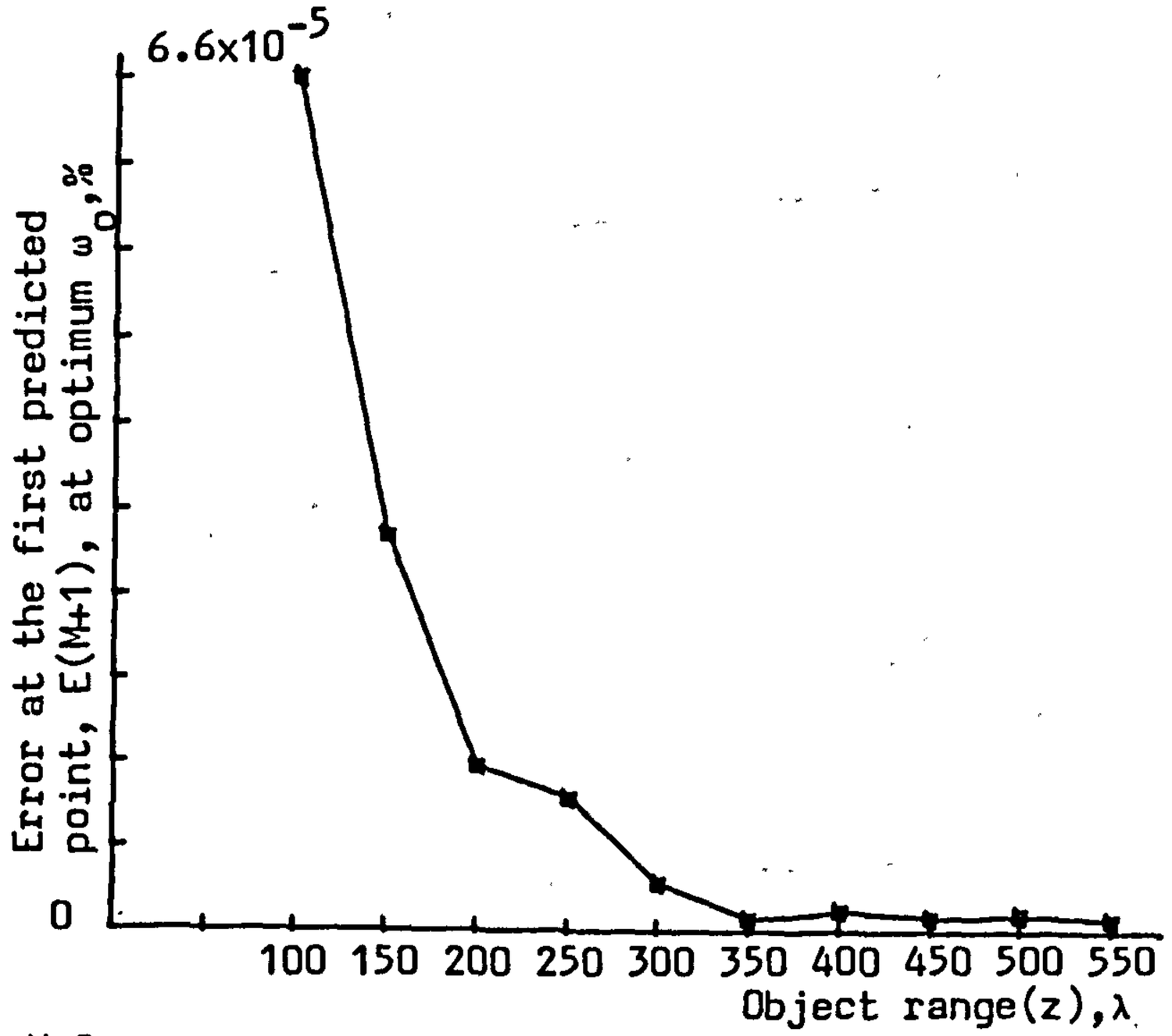


Hologram: Δ=1,M=4,N=8

Object: $x_o$=0

Fig. 4.8 : Relationship between both the optimum frequency of the Fourier series and the optimum prediction error and the range of a 1-point object.

a. For several values of the object range

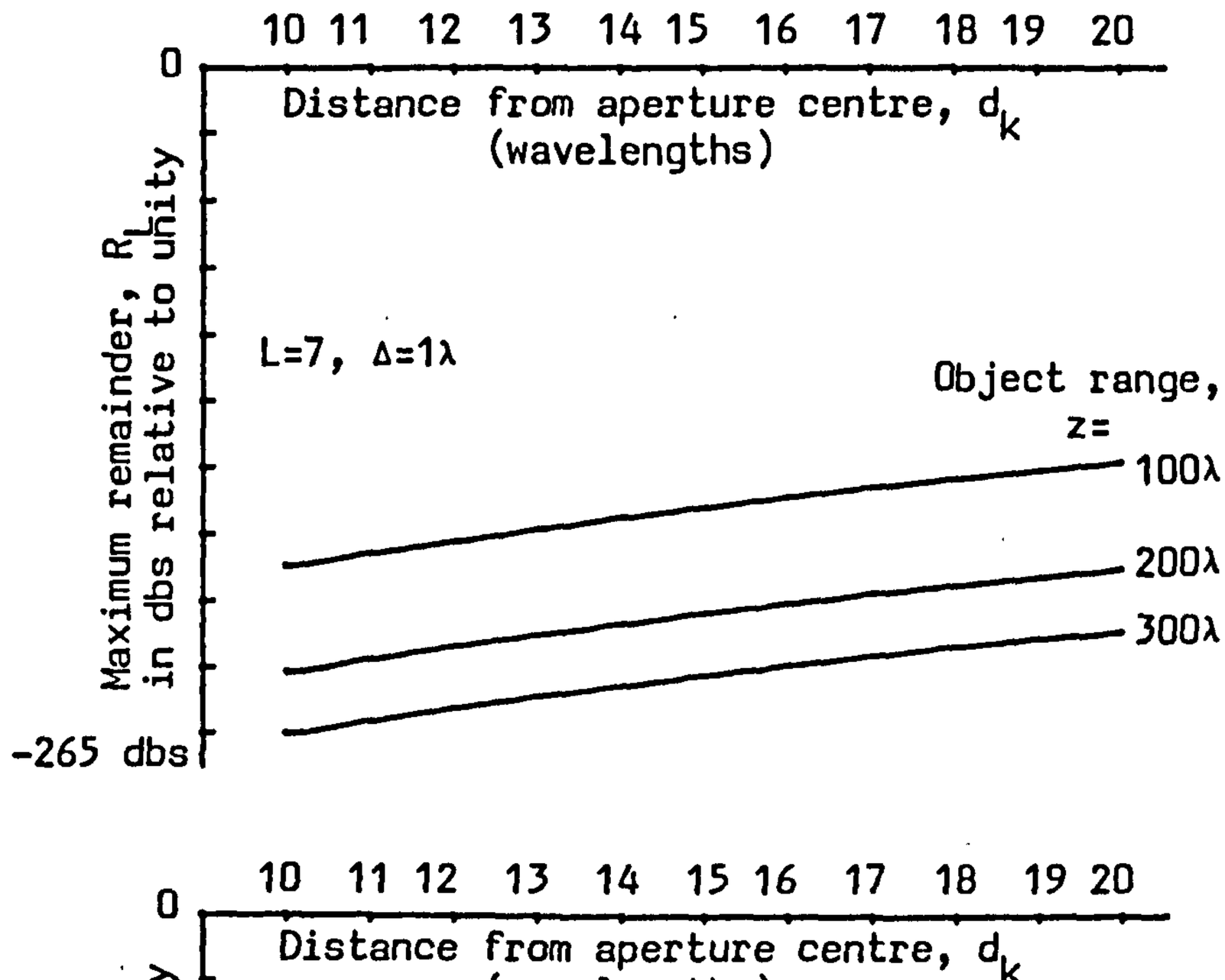


b. For several values of the sample spacing

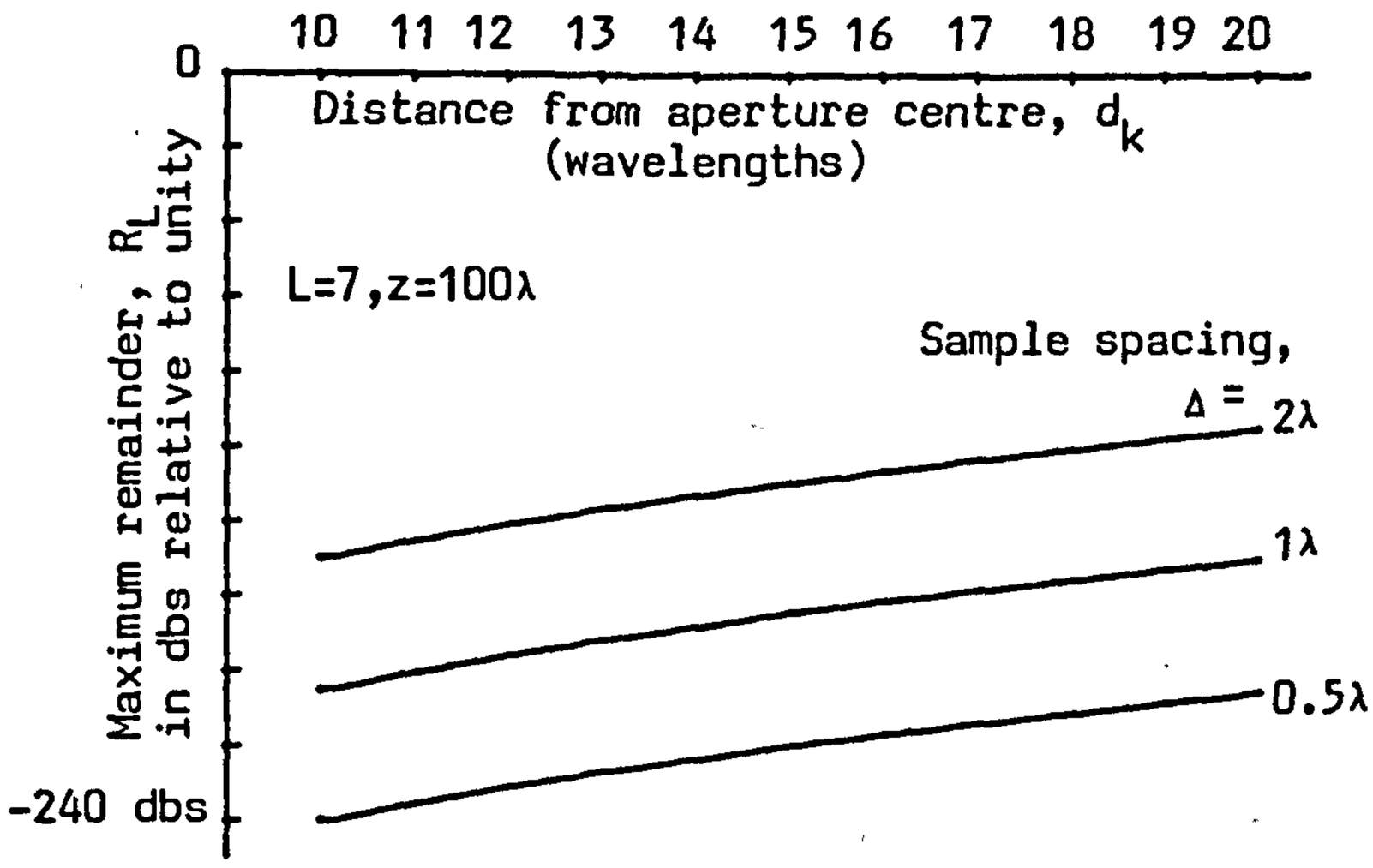


c. For several values of the model order

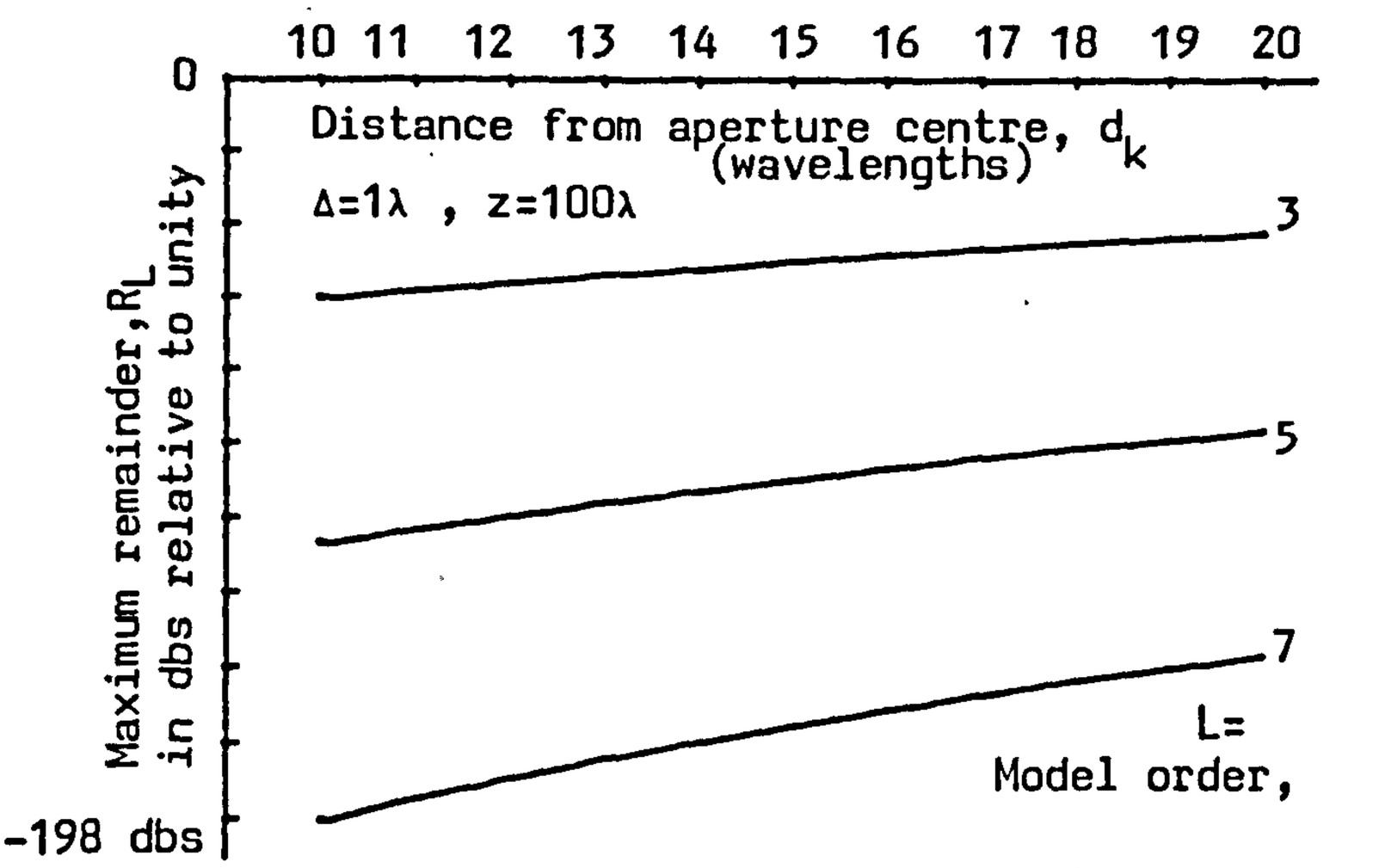


Fig. 4.9 : Maximum remainder, $R_L$, versus distance over the aperture

a. For several values of the sample spacing

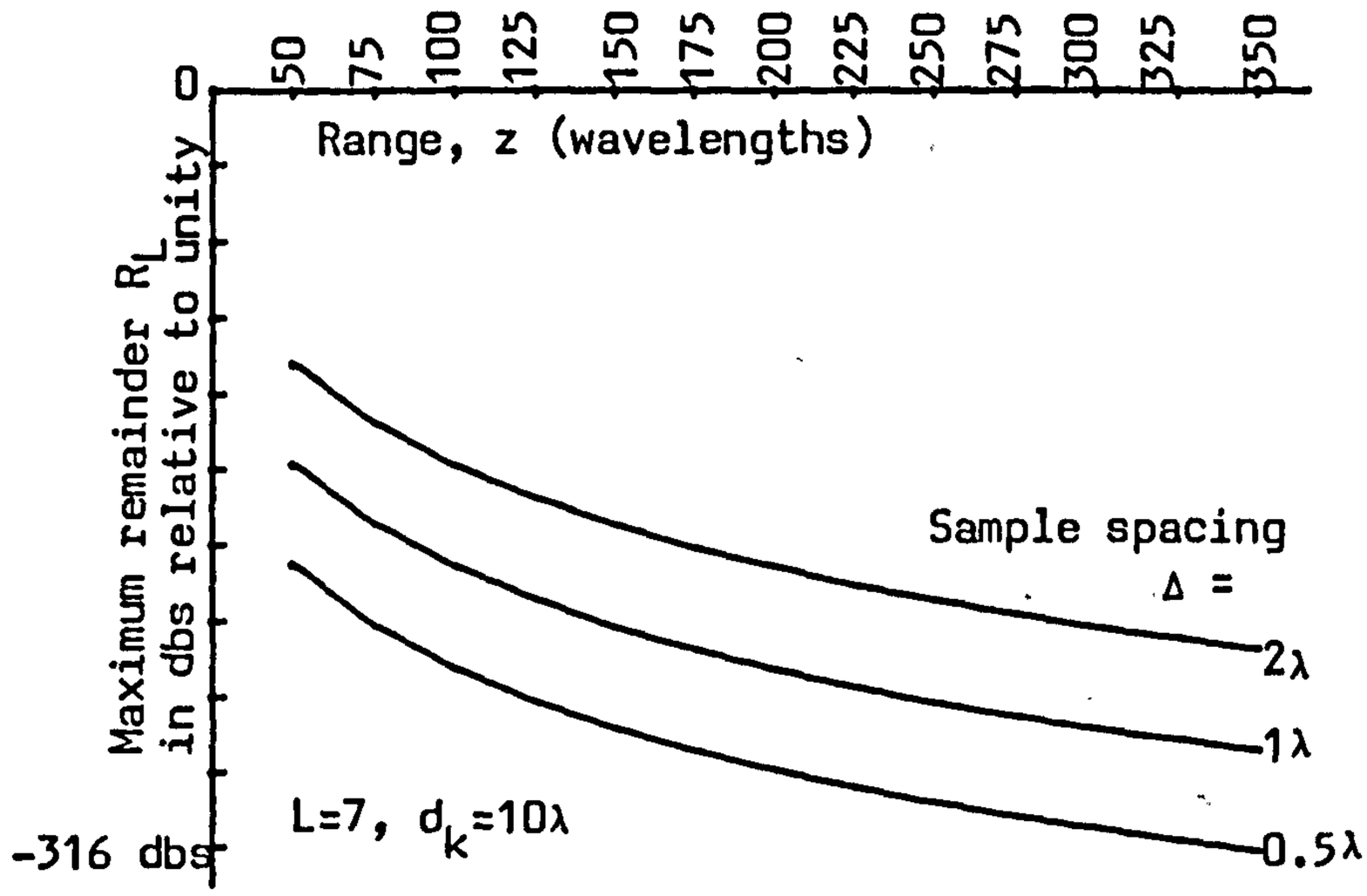


b. For several values of the distance over the aperture

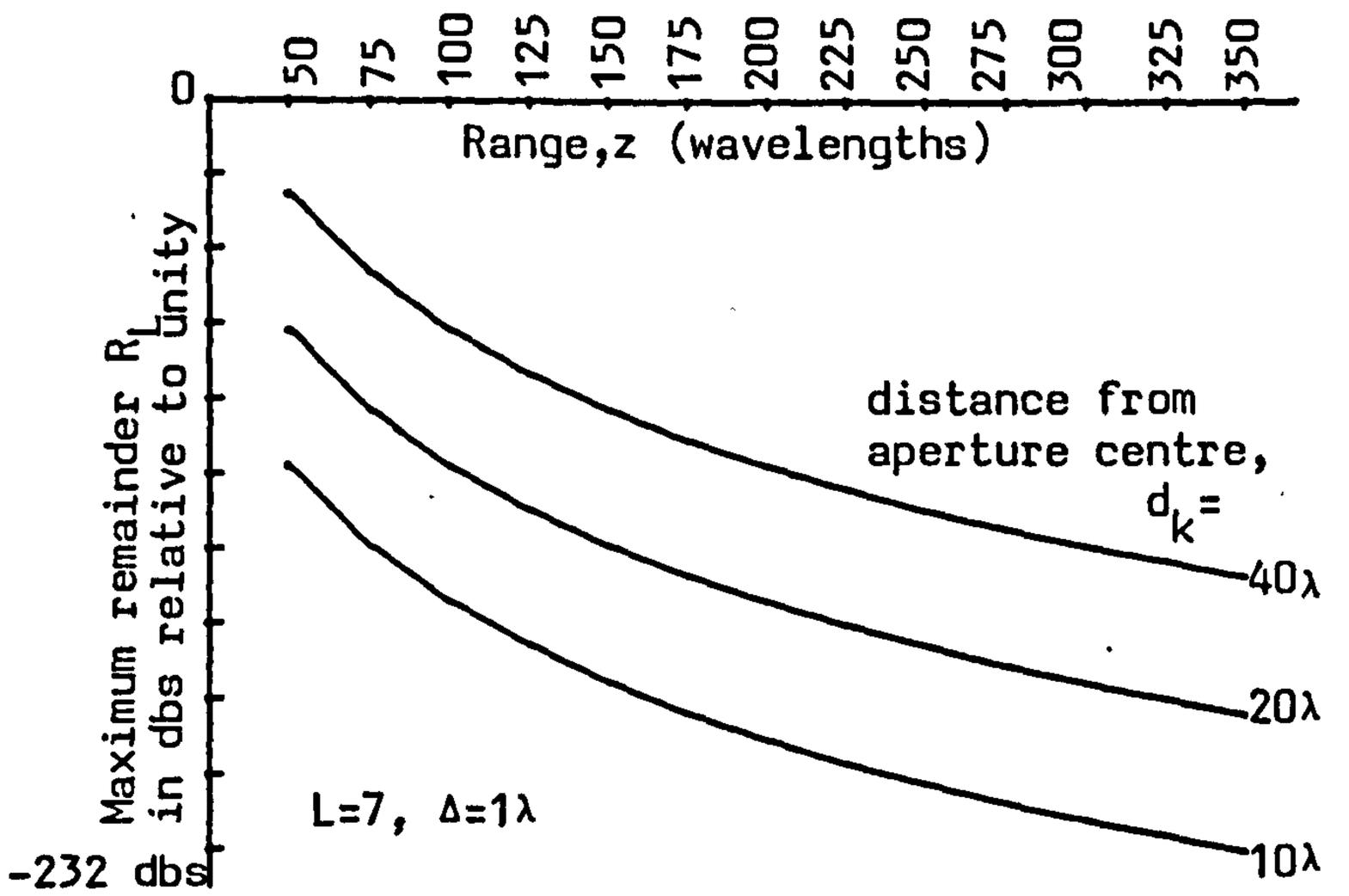


c. For several values of the model order

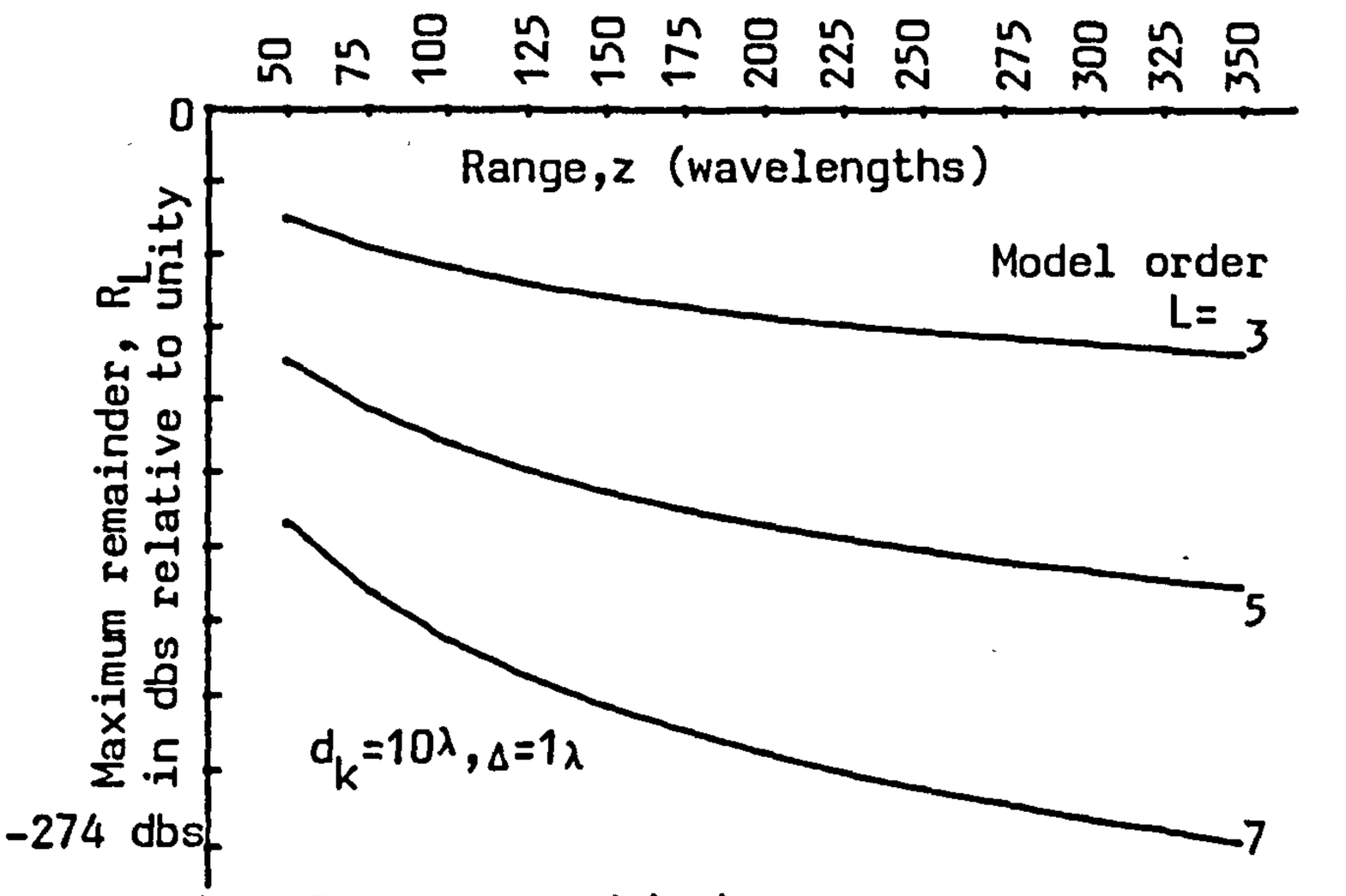


Fig. 4.10 : Maximum remainder, $R_L$, versus object range

a. For several values of the object ranges

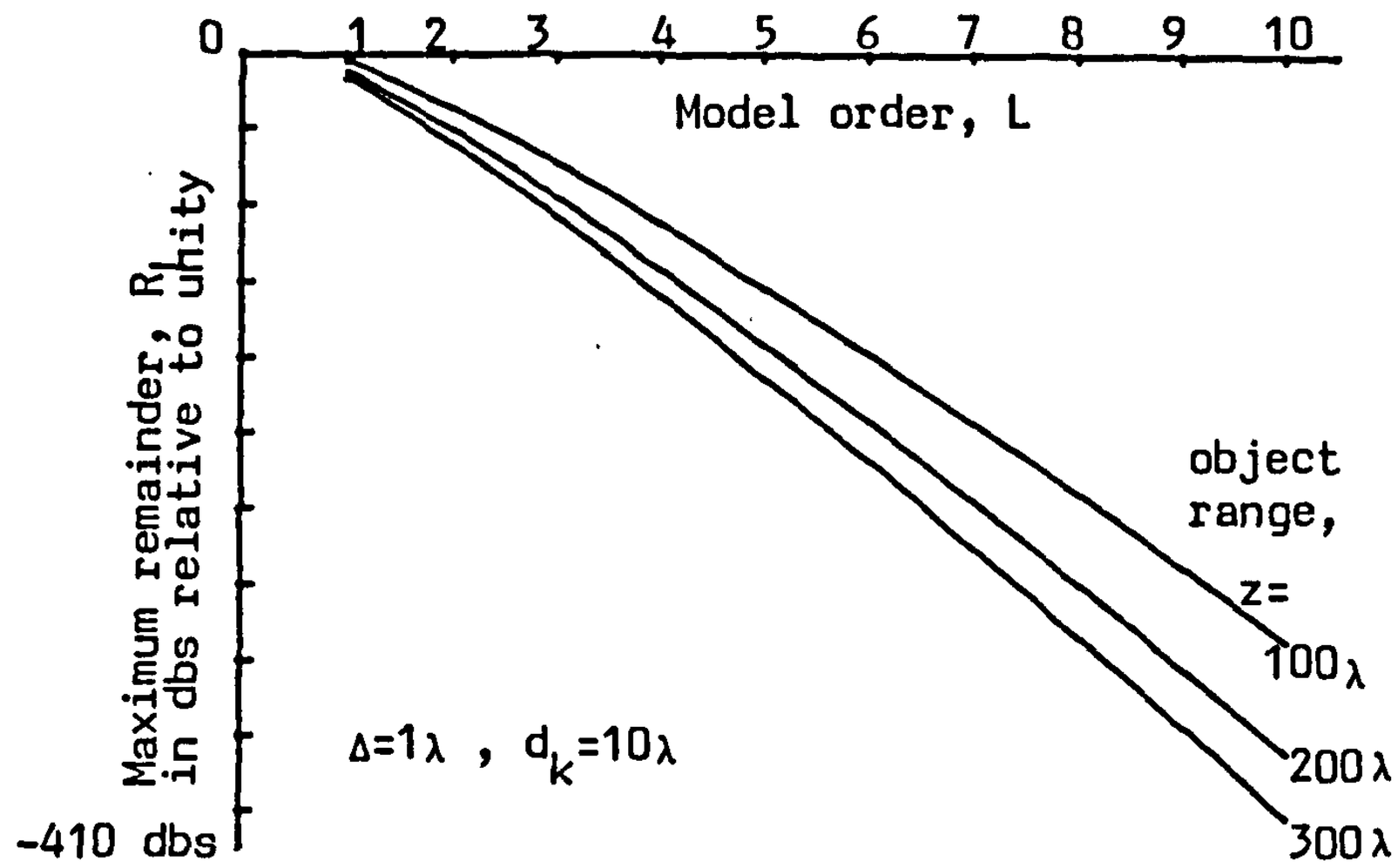


b. For several values of the sample spacing

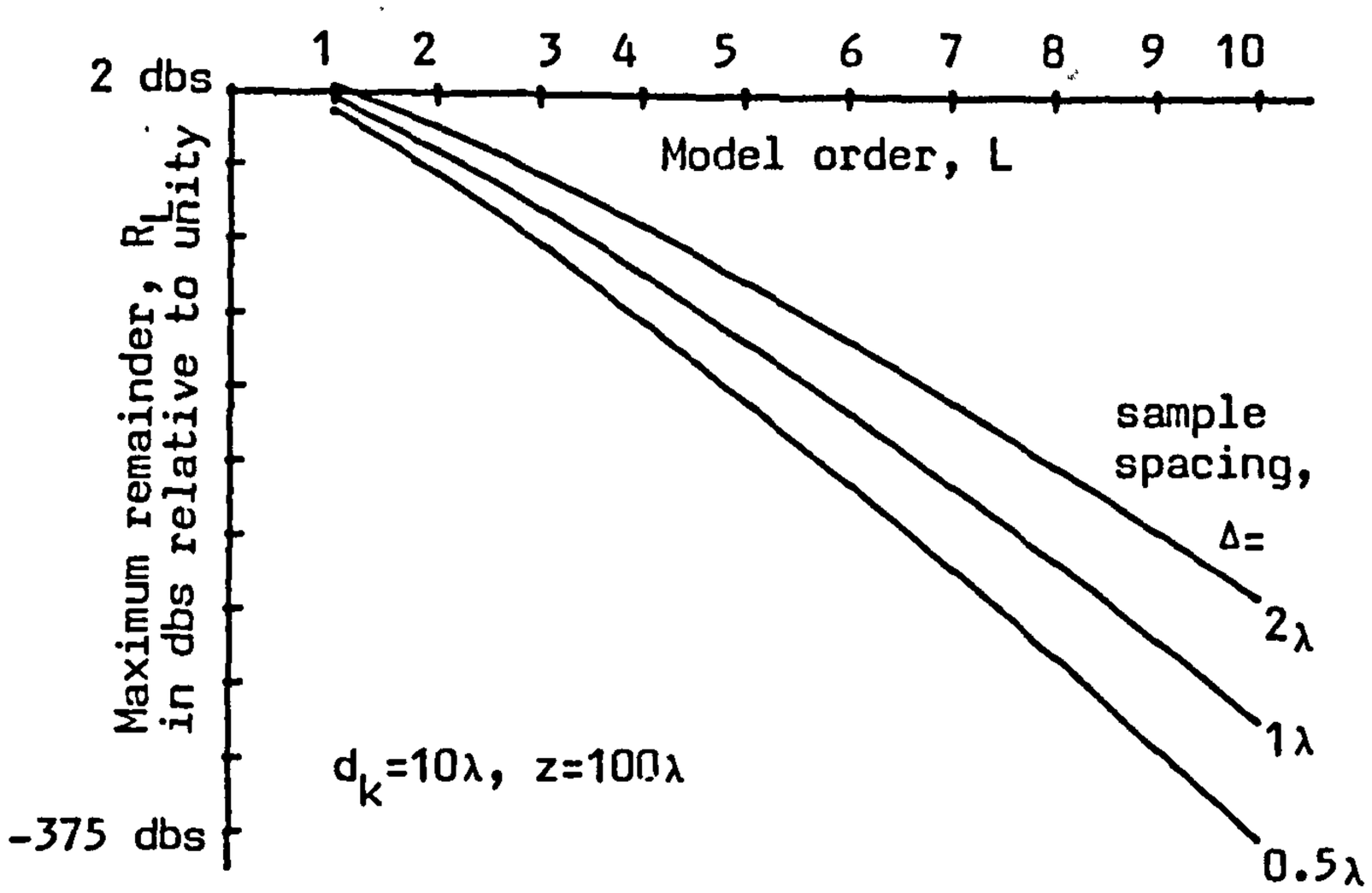


c. For several values of the distance over the aperture

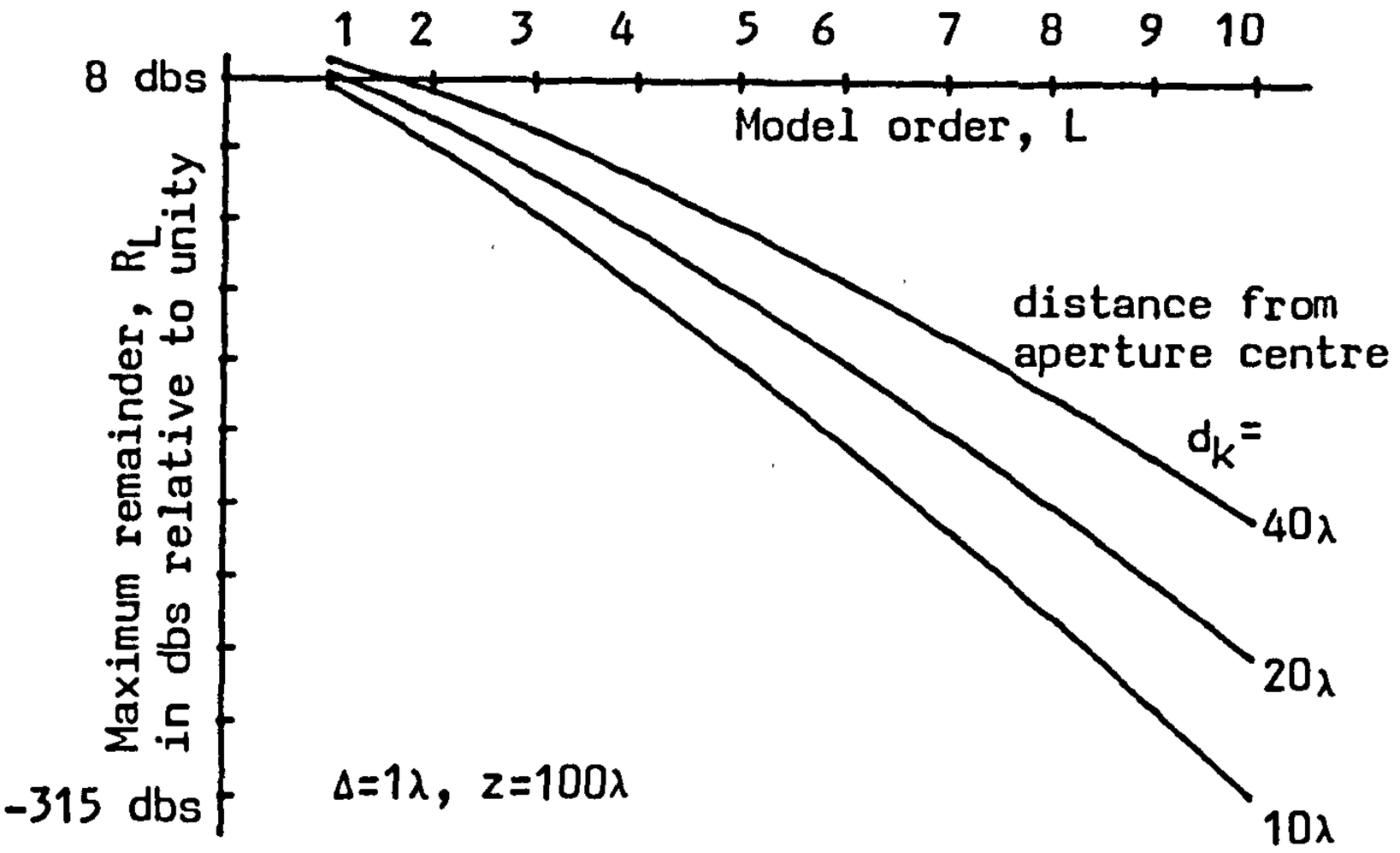


Fig. 4.11 : Maximum remainder, $R_L$, versus model order

a. Prediction error over the aperture

<u>Hologram:</u>

Δ=1
M=8
N=16

<u>Object:</u>

$x_{o1}=2.6\lambda$
$x_{o2}=-2.6\lambda$
$z = 105\lambda$

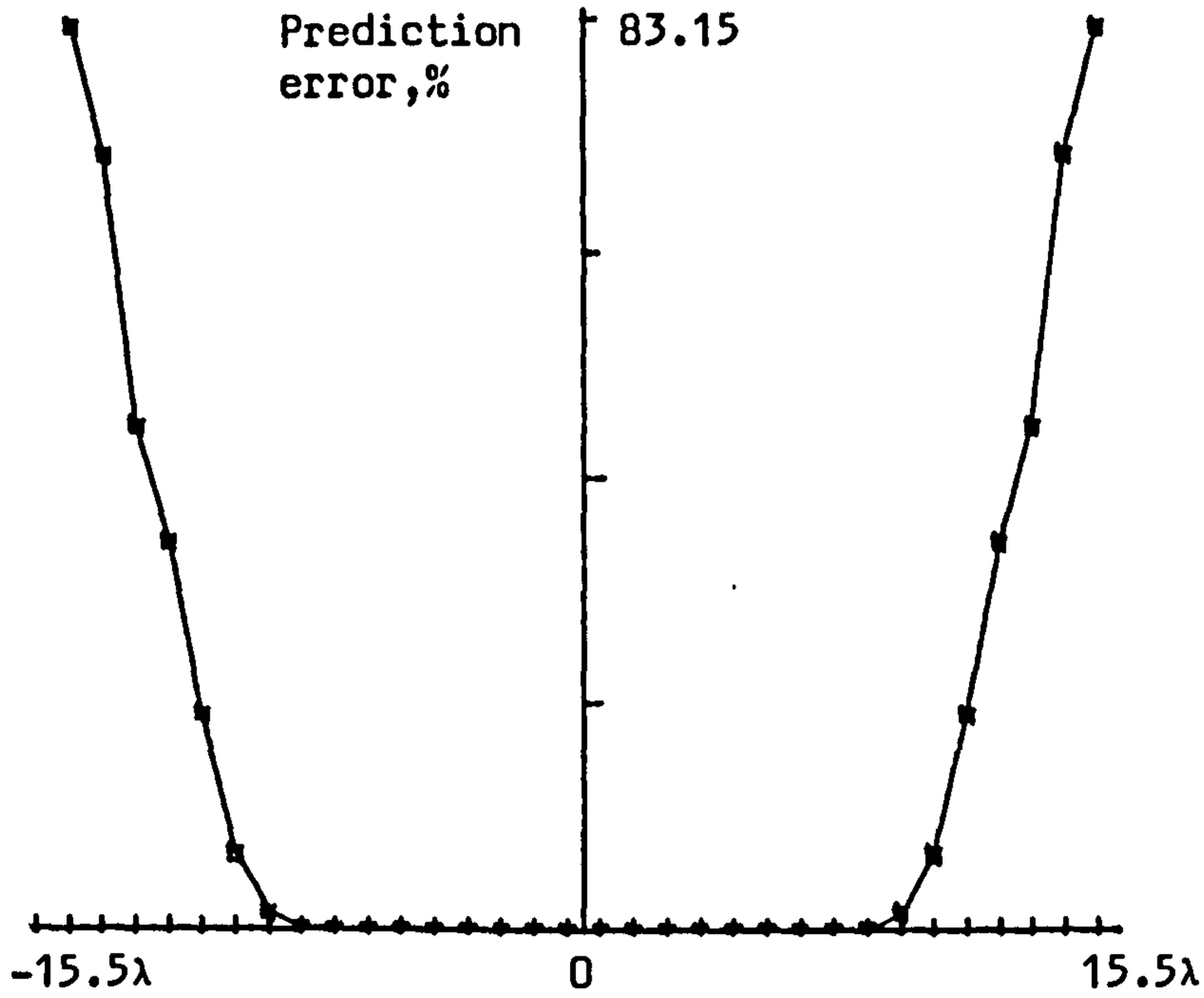


b. Reconstructed images

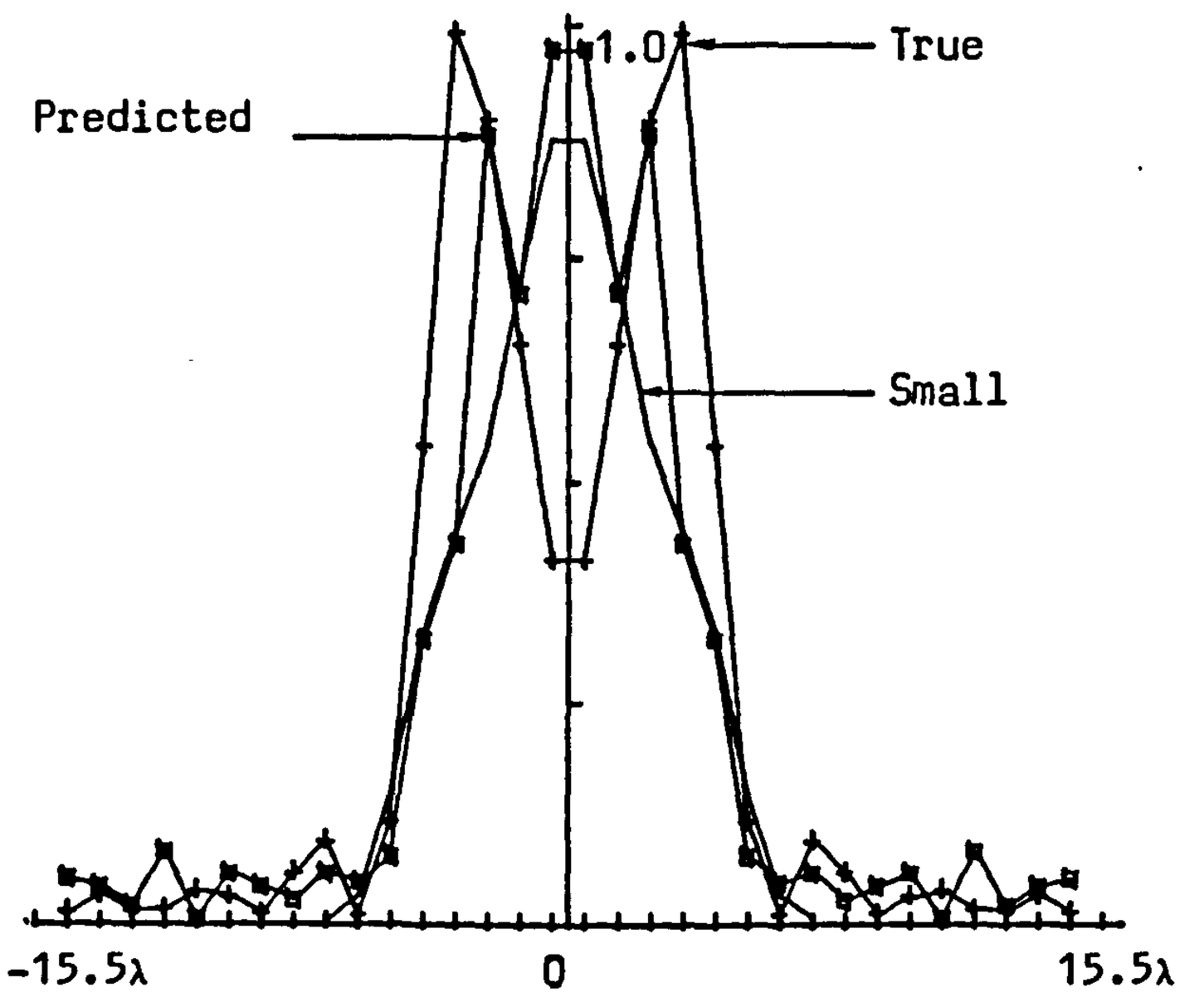


Fig. 4.12 : Prediction errors and reconstructed images obtained when using a power series polynomial model to expand the hologram of a 2-point object.

a. Prediction errors over the aperture for the hologram of a 1-point object

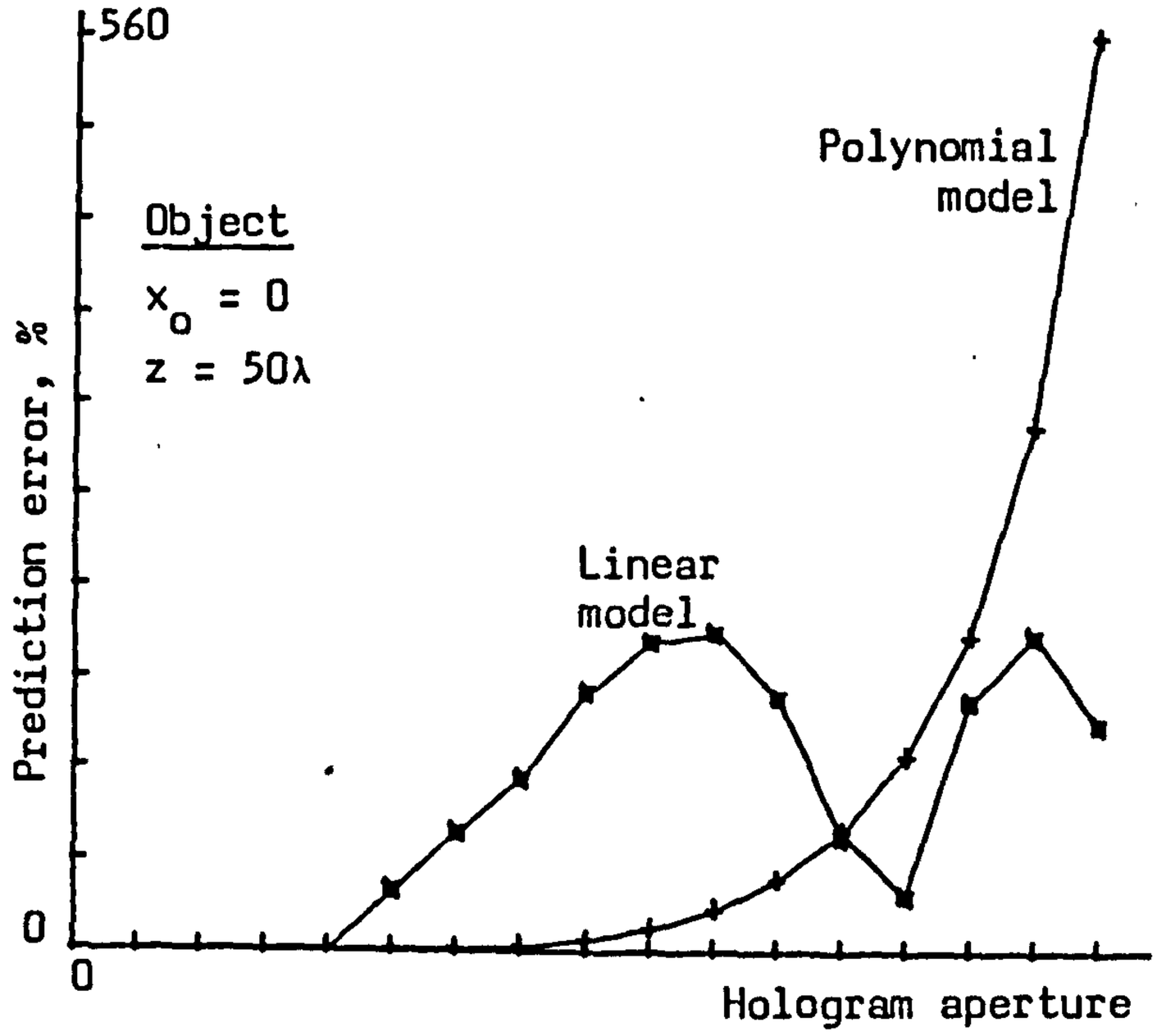


b. Prediction errors over the aperture for the hologram of a 2-point object

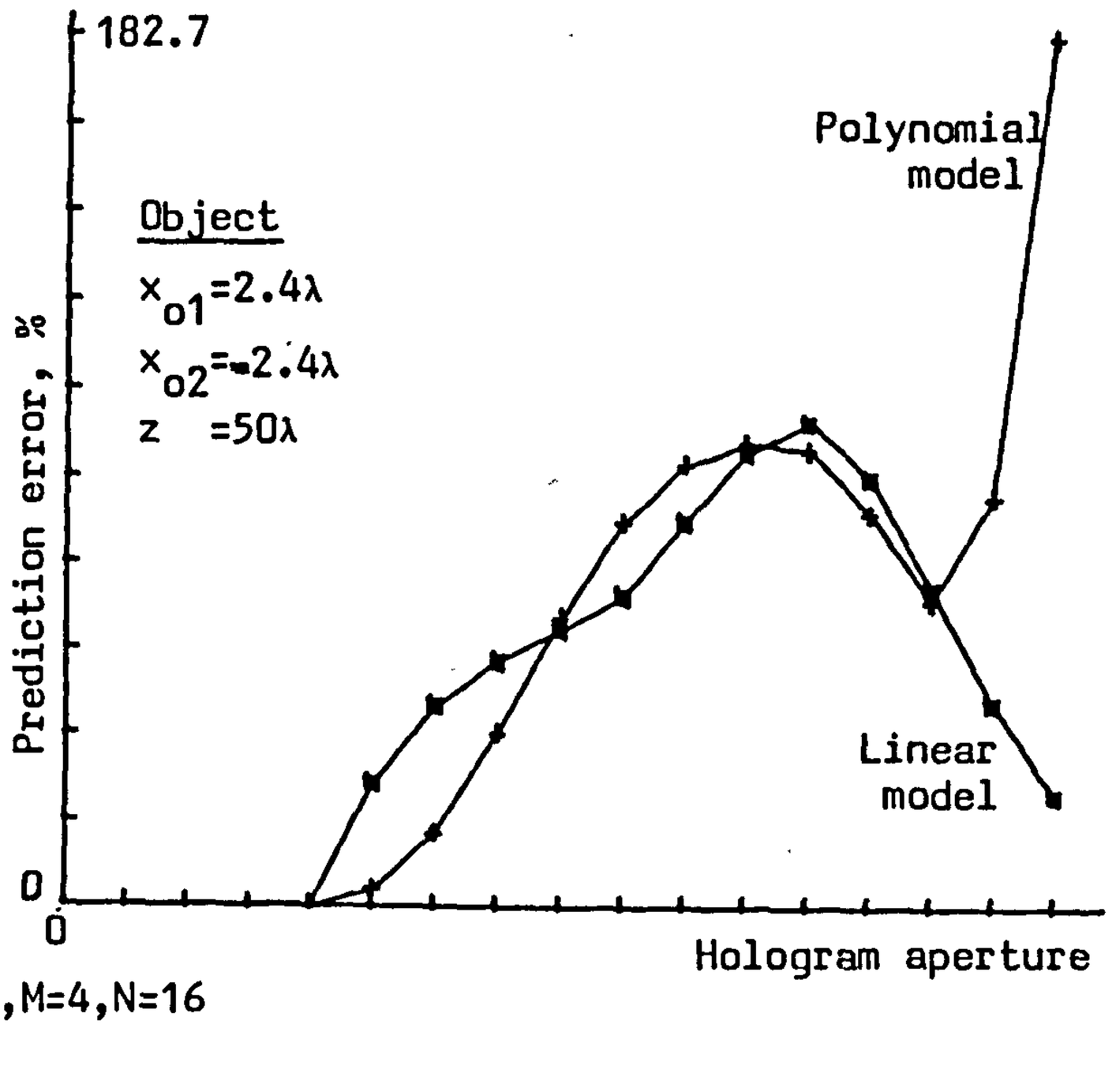


Hologram: $\Delta=1, M=4, N=16$

Fig. 4.13 : Comparison between the performance of the polynomial model and the linear model when expanding the holograms of 1-point and 2-point objects.

a. Prediction error over the aperture

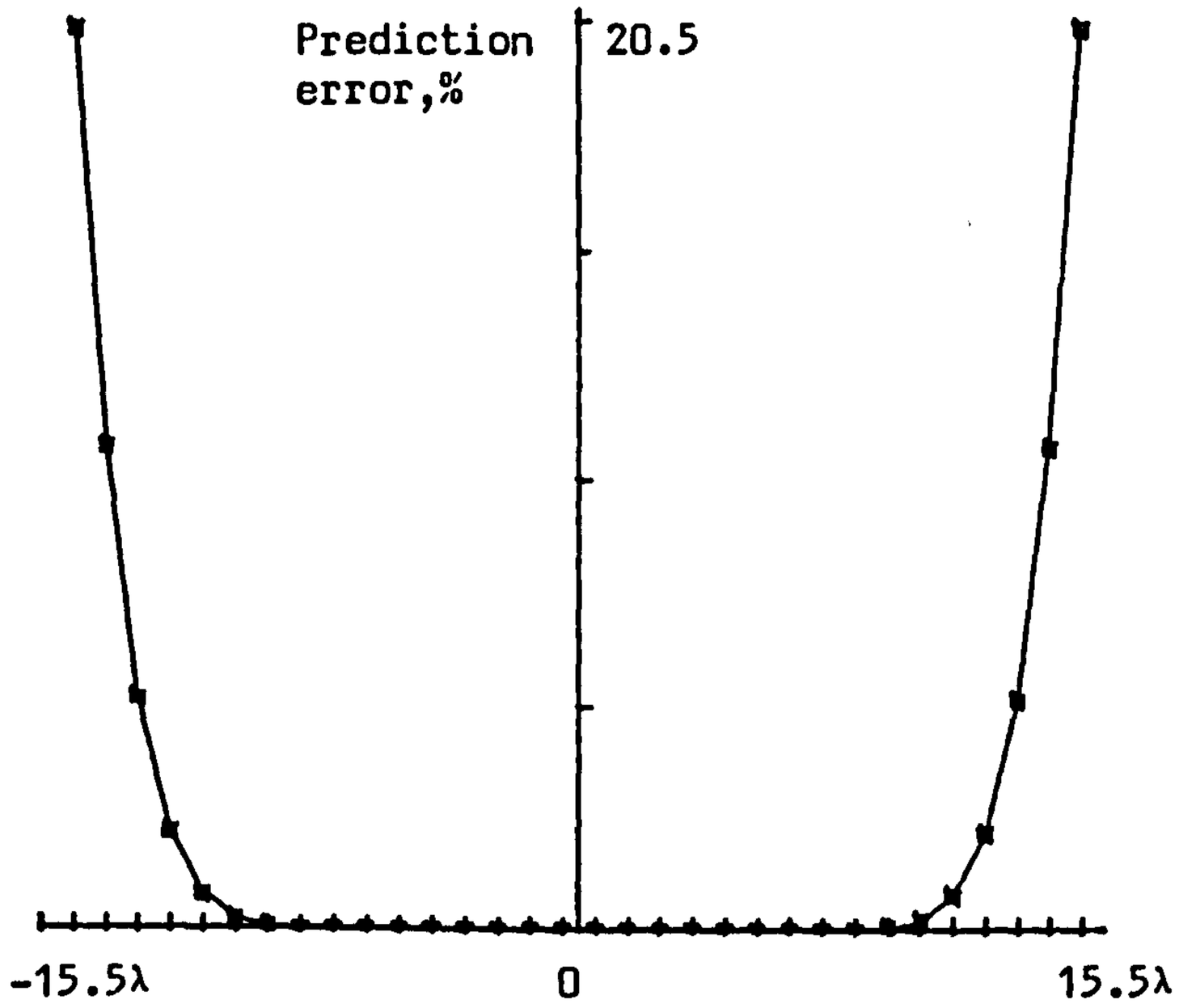


Hologram:

Δ=1
M=8
N=16

Object:

$x_{o1}=3\lambda$
$x_{o2}=-3\lambda$
$z = 105\lambda$

b. Reconstructed images

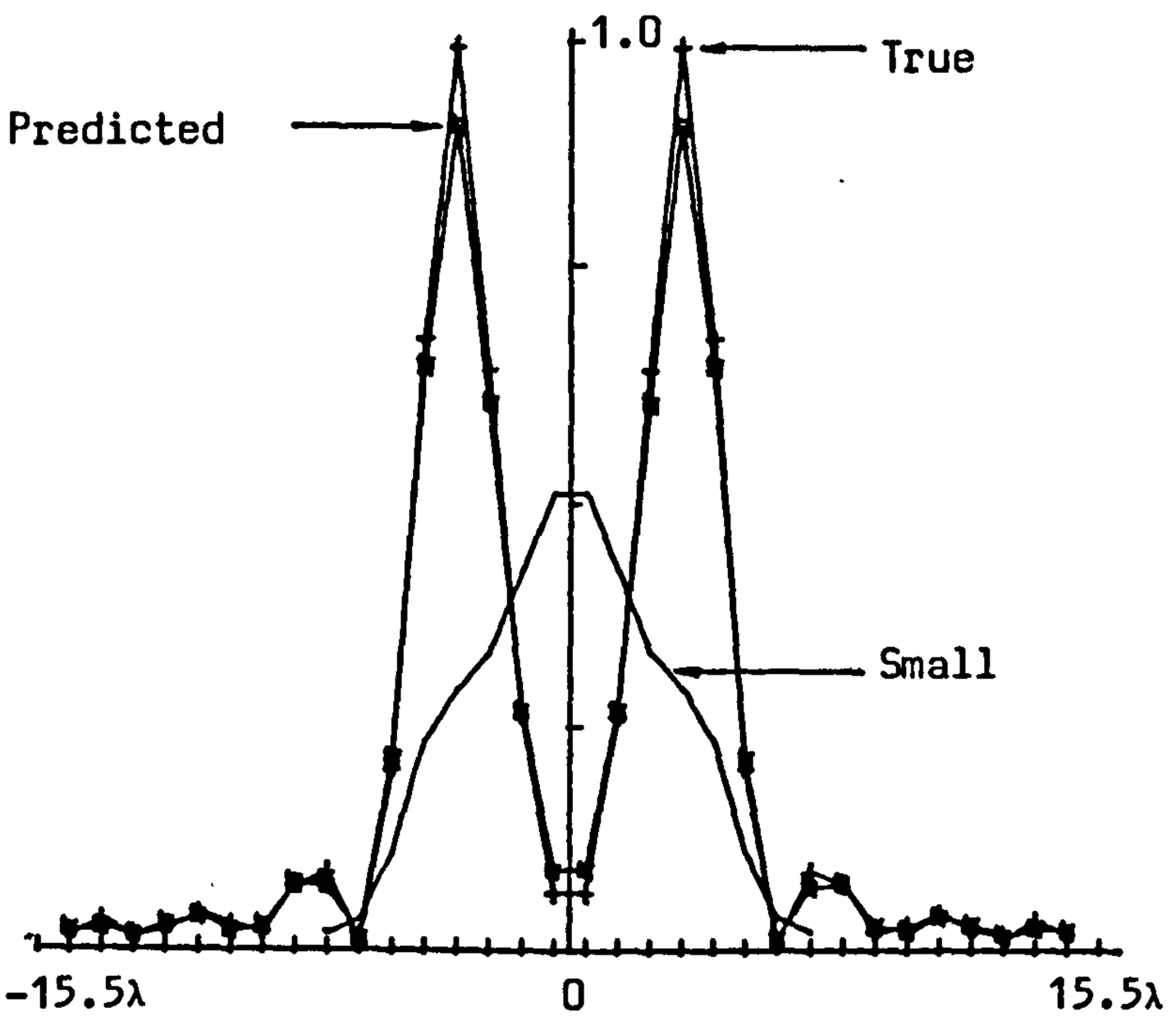


Fig. 4.14 : Prediction errors and reconstructed images obtained when using the optimum hybrid model (p=5,q=2) to double the size of a 16-point hologram of a 2-point object.

a. Reconstructed images with prediction performed using the power series polynomial model

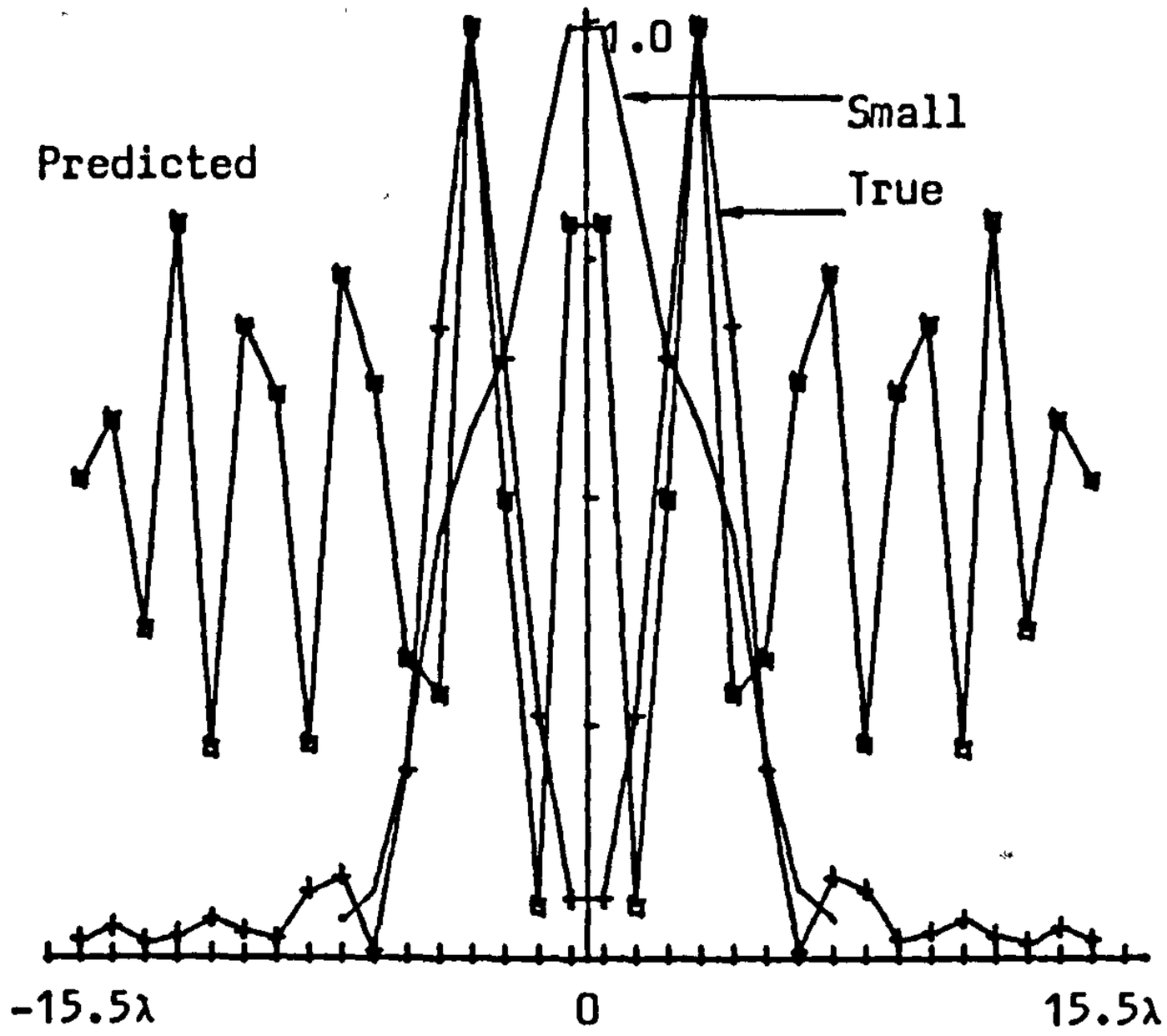


b. Reconstructed images with prediction performed using the linear model

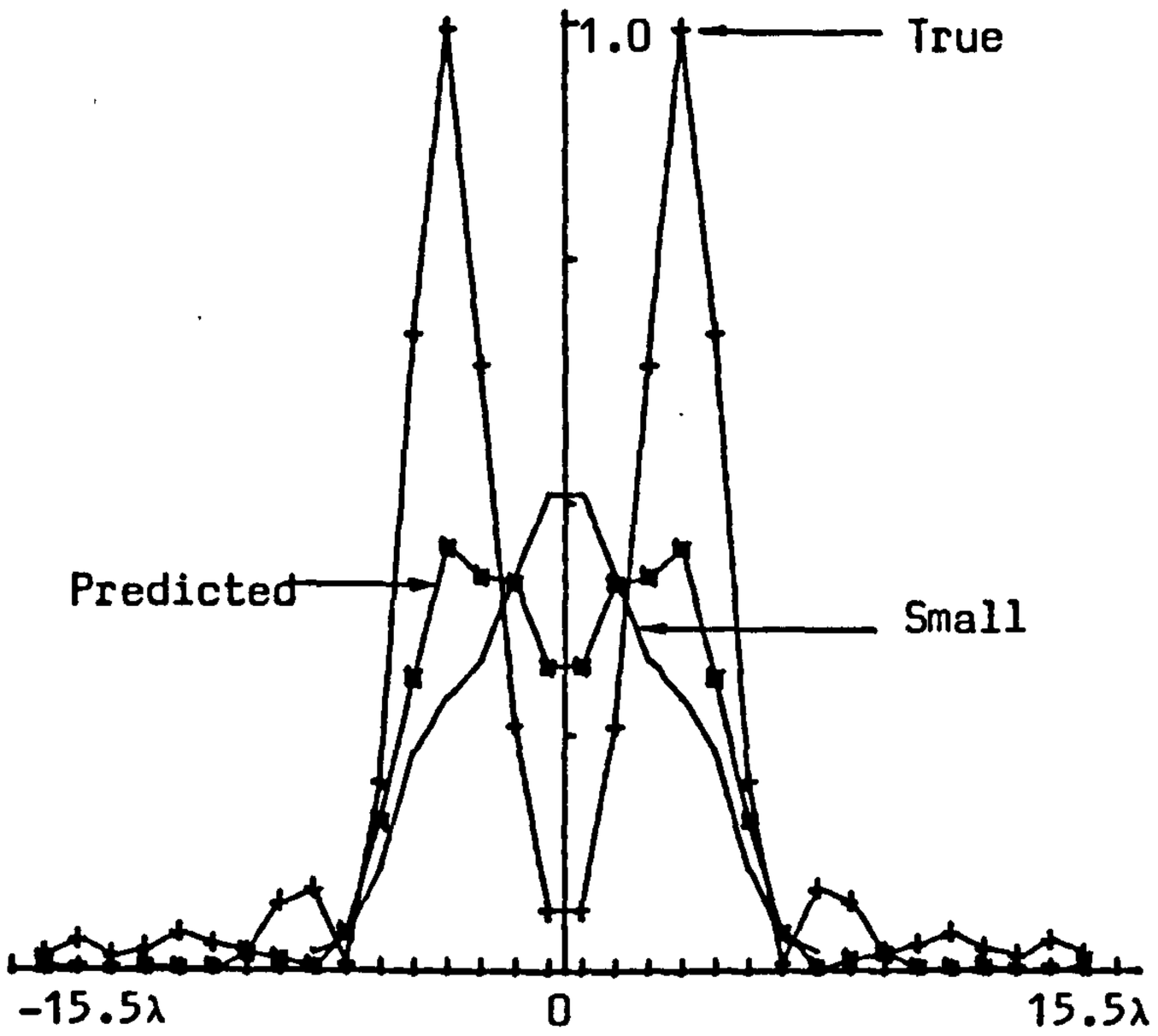


Hologram: Δ=1, M=8, N=16

Object: $x_{o1}=3\lambda$ , $x_{o2}=-3\lambda$ , $z=105\lambda$

Fig. 4.15 : Reconstructed images obtained when using the polynomial and linear models to expand the hologram of Fig. 4.14 for a 2-point object.

a. Prediction error over the aperture

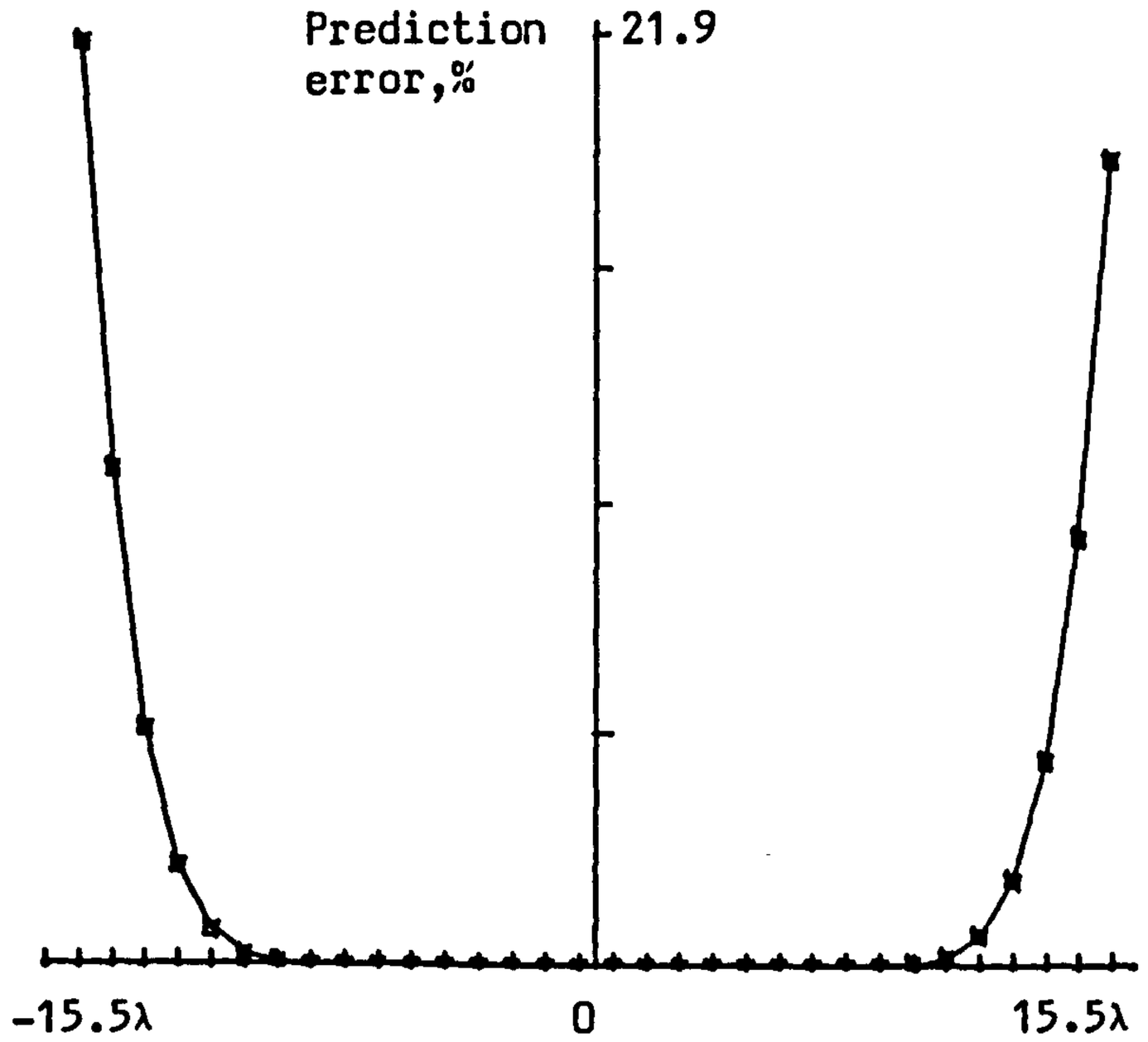


Hologram:

Δ=1
M=8
N=16

Object:

$x_{o1}=3\lambda$
$x_{o2}=-3\lambda$
$z_{o2}=105\lambda$

b. Reconstructed images

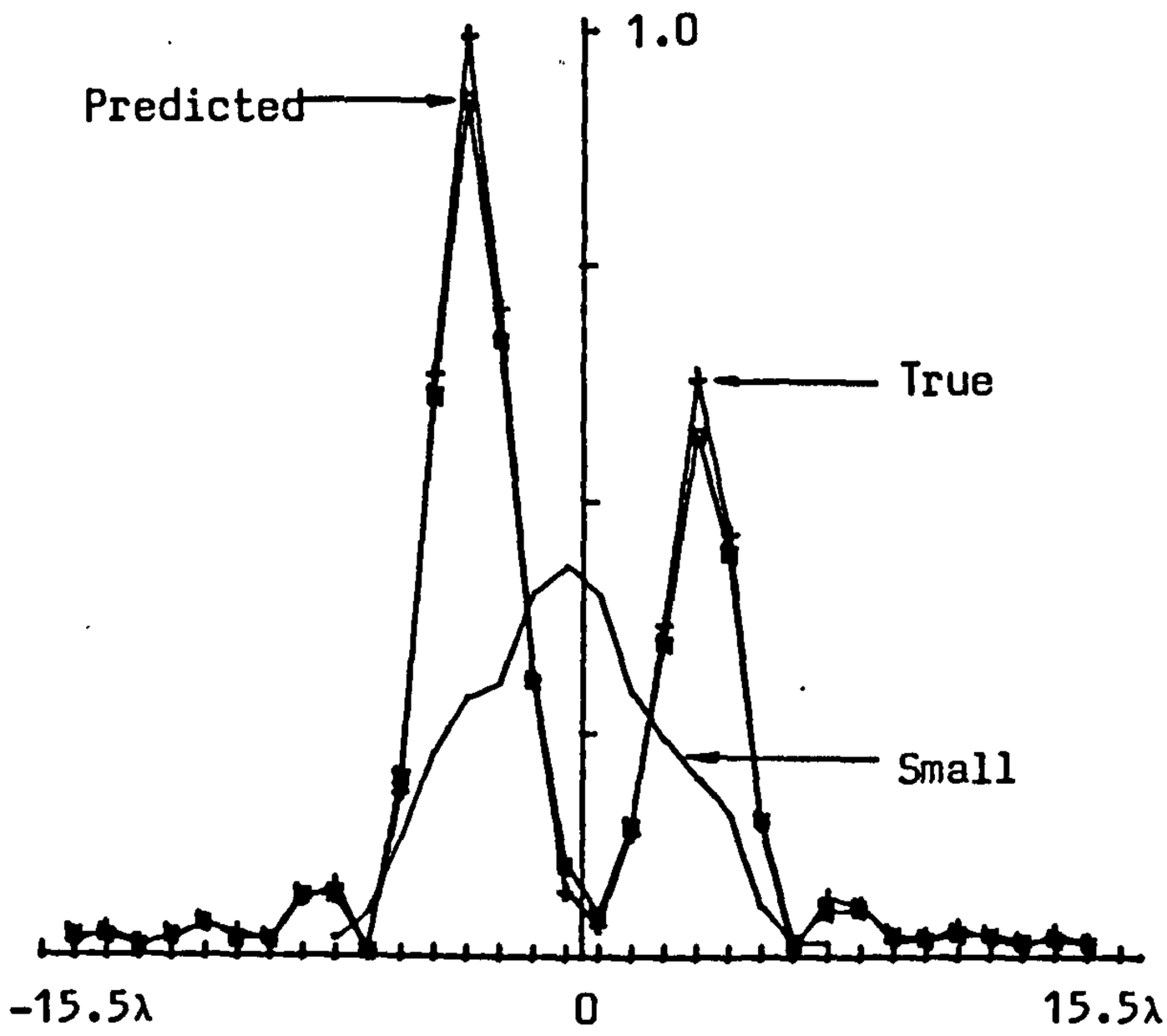


Fig. 4.16 : Prediction errors and reconstructed images obtained when using a 5/2 hybrid model to double the hologram of two points with different radiation strengths. The point at the R.H.S. has 0.8 the radiation strength of the other point.

a. Reconstructed images obtained when using a power series expansion

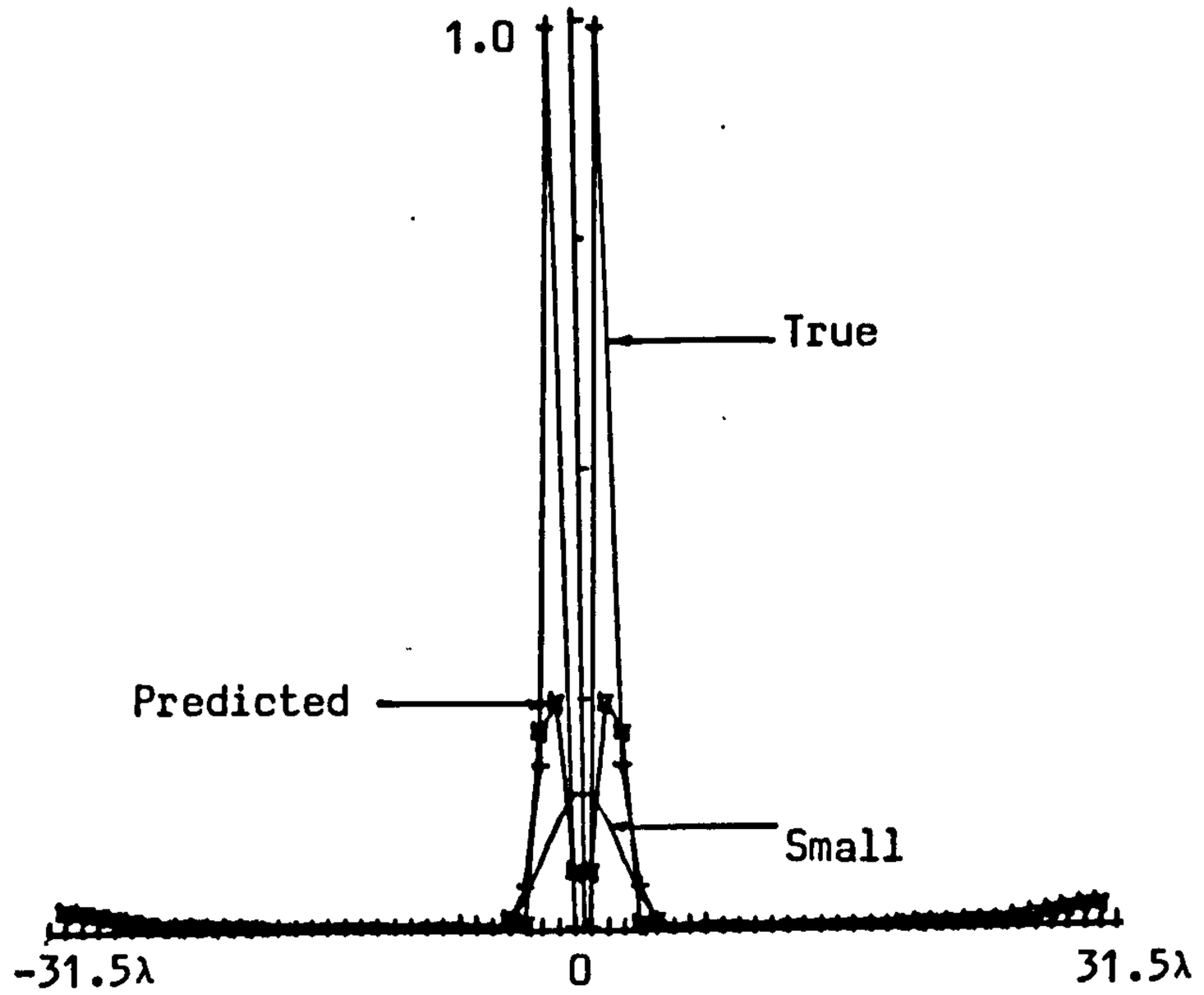


b. Reconstructed images obtained when using a Fourier series expansion of the optimum fundamental spatial frequency; $\alpha_{optimum}$=0.104, cf. eqn. (4.44)

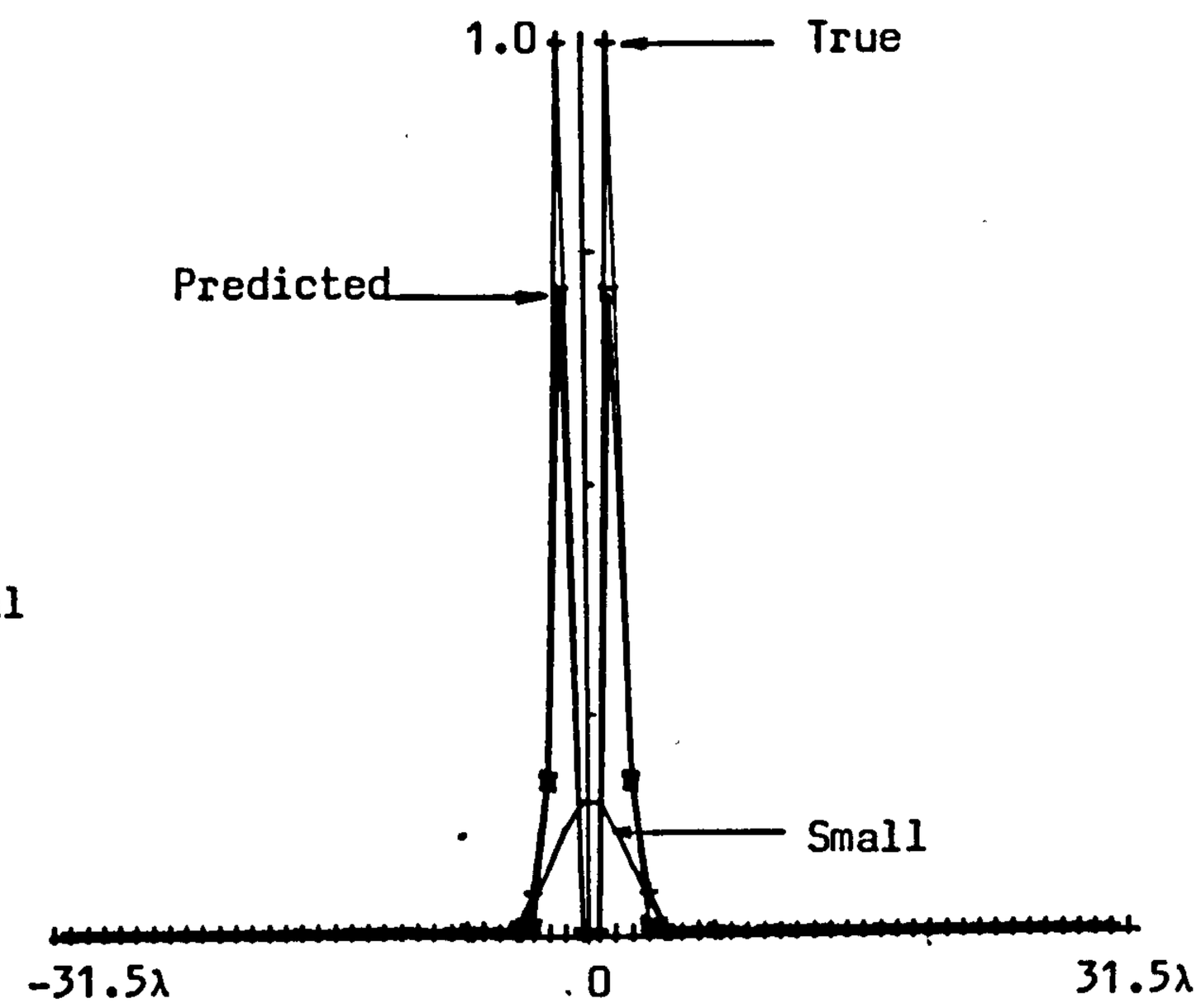


Hologram: Δ=1,M=8,N=32

Object: $x_{o1}$=1.7λ, $x_{o2}$=-1.7λ, z=80λ

Fig. 6.17 : Comparison between the performance of the power series and Fourier series expansions in the polynomial part of a 5/2 hybrid model when used to expand the hologram of a 2-point object four times.

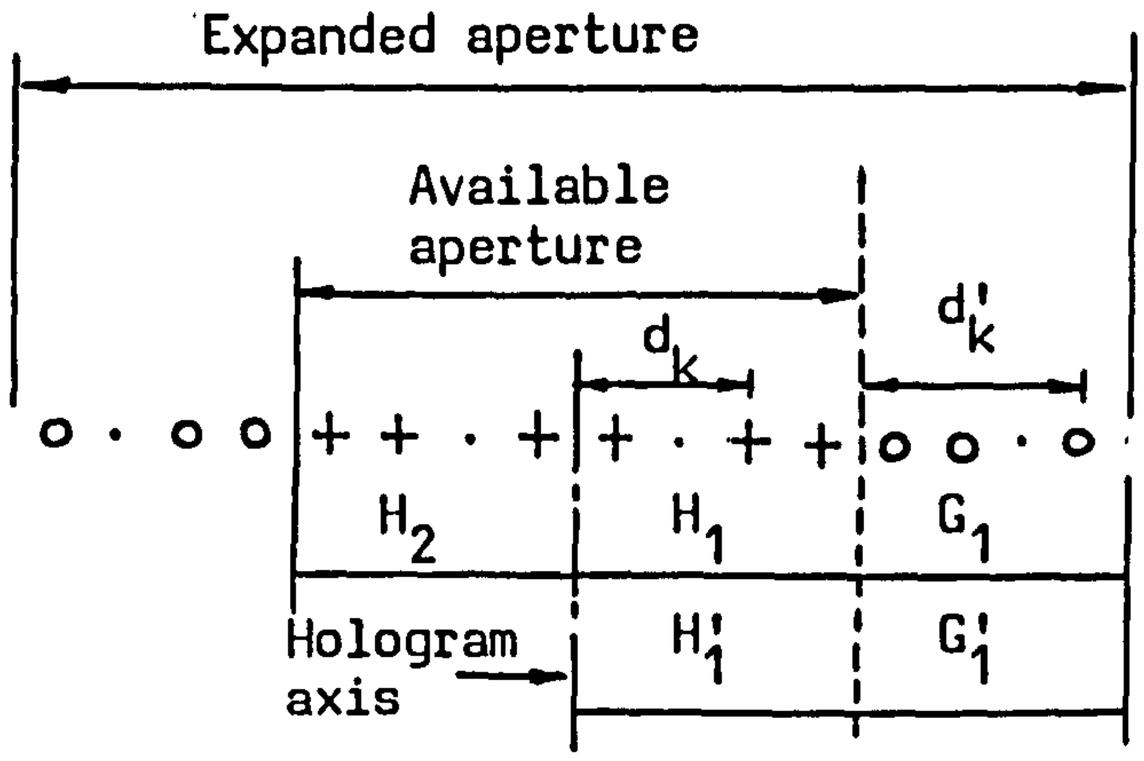


Fig. 4.18 : Hologram geometry for constructing and using the corrective model

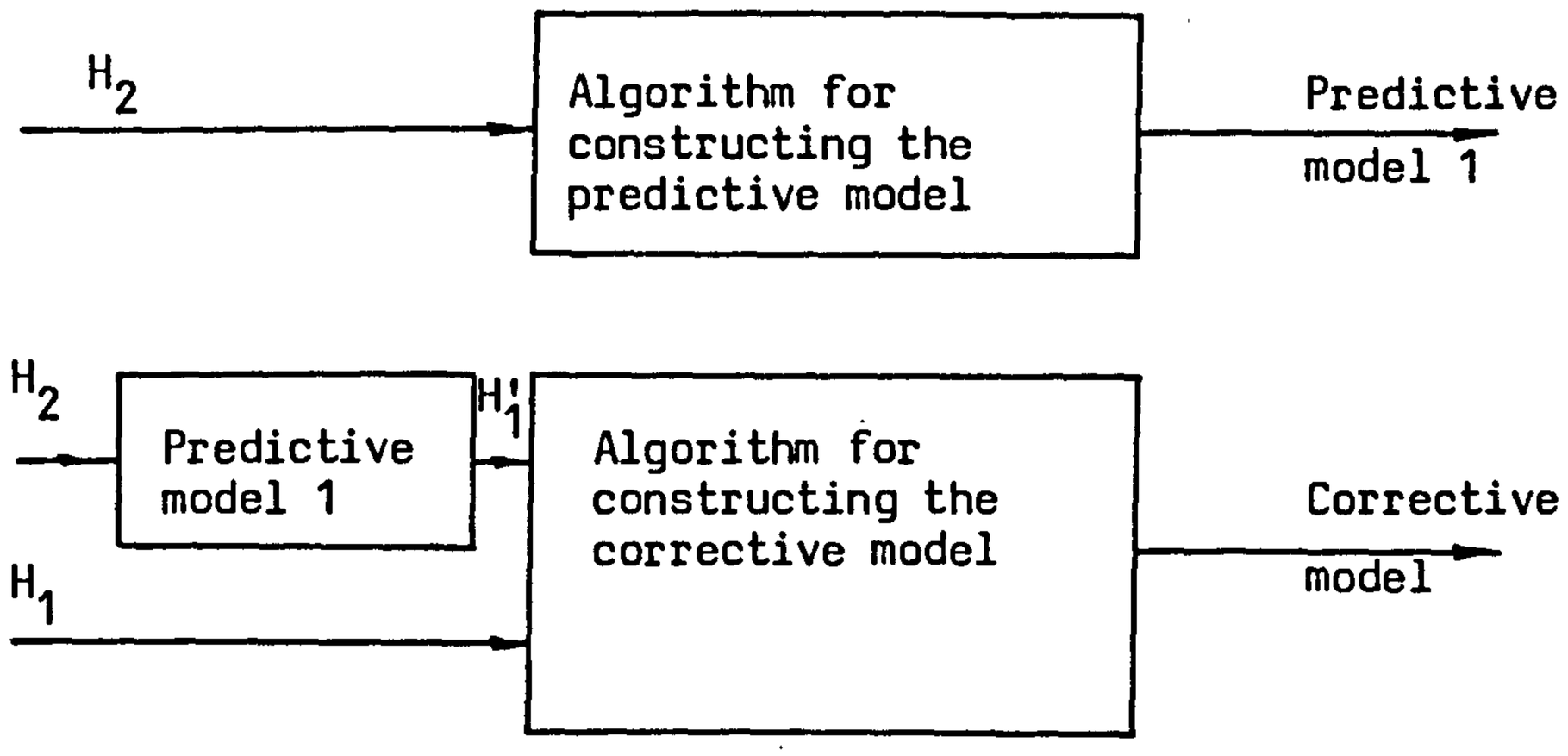


a. Constructing the corrective model

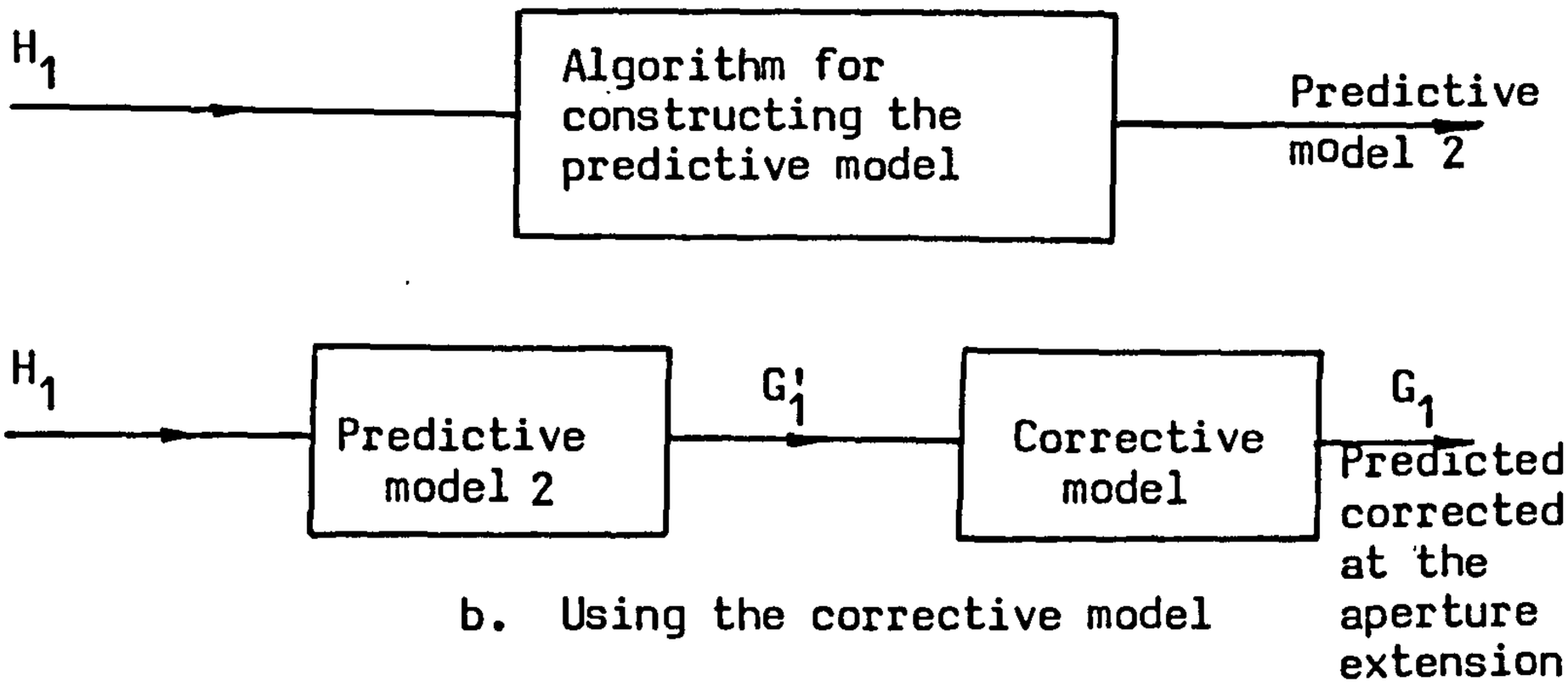


b. Using the corrective model

Fig. 4.19 : Constructing and using the corrective model

a. Errors over the aperture in the predicted and corrected holograms

Object:

$x_o$=0

z = 100λ

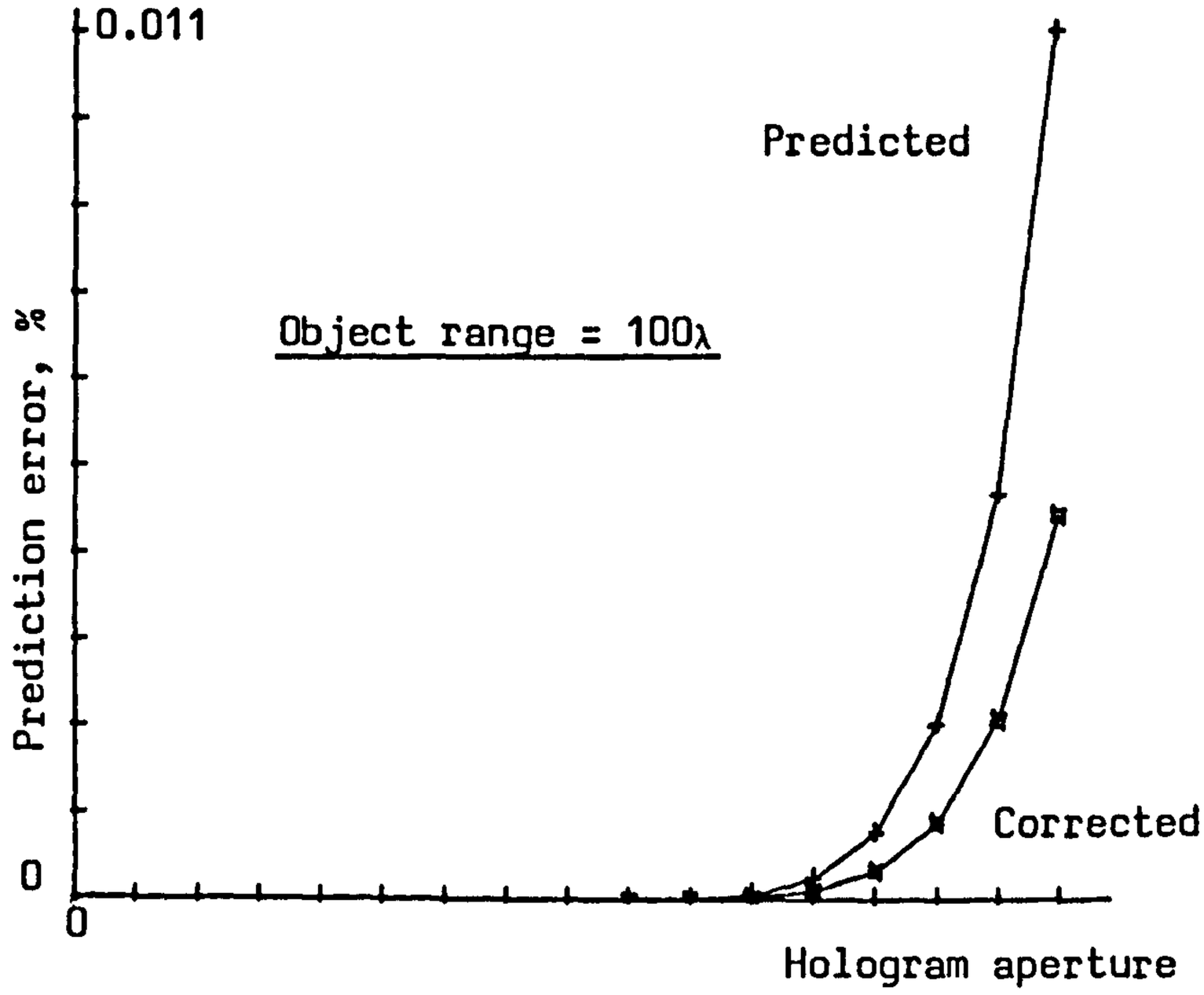


b. Errors over the aperture in the predicted and corrected holograms

Object:

$x_o$=0

z = 60λ

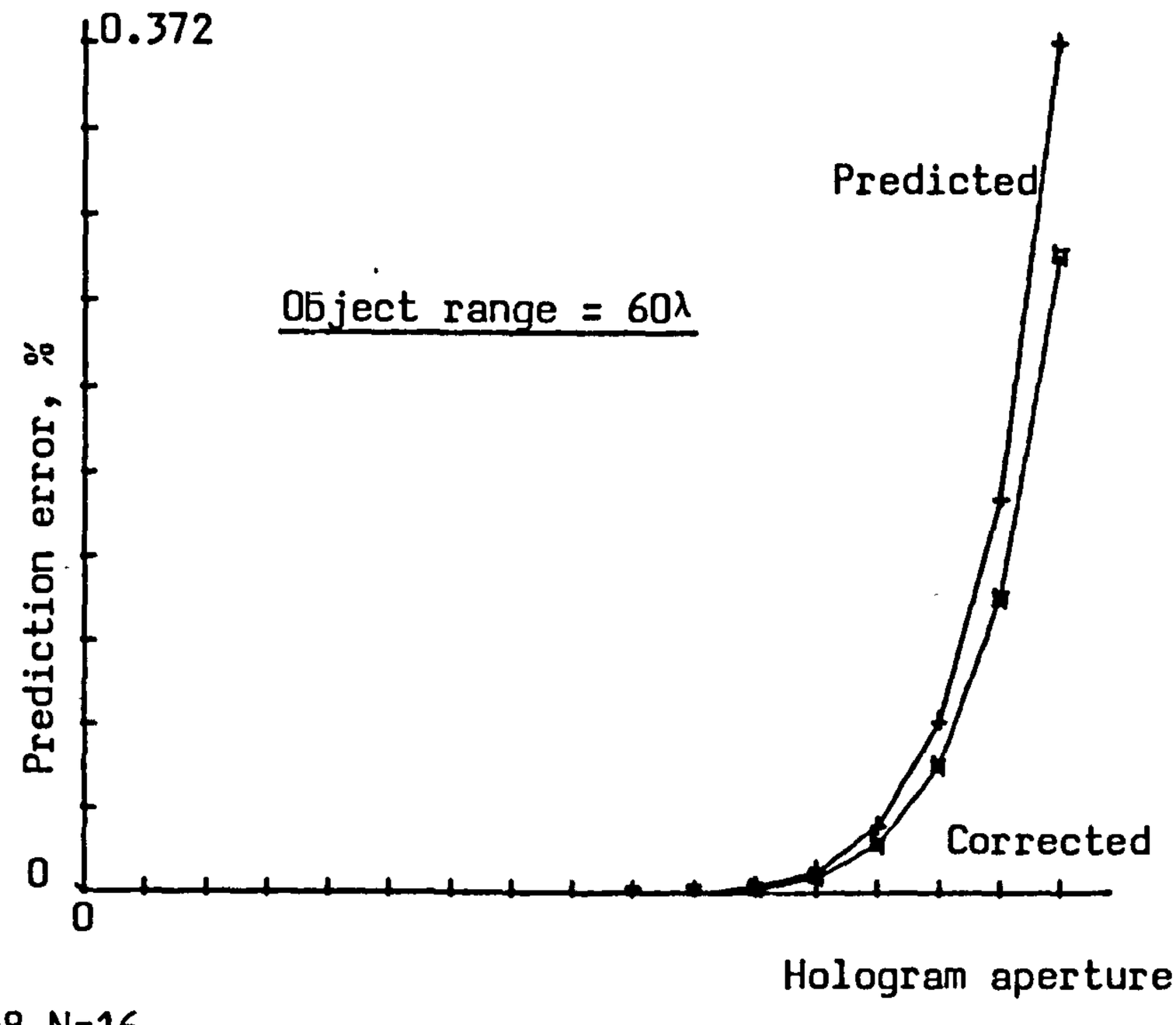


Hologram :Δ=1λ, M=8,N=16

Object : 1-point on the hologram axis

Fig. 4.20 : Effect of object range on the improvement in prediction accuracy obtained using the corrective model for the case of a 1-point object.

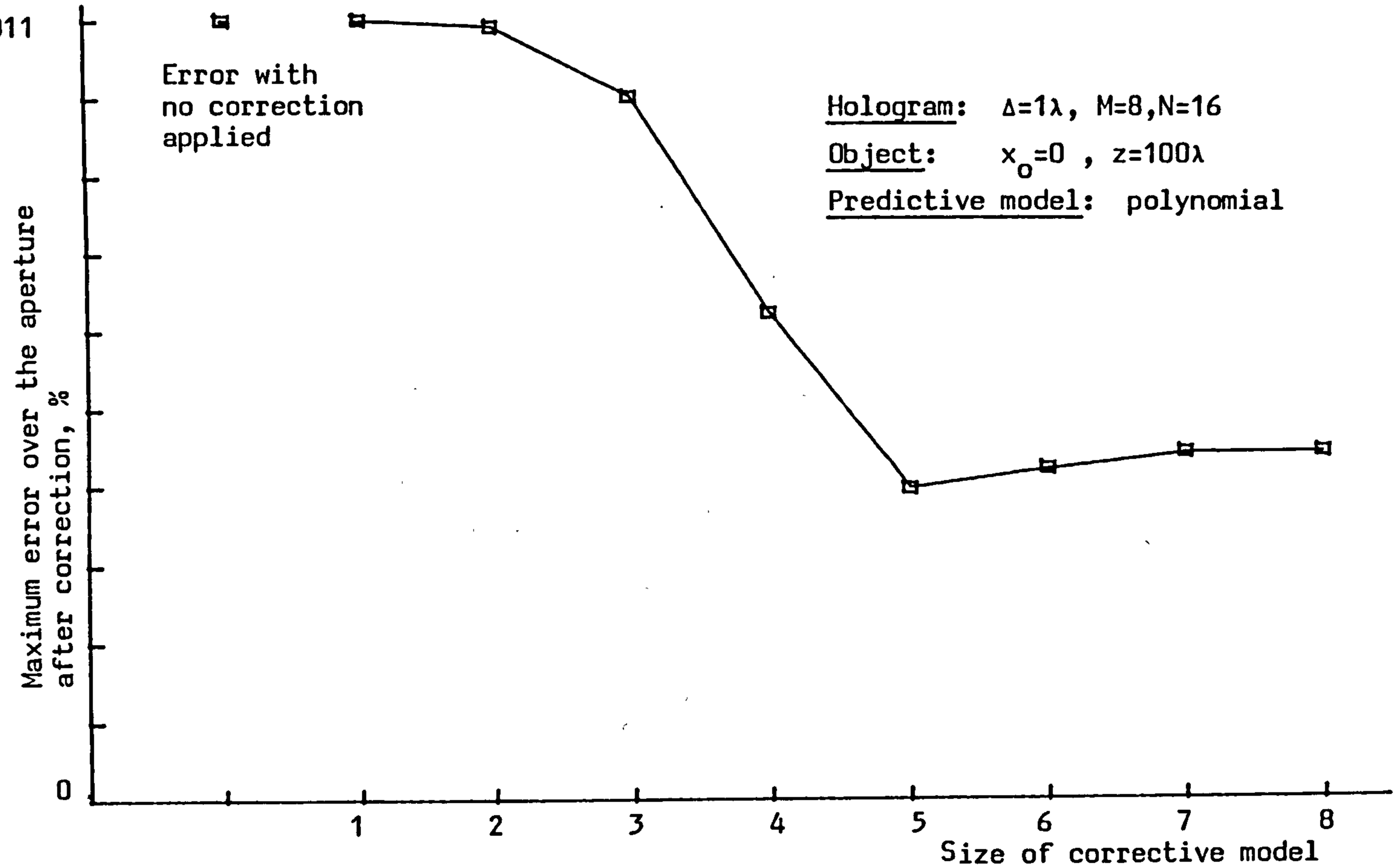


Fig. 4.21 : Effect of the size of a polynomial corrective model on the improvement in prediction accuracy obtained by correction for the case of a 1-point object

a. <u>Predictive model</u>:

Polynomial

<u>Object</u>: 1 point;

$x_o = 0$

$z = 100\lambda$

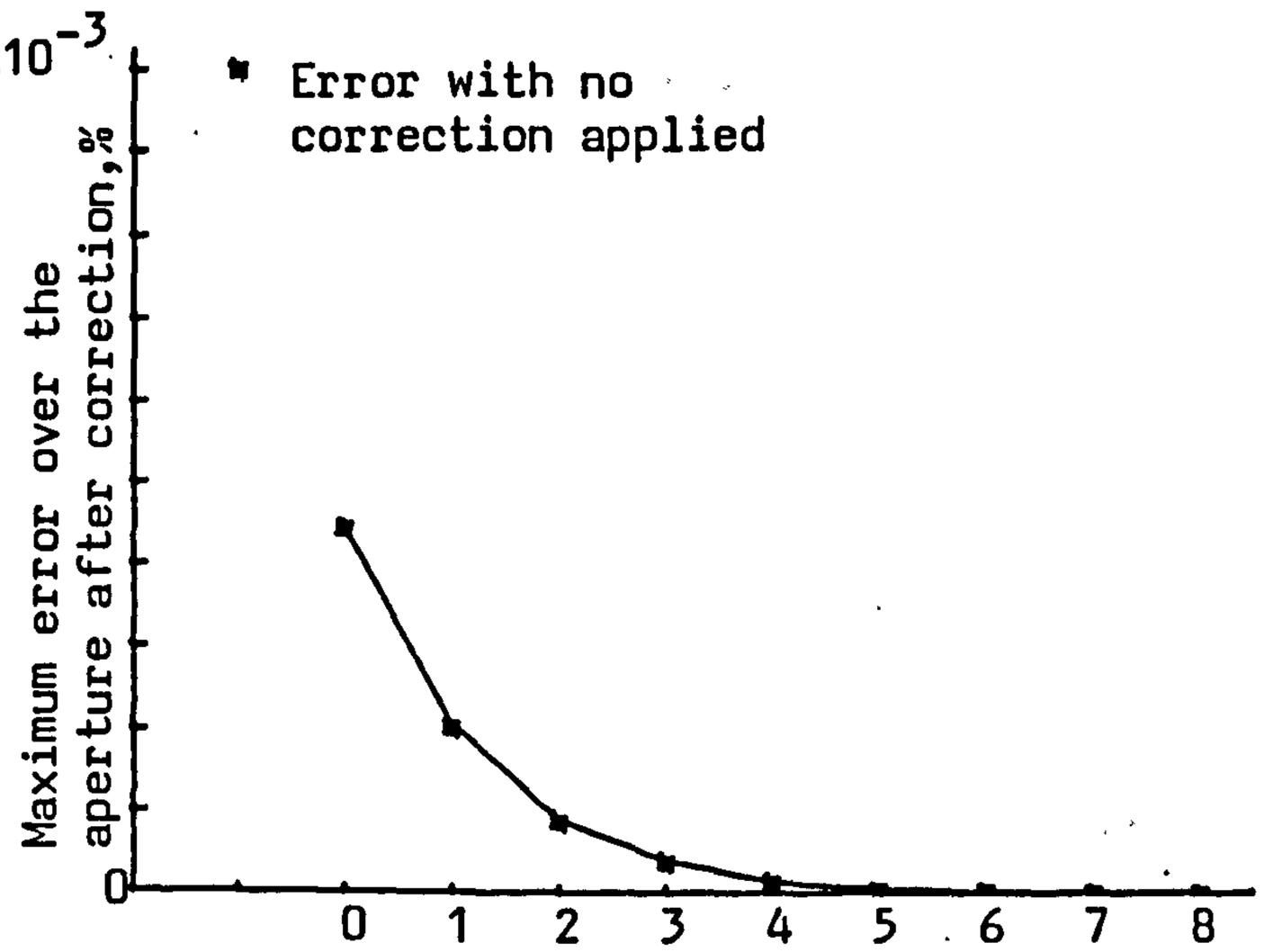


b. <u>Predictive model</u>:

5/2 hybrid

<u>Object</u>: 2 points;

$x_{o1} = 3\lambda$

$x_{o2} = -3\lambda$

$z = 100\lambda$

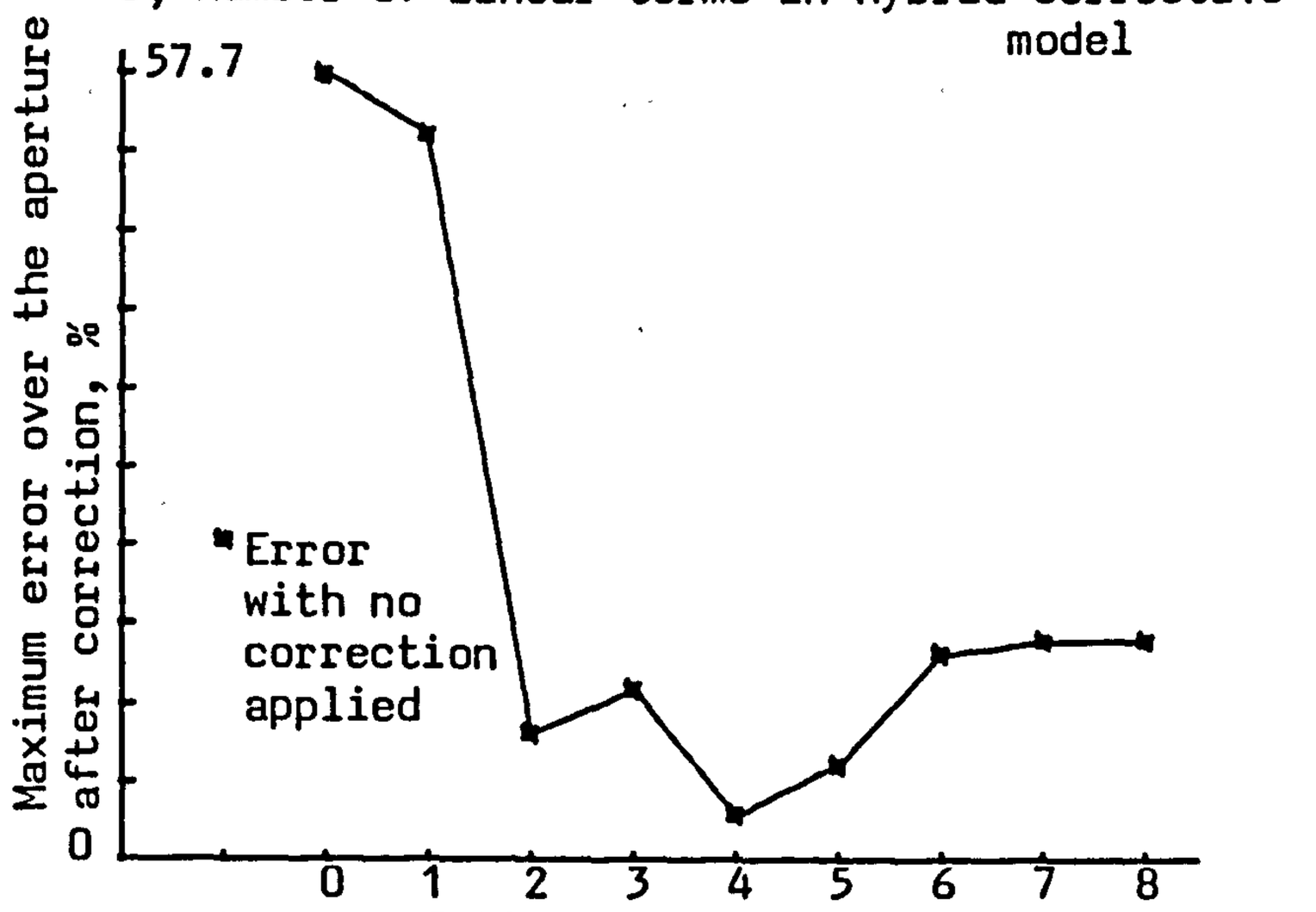


c. <u>Predictive model</u>:

Linear

<u>Object</u>: 2 points;

$x_{o1} = 3\lambda$, $x_{o2} = -3\lambda$

$z = 100\lambda$

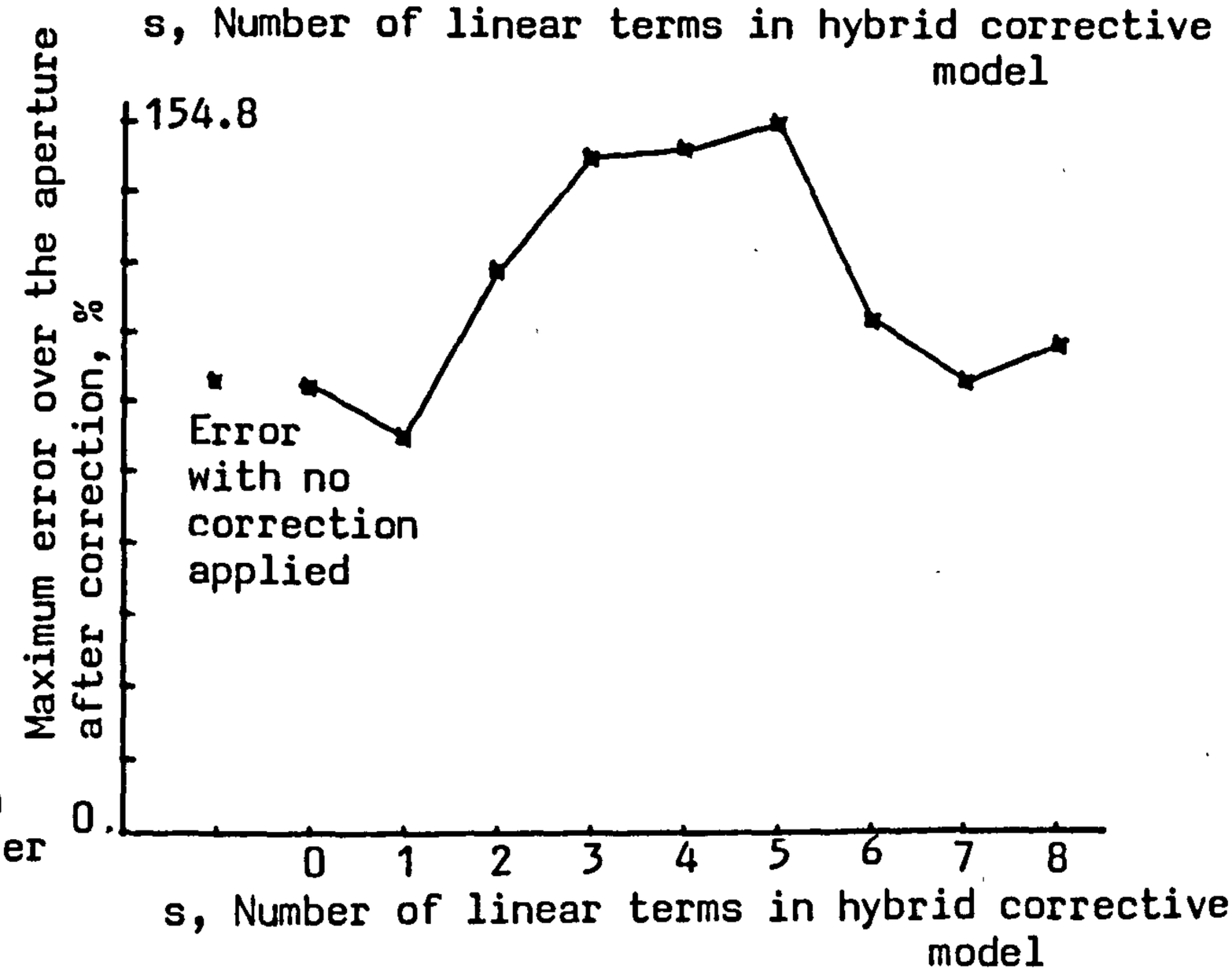


Fig. 4.22 : Effect of the composition of a hybrid corrective model on the correction performance with a number of predictive models

<u>Hologram</u> :Δ=1,M=8,N=16

a. Errors over the aperture in the predicted and corrected holograms,%

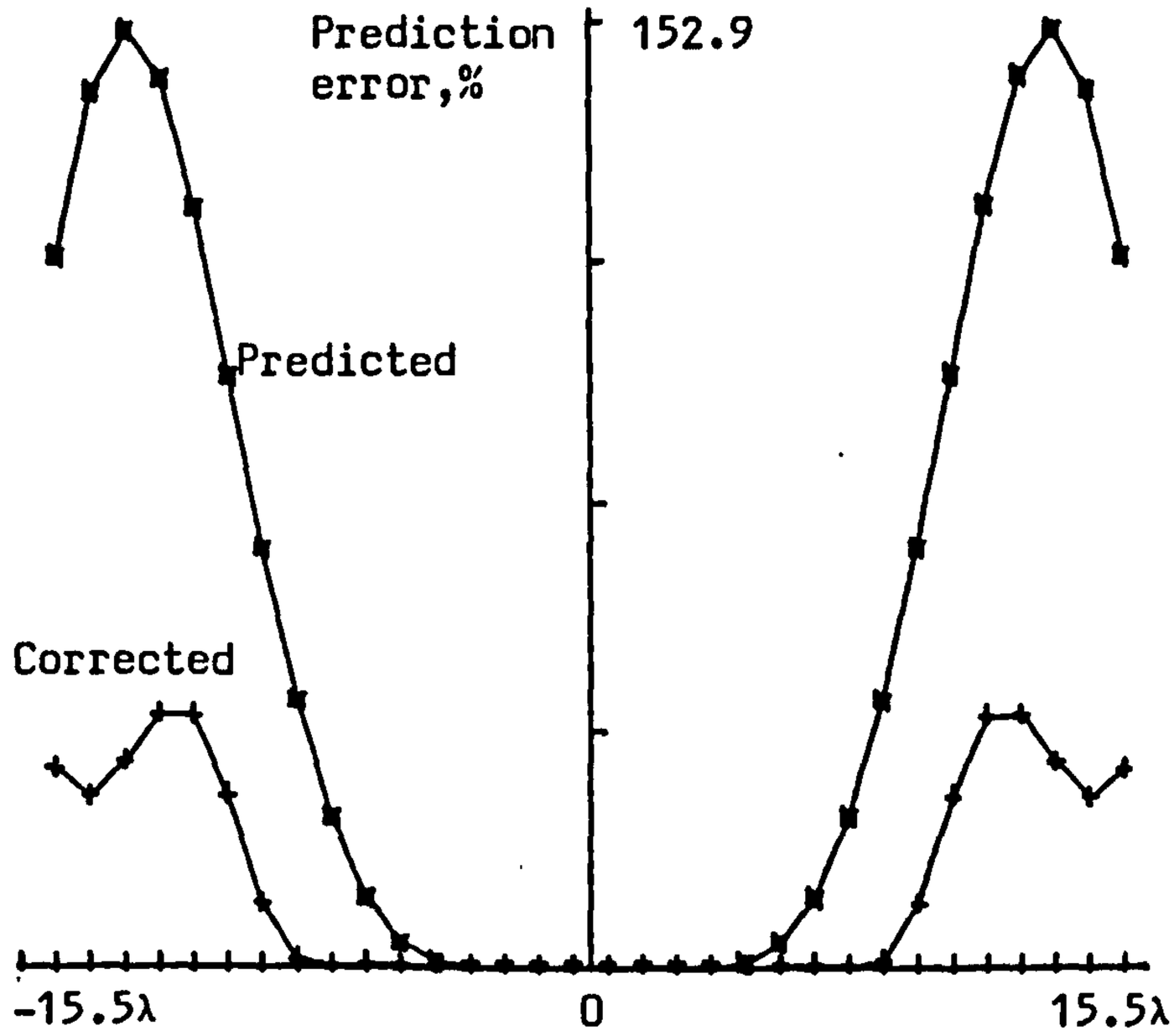


<u>Hologram</u>:

Δ=1,M=4,N=16

<u>Object</u>:

$x_{o1}$=2.5λ

$x_{o2}$=-2.5λ

z = 100λ

b. Reconstructed images from the small, true, predicted and corrected apertures

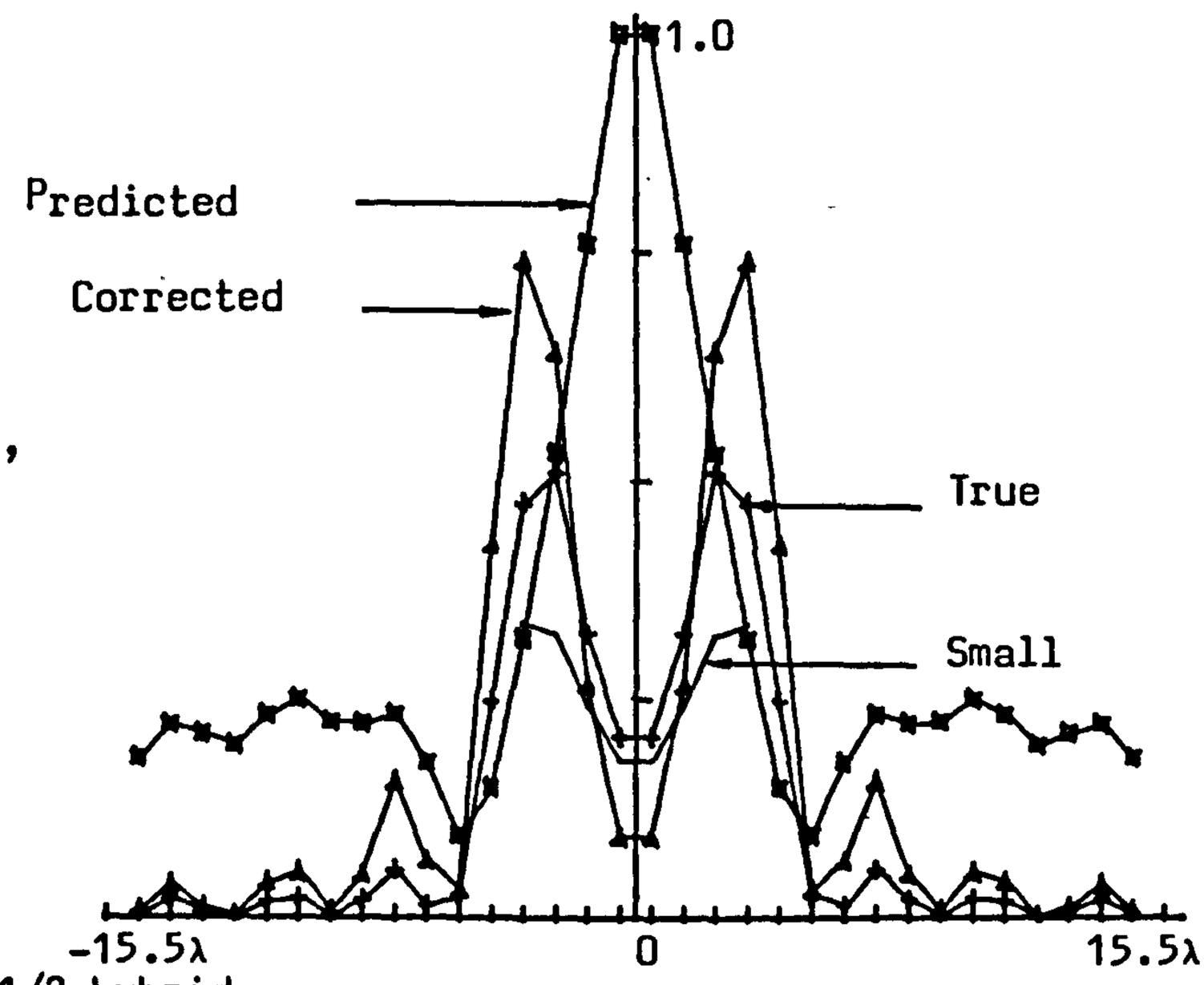


<u>Predictive model</u> : 1/2 hybrid

<u>Corrective model</u> : 0/4 (linear)

Fig. 4.23 : Improvement in resolution obtained through the use of a corrective model. The two points in the object can be resolved only after the predicted data is corrected.

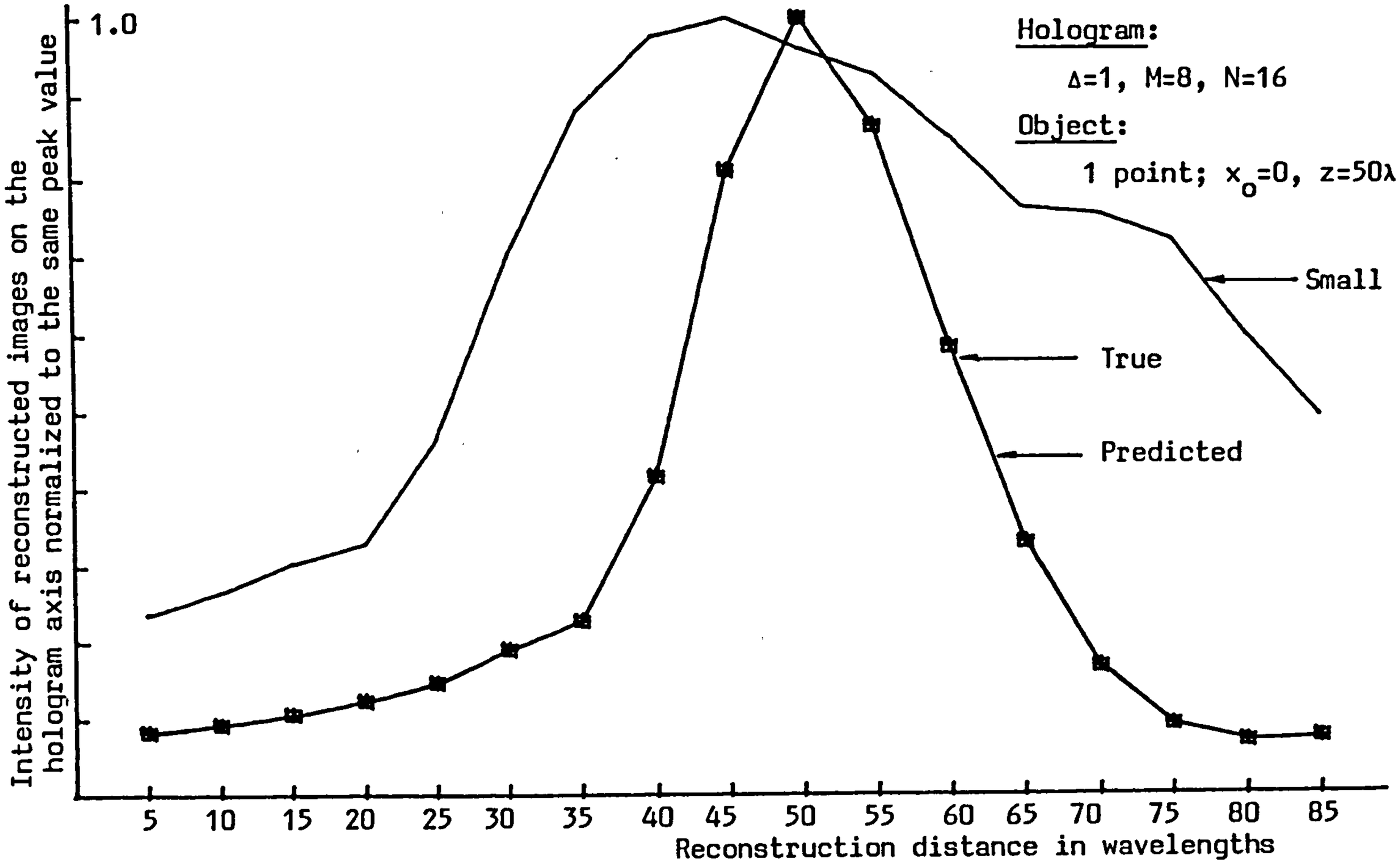


Fig. 4.24 : Reconstructed images in range for a 1-point object. Predictive model: polynomial.

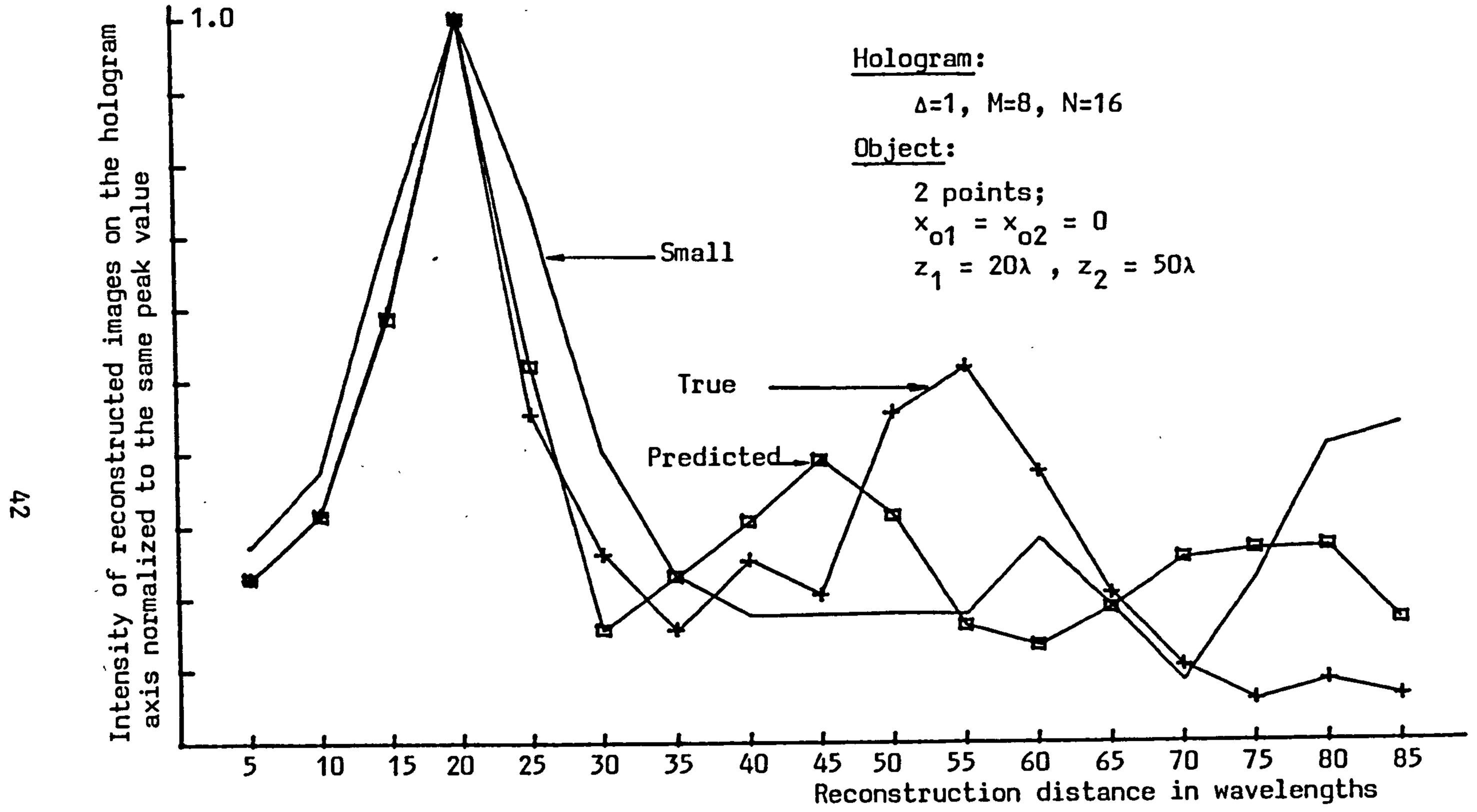


Fig. 4.25 : Reconstructed images in range for a 2-point object. Predictive model: 4/3 hybrid.

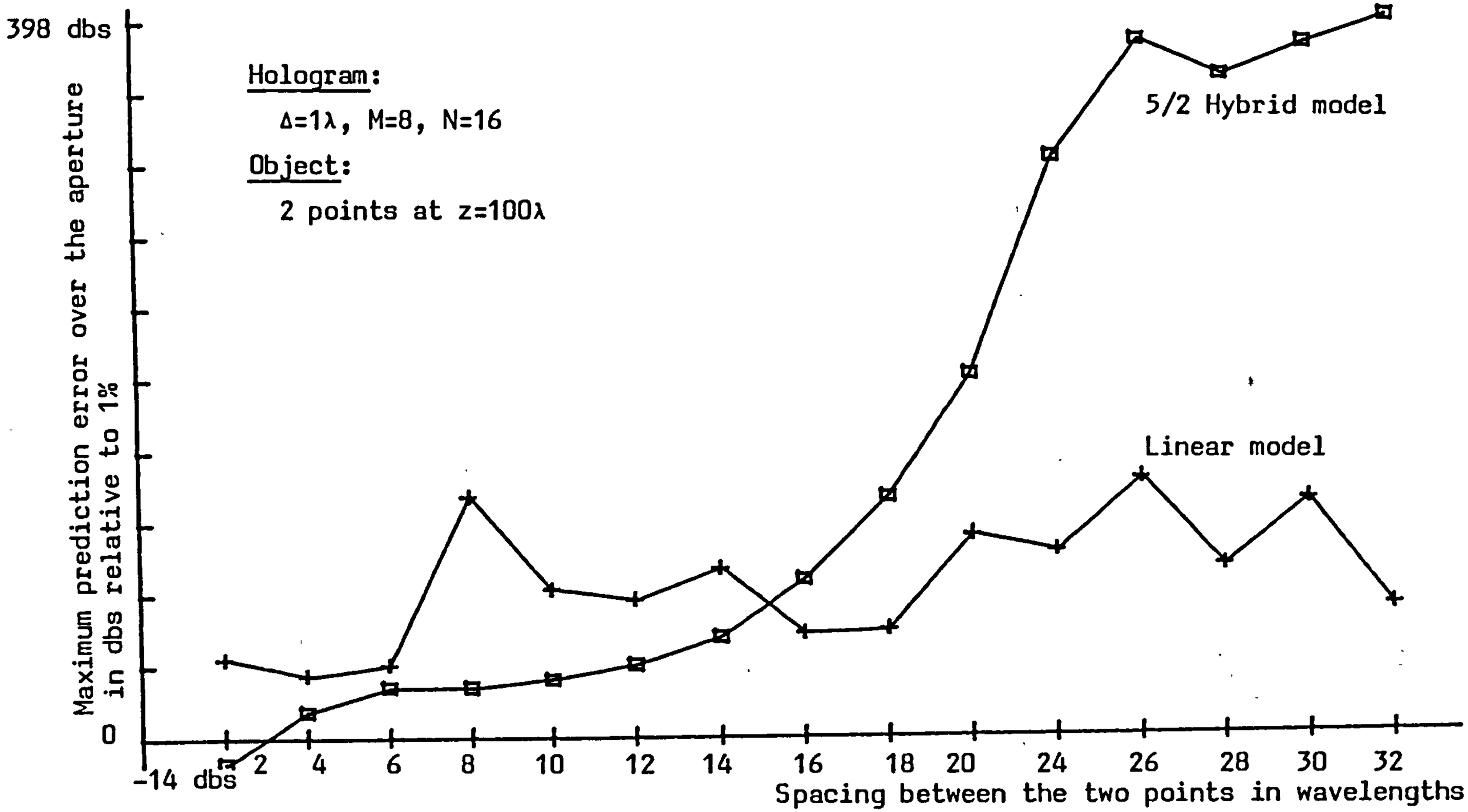


Fig. 4.26 : Effect of increasing the spacing between the points in a 2-point object on the performance of the linear and the hybrid predictive model

a. Effect on the 5/2 hybrid predictive model

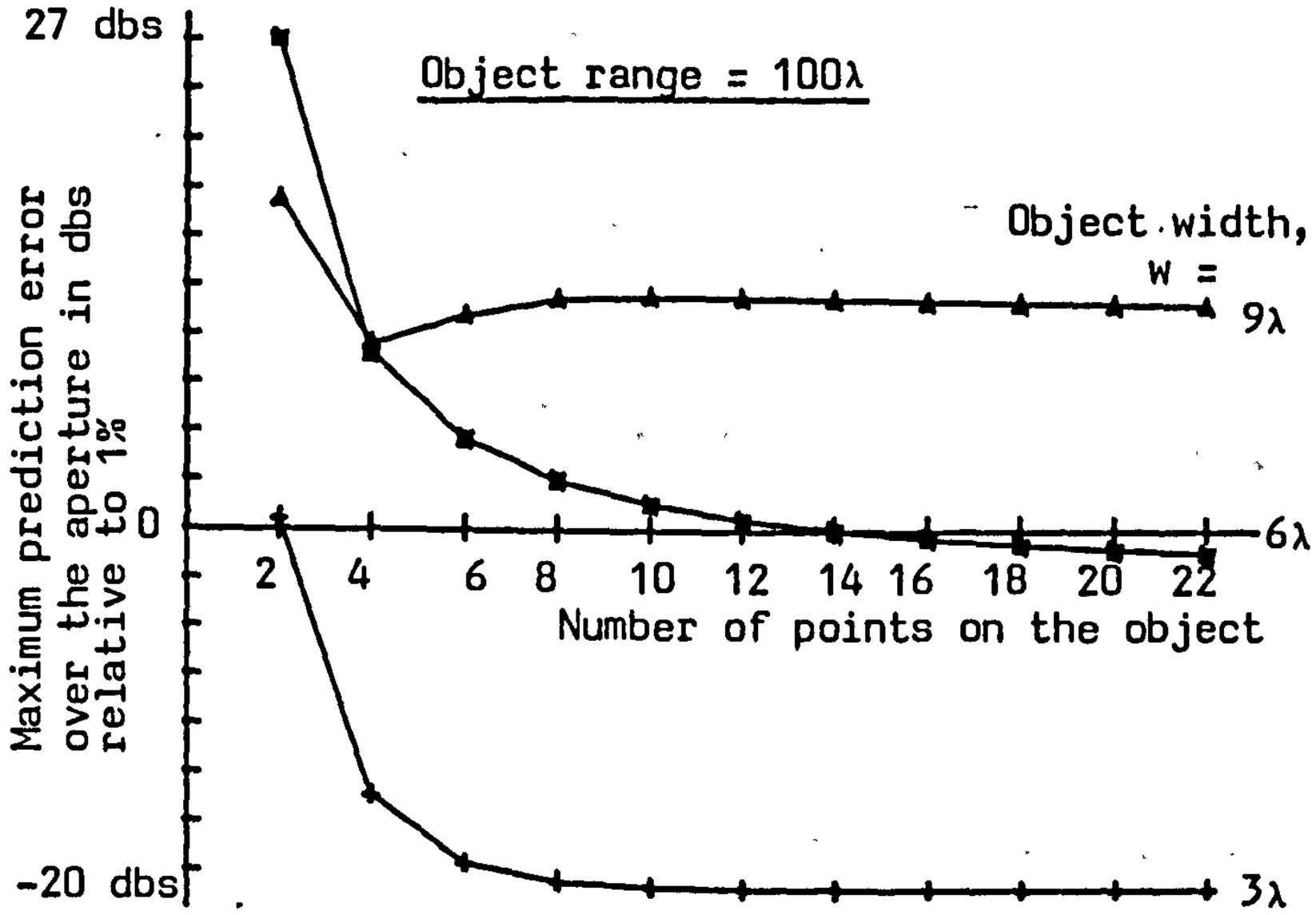


b. Effect on the linear predictive model

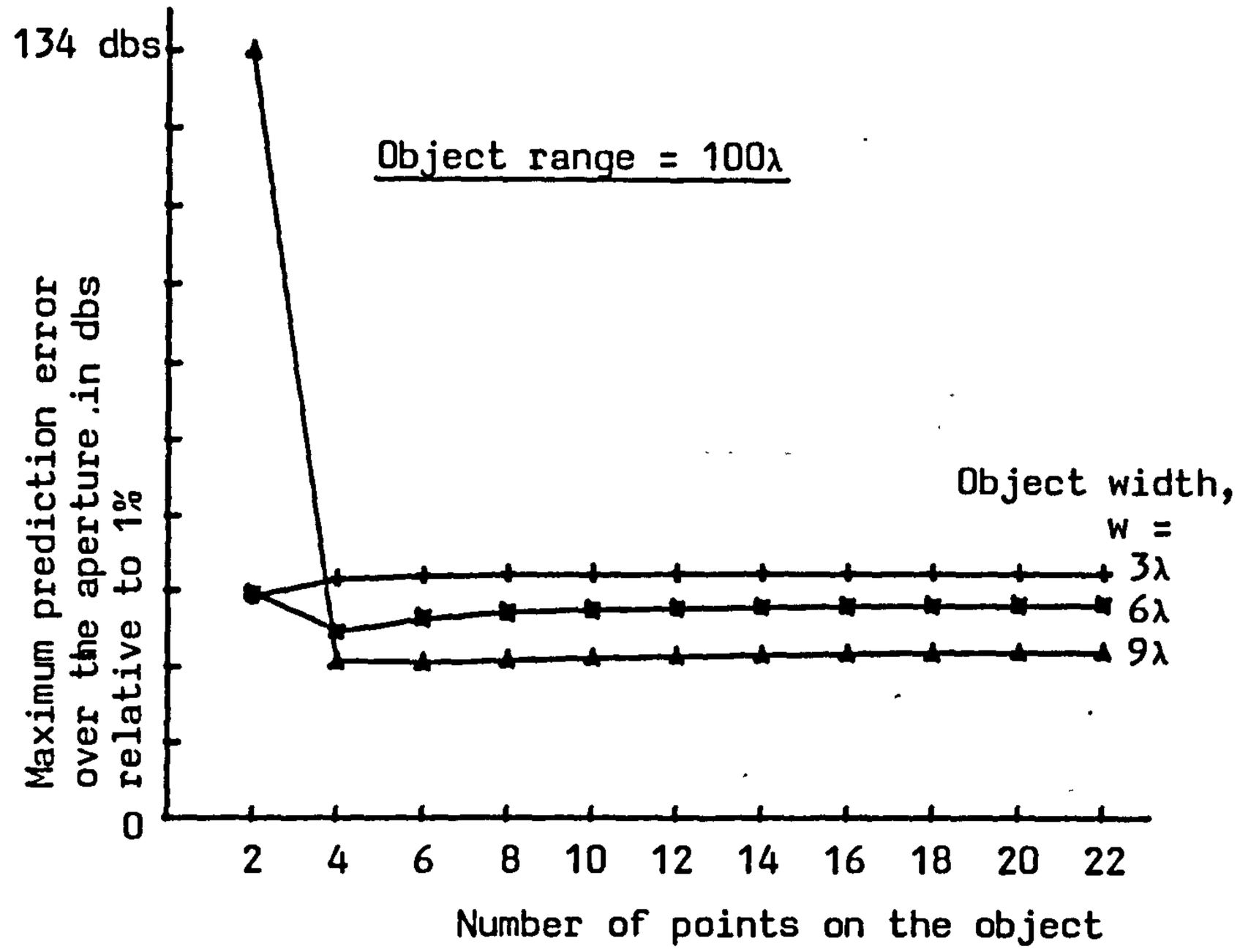


Hologram: Δ=1, M=8, N=16

Fig. 4.27 : Effect of increasing the points taken to represent an object of a given width on the performance of the hybrid and linear models. The plots are for a number of object widths at the same range.

a. Effect on the 5/2 hybrid predictive model

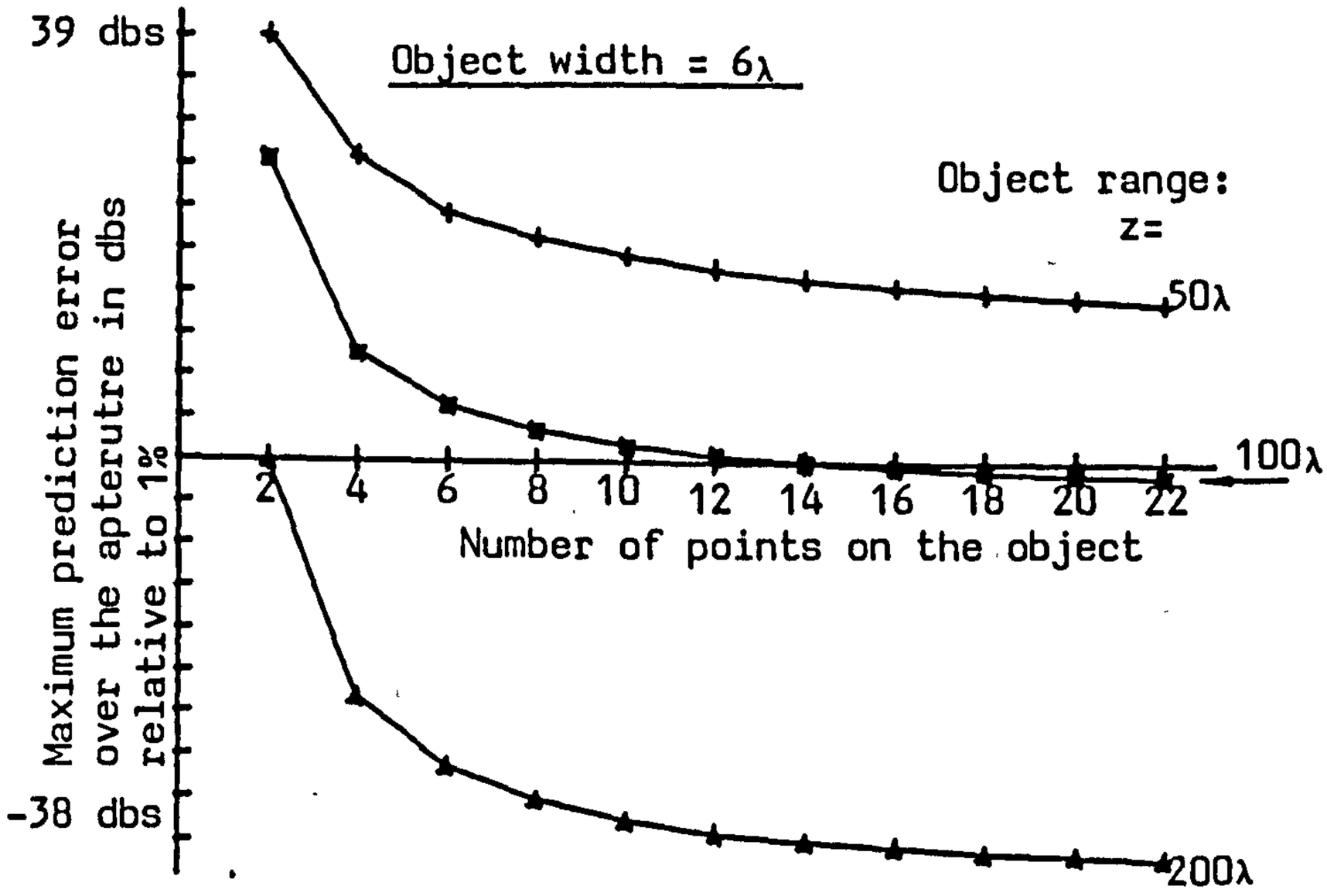


b. Effect on the linear predictive model

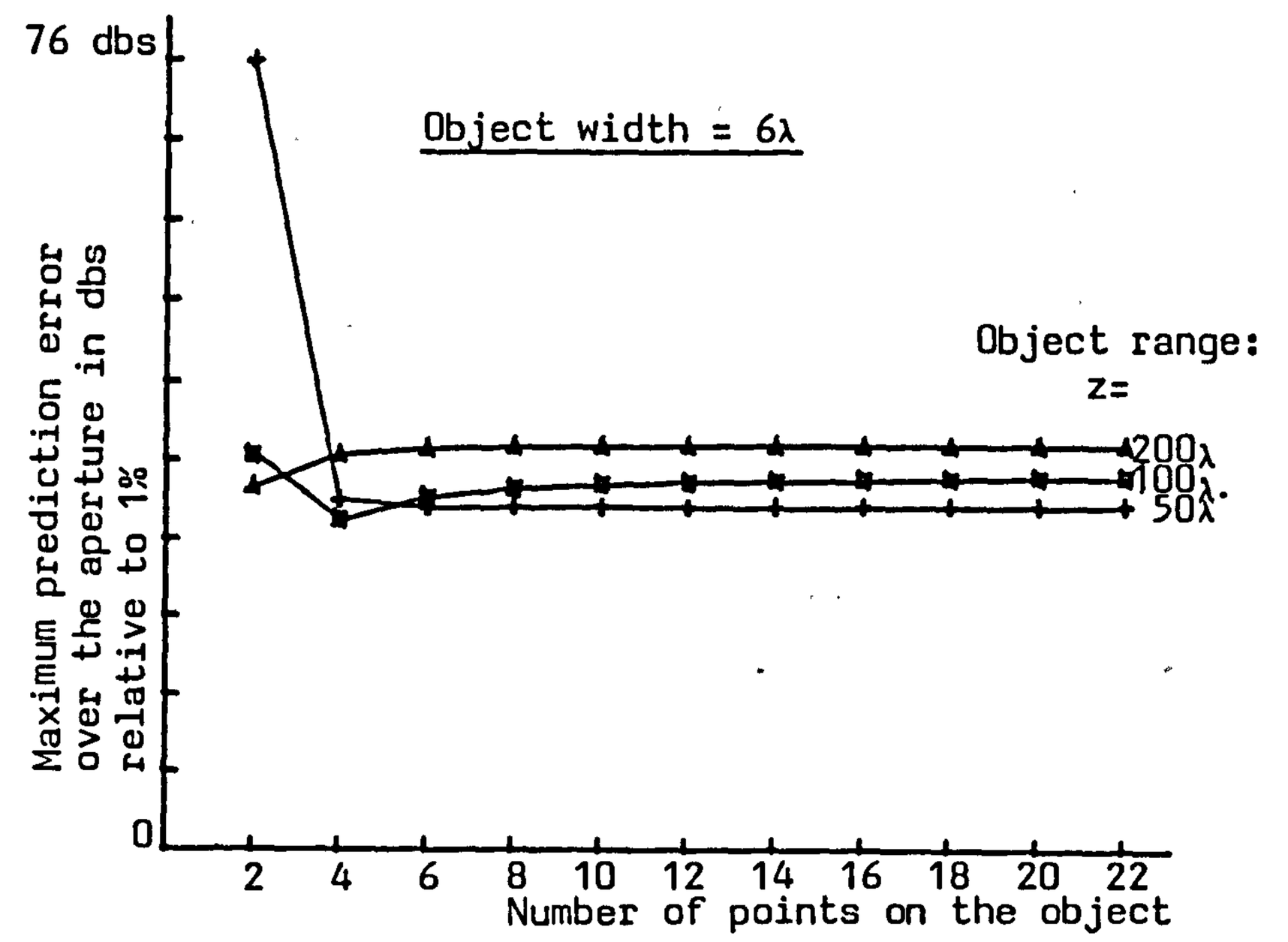


Hologram: Δ=1, M=8, N=16

Fig. 4.28 : Effect of increasing the points taken to represent an object of a given width on the performance of the hybrid and linear models. The plots are for a given object width at a number of values for the range.

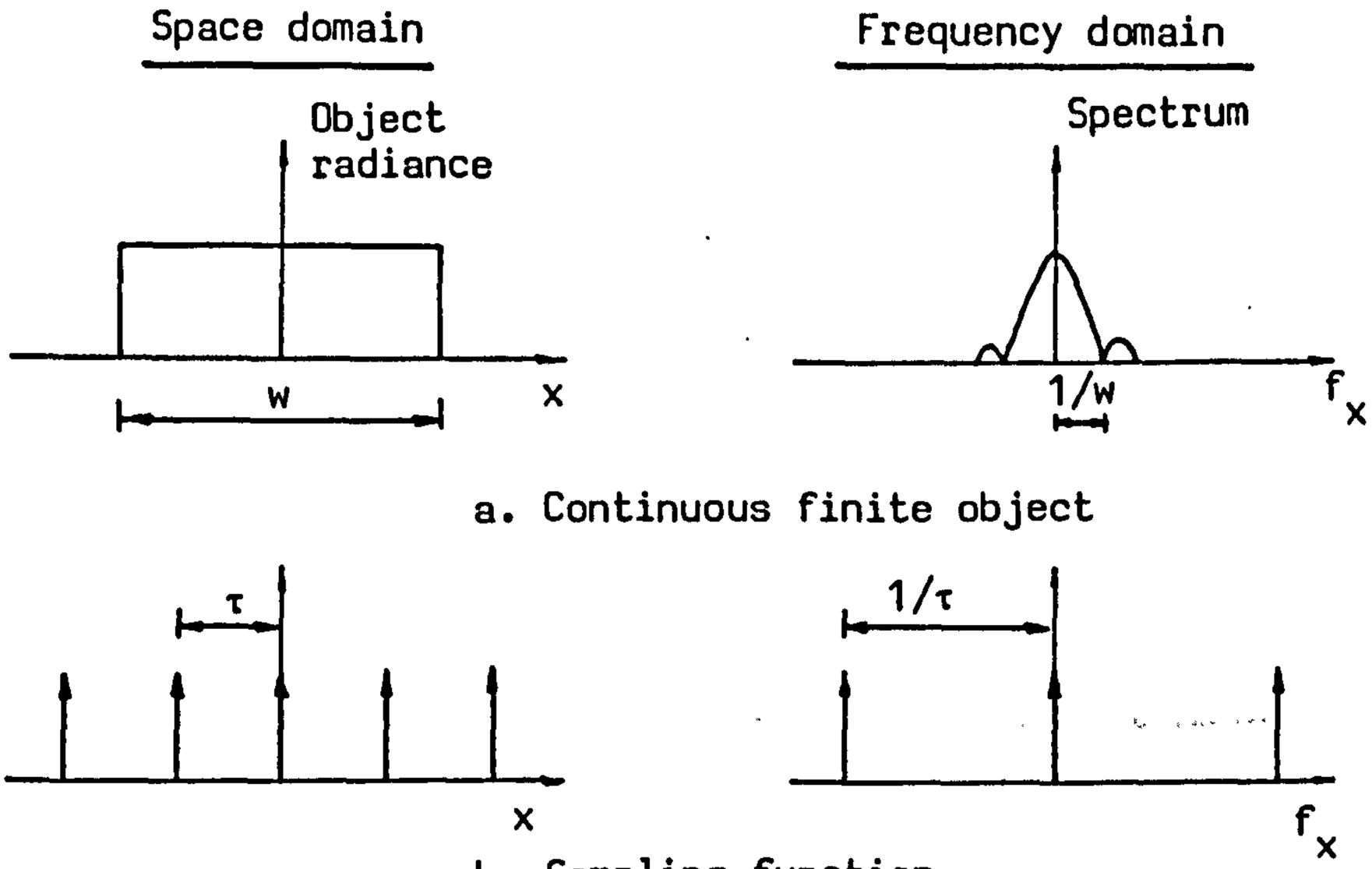


Fig. 4.29 : Spatial and angular spectra of discrete objects

a. Prediction error over the aperture

<u>Hologram</u>:

$\Delta=1\lambda$
M=8
N=16

<u>Object</u>:

two points;

range = $95\lambda$
$d_o = 5.6\lambda$

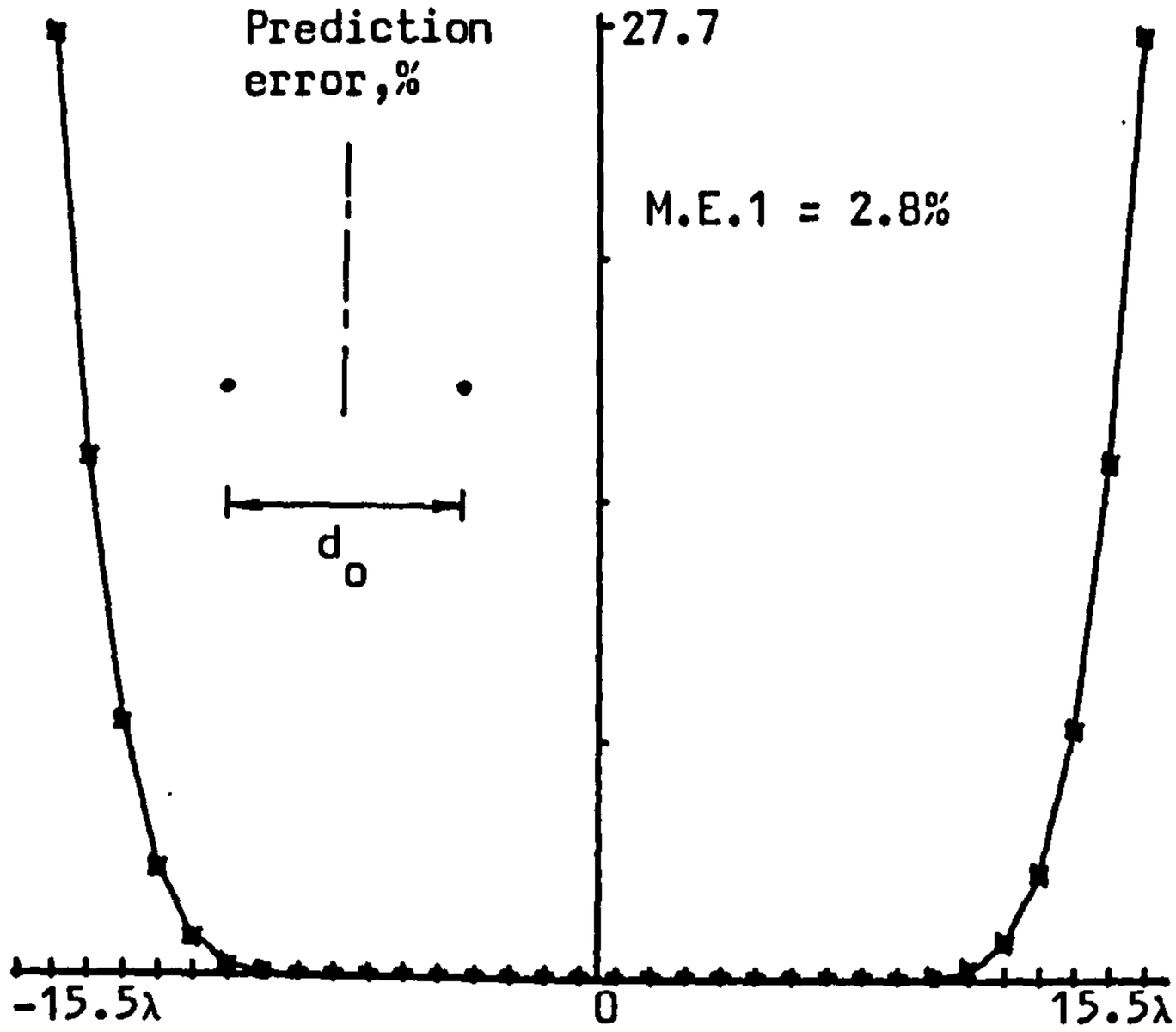


b. Reconstructed images

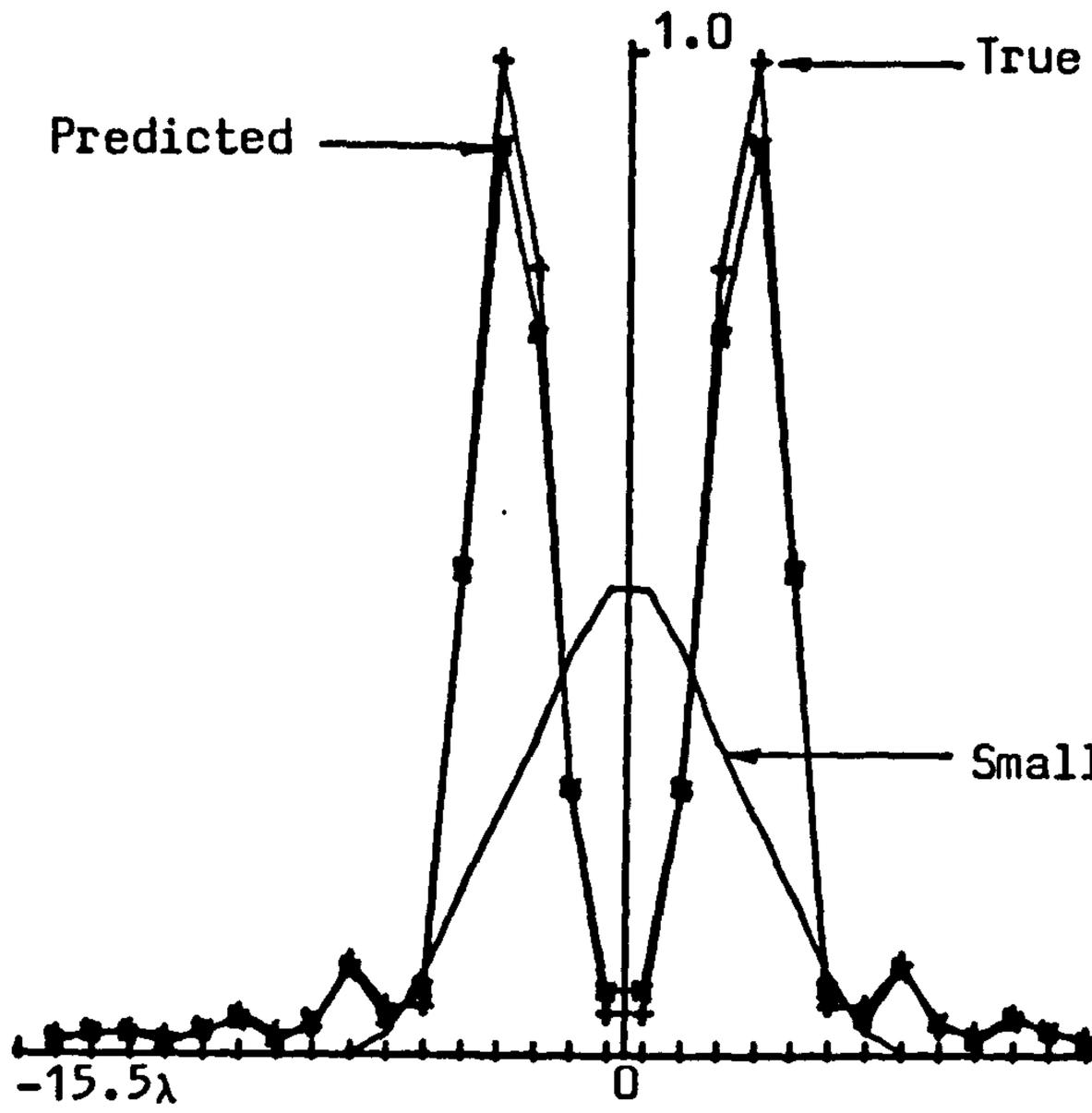


Fig. 4.30 : Prediction errors and reconstructed images obtained when using the 5/2 hybrid model to double the size of the hologram of two points symmetrically positioned about the hologram axis.

a. Prediction error over the aperture

Hologram:

Δ=1λ
M=8
N=16

Object:

two points;

range = 95λ
$d_o$ = 5.6λ

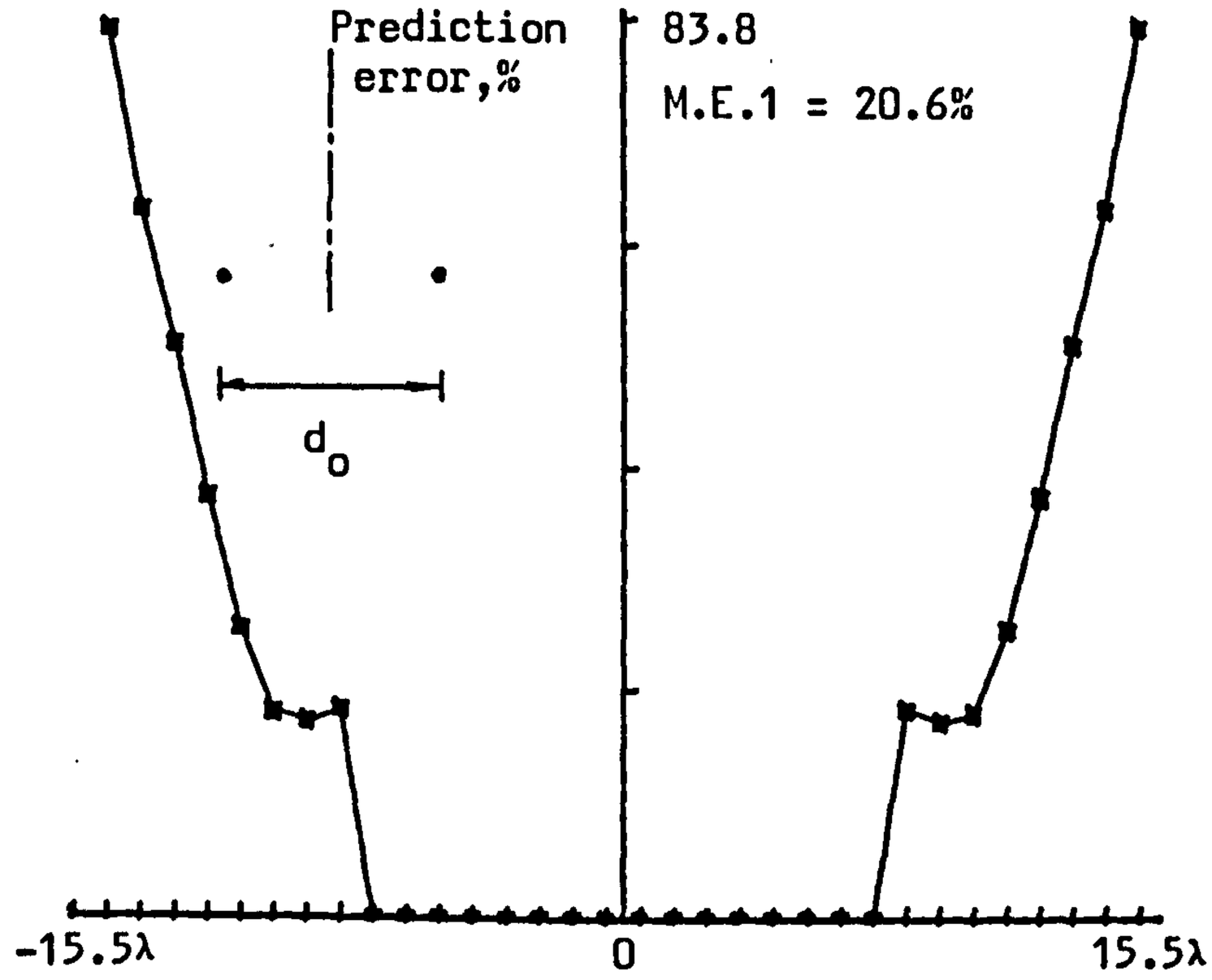


b. Reconstructed images

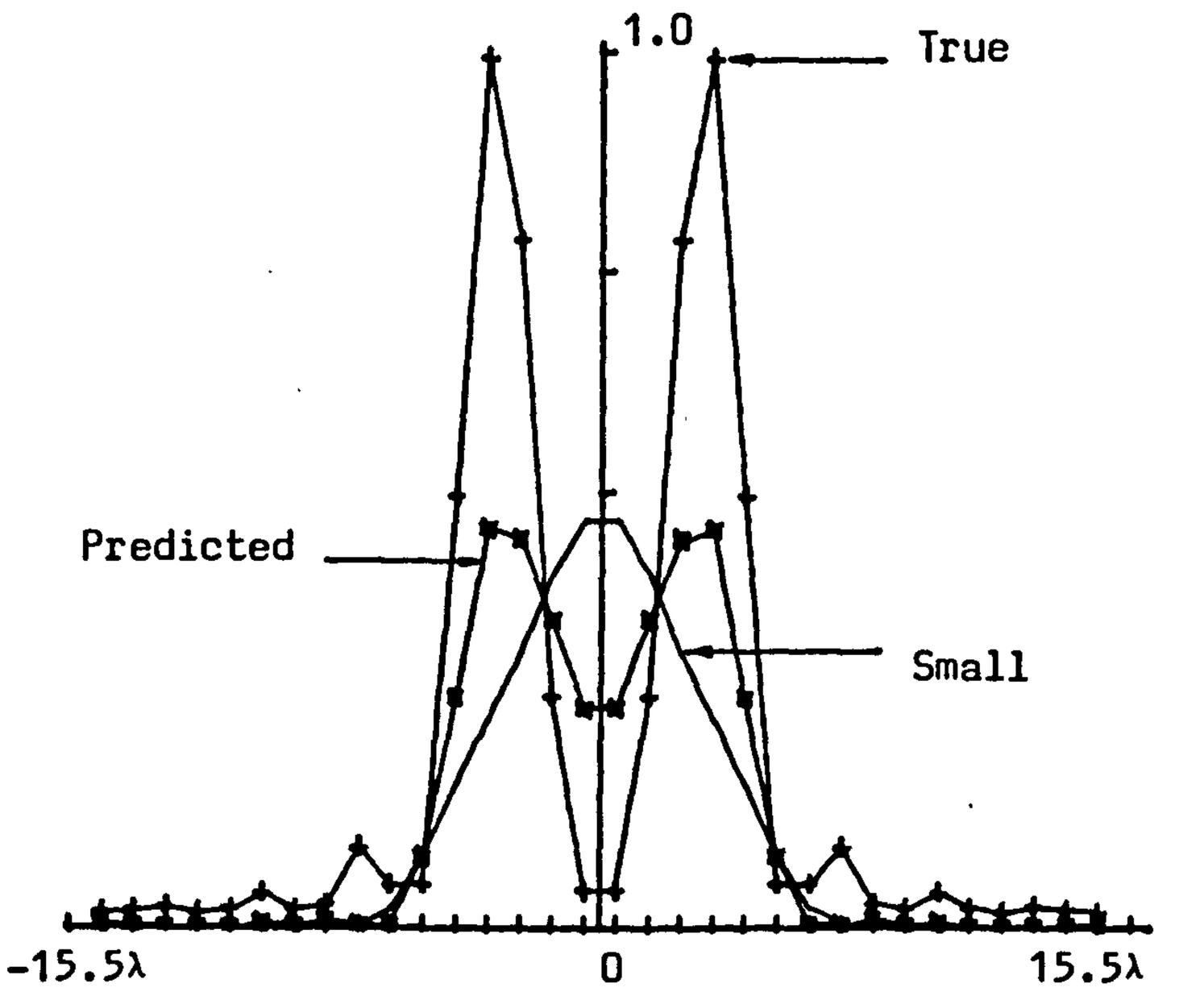


Fig. 4.31 : Prediction errors and reconstructed images obtained when using the linear model to double the size of the hologram of two points symmetrically positioned about the hologram axis.

a. Prediction error over the aperture

Hologram:

Δ=1λ
M=8
N=16

Object:

range = 95λ
$d_o$ = 5.6λ
$w_o$ = 4λ
ρ = 25 points/λ

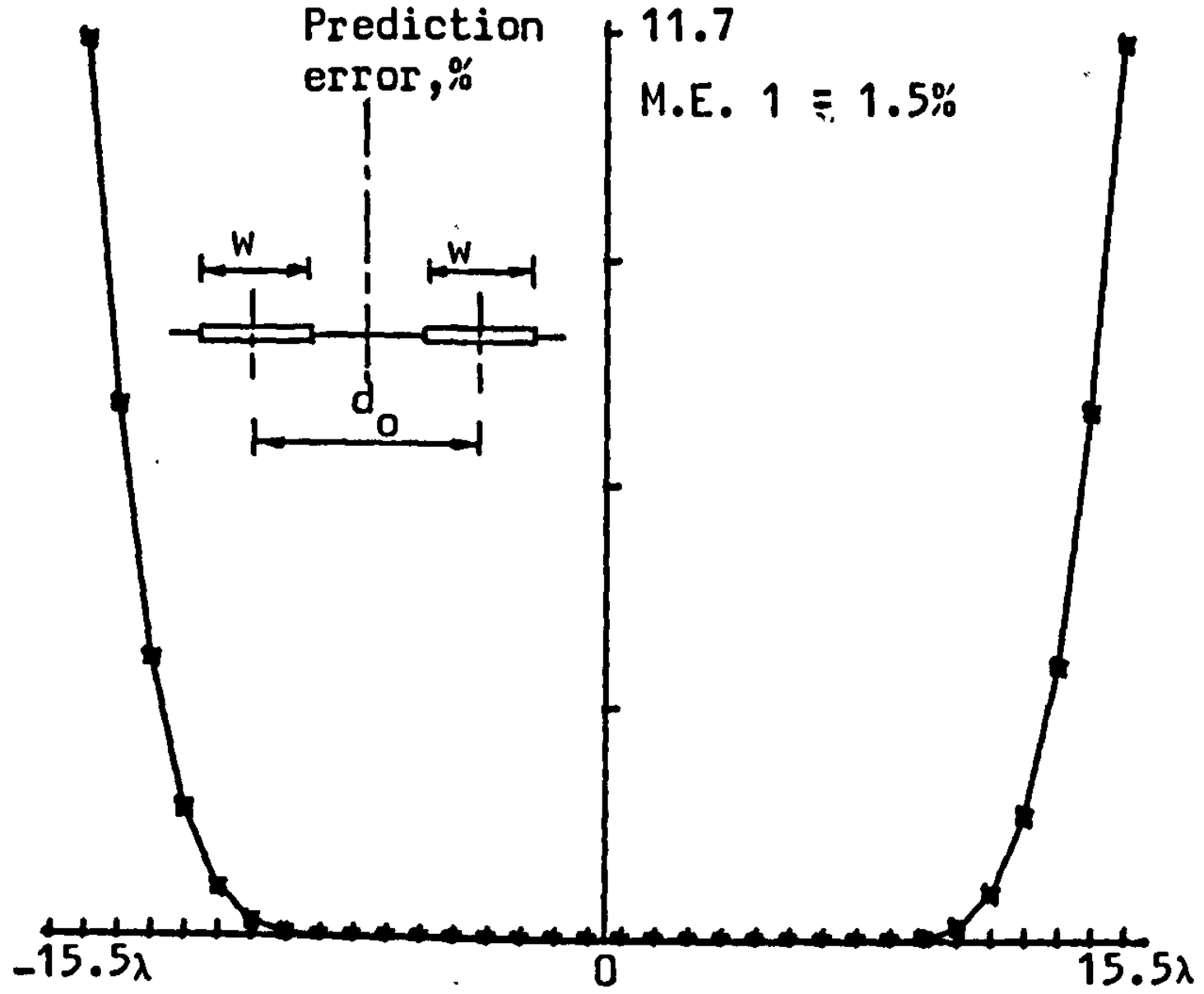


b. Reconstructed images

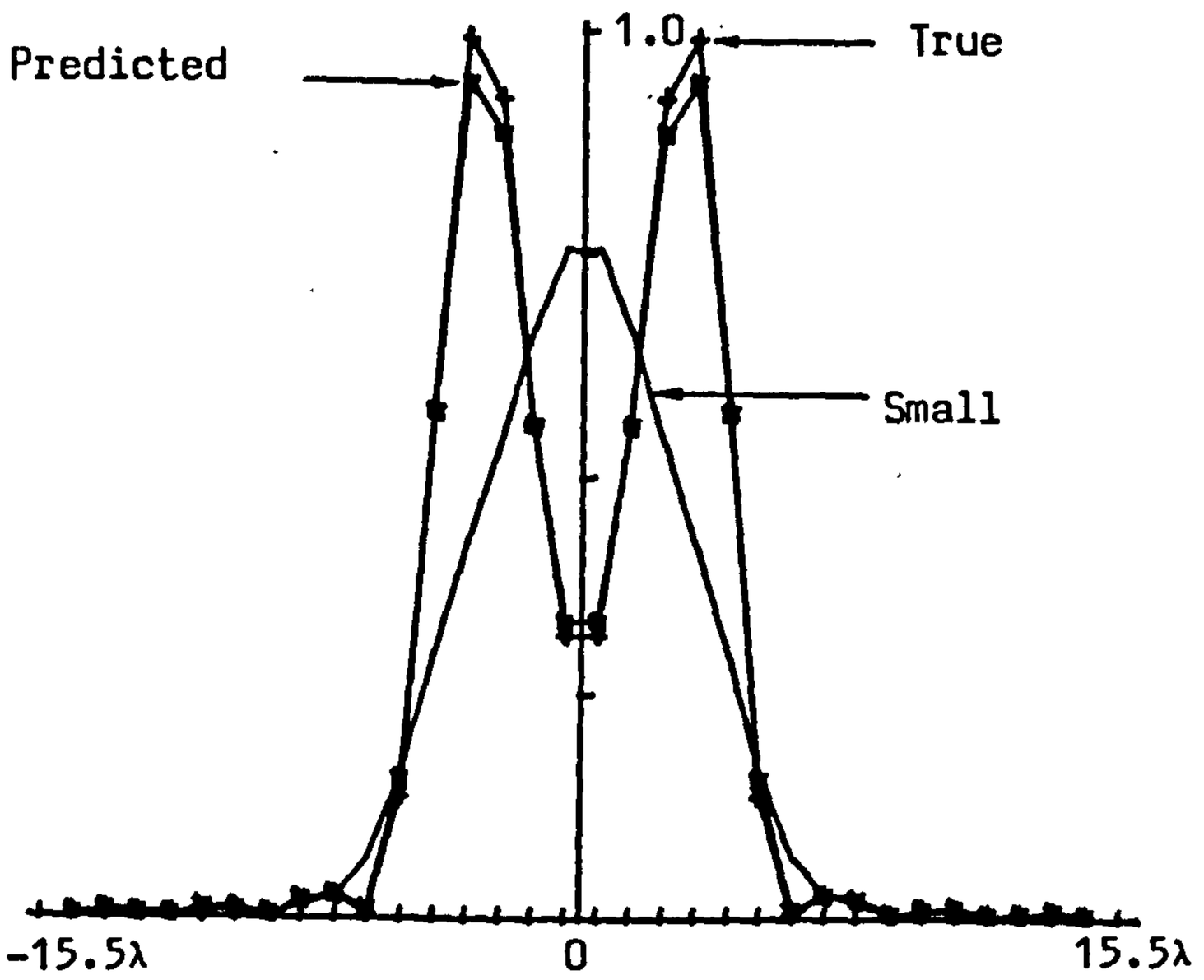


Fig. 4.32: Prediction errors and reconstructed images obtained when using the 5/2 hybrid model to double the size of the hologram of two quasi-continuous segments symmetrically positioned about the hologram axis.

a. Prediction error over the aperture

Hologram:

Δ=1λ
M=8
N=16

Object:

range = 95λ
$d_o$ = 5.6λ
$w_o$ = 4λ
ρ = 25 points/λ

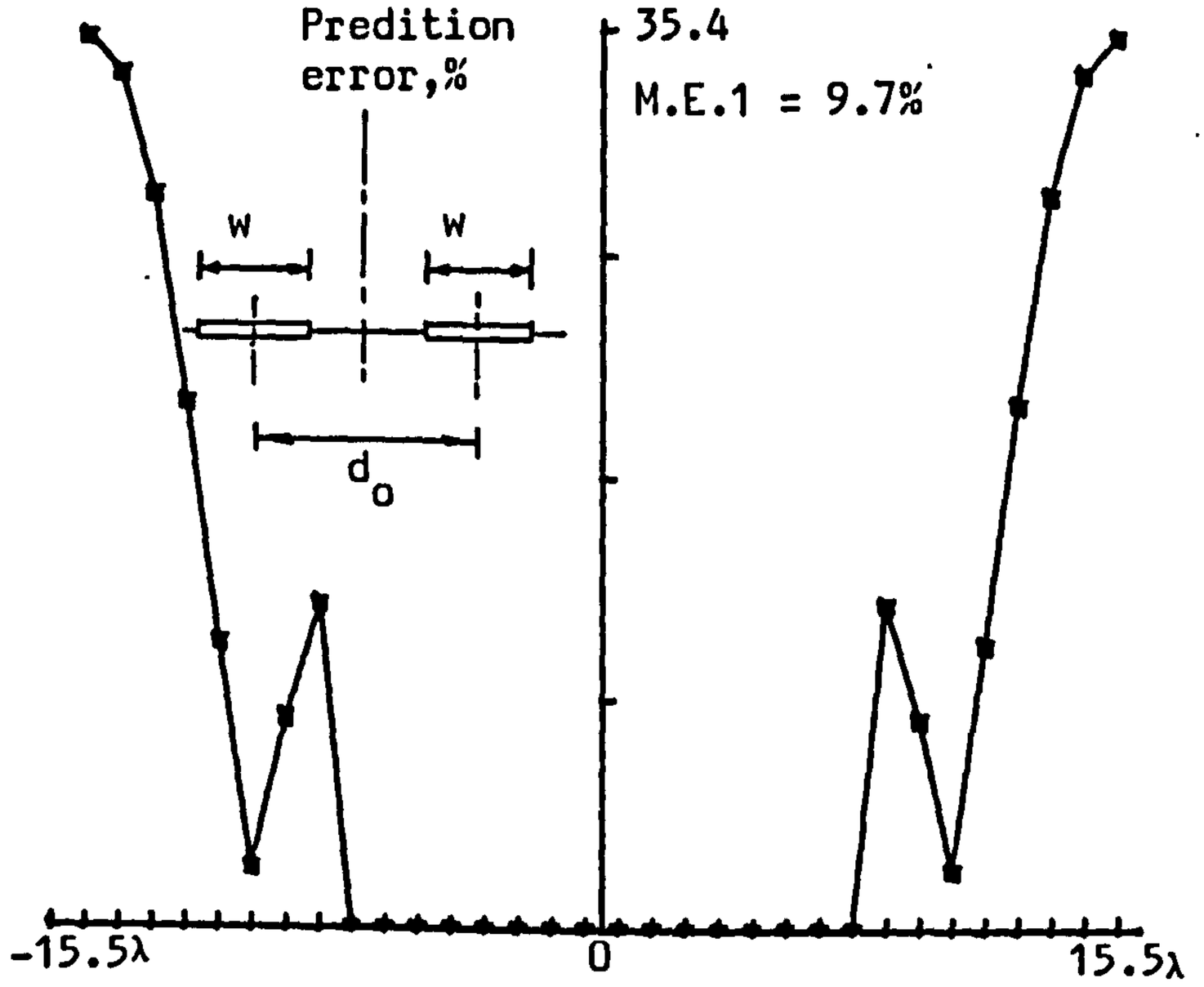


b. Reconstructed images

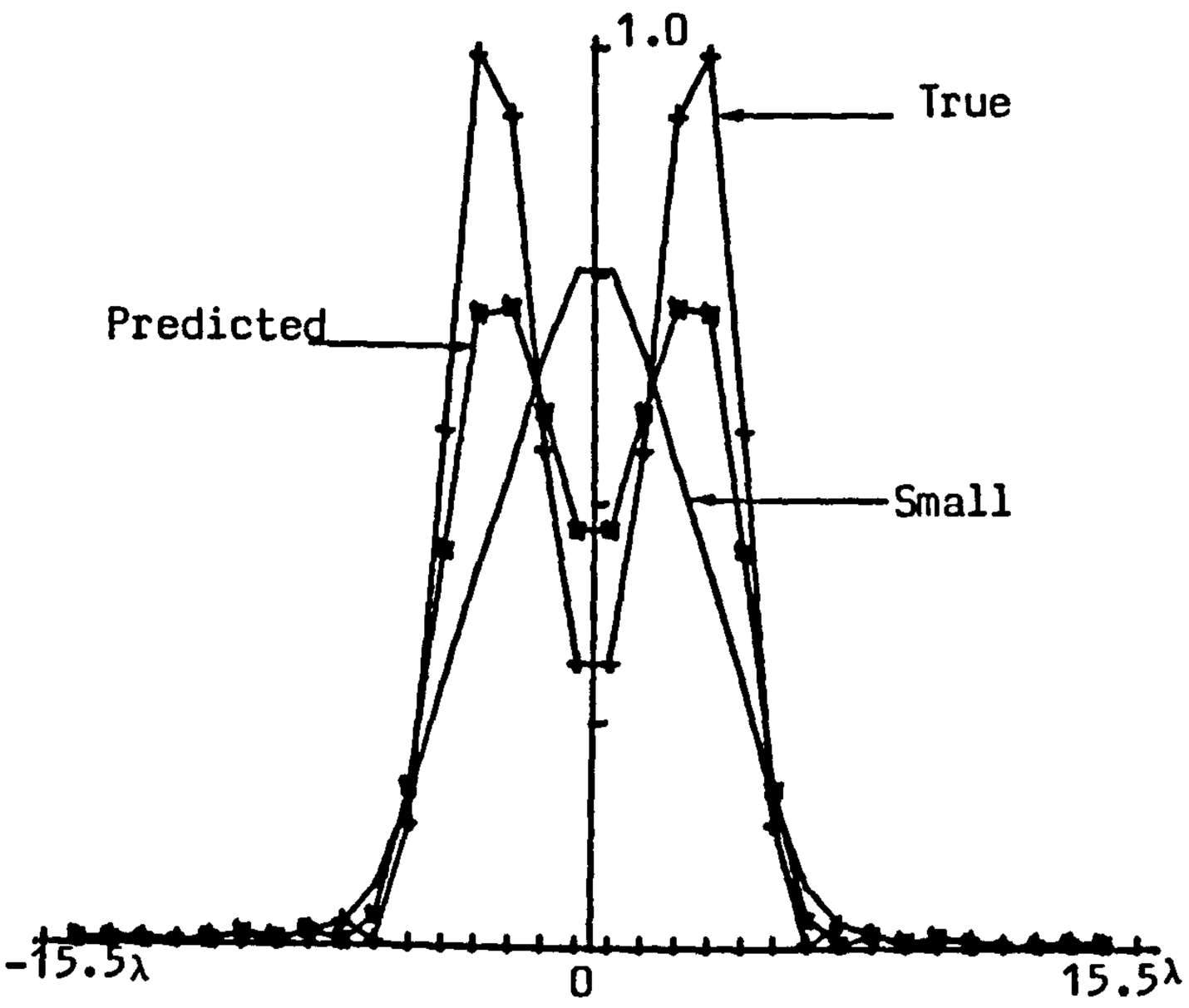


Fig. 4.33 : Prediction errors and reconstructed images obtained when using the linear model to double the size of the hologram of two quasi-continuous segments symmetrically positioned about the hologram axis.

a. Prediction error over the aperture

<u>Hologram</u>:

$\Delta=1\lambda$
M=8
N=16

<u>Object</u>:

range = $95\lambda$
$d_o$ = $5.6\lambda$
$w_o$ = $4\lambda$
$\rho$ = 50points/$\lambda$

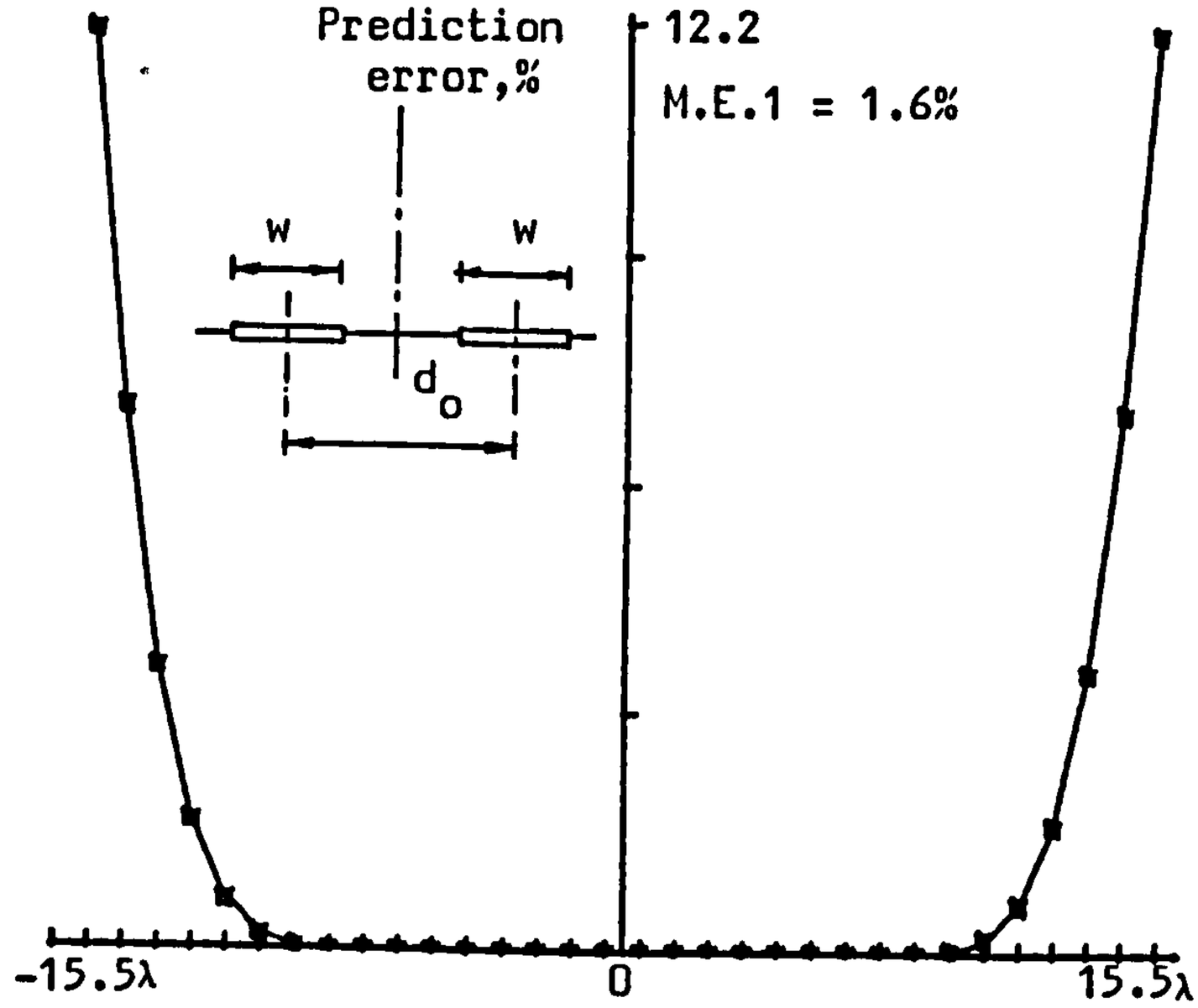


b. Reconstructed images

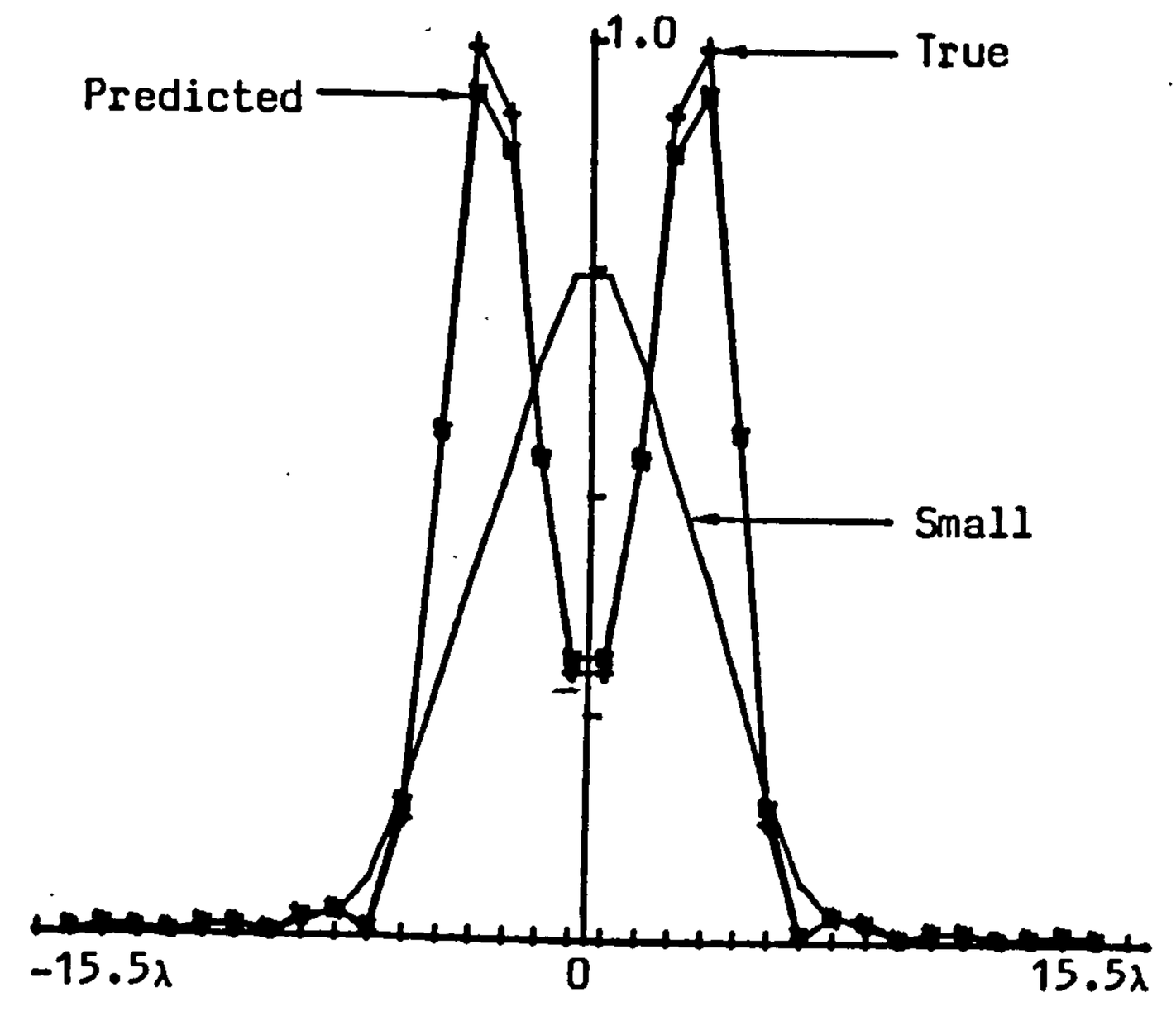


Fig. 4.34 : Prediction errors and reconstructed images obtained when using the 5/2 hybrid model to double the size of the hologram of two quasi-continuous segments symmetrically positioned about the hologram axis.

a. Prediction error over the aperture

<u>Hologram</u>:

$\Delta = 1\lambda$
M=8
N=16

<u>Object</u>:

range = $95\lambda$
$d_o$ = $5.6\lambda$
$w_o$ = $4\lambda$
$\rho$ = 50points/$\lambda$

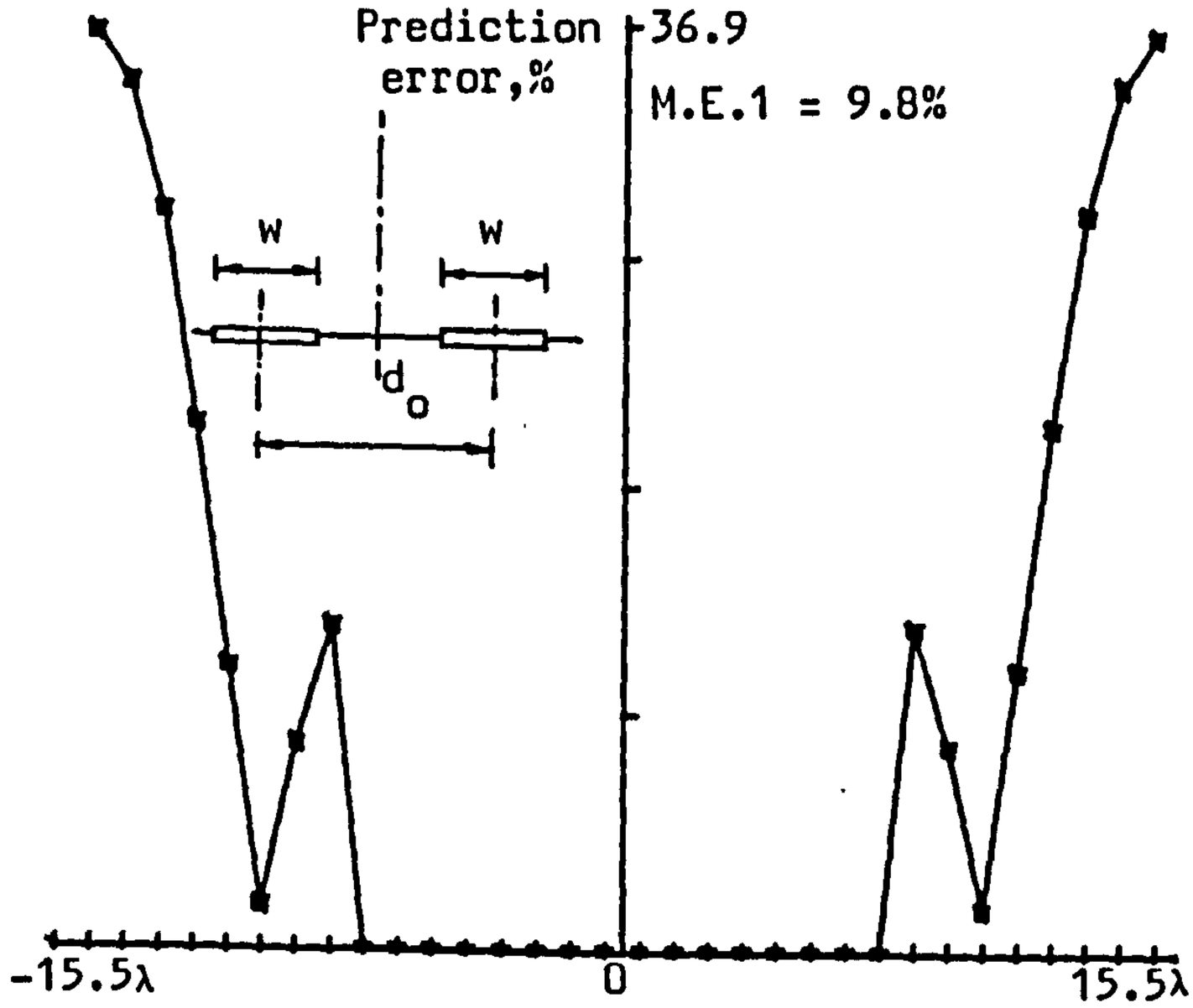


b. Reconstructed images

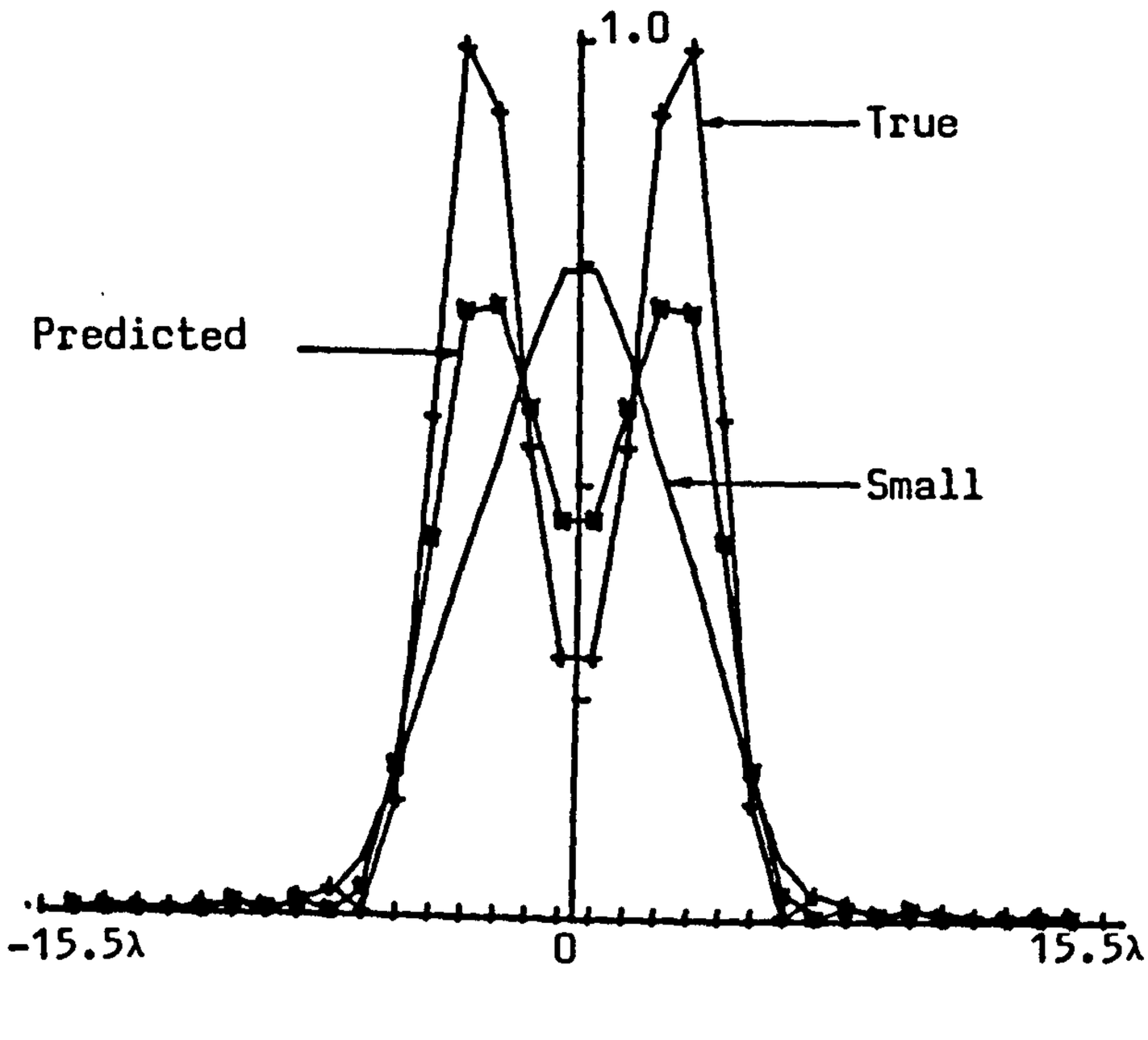


Fig. 4.35 : Prediction errors and reconstructed images obtained when using the linear model to double the size of the hologram of two quasi-continuous segments symmetrically positioned about the hologram axis.

# Figures for Chapter 5

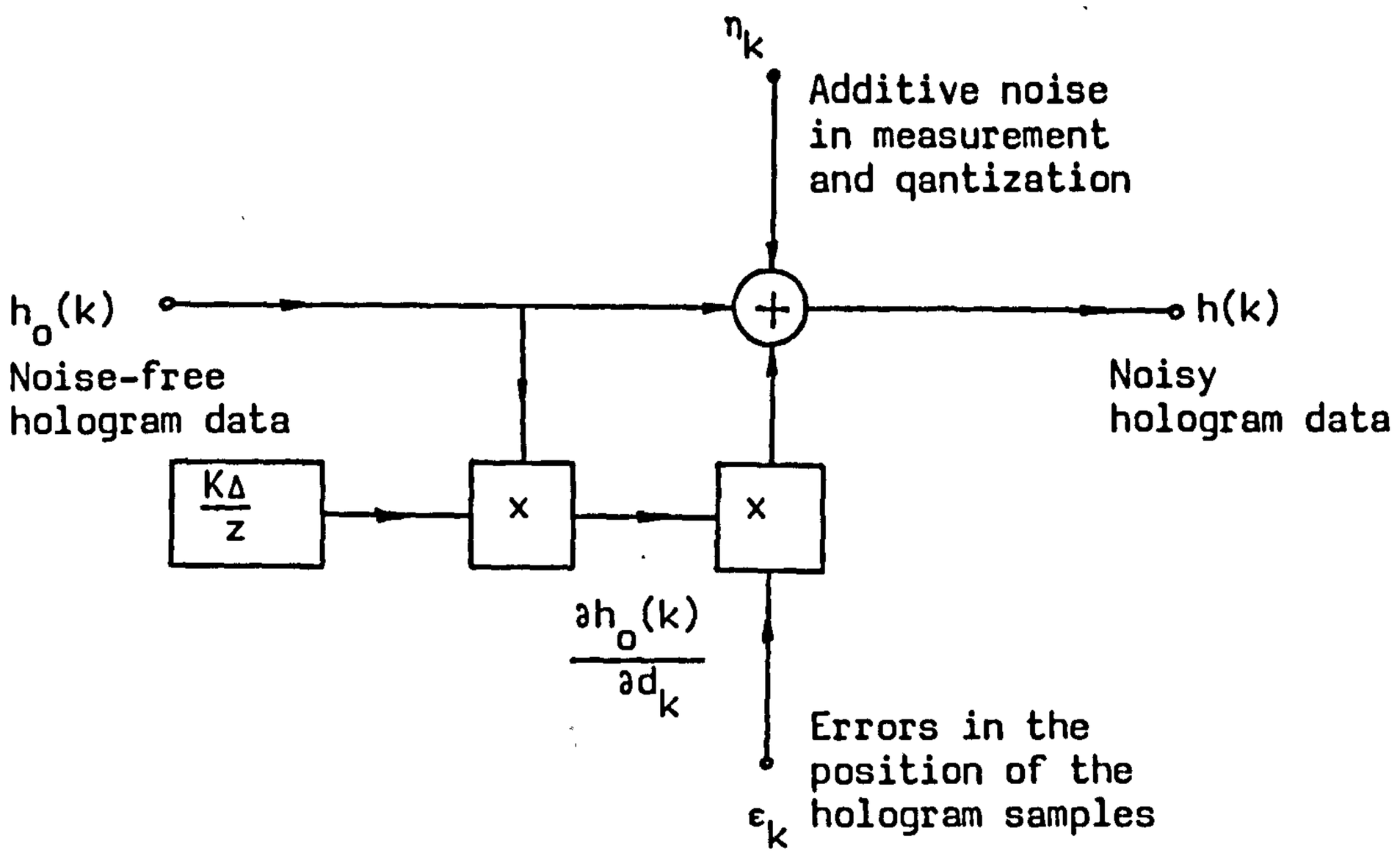


Fig. 5.1 : A model representing the effects of additive noise and distance errors

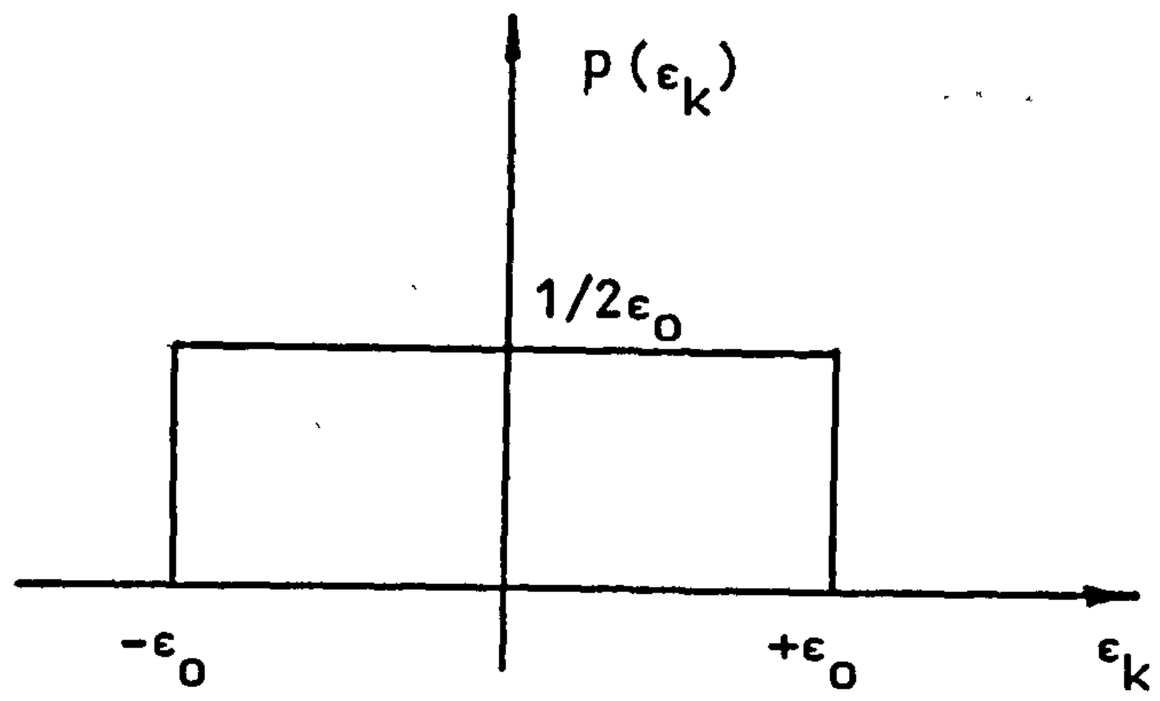


Fig. 5.2 : Probability distribution of the distance error $\epsilon_k$

a. Effect on the prediction error without noise

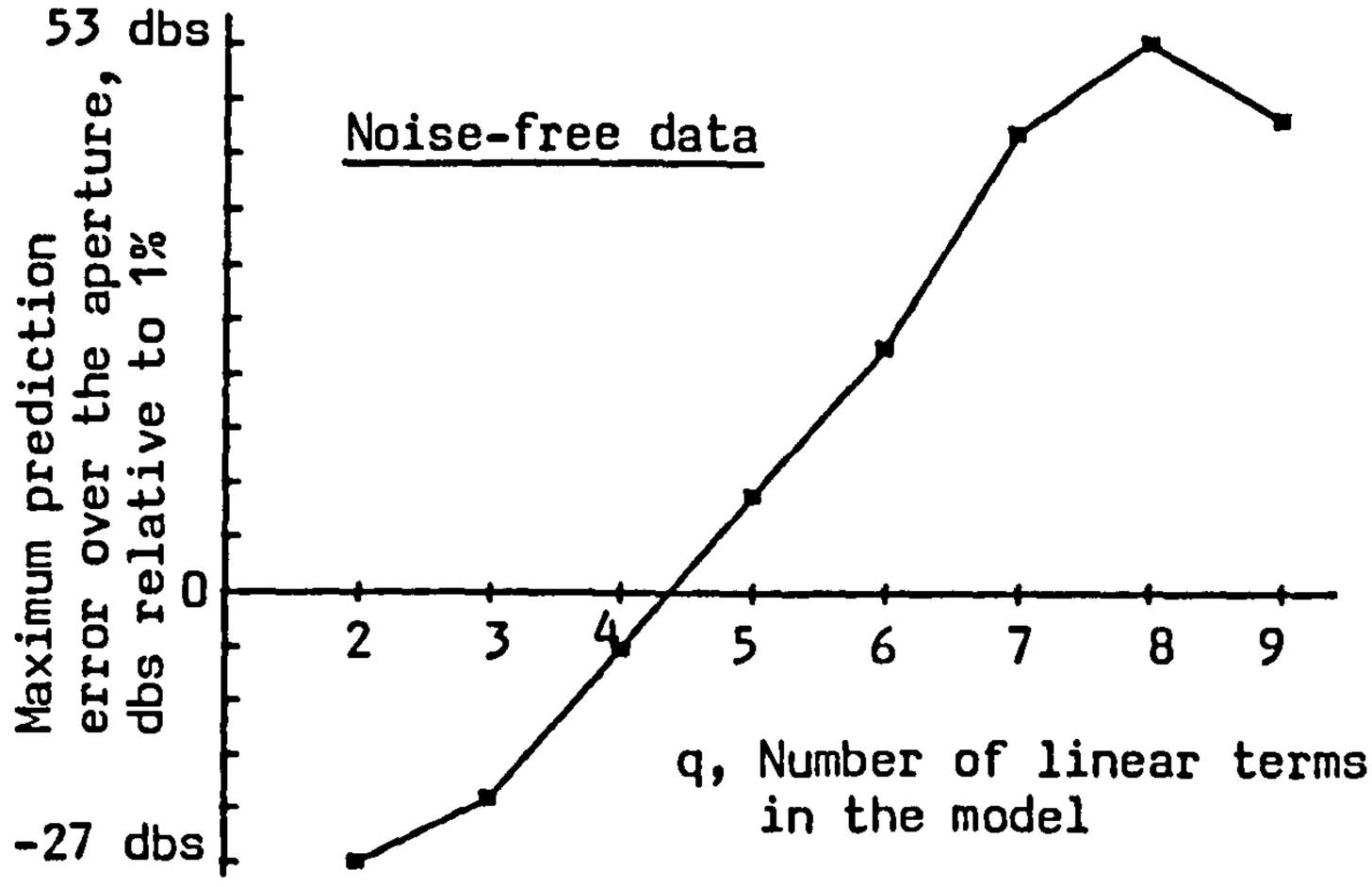


b. Effect on the prediction error with noise

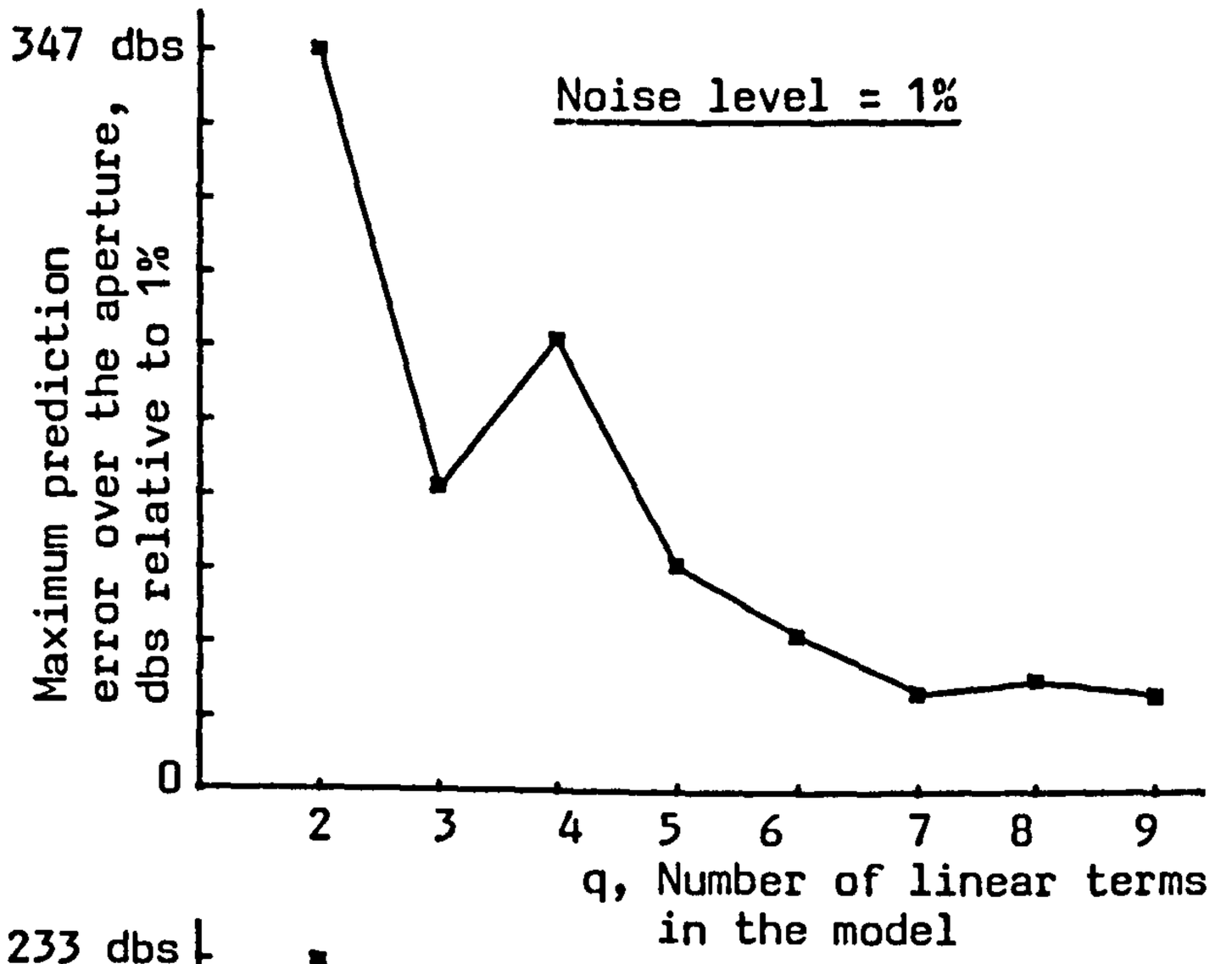


c. Effect on the norm of the inverse matrix

Hologram:

$\Delta=1\lambda, M=10, N=20$

Object:

$x_o=0,\ z=100\lambda$

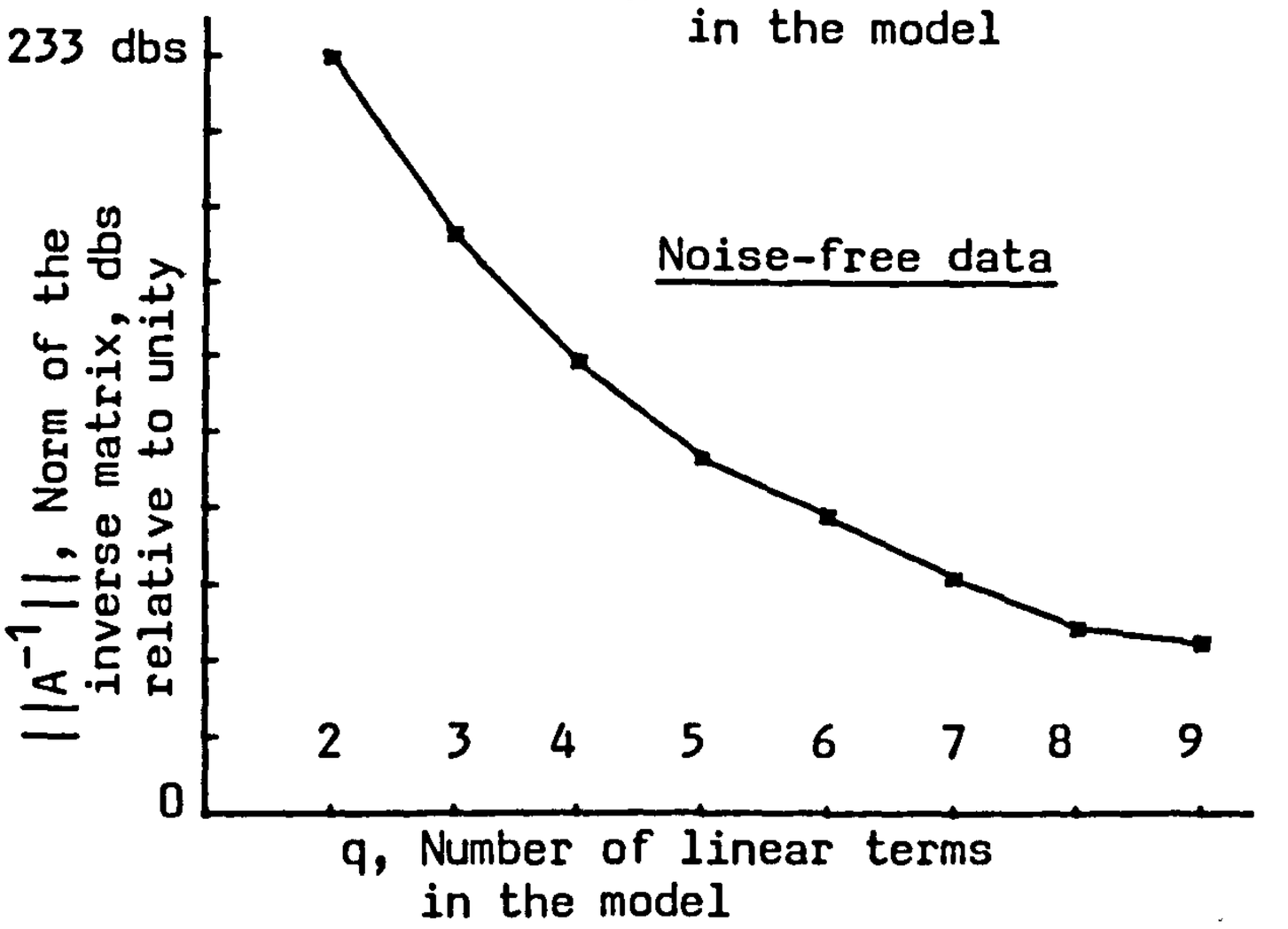


Fig. 5.3 : Effect of the composition of the hybrid predictive model on the performance of the model with and without noise.

a. Square model: Effect of sample spacing

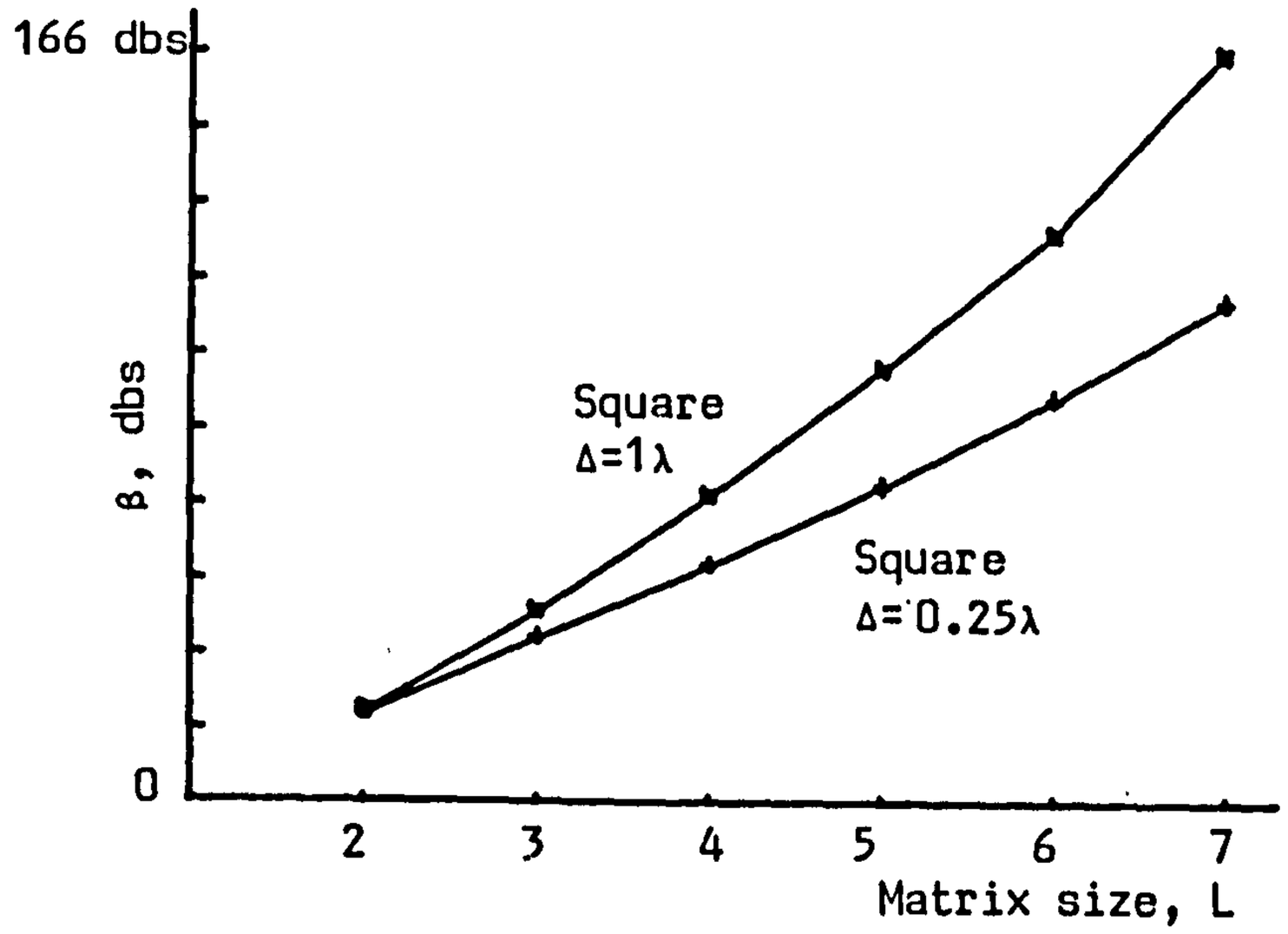


b. Comparison between the performance of the square and triangular models for the same sample spacing

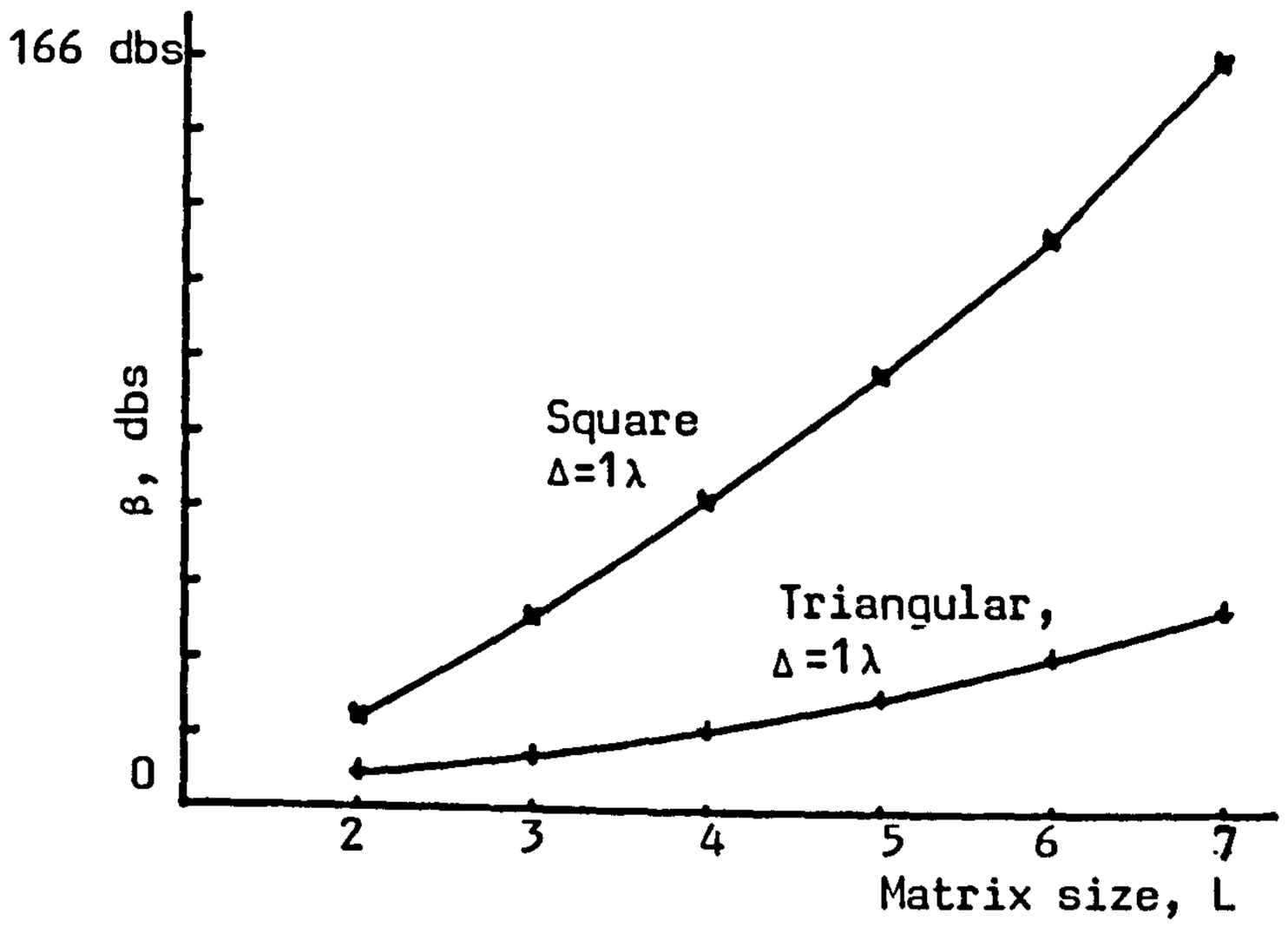


c. Triangular model: Effect of sample spacing

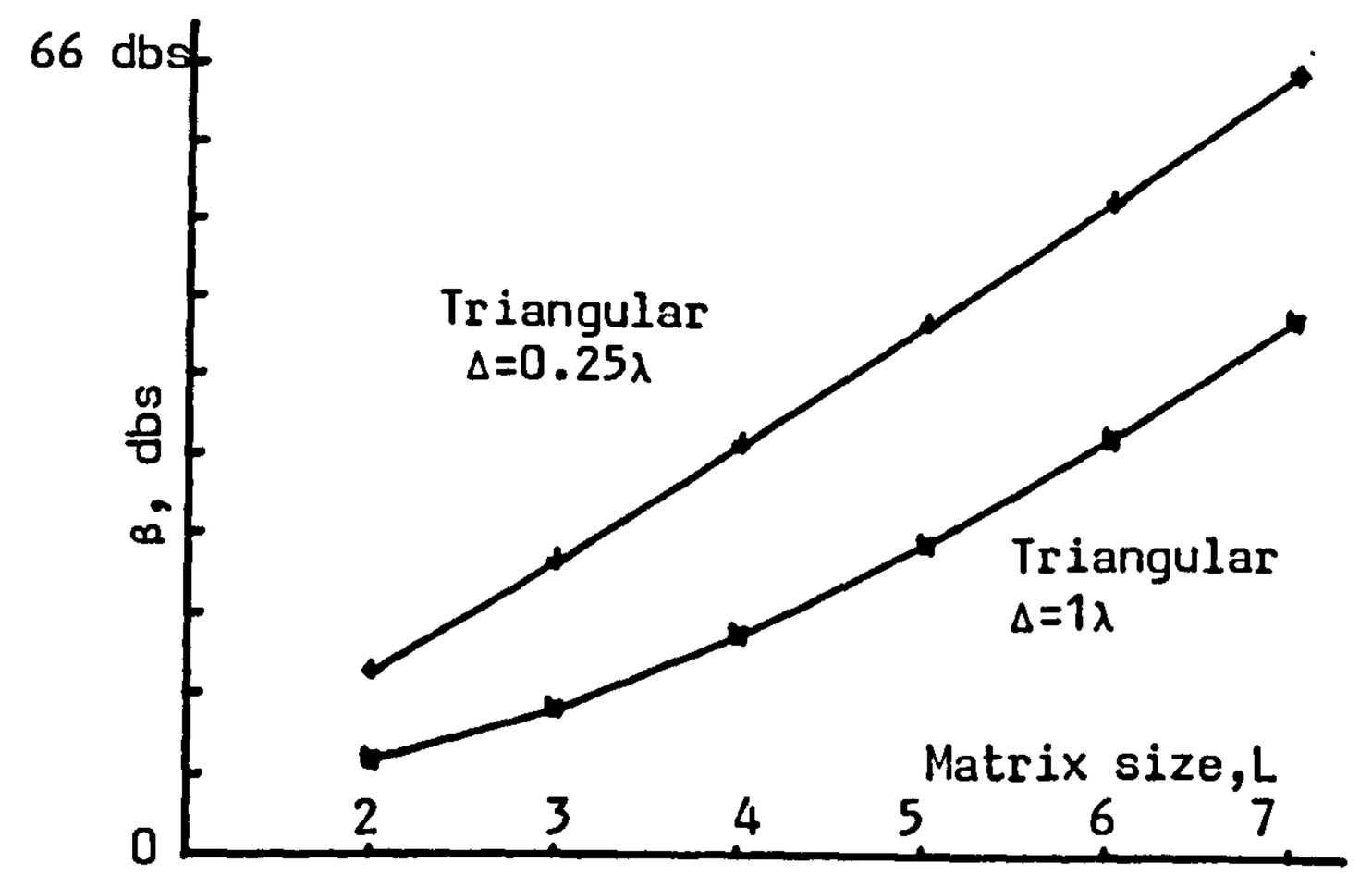


Fig. 5.4 : Effect of the matrix size on the error magnifying parameter β for the square and triangular polynomial models for various values of the sample spacing Δ, cf. eqn. (5.62).

a. Square model: Effect of sample spacing

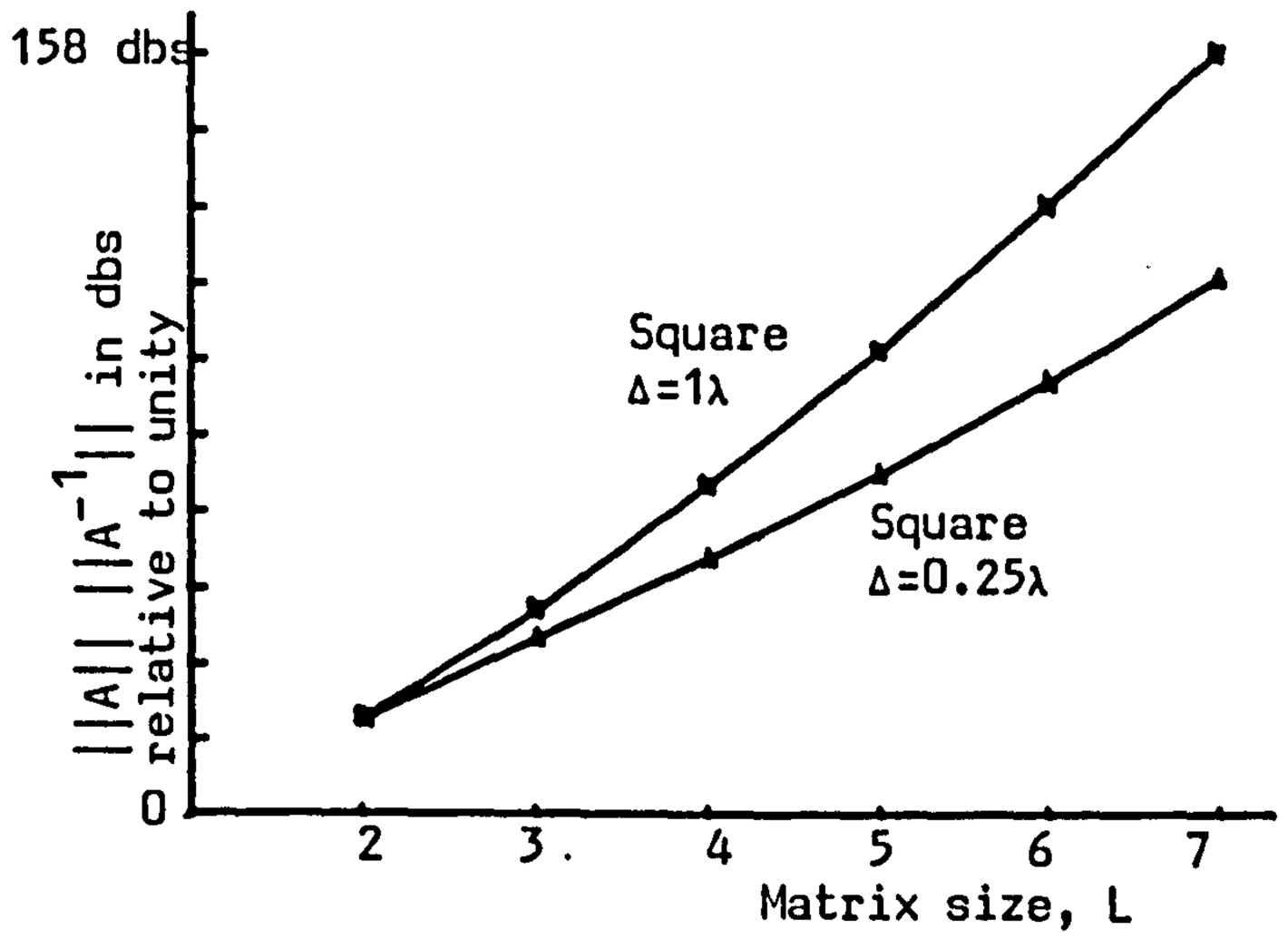


b. Comparison between the performance of the square and triangular models for the same sample spacing

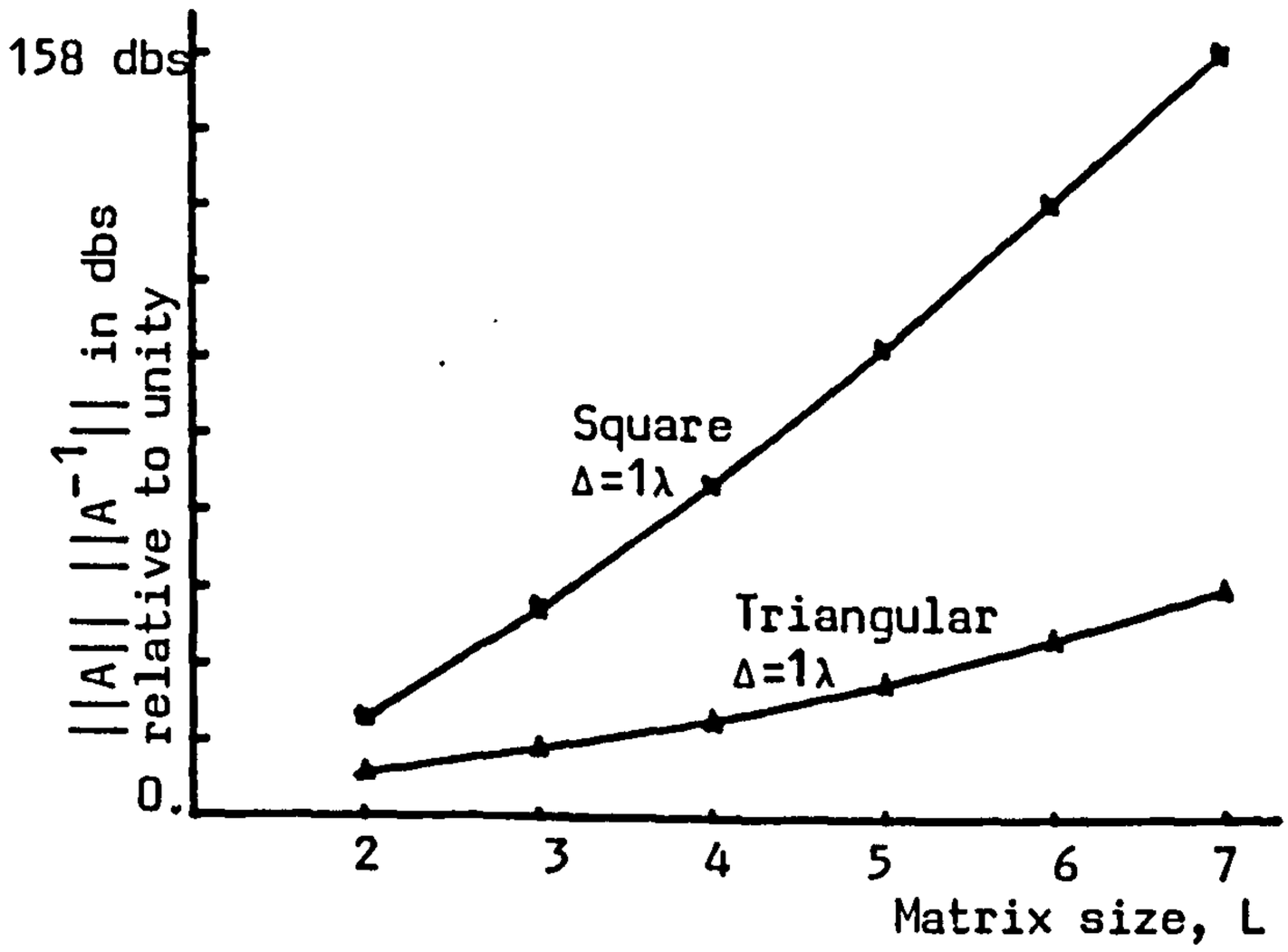


c. Triangular model: Effect of sample spacing

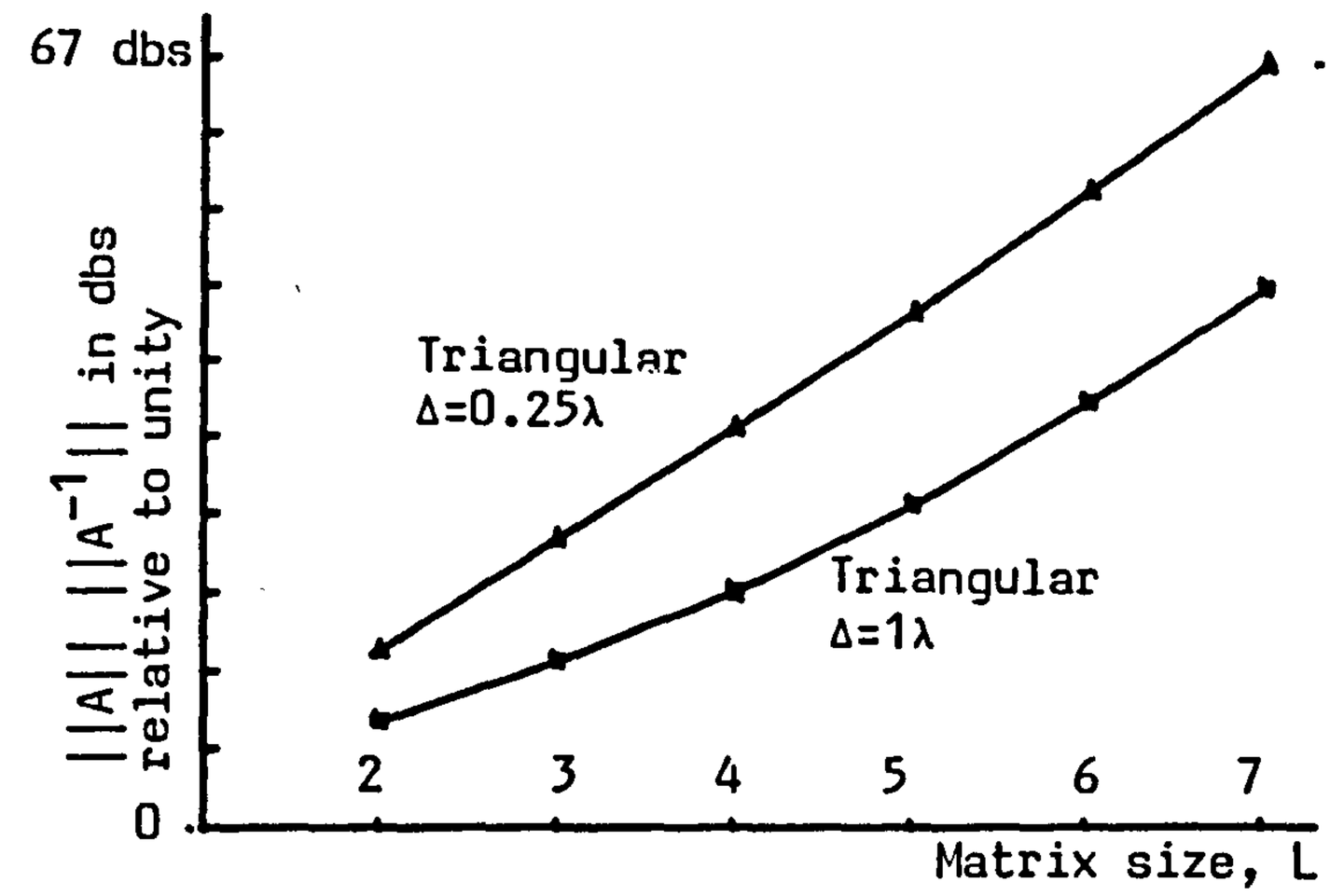


Fig. 5.5 : Effect of the matrix size on the norm product $||A||\ ||A^{-1}||$ for the square and triangular polynomial models for various values of the sample spacing Δ.

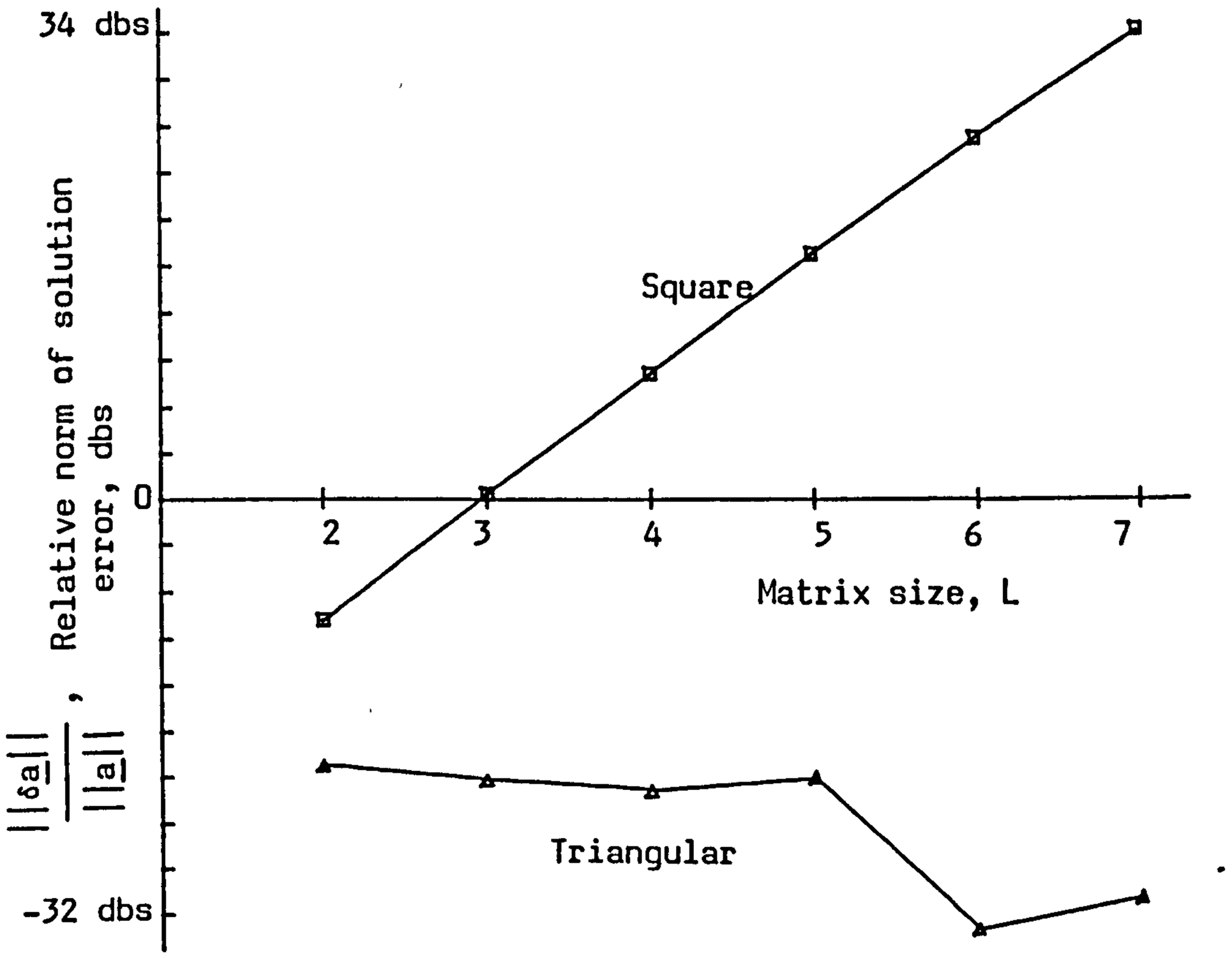


Hologram: $\Delta=1\lambda$, $M=L+1$, $N=2M$

Object: 1-point; $x_o=0$, $z=100\lambda$

Fig. 5.6 : Effect of matrix size on the relative norm of the solution error for both the square and the triangular polynomial predictive models. Noise level : 10%

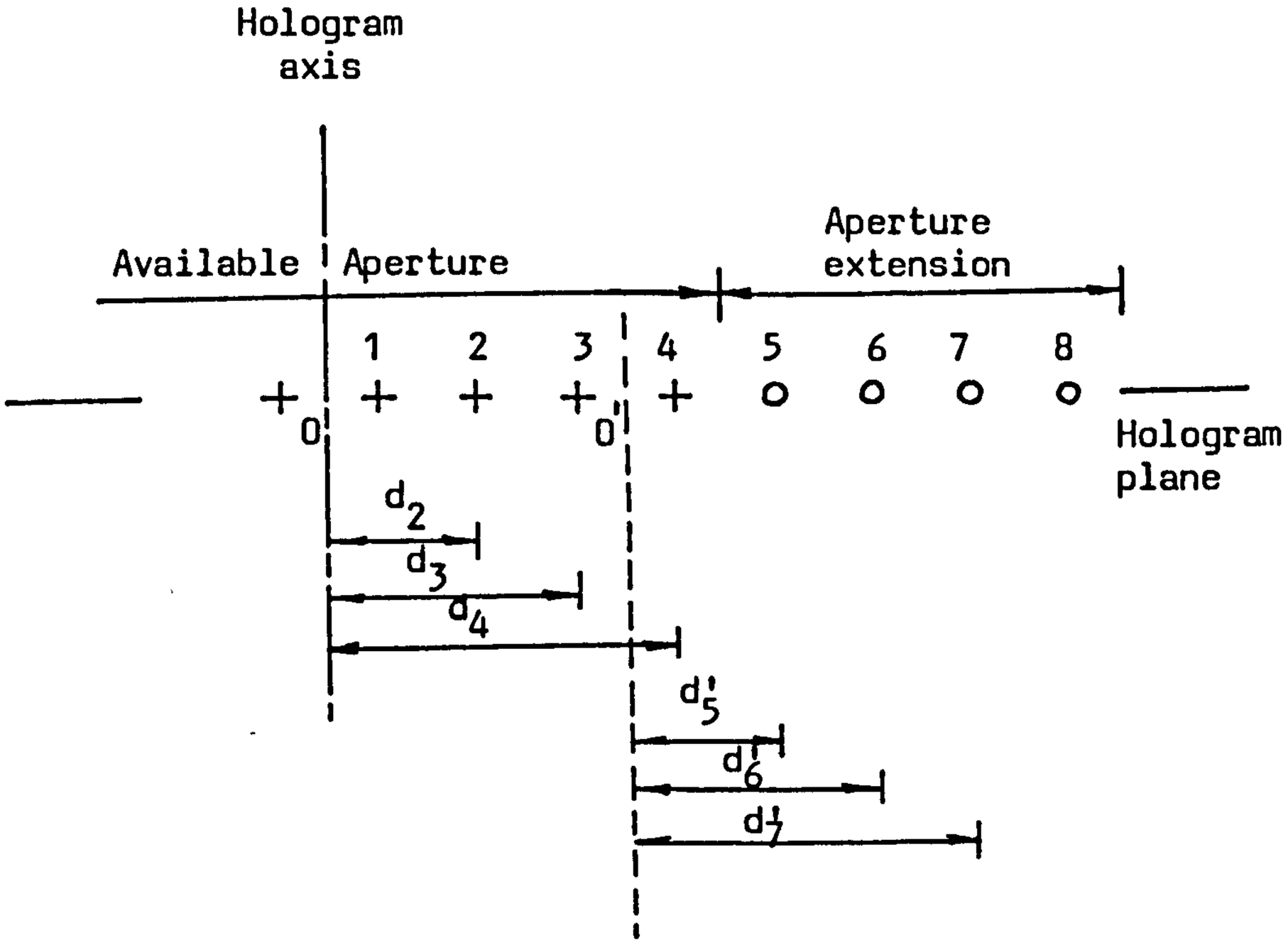


Fig. 5.7 : Geometry for constructing and using the triangular predictive model

a. Noise-free hologram data

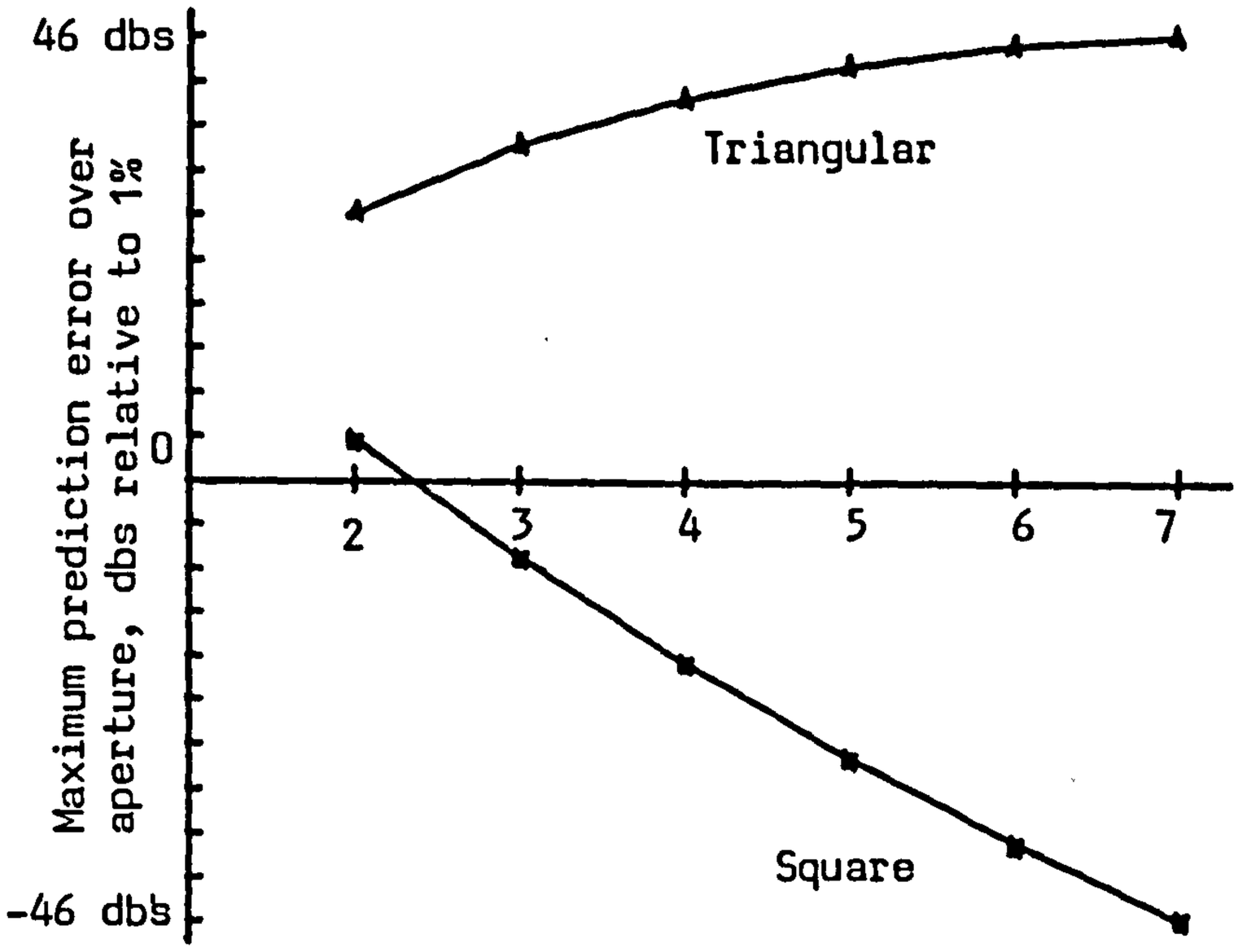


b. Noisy hologram data
Noise level= 10%

Hologram:

$\Delta=1\lambda$
M=L+1
N=2M

Object:

1-point;
$x_o=0$
$z^o= 100\lambda$

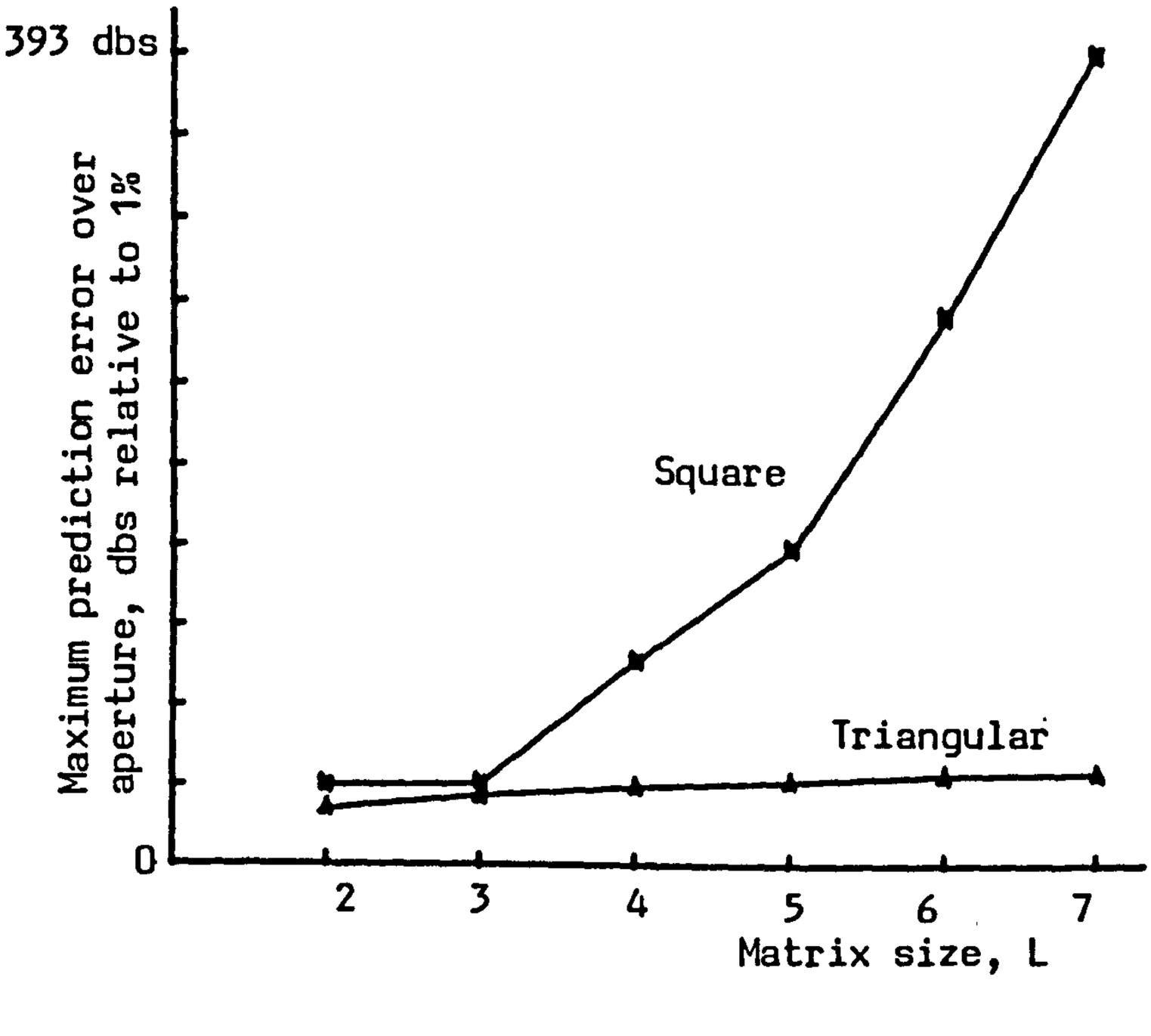


Fig. 5.8 : Effect of matrix size on the prediction accuracy of both the square and triangular polynomial predictive models for noise-free and noisy hologram data.

a. Effect on the norm of the solution error

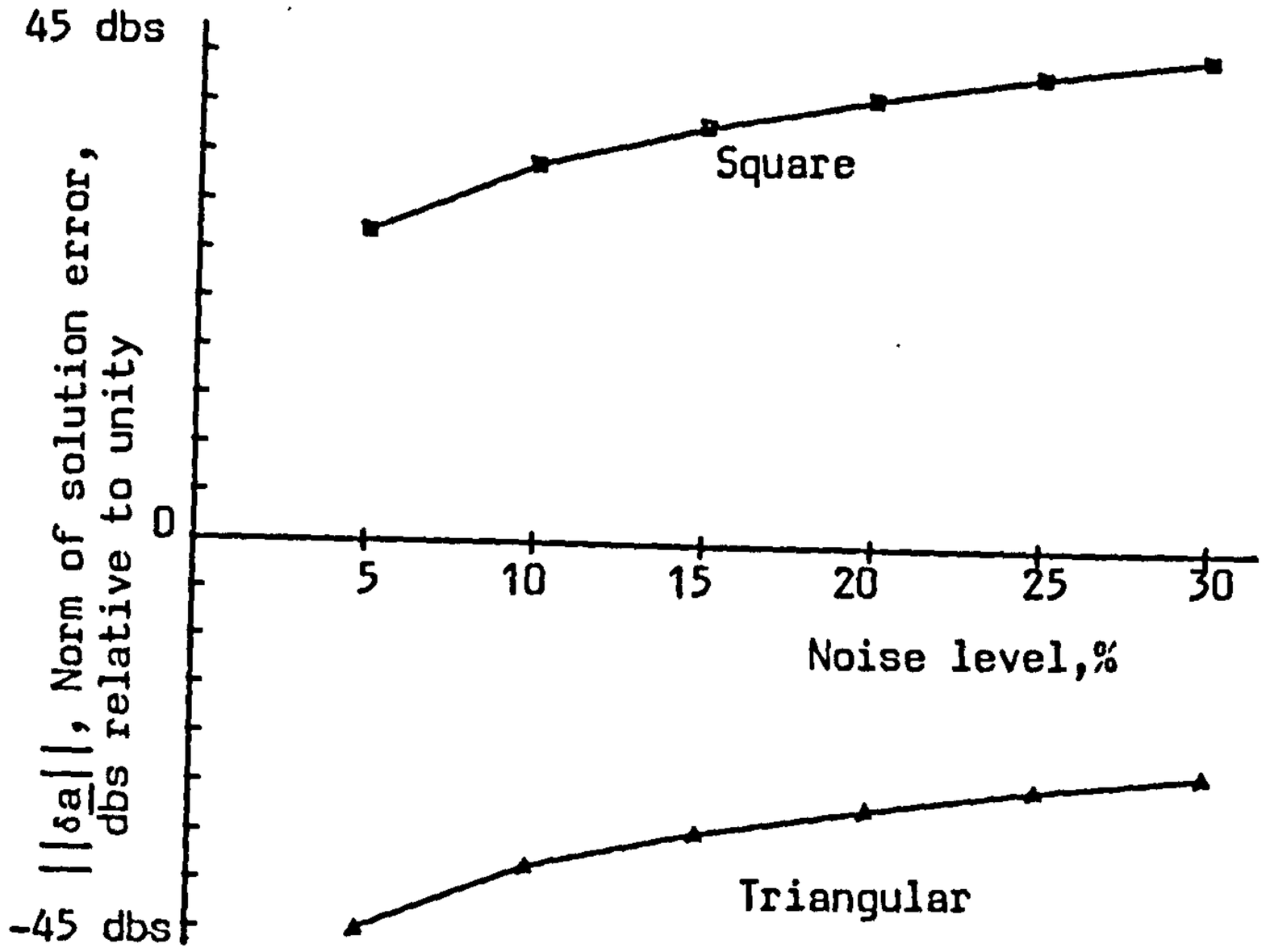


b. Effect on the prediction error

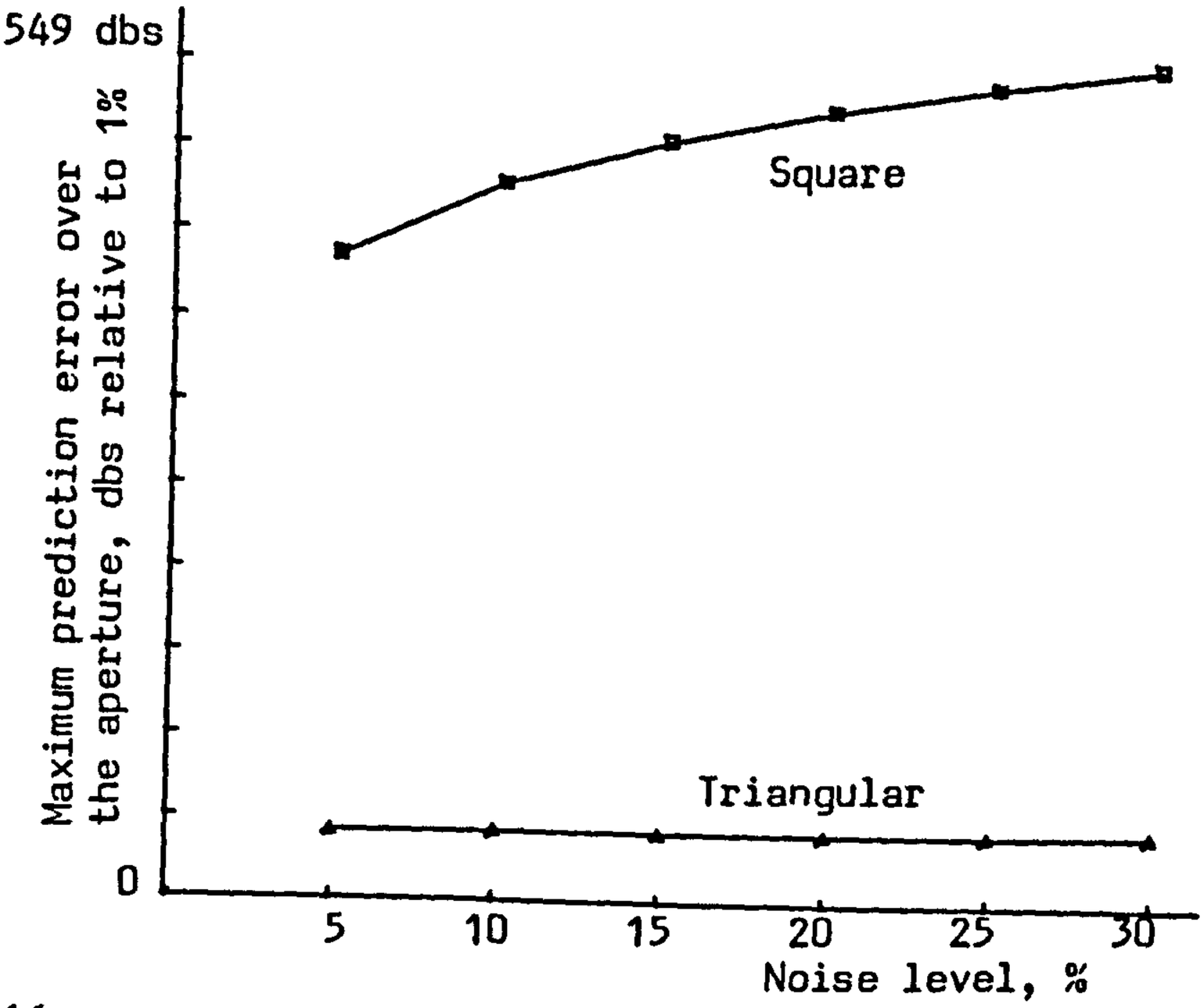


Hologram: Δ=1,M=8,N=16

Fig. 5.9 : Effect of the noise level on the performance of the square and the triangular polynomial predictive models.

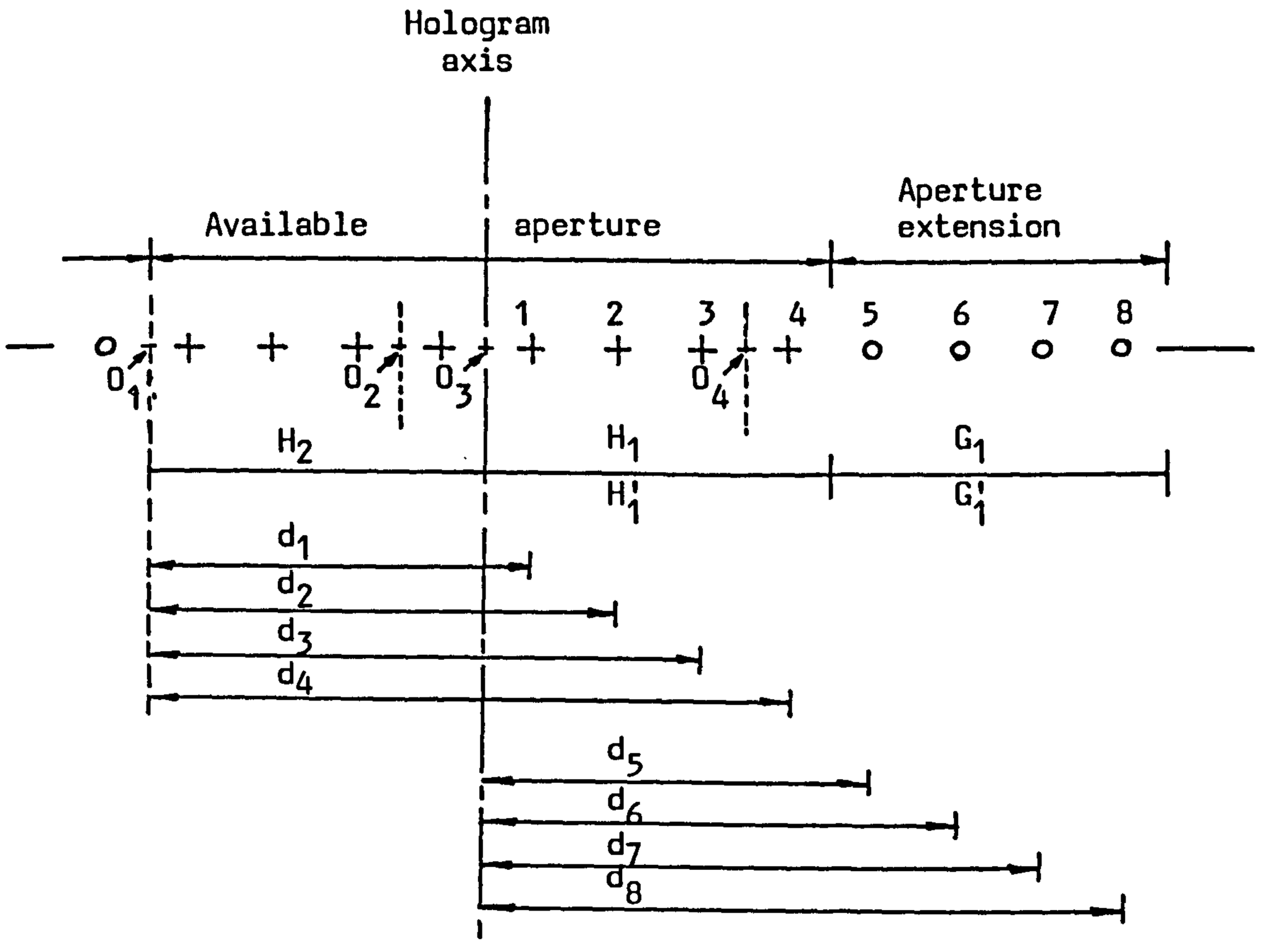


Fig. 5.10 : Geometry for constructing and using the triangular corrective model

a. Noiseless data

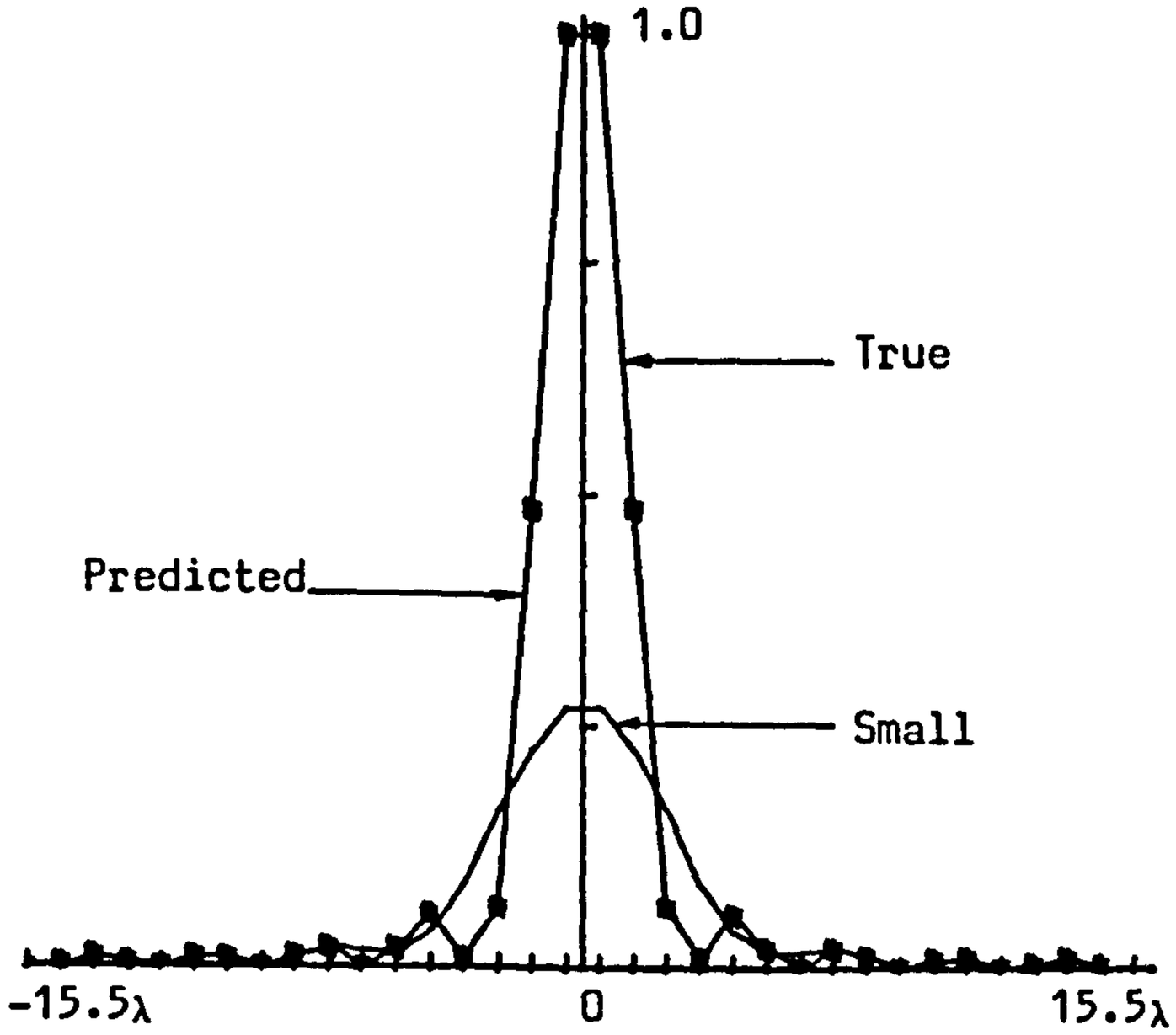


b. Noise level:
0.1%

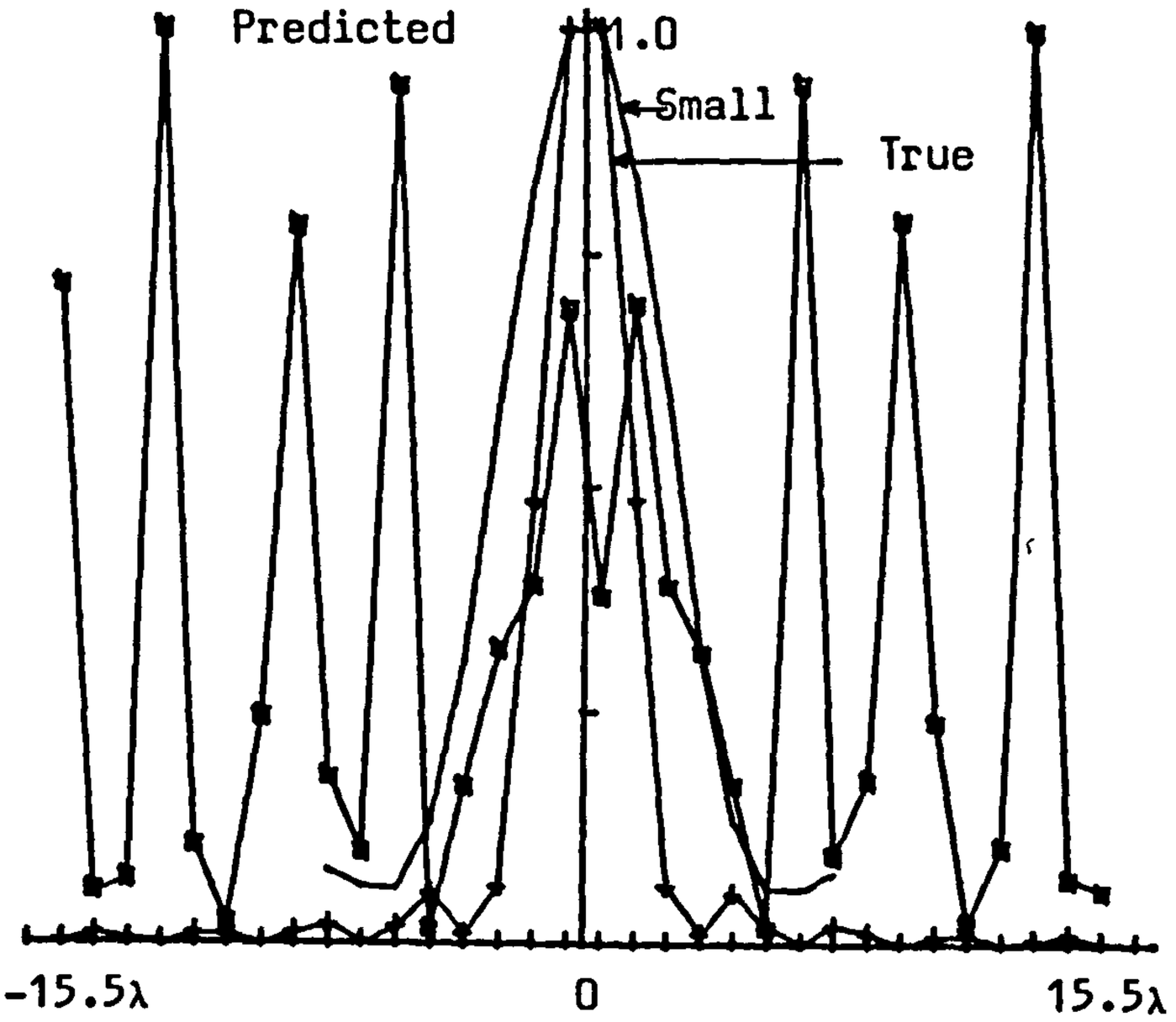


Hologram: Δ=1, M=8, N=16

Object: $x_o$=0, z=100λ

Fig. 5.11 : Effect of noise of 0.1% relative amplitude in the hologram signal on the reconstructed images obtained using the square polynomial predictive model.

a. Prediction errors over the aperture

Hologram:

Δ=1λ
M=8
N=16

Object:

$x_o$=0
$z^o$=100λ

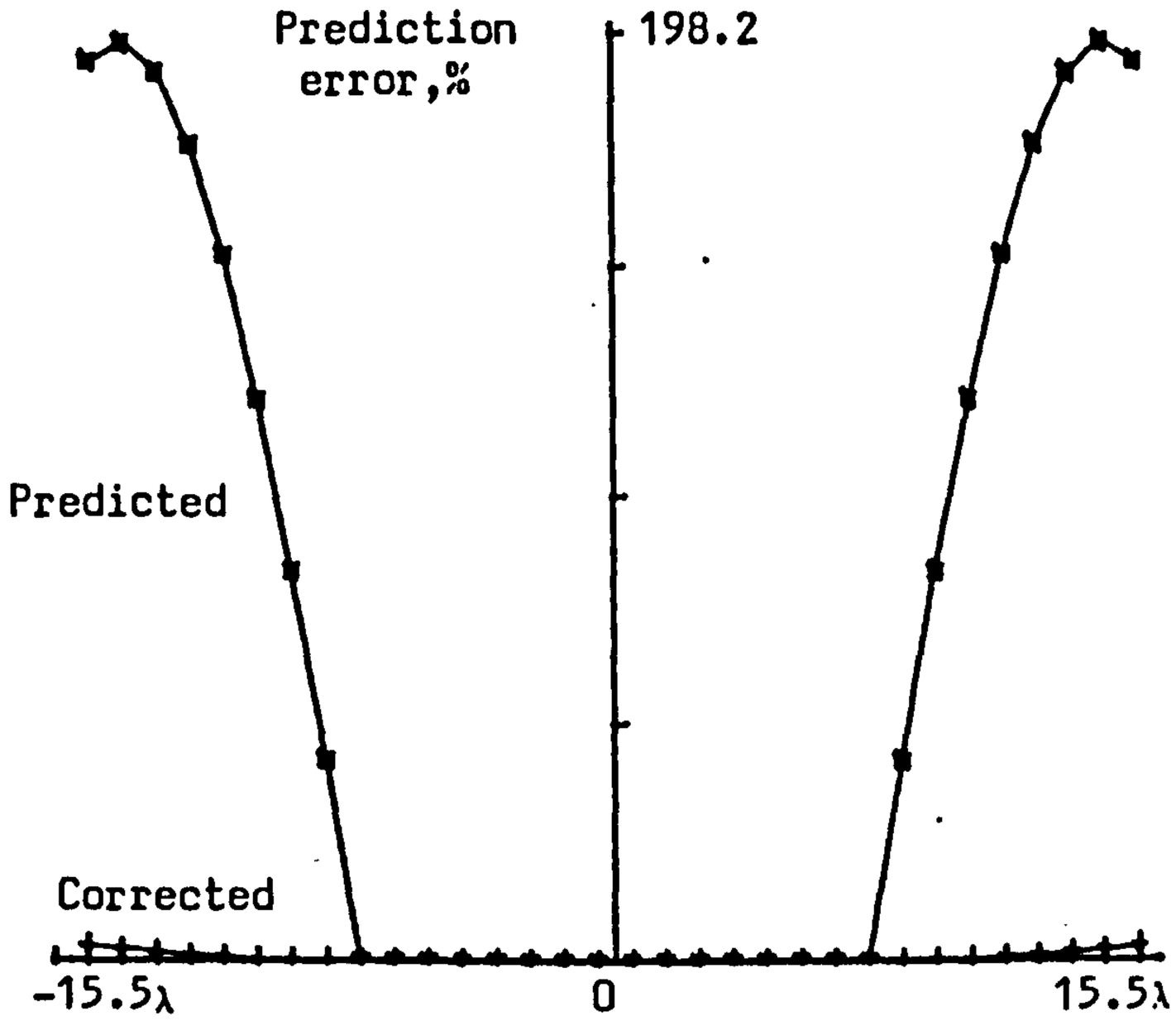


b. Reconstructed images from the small, true, predicted, and corrected holograms.

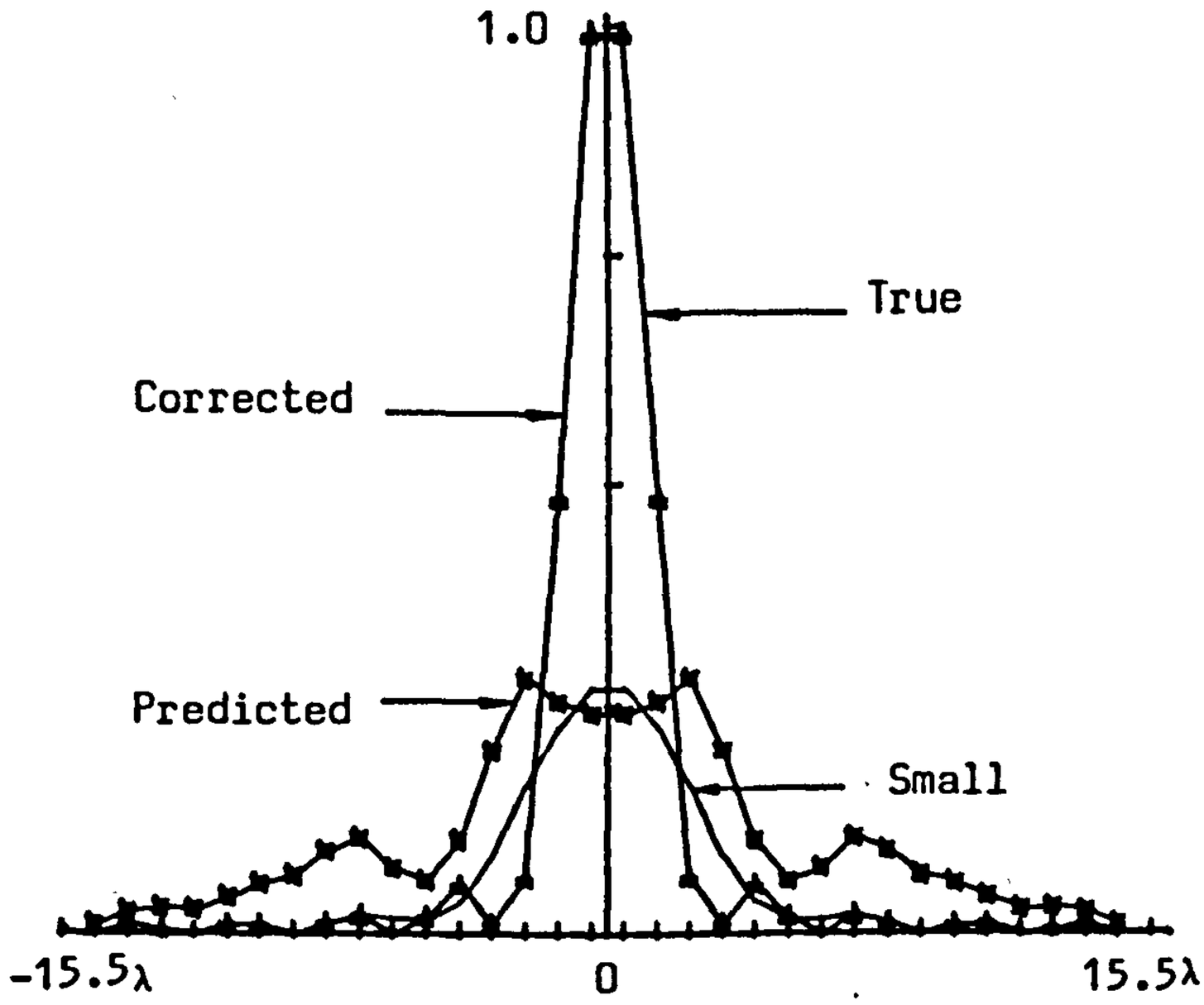


Fig. 5.12 : Prediction errors and reconstructed images obtained when using triangular predictive and corrective models to double the aperture size to image a 1-point object with noiseless data.

a. Prediction errors over the aperture

Hologram:

Δ=1
M=8
N=16

Object:

$x_o$=0
z =100λ

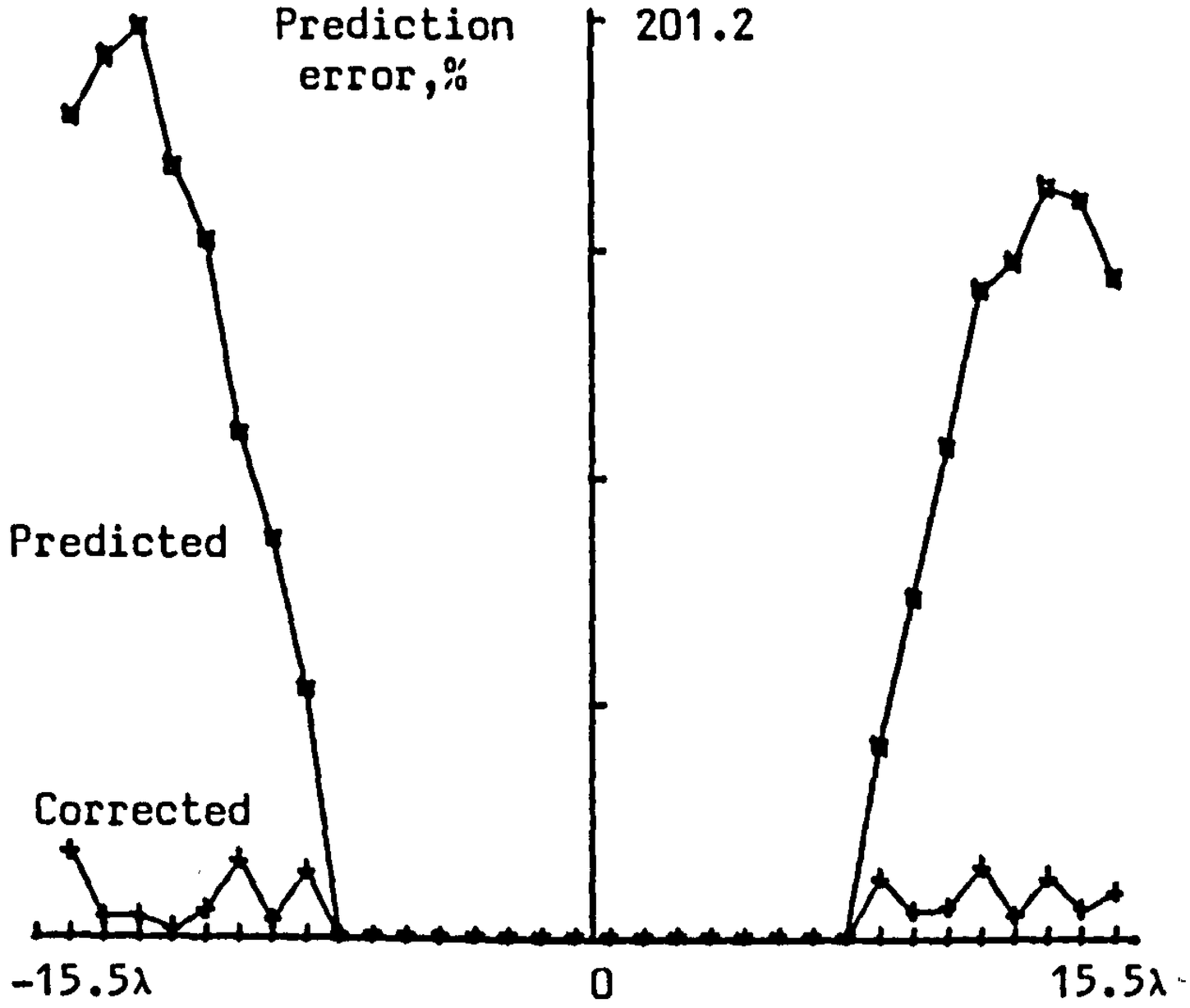


b. Reconstructed images

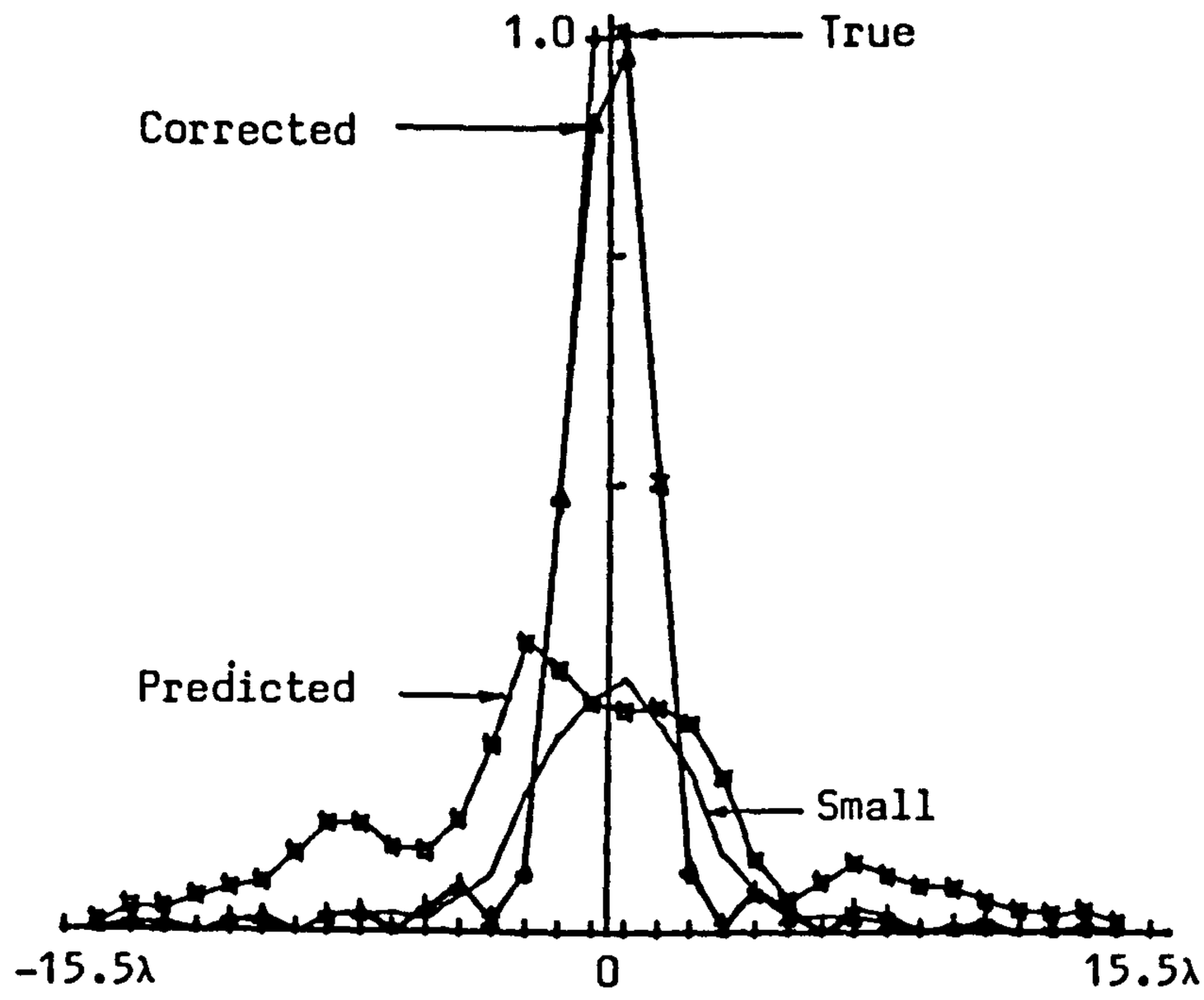


Fig. 5.13 : Effect of noise of 10% relative amplitude in the hologram signal on the prediction errors and reconstructed images obtained when the hologram of a 1-point object is doubled in size using polynomial predictive and corrective models of the triangular type.

a. Reconstructed images,

noise level = 20%

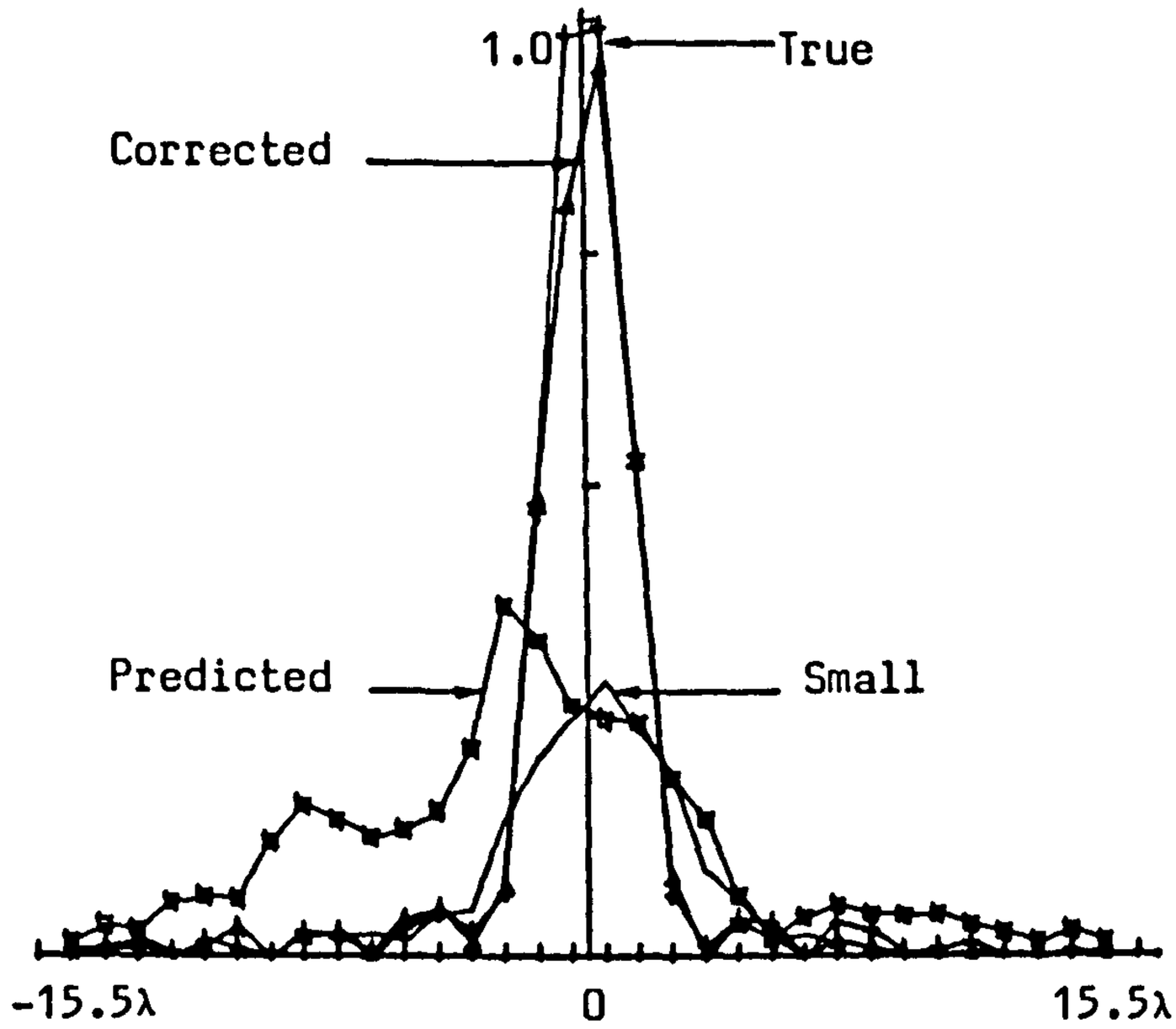


b. Reconstructed images,

noise level = 30%

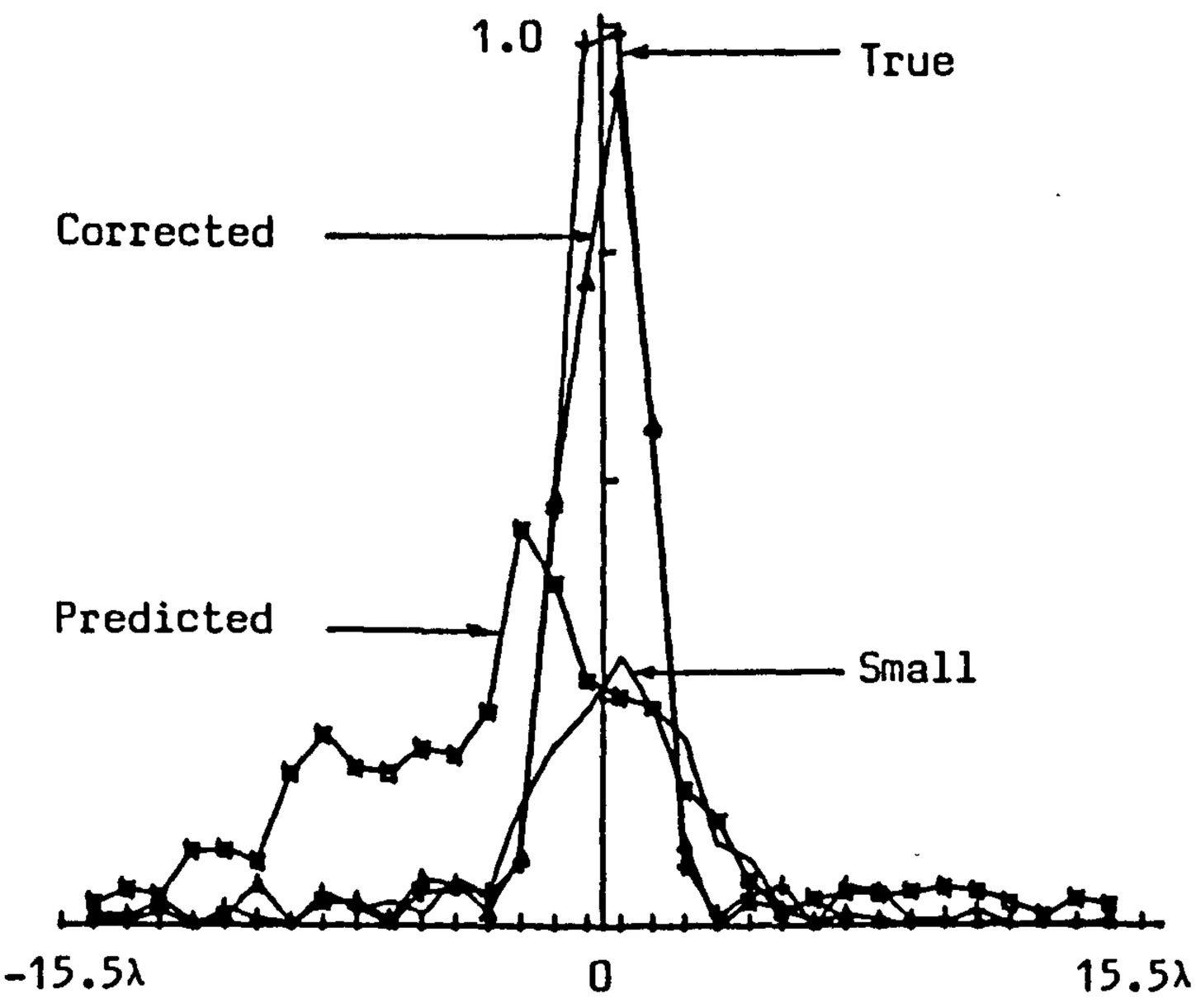


Hologram: Δ=1λ, M=8, N=16

Object: $x_o$=0, z=100λ

Fig. 5.14 : Effect of increasing the noise level on the reconstructed images of a 1-point object. Predictive and corrective models : Triangular polynomial type.

a. Reconstructed images,

noise level = 20%

Noise values:

set 1

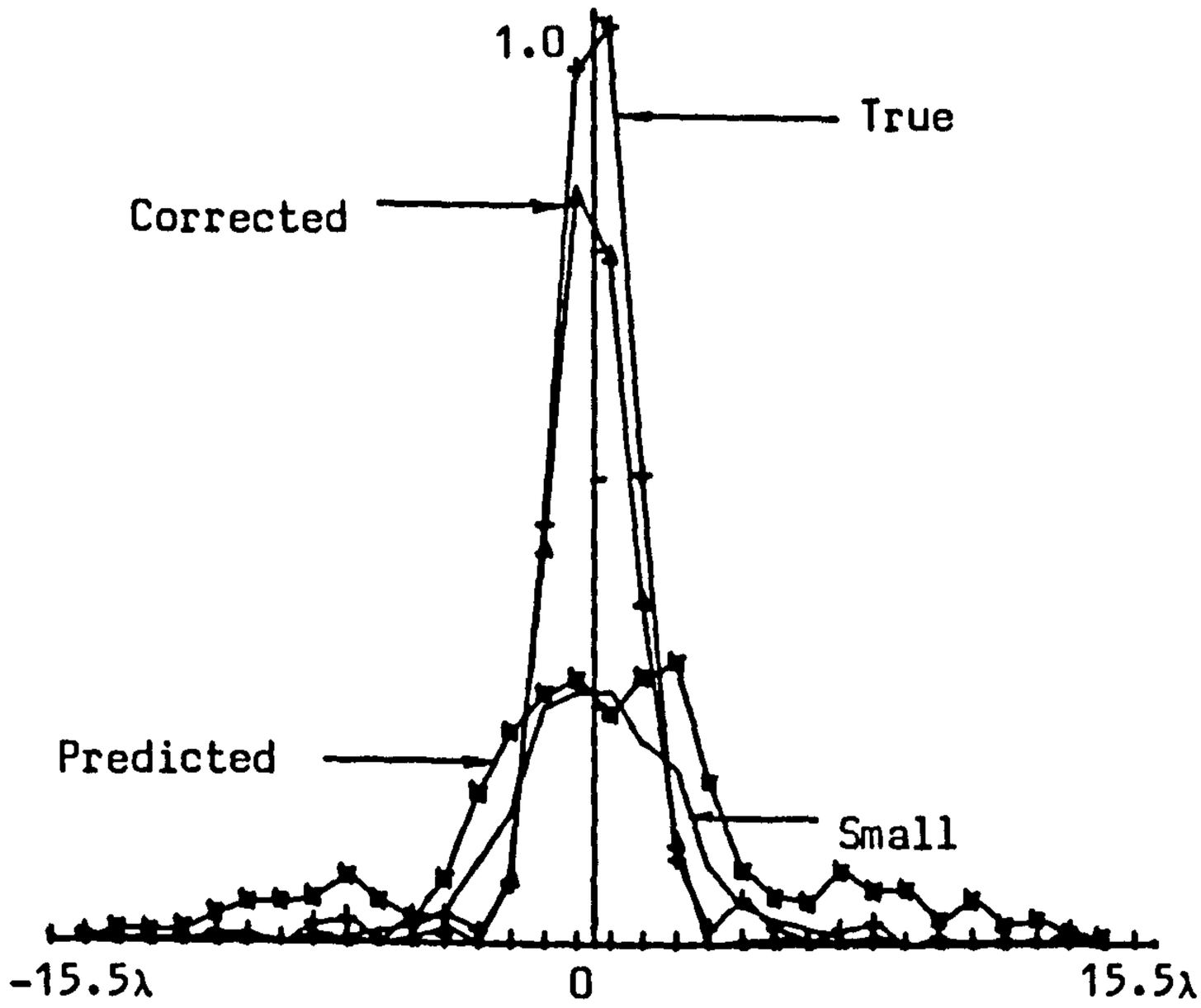


b. Reconstructed images

noise level = 20%

Noise values:

set 2

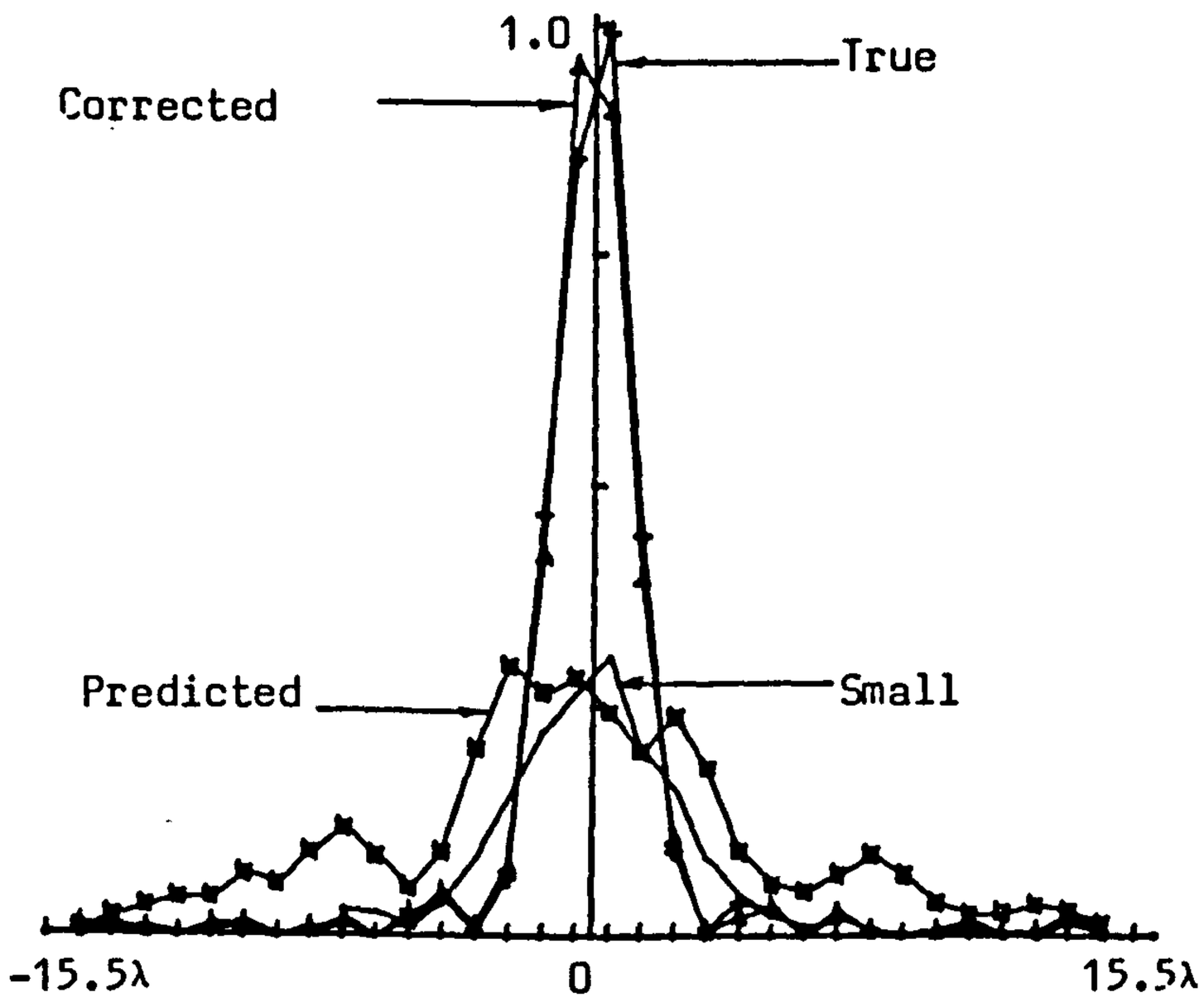


Hologram: $\Delta=1\lambda$, M=8, N=16

Object: $x_o=0$ , $z=100\lambda$

Fig. 5.15 : Effect of using different random values to simulate noise in the hologram on the reconstructed images for a 1-point object. Models: triangular polynomial type.

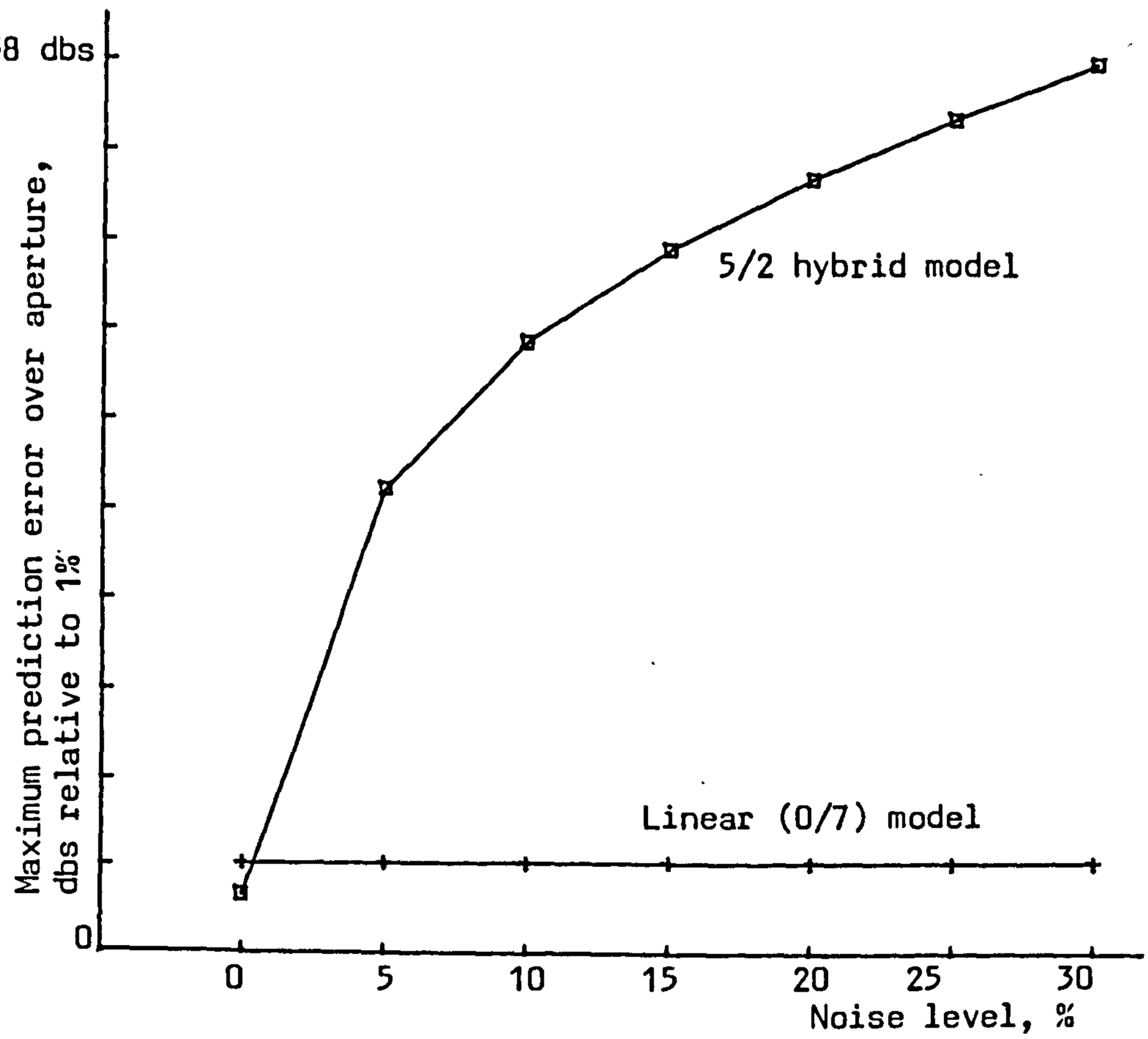


Hologram: $\Delta=1\lambda$, M=8, N=16

Object: 2-points; $x_{o1}=2.6\lambda$, $x_{o2}=-2.6\lambda$, $z=105\lambda$

Fig. 5.16 : Effect of the noise level on the performance of the hybrid and the linear predictive models.

a. Prediction error over the aperture

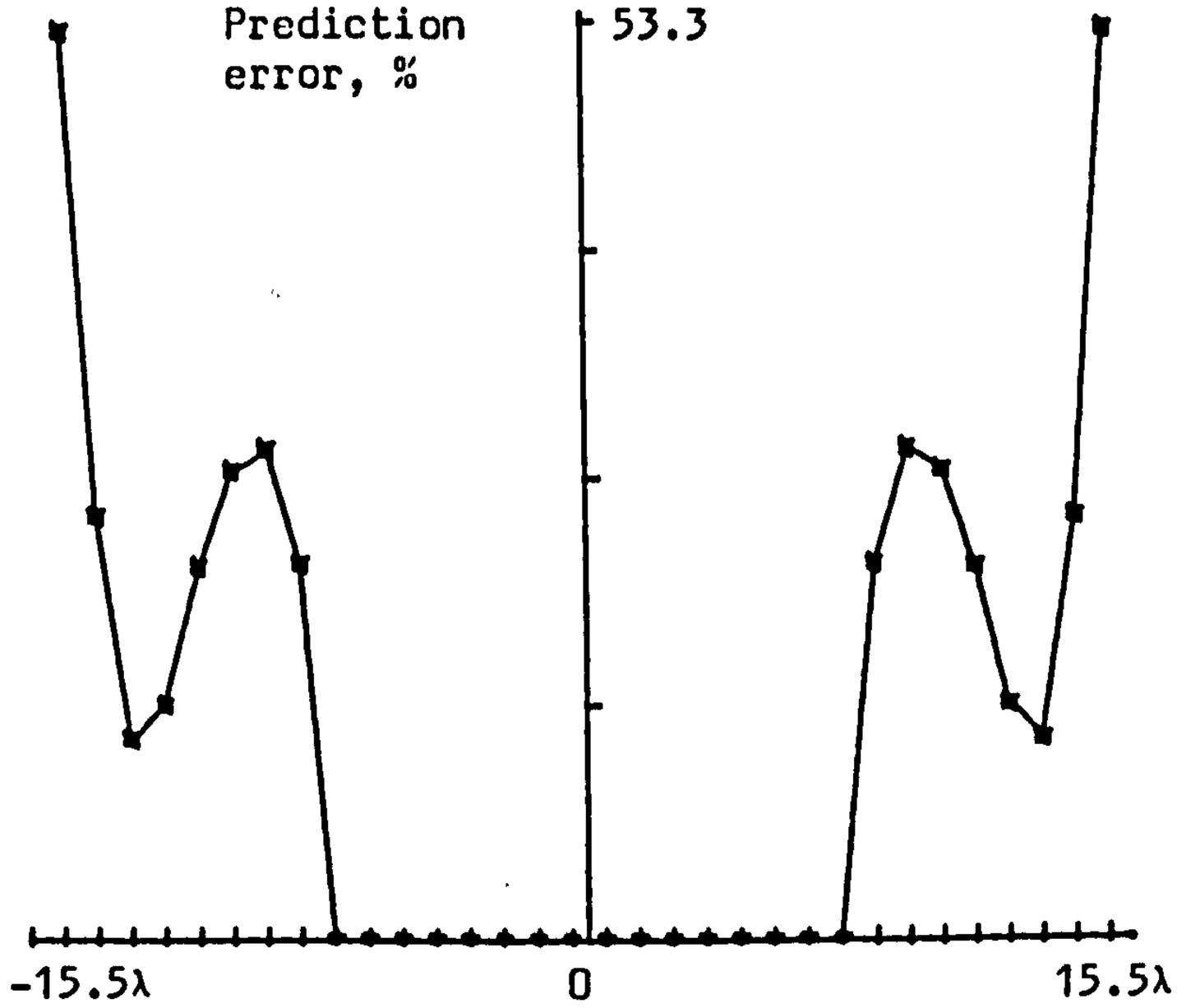


Hologram:

Δ=1λ
M=8
N=16

Object:

$x_{o1}$=2.6λ
$x_{o2}$=-2.6λ
z = 105λ

b. Reconstructed images

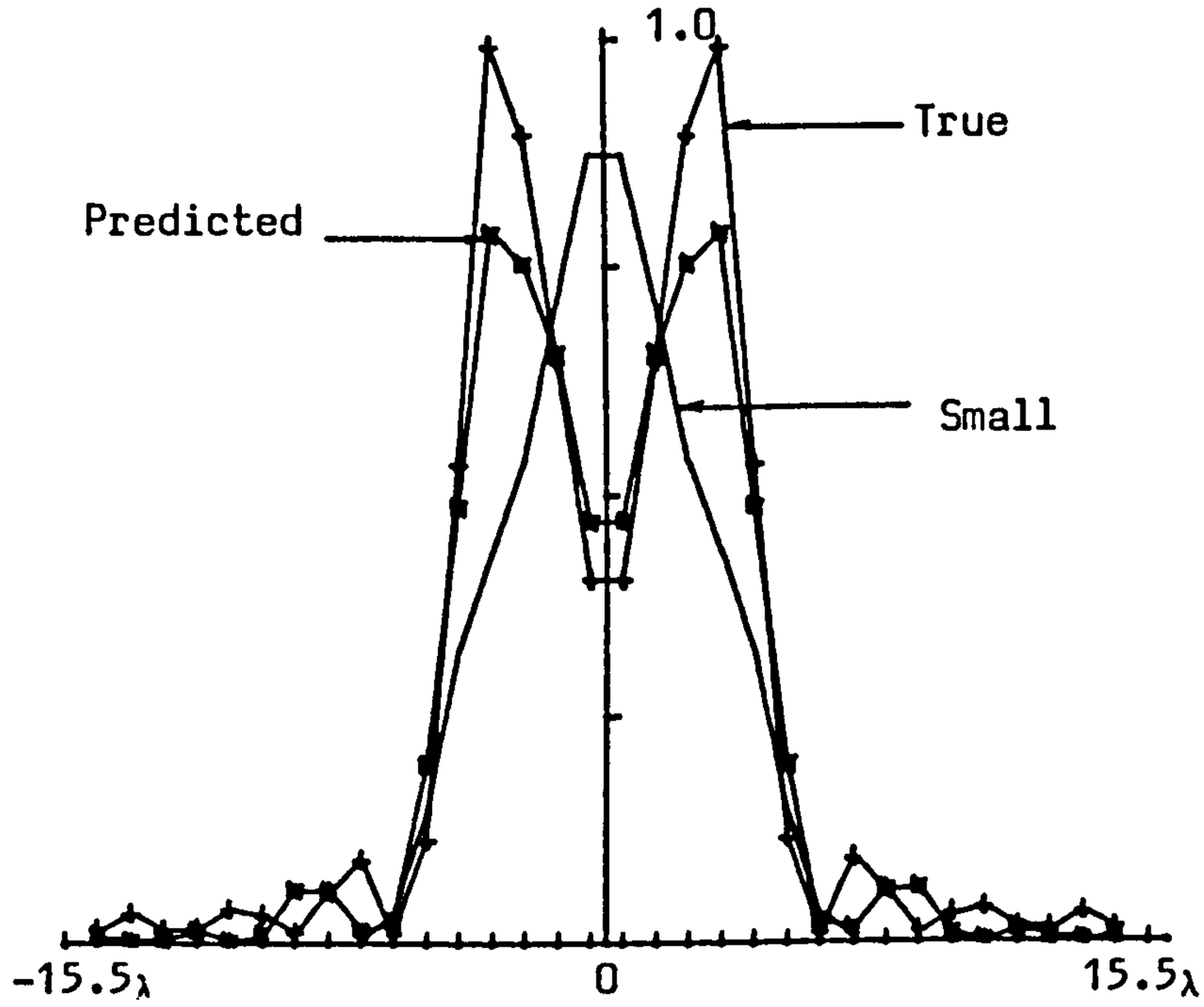


Fig. 5.17 : Results obtained when the linear predictive model is used to double the size of a 2-point object assuming noiseless data.

a. Prediction error over the aperture

<u>Hologram</u>:

Δ=1
M=8
N=16

<u>Object</u>:

$x_{o1}=2.6\lambda$
$x_{o2}=-2.6\lambda$
$z = 105\lambda$

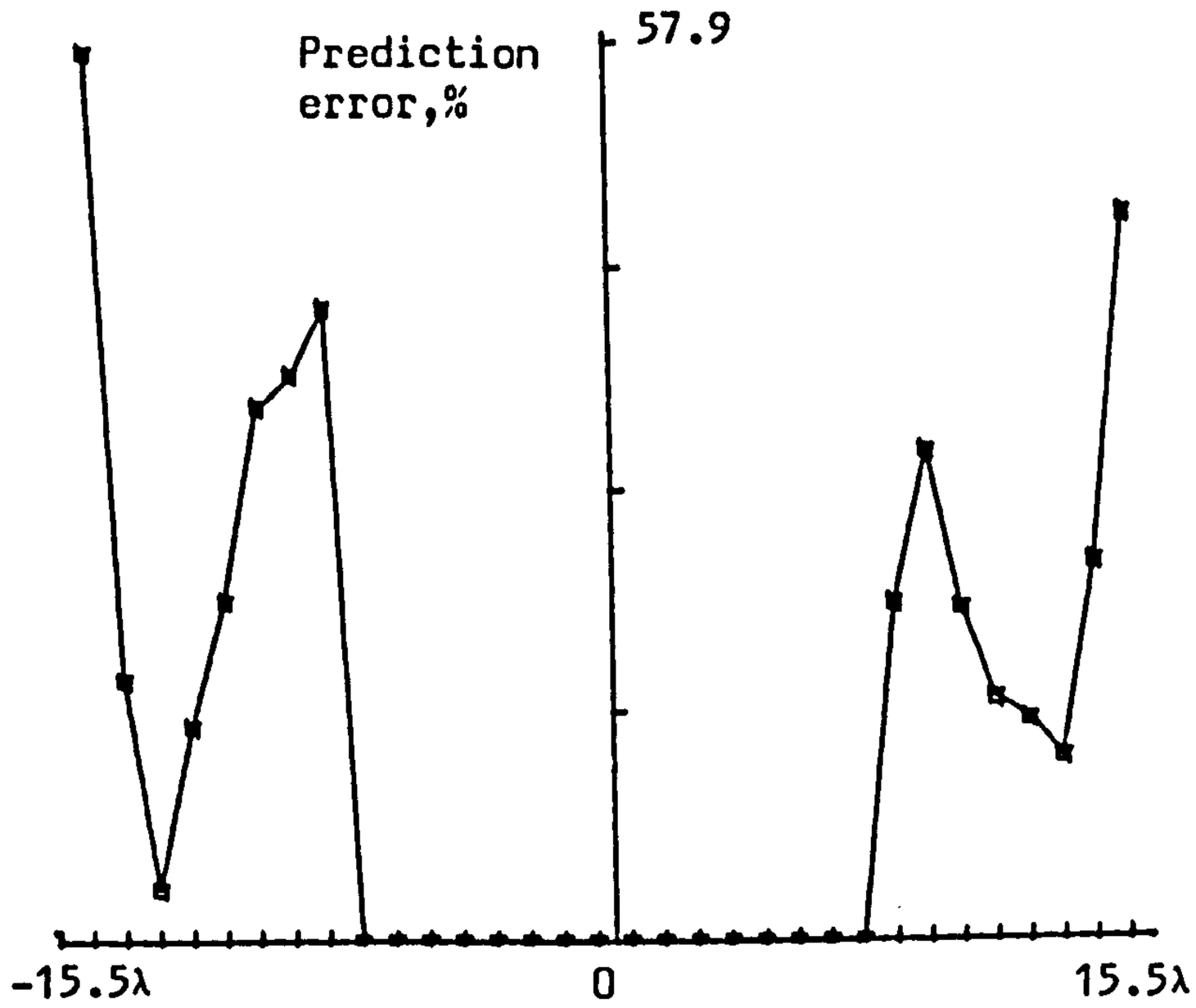


b. Reconstructed images

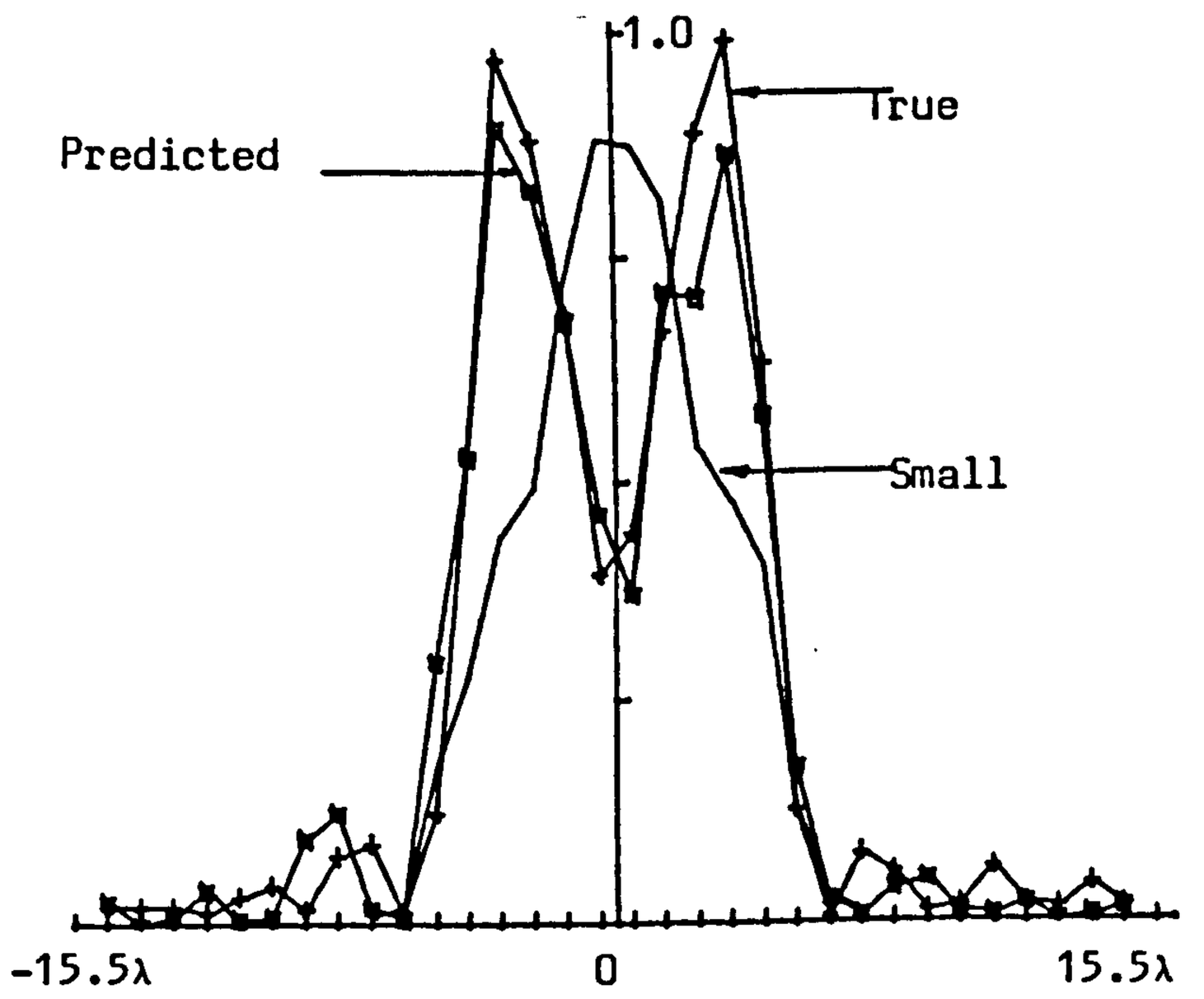


Fig. 5.18 : Effect of 10% noise in the hologram data of Fig. 5.17 on the prediction errors and reconstructed images when the linear model is used for prediction.

a. Reconstructed images with 20% noise

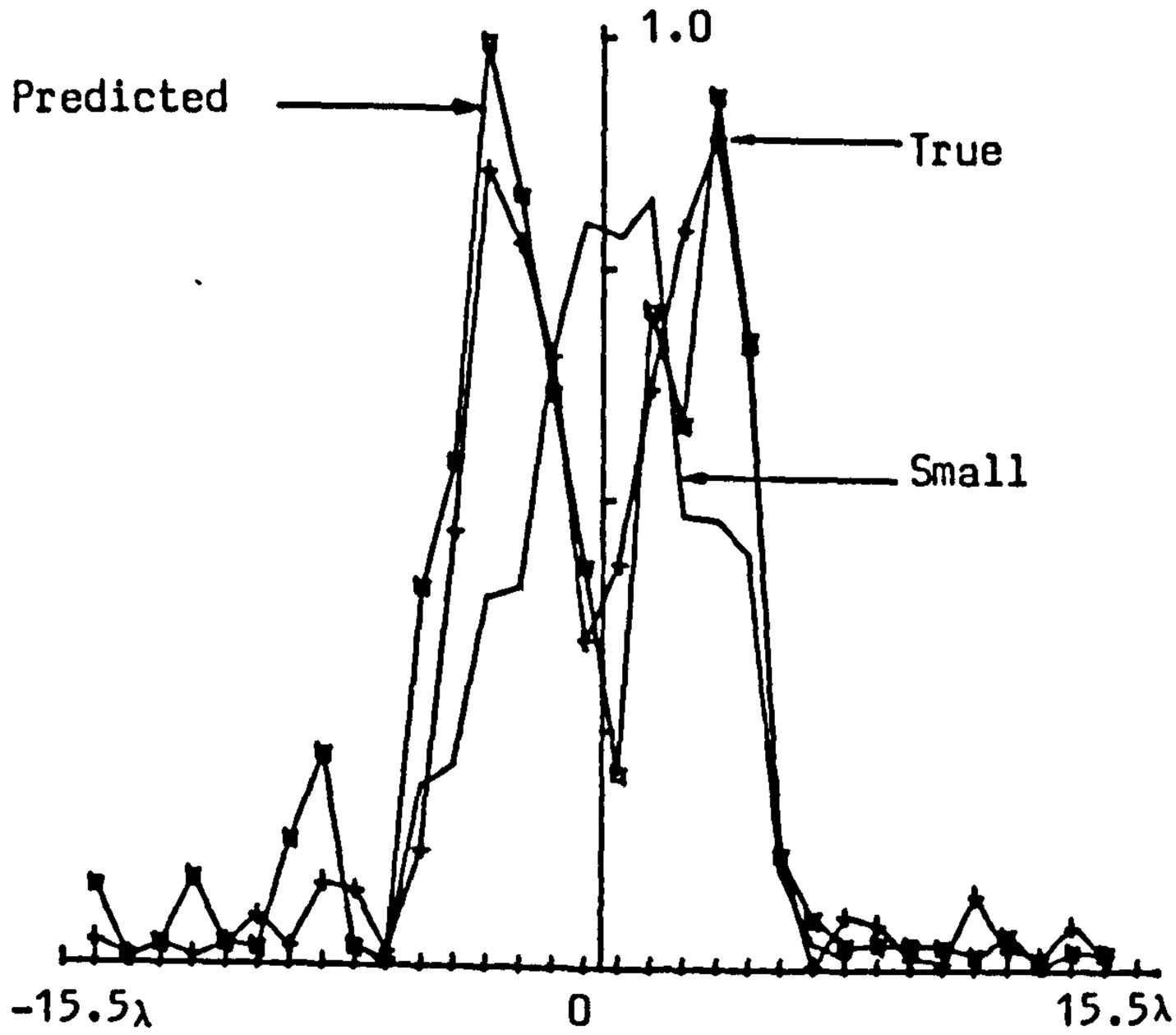


b. Reconstructed images with 30% noise

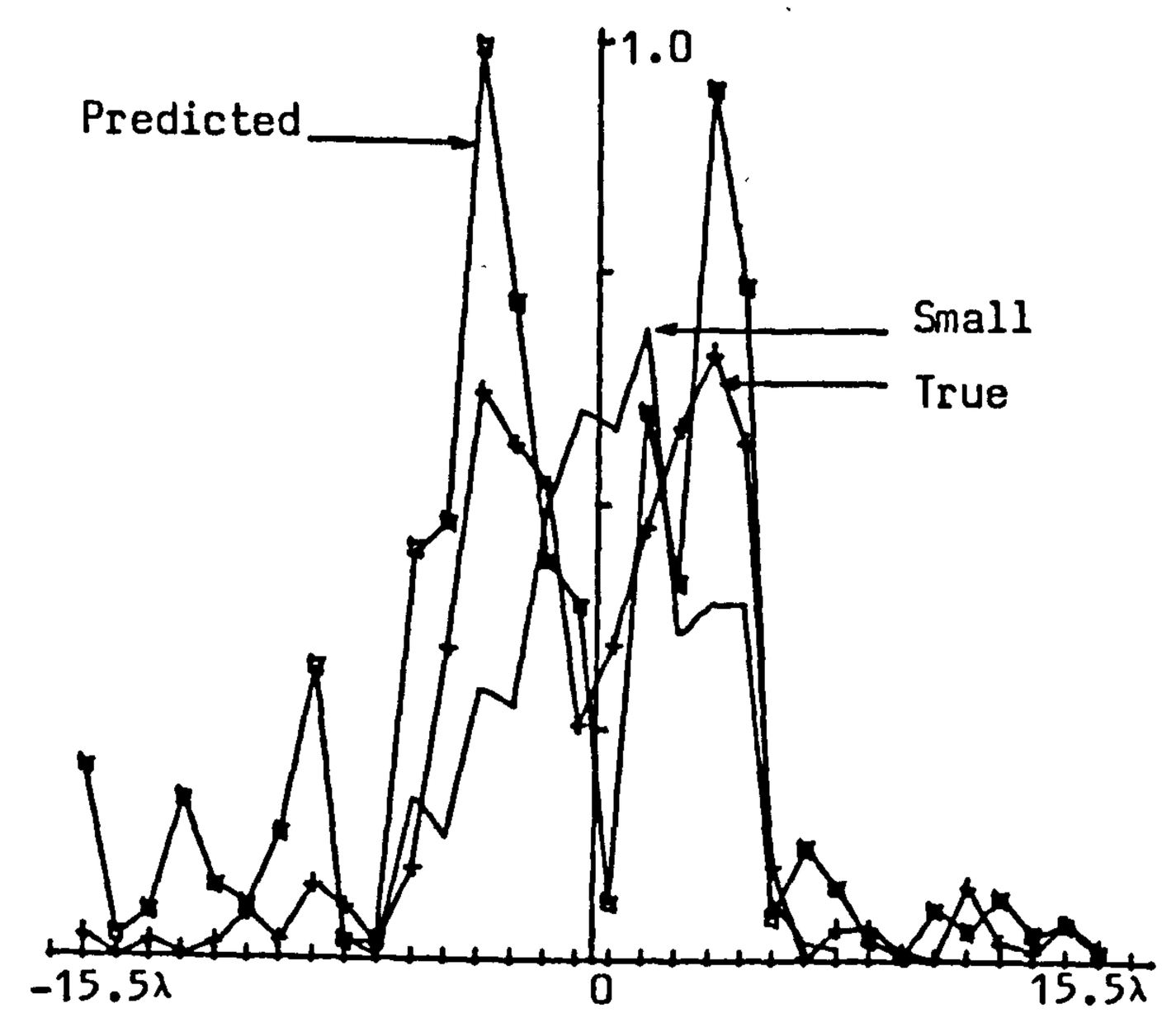


Hologram: Δ=1, M=8, N=16

Object: $x_{o1}=2.6\lambda$, $x_{o2}=-2.6\lambda$, $z=105\lambda$

Fig. 5.19 : Effect of increasing the noise level on the reconstructed images of the 2-point object in Fig. 5.17 and Fig. 5.18. Predictive model: linear.

a. Reconstructed images with 20% noise. Noise values: set 1

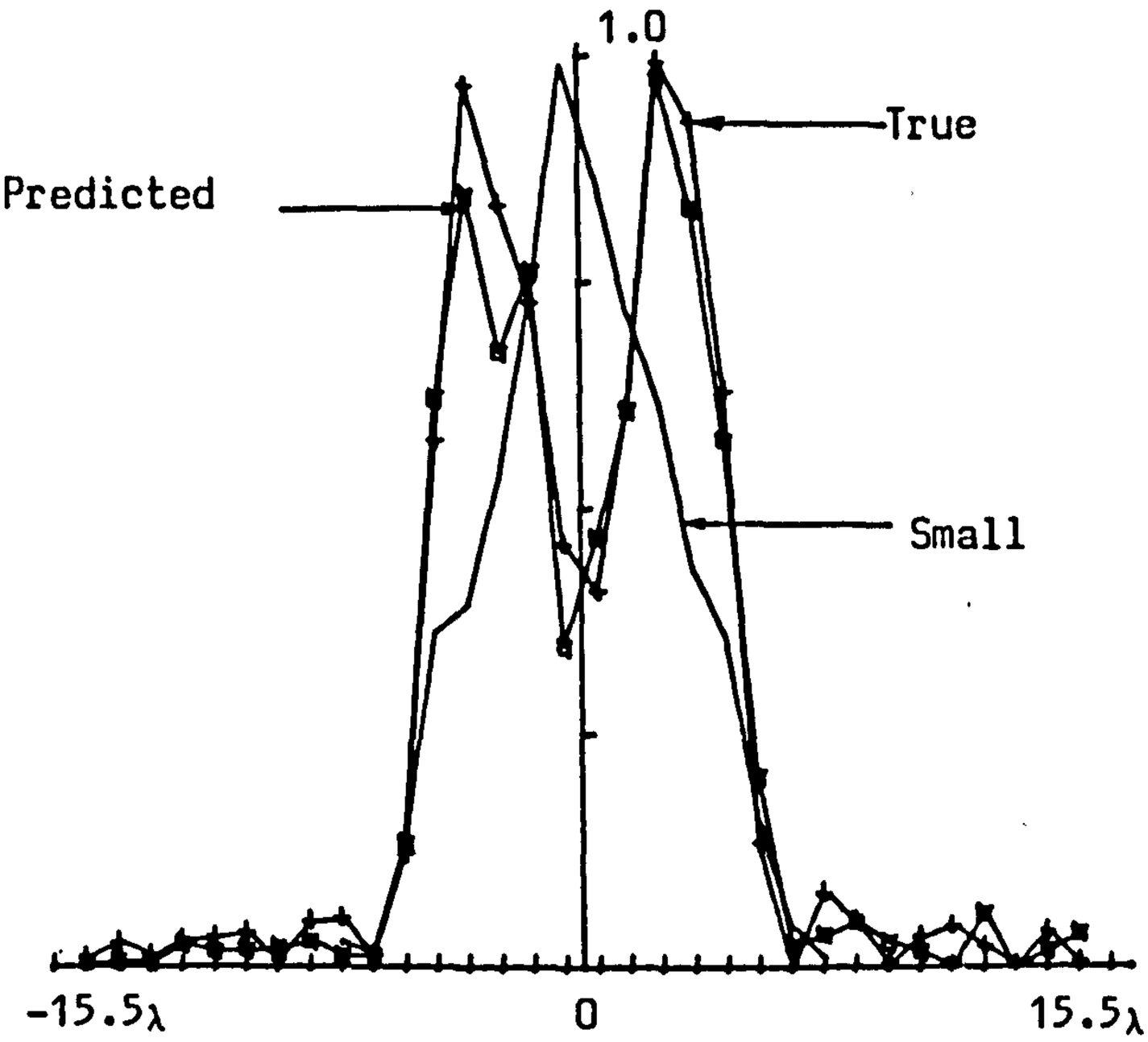


b. Reconstructed images with 20% noise. Noise values: set 2.

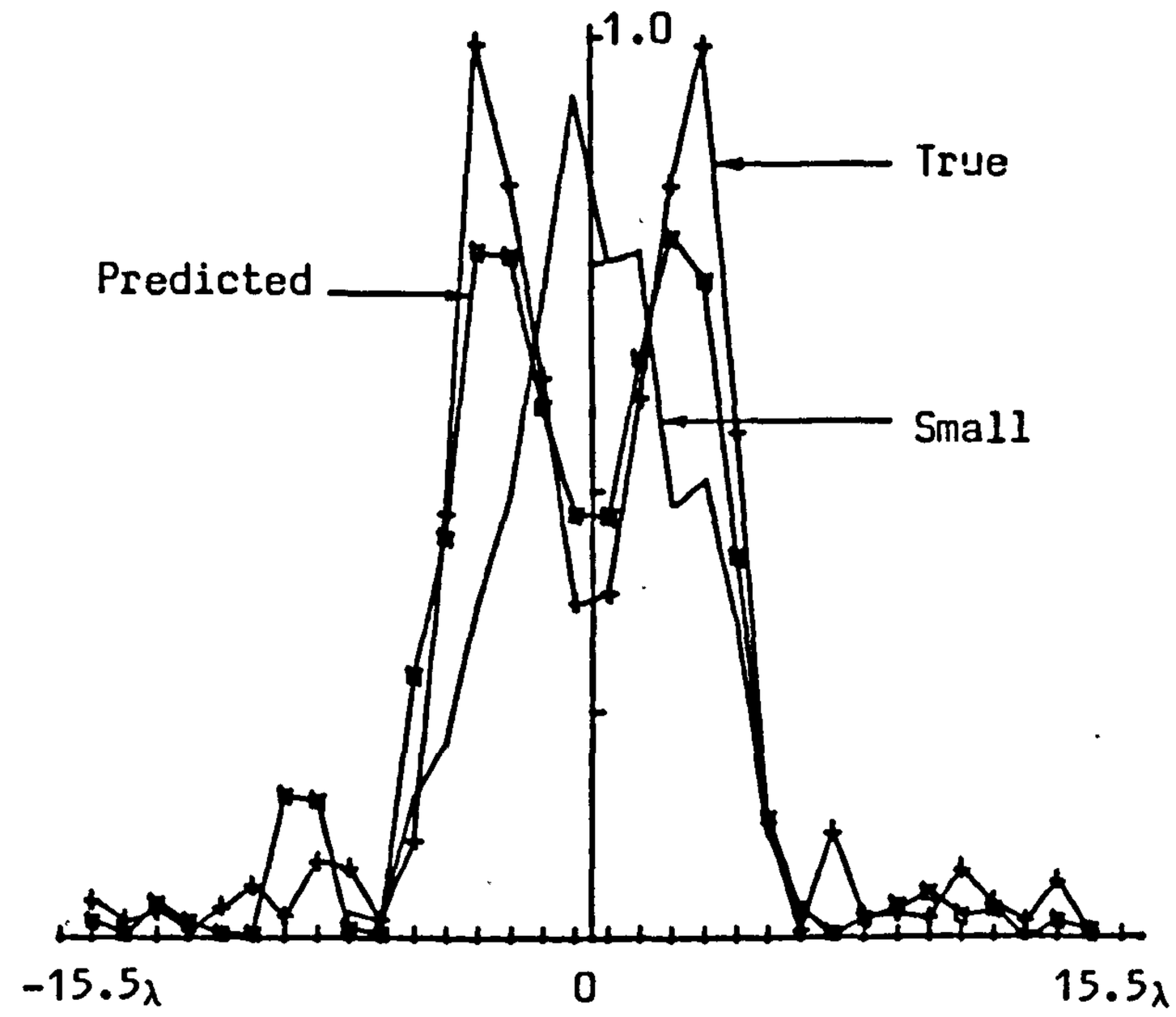


Hologram: Δ=1, M=8, N=16

Object: $x_{o1}=2.6\lambda$, $x_{o2}=-2.6\lambda$, $z=105\lambda$

Fig. 5.20 : Effect of using different values for the random components representing noise on the performance of the linear predictive model for the imaging configuration used in Figs. 5.17-19.

a. Object range = 40λ

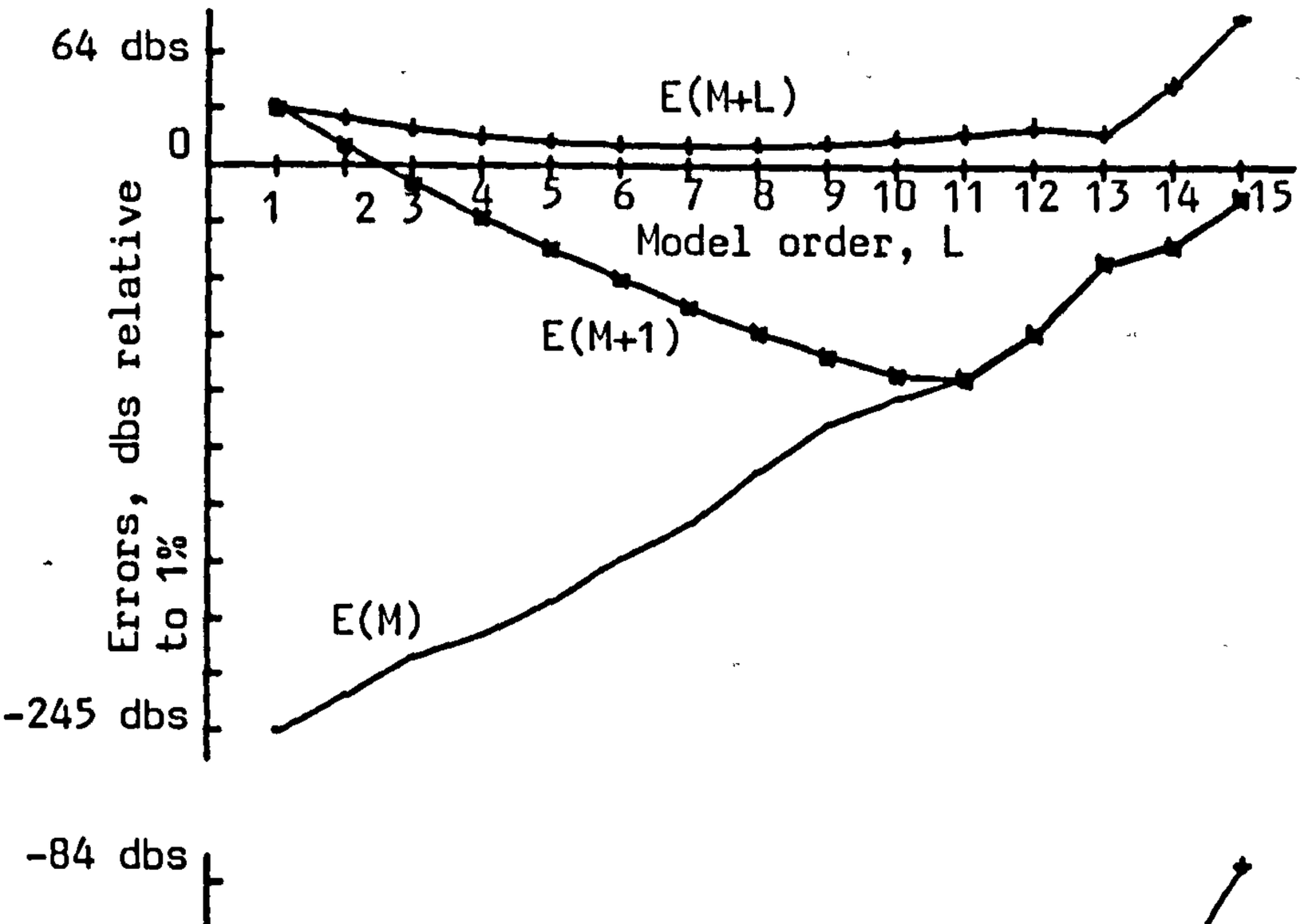


b. Object range = 80λ

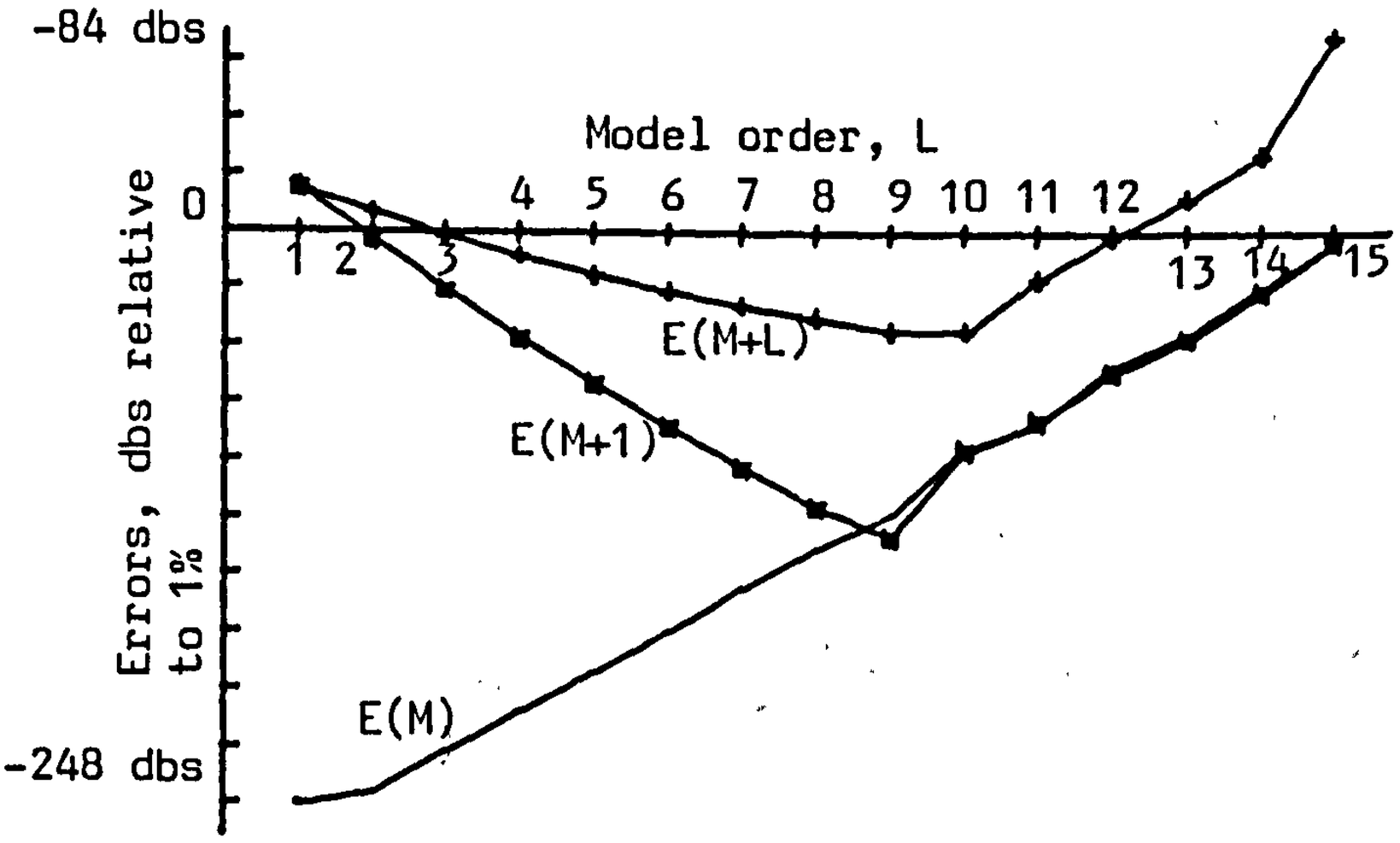


c. Object range = 160λ

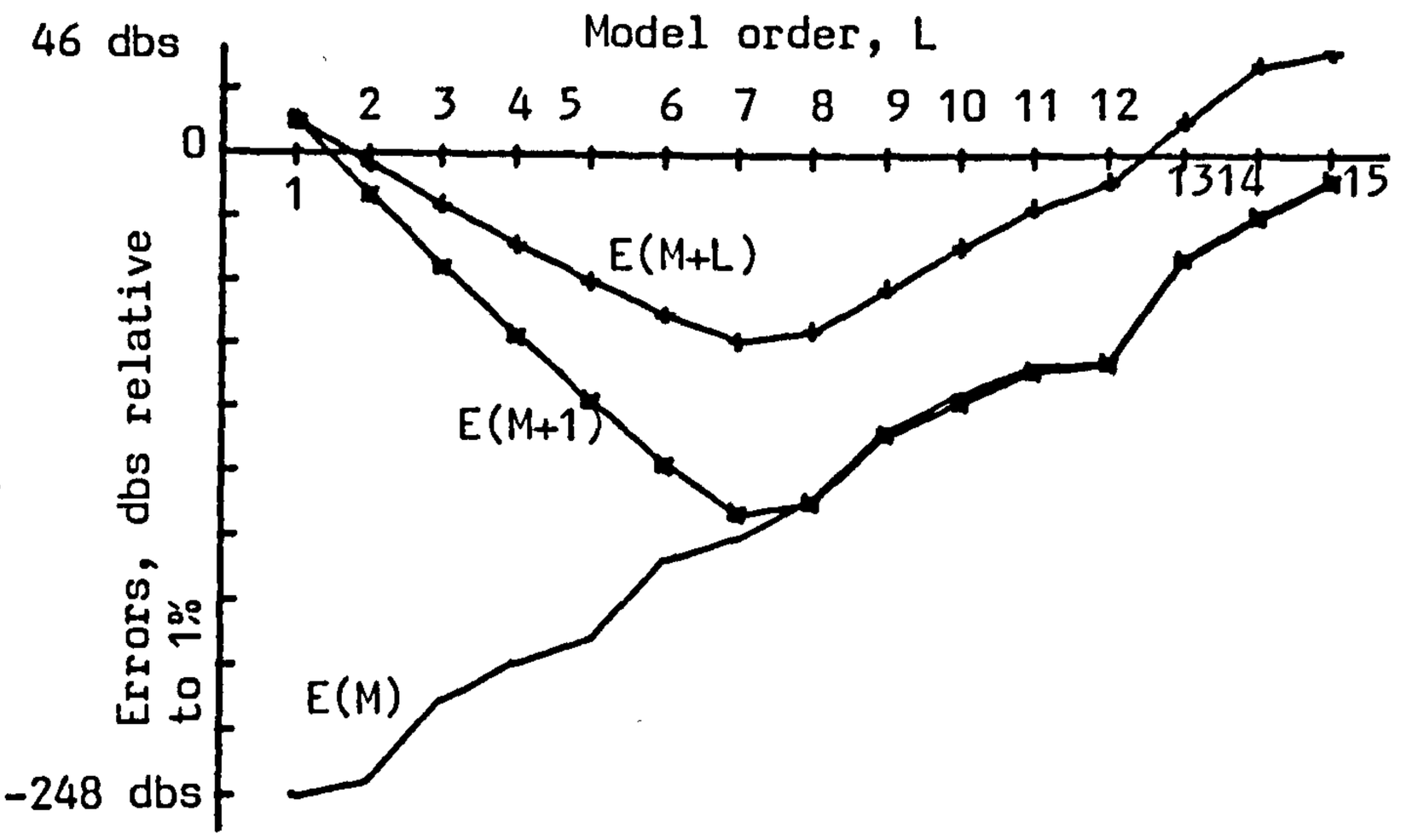


Sample spacing , Δ=1λ  Object = 1-point on the hologram axis

Fig. 5.21 : Errors versus model order using the square model on the 4051 minicomputer

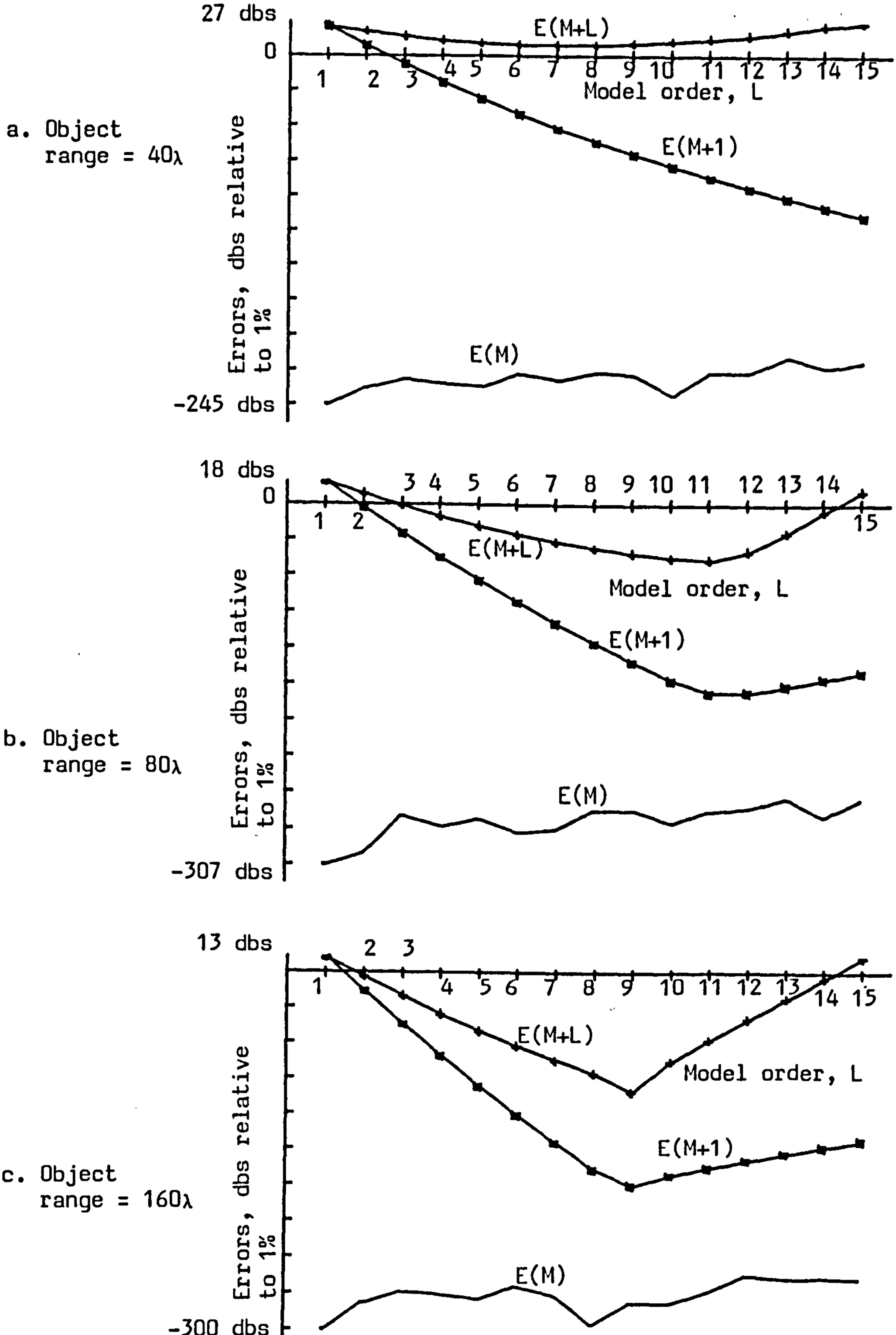


Sample spacing , Δ=1λ Object = 1 point on the hologram axis

Fig. 5.22 : Error versus model order using the square model on the Nova 2 computer

a. Object range = 40λ

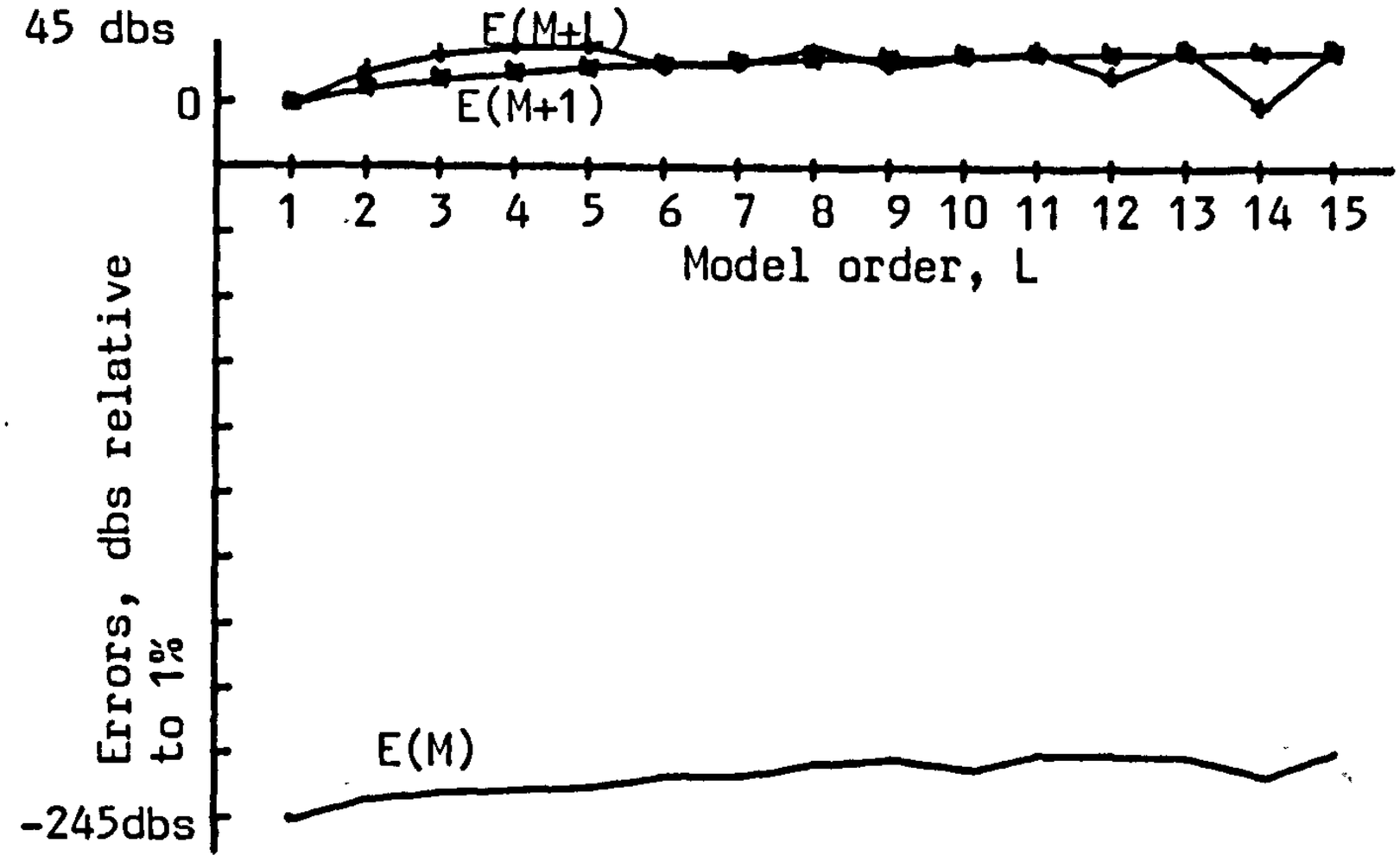


b. Object range = 80λ

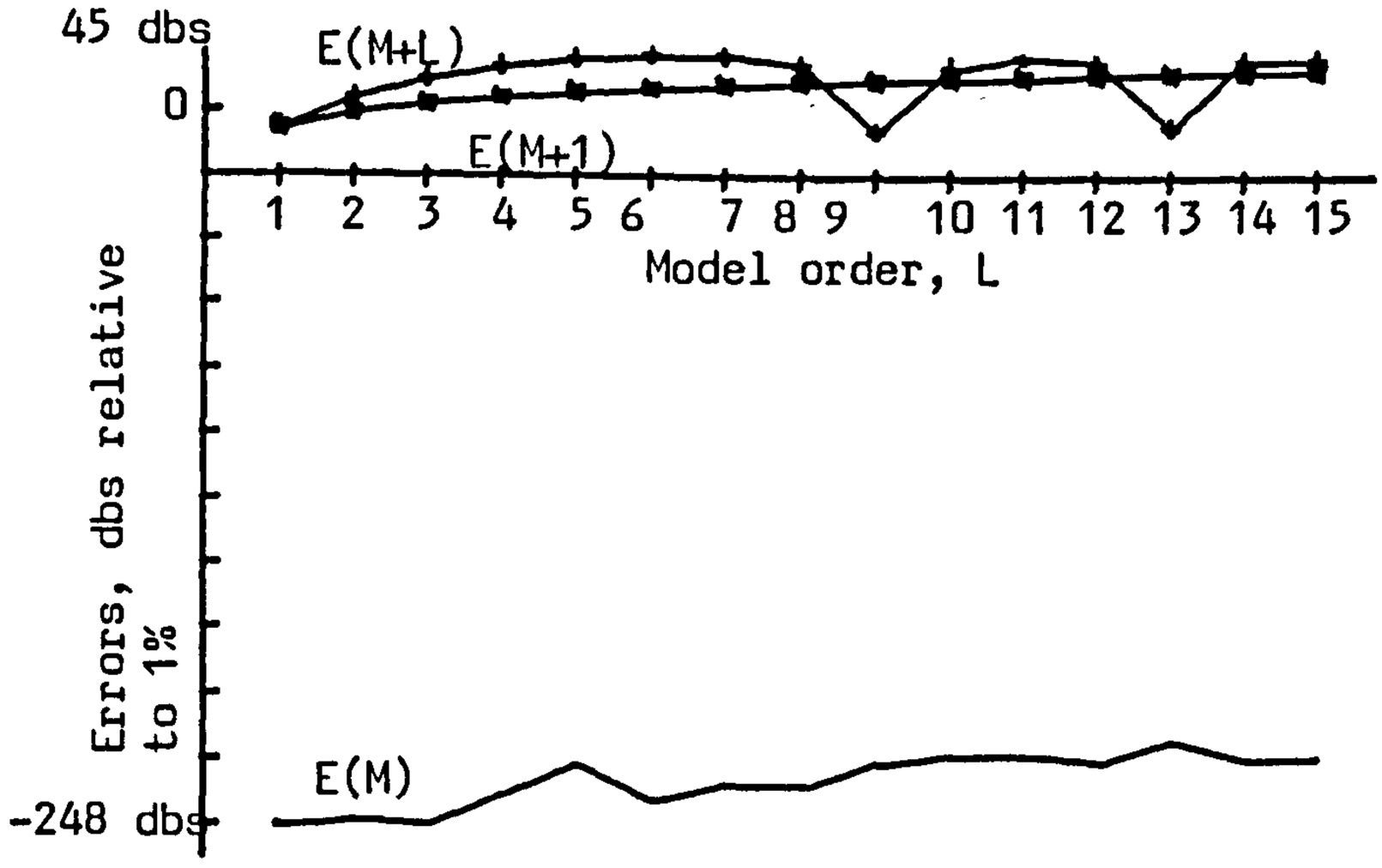


C. Object range = 160λ

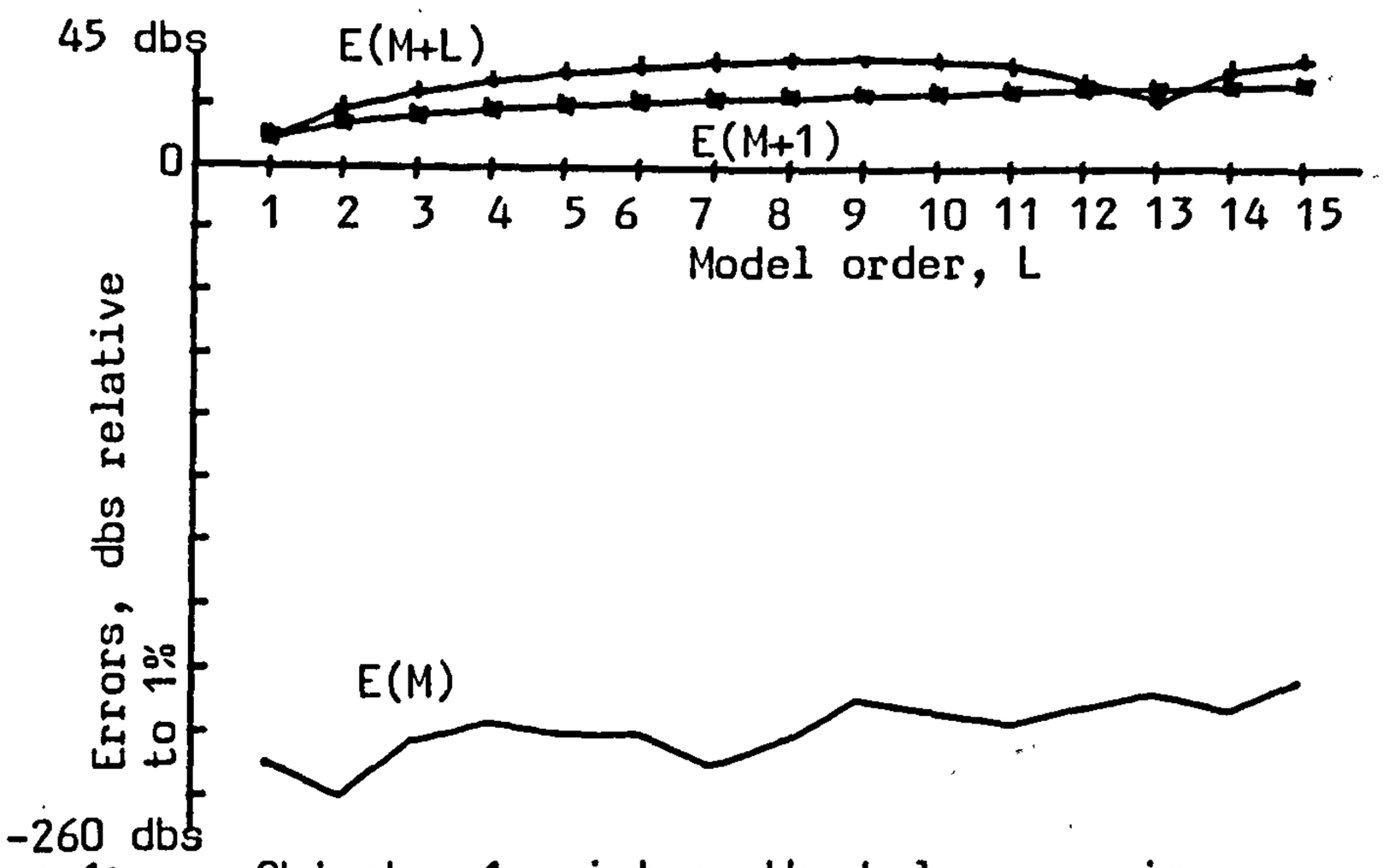


Sample spacing, Δ=1λ  Object = 1-point on the hologram axis

Fig. 5.23 : Errors versus model orders using the triangular model on the 4051 minicomputer

a. Object range = 40λ

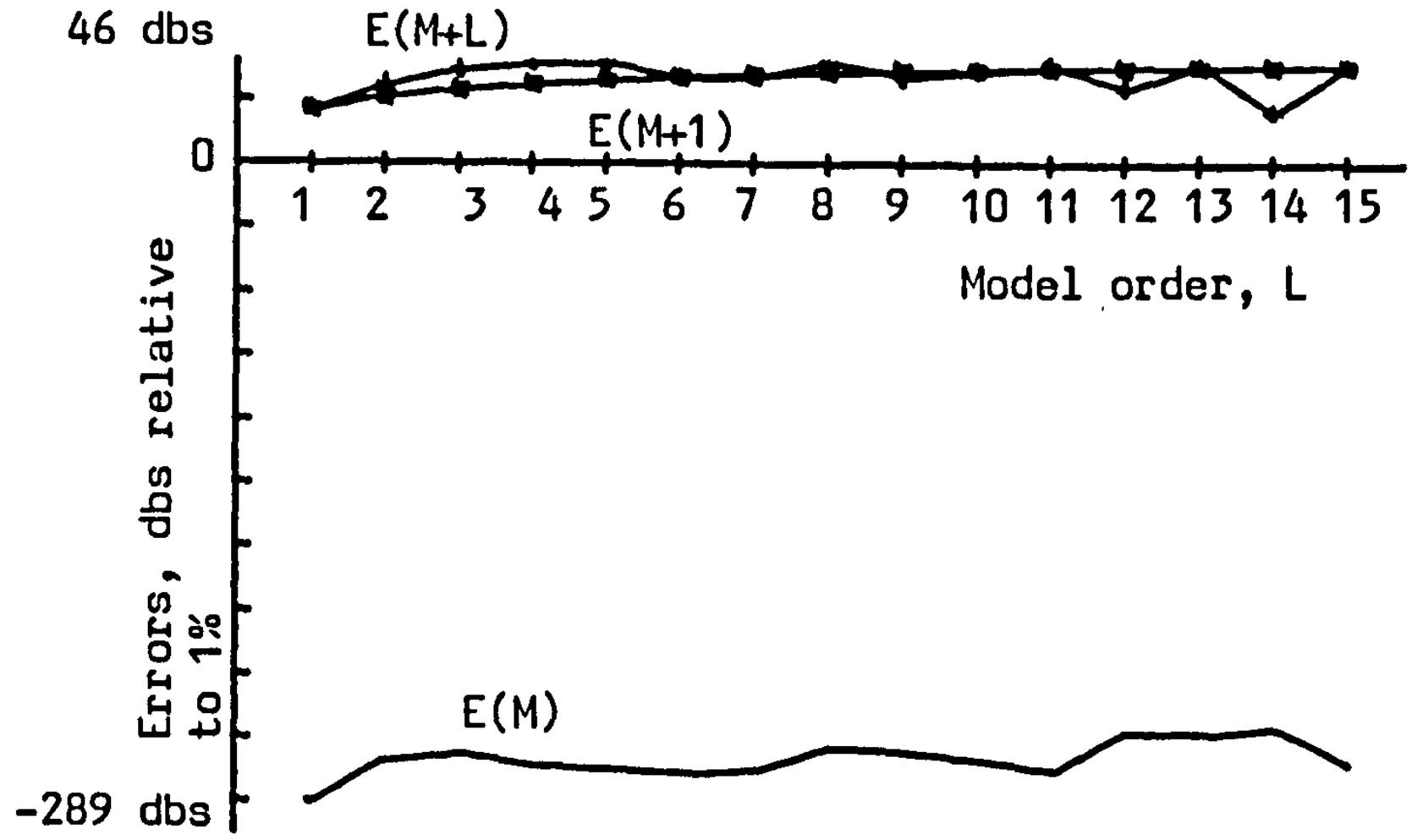


b. Object range = 80λ

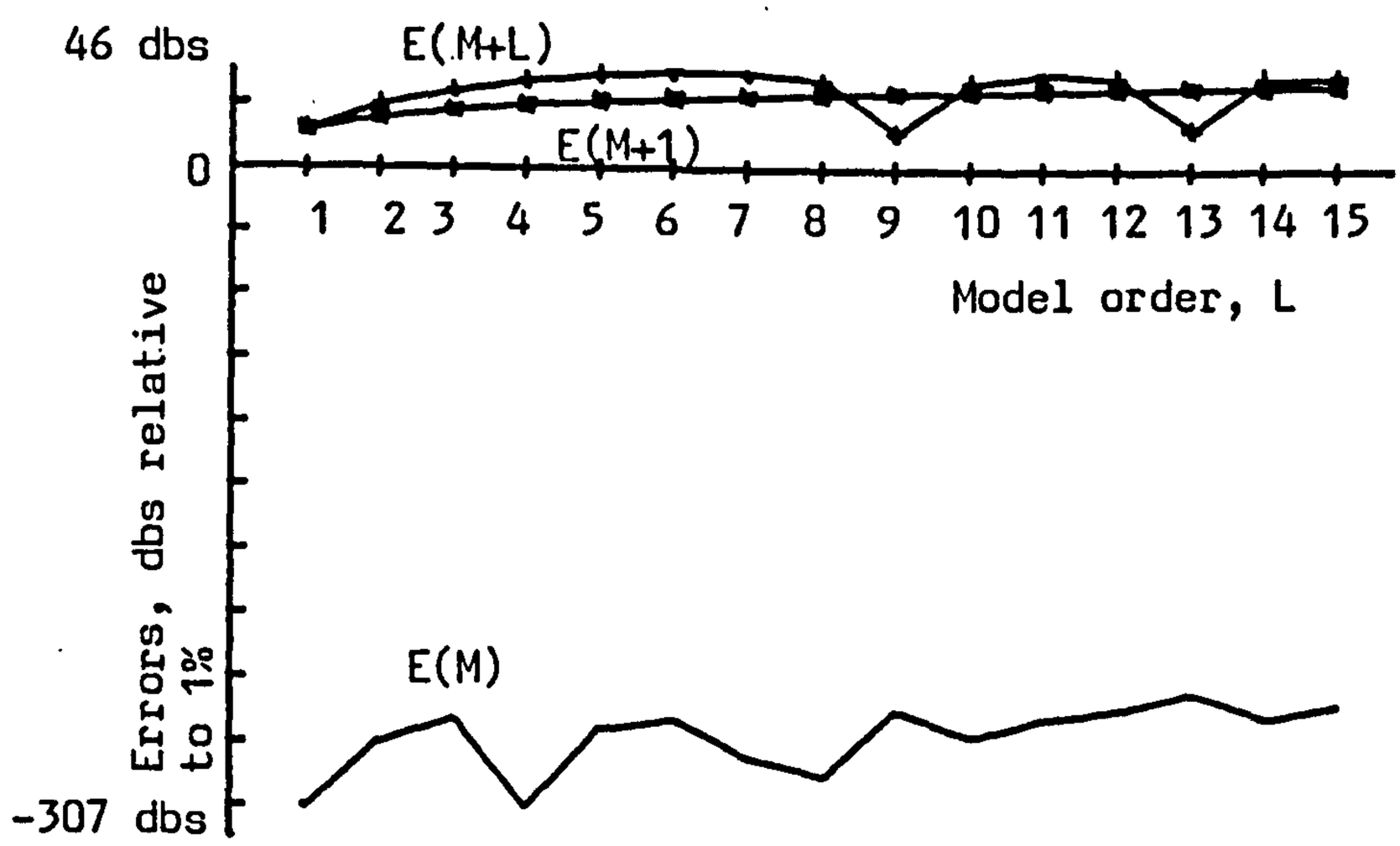


c. Object range = 160λ

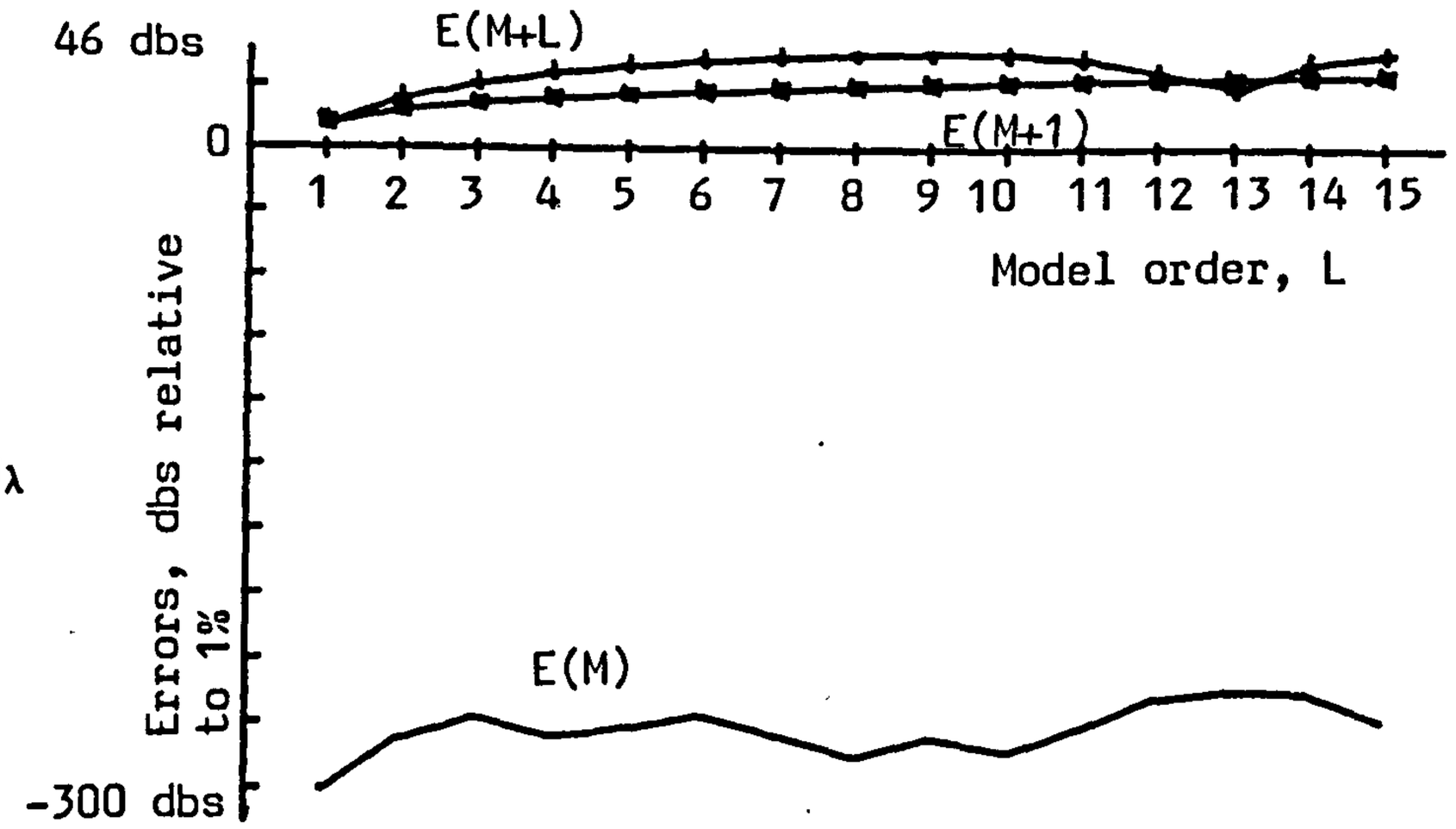


Sample spacing, Δ=1λ  Object : 1 point on the hologram axis

Fig 5.24 : Errors versus model order using the triangular model on the Nova 2 computer

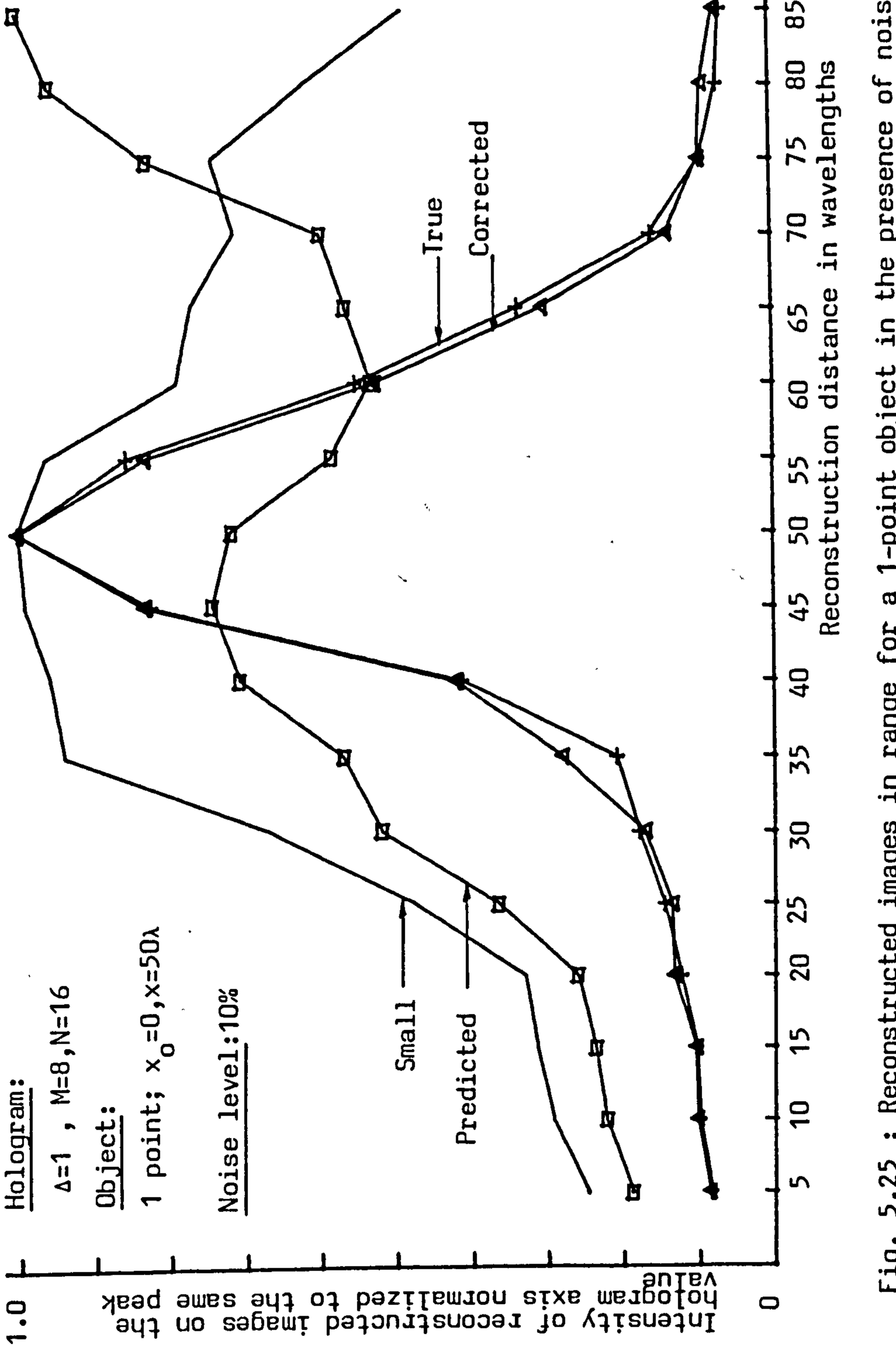


Fig. 5.25 : Reconstructed images in the presence of noise.
Prediction and correction performed using triangular polynomial models.

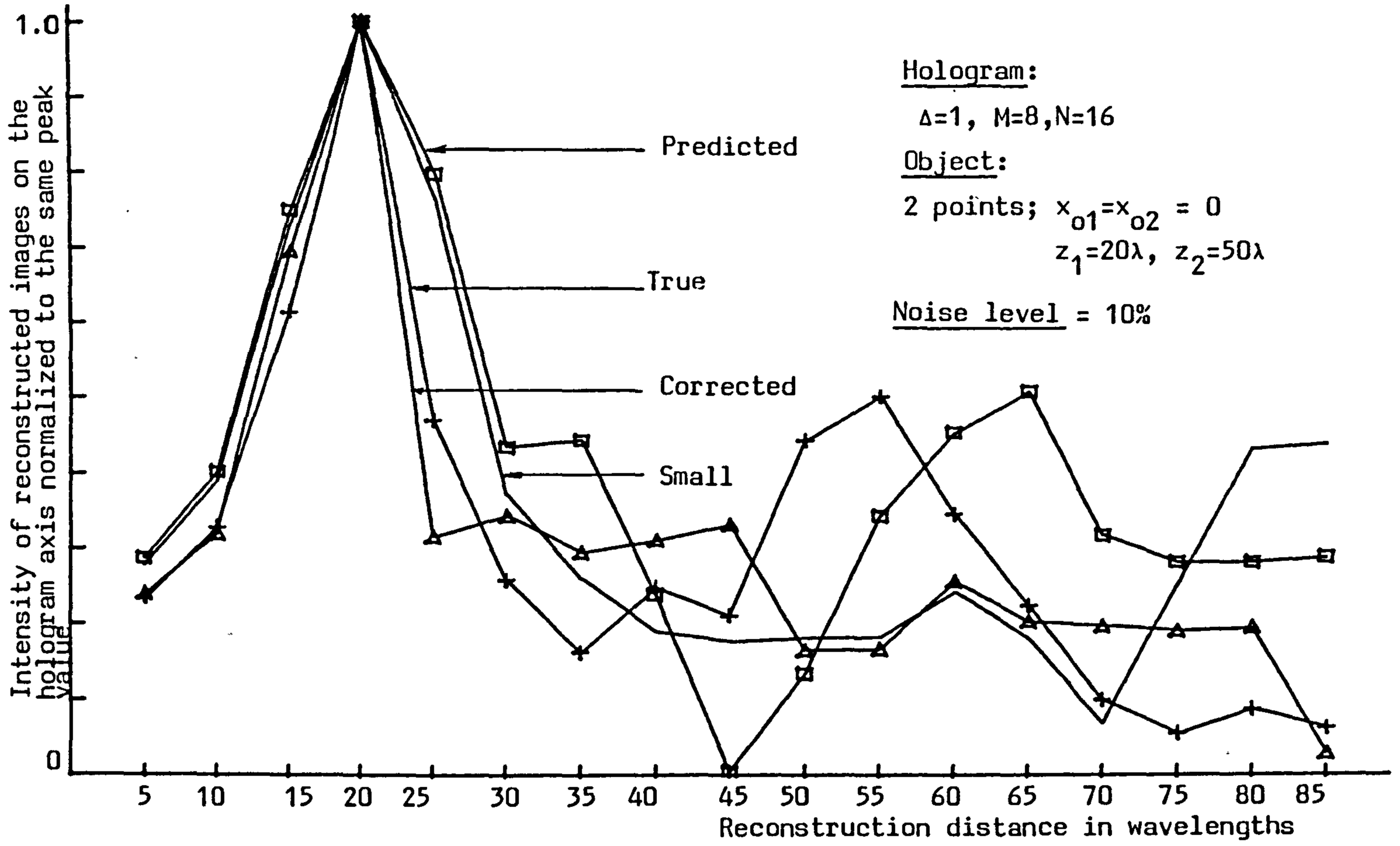


Fig. 5.26 : Reconstructed images in range for 1 2-point object in the presence of noise. Prediction and correction performed using triangular polynomial models .

a. Prediction error over the aperture

Hologram:

Δ=1λ
M=8
N=16
Noise level=10%

Object:

range = 95λ
$d_o$ = 5.6λ
$w_o$ = 4λ
ρ = 50 points/λ

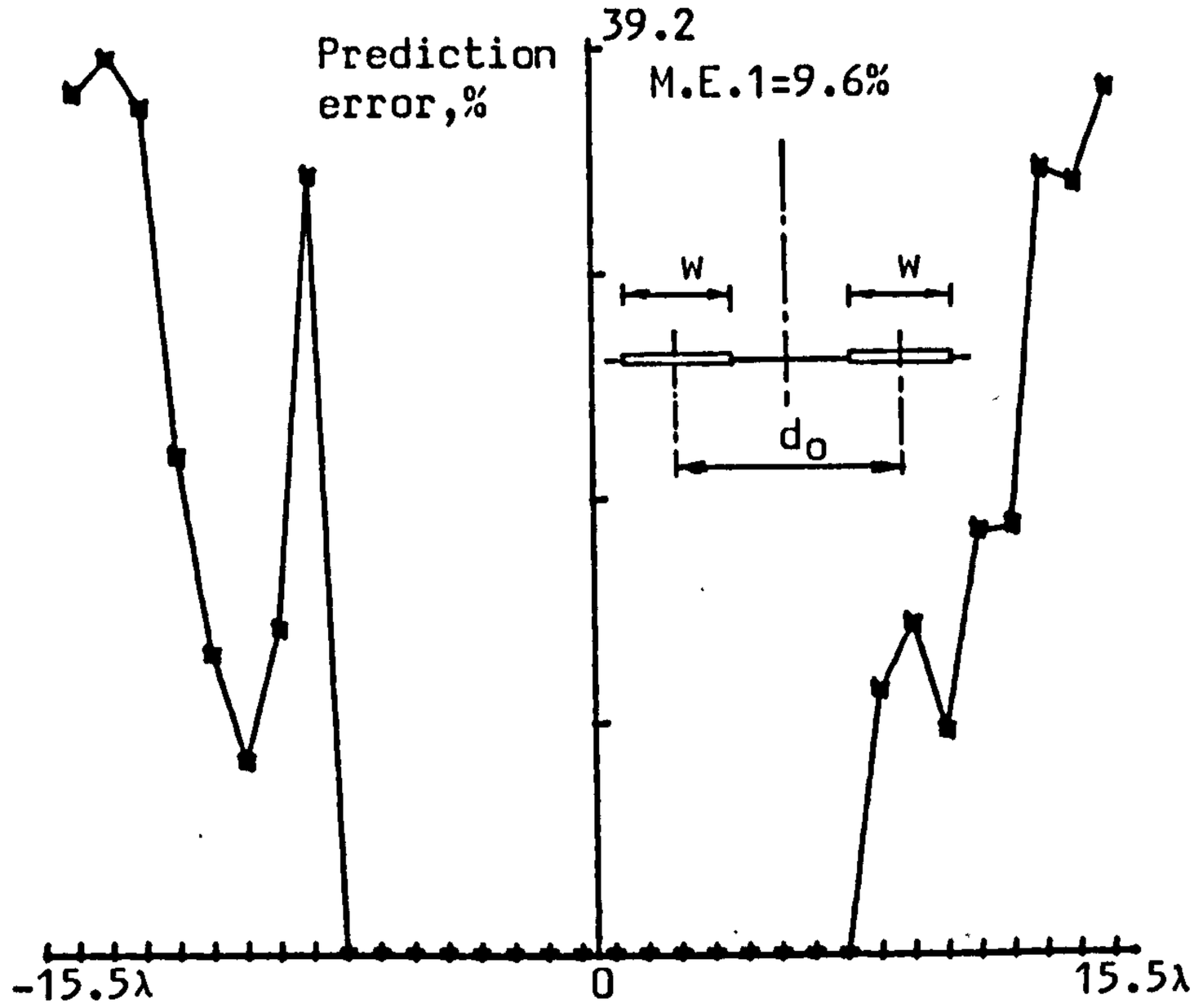


b. Reconstructed images

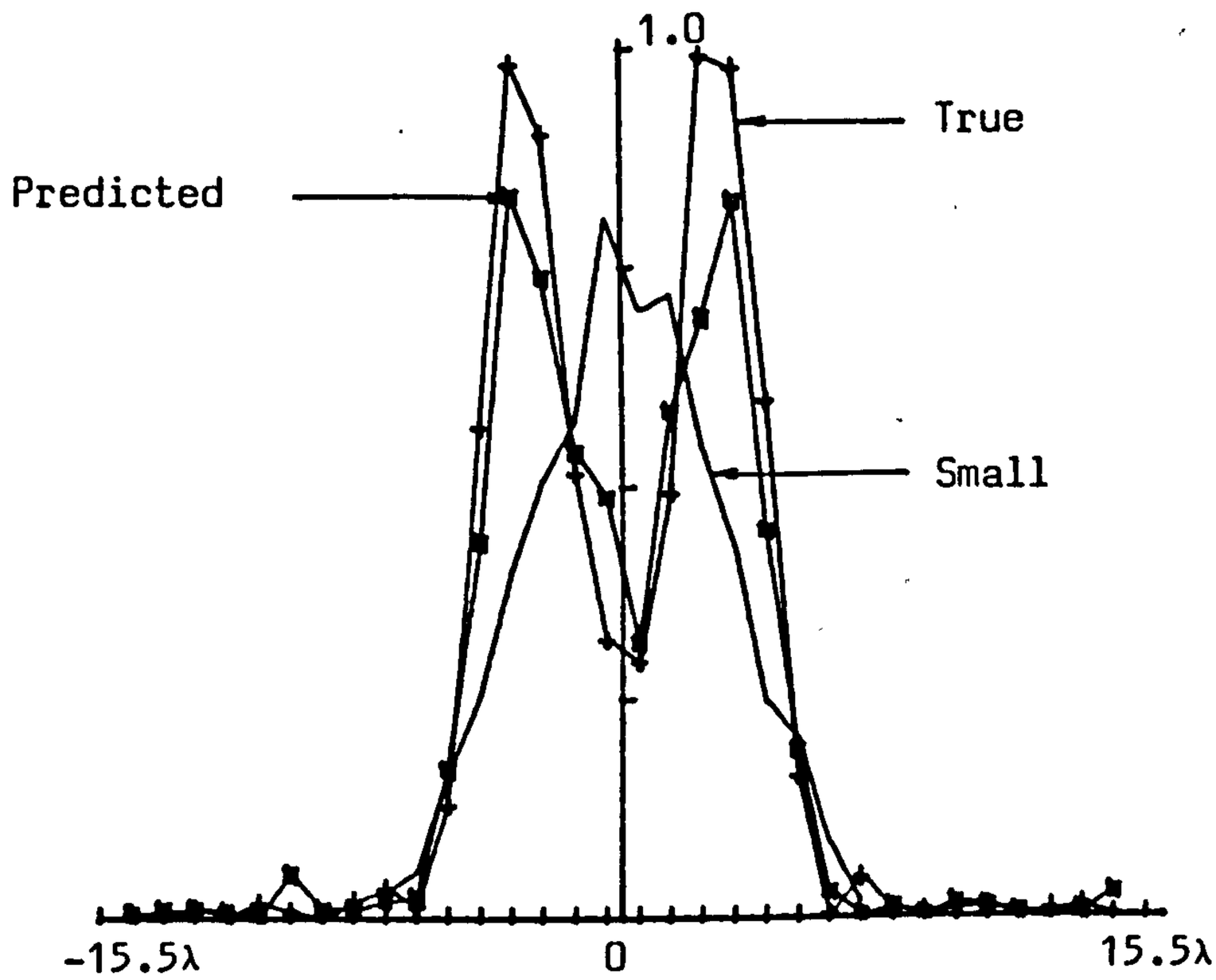


Fig. 5.27 : Results obtained when using the linear model to double the size of the hologram of two quasi-continuous segments in the presence of noise.

a. Prediction error over the aperture

Hologram:

Δ=1λ
M=8
N=16

Object:

$x_{01}$=2.6λ
$x_{02}$=-2.6λ
z = 105λ

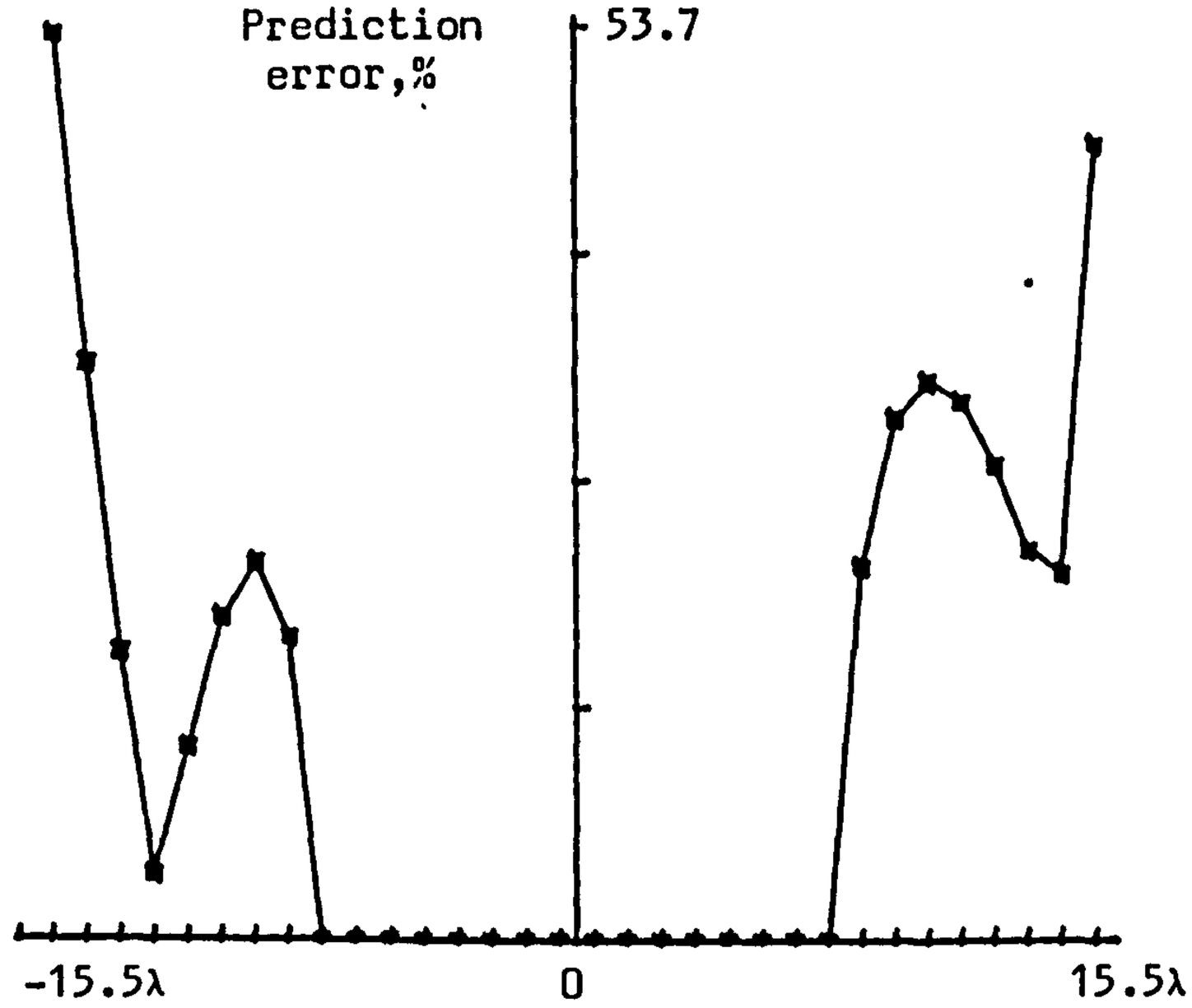


b. Reconstructed images

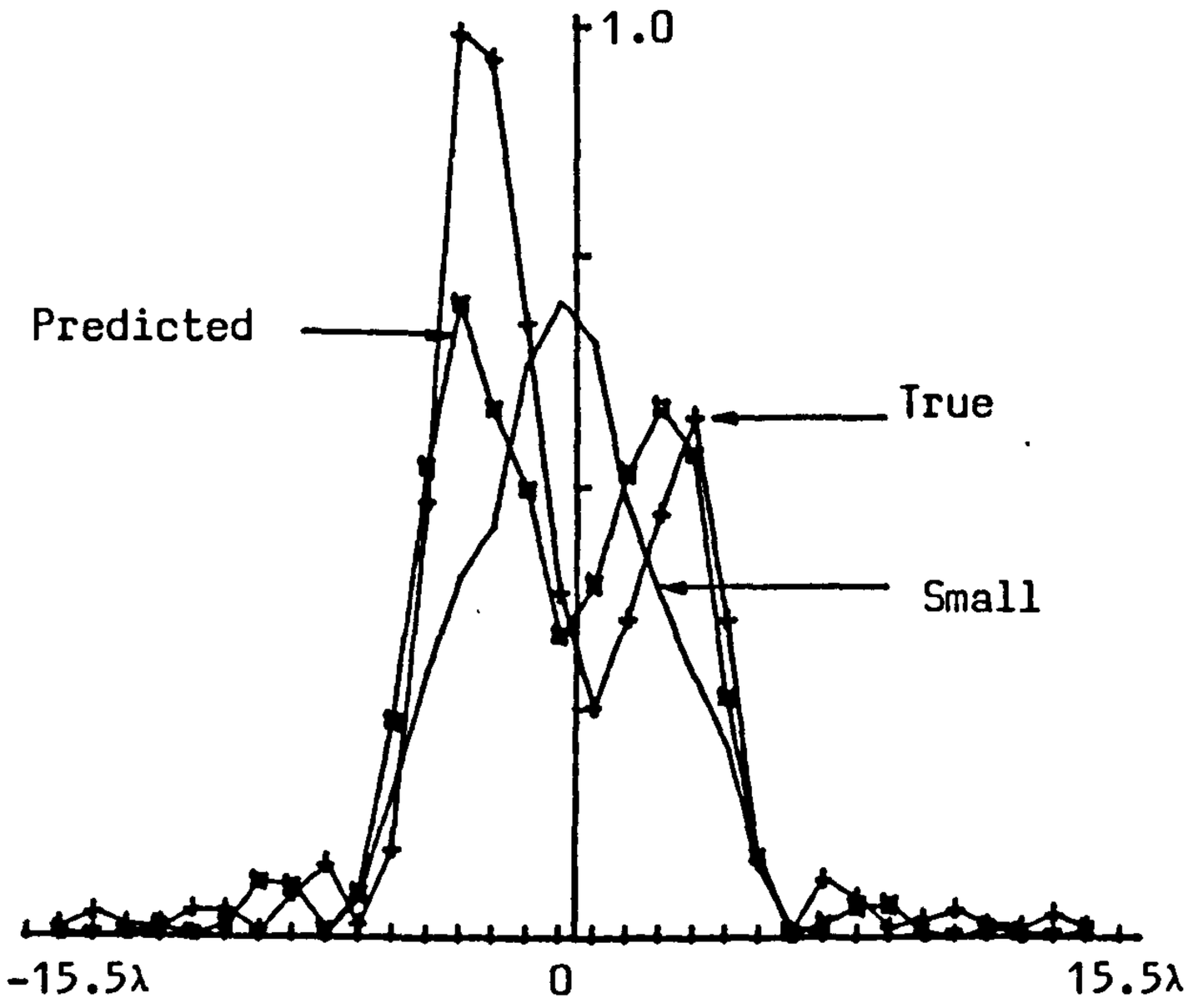


Fig. 5.28 : Imaging of two points with different radiation strengths by doubling the size of the aperture using a linear model in the presence of 10% noise. Relative radiation strength between two points is 0.8.

# Figures for Chapter 6

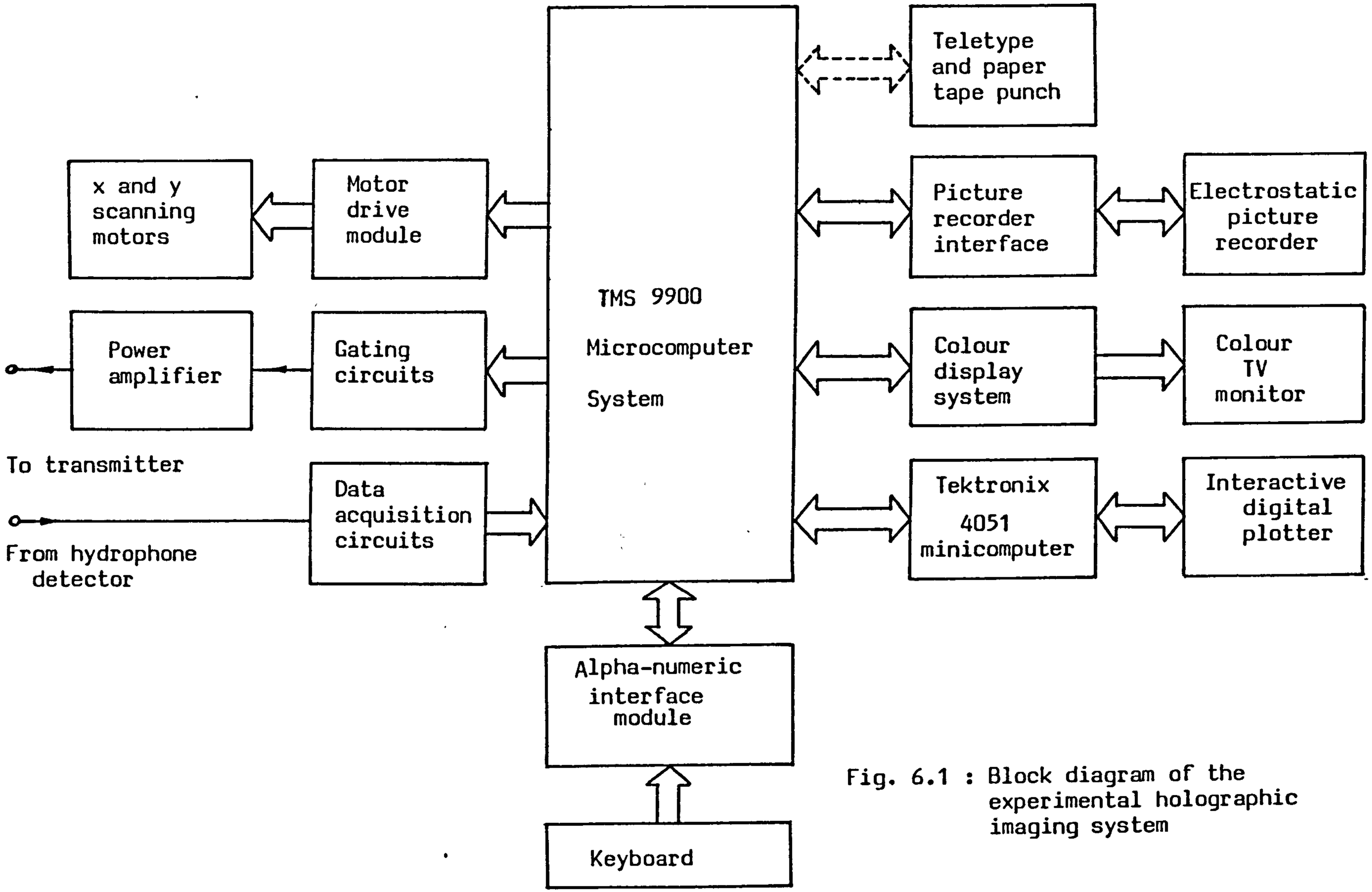


Fig. 6.1 : Block diagram of the experimental holographic imaging system

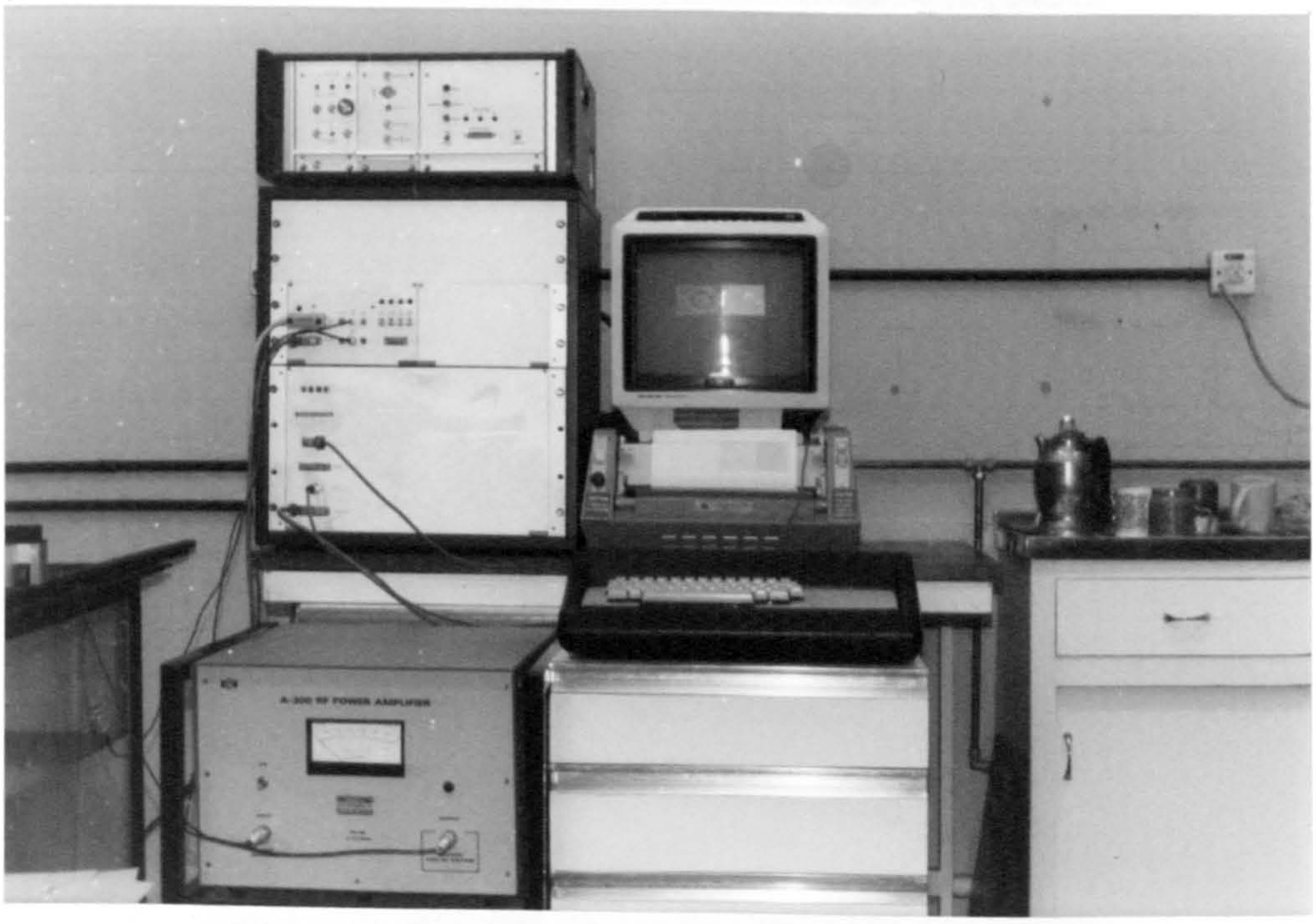


Fig. 6.2 : An overall view of the Experimental Holographic Imaging System

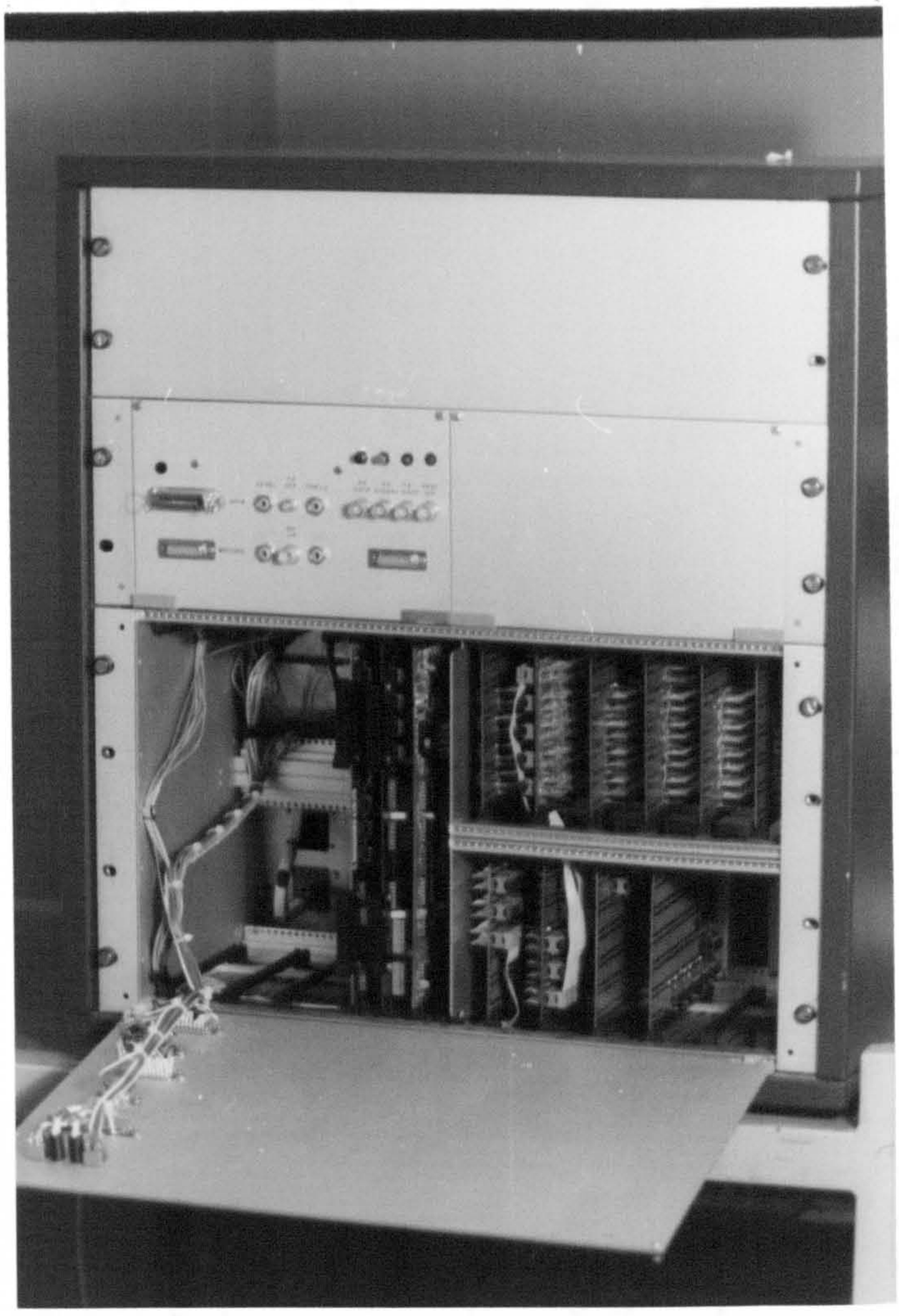

Fig. 6.3 : Electronic circuits for the Experimental Holographic Imaging System

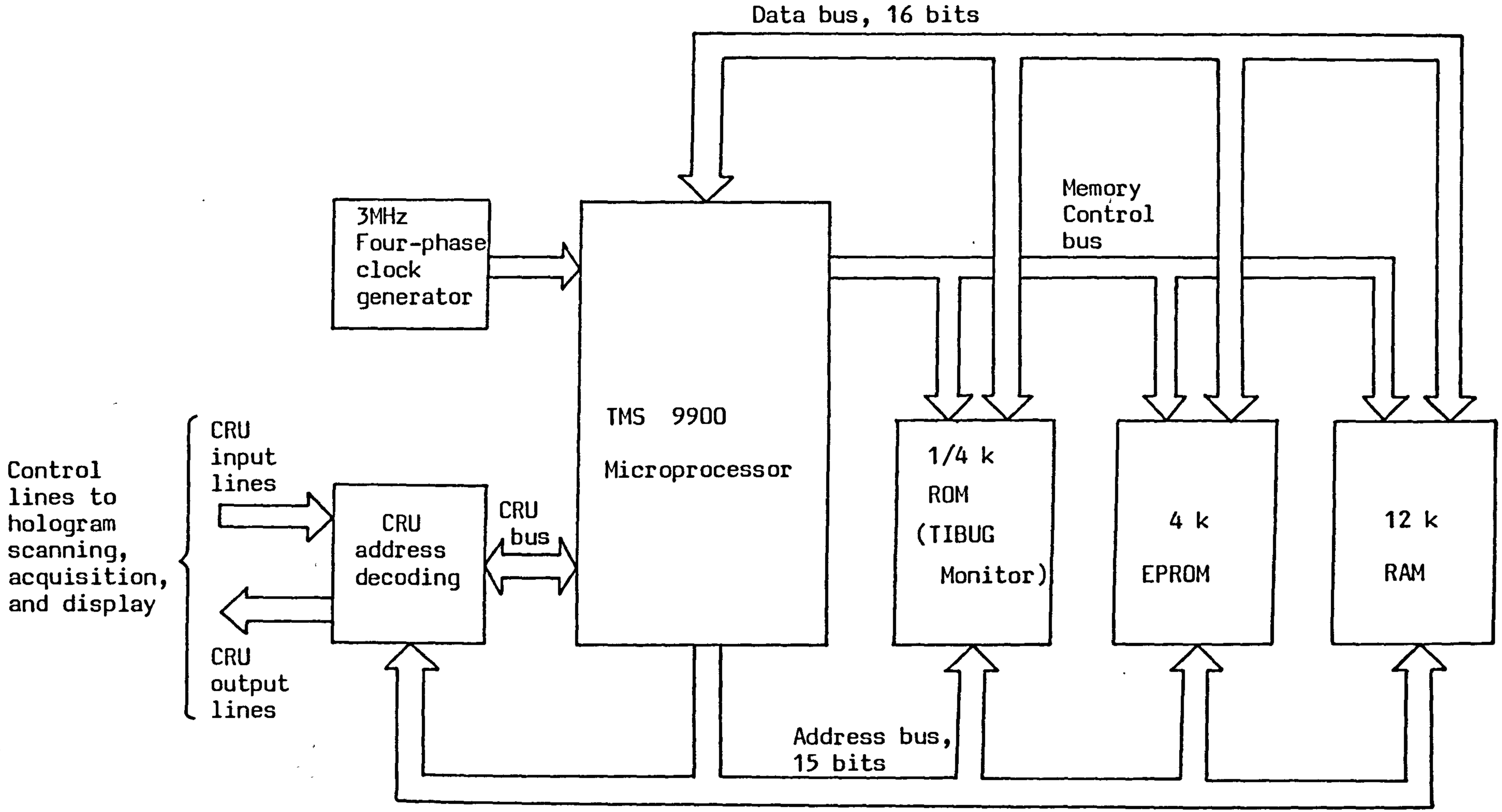


Fig. 6.4 : Functional diagram of the TMS 9900 microcomputer system

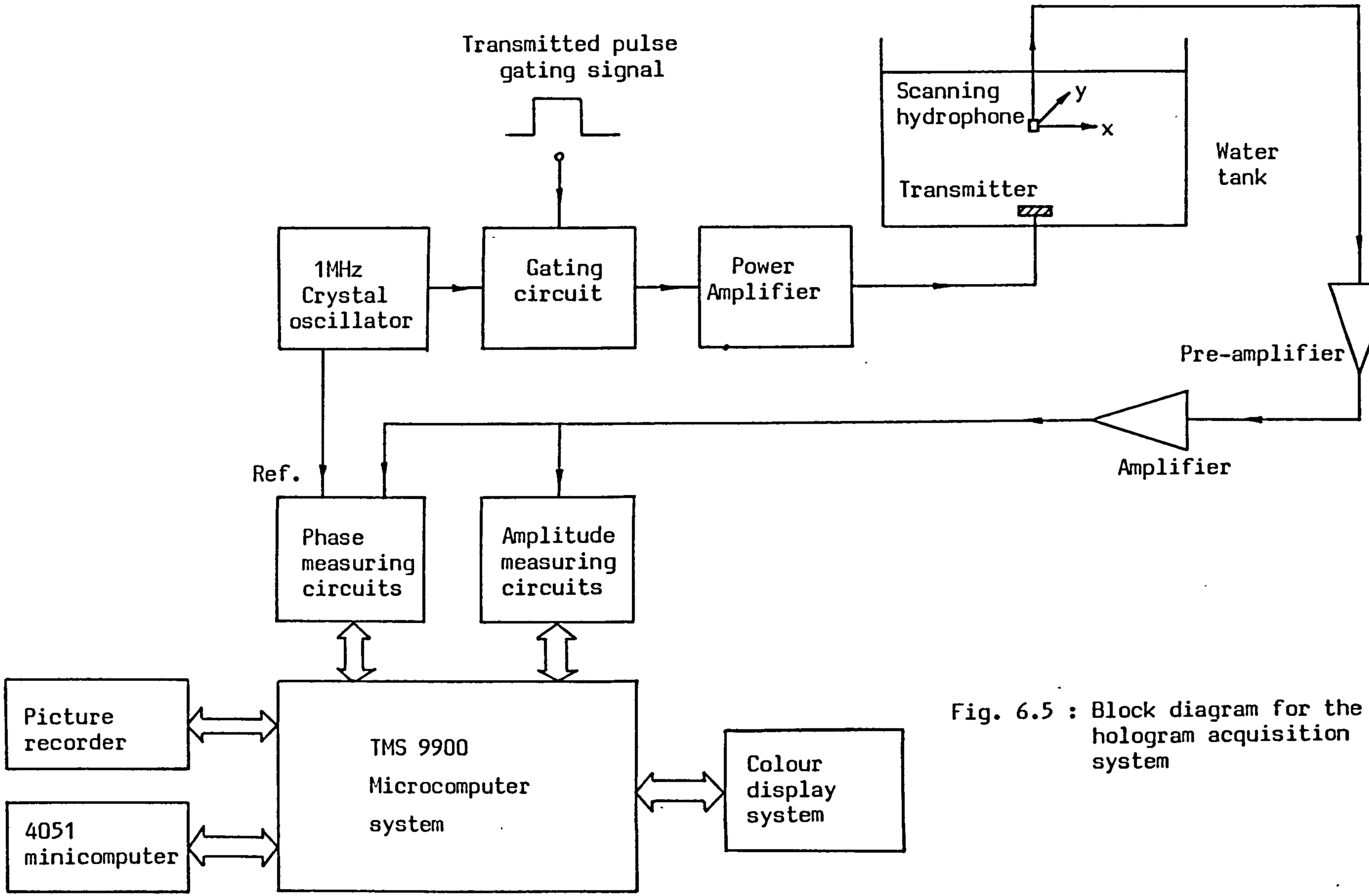


Fig. 6.5 : Block diagram for the hologram acquisition system

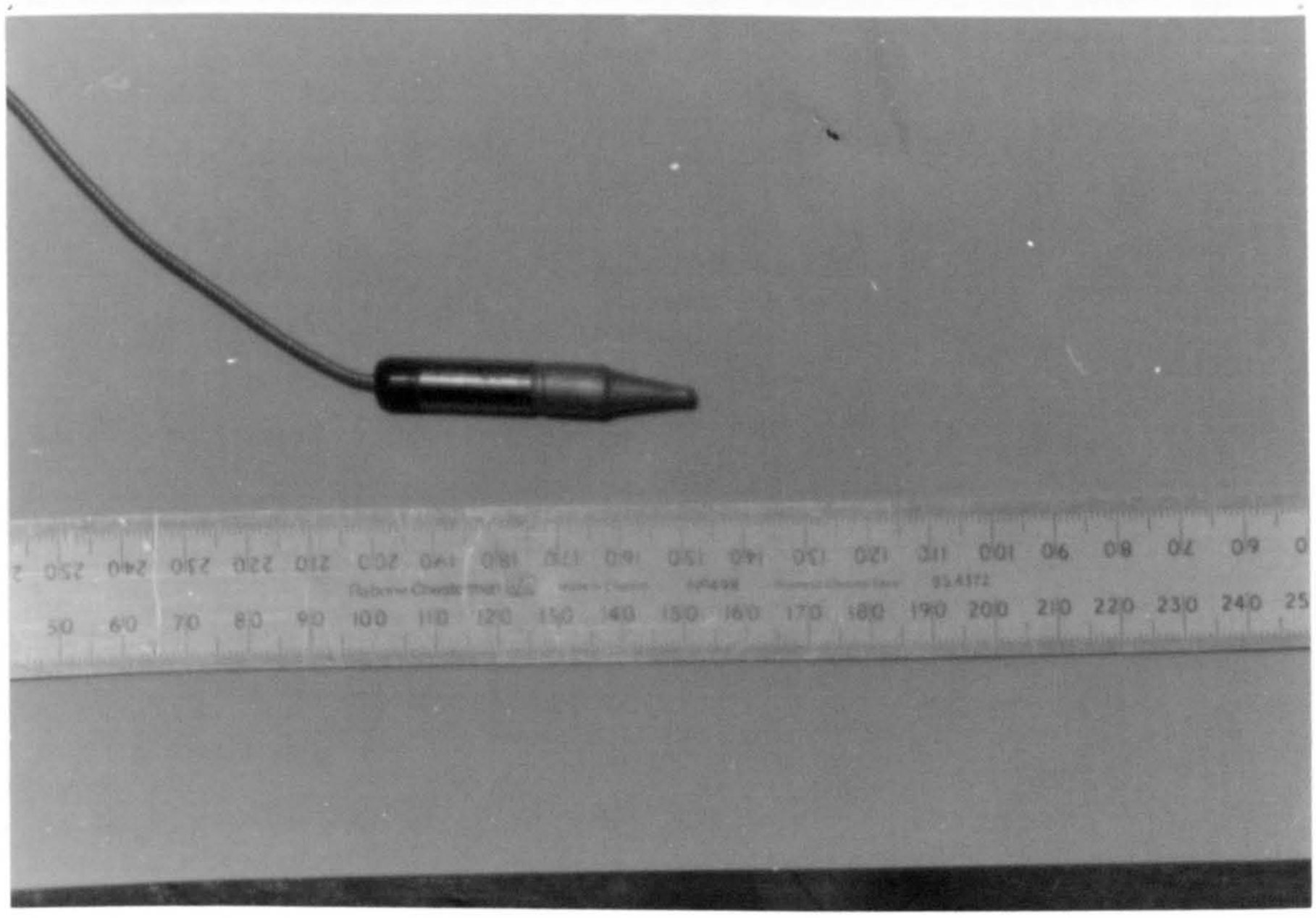

Fig. 6.6 : The hydrophone detector

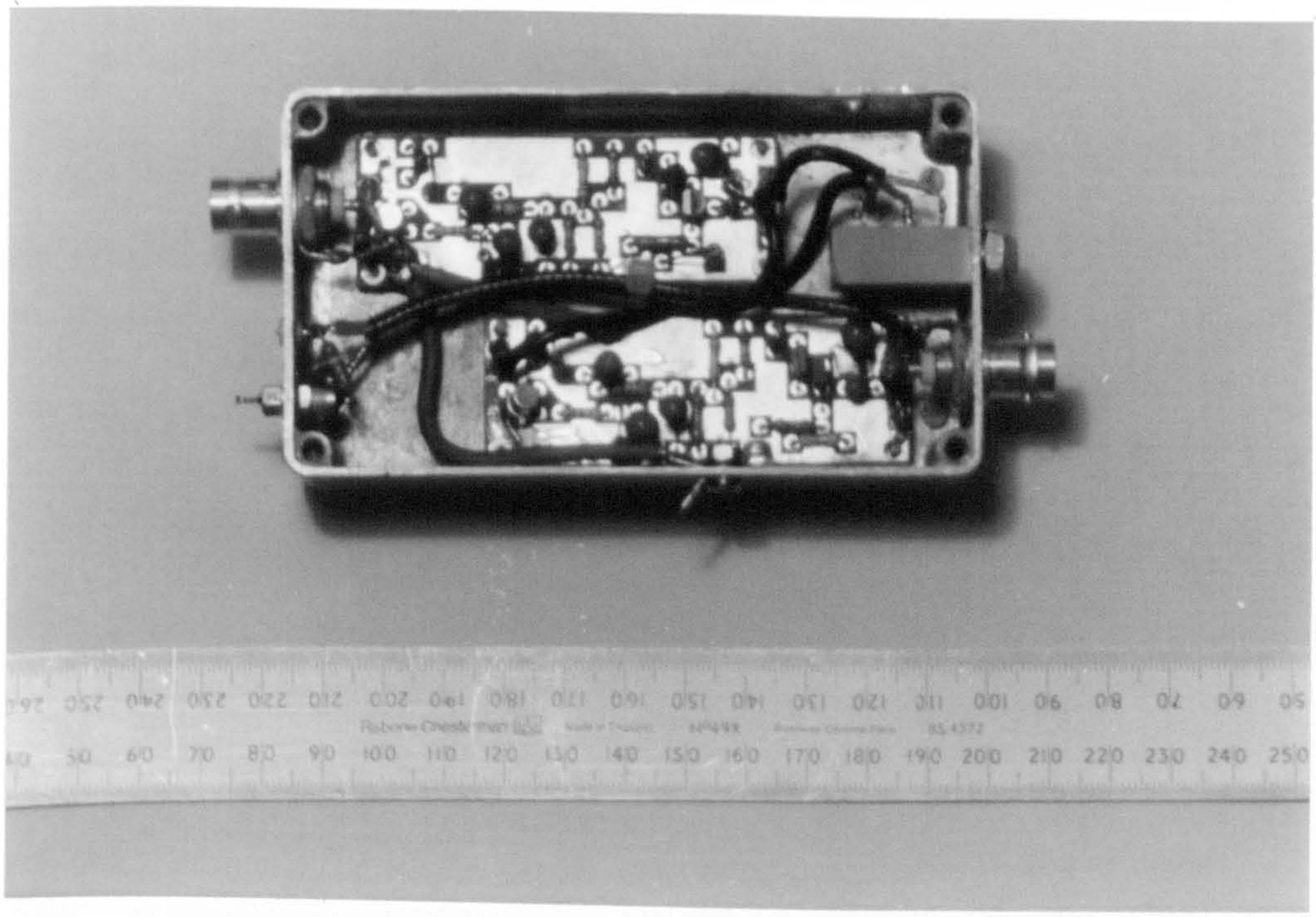

Fig. 6.7 : The low-noise pre-amplifier

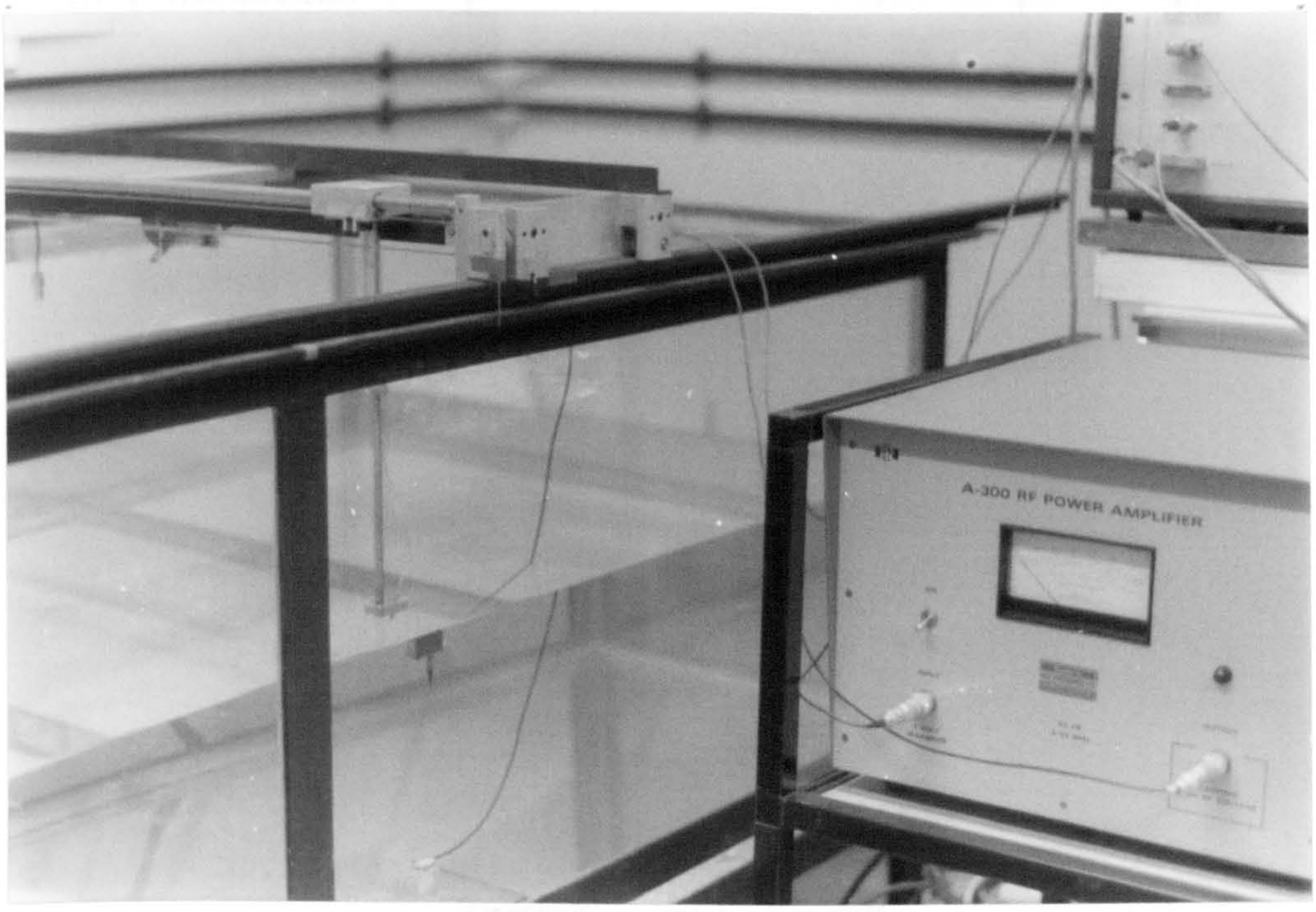


Fig. 6.8 : Experimental set-up and the mechanical scanning arrangement

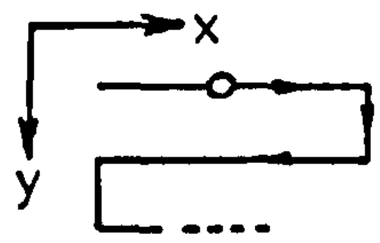


N : Number of scan points in both x and y directions

Δx : Increment in x direction

Δy : Increment in y direction

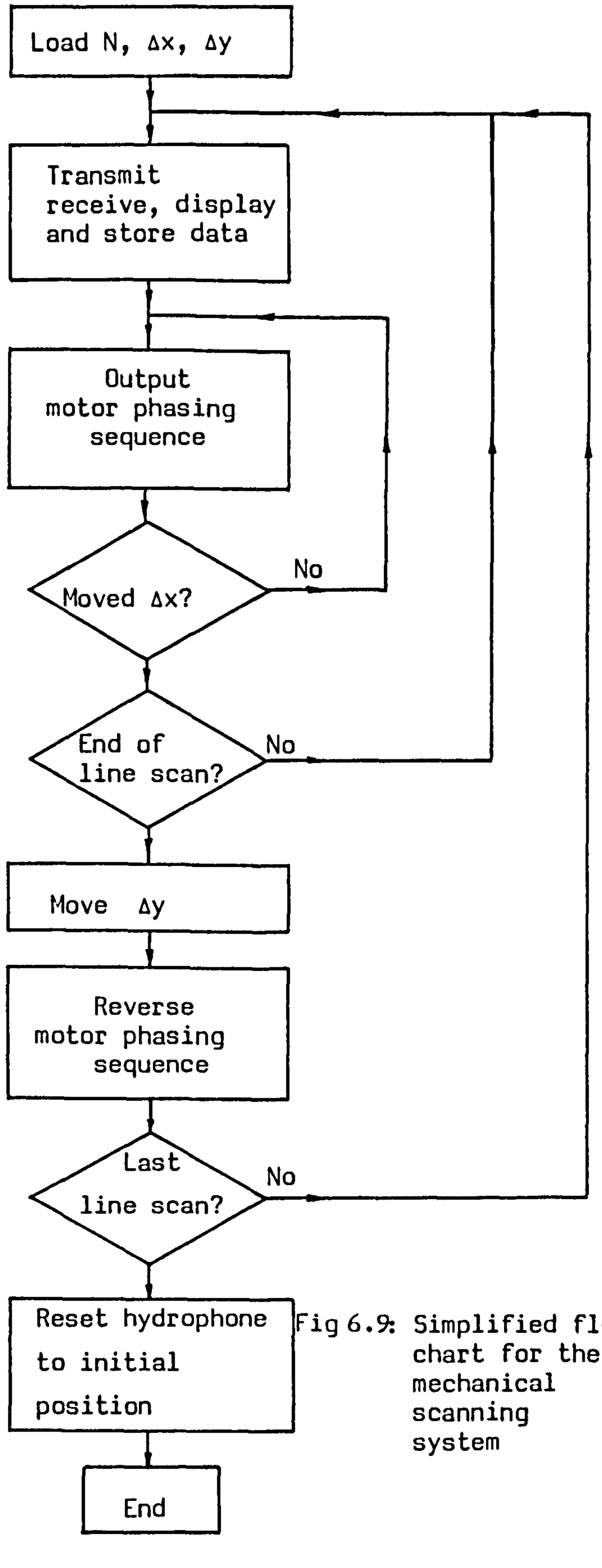


Fig 6.9: Simplified flow chart for the mechanical scanning system

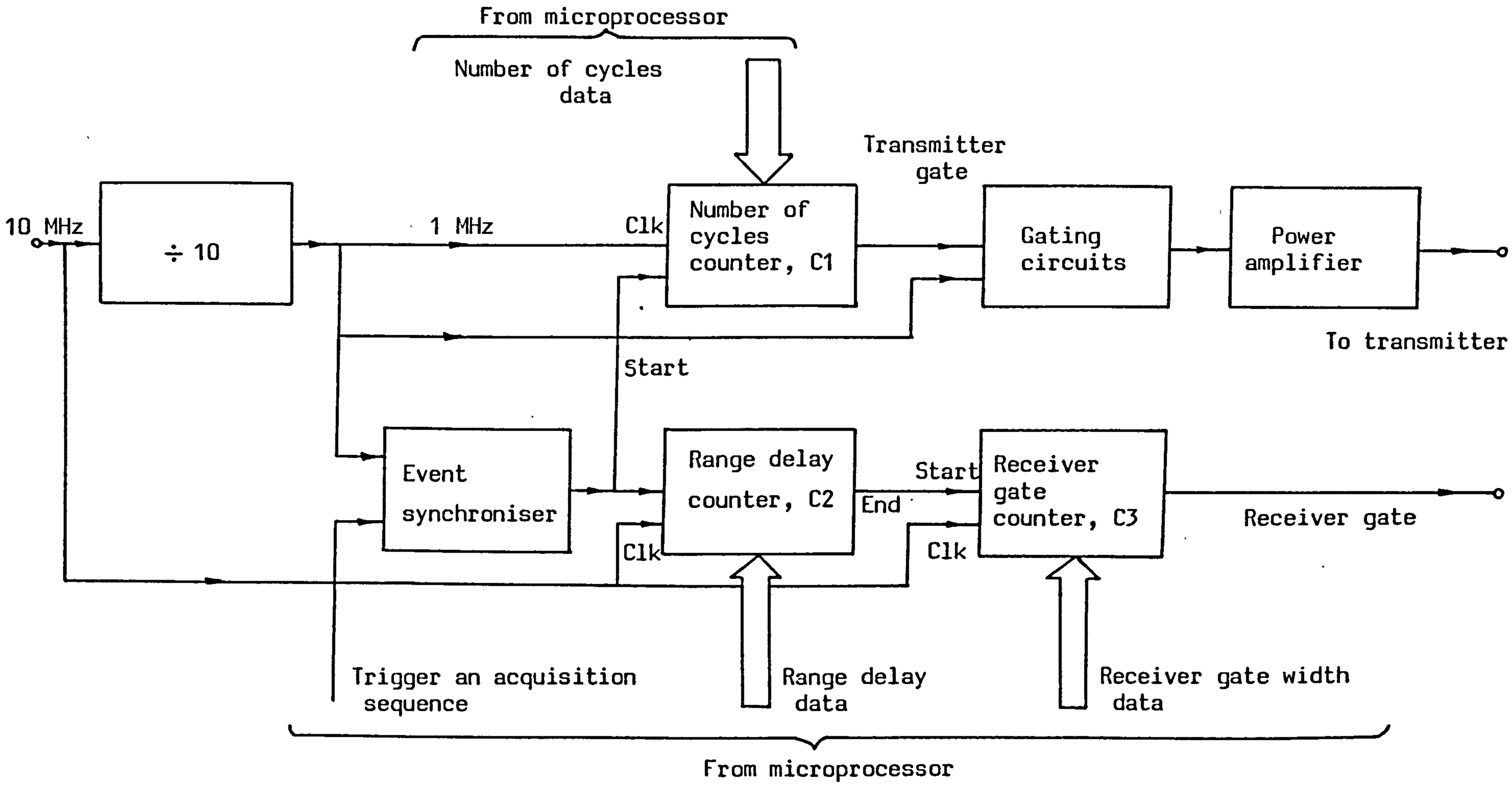


Fig. 6.10 : Transmission and range gating circuits

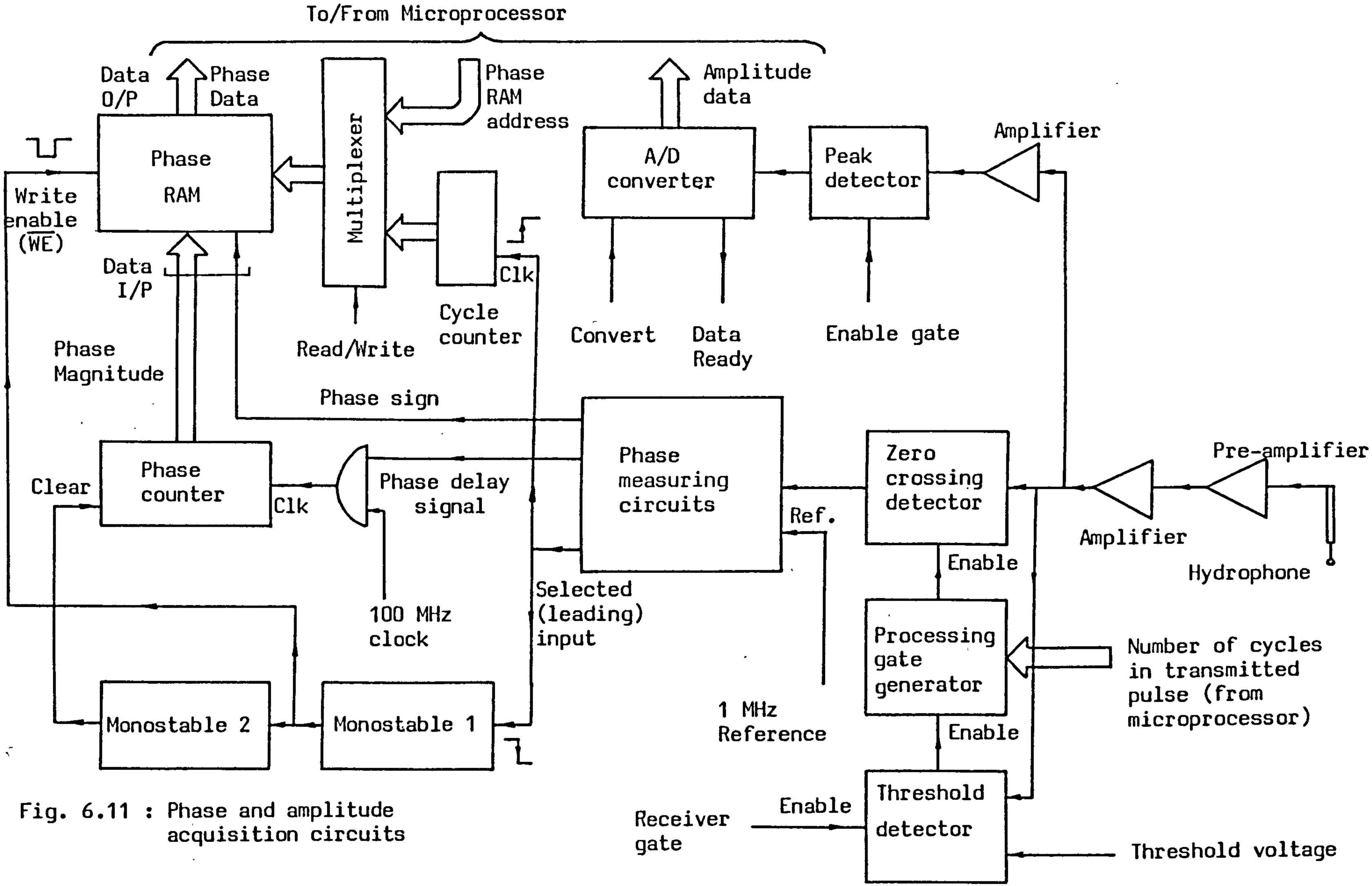


Fig. 6.11 : Phase and amplitude acquisition circuits

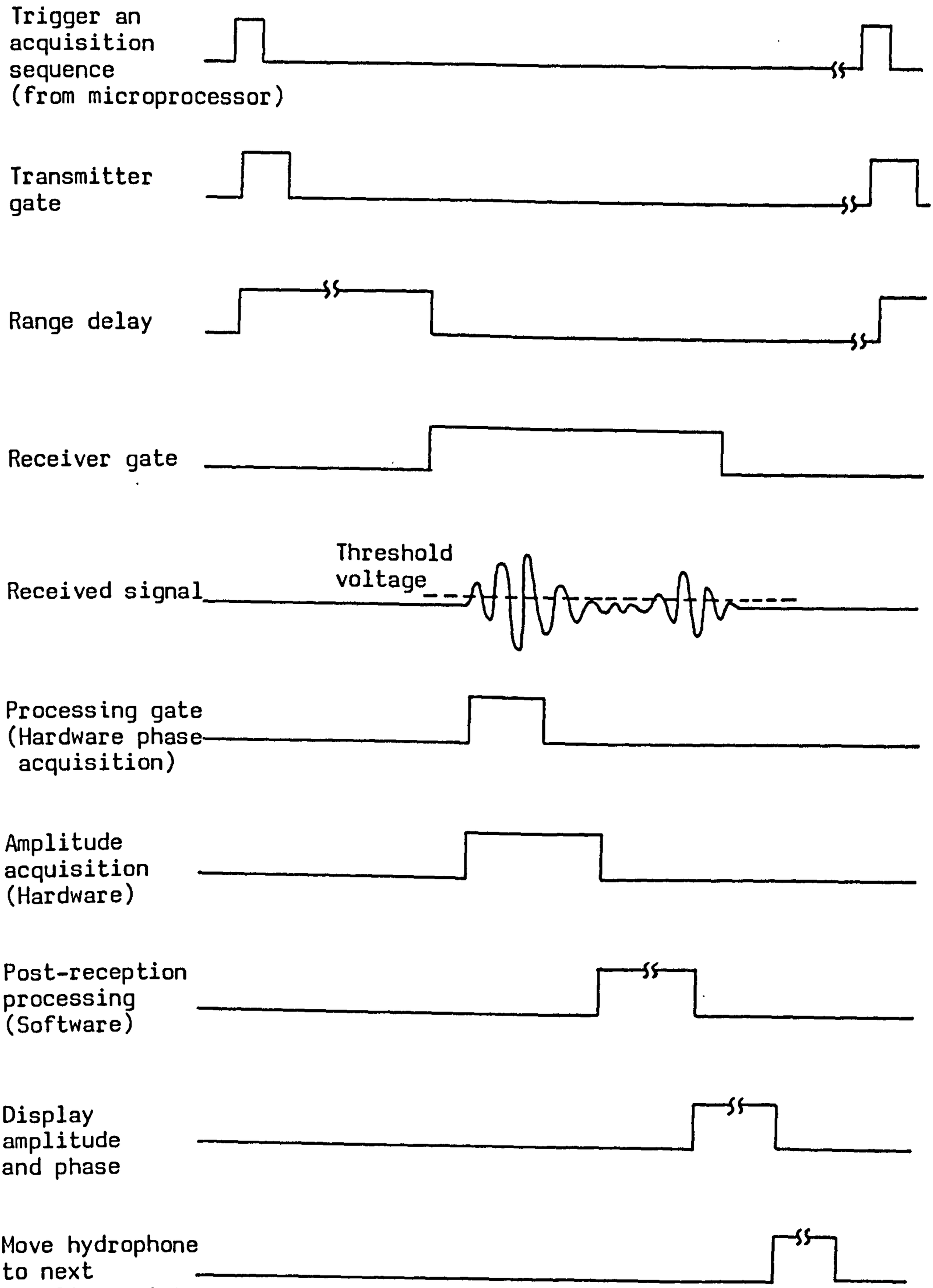


Fig. 6.12 : Sequence for hologram data acquisition

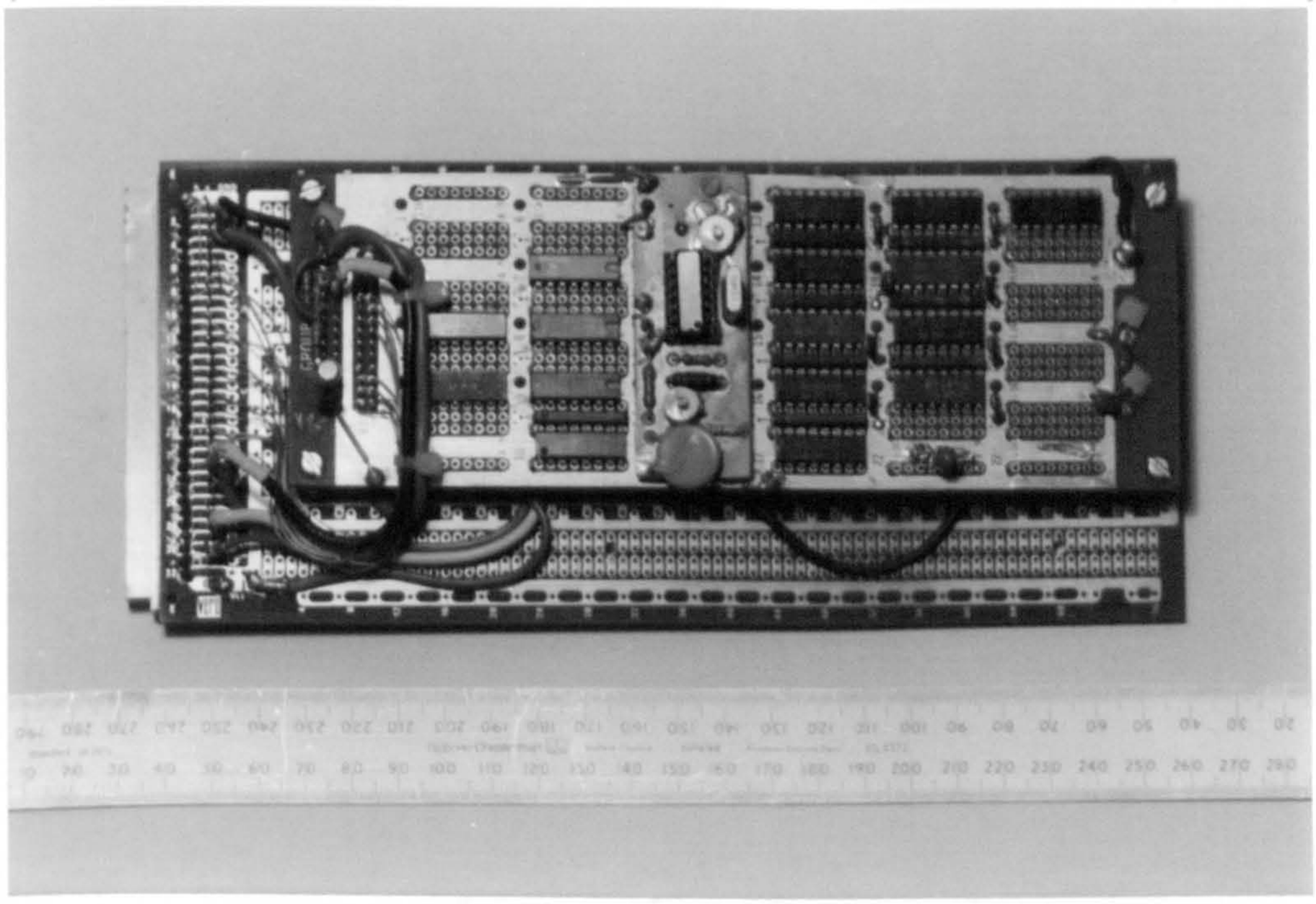

Fig. 6.13 : The ECL board

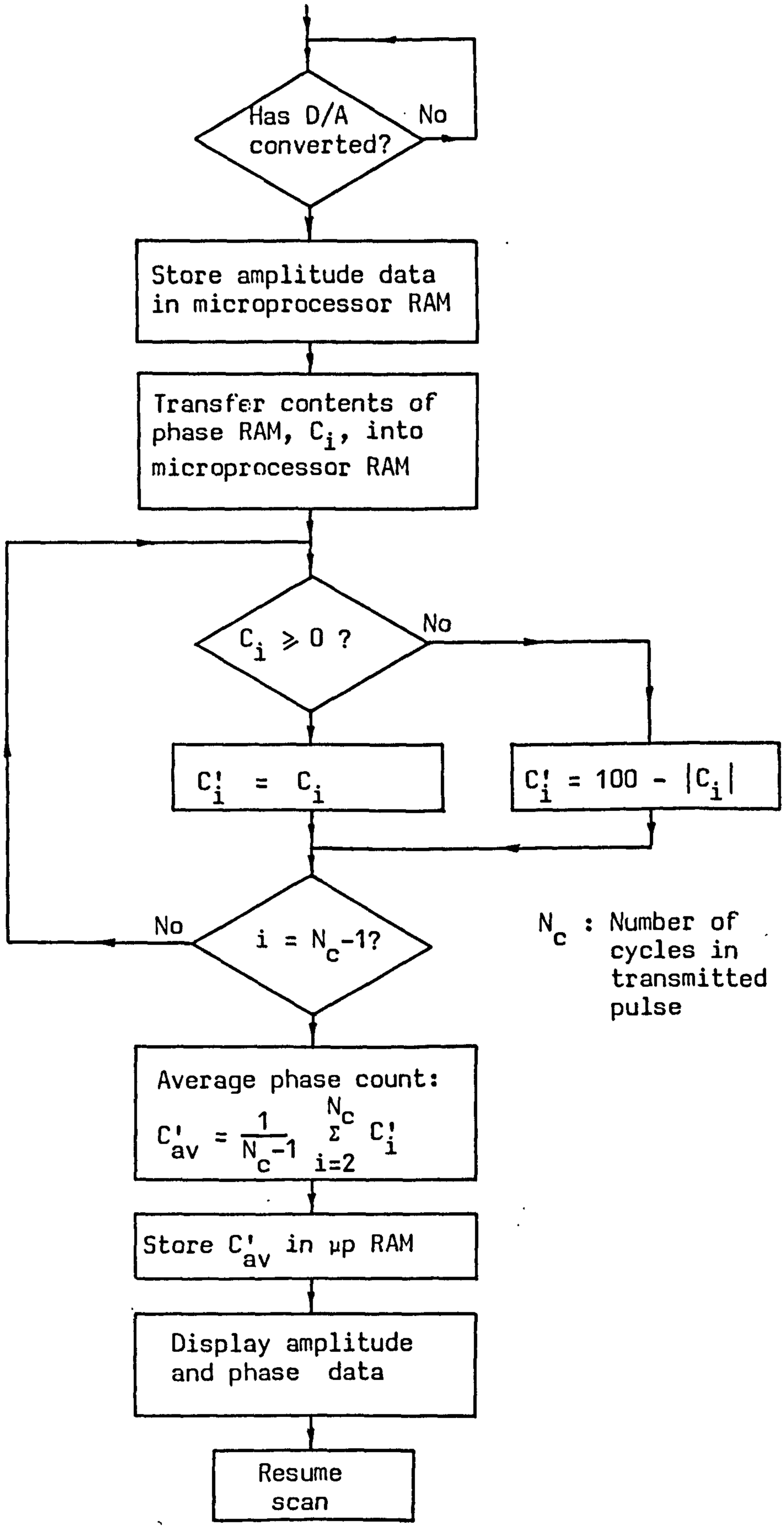


Fig. 6.14 : Flow chart for post-reception software processing

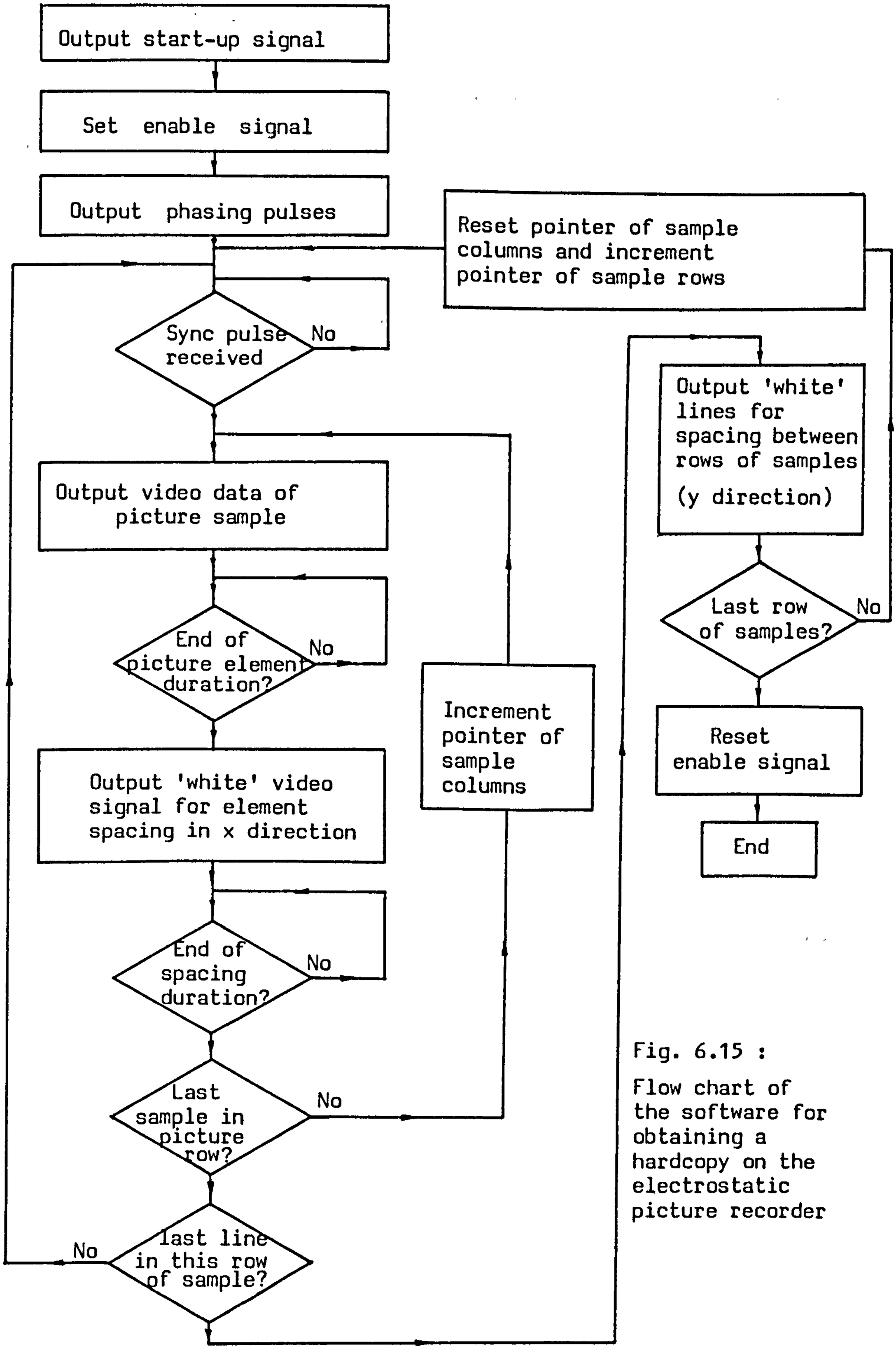


Fig. 6.15 :

Flow chart of the software for obtaining a hardcopy on the electrostatic picture recorder

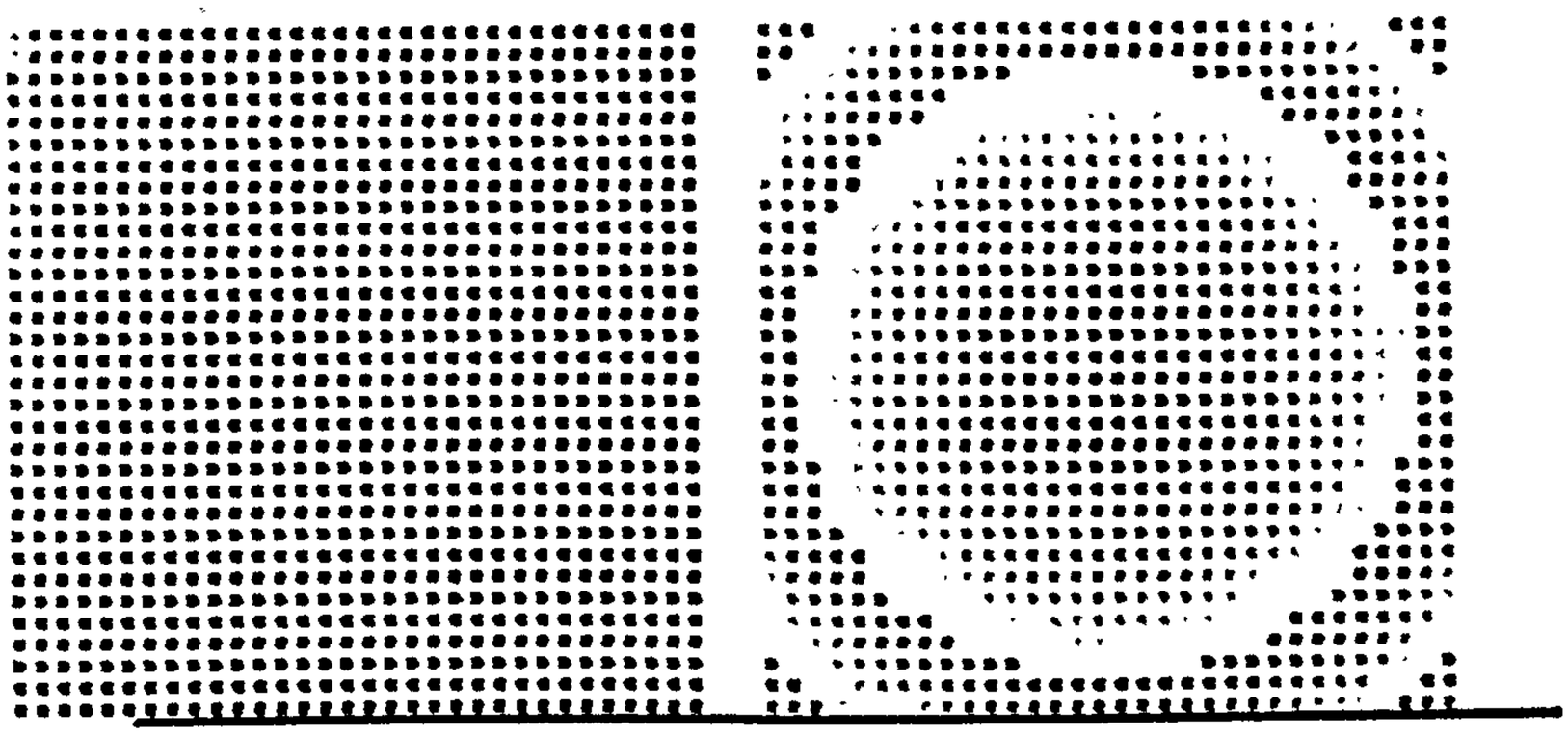

Amplitude Phase

Hologram : Number of samples = 32x32 Sample spacing=1λ

Object : 1 point on the hologram axis, range = 100λ

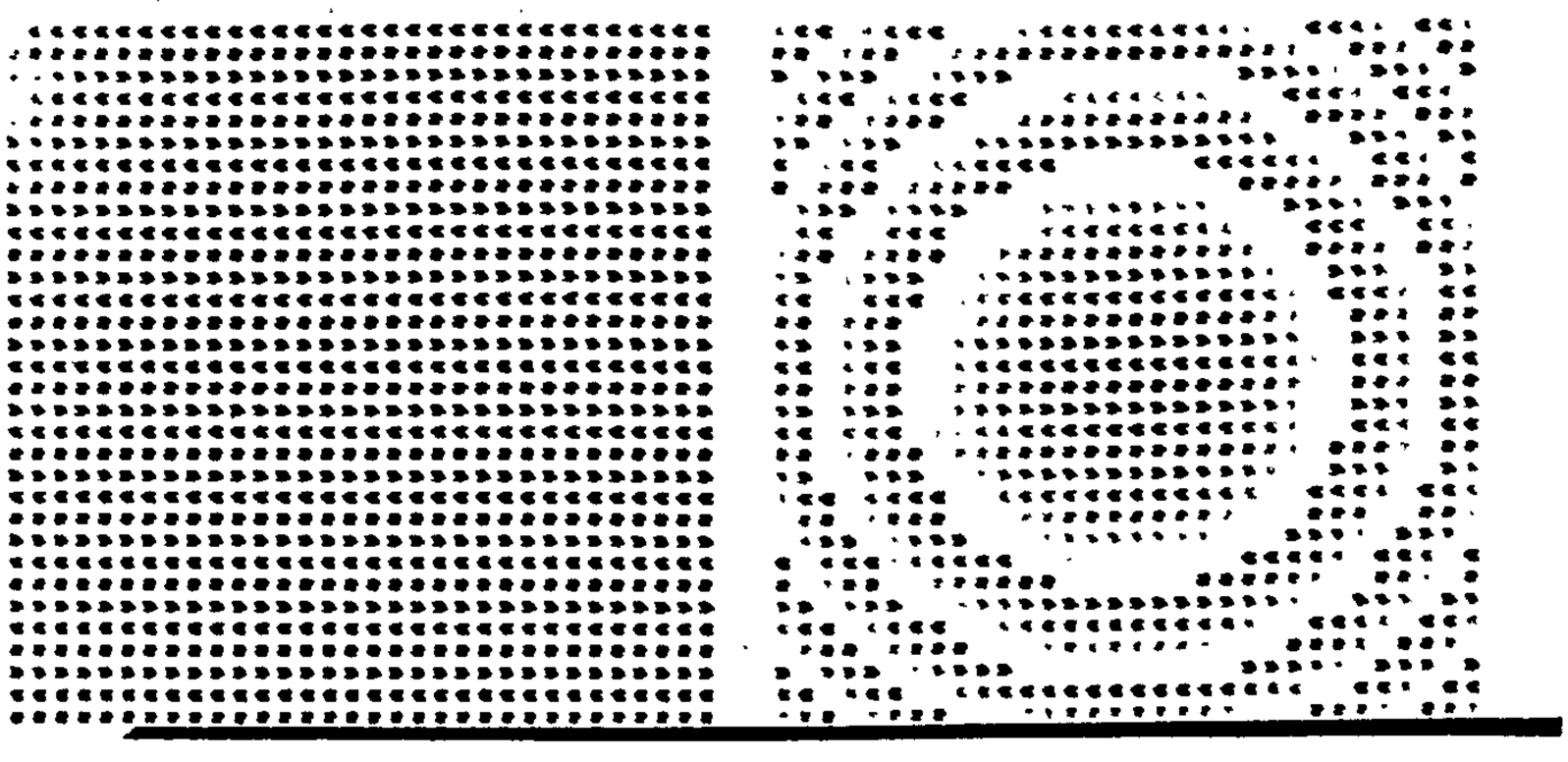

Amplitude Phase

Hologram : Number of samples = 32x32 Sample spacing=1λ

Object : 1 point on the hologram axis, range = 50λ

Fig 6.16: Samples of hardcopies obtained using the electrostatic picture recorder. The two examples are for simulated holograms

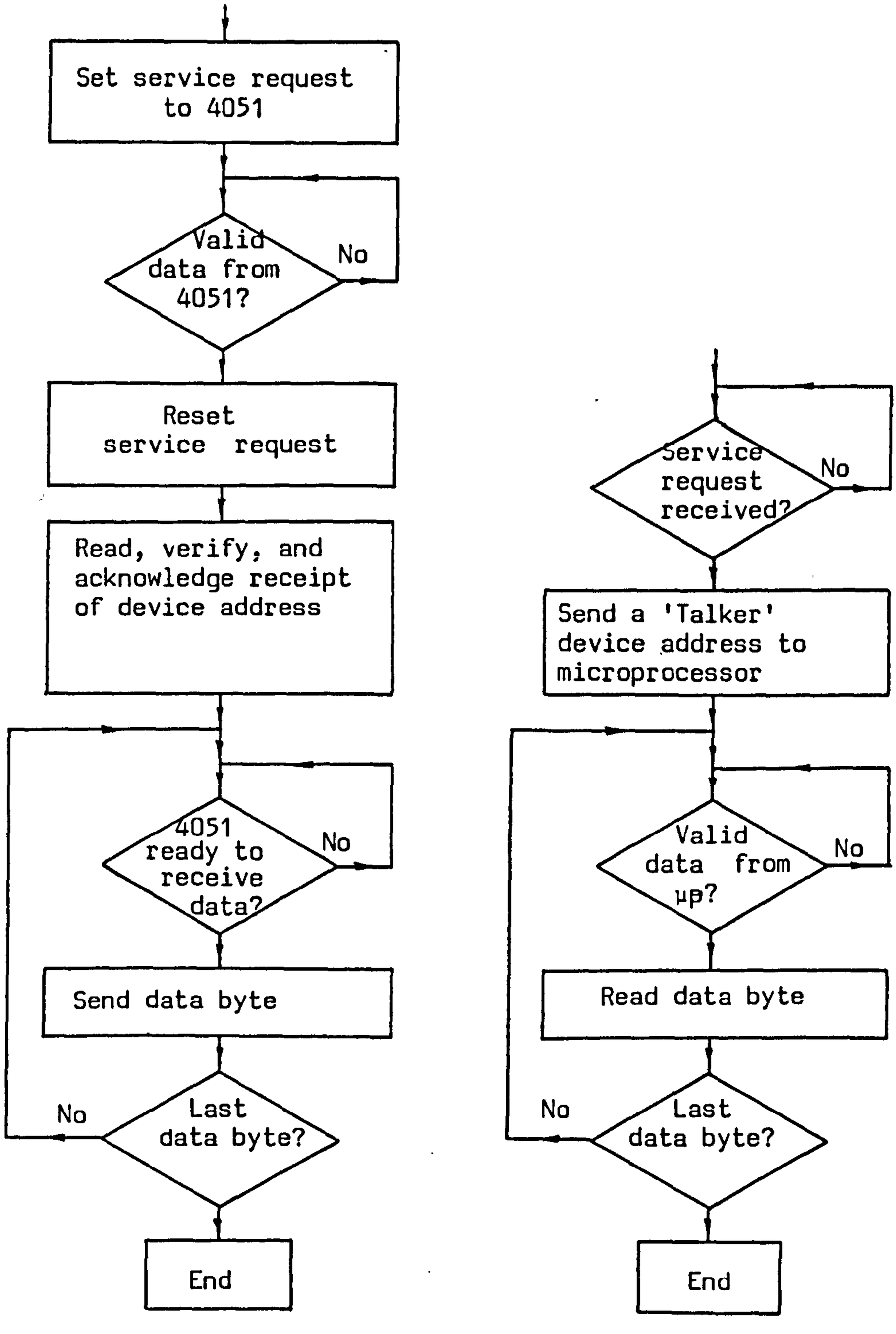


Microprocessor side 4051 side

Fig. 6.17 : Flow charts for the interface software between the microprocessor and the Tektronix 4051 minicomputer

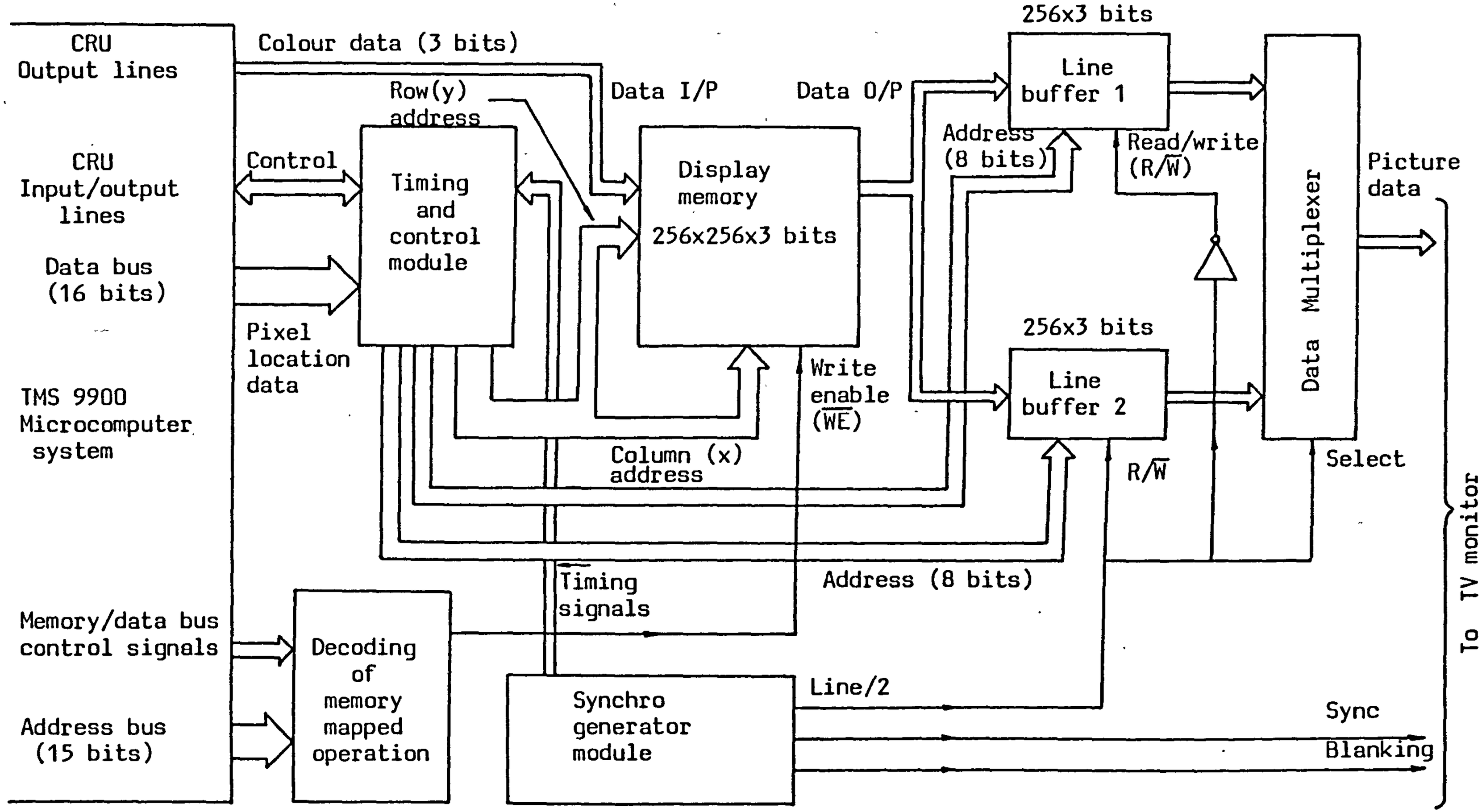


Fig. 6.18 : Block diagram for the colour display system

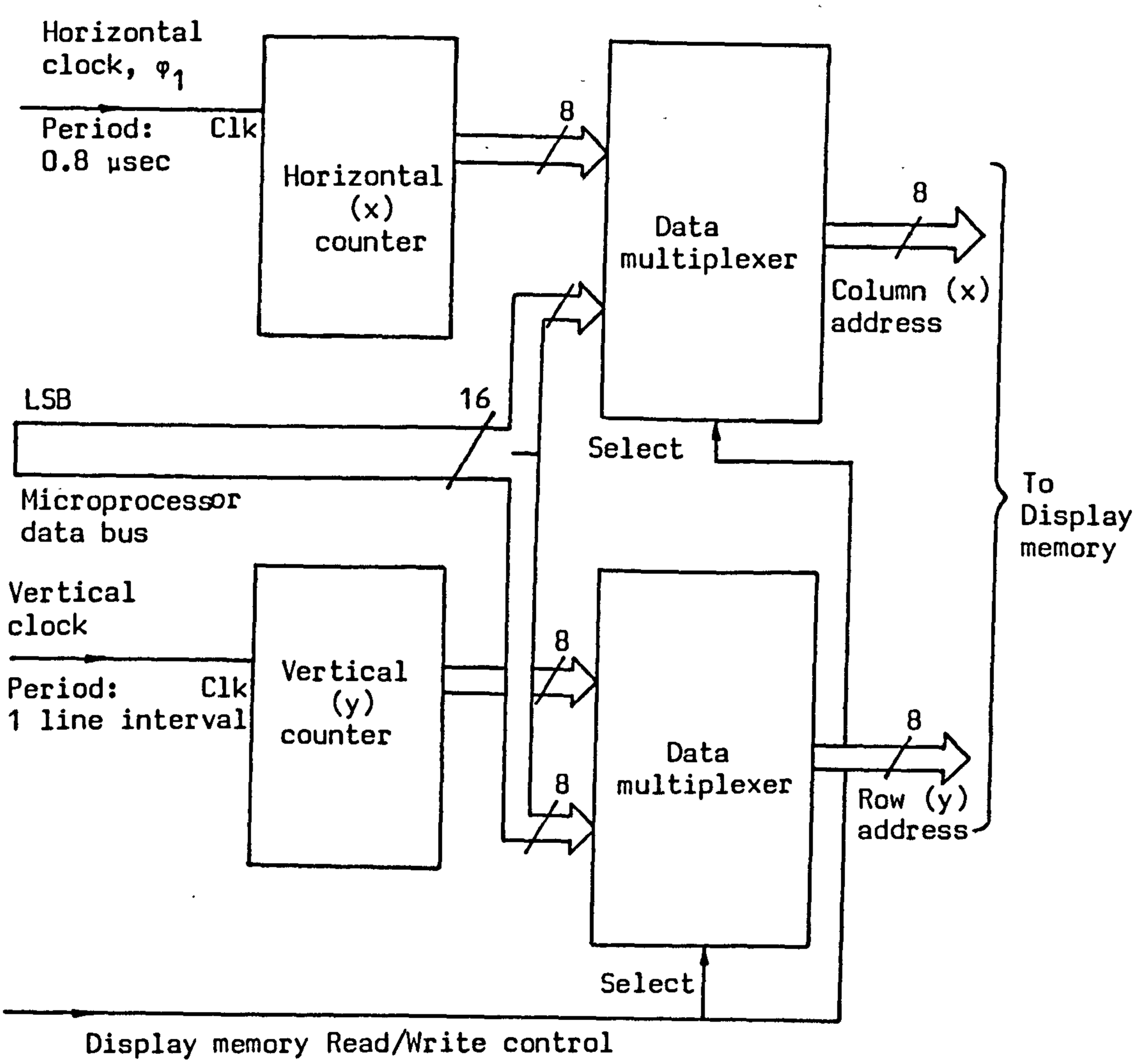


Fig. 6.19 : Derivation of the display memory address

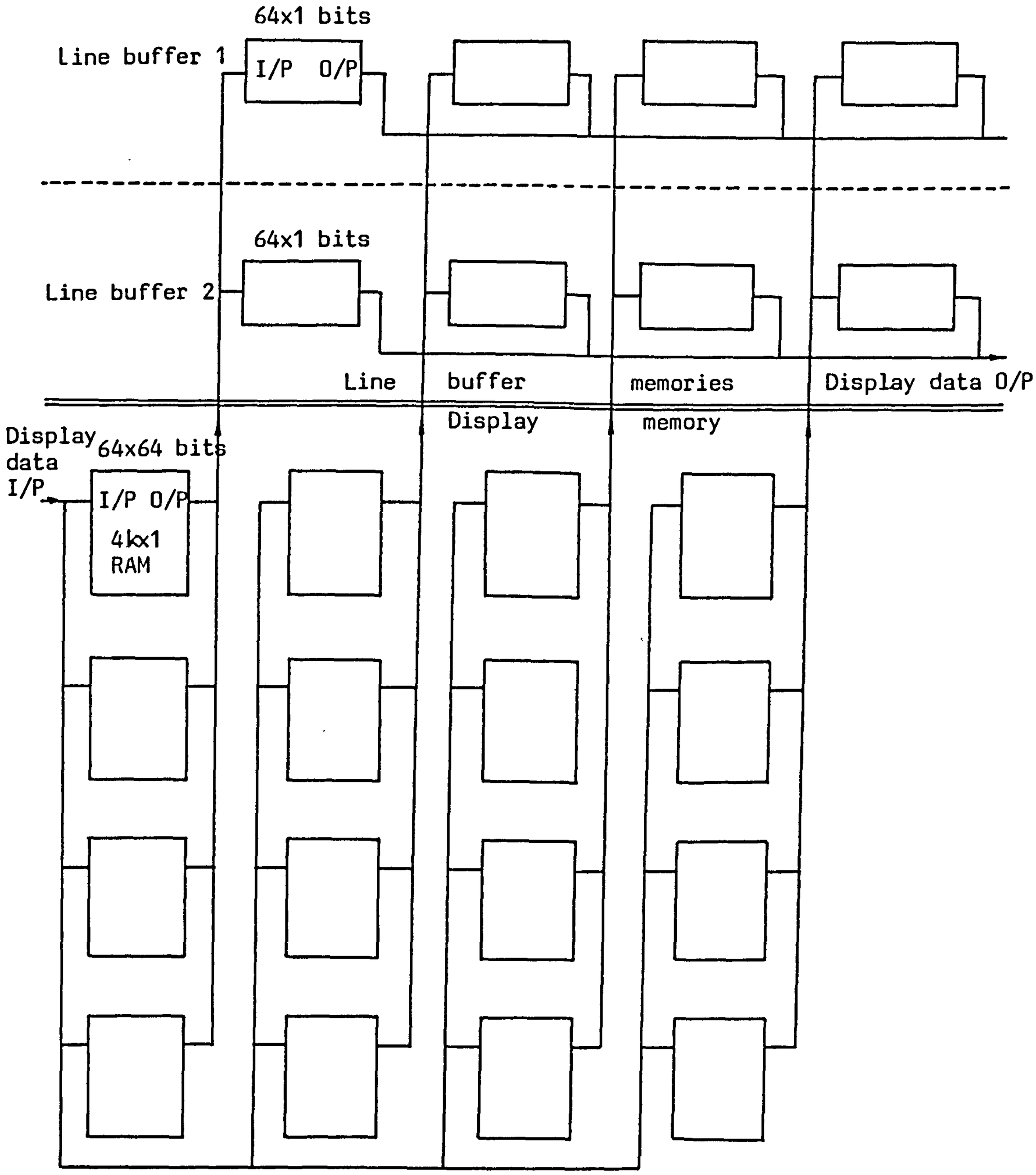


Fig. 6.20 : Layout of the arrangement used for reducing the speed requirements on the display memory by using two line buffers each made up of 4 separate RAMs.

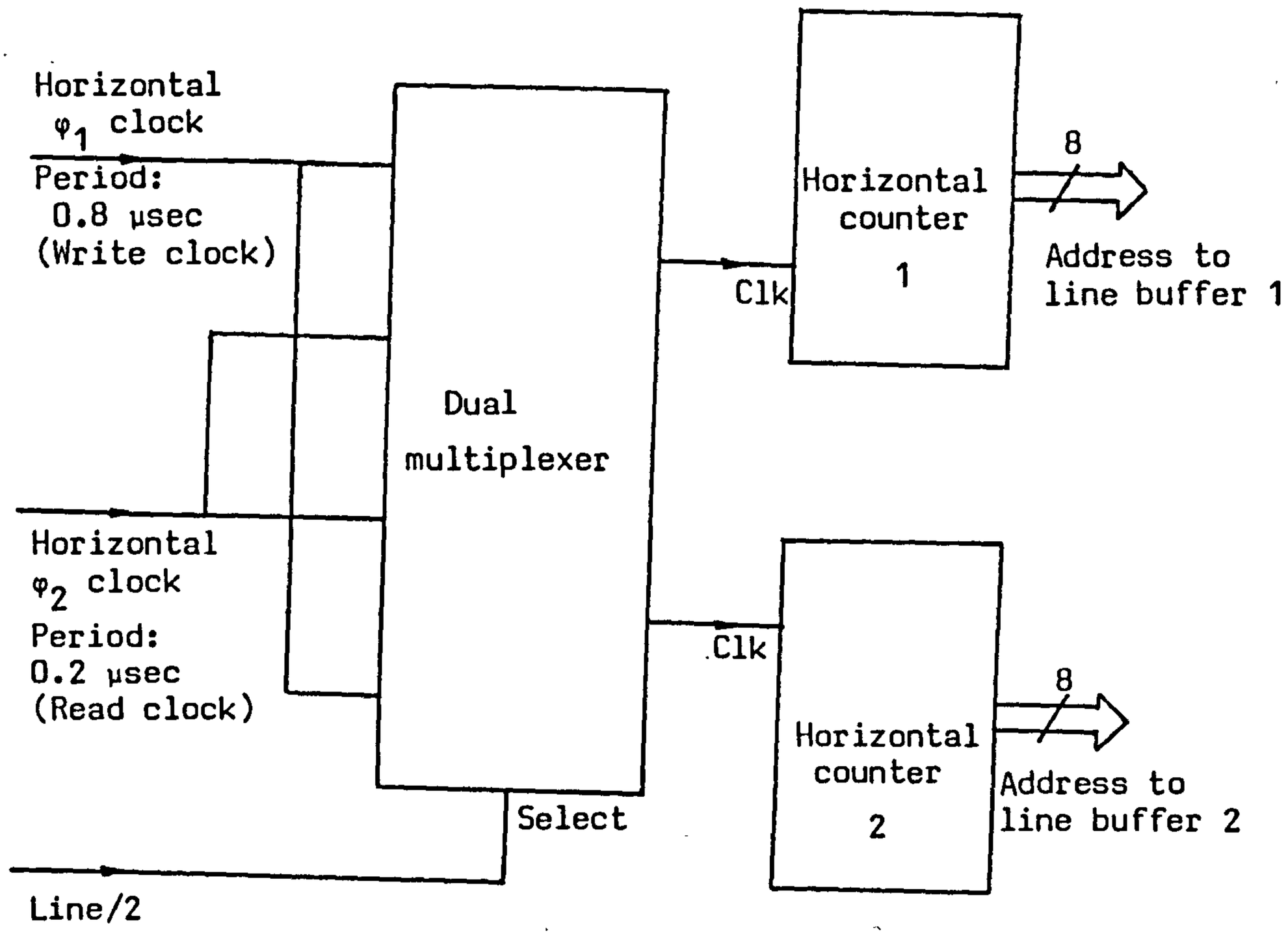


Fig. 6.21 : Derivation of the Read/Write addresses for the two line buffer memories

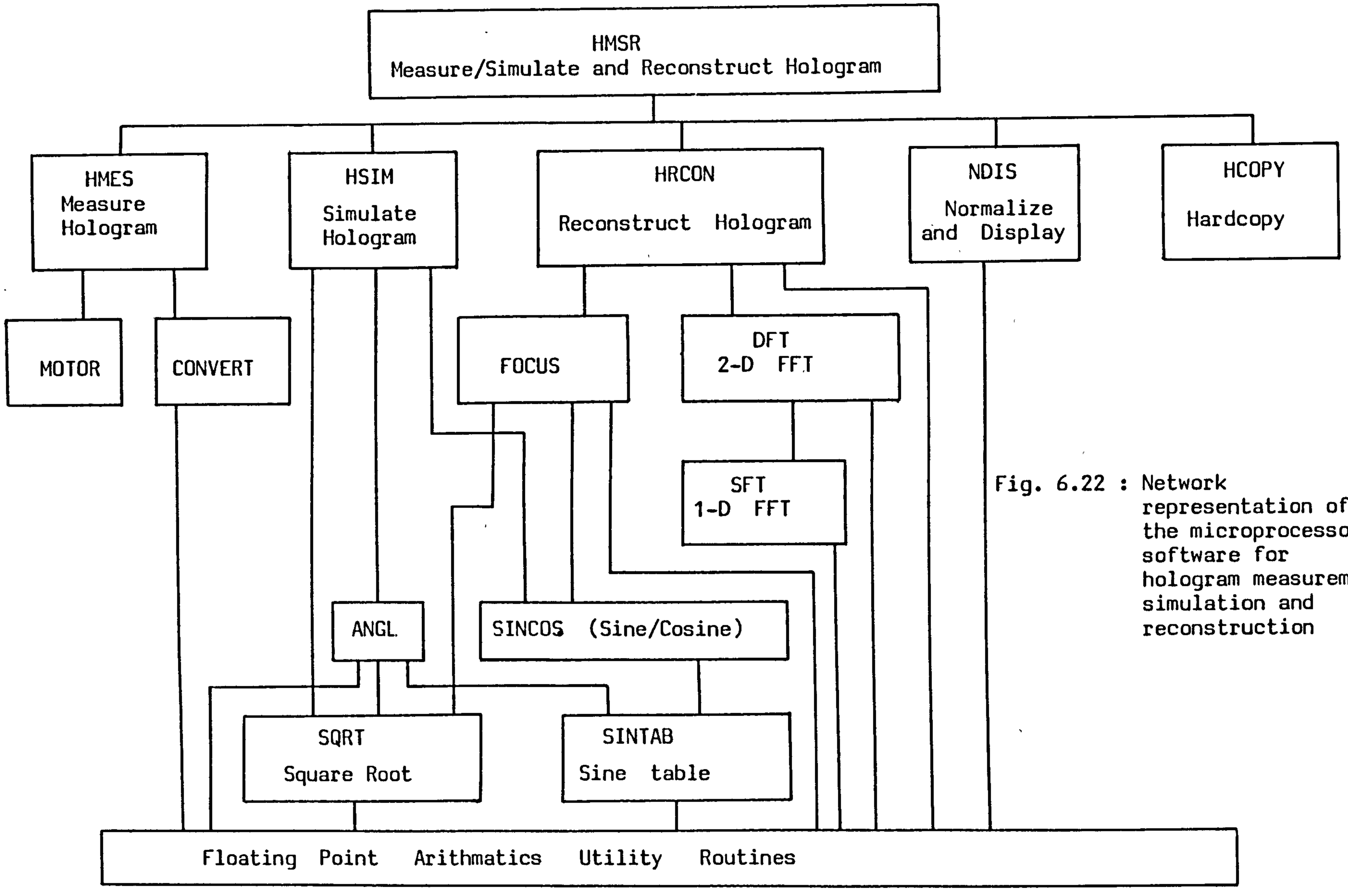


Fig. 6.22 : Network representation of the microprocessor software for hologram measurement/ simulation and reconstruction

N: Size of data matrix

T: Type of transform (forward /inverse)

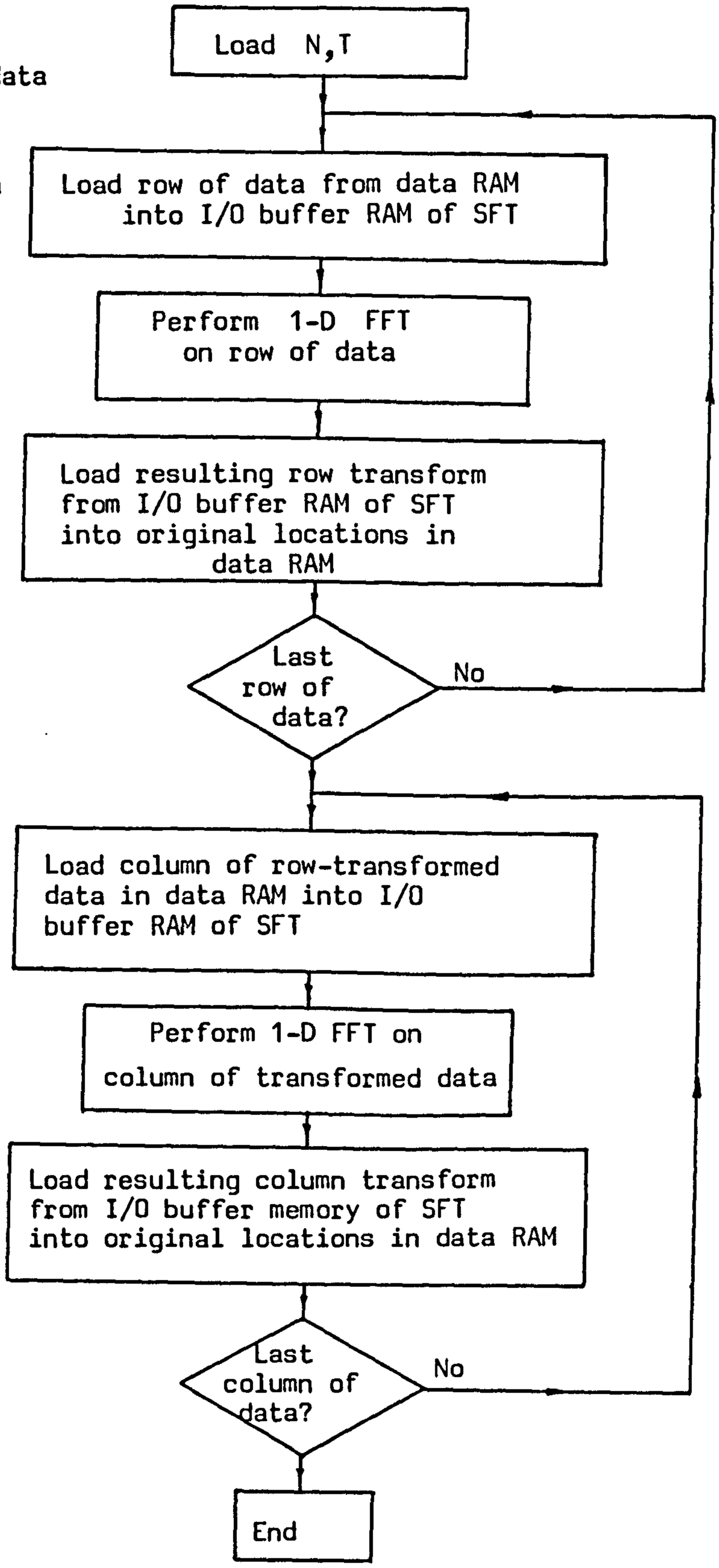


Fig. 6.23 : Flow chart for the 2-D FFT routine (DFT)

# Figures for Chapter 7

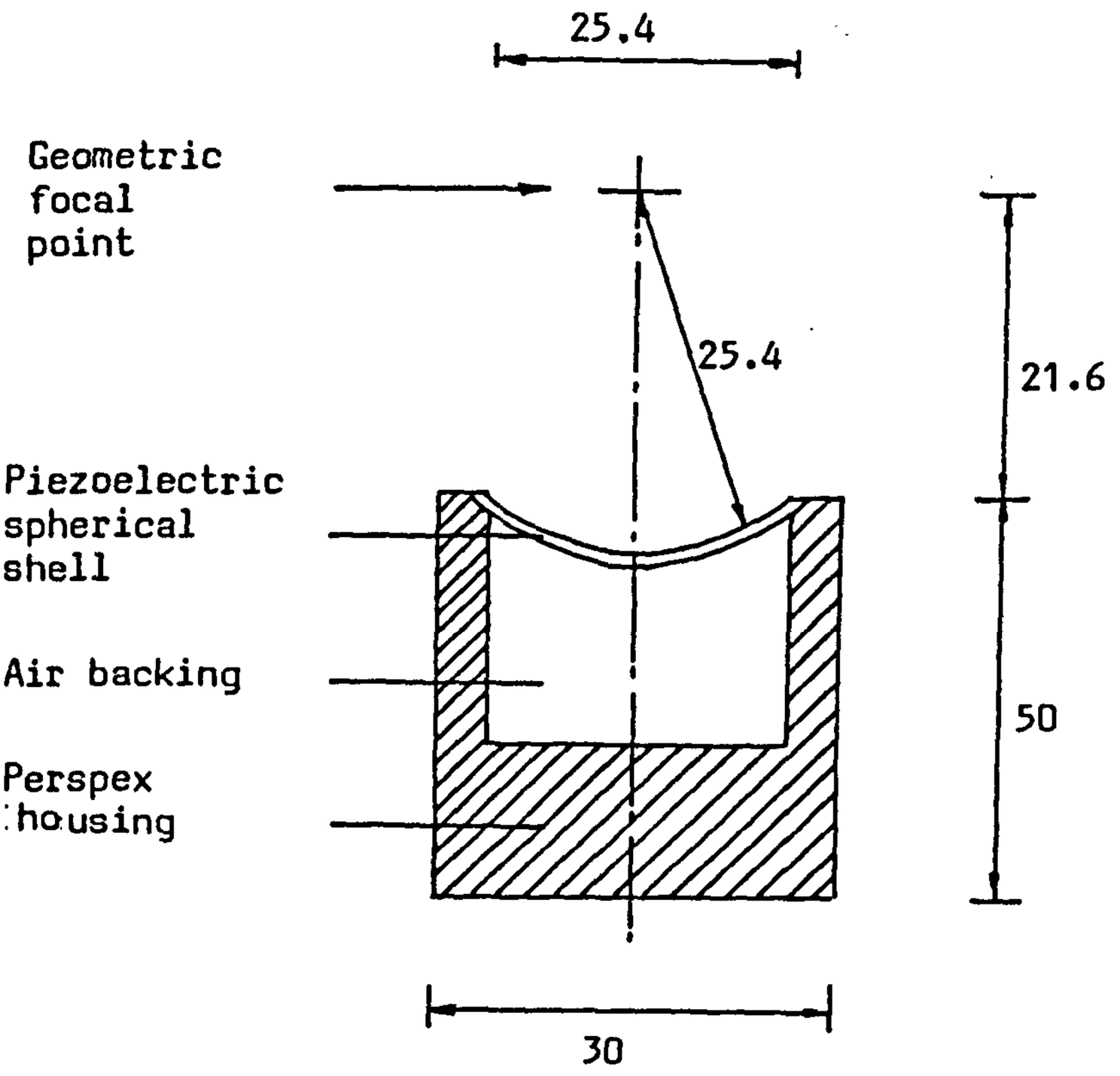


Fig. 7.1 : Construction of the focused transducer
(Dimensions in mm)

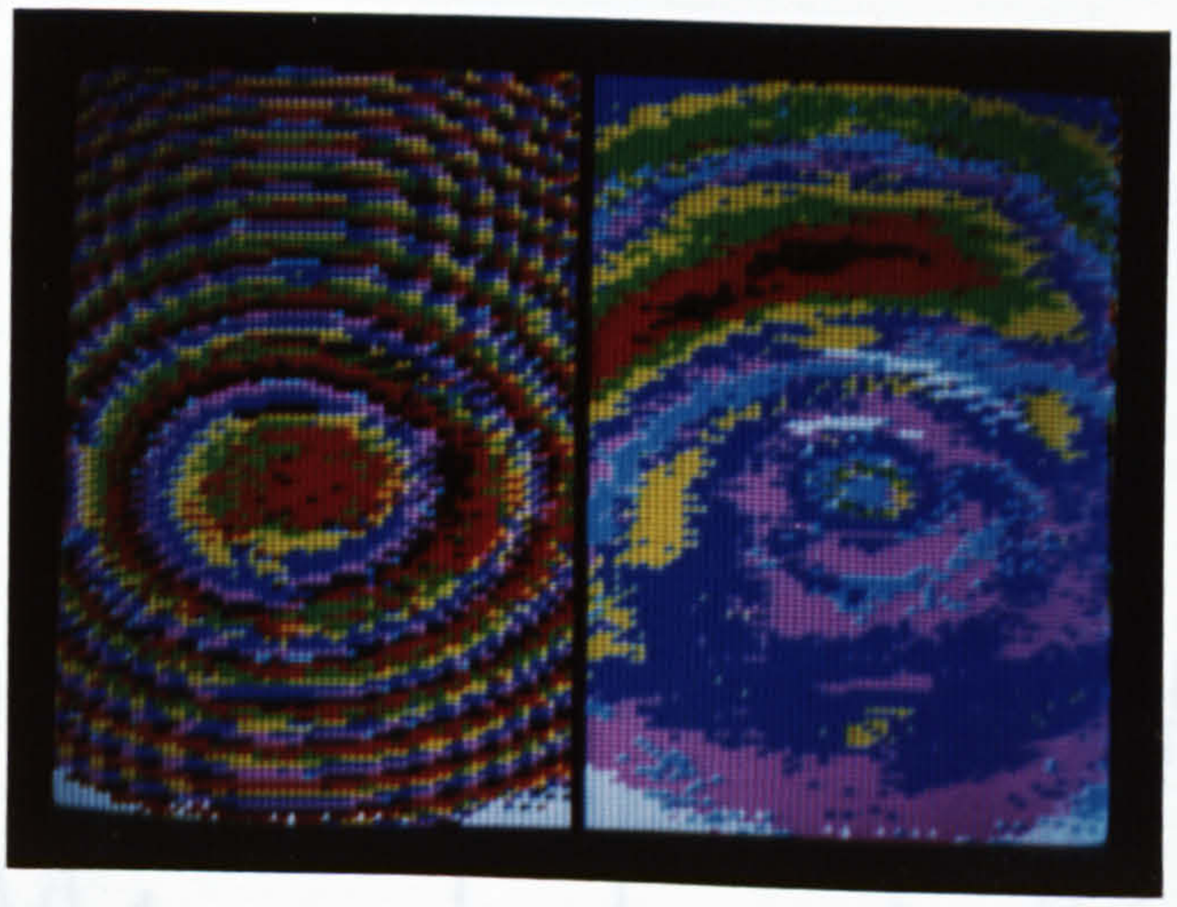

. Phase  . Amplitude

Hologram : $\Delta=0.5\lambda$, Number of samples : 64 and 128 in x and y directions resepctively

Object : 1-point located at a distance of $60\lambda$ from the hologram

Fig. 7.2 : Effect of relative tilt between the hologram and object planes on a measured two-dimensional hologram

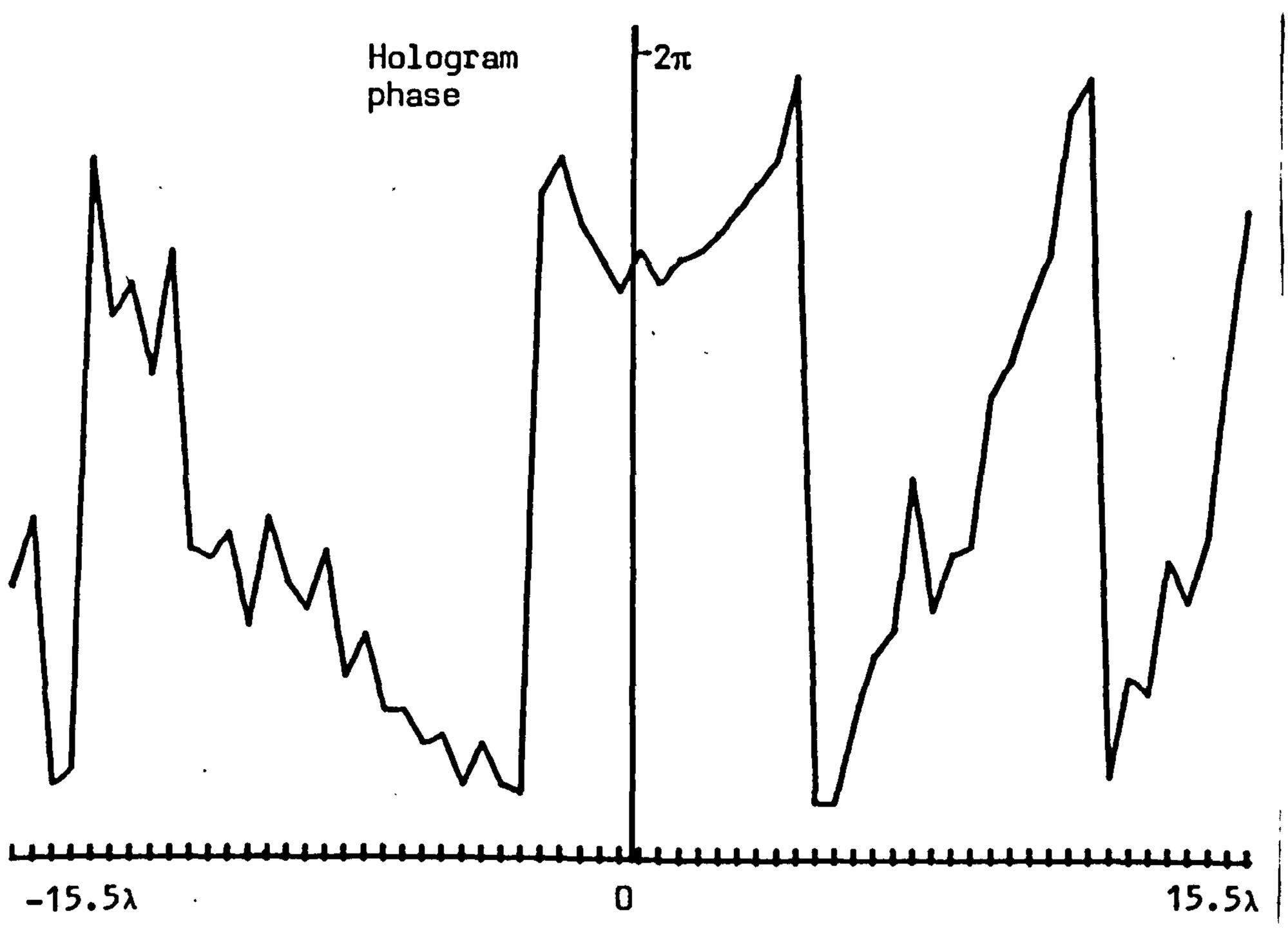


Hologram :Δ=1.11λ, 32 samples

Object : 1-point located at a distance of 120λ from the hologram

Fig. 7.3 : Effect of relative tilt between the hologram and object planes on the phase function of a measured line hologram.

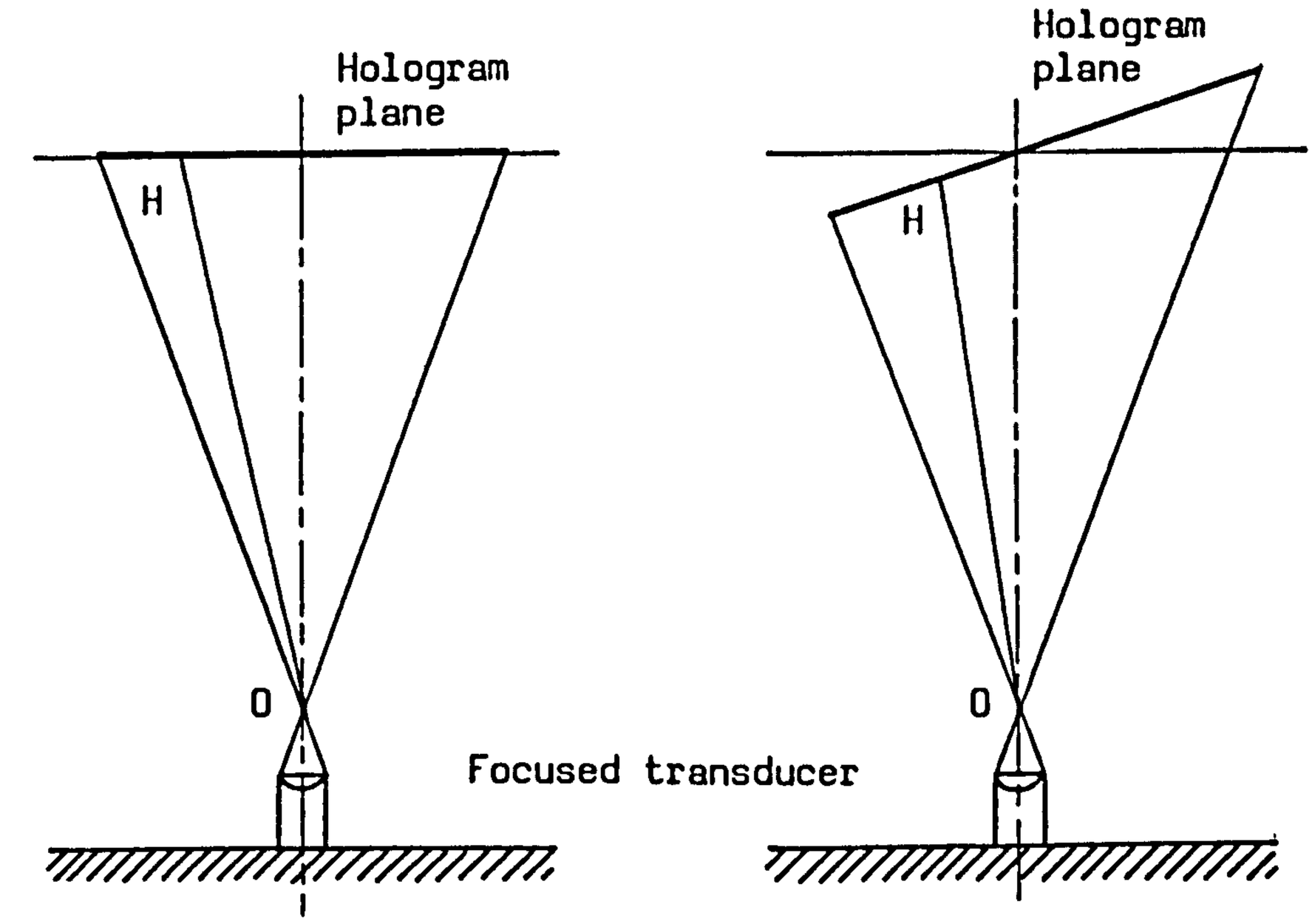


a. Proper Alignment

b. Exaggerated tilt in the hologram plane

Fig. 7.4 : Alignment between the hologram plane and the base of the acoustic transducer

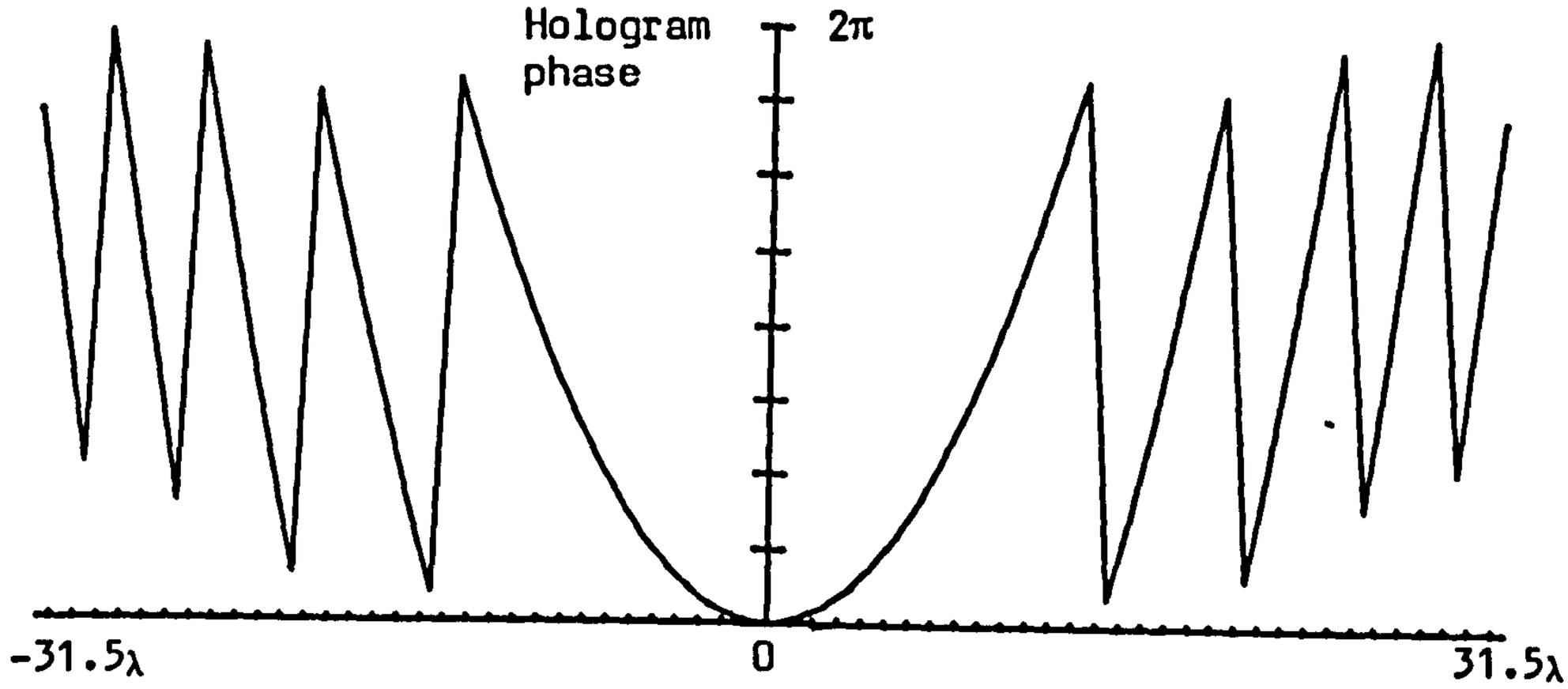


a. Tilt angle : $0^o$

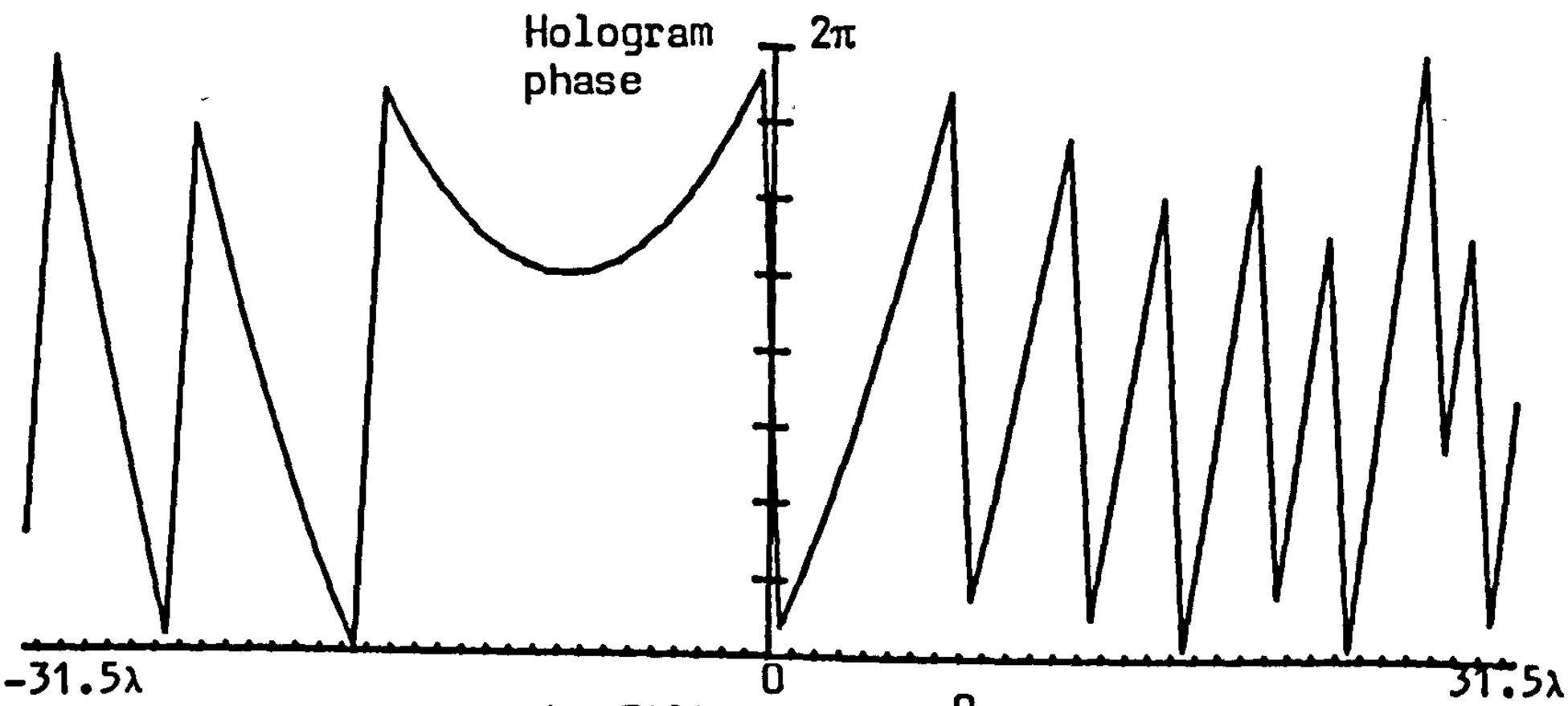


b. Tilt angle : $5^o$

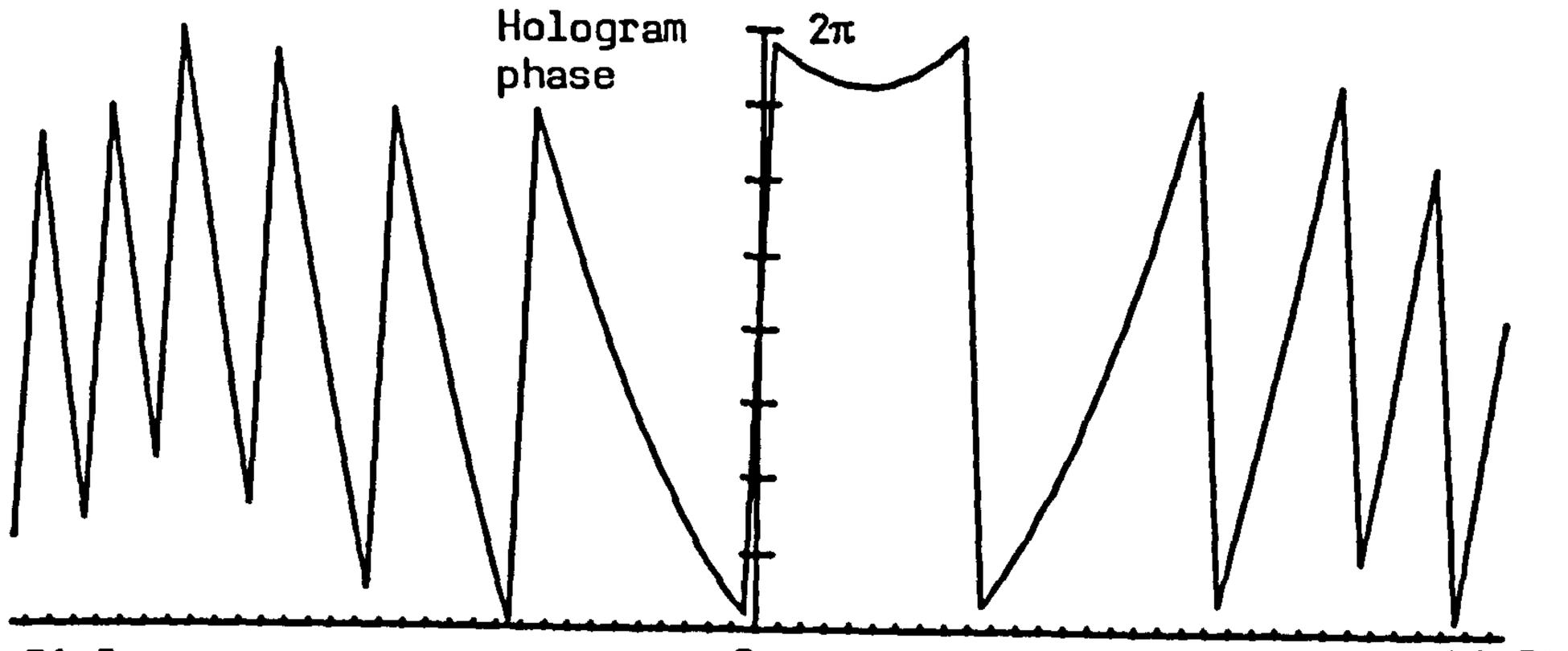


c. Tilt angle : $-2.5^o$

Hologram: $\Delta=1\lambda$, 64 samples. Object: 1-point; $x_o=y_o=0$, $z=100\lambda$

Fig. 7.5 : Effect of hologram tilt on the phase function

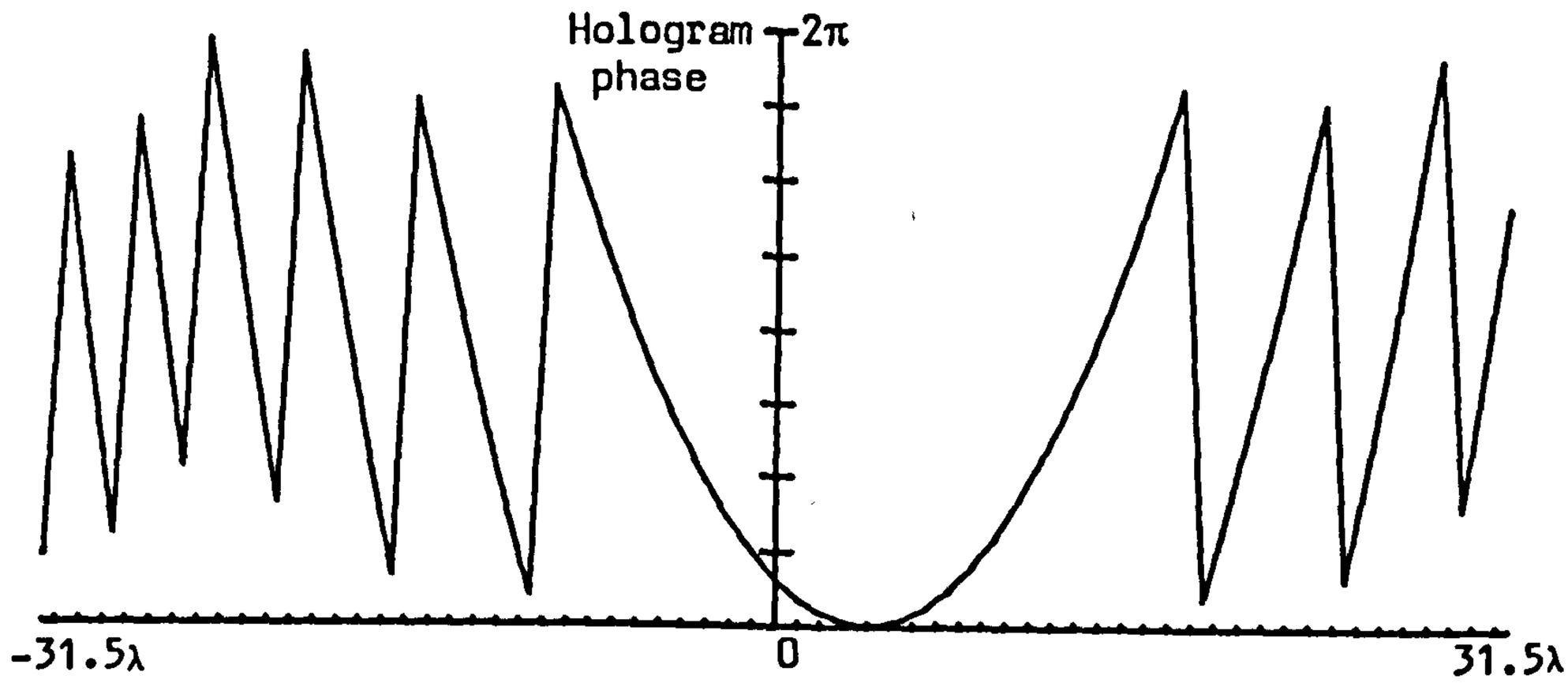


a. Shift in the direction parallel to the line hologram:
$x_o=4\lambda, y_o=0$

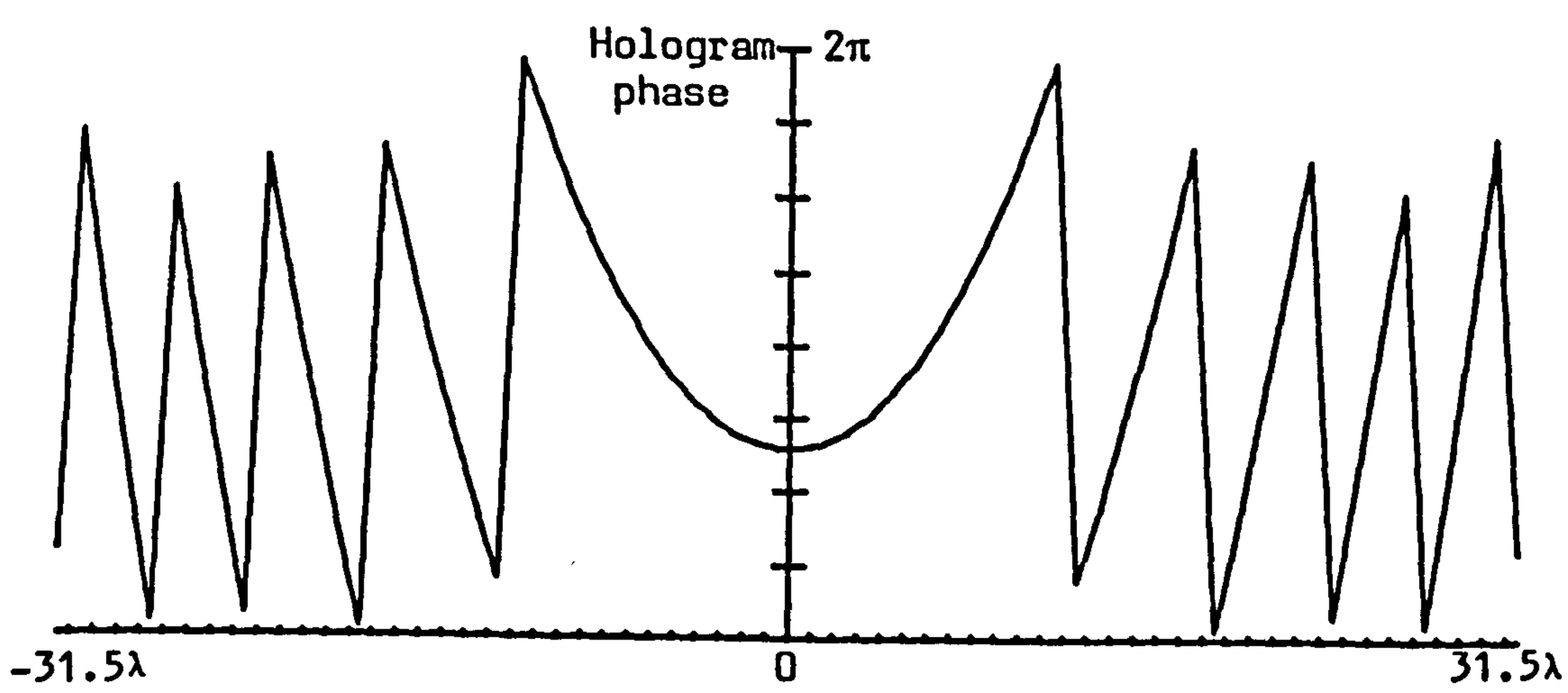


b. Shift in the direction perpendicular to the line hologram: $x_o=0, y_o=8\lambda$

Hologram: $\Delta=1\lambda$, 64 samples. Object: 1-point; $z=100\lambda$

Fig. 7.6 : Effect of lateral shifts in the position of a point object on the hologram phase function

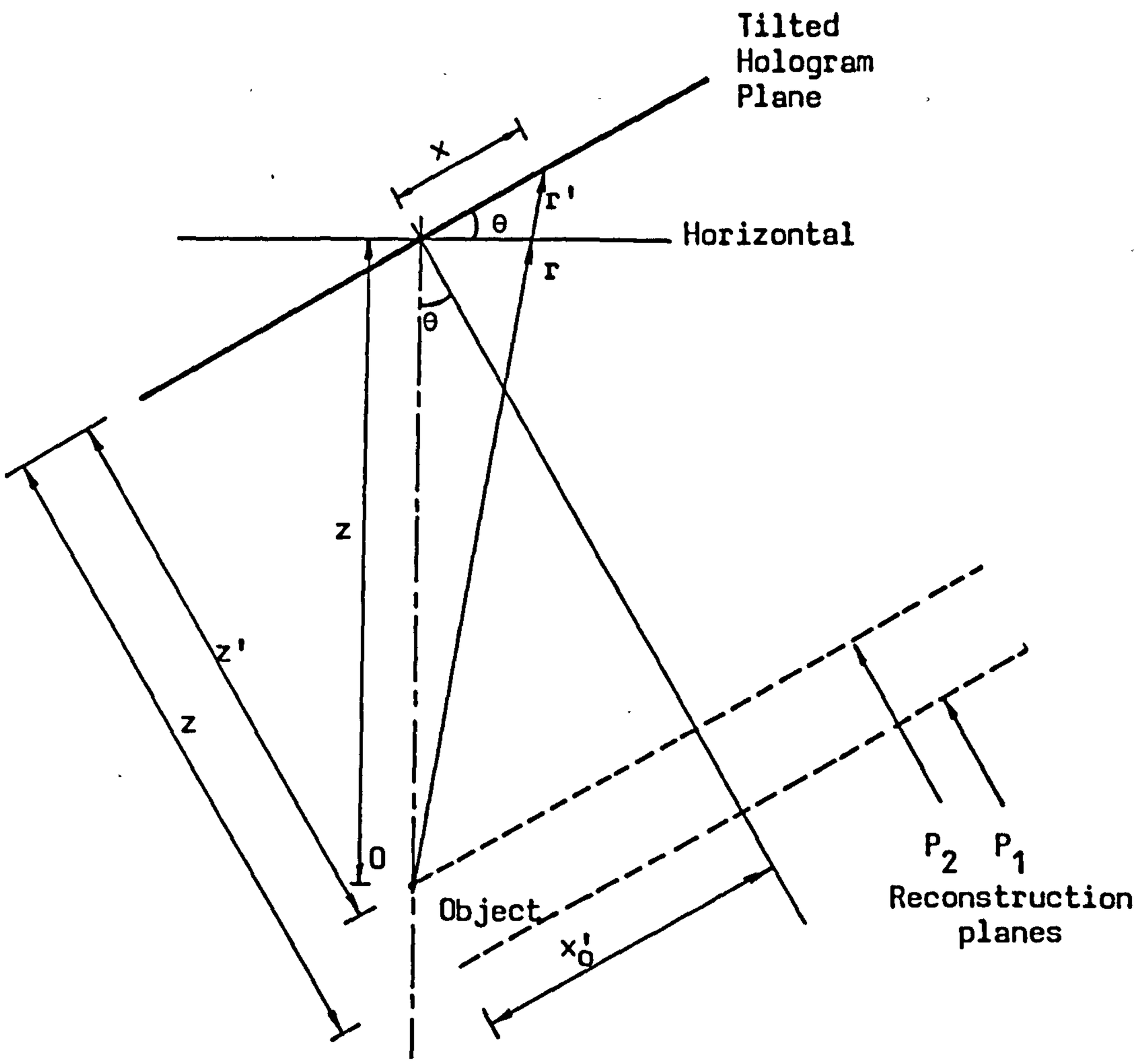


Fig. 7.7 : Geometry for recording and reconstructing a tilted hologram of a 1-point object

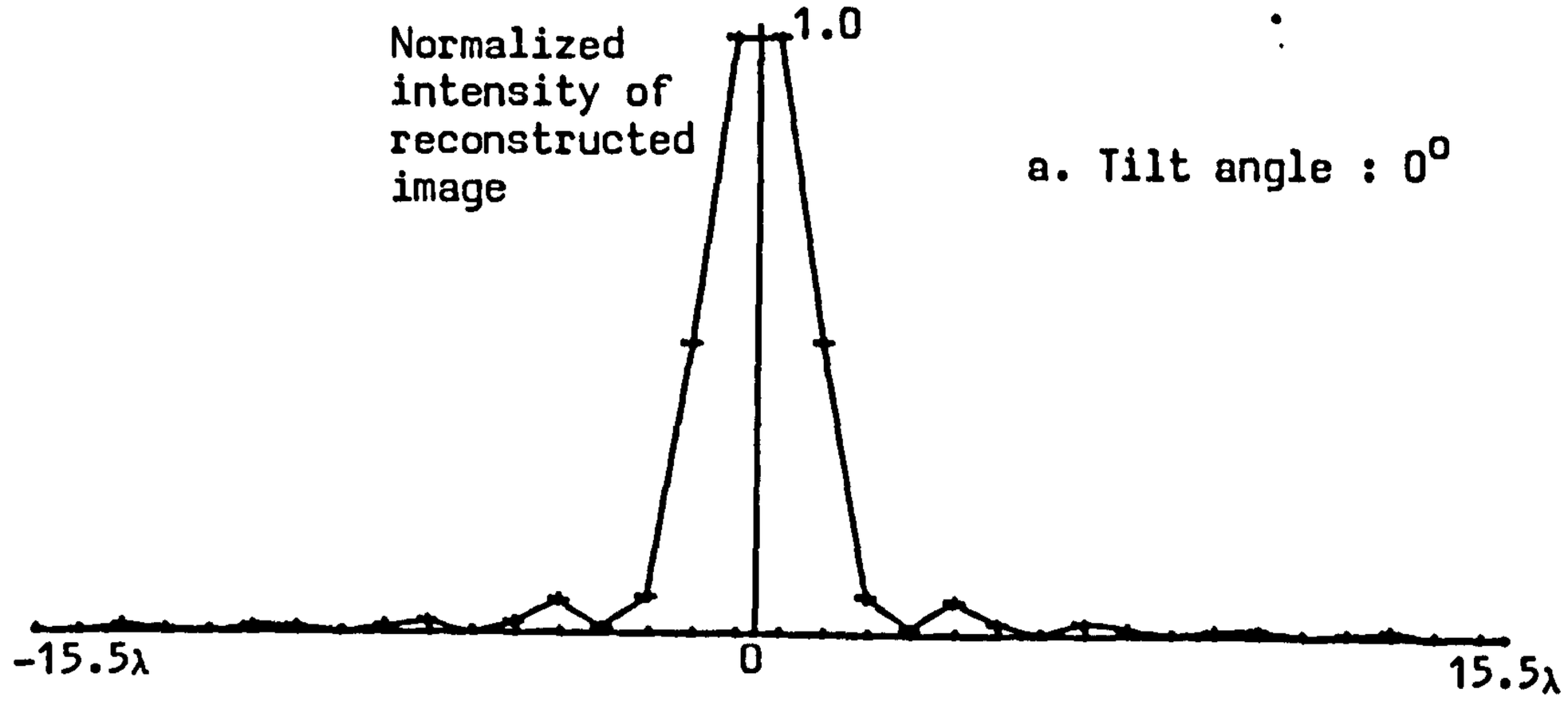


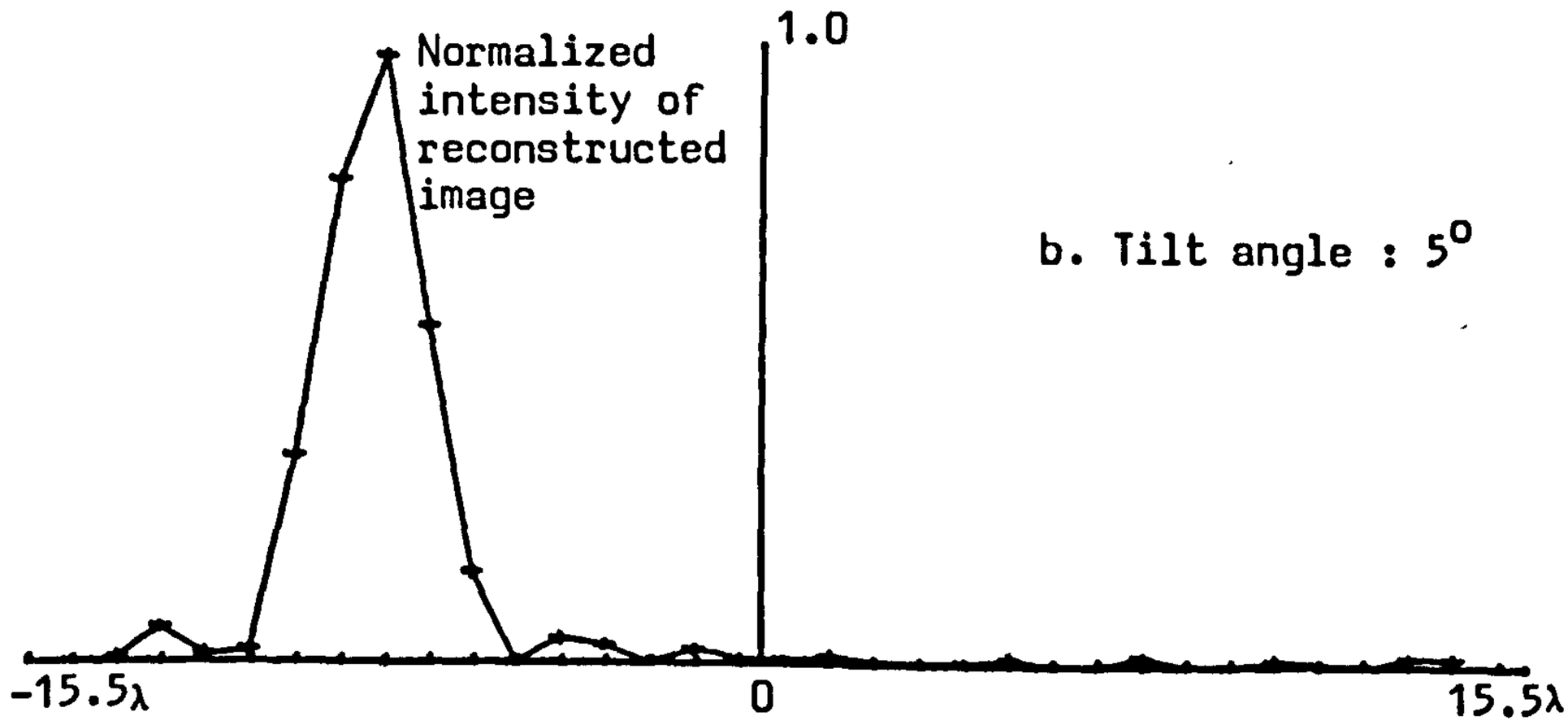


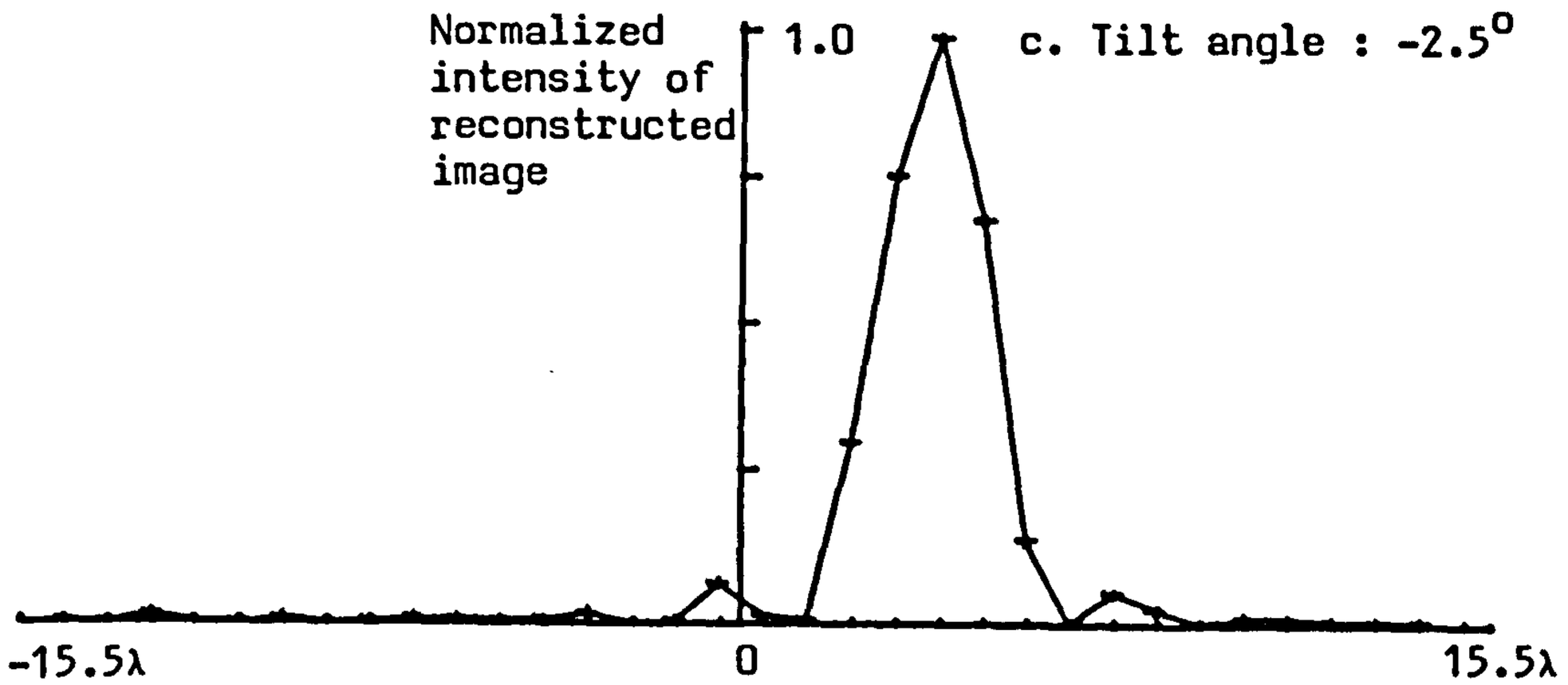


Hologram: $\Delta=1\lambda$, 32 samples. Object: $x_o=y_o=0$, $z=100\lambda$

Reconstruction distance : $100\lambda$

Fig. 7.8 : Effect of hologram tilt on the reconstructed image for the case of a 1-point object on the hologram axis.

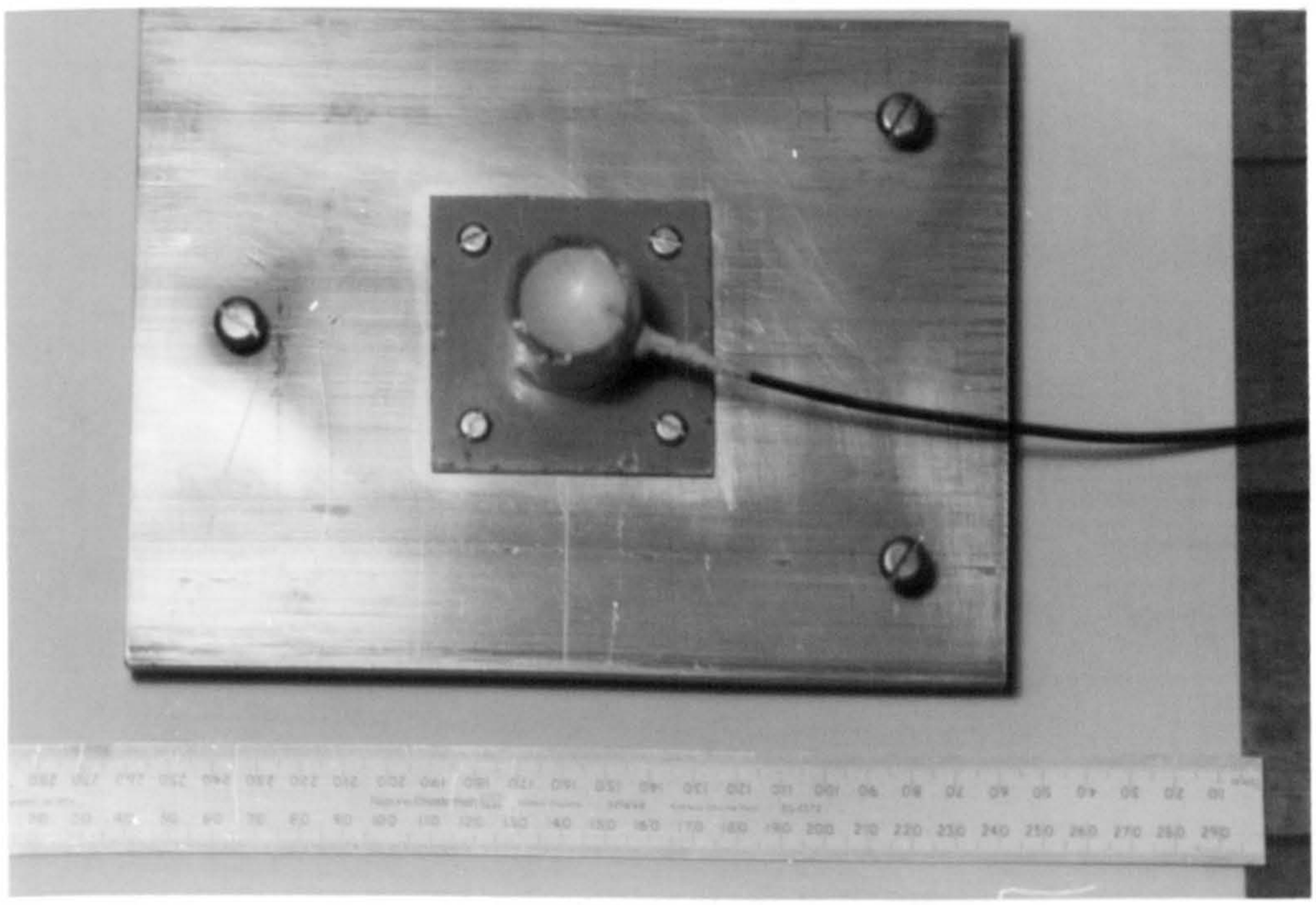

Fig. 7.9 : The focused acoustic transducer mounted on a brass plate with three adjustment screws in a tripod arrangement.

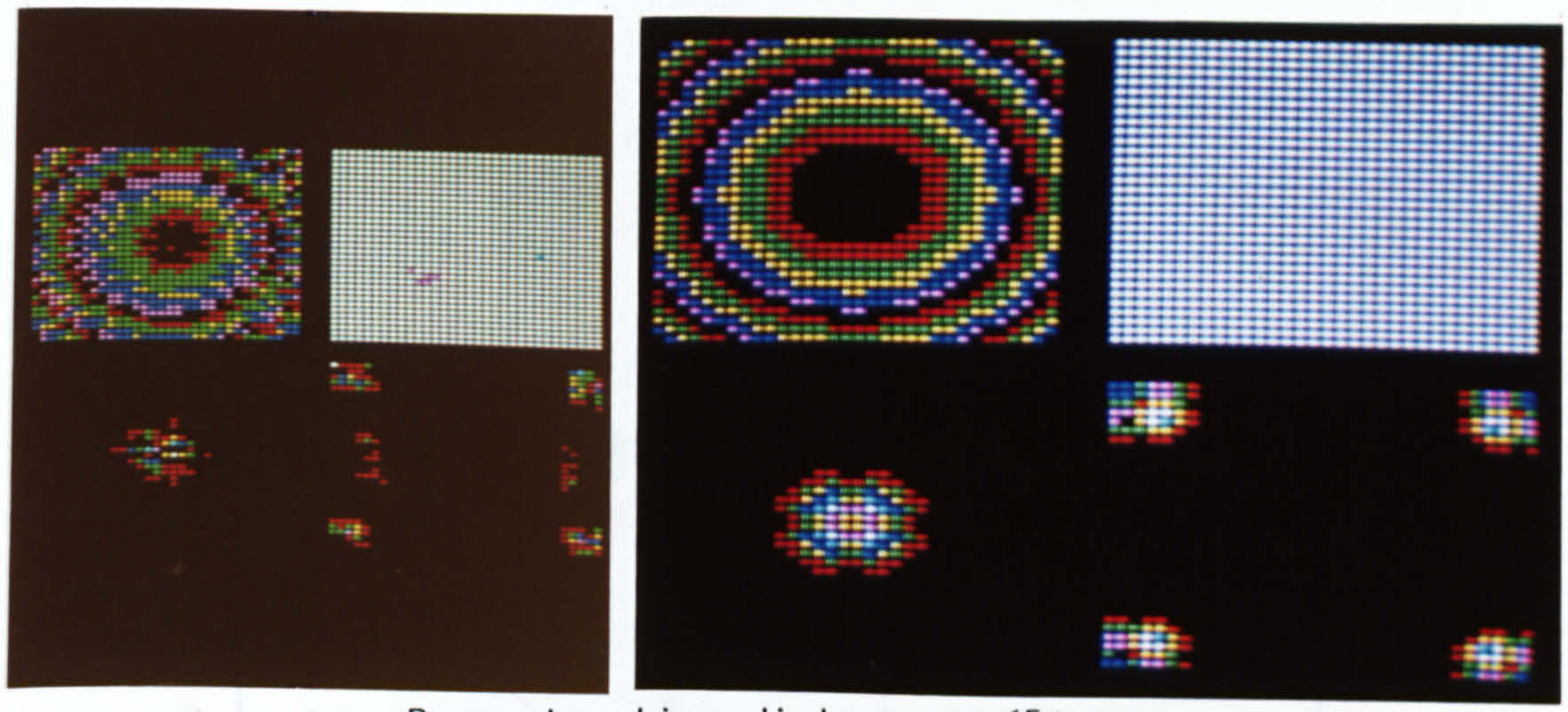

a. Reconstruction distance = 65λ

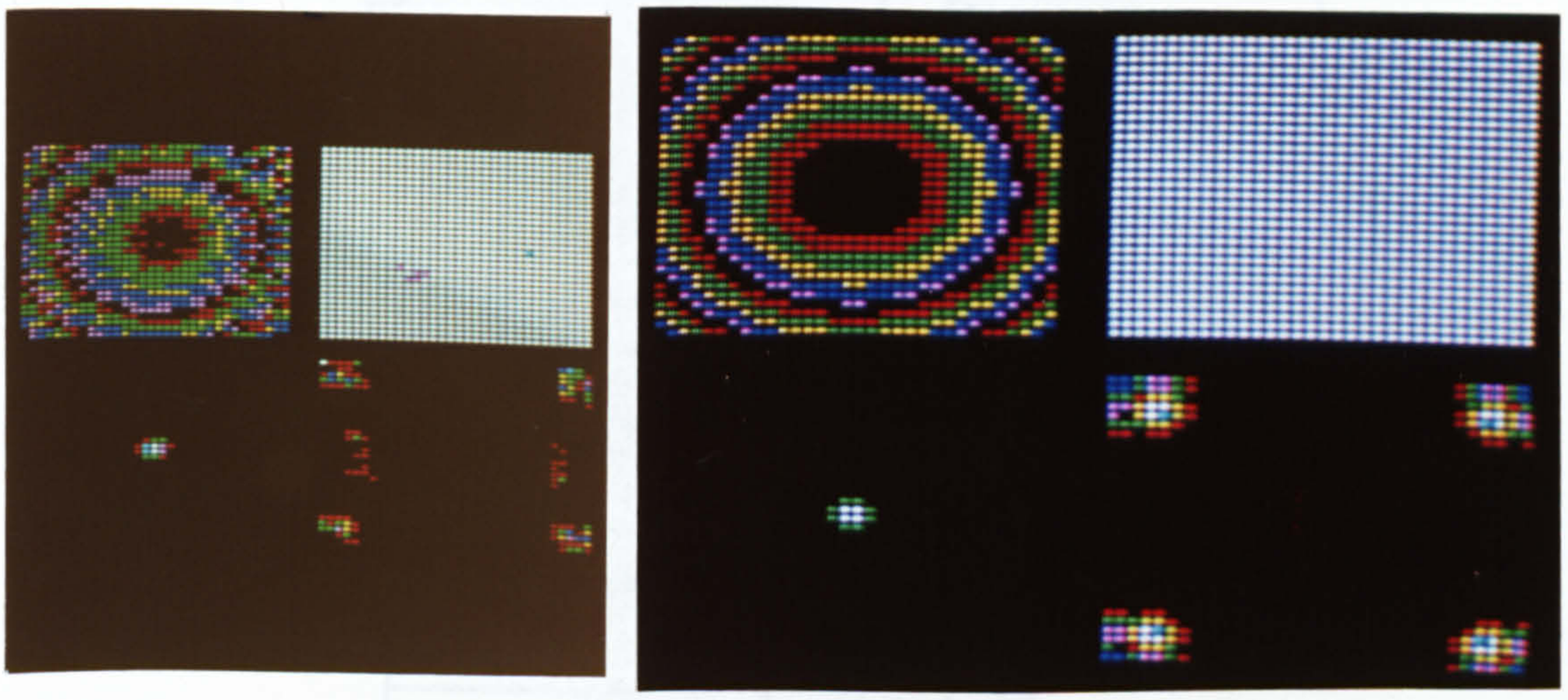

b. Reconstruction distance = 97λ (object in focus)

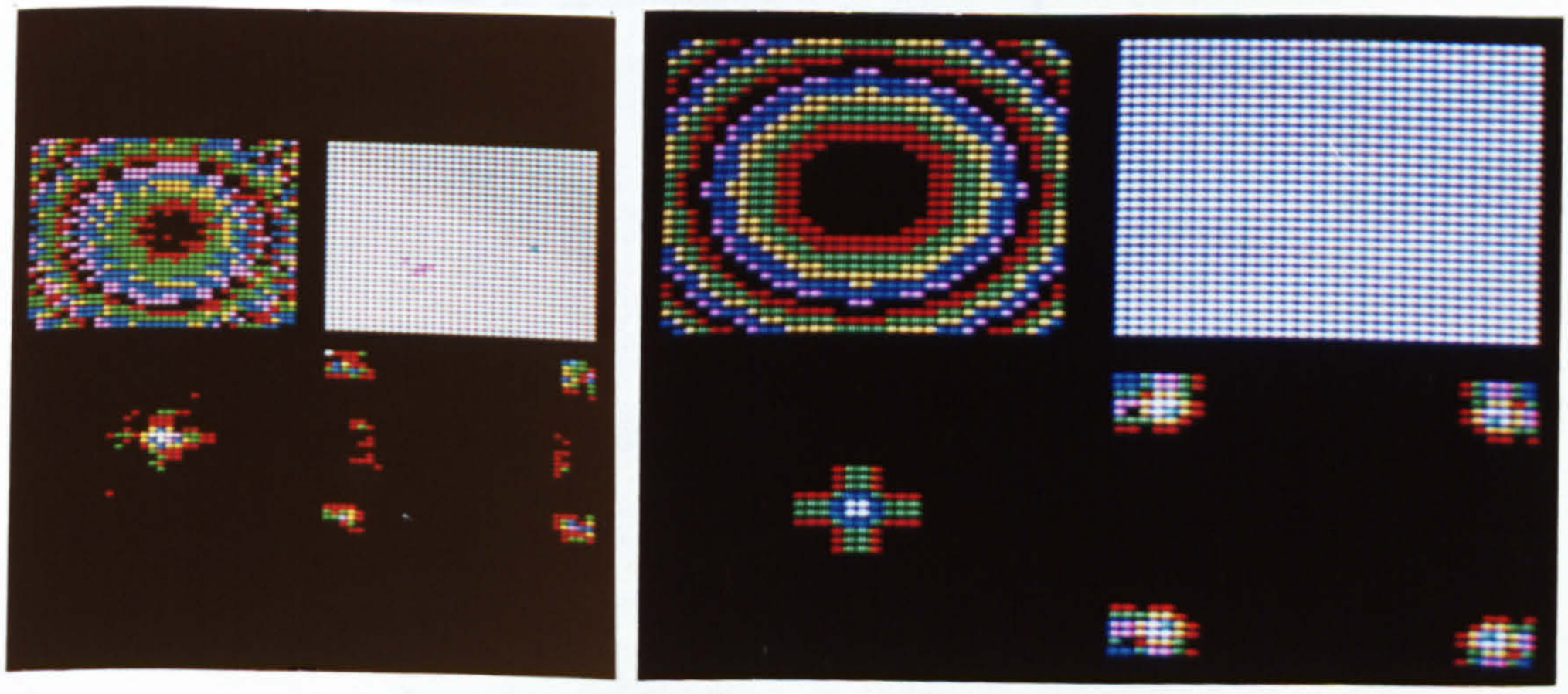

c. Reconstruction distance = 129λ

Fig. 7.10 : Measured (left) and simulated hologram and reconstructed images at 3 distances. Hologram : $\Delta=1.11\lambda$, 32x32 samples. Object: 1-point; $x_o=0, y_o=0$, $z=97\lambda$

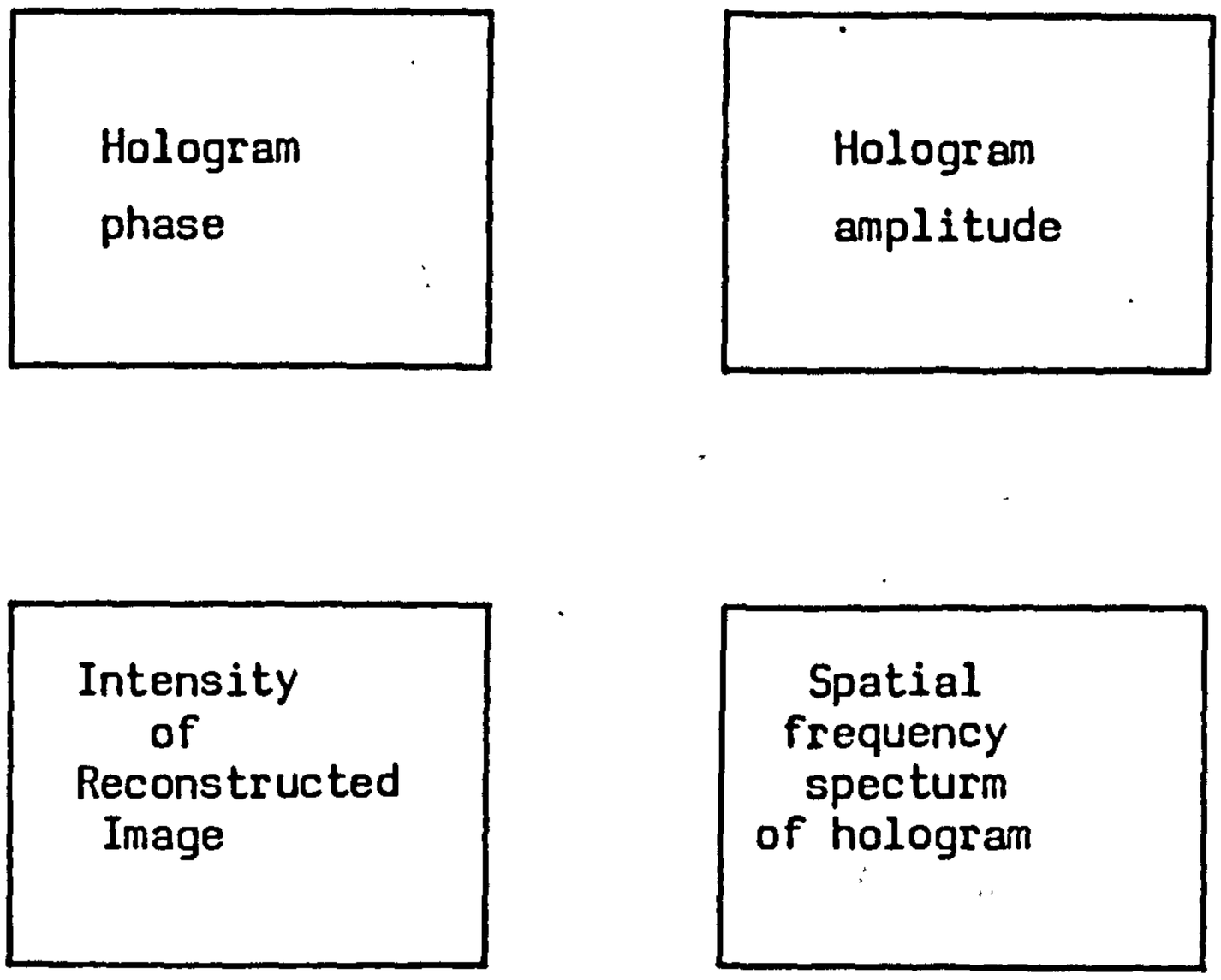


a. Picture Layout

| Colour | Data Value |
|---|---|
| Black | 0 |
| Red | 1 |
| Green | 2 |
| Yellow | 3 |
| Blue | 4 |
| Magenta | 5 |
| Cayan | 6 |
| White | 7 |

b. Colour code

Fig. 7.11 : Layout and colour code for the photographs of the two-dimensional holograms and images in Figs. 7.10, 12,13 and 31-38.

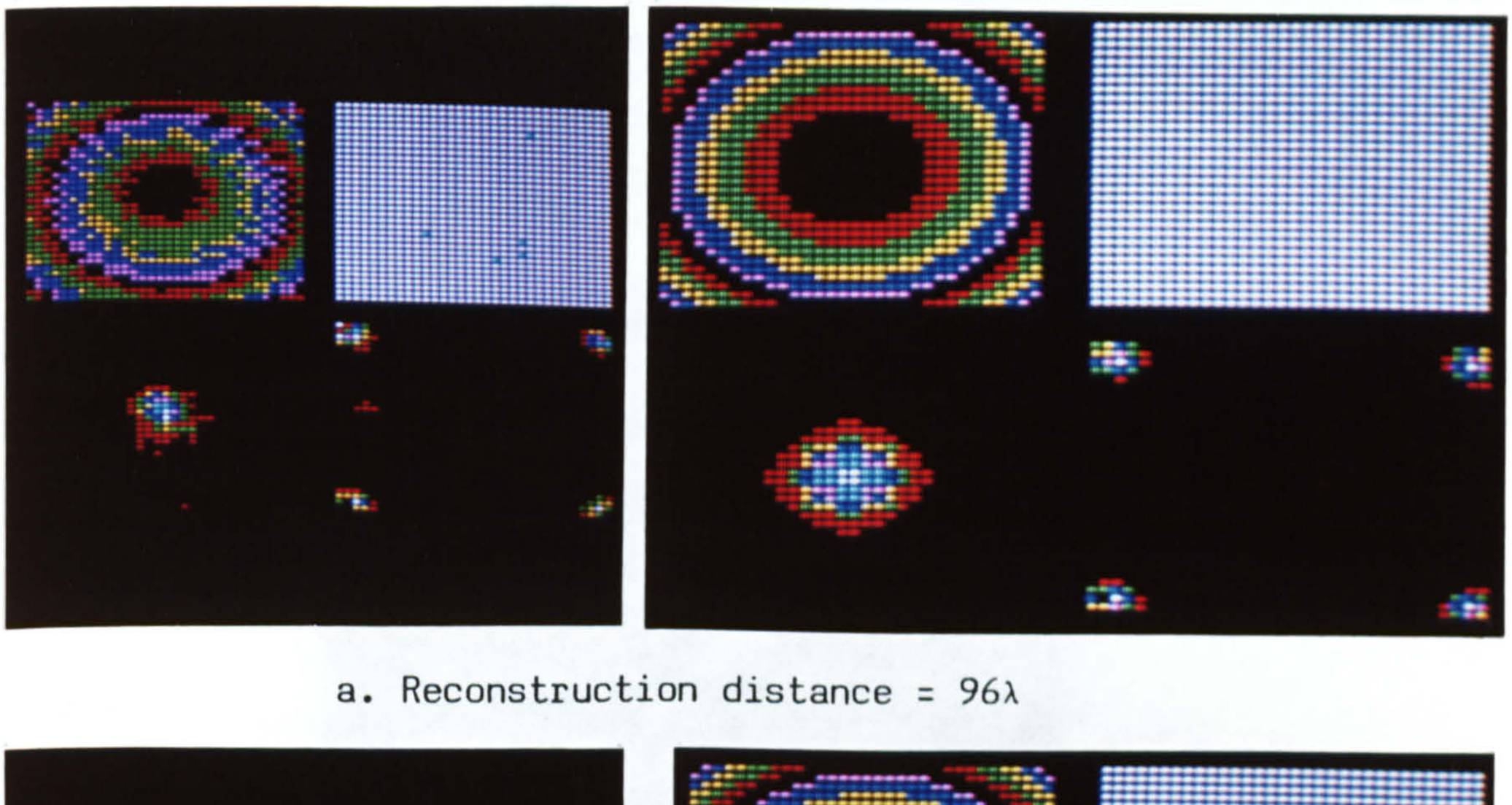

a. Reconstruction distance = 96λ

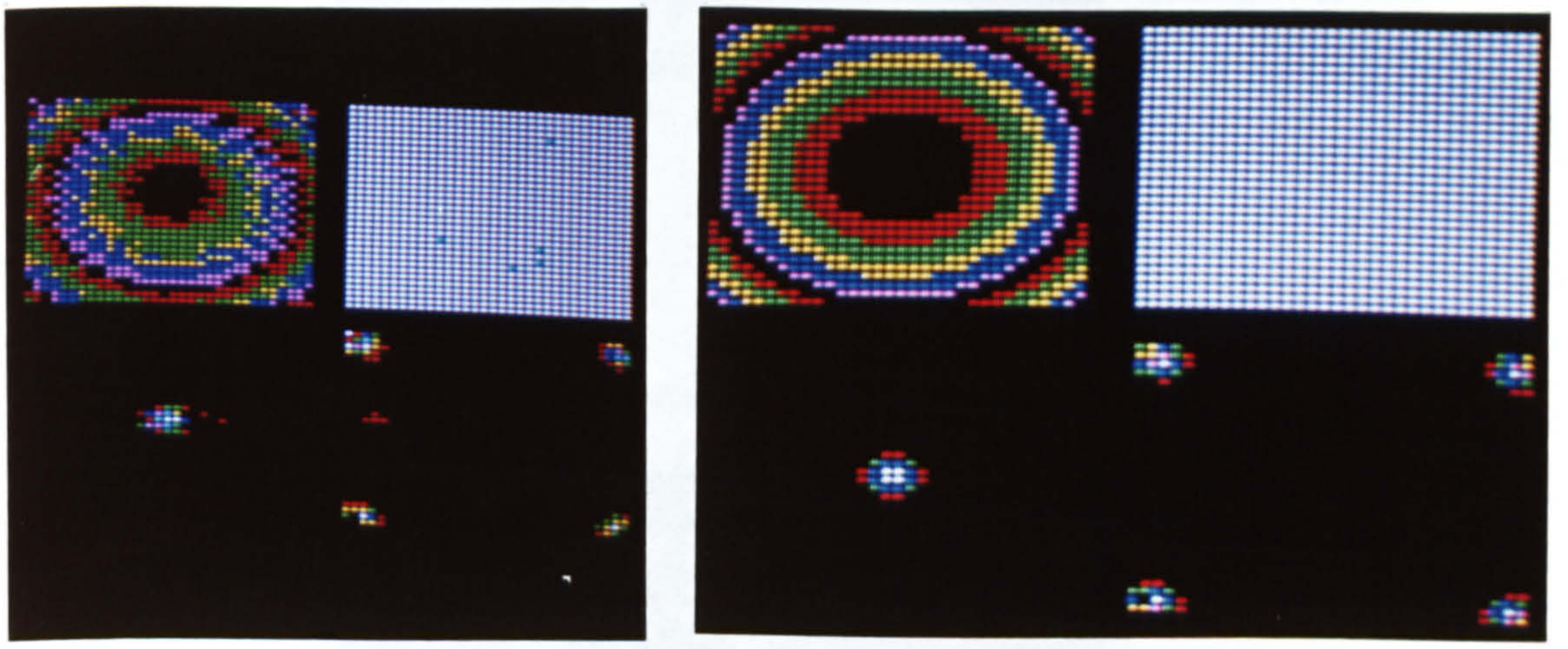

b. Reconstruction distance = 144λ (object in focus)

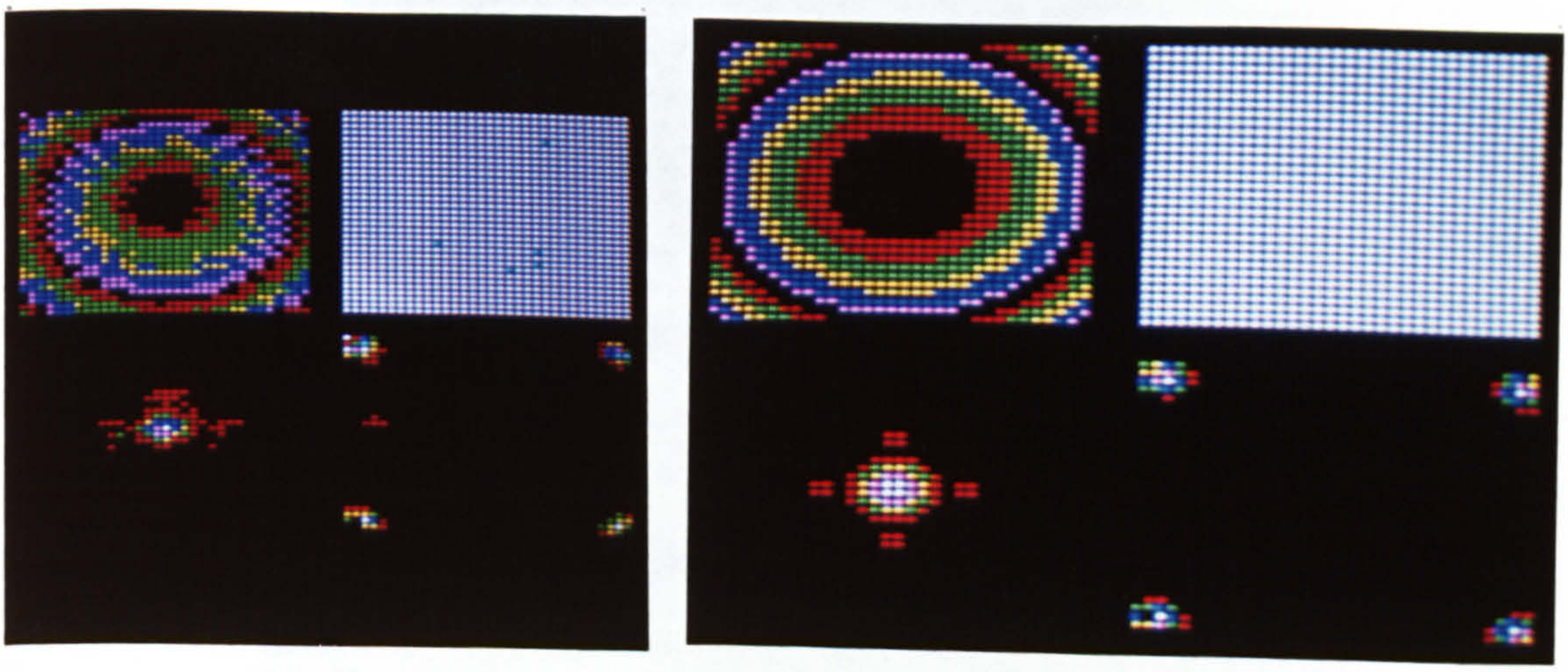

c. Reconstruction distance = 192λ

Fig. 7.12 : Measured (left) and simulated hologram and reconstructed images at 3 distances. Hologram : $\Delta$=1.11λ, 32x32 samples. Object: 1-point; $x_o$=0, $y_o$=0, z=144λ

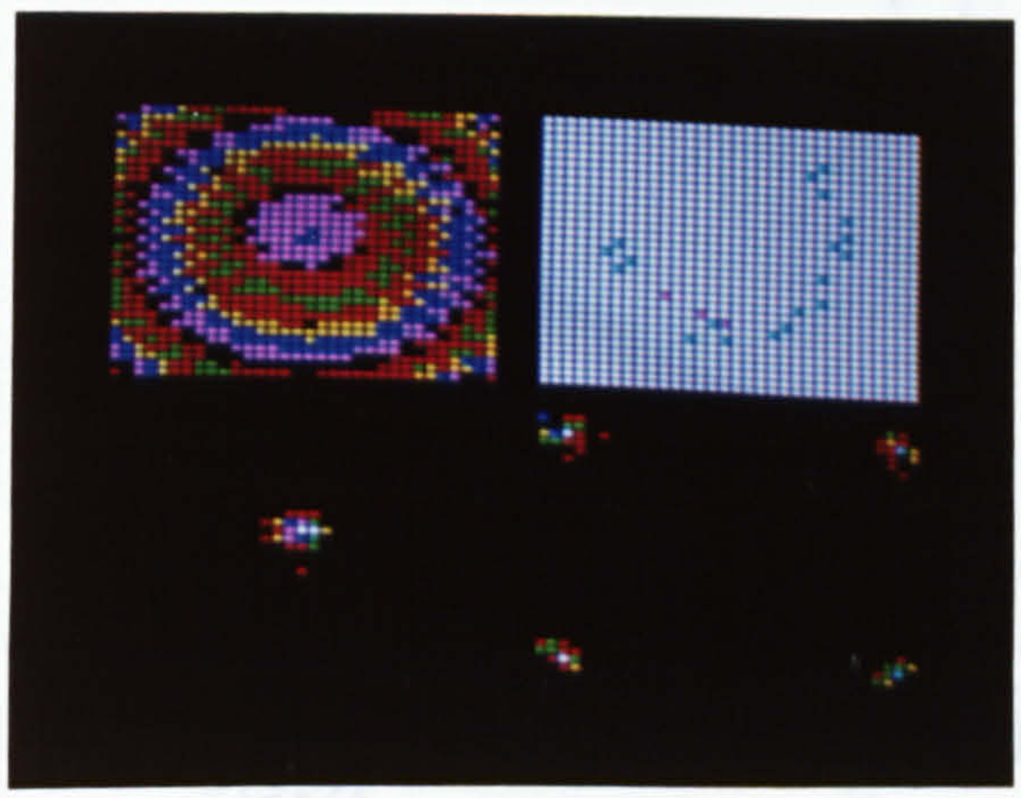

a. Pulse width : 4 cycles

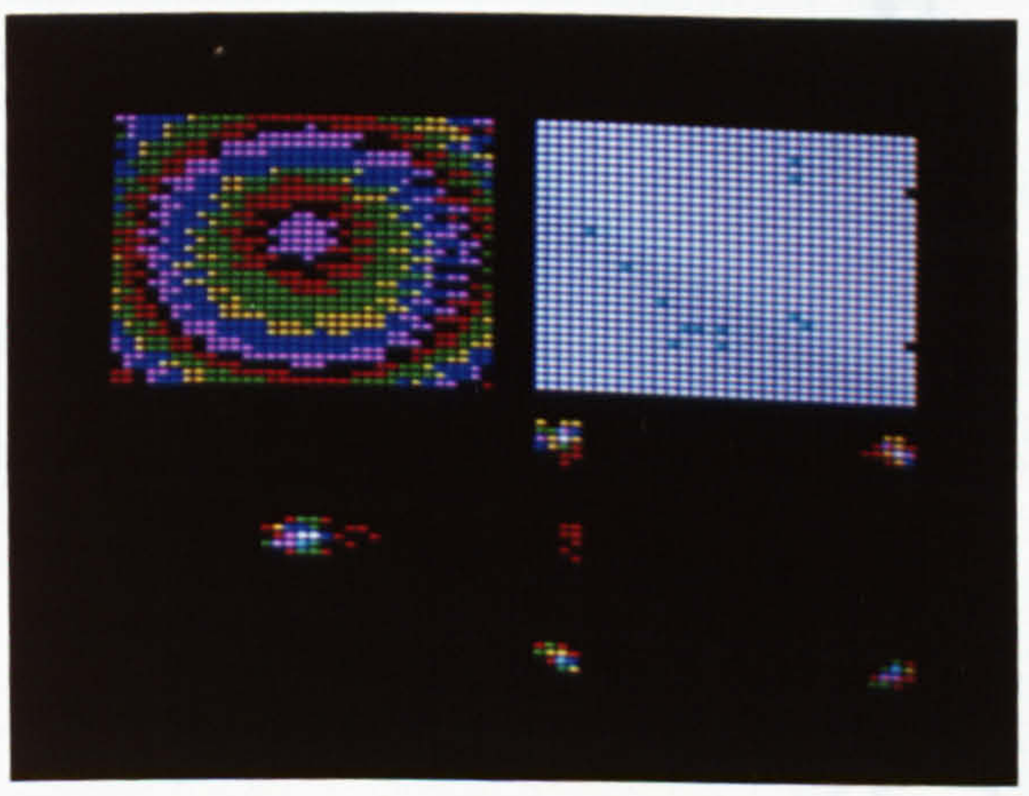

b. Pulse width : 15 cycles

Fig. 7.13 : Effect of the width of the transmitted acoustic pulse on the accuracy of the measured hologram and the quality of the reconstructed image. Hologram: $\Delta=1.11\lambda$, 32x32 samples. Object: 1-point; $x_o=0, y_o=0, z=144\lambda$

a. Intensity of image reconstructed at 93λ

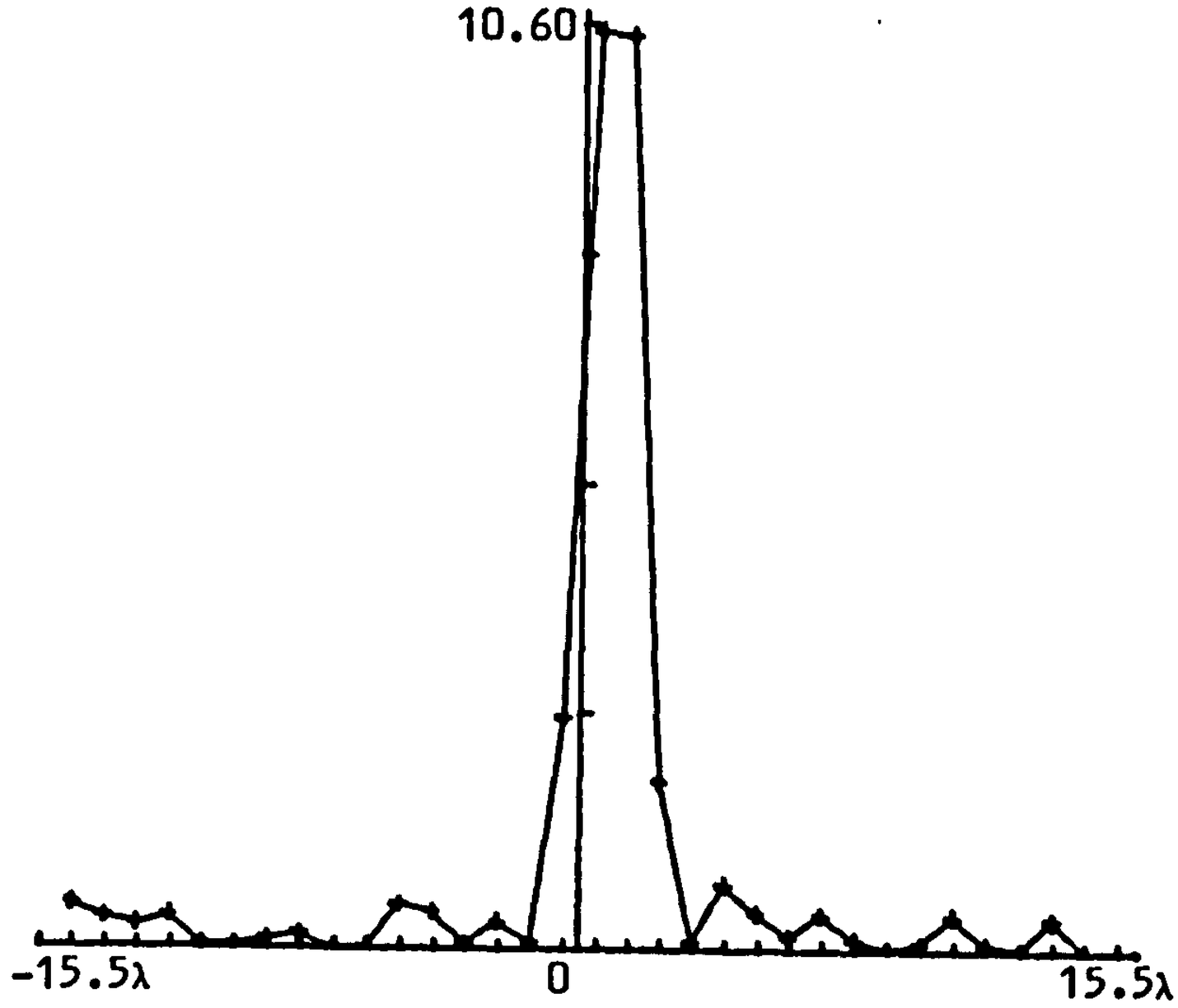


b. Intensity of optimum image, reconstructed at 90λ

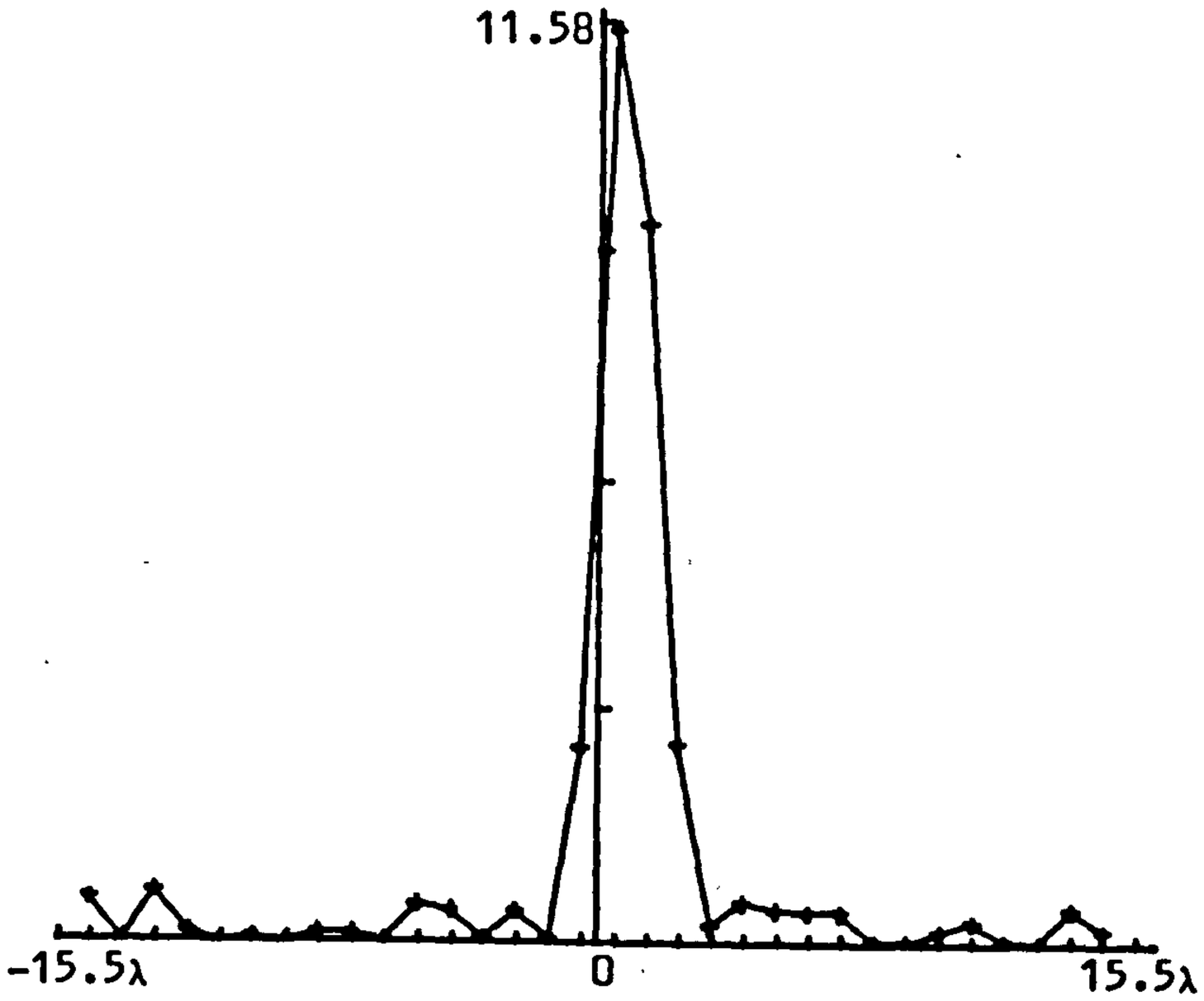


Hologram:Δ=1,32 samples. Object: 1-point; $x_o$=0,z=93λ

Fig. 7.14 : Reconstructed images from the hologram recorded at 93λ at both the measured and the optimum values of the range.

a. Intensity of image reconstructed at 144λ

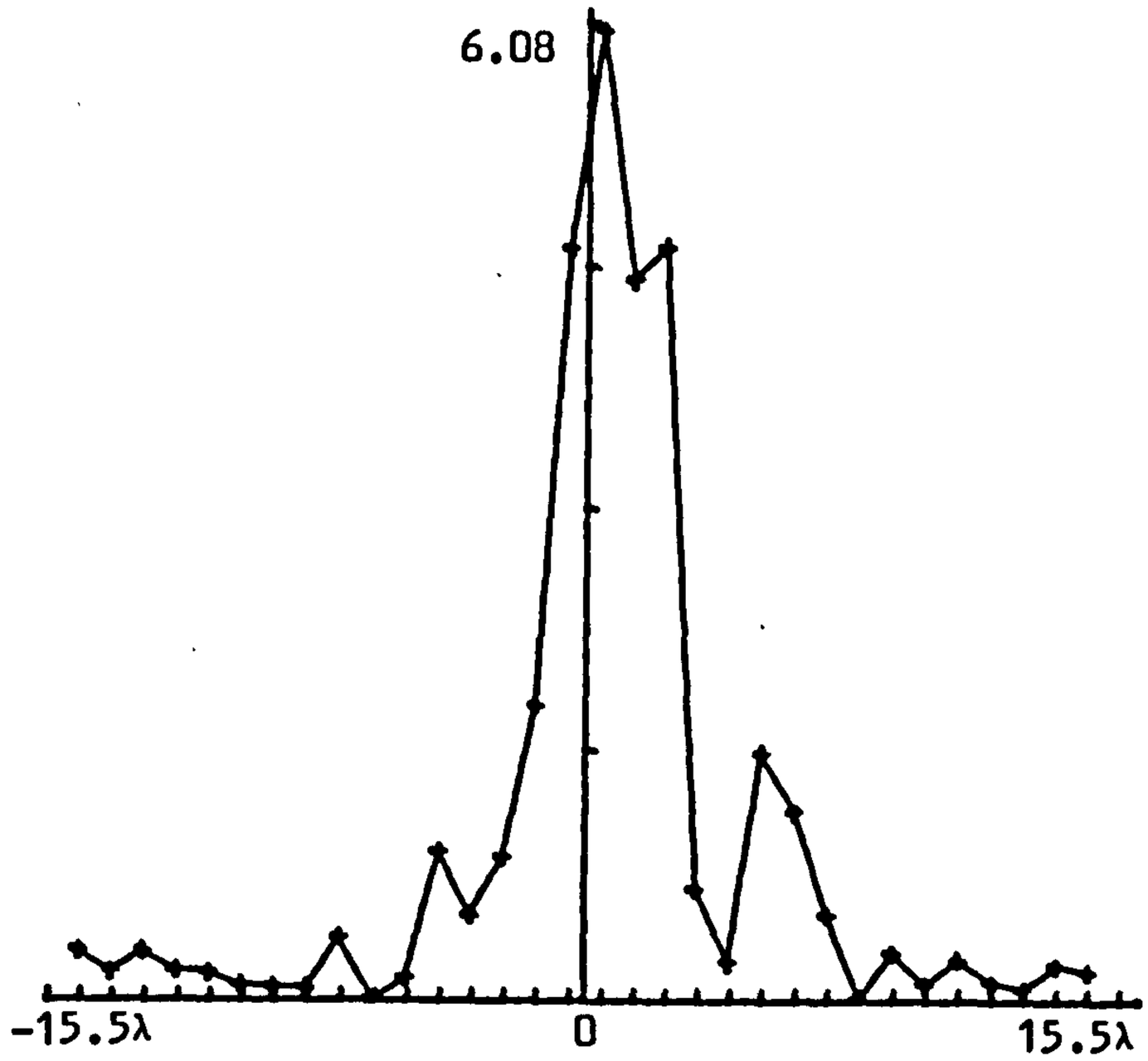


b. Intensity of optimum image, reconstructed at 132λ

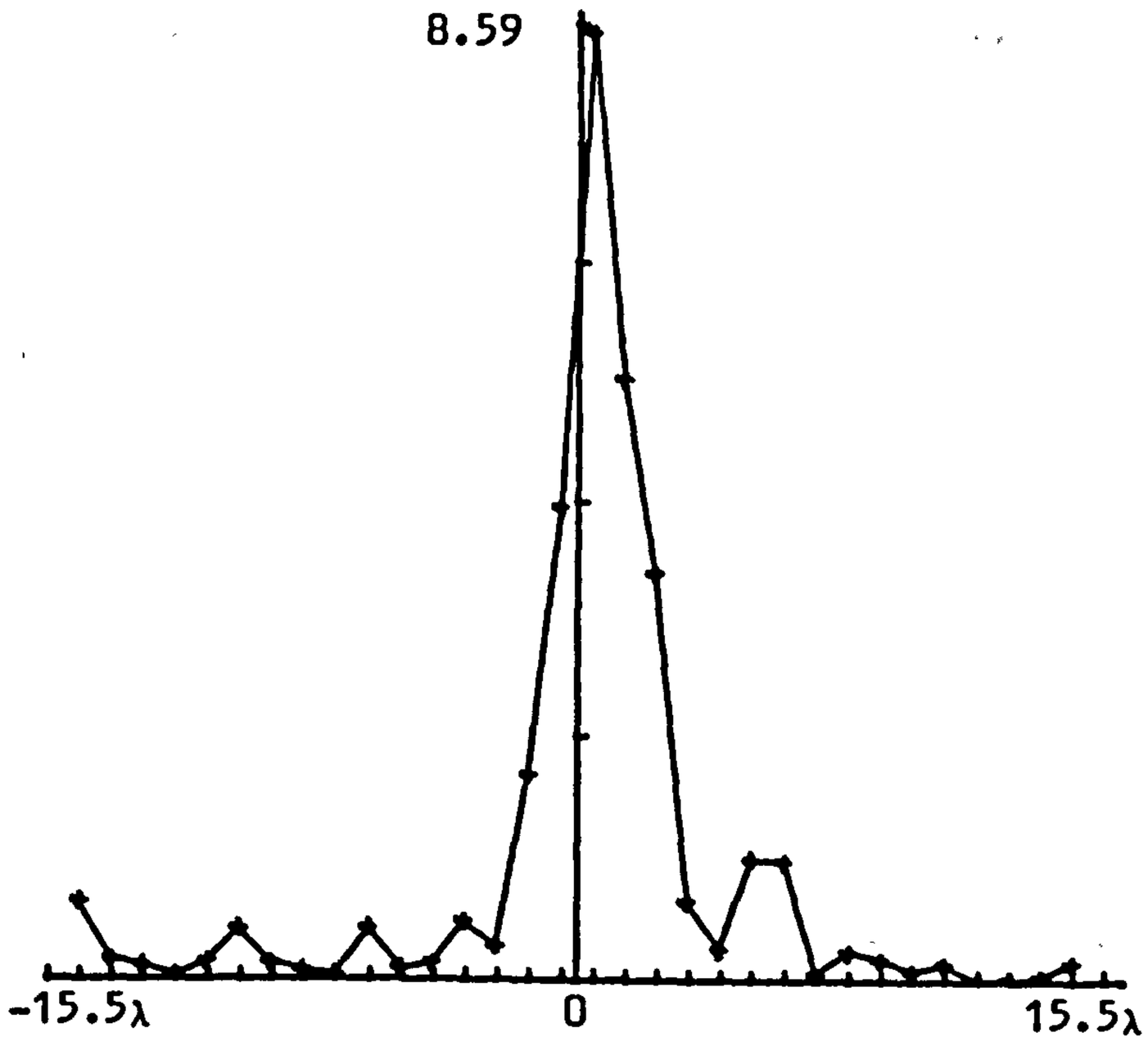


Hologram: Δ=1, 32 samples. Object : 1-point; $x_o$=0, z=144λ

Fig. 7.15 : Reconstructed images from the hologram recorded at 144λ at both the measured and the optimum values of the range.

a. Hologram phase

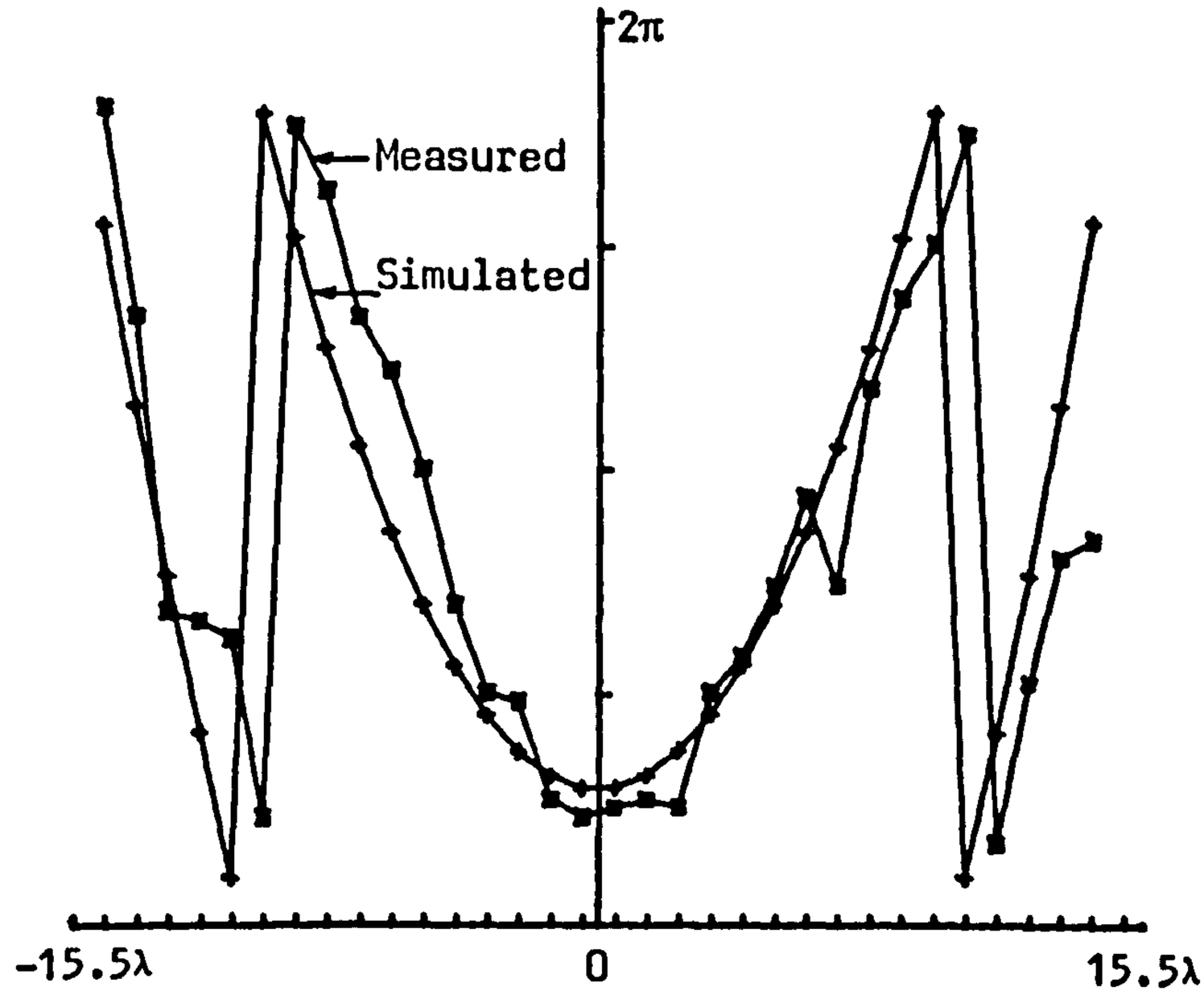


b. Normalized hologram amplitude

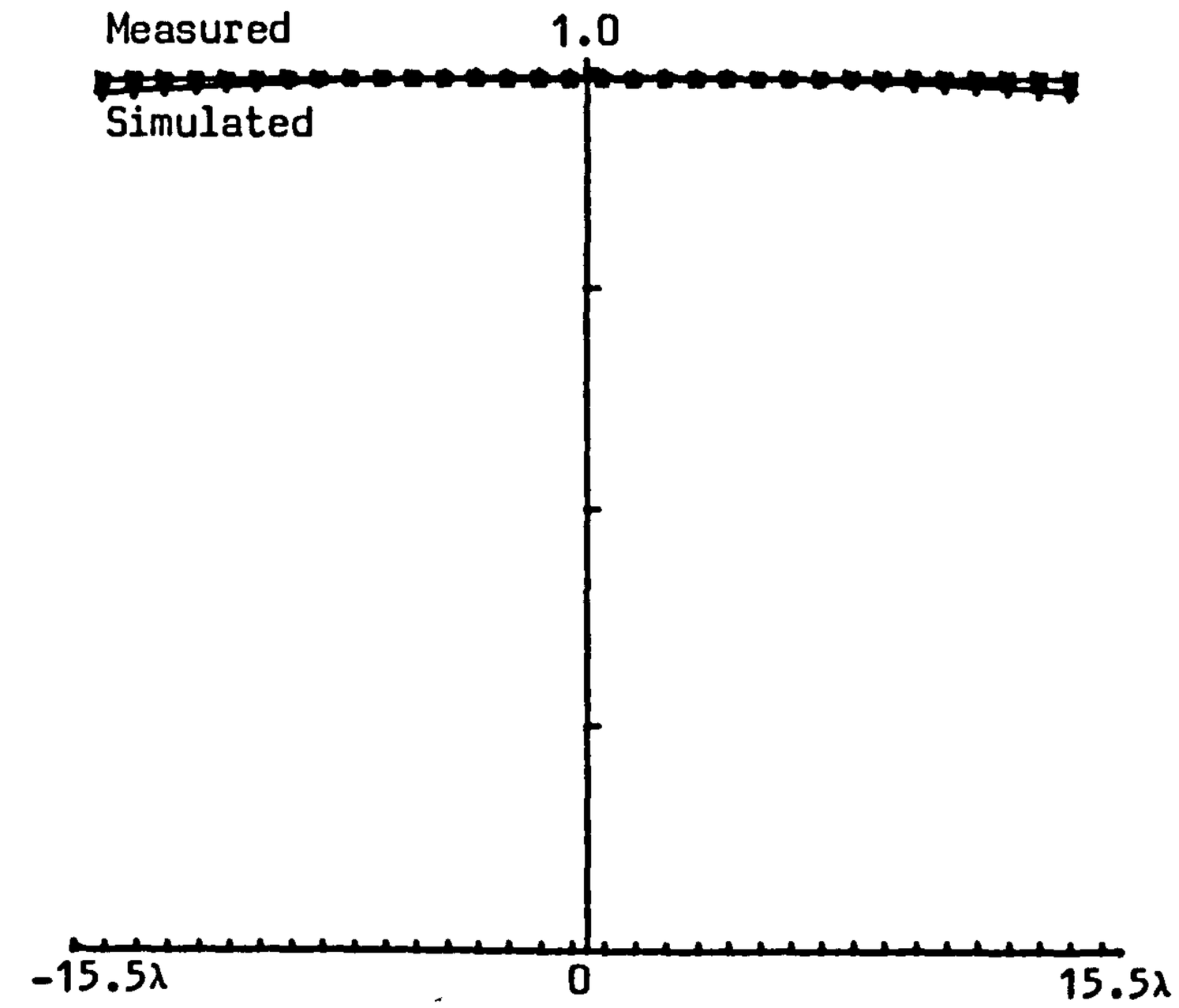


Measured and simulated holograms: Δ=1, 32 samples

Object for Measured hologram: $x_o$=0, z= 93λ

Object for Simulated hologram: $x_o$=0, z=90.15λ

Fig. 7.16 : Measured phase and amplitude of the hologram recorded at 93λ together with those of a simulated hologram for an object at a distance approximately equal to the optimum range of the measured hologram.

a. Hologram phase

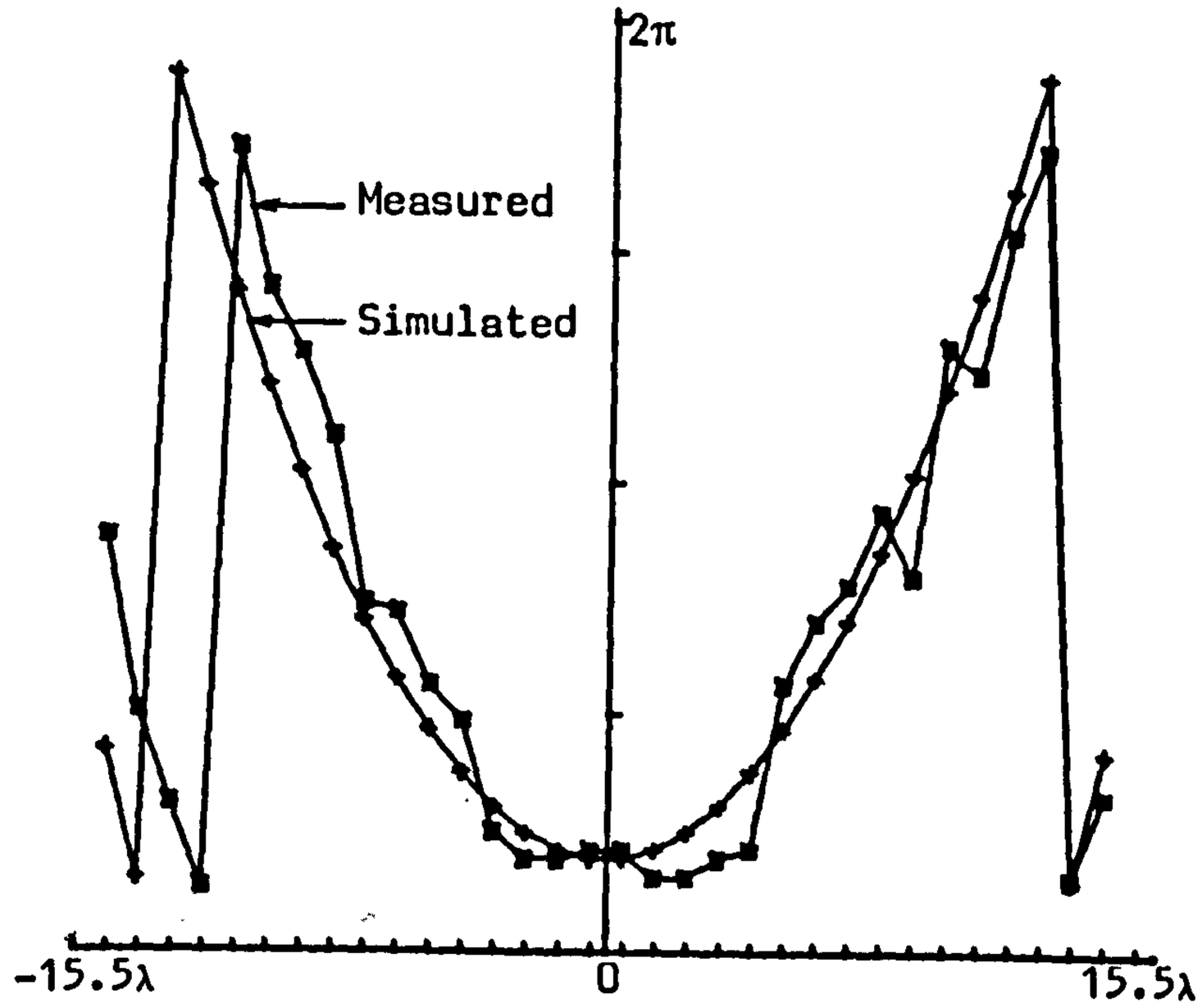


b. Normalized hologram amplitude

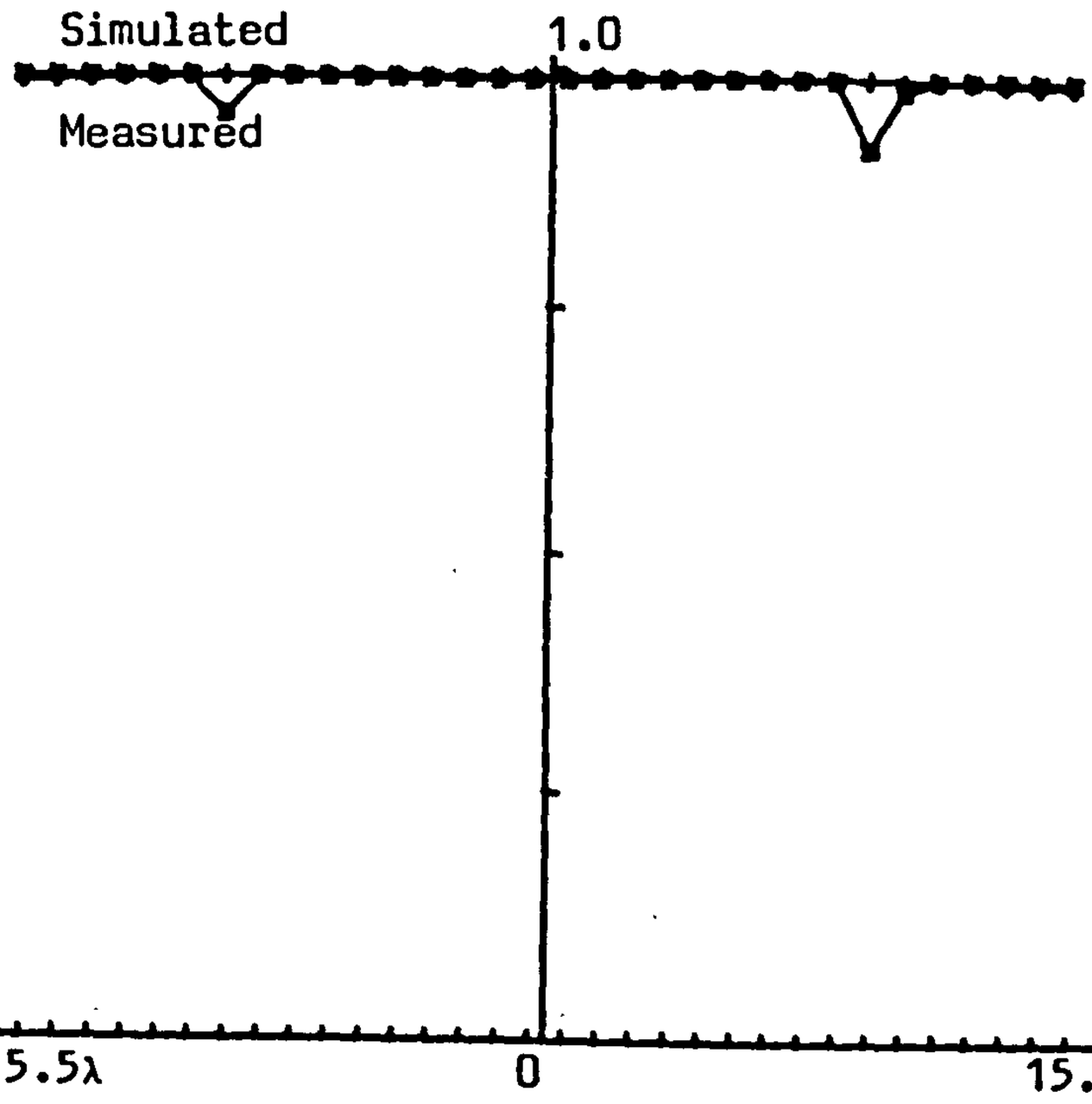


Measured and simulated holograms: Δ=1, 32 samples

Object for measured hologram: $x_o$=0, z=144λ

Object for simulated hologram: $x_o$=0, z=132.1λ

Fig. 7.17 : Measured phase and amplitude of the hologram recorded at 144λ together with those of a simulated hologram for an object at a distance approximately equal to the optimum range of the measured hologram.

a. Intensity of the reconstructed image with a simulated error of 5% in the sample spacing.

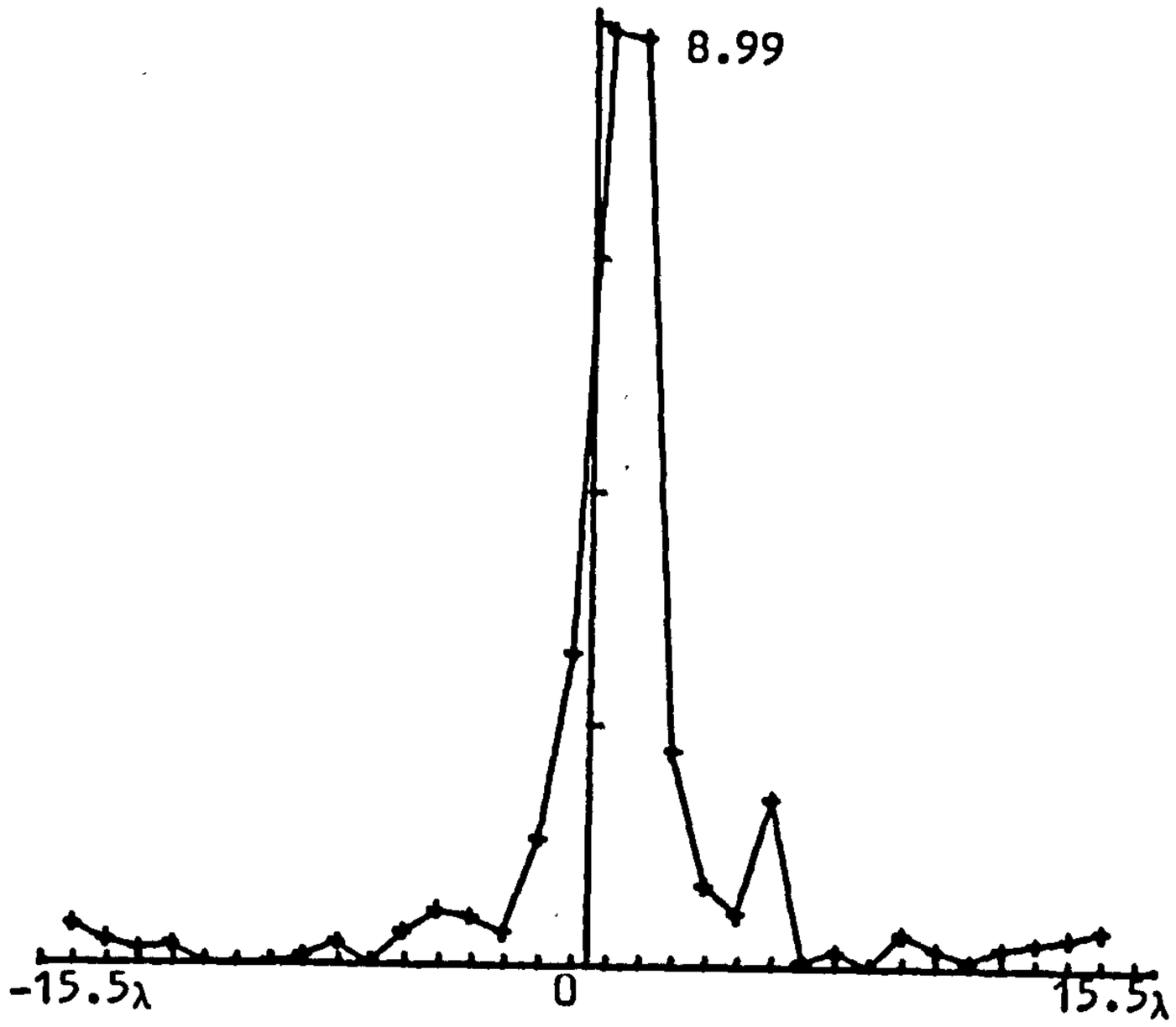


b. Intensity of the reconstructed image with a simulated error of -5% in the sample spacing.

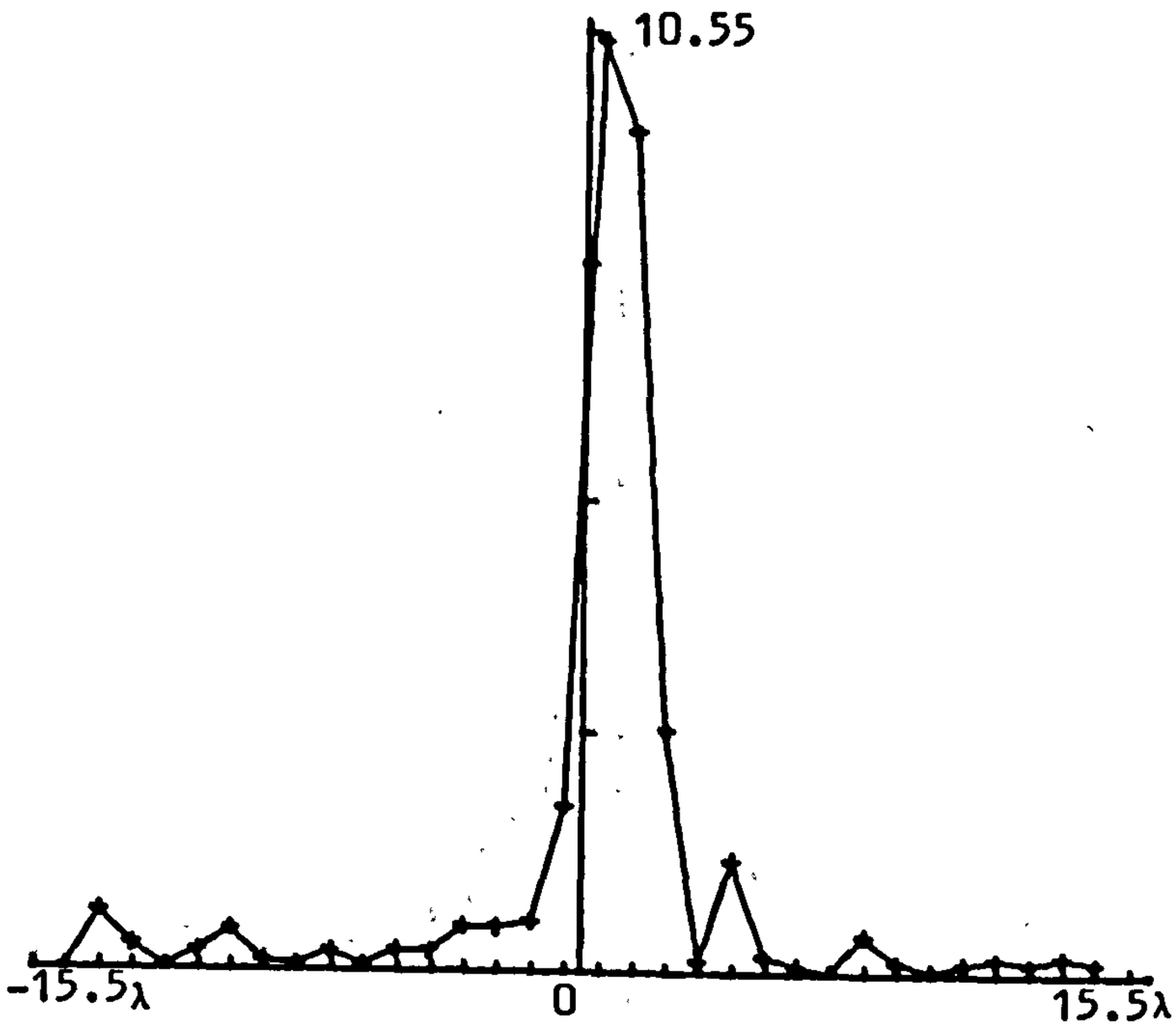


Hologram: Δ=1, 32 samples

Object: $x_o$=0, z=93λ

Fig. 7.18 : Effect of error in the sample spacing on the reconstructed image for the hologram measured at 93λ

a. Intensity of the reconstructed image with a simulated error of 5% in the sample spacing.

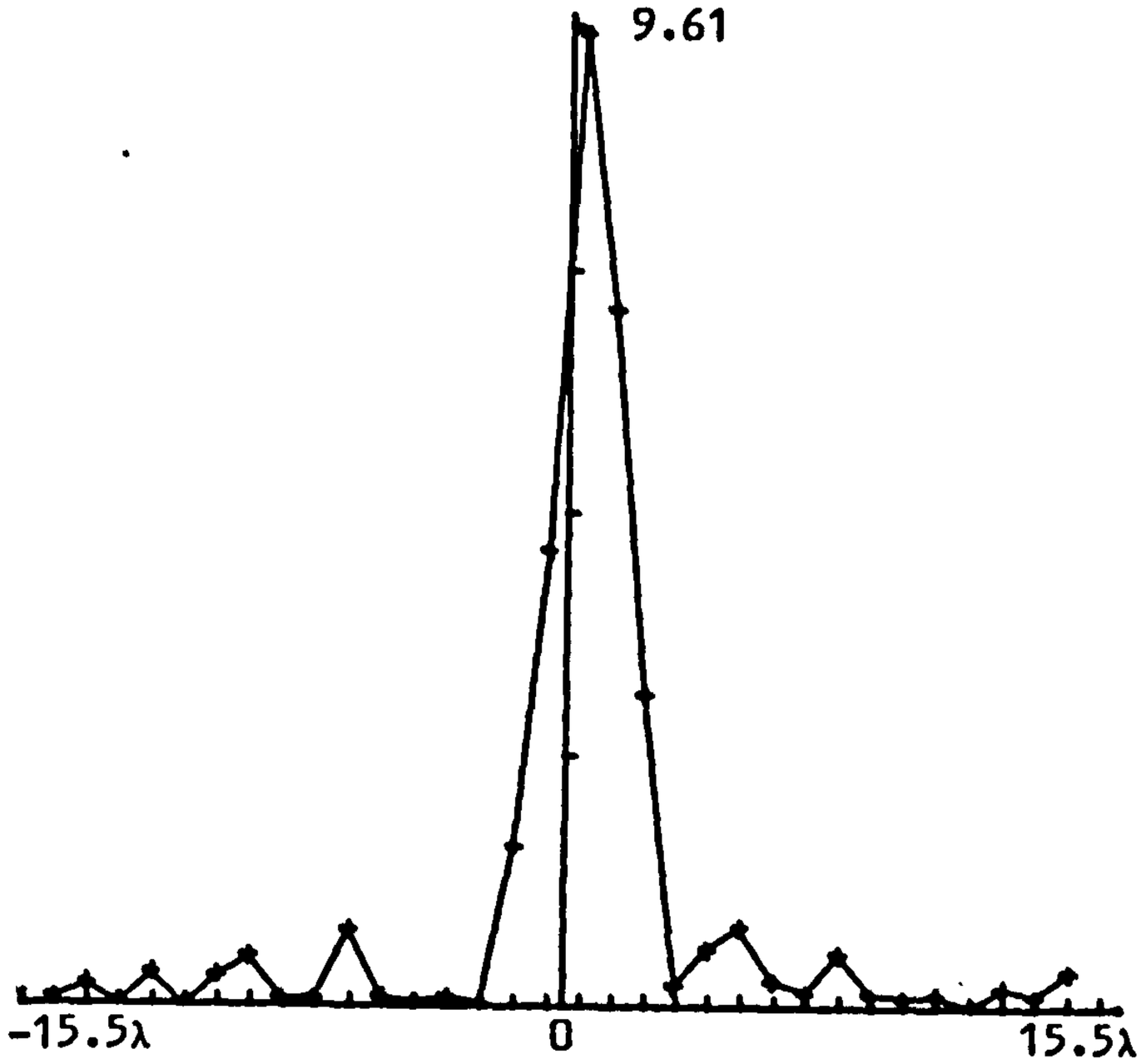


b. Intensity of the reconstructed image with a simulated error of -5% in the sample spacing.

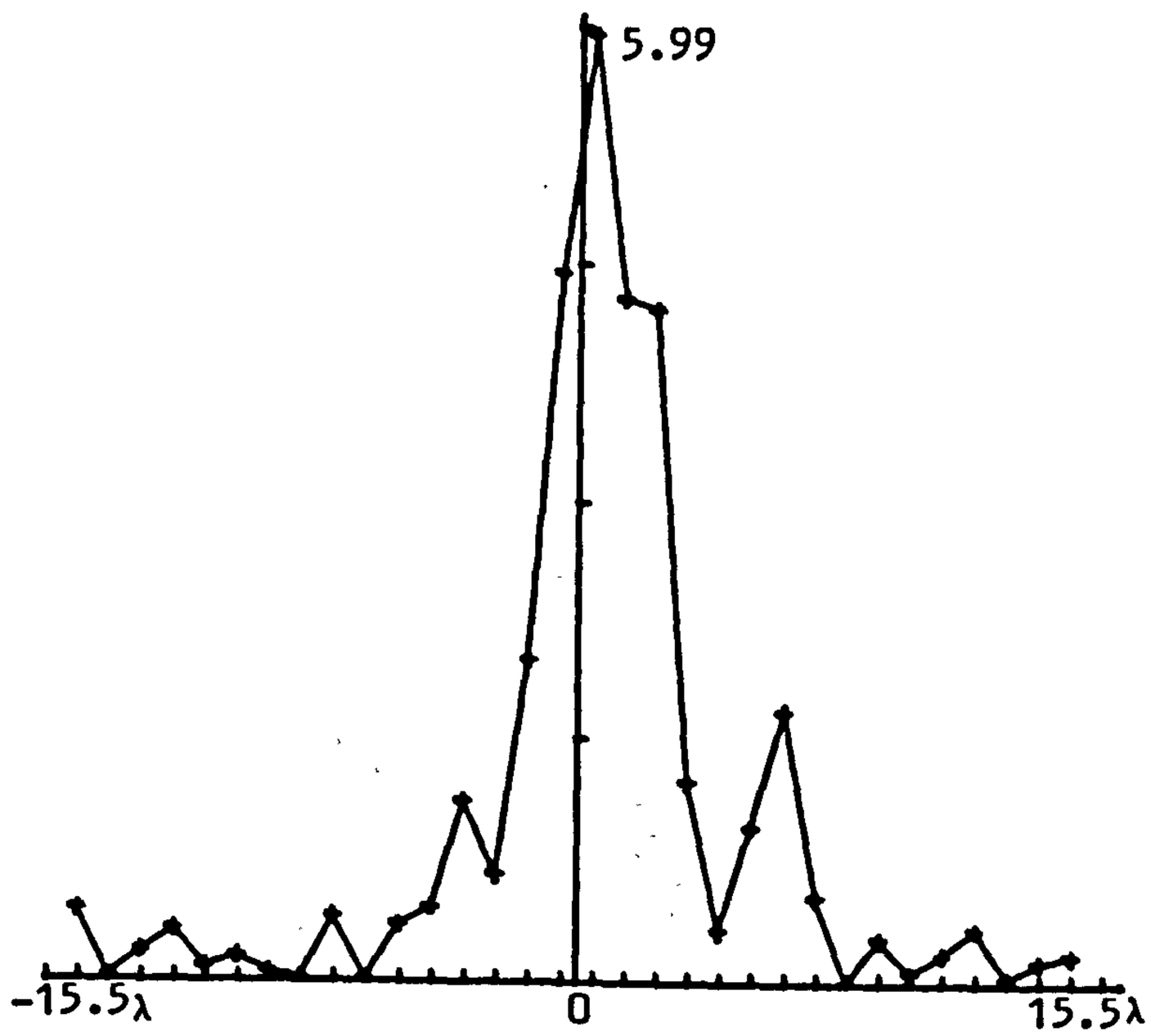


Hologram: Δ=1, 32 samples

Object: $x_o$=0, z=144λ

Fig. 7.19 : Effect of error in the sample spacing on the reconstructed image for the hologram measured at 144λ

a. Prediction errors over the aperture

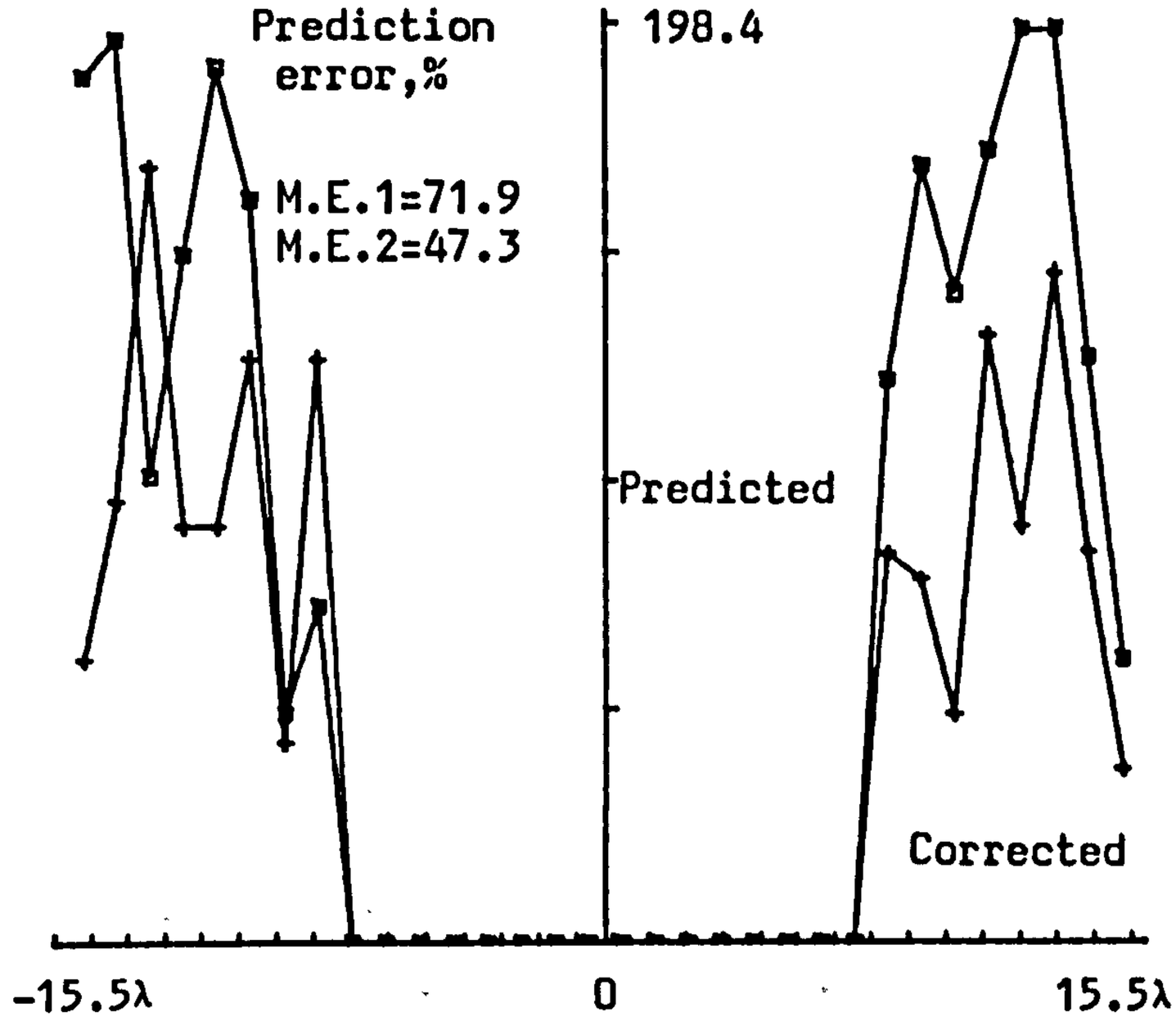


b. Normalized intensities of the images from the small, true, predicted, and corrected apertures reconstructed at the optimum range of 90λ

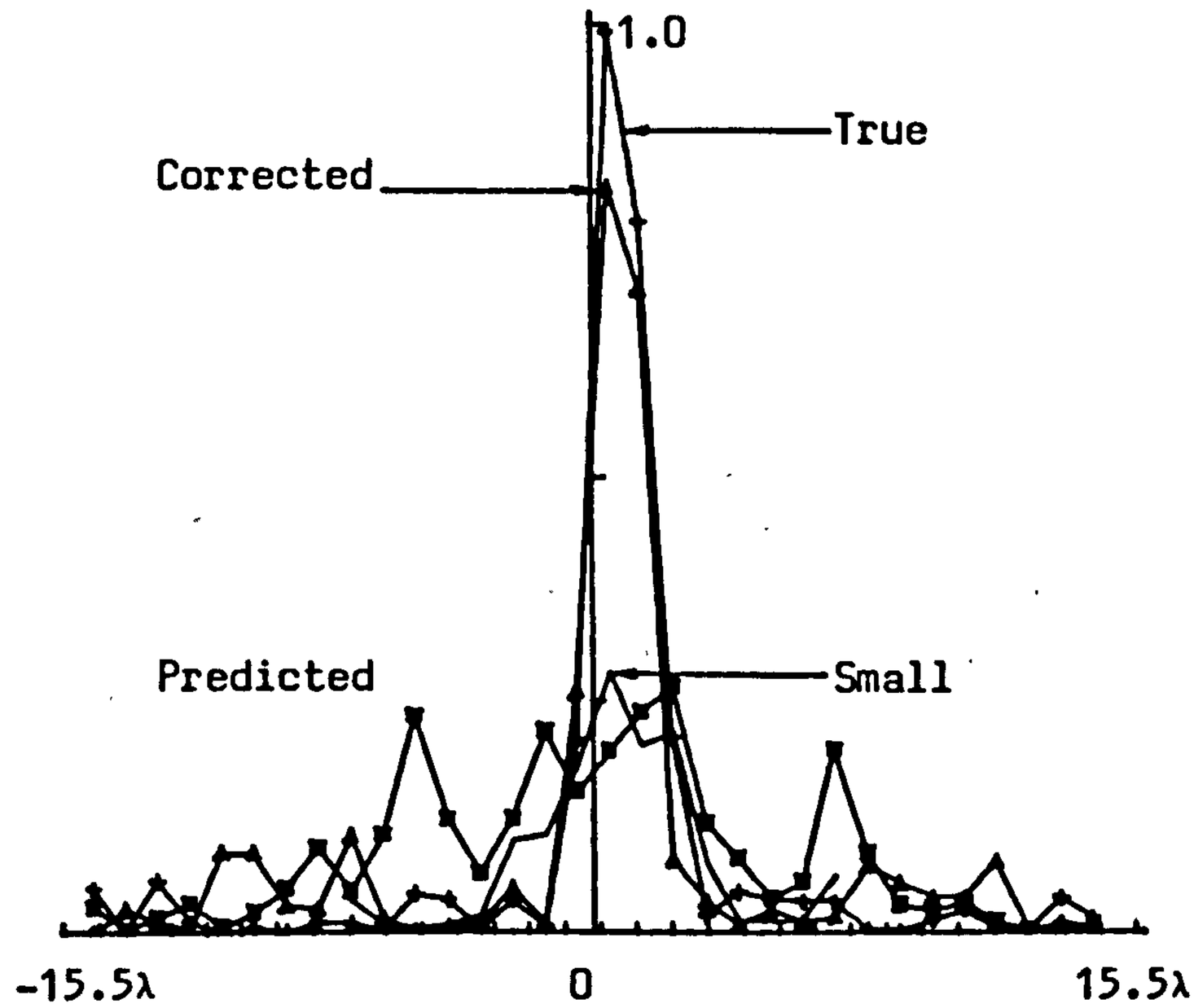


Hologram: Δ=1, M=8,N=16 Object: $x_o$=0 , z=93λ

Fig. 7.20 : Prediction errors and reconstructed image obtained when the inner half of the measured hologram at 93λ is expanded to twice its size using triangular polynomial models for prediction and correction.

a. Prediction errors over the aperture

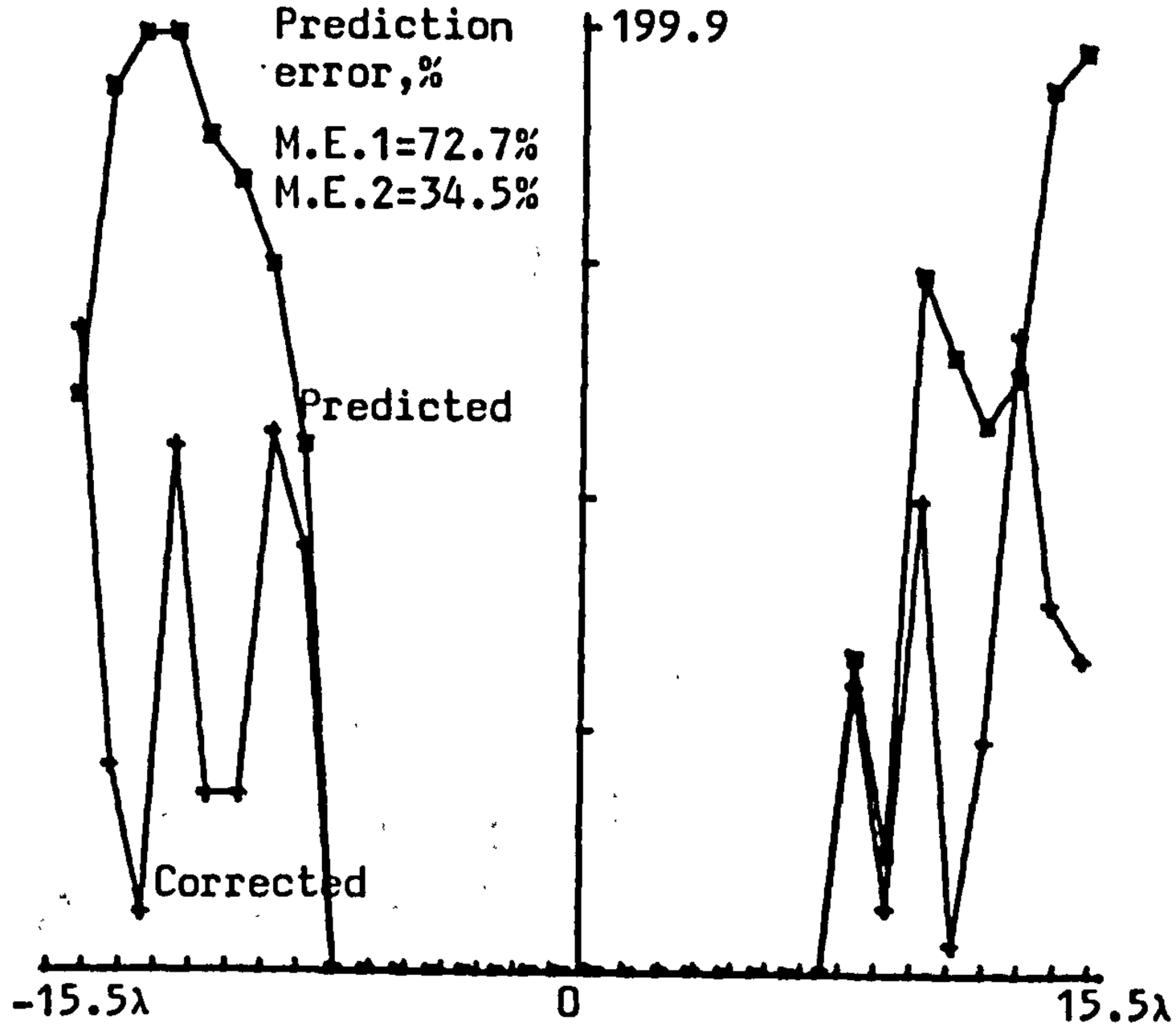


b. Normalized intensities of the images from the small, true, predicted, and corrected apertures reconstructed at the optimum range of 132λ

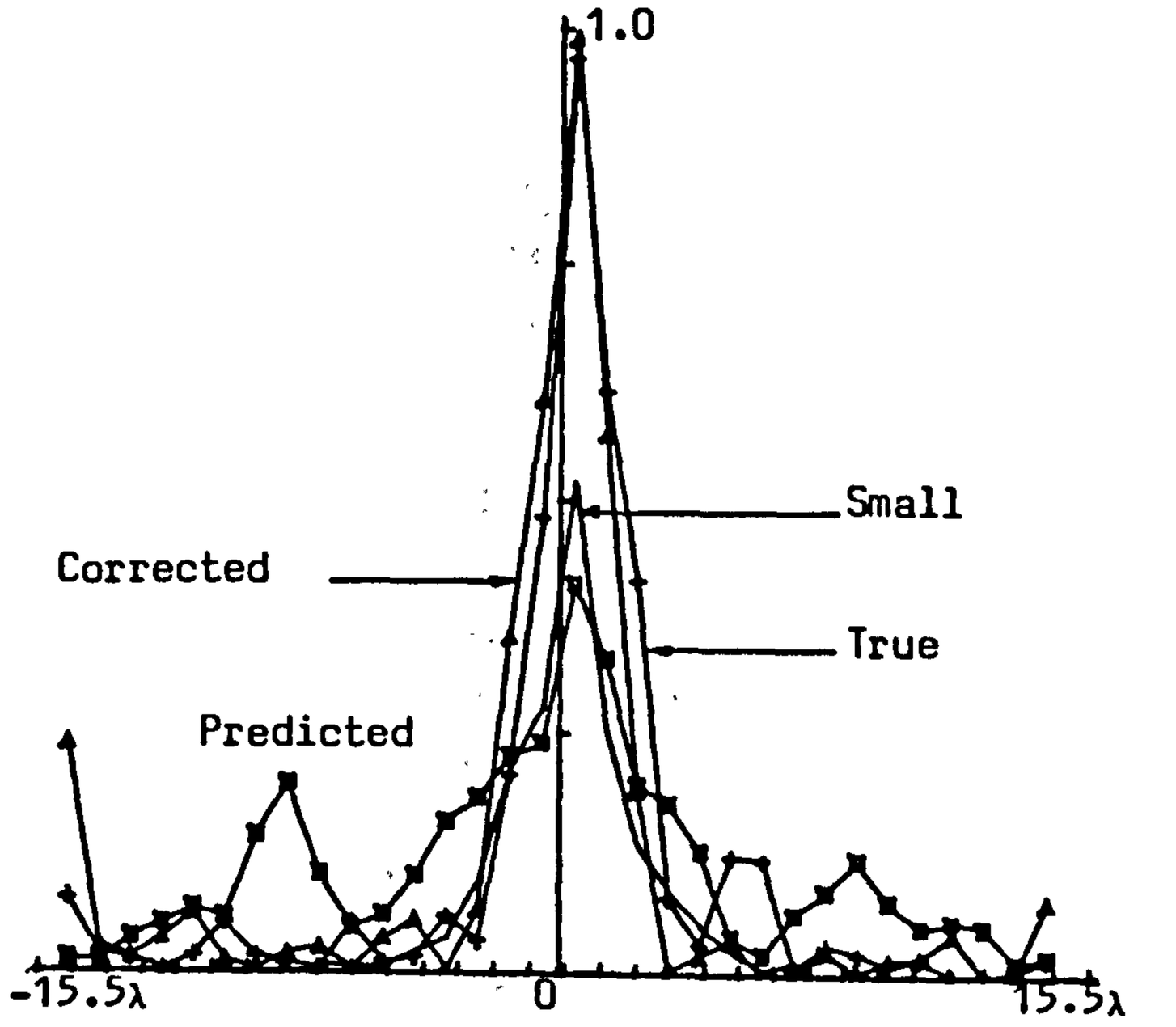


Hologram : Δ=1, M=8,N=16 Object: $x_o$=0 , z=144λ

Fig. 7.21: Prediction errors and reconstructed images obtained when the inner half of the measured hologram at 144λ is expanded to twice its size using triangular polynomial models for prediction and correction.

a. Intensity of reconstructed images at 93λ

Hologram:

Δ=1,M=8,N=16

Object:

$x_o$=0, z=93λ

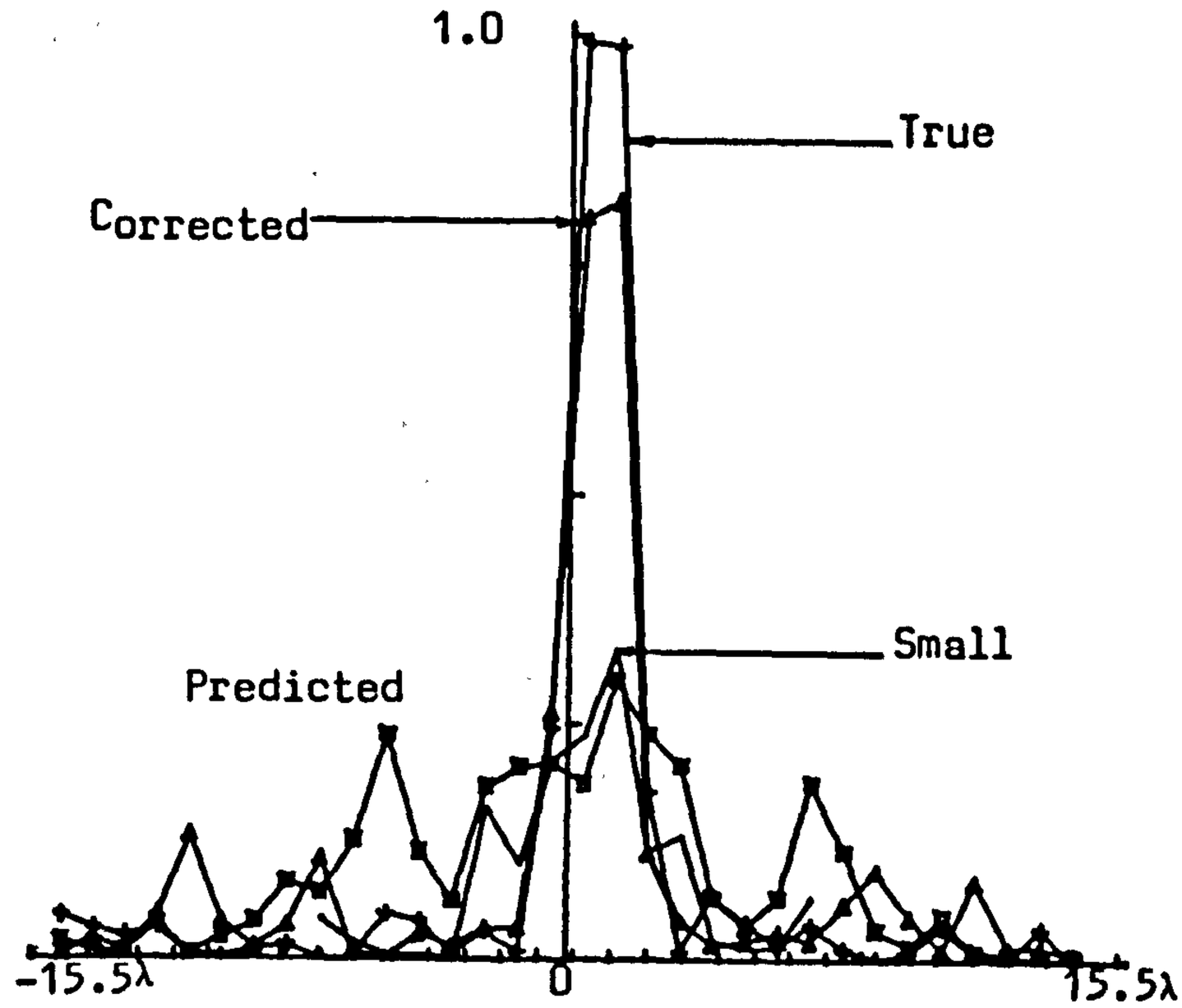


b. Intensity of reconstructed images at 144λ

Hologram:

Δ=1,M=8,N=16

Object:

$x_o$=0, z=144λ

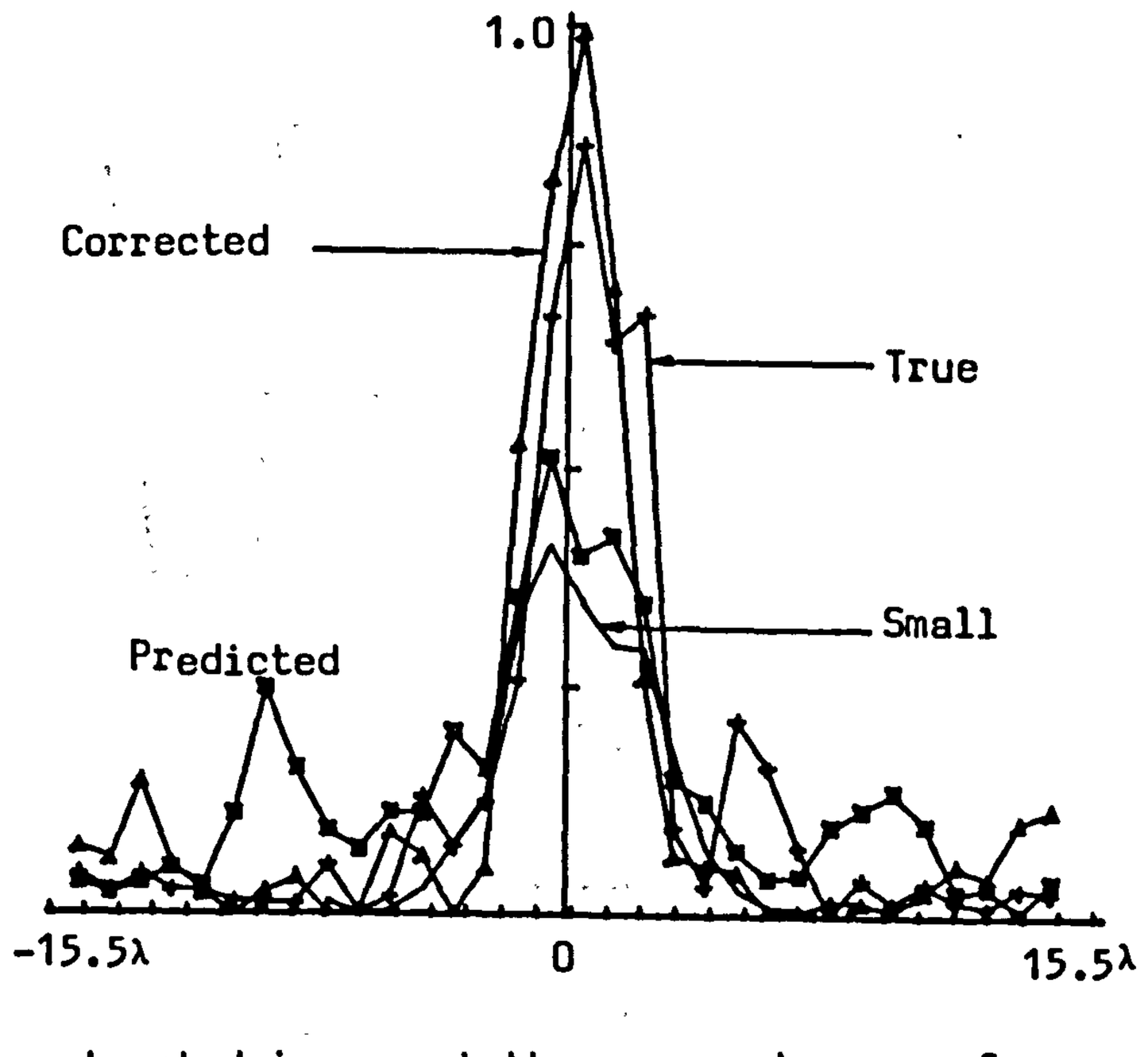


Fig. 7.22 : Reconstructed images at the measured ranges from the small, true, predicted apertures for the holograms measured at 93λ and 144λ. Predictive and corrective models : Triangular polynomial type.

a. Smoothed function of the hologram phase over the middle half of the measured hologram obtained with a smoothing factor s=300. The plot also shows the original ohase data.

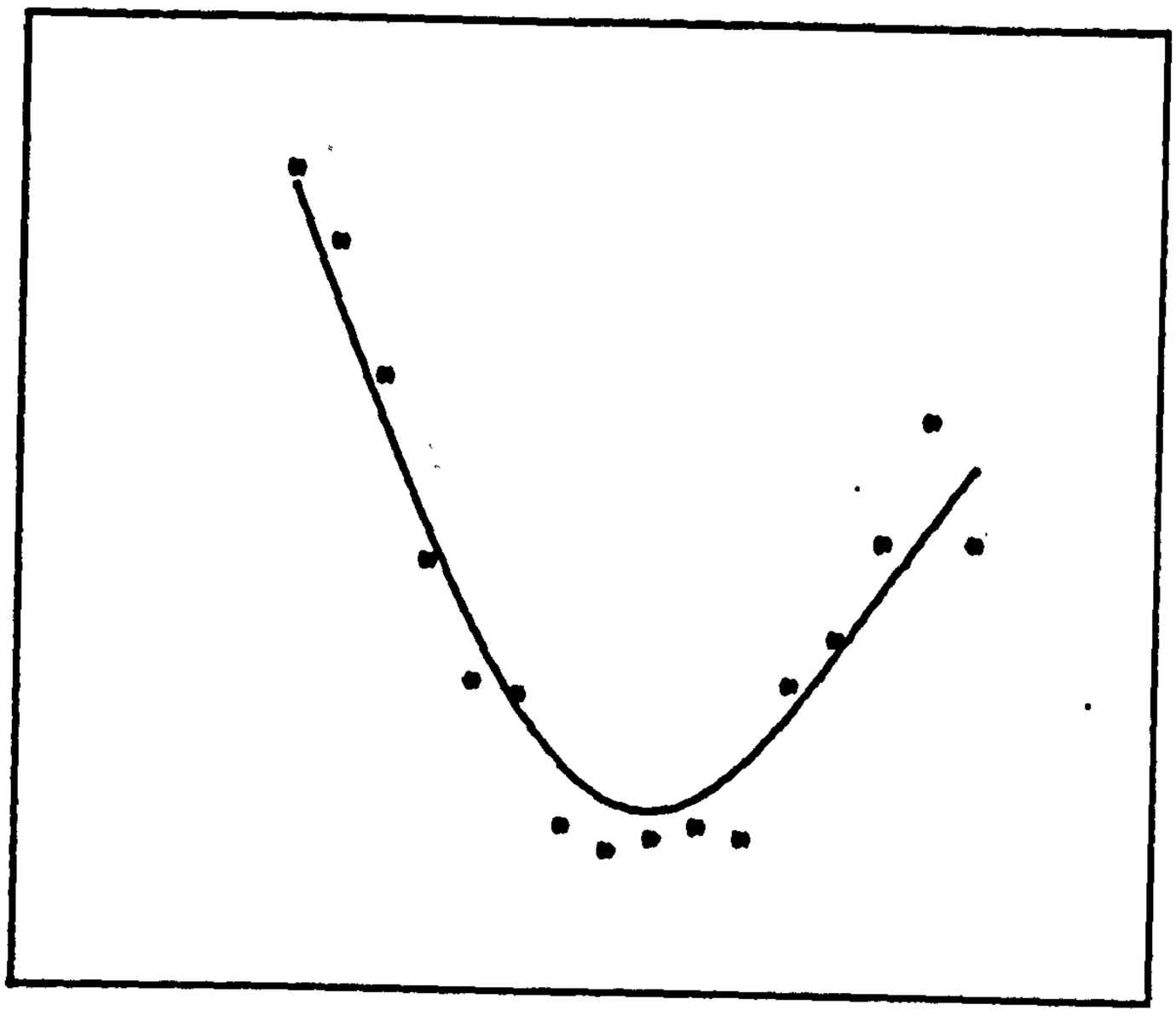

b. Hologram phase over the total apertures with the values at the middle half replaced by the corresponding values of the smoothed function in (a) above.

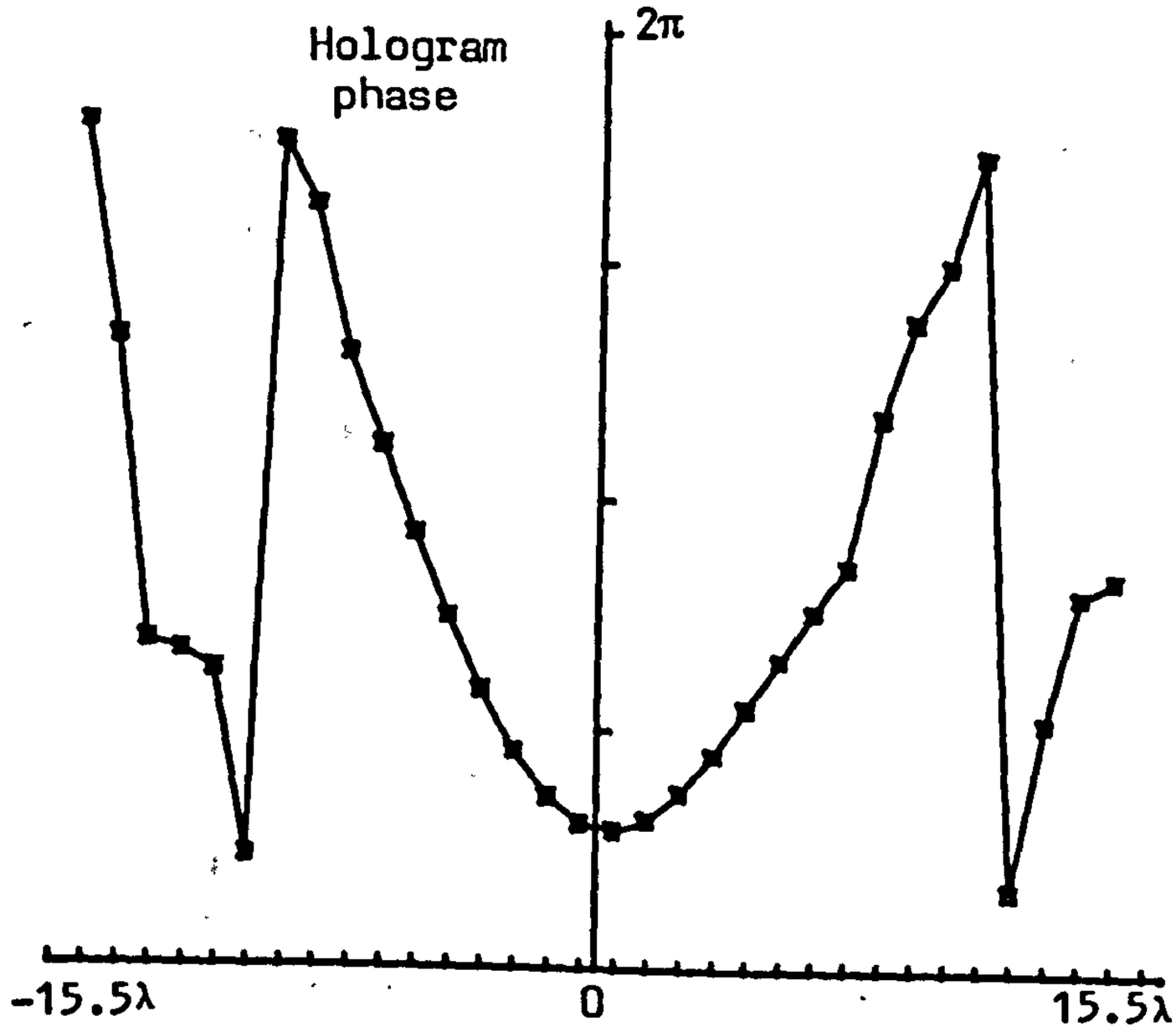


Hologram: Δ=1λ, 32 samples  Object: $x_o$=0, z=93λ

Fig. 7.23 : Smoothing the phase function over the middle half of the hologram measured at 93λ

a. Smoothed function of the hologram phase over the middle half of the measured hologram obtained with a smoothing factor s=200. The plot also shows the original phase data.

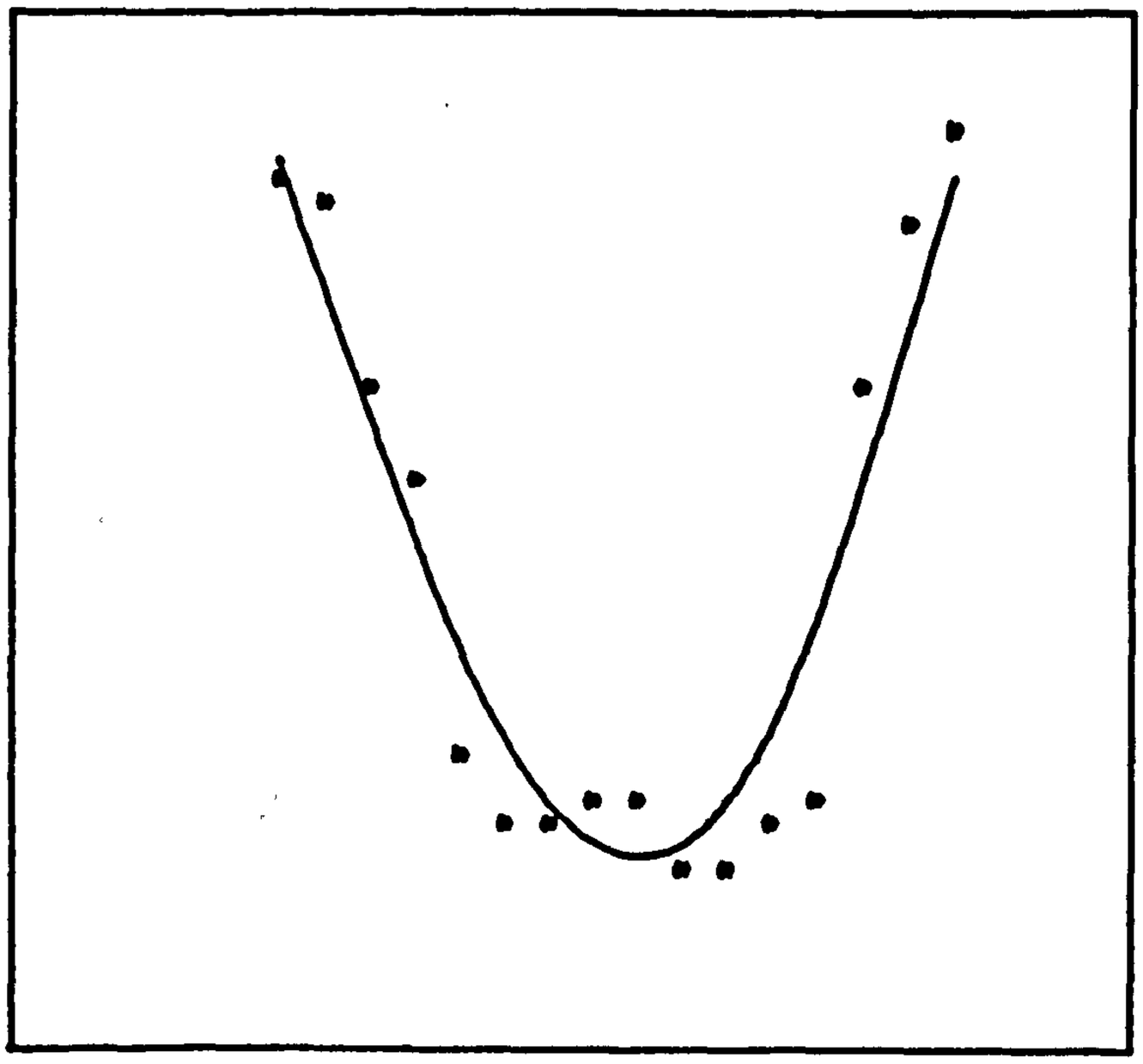

b. Hologram phase over the total aperture with the values at the middle half replaced by the corresponding values of the smoothed function in (a) above.

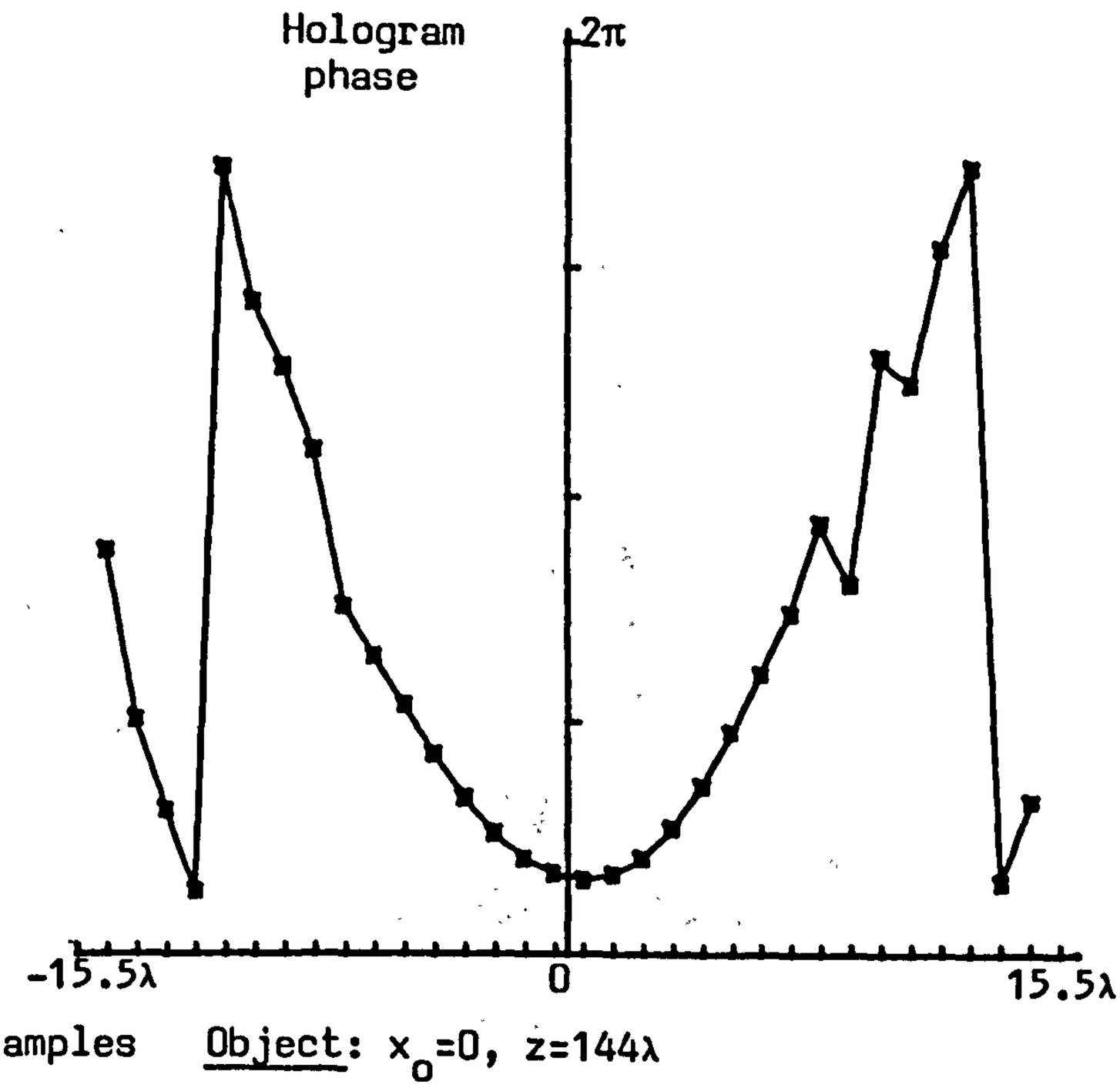


Hologram: Δ=1λ, 32 samples  Object: $x_o$=0, z=144λ

Fig. 7.24 : Smoothing the phase function over the middle half of the hologram measured at 144λ

a. Prediction errors over the aperture

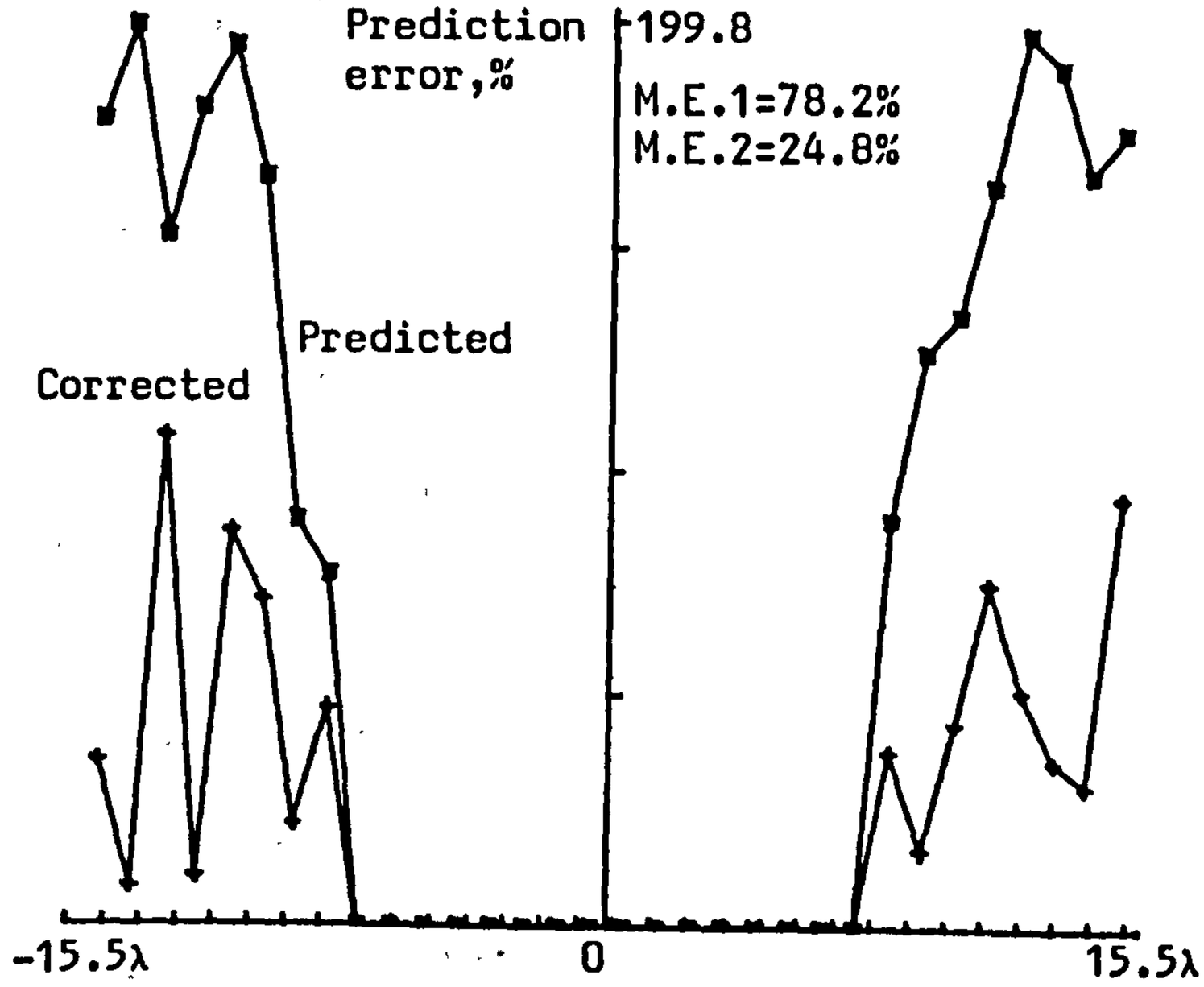


b. Reconstructed images at the optimum range of 90λ

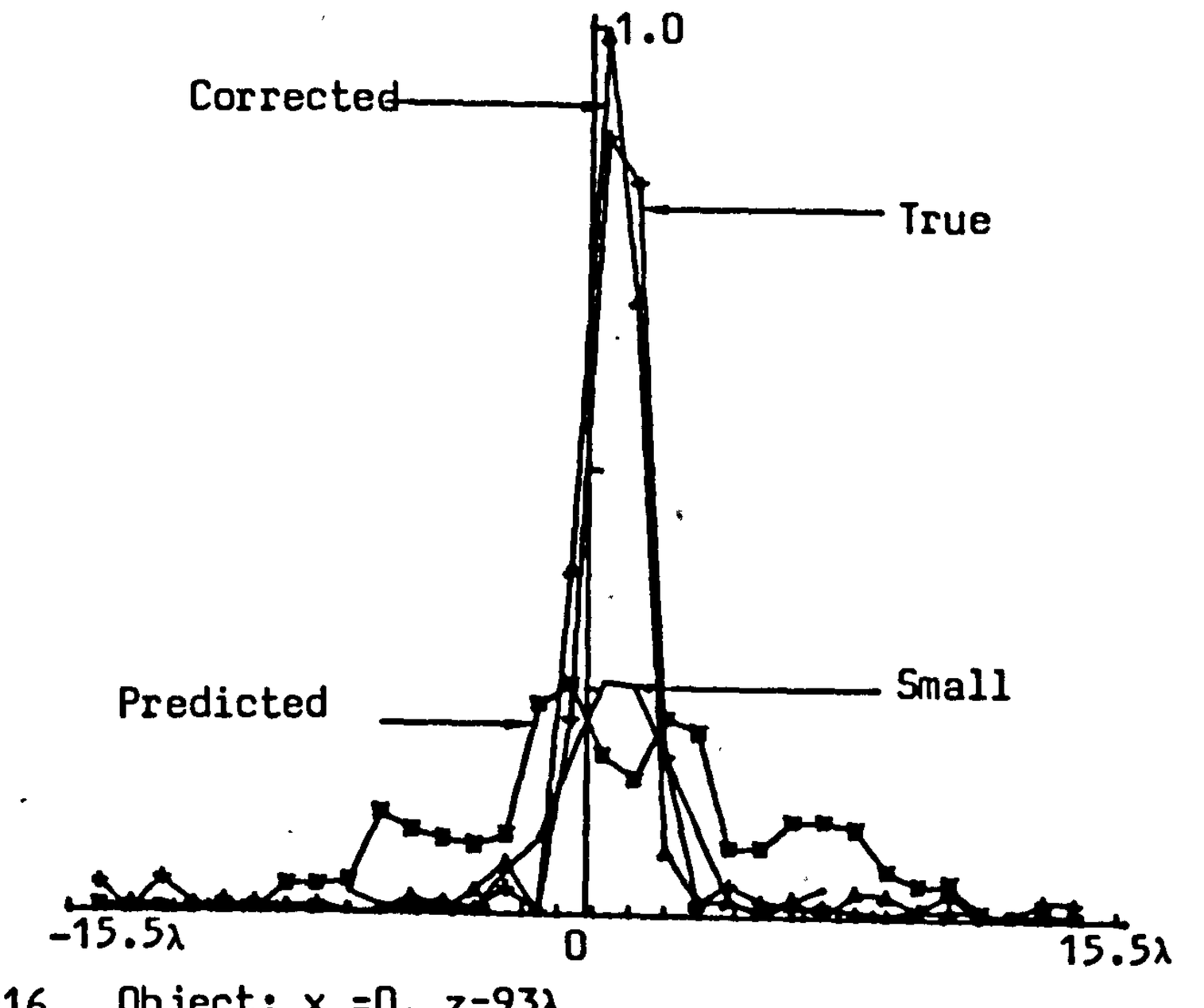


Hologram: Δ=1λ, M=8,N=16 Object: $x_o$=0, z=93λ

Fig. 7.25 : Improvement in the correction accuracy and in the quality of the image reconstructed from the corrected hologram as a result of smoothing the 16-point 'available' aperture as shown in Fig. 7.23 for the hologram measured at 93λ

a. Prediction errors over the aperture

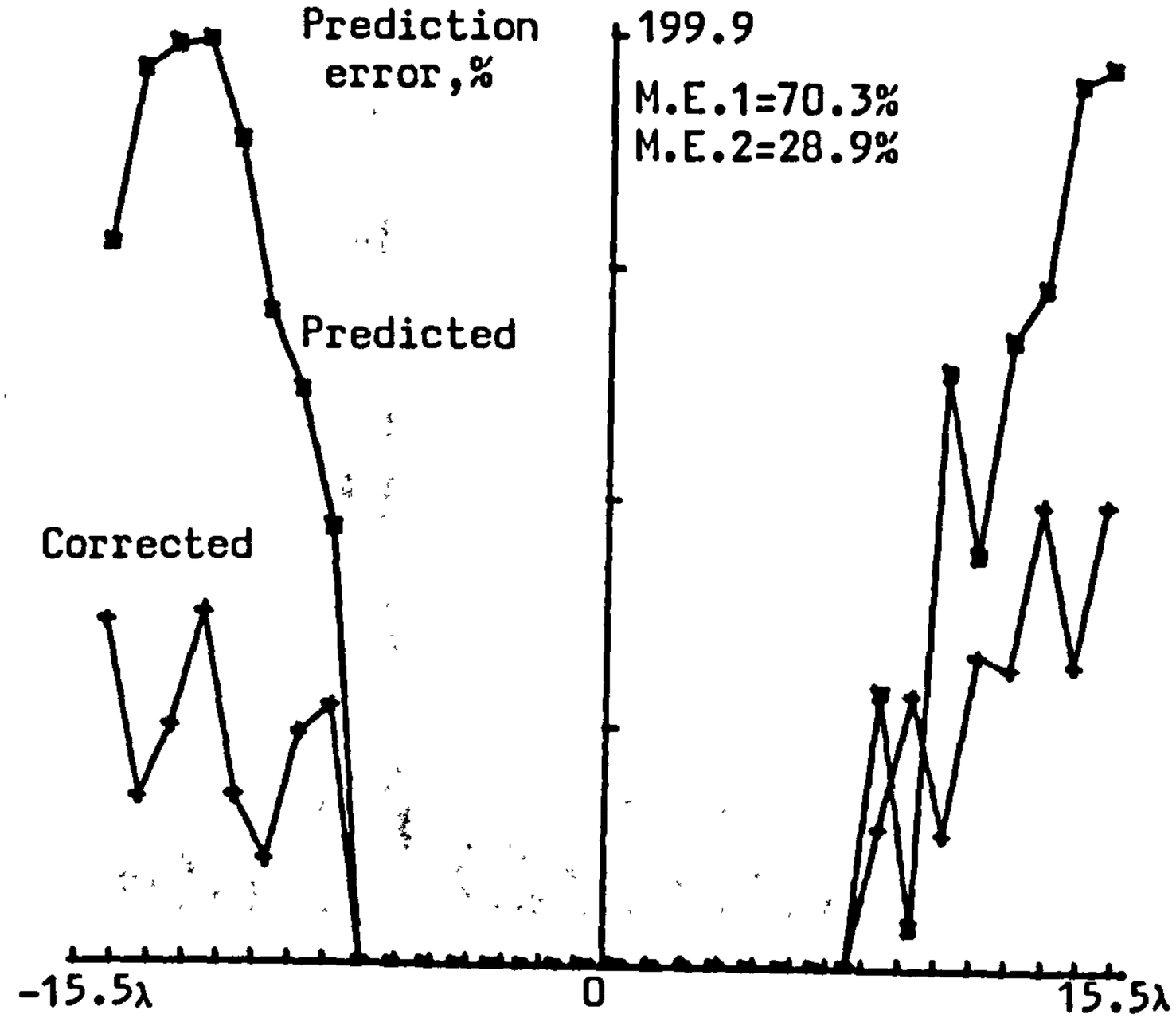


b. Reconstructed images at the optimum range of 132λ

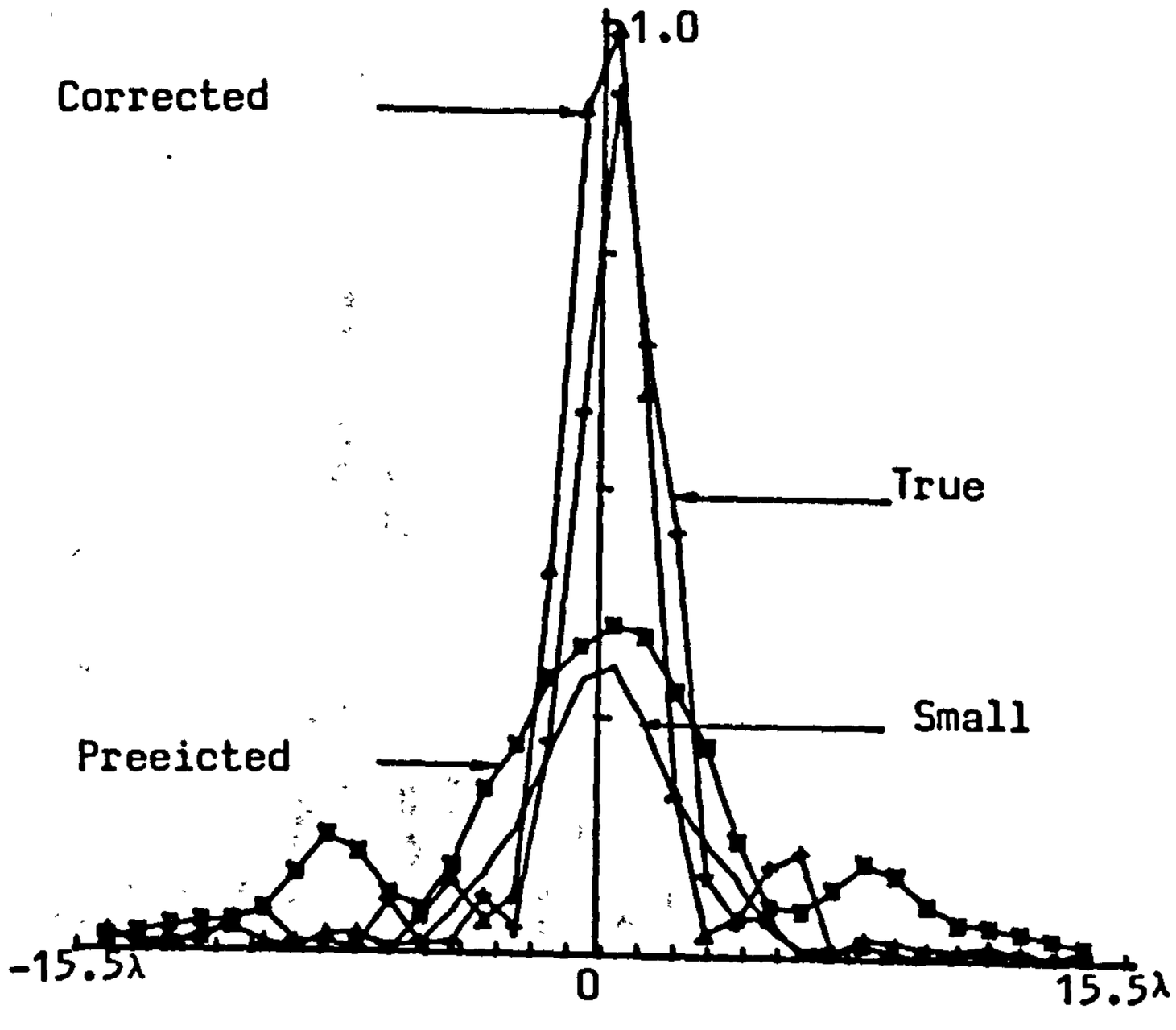


Hologram: Δ=1, M=8, N=16 Object: $x_o$=0, z=144λ

Fig. 7.26 : Improvement in the correction accuracy and in the quality of the image reconstructed from the corrected hologram as a result of smoothing the 16-point 'available' aperture as shown in Fig. 7.24 for the hologram measured at 144λ

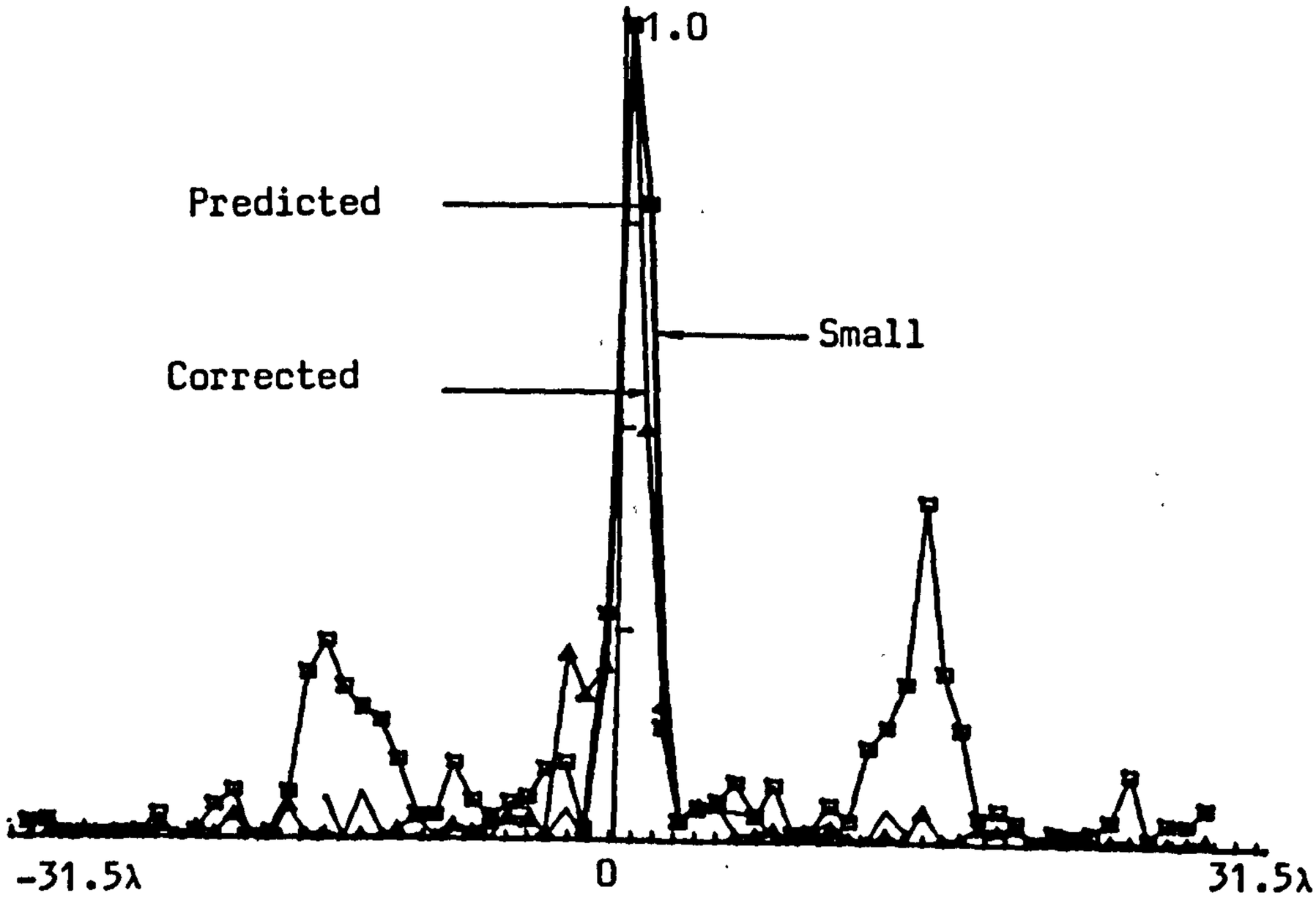


a. Images reconstructed at 90λ for the hologram recorded at 93λ

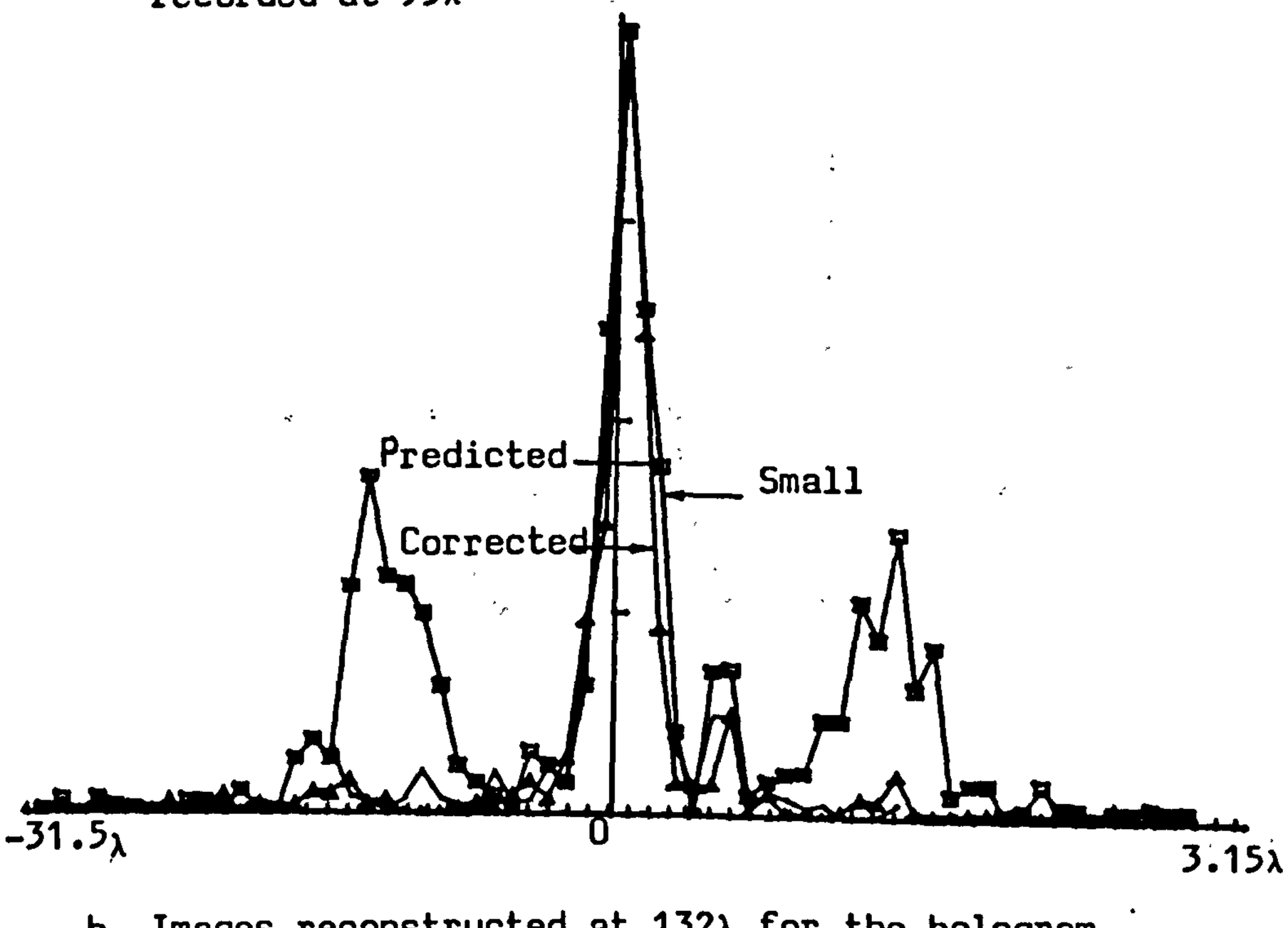


b. Images reconstructed at 132λ for the hologram recorded at 144λ

Hologram in both cases: Δ=1, M=16, N=32

Fig. 7.27 : Reconstructed images obtained at the optimum ranges from the holograms recorded at 93λ and 144λ when the measured 32-point hologram is doubled in size through prediction and correction using triangular polynomial models.

a. Smoothed phase function over the whole of the measured hologram obtained using a smoothing factor of s=2000. The plot also shows the original phase data.

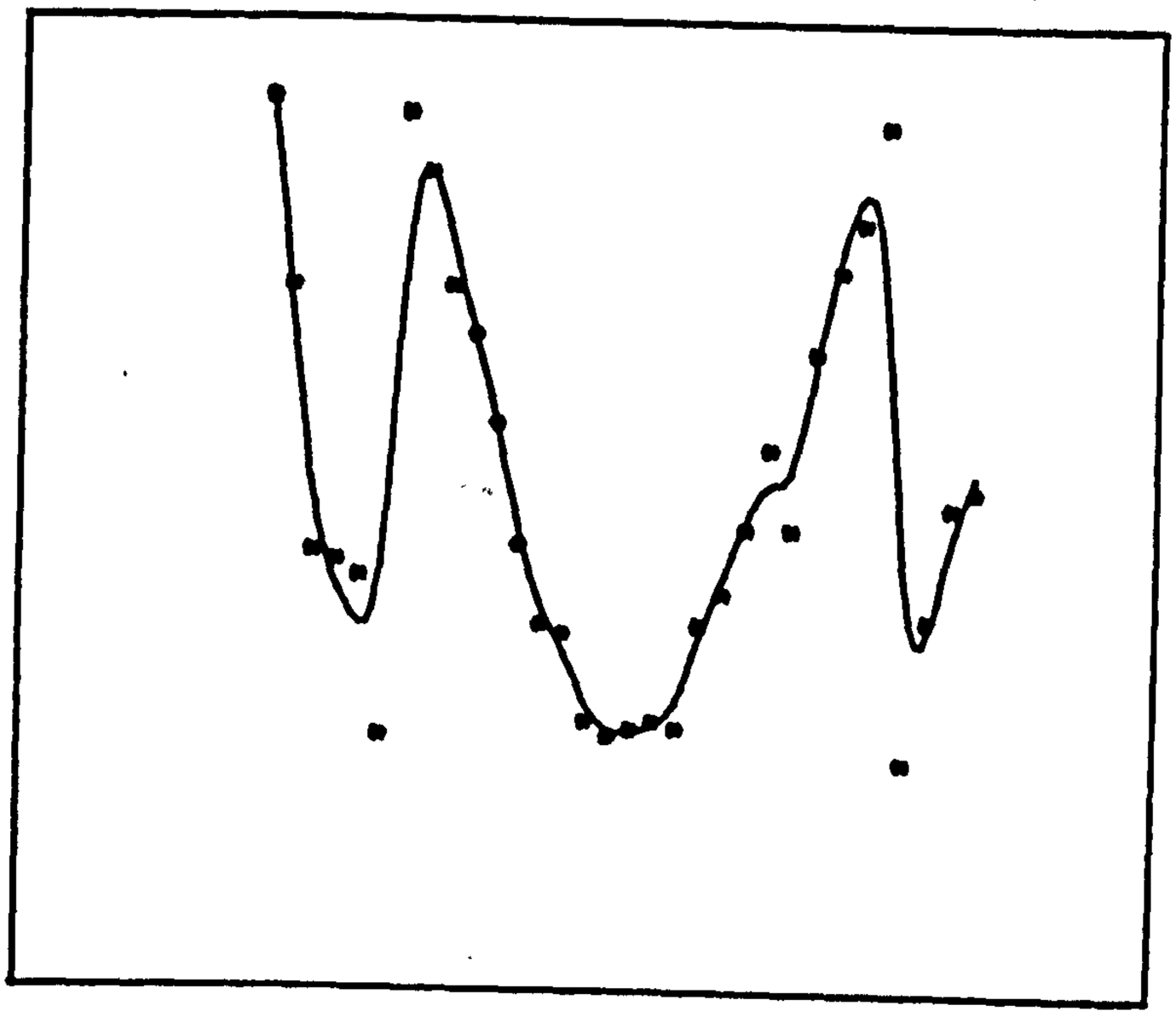

b. Hologram phase over the total aperture with the values at the sampling points replaced by the corresponding values of the smoothed function in (a) above

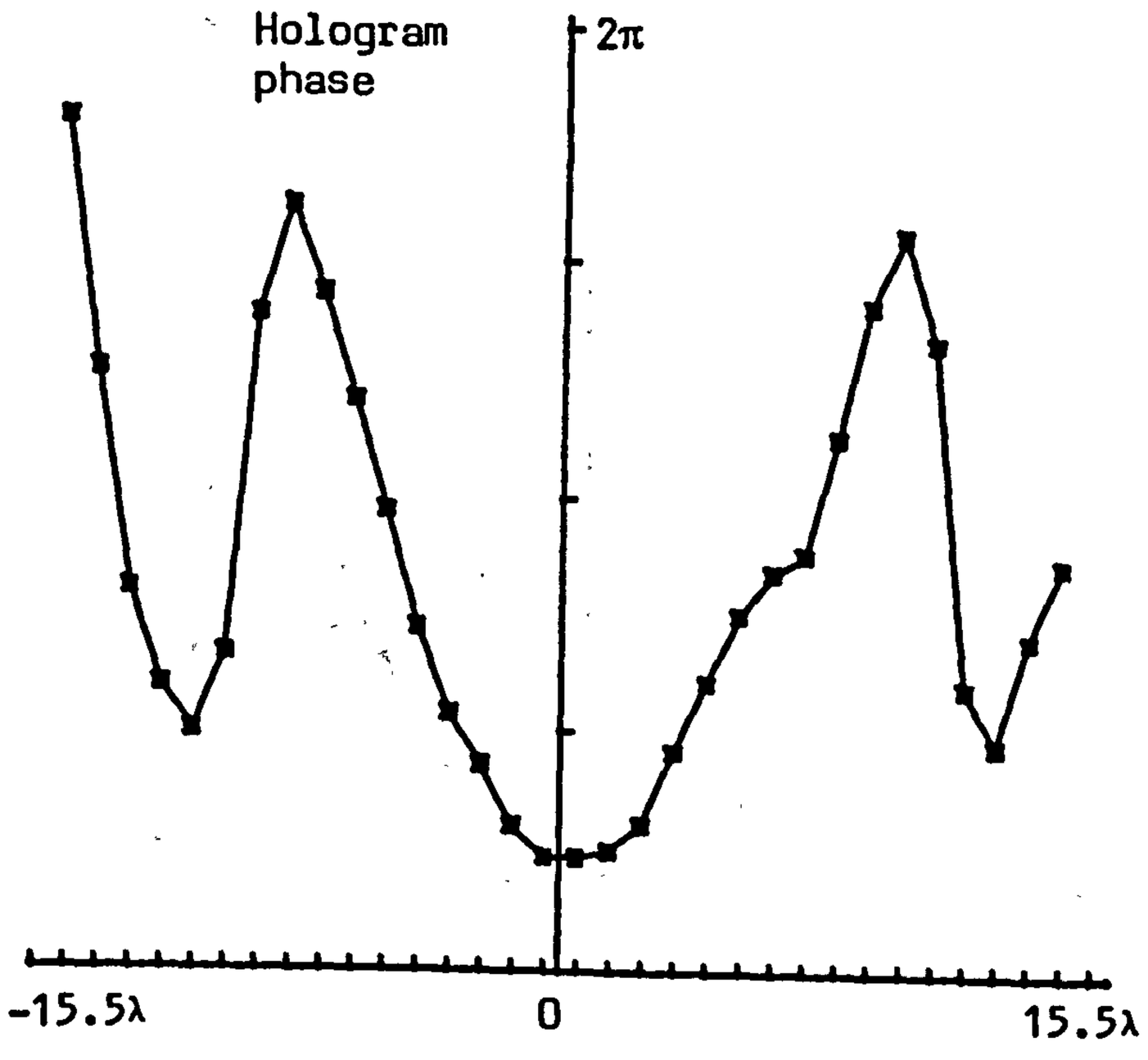


Hologram: Δ=1, 32 samples Object: $x_o$=0 , z=93λ

Fig. 7.28 : Smoothing the phase function over the whole of the hologram measured at 93λ

a. Smoothed phase function over the whole of the measured hologram obtained using a smoothing factor of s=2000. The plot also shows the original phase data.

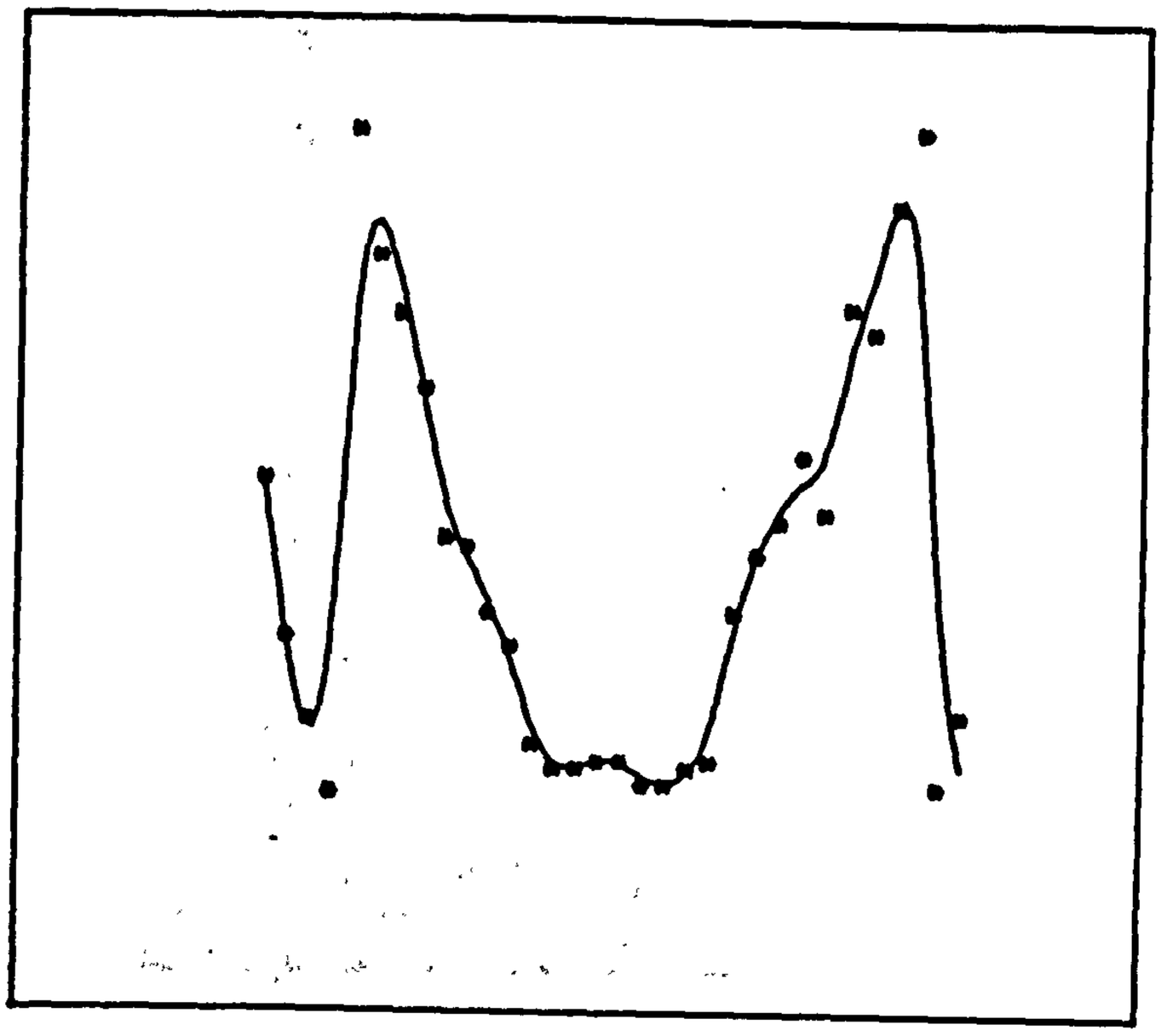

b. Hologram phase over the total aperture with the values at the sampling points replaced by the corresponding values of the smoothed function in (a) above

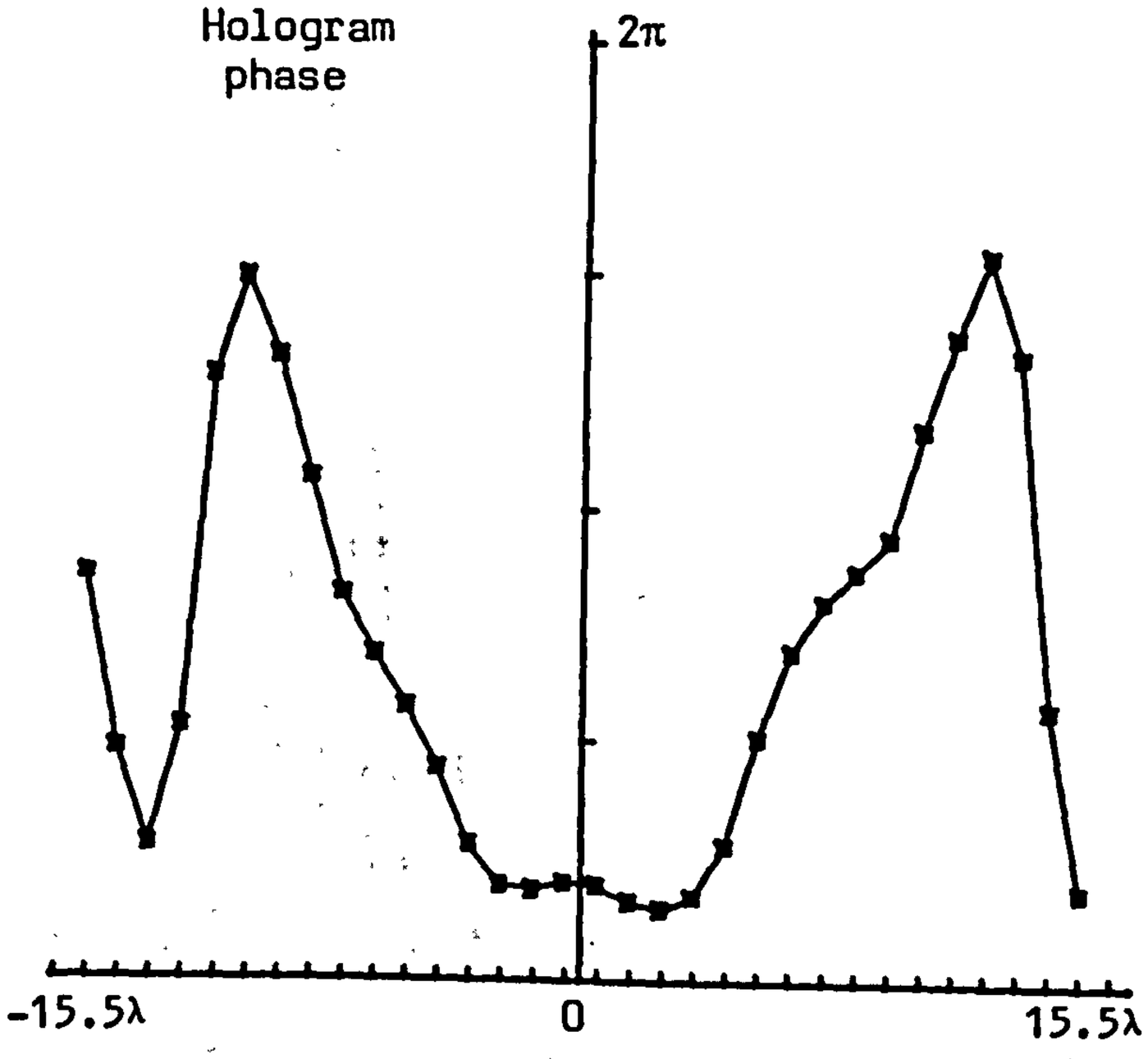


Hologram: Δ=1, 32 samples  Object: $x_o$=0 , z=144λ

Fig. 7.29 : Smoothing the phase function over the whole of the hologram measured at 144λ

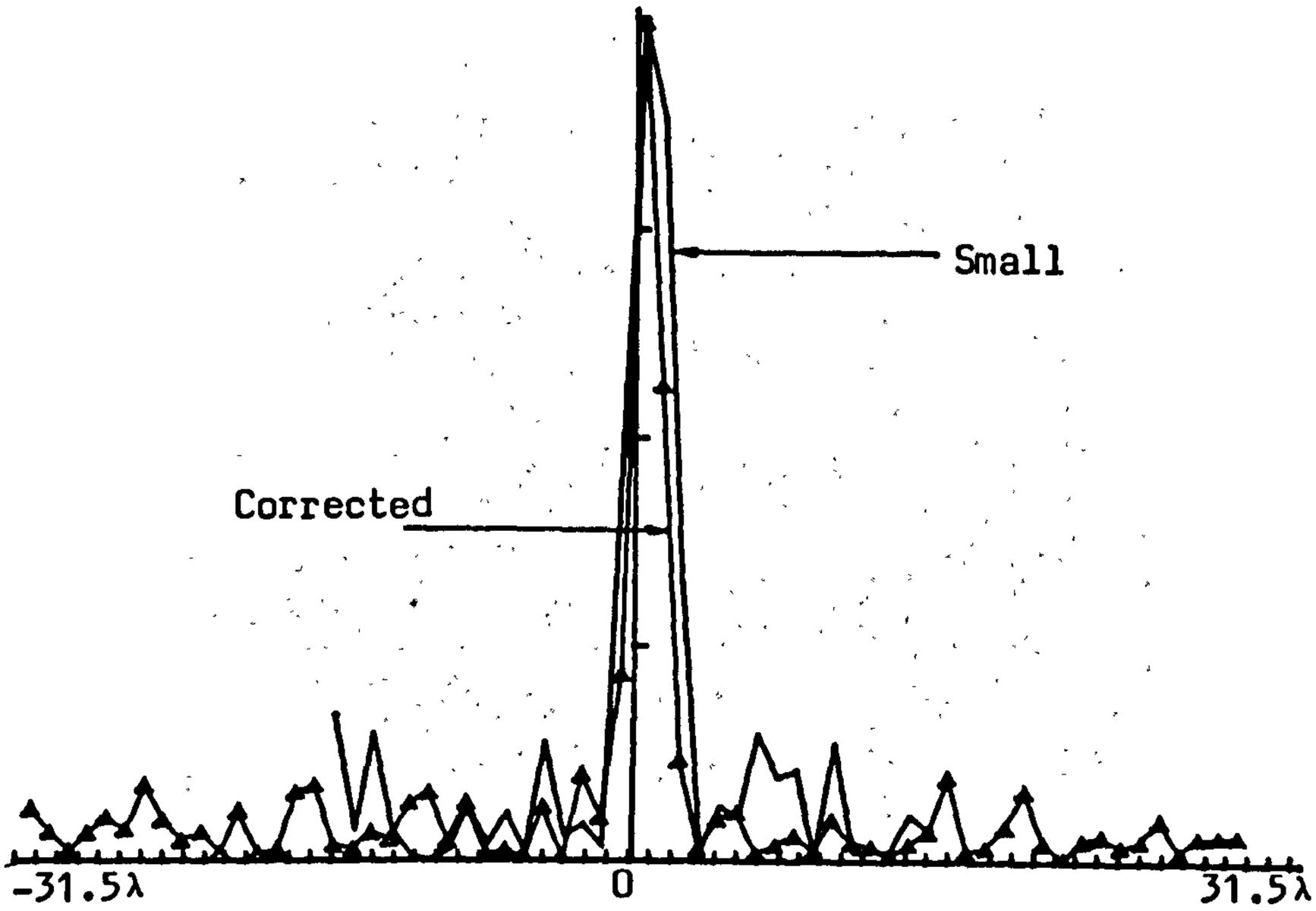


a. Images reconstructed at 90λ from the small and corrected apertures of the hologram recorded at 93λ after smoothing.

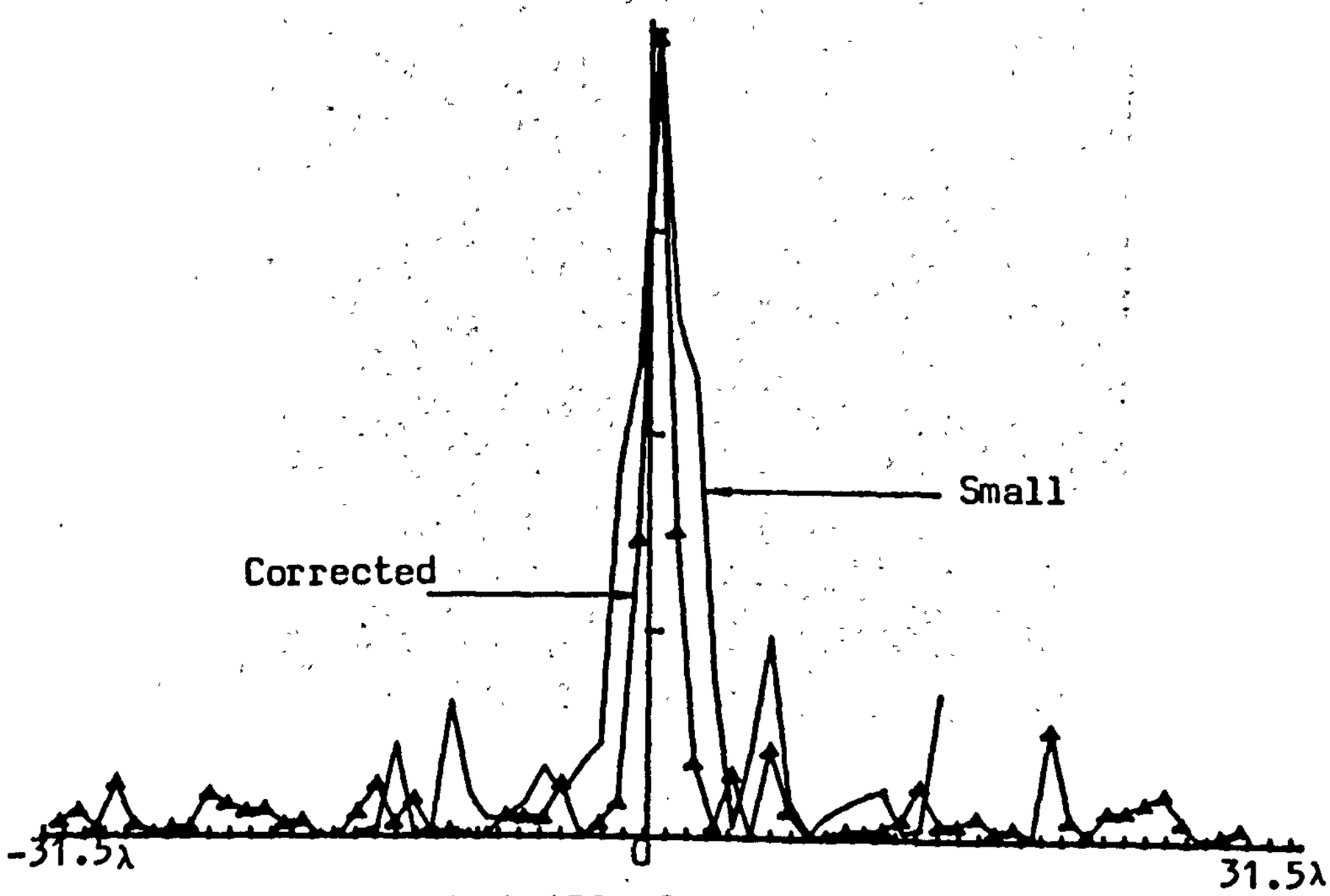


b. Images reconstructed at 132λ from the small and corrected apertures of the hologram recorded at 144λ after smoothing.

Hologram in both cases: Δ=1, M=16, N=32

Fig. 7.30 : Reconstructed images obtained at the optimum ranges from the holograms recorded at 93λ and 144λ when the smoothed 32-point holograms, Figs. 7.28 and 7.29 respectively, are doubled in size through prediction and correction using triangular polynomial models.

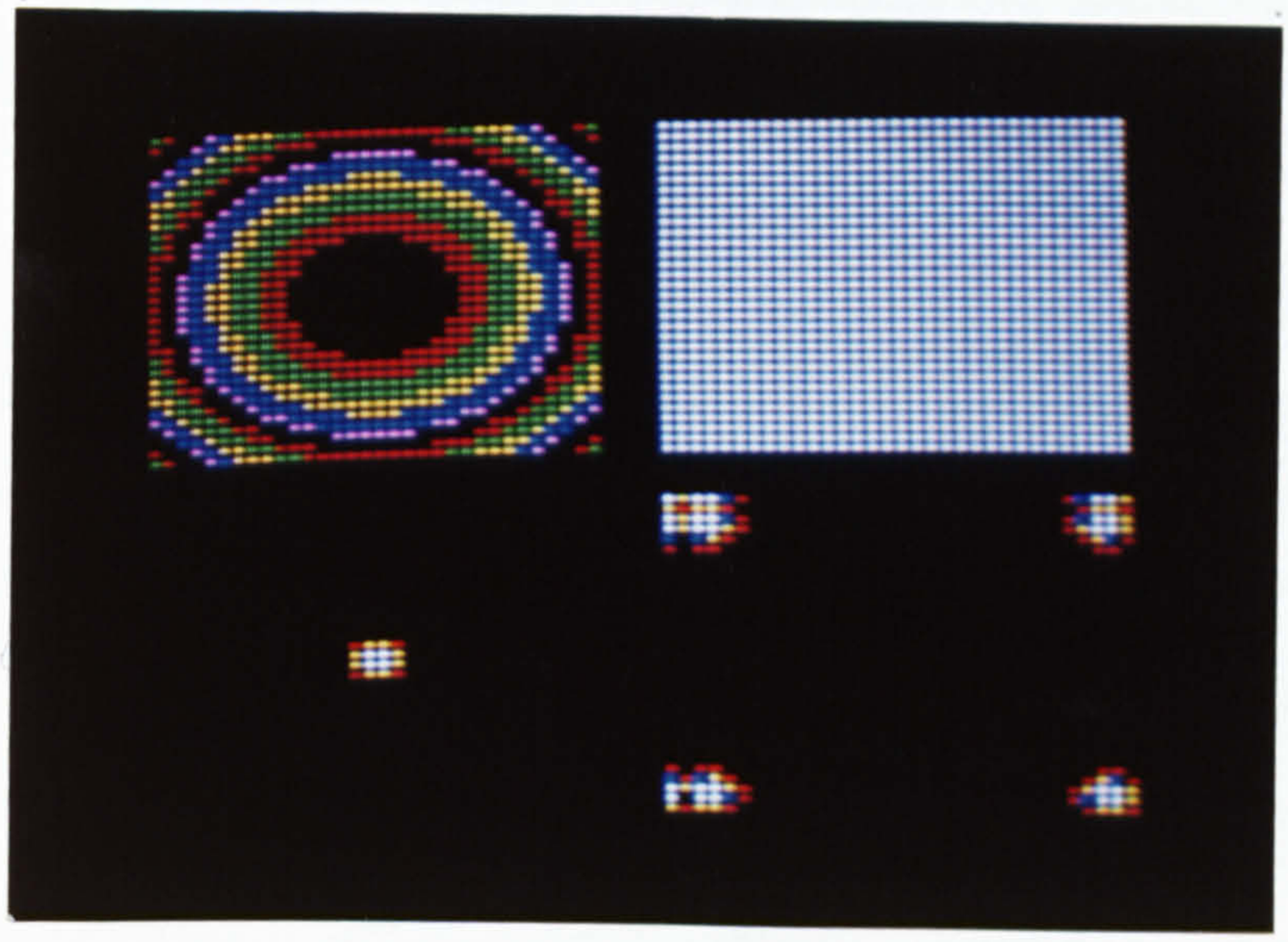

Object on the hologram axis:

$x_o=0$ , $y_o=0$, $z=96\lambda$

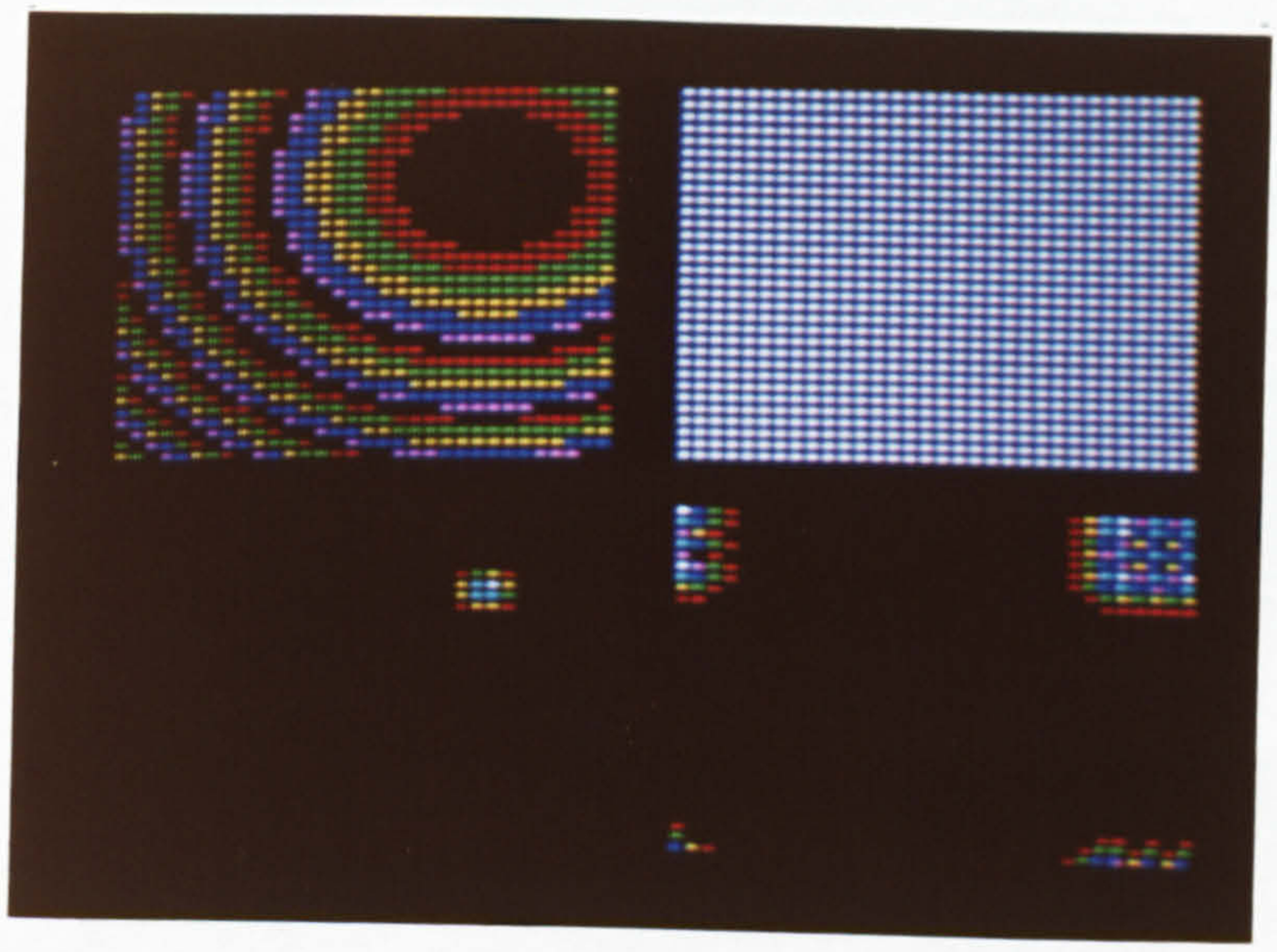

Offset object:

$x_o=8\lambda$, $y_o=8\lambda$, $z=96\lambda$

Fig. 7.31 : Effect of a lateral shift in the object position on the hologram of one point. Hologram: $\Delta=1\lambda$, 32x32 samples

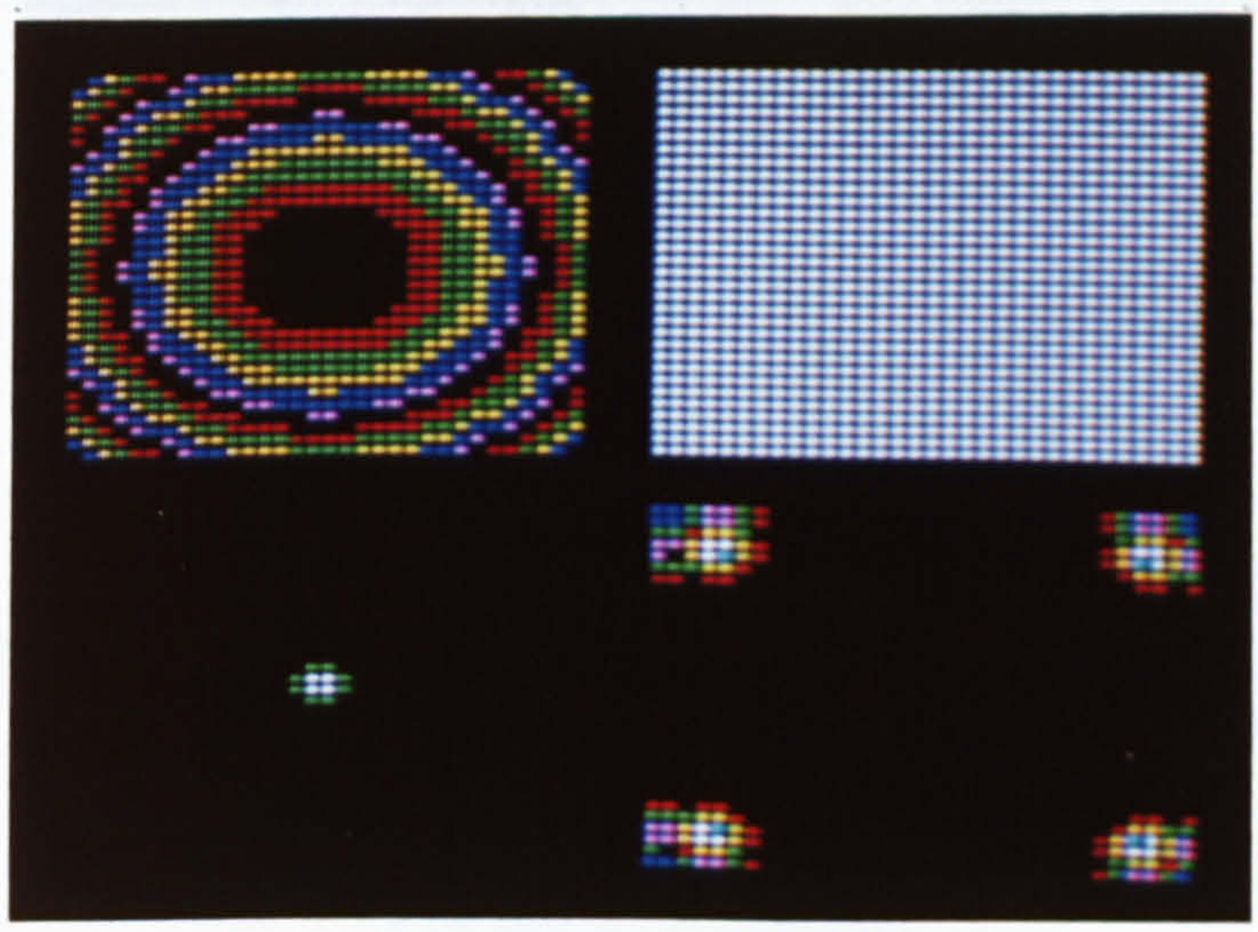

a. Object : $x_o$=0, $y_o$=0, z=97λ

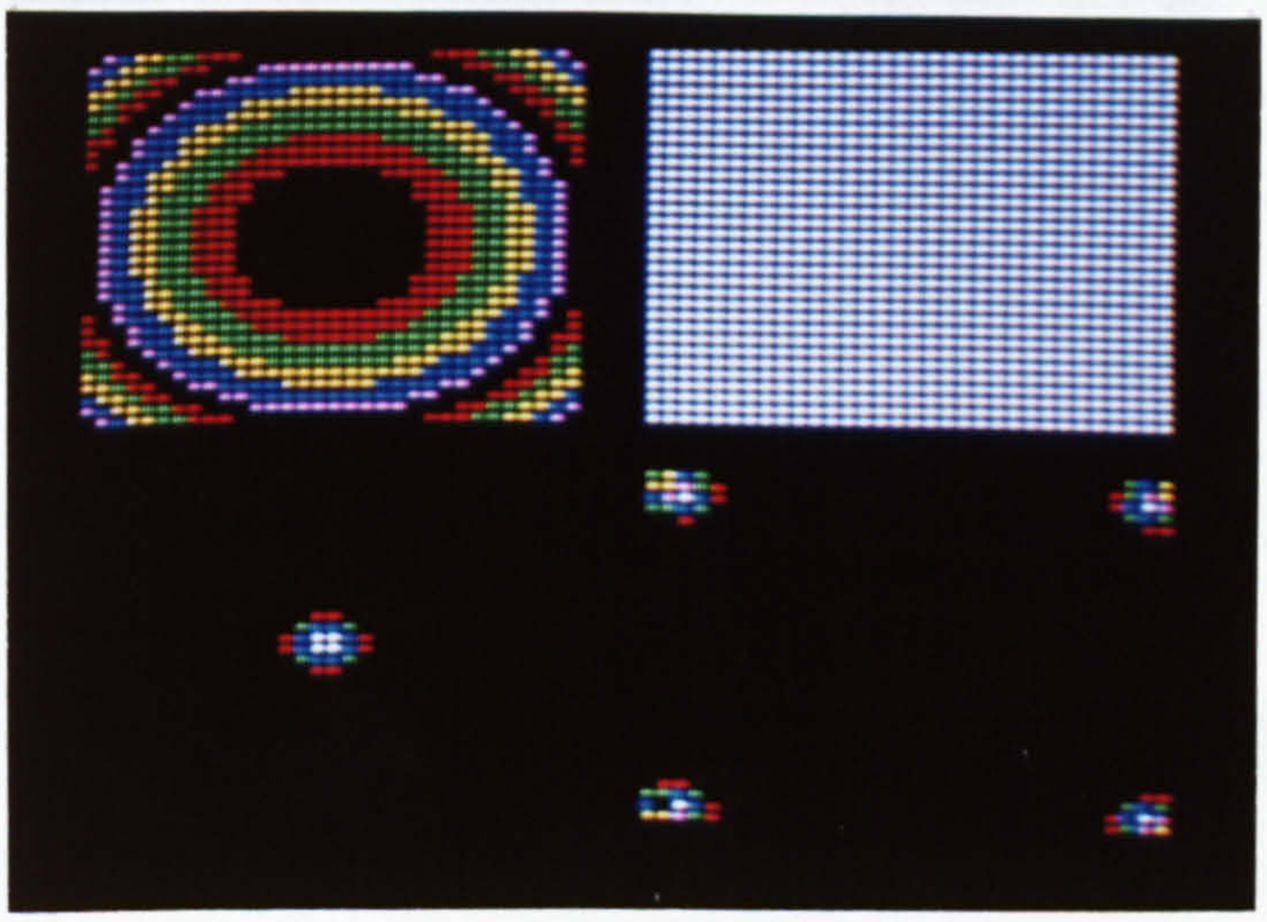

b. Object : $x_o$=0, $y_o$=0, z=144λ

Fig. 7.32 : Effect of increasing the object range on the resolution and the spatial frequency bandwidth of the hologram of a 1-point object. Hologram: Δ=1.11λ, 32x32 samples

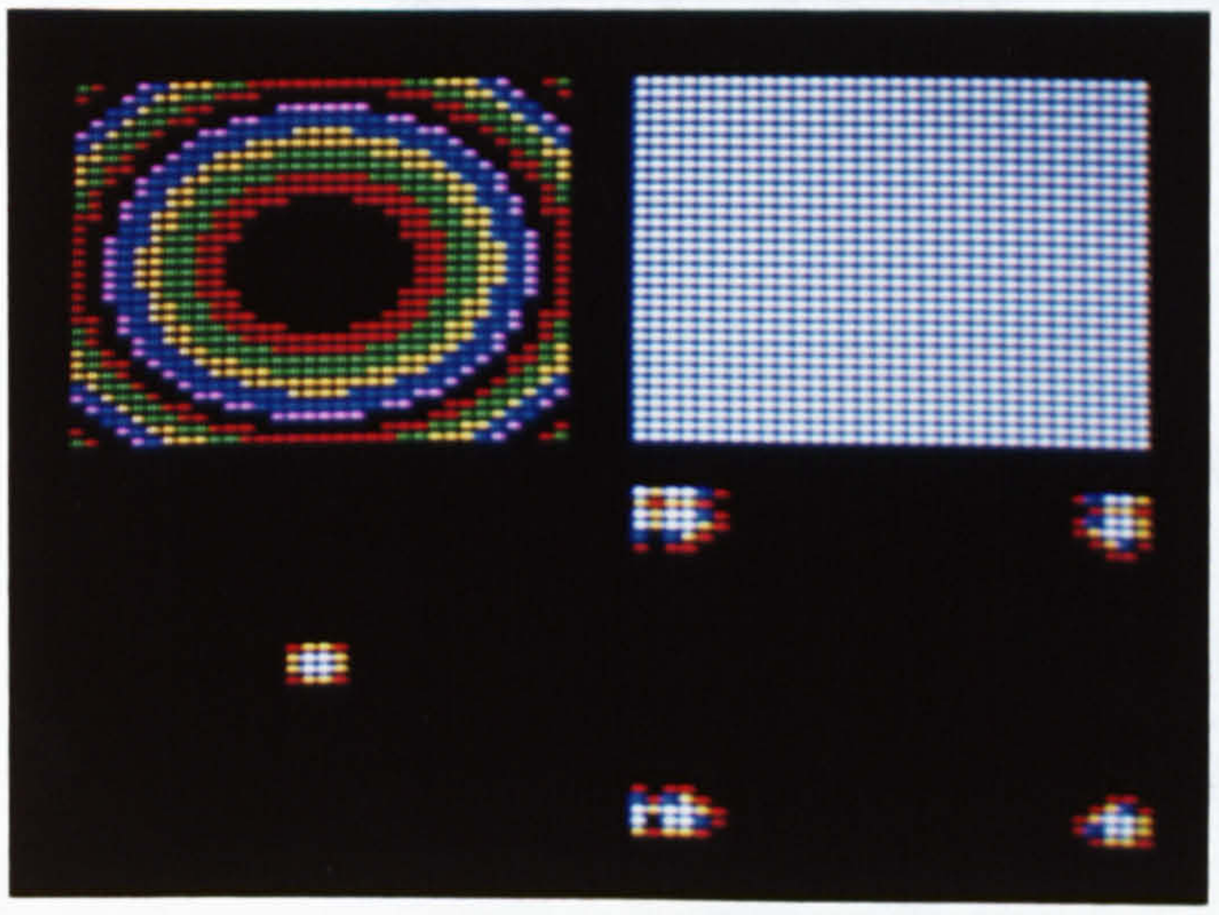

a. Properly sampled hologram:
object: $x_o$=0, $y_o$=0, z=96λ

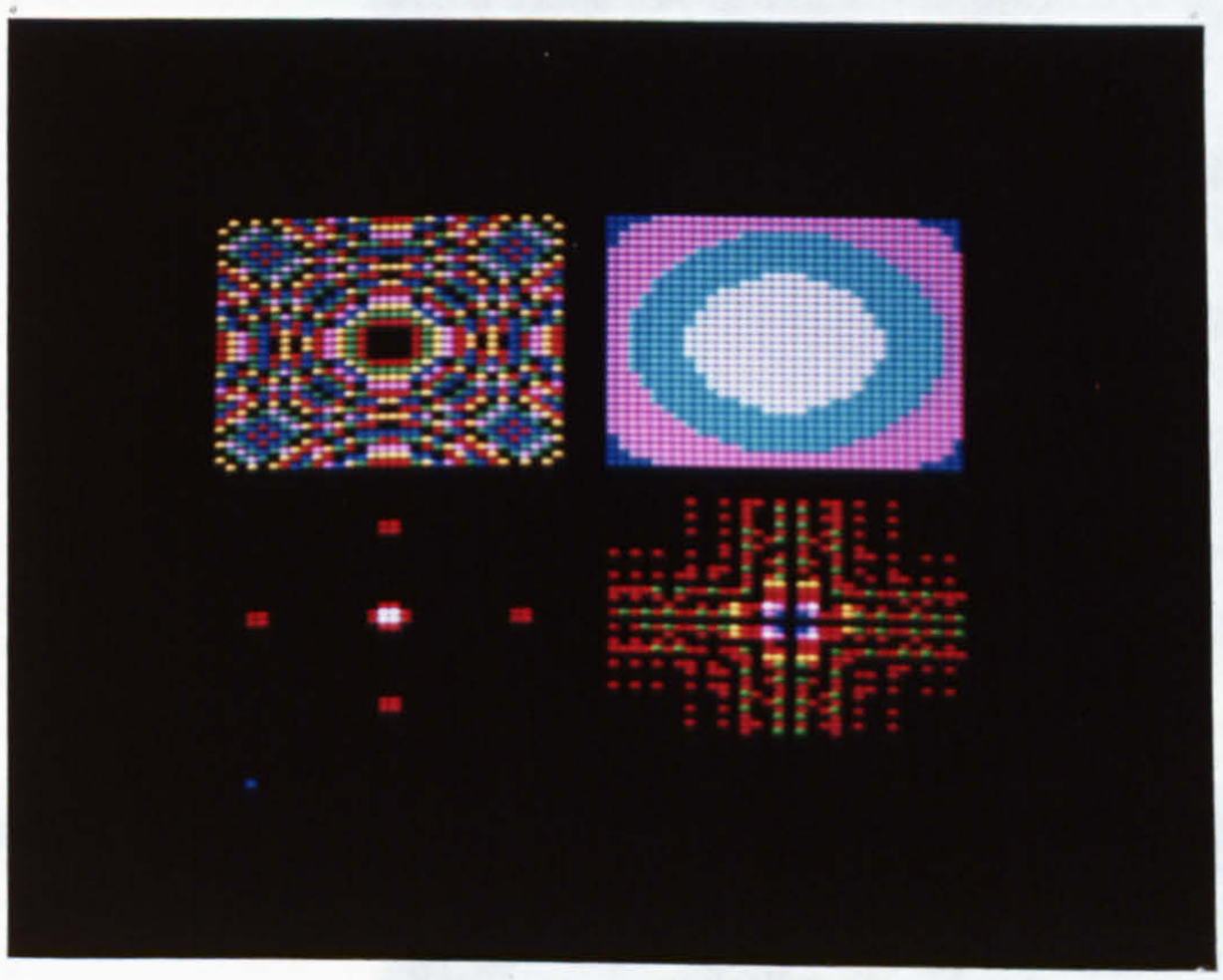

b. Undersampled hologram :
object: $x_o$=0, $y_o$=0, z=16λ

Fig. 7.33 : Effect of undersampling of the hologram and the generation of multiple images. Hologram: Δ=1λ 32x32 samples.

a. Reconstruction distance : 80λ

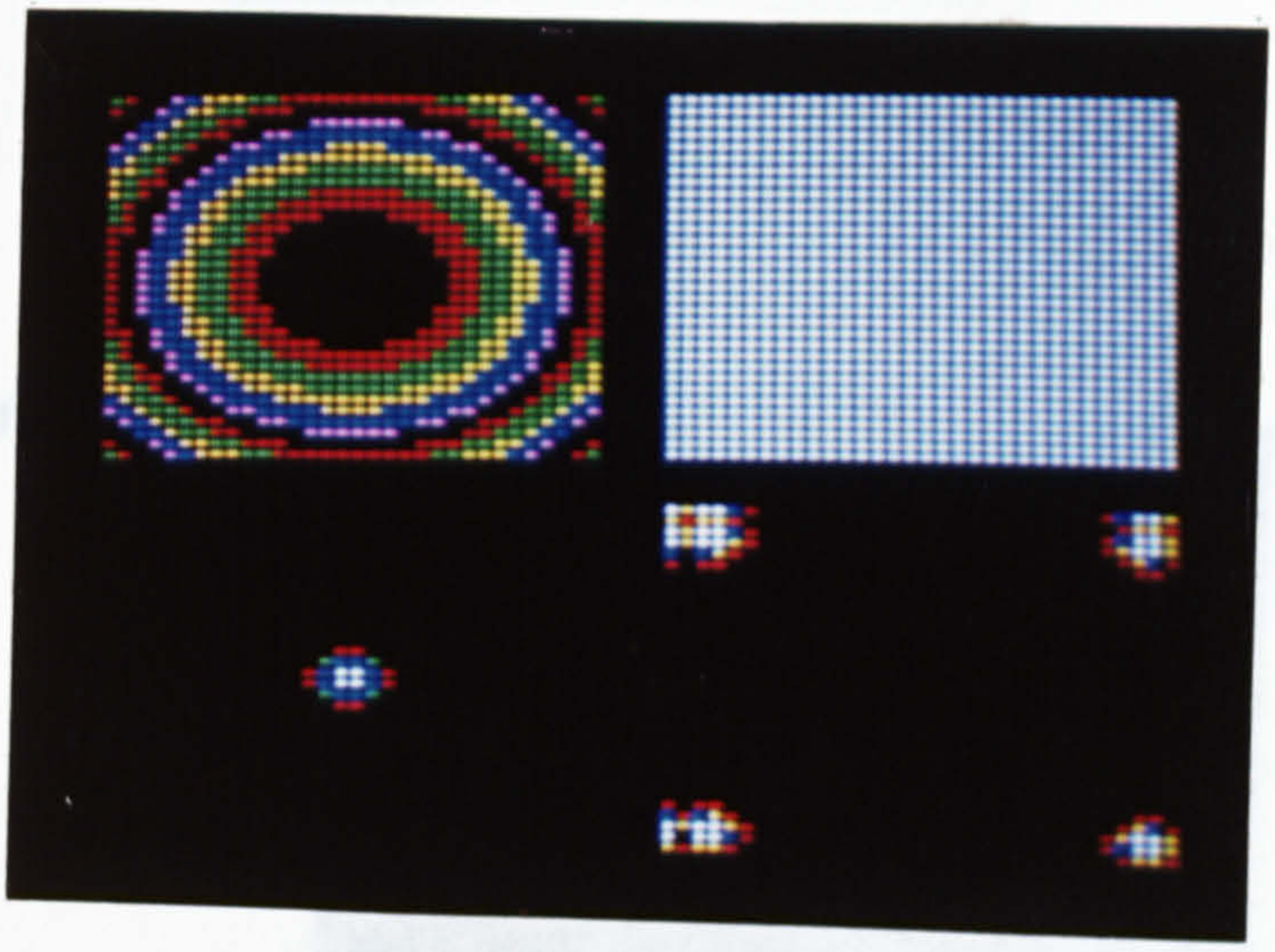

b. Reconstruction distance : 96λ

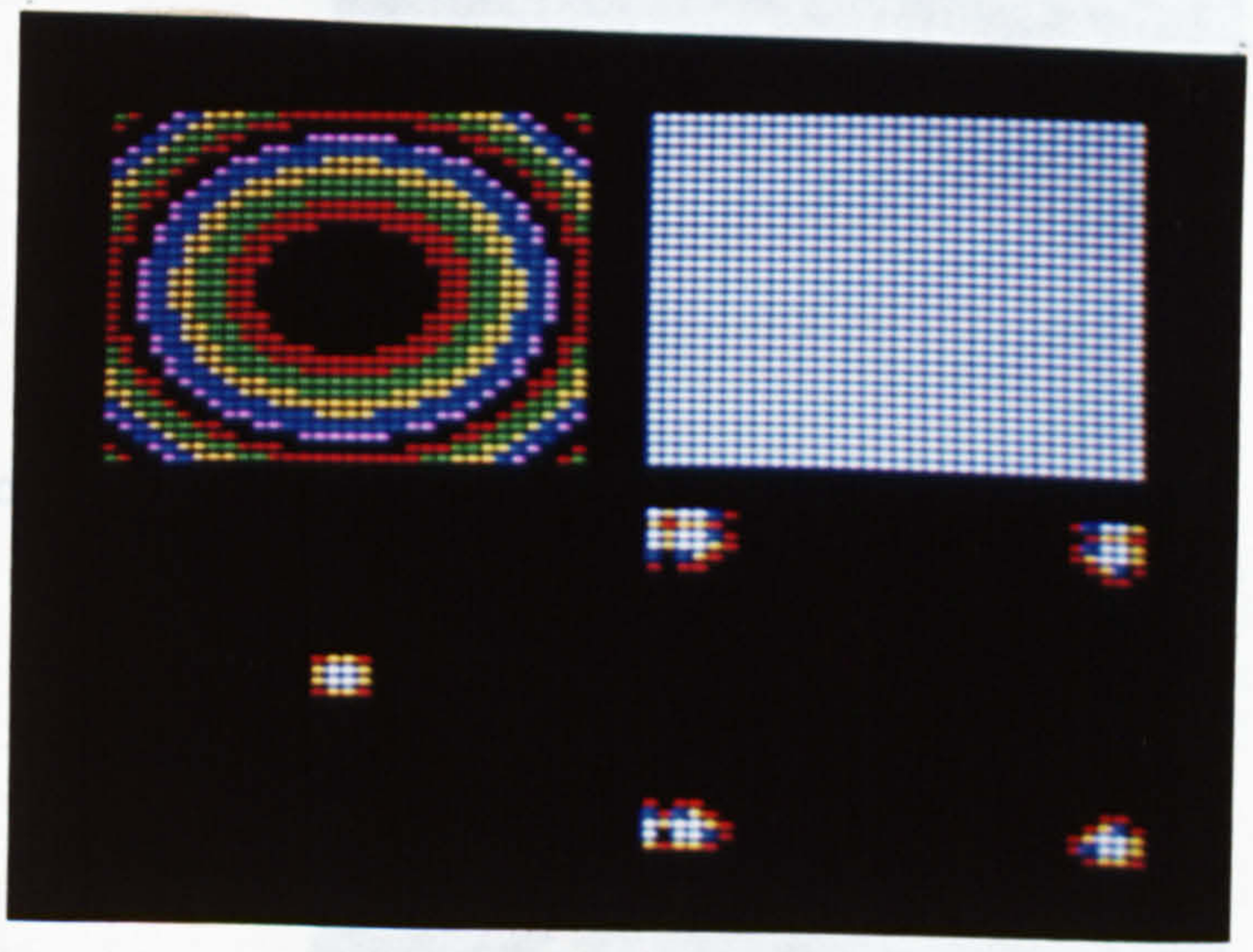

c. Reconstruction distance : 112λ

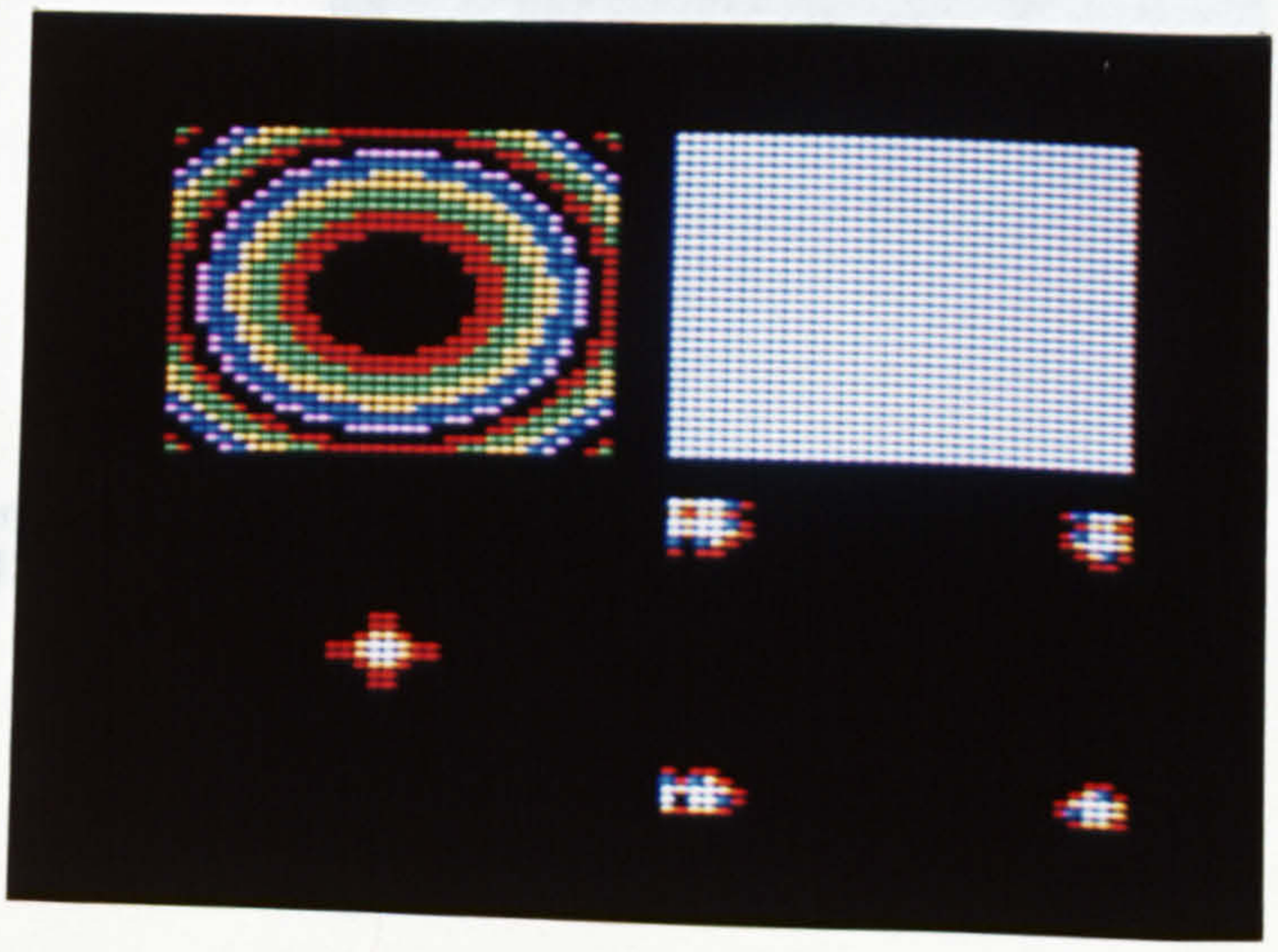

Fig. 7.34: Images obtained at a number of reconstruction distances to indicate the depth of focus of a given hologram.
Hologram:Δ=1λ,
32x32 samples

Object: $x_o$=0,$y_o$=0,
z=96λ

a. Object points separated in the x direction.

Object

$x_{o1} = -3\lambda$
$x_{o2} = 3\lambda$
$y_{o1}, y_{o2} = 0$
$z_{o2} = 96\lambda$

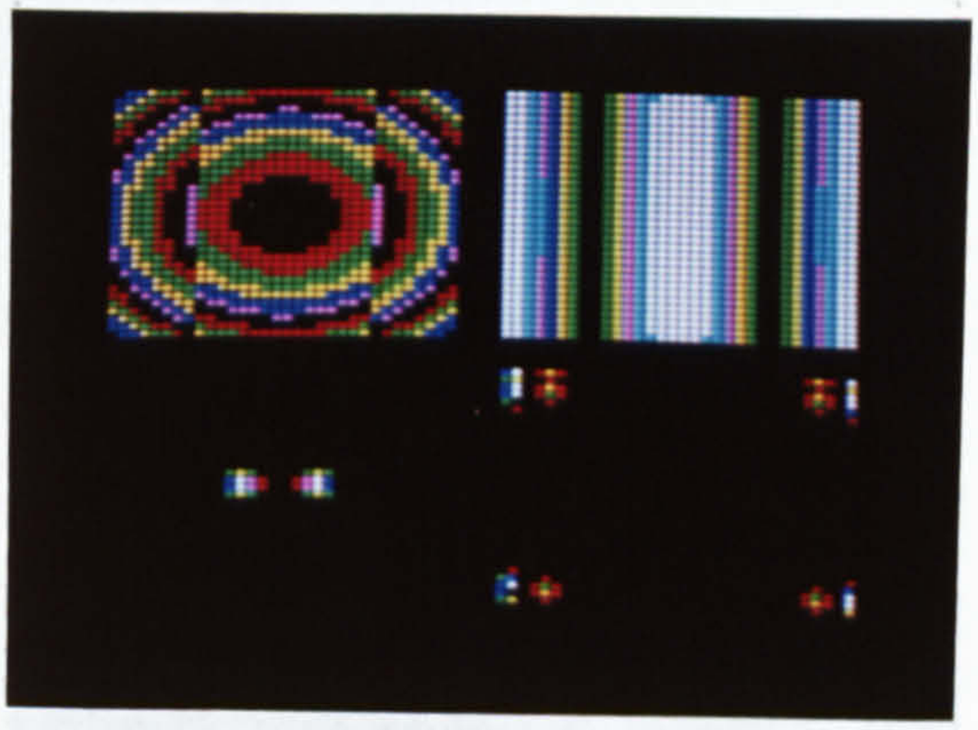

b. Object points separated in the y direction.

Object

$x_{o1}, x_{o2} = 0$
$y_{o1} = -3\lambda$
$y_{o2} = 3\lambda$
$z_{o2} = 96\lambda$

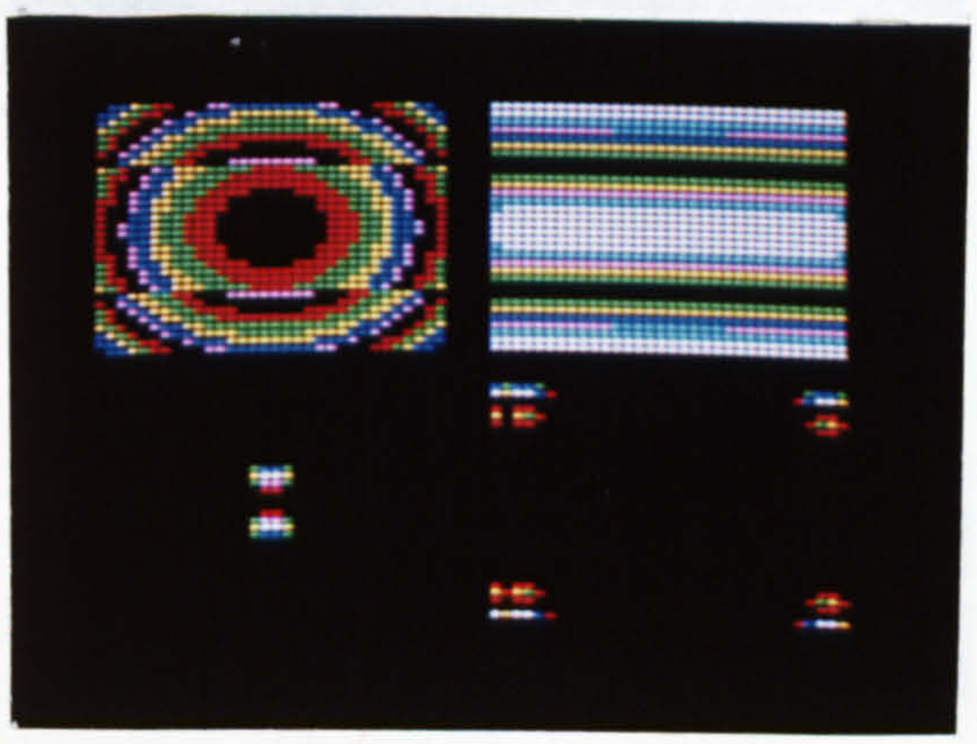

Fig. 7.35 : Resolving two points in the lateral dimension
Hologram: $\Delta = 1\lambda$, 32x32 samples.

a. Spacing = 4λ,
points unresolved.

<u>Object</u>

$x_{o1}, x_{o2} = 0$
$y_{o1} = -2\lambda$
$y_{o2} = 2\lambda$
$z_{o2} = 96\lambda$

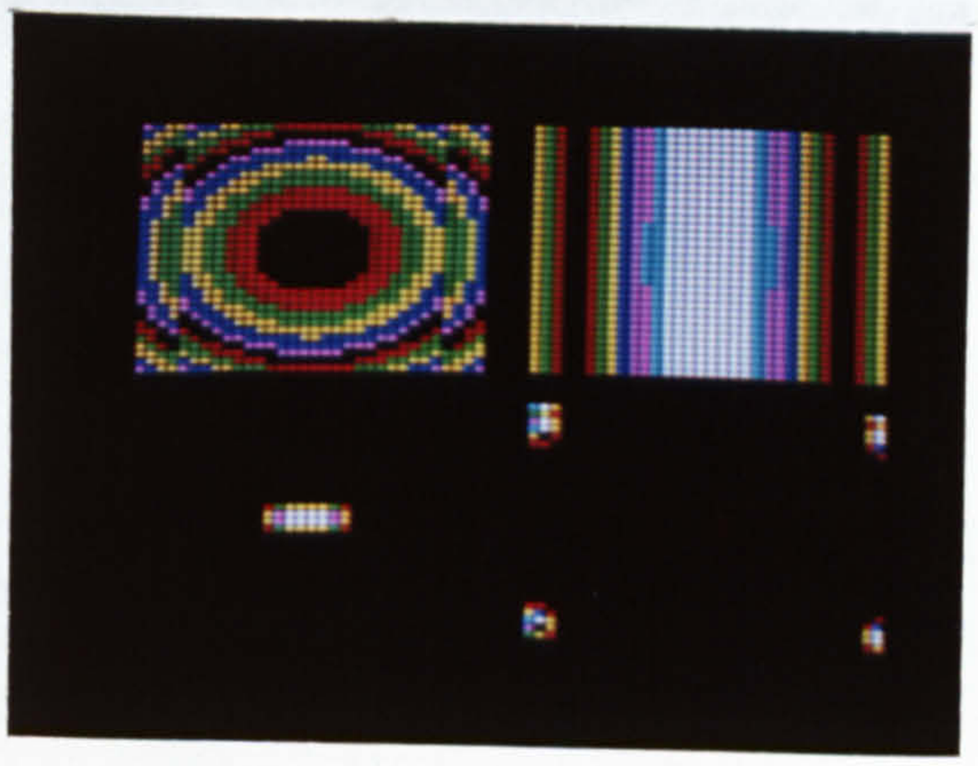

b. Spacing = 6λ,
points resolved.

<u>Object</u>

$x_{o1}, x_{o2} = 0$
$y_{o1} = -3\lambda$
$y_{o2} = 3\lambda$
$z_{o2} = 96\lambda$

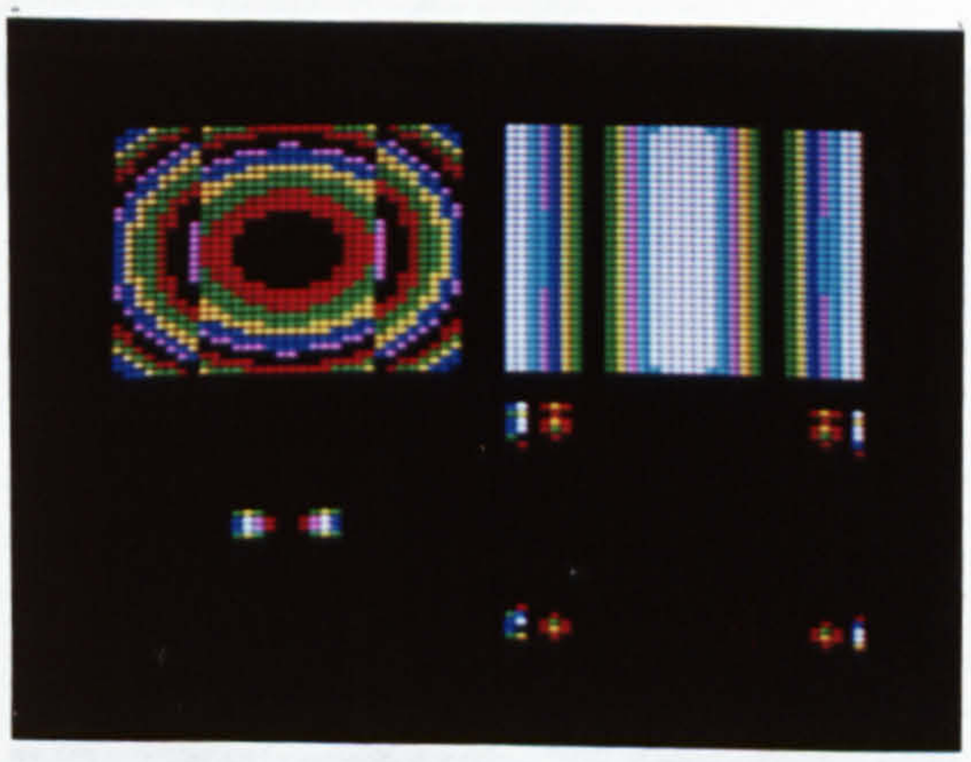

Fig. 7.36 : Effect of point spacing on the resolution of two points
<u>Hologram</u>: Δ=1λ, 32x32 samples.

a. Number of samples:16x16 ,
points unresolved.

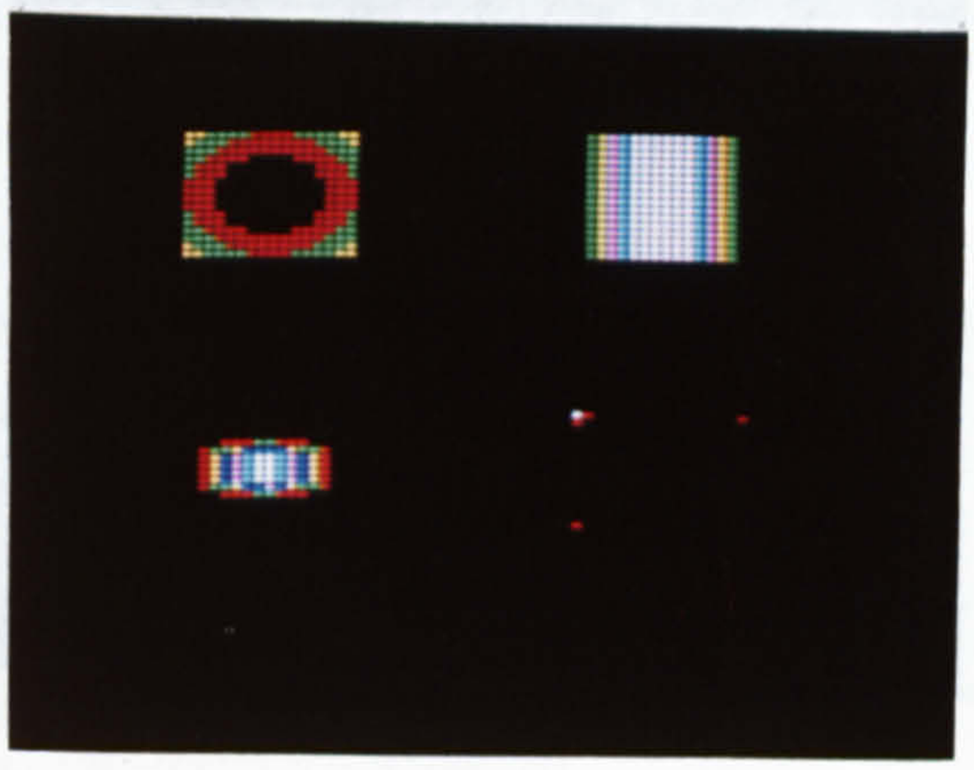

b. Number of samples:32x32 ,
points resolved.

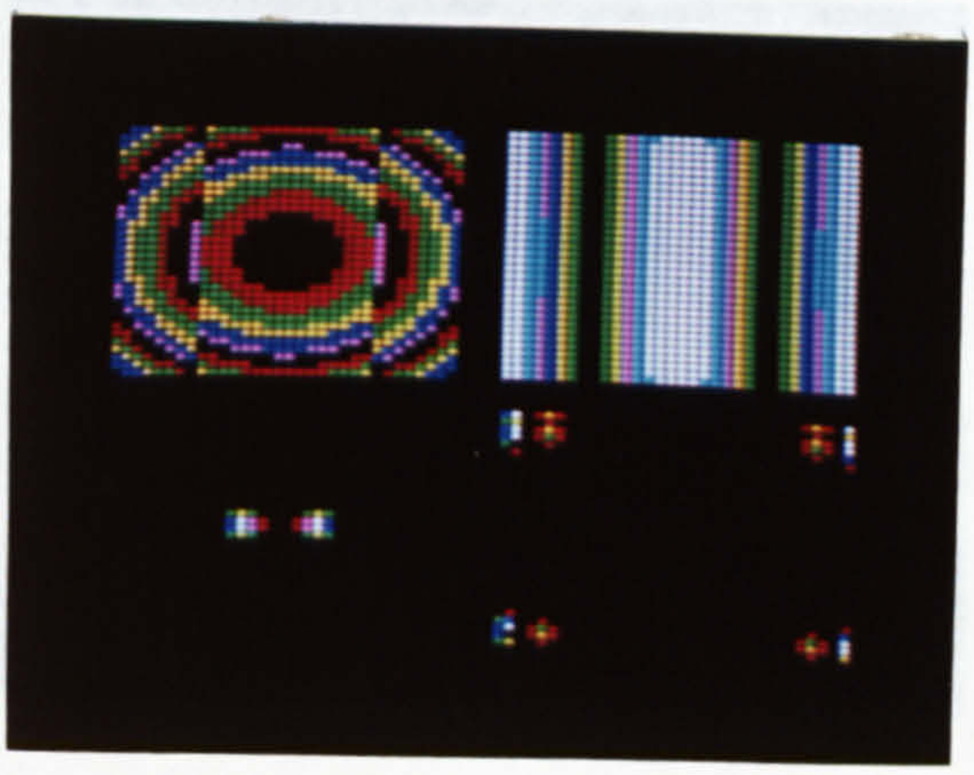

Fig. 7.37 : Effect of doubling the linear dimensions of the hologram aperture on the resolution of two points. Both Holograms: $\Delta=1\lambda$. Object: $x_{o1}=-3\lambda, x_{o2}=3\lambda$, $y_{o1}, y_{o2}=0$, $z=96\lambda$

a. Focusing at point 1,
Reconstruction distance:
48λ

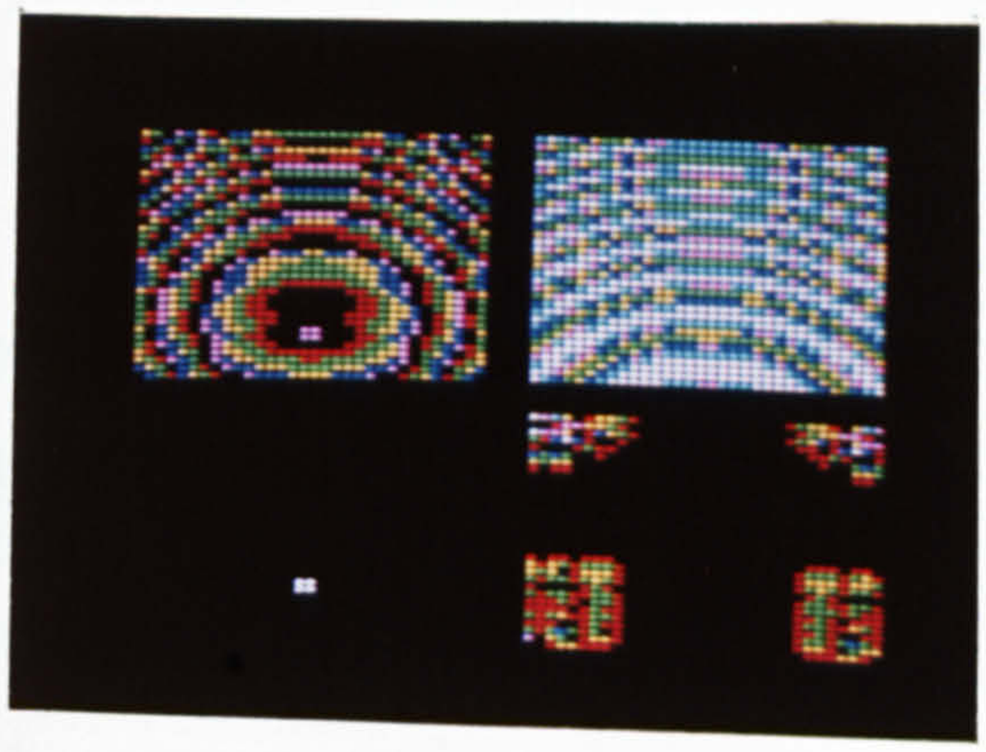

b. Focusing at point 2,
Reconstruction distance:
96λ

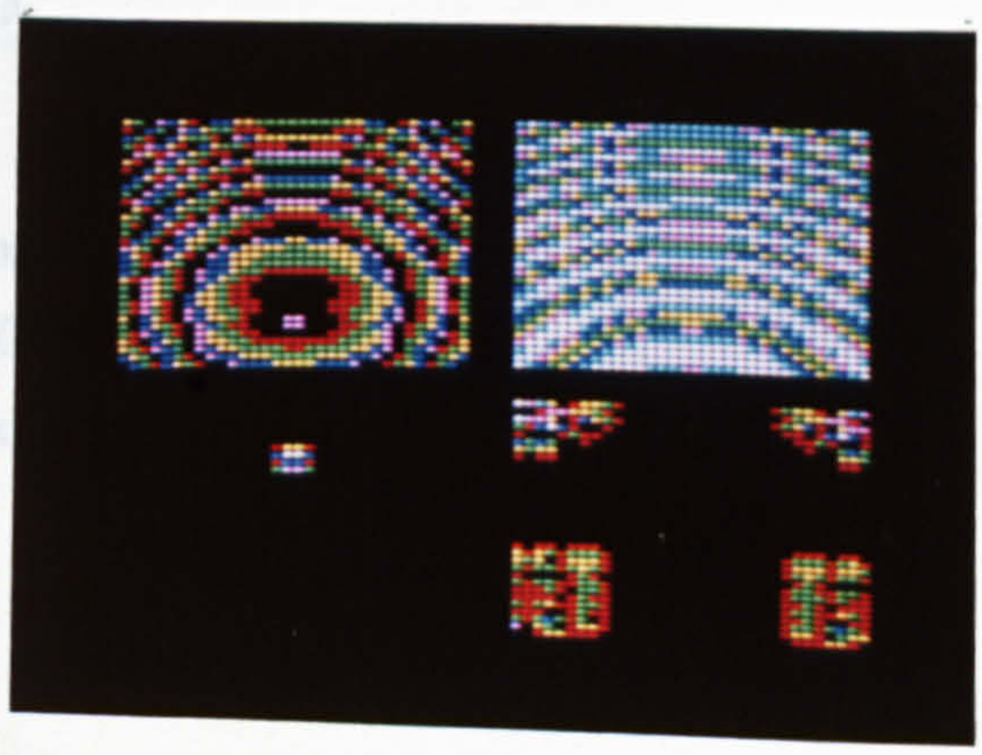

Fig. 7.38 : Resolving two points in the range dimension

Object: point 1 : $x_{o1}$=0, $y_{o1}$=-8λ, $z_1$=48λ

point 2 : $x_{o1}$=0, $y_{o2}$= 8λ, $z_2$=96λ

Hologram: Δ=1λ, 32x32 samples.

# Appendix A

## Listing of an Interactive Program in BASIC for the Simulation and Expansion of the Hologram of 1-point Objects Using a Power Series Predictive Model

```
100 REM **HOLOGRAM EXPANSION:1-POINT OBJECT:POLYNOMIAL MODEL
110 REM *ARRAY R CONTAINS PREDICTION ERORRS
120 INIT
130 PRINT "TOTAL NO OF POINTS IN EXPANDED APERTURE ";
140 INPUT N2
150 PRINT "SPACING IN W.L ";
160 INPUT B
170 A=(N2-1)*B
180 PRINT "HOLOGRAM APERTURE=";
190 PRINT A
200 PRINT "ENTER X,Z OF POINT SOURCE ";
210 INPUT X0,Z0
220 PRINT "NO OF POINTS IN HALF THE APERTURE IS: ";N2/2
230 PRINT "ENTER HALF THE NO OF POINTS IN REDUCED APRETURE";
240 INPUT N1
250 PRINT "ENTER NO. OF LAST PT TO BE PREDICTED ";
260 INPUT N6
270 N=N1-1
280 R8=N
290 M=1
300 REM ****OBTAIN TOTAL HOLOGRAM****
310 DELETE A1,A2,B1,B2,H,G,Y,R
320 DIM A1(N,N),A2(N,N),B1(N,M MAX 1),B2(N,M MAX 1),H(N2/2,2)
330 DIM G(N6,2),Y(N6),R(N6)
340 A2=0
350 A1=0
360 R=0
370 FOR I=1 TO N2/2
380 R1=SQR(Z0^2+((I-1+0.5)*B-X0)^2)
390 P1=2*PI*R1
400 H(I,1)=COS(P1)/R1
410 H(I,2)=SIN(P1)/R1
420 IF I>N1 THEN 450
430 G(I,1)=H(I,1)
440 G(I,2)=H(I,2)
450 NEXT I
460 REM *GET MAX OF MODULUS OF H
470 FOR I=1 TO N6
480 Y(I)=SQR(H(I,1)^2+H(I,2)^2)
490 NEXT I
500 H1=Y(1)
510 FOR J=2 TO N6
520 IF H1=>Y(J) THEN 540
530 H1=Y(J)
540 NEXT J
550 REM*GENERATE DATA VECTOR & COFFT MATRIX FROM REDUCD APRETURE
560 R7=N-R8
570 FOR I=2 TO N1
580 I1=I-1
590 FOR J=1 TO R8
600 J1=J-1
610 A1(I1,J)=((I1+0.5)*B)^J1*H(I1,1)
620 A2(I1,J)=((I1+0.5)*B)^J1*H(I1,2)
630 NEXT J
640 B1(I1,1)=H(I,1)
650 B2(I1,1)=H(I,2)
660 NEXT I
```

```
670 REM◆◆◆◆◆◆◆◆◆◆◆◆◆◆◆◆◆◆◆◆◆◆◆◆◆◆◆◆
680 REM SOLVE MATRIX EQUATION
690 DELETE P8,P9,Q7,D
700 DIM P9(N),P8(N),D(2),Q7(2)
710 REM INITIALIZE DETERMINANT AND PIVOT ELEMENT ARRAY
720 D(1)=1
730 D(2)=0
740 P9=0
750 REM PERFORM SUCCESSIVE PIVOT OPERATIONS (GRAND LOOP)
760 FOR P3=1 TO N
770 REM SEARCH FOR PIVOT ELEMENT AND EXTEND DETERMINANT PRODUCT
780 P5=0
790 FOR P1=1 TO N
800 IF P9(P1)<>0 THEN 890
810 FOR P2=1 TO N
820 IF P9(P2)<>0 THEN 880
830 P4=A1(P1,P2)^2+A2(P1,P2)^2
840 IF P4<P5 THEN 880
850 P6=P1
860 P7=P2
870 P5=P4
880 NEXT P2
890 NEXT P1
900 P8(P3)=4096◆P6+P7
910 P1=P6
920 Q7(1)=A1(P1,P7)
930 Q7(2)=A2(P1,P7)
940 Q1=D(1)
950 D(1)=Q7(1)◆D(1)-Q7(2)◆D(2)
960 D(2)=Q7(1)◆D(2)+Q7(2)◆Q1
970 REM  CHECK FOR SINGULAR MATRIX
980 P9(P7)=P5
990 REM INTERCHANGE ROWS TO PUT PIVOT ELEMENT ON DIAGONAL
1000 IF P6=P7 THEN 1210
1010 D(1)=-D(1)
1020 D(2)=-D(2)
1030 FOR P2=1 TO N
1040 Q1=A1(P1,P2)
1050 Q2=A2(P1,P2)
1060 A1(P1,P2)=A1(P7,P2)
1070 A2(P1,P2)=A2(P7,P2)
1080 A1(P7,P2)=Q1
1090 A2(P7,P2)=Q2
1100 NEXT P2
1110 IF M<=0 THEN 1210
1120 FOR P2=1 TO M
1130 Q1=B1(P1,P2)
1140 Q2=B2(P1,P2)
1150 B1(P1,P2)=B1(P7,P2)
1160 B2(P1,P2)=B2(P7,P2)
1170 B1(P7,P2)=Q1
1180 B2(P7,P2)=Q2
1190 NEXT P2
```

```
1200 REM DIVIDE PIVOT ROW BY PIVOT ELEMENT
1210 Q1=Q7(1)
1220 Q2=Q7(2)
1230 Q8=1/(Q1*Q1+Q2*Q2)
1240 FOR P2=1 TO N
1250 IF P2<>P7 THEN 1280
1260 A1(P7,P2)=1
1270 A2(P7,P2)=0
1280 Q3=A1(P7,P2)
1290 A1(P7,P2)=(A1(P7,P2)*Q1+A2(P7,P2)*Q2)*Q8
1300 A2(P7,P2)=(A2(P7,P2)*Q1-Q3*Q2)*Q8
1310 NEXT P2
1320 IF M<=0 THEN 1390
1330 FOR P2=1 TO M
1340 Q3=B1(P7,P2)
1350 B1(P7,P2)=(B1(P7,P2)*Q1+B2(P7,P2)*Q2)*Q8
1360 B2(P7,P2)=(B2(P7,P2)*Q1-Q3*Q2)*Q8
1370 NEXT P2
1380 REM REDUCE NON-PIVOT ROWS
1390 FOR P1=1 TO N
1400 IF P1=P7 THEN 1560
1410 Q1=A1(P1,P7)
1420 Q2=A2(P1,P7)
1430 A1(P1,P7)=0
1440 A2(P1,P7)=0
1450 FOR P2=1 TO N
1460 Q3=A1(P7,P2)
1470 A1(P1,P2)=A1(P1,P2)-(A1(P7,P2)*Q1-A2(P7,P2)*Q2)
1480 A2(P1,P2)=A2(P1,P2)-(Q3*Q2+A2(P7,P2)*Q1)
1490 NEXT P2
1500 IF M<=0 THEN 1560
1510 FOR P2=1 TO M
1520 Q3=B1(P7,P2)
1530 B1(P1,P2)=B1(P1,P2)-(B1(P7,P2)*Q1-B2(P7,P2)*Q2)
1540 B2(P1,P2)=B2(P1,P2)-(Q3*Q2+B2(P7,P2)*Q1)
1550 NEXT P2
1560 NEXT P1
1570 NEXT P3
1580 REM INTERCHANGE COLUMNS AFTER PERFORMING ALL PIVOT OPERATIONS
1590 FOR Q3=N TO 1 STEP -1
1600 P2=INT(P8(Q3)/4096)
1610 P7=P8(Q3)-4096*P2
1620 IF P2=P7 THEN 1710
1630 FOR P1=1 TO N
1640 Q1=A1(P1,P2)
1650 Q2=A2(P1,P2)
1660 A1(P1,P2)=A1(P1,P7)
1670 A2(P1,P2)=A2(P1,P7)
1680 A1(P1,P7)=Q1
1690 A2(P1,P7)=Q2
1700 NEXT P1
1710 NEXT Q3
```

```
1720 REM **OBTAIN PREDICTED DATA
1730 FOR N3=1 TO N6
1740 IF N3<N1+1 THEN 1850
1750 N4=N3-1
1760 V1=0
1770 V2=0
1780 FOR I=1 TO R8
1790 V1=V1+B1(I,1)*((N4+0.5)*B)^(I-1)
1800 V2=V2+B2(I,1)*((N4+0.5)*B)^(I-1)
1810 NEXT I
1820 G(N3,1)=G(N4,1)*V1-G(N4,2)*V2
1830 G(N3,2)=G(N4,1)*V2+G(N4,2)*V1
1840 R(N3)=100*SQR((G(N3,1)-H(N3,1))^2+(G(N3,2)-H(N3,2))^2)/H1
1850 NEXT N3
1860 END
```

# Appendix B

## Description of the Basic Phase Measuring Circuit

## Appendix B : Description of the basic Phase Measuring Circuit

The basic circuit for measuring the phase is shown schematically in Fig. B.1. The two square wave signals, A and B, for which the relative phase is to be measured are gated to produce two signals $A\bar{B}$ and $\bar{A}B$ . Referring to Fig. B.2a, the signal $A\bar{B}$ represents the phase delay between the two waveforms when A leads B and the positive going pulse in this signal extends from the leading edge of A to the leading edge of B. If A is taken as a reference, the phase in this case is considered positive. When A lags B the phase delay is represented by $\bar{A}B$ which extends from the leading edge of B to the leading edge of A and the phase is negative as shown in Fig. B.2b.

The sign of the phase can be determined using a D-type flip flop whose clock input is driven by signal A while the D-input is driven by signal B, as shown in Fig. B.1. Signal A therefore continuously samples signal B. When A leads B, the Q output of the flip flop is at logic 0 while this output will be at logic 1 if A lags B. Therefore, the Q output represents the sign of the phase. Using a dual multiplexer, the sign signal selects the appropriate $A\bar{B}$ or $\bar{A}B$ signal which represents the phase delay, together with the leading of the two input signals A and B. From Fig. B.2. it is noted that in both cases of positive and negative phase indicated in a and b, the phase delay signal is always enclosed between the leading and the trailing edges of the selected (leading) input signal. Therefore, the trailing edge of the selected input signal can be used to store the value of the phase delay (including the sign) and to clear the phase counter which counts the number of pulses of a high frequency clock for the duration of the selected phase delay signal. The higher the frequency of this clock the greater the accuracy of the phase measurement.

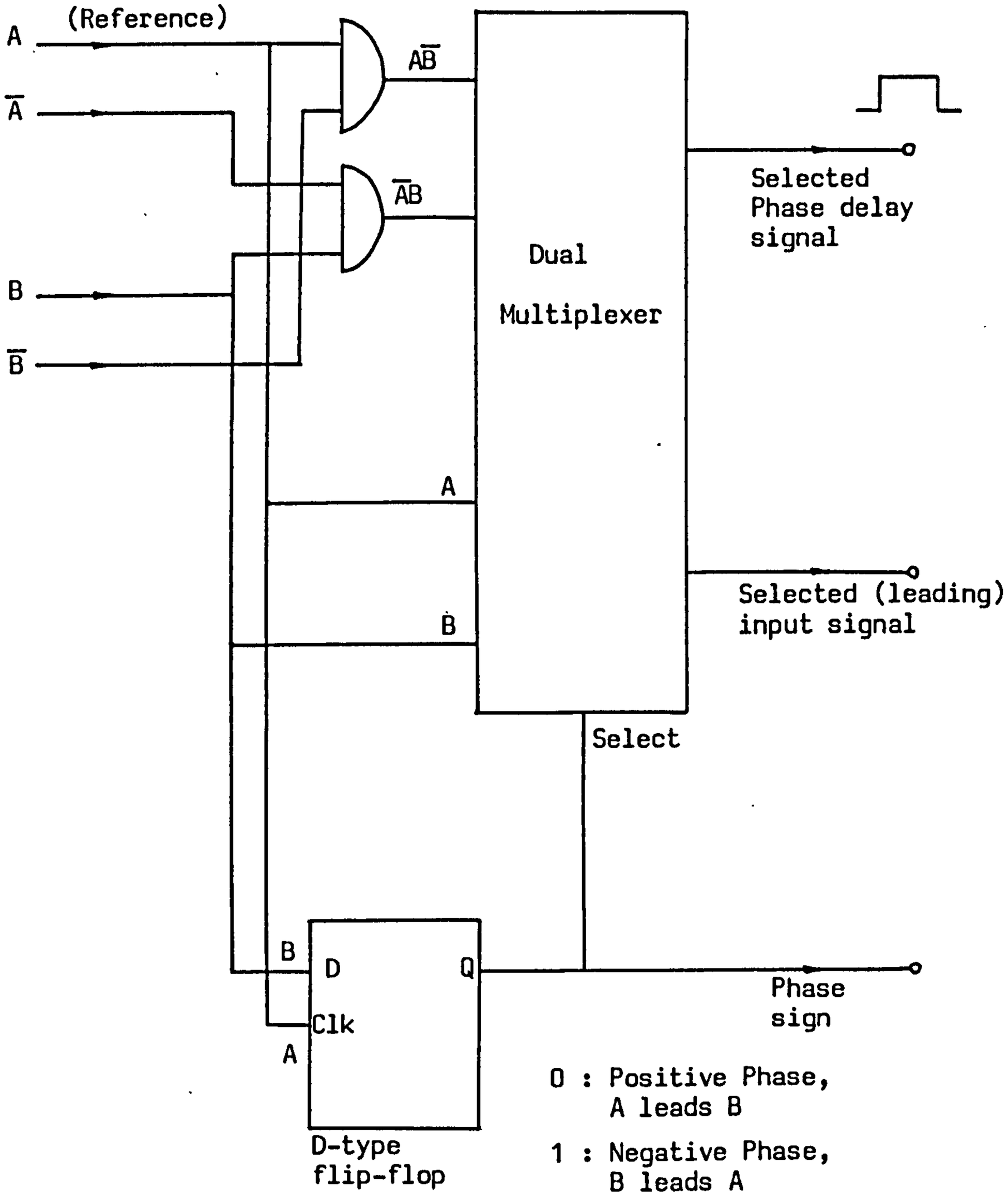


Fig. B.1 : Basic phase measuring circuit

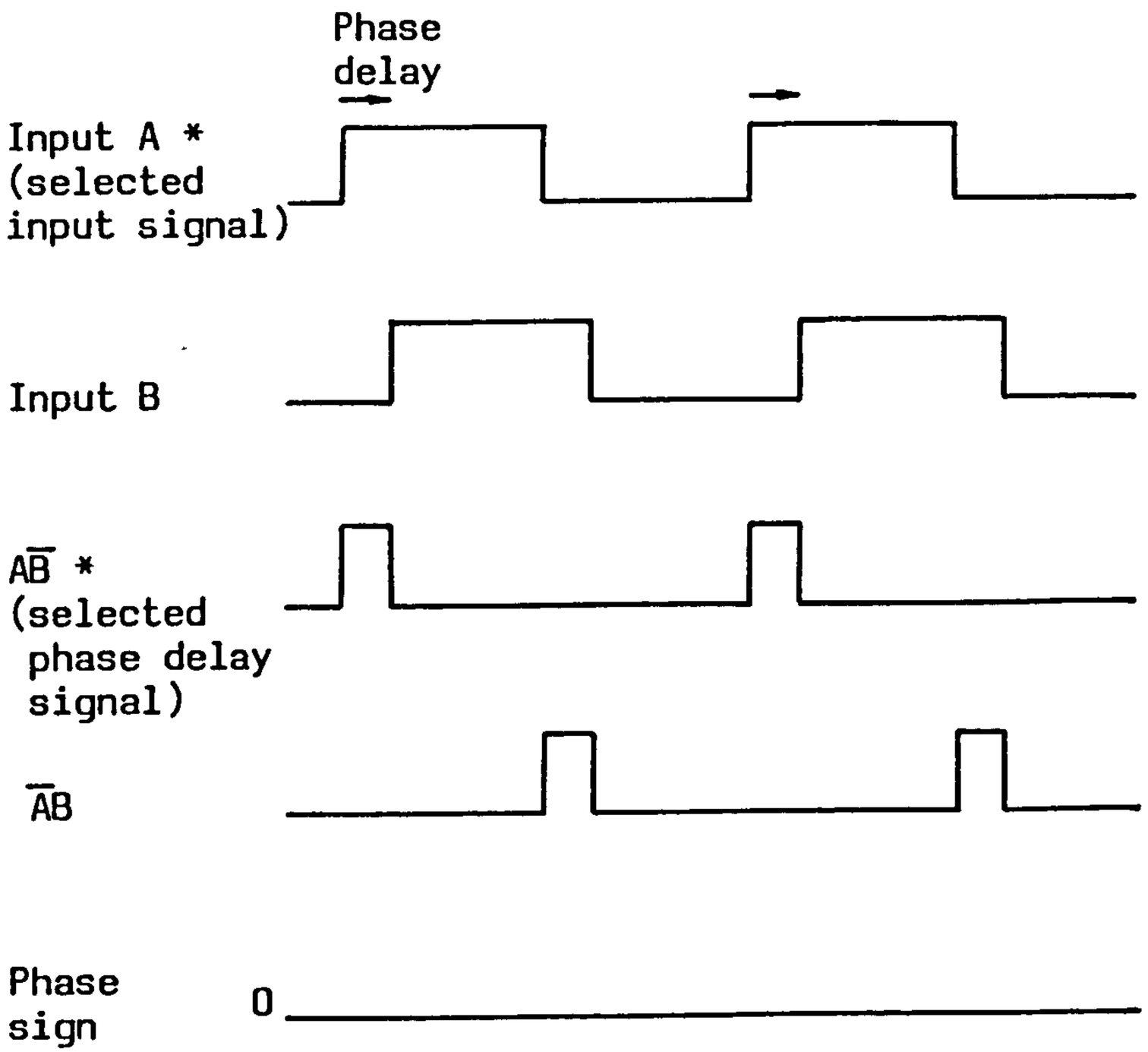


a. Positive phase : A leads B

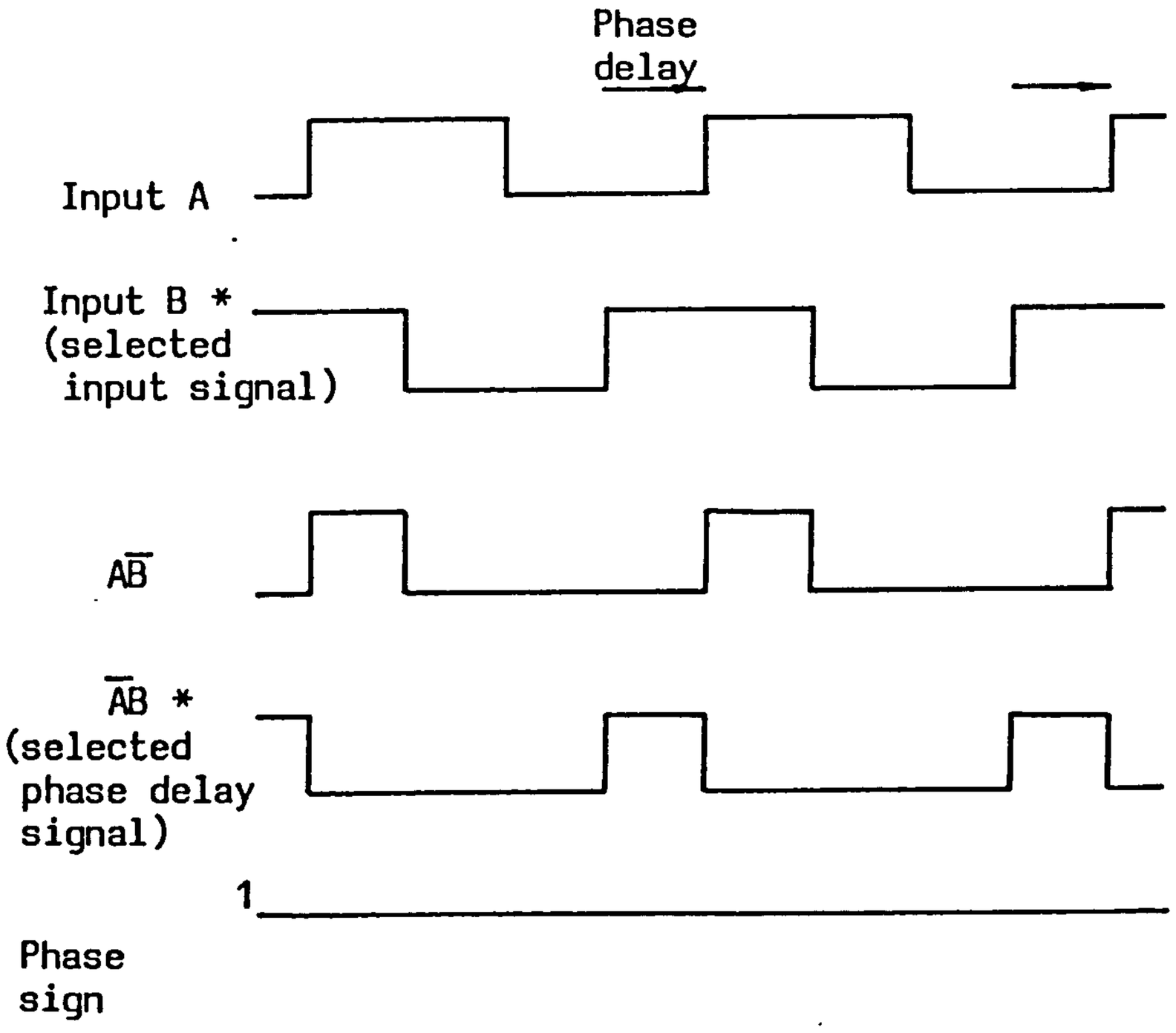


b. Negative phase : B leads A

Note : '*' denotes waveforms of the input and phase delay signals selected by the dual multiplexer, see Fig. B.1.

Fig. B.2 : Waveforms for the basic phase measuring circuit

# Appendix C

## Listing of the TMS 9900 Microprocessor Software for Calculating the Fast Fourier Transform.

## C.1 Listing of the One-dimensional FFT Routine :

```
0001 *FFT PROG DOES ONE DIMENSONAL FFT
0002          IDT 'FFT'
0003          DXOP E,3
0004          DEF NS,ANG,ANG2,ANGLE,ANGLE2,BUFF,BUFF2,RES,RES2
0005          DEF RETURN,RETADR,BUFF4,BUFF6
0006          DEF 0,RE,IM,P1,P2,P3,P9,P8,P92,012,022,09,092
0007          DEF 01,02,03,04,P5M01,P4,P42,P6,P62
0008          DEF 05,052,06,062,07,072,08,082,07STR,07STR2
0009          DEF 08STR,08STR2,SUM1,SUM12,SUM2,SUM22
0010          REF F$XCIR,F$XCPI,F$XAR,F$XSR,F$XMR,F$XDR
0011          REF SINE,COSINE
0012 DBUG     EQU >C970
0013 WSXOP    EQU >E0
0014 *INPUT DATA
0015 NS       BSS 2
0016 0        DATA 0    0:FFT,1:IFT
0017 RE       BSS 128   32PTS (MAX),REAL PART
0018 IM       BSS 128   32PTS (MAX),IMAG PART
0019 *RAM FOR PROGRAM
0020 P1       BSS 2
0021 RETURN   BSS 2
0022 RETADR   BSS 2
0023 R7DIV    BSS 4
0024 P2       BSS 2
0025 P3       BSS 2
0026 P5       BSS 2
0027 P9       BSS 2
0028 P92      BSS 2     P9/2
0029 P8       BSS 2     2^P8=P9=N
0030 01       BSS 2
0031 012      BSS 2
0032 02       BSS 2
0033 022      BSS 2
0034 03       BSS 2
0035 03FP     BSS 2
0036 03FP2    BSS 2
0037 04       BSS 2
0038 09       BSS 2
0039 092      BSS 2
0040 P5M01    BSS 2    P5-01
0041 P4       BSS 2
0042 P42      BSS 2
0043 P6       BSS 2
0044 P62      BSS 2
0045 P9FP     BSS 4
0046 05       BSS 2
0047 052      BSS 2
0048 06       BSS 2
0049 062      BSS 2
0050 07       BSS 2
0051 072      BSS 2
0052 07STR    BSS 2
0053 07STR2   BSS 2
0054 08       BSS 2
0055 082      BSS 2
```

```
0056 08STR    BSS 2
0057 08STR2   BSS 2
0058 SUM1     BSS 2
0059 SUM12    BSS 2
0060 SUM2     BSS 2
0061 SUM22    BSS 2
0062 *RAM FOR USE BY OTHER ROUTINES
0063 ANG      BSS 2
0064 ANG2     BSS 2
0065 ANGLE    BSS 2
0066 ANGLE2   BSS 2
0067 BUFF     BSS 2
0068 BUFF2    BSS 2
0069 BUFF4    BSS 2
0070 BUFF6    BSS 2
0071 RES      BSS 2
0072 RES2     BSS 2
0073 *EPROM FROM HERE
0074 *FIXED DATA
0075 PI         DATA >4132
0076 PI2        DATA >43F1
0077 D180P      DATA >4239
0078 D180P2     DATA >4BB8
0079 ONE        DATA >1
0080 D2         DATA >4120
0081 D22        DATA >0000
0082 D1         DATA >4110
0083 D12        DATA >0000
0084 ZERO       DATA >0000
0085 *SET UP XOP DATA
0086            LI 1,WSXOP
0087            MOV 1,@>4C
0088            LI 1,ERROR
0089            MOV 1,@>4E
0090 *FFT FROM HERE
0091 *CALCULATE THINGS FIRST
0092            MOV @NS,@P9   P9=N
0093            LI 9,P9
0094            LI 10,P9FP
0095            BL @F$XCIR    P9FP HAS P9 IN FP
0096            E 1
0097 *GET P8
0098            MOV @NS,1
0099            CLR 0
0100 SHIFT      SRA 1,1
0101            INC 0
0102            MOV 1,1
0103            JGT SHIFT
0104            DEC 0
0105            MOV 0,@P8
0106 *GET P6
0107            MOV @D1,@ANG
0108            MOV @D12,@ANG2
0109            LI 7,R7DIV
0110            LI 9,P9FP
```

```
0111            LI 10,ANG
0112            BL @F$XDR
0113            E 1
0114            MOV @ANG,@P6
0115            MOV @ANG2,@P62    P6=1/P9
0116 *GET Q6
0117            MOV @P6,@Q6
0118            MOV @P62,@Q62
0119            LI 9,PI
0120            LI 10,Q6
0121            BL @F$XMR    Q6=PI*P6
0122            E 1
0123 *
0124             C @0,@ZERO
0125             JEQ FRWRD
0126             MOV @D1,@P6
0127             MOV @D12,@P62    P6=1
0128             MOV @Q6,0
0129             AI 0,>8000
0130             MOV 0,@Q6    Q6=-Q6(Q6 WAS KNOWN TO BE +IVE)
0131 FRWRD   MOV @P9,@P5
0132         A @ONE,@P5    P5=P9+1
0133         MOV @P9,0
0134         SLA 0,1
0135         MOV 0,@Q1     Q1=2*P9
0136 *GET P9/2
0137             SRA 0,2
0138             MOV 0,@P92
0139 *END OF SET UP PART;DATA STARTS TO MATTER FROM HERE
0140 *3 MAIN NESTED LOOPS
0141           MOV @ONE,@P1    P1=1
0142 LOOP1     MOV @Q1,0
0143           SRA 0,1
0144           MOV 0,@Q1     Q1=Q1/2
0145           SRA 0,1
0146           MOV 0,@Q2     Q2=Q1/2
0147           LI 9,D2
0148           LI 10,Q6
0149           BL @F$XMR    Q6=2.0*Q6
0150           E 1
0151           MOV @ONE,@P2    P2=1
0152           MOV @P5,@P5MQ1
0153           S @Q1,@P5MQ1    P5MQ1 =P5-Q1
0154 LOOP2     MOV @Q6,0
0155           CI 0,>8000
0156           JL POS
0157           LI 1,>8000
0158           S 1,0
0159           JMP FINSH
0160 POS       AI 0,>8000
0161 FINSH     MOV 0,@Q5    Q5=-Q6(GENERAL)
0162           MOV @Q62,@Q52
0163           MOV @P2,@P4
0164           S @ONE,@P4    P4=P2-1
0165           MOV @ONE,@P3    P3=1
```

```
0166 LOOP3   LI 9,Q6
0167         LI 10,Q5
0168         BL @F$XAR    Q5=Q5+Q6
0169         E 1
0170         MOV @P4,@Q3
0171         A @P3,@Q3    Q3=P3+P4
0172         MOV @Q3,@Q4
0173         A @Q2,@Q4    Q4=Q2+Q3
0174         MOV @Q5,@ANG
0175         MOV @Q52,@ANG2
0176         LI 9,D180P
0177         LI 10,ANG
0178         BL @F$XMR   ANG HAS Q5*180/PI
0179         E 1
0180         BL @SINE
0181         MOV @RES,@Q8
0182         MOV @RES2,@Q82
0183         MOV @RES,@Q8STR
0184         MOV @RES2,@Q8STR2    BOTH Q8,Q8STR HAS SIN(Q5)
0185         BL @COSINE
0186         MOV @RES,@Q7
0187         MOV @RES2,@Q72
0188         MOV @RES,@Q7STR
0189         MOV @RES2,@Q7STR2    BOTH Q7,Q7STR HAS COS(Q5)
0190 *
0191         MOV @Q3,@BUFF
0192         MOV @Q4,@BUFF2   Q3,Q4 ARE ARRAY POINTERS
0193         BL @CONVRT  R13 HAS EQUIV(Q3),R14 HAS EQUIV(Q4)
0194 *
0195         MOV @RE(13),@ANG
0196         MOV @IM(13),@ANGLE
0197         INCT 13
0198         MOV @RE(13),@ANG2
0199         MOV @IM(13),@ANGLE2    ANG HAS P(Q3,1),ANGLE HAS P(Q3,2)
0200         MOV @RE(14),@RES
0201         MOV @IM(14),@BUFF
0202         INCT 14
0203         MOV @RE(14),@RES2
0204         MOV @IM(14),@BUFF2    RES HAS P(Q4,1),BUFF HAS P(Q4,2)
0205         MOV @ANG,@SUM1
0206         MOV @ANG2,@SUM12    SUM1 HAS P(Q3,1)
0207         LI 9,RES
0208         LI 10,ANG
0209         BL @F$XSR    ANG HAS P(Q3,1)-P(Q4,1)
0210         E 1
0211         LI 9,RES
0212         LI 10,SUM1
0213         BL @F$XAR    SUM1 HAS P(Q3,1)+P(Q4,1)
0214         E 1
0215         LI 9,ANG
0216         LI 10,Q7
0217         BL @F$XMR    Q7 HAS Q7*(P(Q3,1)-P(Q4,1))
0218         E 1
0219         MOV @BUFF,@SUM2
0220         MOV @BUFF2,@SUM22    SUM2 HAS P(Q4,2)
```

```
0221            LI 9,ANGLE
0222            LI 10,BUFF
0223            BL @F$XSR    BUFF HAS P(Q4,2)-P(Q3,2)
0224            E 1
0225            LI 9,ANGLE
0226            LI 10,SUM2
0227            BL @F$XAR    SUM2 HAS P(Q3,2)+P(Q4,2)
0228            E 1
0229            LI 9,BUFF
0230            LI 10,Q8
0231            BL @F$XMR    Q8 HAS Q8*(P(Q4,2)-P(Q3,2))
0232            E 1
0233            MOV @Q7,@Q9
0234            MOV @Q72,@Q92
0235            LI 9,Q8
0236            LI 10,Q9
0237            BL @F$XAR    Q9 HAS Q7*(P(Q3,1)-P(Q4,1))+Q8(P(Q4,2)-P(Q3,2)
0238            E 1
0239            LI 9,ANG
0240            LI 10,Q8STR
0241            BL @F$XMR    Q8STR HAS Q8*(P(Q3,1)-P(Q4,1))
0242            E 1
0243            LI 9,BUFF
0244            LI 10,Q7STR
0245            BL @F$XMR    Q7STR HAS Q7*(P(Q4,2)-P(Q3,2))
0246            E 1
0247            MOV @Q8STR,@Q8
0248            MOV @Q8STR2,@Q82
0249            LI 9,Q7STR
0250            LI 10,Q8
0251            BL @F$XSR    Q8 HAS Q8*(P(Q3,1)-P(Q4,1))-Q7*(P(Q4,2)-P(Q3,2
0252            E 1
0253 *TFER CALCULATED QUANTITIES TO THEIR POSNS
0254 *1ST: POSITION Q3
0255            MOV @SUM12,@RE(13)    2ND WORD 1ST(R13 WAS STILL POINTING T
0256            MOV @SUM22,@IM(13)
0257            DECT 13
0258            MOV @SUM1,@RE(13)     NOW 2ND WORDS
0259            MOV @SUM2,@IM(13)
0260 *THEN @POSN Q4
0261            MOV @Q92,@RE(14)
0262            MOV @Q82,@IM(14)
0263            DECT 14
0264            MOV @Q9,@RE(14)
0265            MOV @Q8,@IM(14)
0266 *END OF 1ST 3 LOOPS
0267            A @ONE,@P3
0268            C @P3,@Q2
0269            JGT OP3
0270            B @LOOP3
0271 OP3       A @Q1,@P2
0272            C @P2,@P5MQ1
0273            JGT OP2
0274            B @LOOP2
0275 OP2       A @ONE,@P1
```

```
0276            C @P1,@P8
0277            JGT DP1
0278            B @LOOP1
0279 *
0280 *NOW TWO NESTED LOOPS
0281 DP1        MOV @ONE,@P1    P1=1
0282 LOP1       MOV @P1,@Q3
0283            S @ONE,@Q3    Q3=P1-1
0284            CLR @Q4    Q4=0
0285            MOV @ONE,@P2    P2=1
0286 LOP2       MOV @Q4,0
0287            SLA 0,1
0288            MOV 0,@Q4    Q4=2*Q4
0289            LI 9,Q3
0290            LI 10,Q3FP
0291            BL @F$XCIR    GET Q3FP
0292            E 1
0293            LI 9,D2
0294            LI 10,Q3FP
0295            LI 7,R7DIV
0296            BL @F$XDR    Q3FP HAS Q3/2.0
0297            E 1
0298            MOV @Q3FP,@P4
0299            MOV @Q3FP2,@P42    P4 HAS Q3/2.0
0300            LI 9,P4
0301            LI 10,ANG
0302            BL @F$XCRI    ANG HAS NINT(P4),KEEP IT
0303            E 1
0304            LI 9,ANG
0305            LI 10,BUFF
0306            BL @F$XCIR    BUFF HAS NINT(P4) IN FP
0307            E 1
0308            C @BUFF,@P4
0309            JNE NE
0310            C @BUFF2,@P42
0311            JNE NE
0312            JMP EQ
0313 NE         A @ONE,@Q4    Q4=Q4+1 ONLY IF P4><NINT(P4)
0314 EQ         MOV @ANG,@Q3    Q3=NINT(P4) AT ANY CASE
0315            A @ONE,@P2
0316            C @P2,@P8
0317            JLE LOP2    END OF LOP2
0318            A @ONE,@Q4
0319            C @Q4,@P1
0320            JLE OUTSID
0321            MOV @P1,@BUFF    1ST POINTER IS P1
0322            MOV @Q4,@BUFF2  2ND POINTER IS Q4
0323            BL @CONVRT
0324            MOV @RE(13),@Q9
0325            MOV @IM(13),@Q8
0326            INCT 13
0327            MOV @RE(13),@Q92
0328            MOV @IM(13),@Q82    Q9 HAS P(P1+1),Q8 HAS P(P1+2)
0329            DECT 13
0330 *SWAP Q4 PLACE INTO P1 PLACE
```

```
0331            MOV @PE(14),@RE(13)
0332            MOV @IM(14),@IM(13)
0333            INCT 13
0334            INCT 14
0335            MOV @RE(14),@RE(13)
0336            MOV @IM(14),@IM(13)    NOW P(P1,1)=P(Q4,1),P(P1,2)=P(Q4,2)
0337            DECT 13
0338            DECT 14
0339 *
0340            MOV @Q9,@RE(14)
0341            MOV @Q8,@IM(14)
0342            INCT 14
0343            MOV @Q92,@RE(14)
0344            MOV @Q82,@IM(14)      P(Q4,1)=Q9,P(Q4,2)=Q8
0345 OUTSID     A @ONE,@P1
0346            C @P1,@P9
0347            JGT OP11     END OF LOPS
0348            B @LOP1
0349 ***
0350 OP11       C @P6,@D1
0351            JNE OK
0352            C @P62,@D12
0353            JEQ LAST
0354 OK         MOV @ONE,@P1    P1=1
0355 LP6        MOV @P1,@BUFF
0356            BL @CONVRT      P1 IS THE POINTER(ONLY 1)
0357            MOV @RE(13),@ANG
0358            MOV @IM(13),@ANGLE
0359            INCT 13
0360            MOV @RE(13),@ANG2
0361            MOV @IM(13),@ANGLE2    ANG HAS P(P1,1),ANGLE HAS P(P1,2)
0362            LI 9,P6
0363            LI 10,ANG
0364            BL @F$XMR    ANG HAS P(P1,1)*P6
0365            E 1
0366            LI 9,P6
0367            LI 10,ANGLE
0368            BL @F$XMR    ANGLE HAS P(P1,2)*P6
0369            E 1
0370            MOV @ANG2,@RE(13)
0371            MOV @ANGLE2,@IM(13)
0372            DECT 13
0373            MOV @ANG,@RE(13)
0374            MOV @ANGLE,@IM(13)    NOW NEW VALUES ARE IN P(P1,1),P(P1,2
0375            A @ONE,@P1
0376            C @P1,@P9
0377            JLE LP6      END OF LP6
0378 *NOW LAST LOOP L7
0379 LAST       MOV @P9,@P2
0380            LI 0,2
0381            MOV 0,@P1
0382 L7         MOV @P1,@BUFF
0383            MOV @P2,@BUFF2
0384            BL @CONVRT    CONVERT POINTERS P1,P2
0385            MOV @RE(13),@Q1
```

```
0386            MOV @IM(13),@02
0387            INCT 13
0388            MOV @RE(13),@012
0389            MOV @IM(13),@022    01=P(P1,1),02=P(P1,2)
0390            DECT 13
0391 *SWAP 14 INTO 13
0392            MOV @RE(14),@RE(13)
0393            MOV @IM(14),@IM(13)    P(P1,1)=P(P2,1),P(P1,2)=P(P2,2)
0394            INCT 13
0395            INCT 14
0396            MOV @RE(14),@RE(13)
0397            MOV @IM(14),@IM(13)
0398            DECT 13
0399            DECT 14
0400            MOV @01,@RE(14)
0401            MOV @02,@IM(14)
0402            INCT 14
0403            MOV @012,@RE(14)
0404            MOV @022,@IM(14)    P(P2,1)=01,P(P2,2)=02
0405            S @ONE,@P2
0406            A @ONE,@P1
0407            C @P1,@P92
0408            JLE L7
0409 *END OF FFT
0410            B @DBUG
0411 *CONVERSION SUB ; CONVERTS ARRAY PARAMETERS L1,L2 IN BUFF,BUFF2
0412 *INTO MEMORY AIRES INDICES M1,M2 IN R13,R14 RESPECTIVELY,M=(P-1)*4
0413 CONVRT  MOV @BUFF,13
0414            DEC 13
0415            SLA 13,2
0416            MOV @BUFF2,14
0417            DEC 14
0418            SLA 14,2
0419            RT
0420 *ERROR SUB
0421 ERROR     LI 12,>600
0422            SBO 14
0423            LI 1,DBUG
0424            MOV 1,14
0425            RTWP
0426            END
```

## C.2 Listing of the SINCOS Routine :

```
0001          IDT  'SINCOS'
0002           DXOP E,3
0003          DEF  SINE,COSINE
0004           REF   SIN,COS
0005          REF  F$XCRI,F$XCIR,F$XSR,F$XAR,F$XMR
0006           REF ANG,ANG2,ANGLE,ANGLE2,BUFF,RES,RETURN
0007 * ALGORITHM TO EVALUATE SINE AND COSINE
0008 * OF A REAL ANGLE SPECIFIED IN FLOATING POINT FORMAT
0009 * THE ANGULAR VALUE(IN DEGREES) SHOULD BE CONTAINED
0010 * AT THE ADDRESS @ANGLE , @ANGLE+2
0011 * A FOUR WORD BUFFER BLOCK SHOULD BE MADE AVAILABLE ADDRESSED
0012 * BY BUFF , PROVISION FOR INTERMEDIATE STORAGE OF RETURN VECTOR
0013 * SHOULD BE MADE VIA A ONE WORD LOCATION LABELLED RETURN
0014 * THE RESULT OF THE FUNCTION WILL BE RETURNED
0015 * IN A TWO WORD BLOCK LABELLED RES
0016 * TOTAL RAM REQUIREMENT(IN EXCESS OF WORKSPACE)=9 WORDS
0017 * SINE(ANGLE)=SINE(X+@) ; X=INT(ANGLE),@=ANGLE-X
0018 *              =SINE(X)+@*COS(X)
0019 * COSINE(ANGLE)=SINE(ANGLE+90.0)
0020 *
0021 NINTY   DATA >425A,0
0022 PI180   DATA >3F47,>7D1B  *PI/180
0023 * START WITH SINE
0024 * FORM THE INTEGER ANGLE
0025 SINE    MOV 11,@RETURN
0026         MOV @ANG,@ANGLE
0027         MOV @ANG2,@ANGLE2
0028 COSE    LI   9,ANGLE
0029         LI   10,BUFF
0030         BL   @F$XCRI        EVALUATE  X
0031         E 1
0032         LI   1,BUFF
0033         AI   1,4
0034         MOV  @BUFF,*1
0035 * CONVERT X BACK TO FLOATING POINT FORMAT
0036         LI   9,BUFF
0037         LI   10,BUFF
0038         BL   @F$XCIR
0039         E 1
0040 * EVALUATE @=ANGLE-X
0041         LI   1,ANGLE
0042         LI   2,RES
0043         MOV  *1+,*2+
0044         MOV  *1,*2
0045         LI   10,RES
0046         LI   9,BUFF
0047         BL   @F$XSR
0048         E 1
0049 * CONVEPT TO RADIANS
0050         LI   10,RES
0051         LI   9,PI180
0052         BL   @F$XMR
0053         E 1
0054 *** RES = @
0055 * EVALUATE SINE AND COSINE
```

```
0056          LI    1,BUFF
0057          AI    1,4
0058          MOV   *1,7
0059          BL    @SIN
0060          LI    1,BUFF   RELOCATE BUFF
0061          MOV   7,*1+
0062          MOV   8,*1+
0063          MOV   *1,7
0064          BL    @COS
0065          MOV   7,*1+
0066          MOV   8,*1  PLACE COS IN BUFF+4,+6
0067          LI    10,RES
0068          DECT  1
0069          MOV   1,9
0070          BL    @F$XMR
0071          E 1
0072          LI    10,RES
0073          LI    9,BUFF
0074          BL    @F$XAR
0075          E 1
0076 * RES NOW CONTAINS SINE(X)
0077 OUT       MOV @RETURN,11
0078           RT
0079 *COSINE..ADD 90 TO ANGLE 1ST
0080 COSINE   MOV 11,@RETURN
0081          MOV  @ANG,@ANGLE
0082          MOV @ANG2,@ANGLE2
0083          LI    10,ANGLE
0084          LI    9,NINTY
0085          BL    @F$XAR
0086          E 1
0087          JMP   COSE
0088 *RES NOW CONTAINS COS(X)
0089 * COSINE ADD 90 TO ANGLE FIRST
0090          END
```

## C.3 Listing of the SINTAB Routine :

```
0001          IDT   'SINTAB'
0002          DEF   SIN,COS,TABL
0003 SINE     DATA  >0,>0478,>08EF,>0D66,>11DC,>1650,>1AC2
0004          DATA  >1F33,>23A1,>280C,>2C74,>30D9,>353A,>3996
0005          DATA  >3DEF,>4242,>4690,>4AD9,>4F1A,>5358,>578F
0006          DATA  >5BBE,>5FE6,>6407,>6820,>6C31,>7039,>7439
0007          DATA  >782F,>7C1C,>8000,>83DA,>87A9,>8B6D,>8F27
0008          DATA  >92D6,>9679,>9A11,>9D9C,>A11B,>A48E,>A7F3
0009          DATA  >AB4C,>AE97,>B1D5,>B505,>B827,>BB3A,>BE3F
0010          DATA  >C135,>C41B,>C6F3,>C9BB,>CC73,>CF1C,>D1B4
0011          DATA  >D43C,>D6B3,>D91A,>DB6F,>DDB4,>DFE7,>E209
0012          DATA  >E419,>E617,>E804,>E9DE,>EBA6,>ED5A,>EEFF
0013          DATA  >F086,>F20E,>F378,>F4D0,>F615,>F747,>F865
0014          DATA  >F970,>FA68,>FB4C,>FC1C,>FCD9,>FD82,>FE18
0015          DATA  >FE99,>FF07,>FF60,>FFA6,>FFD8,>FFF6,>FFFF  SIN(90)
0016 TABL     EQU   SINE
0017 SIN      MOV   7,8
0018          LI    2,2
0019          LI    3,180
0020          LI    4,360
0021          CI    7,0
0022          JLT   NEGT
0023          JEQ   OUT
0024          LI    7,>4000
0025 OK       CI    8,90
0026          JGT   OT
0027          JEQ   NTY
0028          SWPB  7
0029          MPY   8,2
0030          MOV   @SINE(3),9
0031          MOVB  9,7
0032          SWPB  7
0033          SWPB  9
0034          CLR   8
0035          MOVB  9,8
0036          RT
0037 NTY      AI    7,>0110
0038          CLR   8
0039          RT
0040 NEGT     LI    7,>C000
0041          NEG   8
0042          JMP   OK
0043 OT       CI    8,180
0044          JGT   OT1
0045          S     8,3
0046          MOV   3,8
0047          JMP   OK
0048 OT1      CI    8,270
0049          JGT   OT2
0050          S     3,8
0051          NEG   7
0052          JMP   OK
0053 OT2      CI    8,360
0054          JGT   OT3
0055          JEQ   OUT
```

```
0056          S     8,4
0057          MOV   4,8
0058          NEG   7
0059          JMP   OK
0060 COS      AI    7,90
0061          JMP   SIN
0062 OT3      AI    8,-360
0063          JMP   OK
0064          RT
0065 OUT      CLR   7
0066          CLR   8
0067          RT
0068          END
```

# Appendix D

## Publications

Reprinted from: Acoustical Imaging, Vol 12,
Plenum Press, New York, 1982.

# EXPANSION OF ACOUSTIC HOLOGRAM APERTURES USING ARMA MODELLING TECHNIQUES

R E Abdel-Aal, C J Macleod and T S Durrani

Department of Electronic and Electrical Engineering
University of Strathclyde
Glasgow G1 1XW, Scotland

## ABSTRACT

As distinct from optical holography, the wavelengths in acoustic holography are large and therefore the numerical aperture is small for a given physical aperture. Further, the number of points at which the hologram can be sampled is limited due to time considerations when mechanical scanning is used and the high cost of building large arrays to sample the hologram. In order to achieve adequate resolution large apertures are necessary, therefore, a requirement exists for investigating signal processing techniques for increasing aperture size from available data.

In this paper a method is proposed for enlarging a limited hologram aperture in the space domain by extrapolating, computationally, additional points outside the available aperture using estimation techniques. The paper is concerned with two particular aspects of hologram extrapolation:

(i) Moving Average (MA)/Autoregressive (AR) processing techniques based on the available data.

(ii) The effect of disturbing noise in the measured hologram signals on the estimation accuracy.

Results obtained by computer simulation show the effectiveness of this method for enlarging the aperture with corresponding improvement in resolution with and without disturbing noise.

## INTRODUCTION

Signal processing aimed at increasing lateral resolution is of particular importance in acoustic imaging because numerical apertures (i.e. aperture values expressed in terms of multiples of the wavelength) are normally much smaller than those available in optical imaging. Improving the resolution in this way would achieve considerable savings in time and cost by reducing the area over which the data is collected. Moreover, situations arise in the field of acoustic imaging where the available aperture is physically restricted, for example, when imaging the inside of the chest through narrow spaces between the ribs. A considerable amount of such signal processing can be conveniently carried out using a digital computer, which most holographic imaging systems use nowadays for reconstructing images.

The possibility of resolution beyond the diffraction limit has been recognised in optics for a number of years (1), and several techniques have been developed for this purpose (2). These include a process of analytic continuation on the spatial frequency spectrum of the image (3), and an object restoration technique based on expanding the aperture function in terms of prolate spheroidal wave functions (4). Other methods which are more robust against noisy environments include the error energy reduction method proposed by Gerchberg (5) and the maximum entropy technique by Frienden (6).

A number of techniques to improve lateral resolution in acoustic holography have been reported in the literature. A sequential estimation method based on the minimization of a mean square criterion function in the frequency domain have been used by Takuso Sato et al (7) to expand the hologram aperture. Other methods attempt to improve resolution without expanding the available aperture, such as a more exact reconstruction method proposed by Williams et al (8), (9). Another method is that suggested by Ikeda et al (10) where the resolution is improved by artificially increasing the frequency of the hologram signals before reconstruction.

This paper describes a new method for enlarging a limited hologram aperture in the space domain using estimation techniques. The method is based on modelling the hologram signal over the available aperture and using the model so constructed to predict new points outside that aperture. The models used are in general of the ARMA type containing both space variant and space invariant terms. The paper also describes a technique for correcting the predicted signals in order to improve the prediction accuracy. The effect of noise in the hologram signals is discussed and numerical examples are given to illustrate the effectiveness of the method as a tool for improving resolution when imaging single or multiple-point objects with and without disturbing noise.

## NATURE OF THE PROBLEM

### Hologram signal and simulation of noise

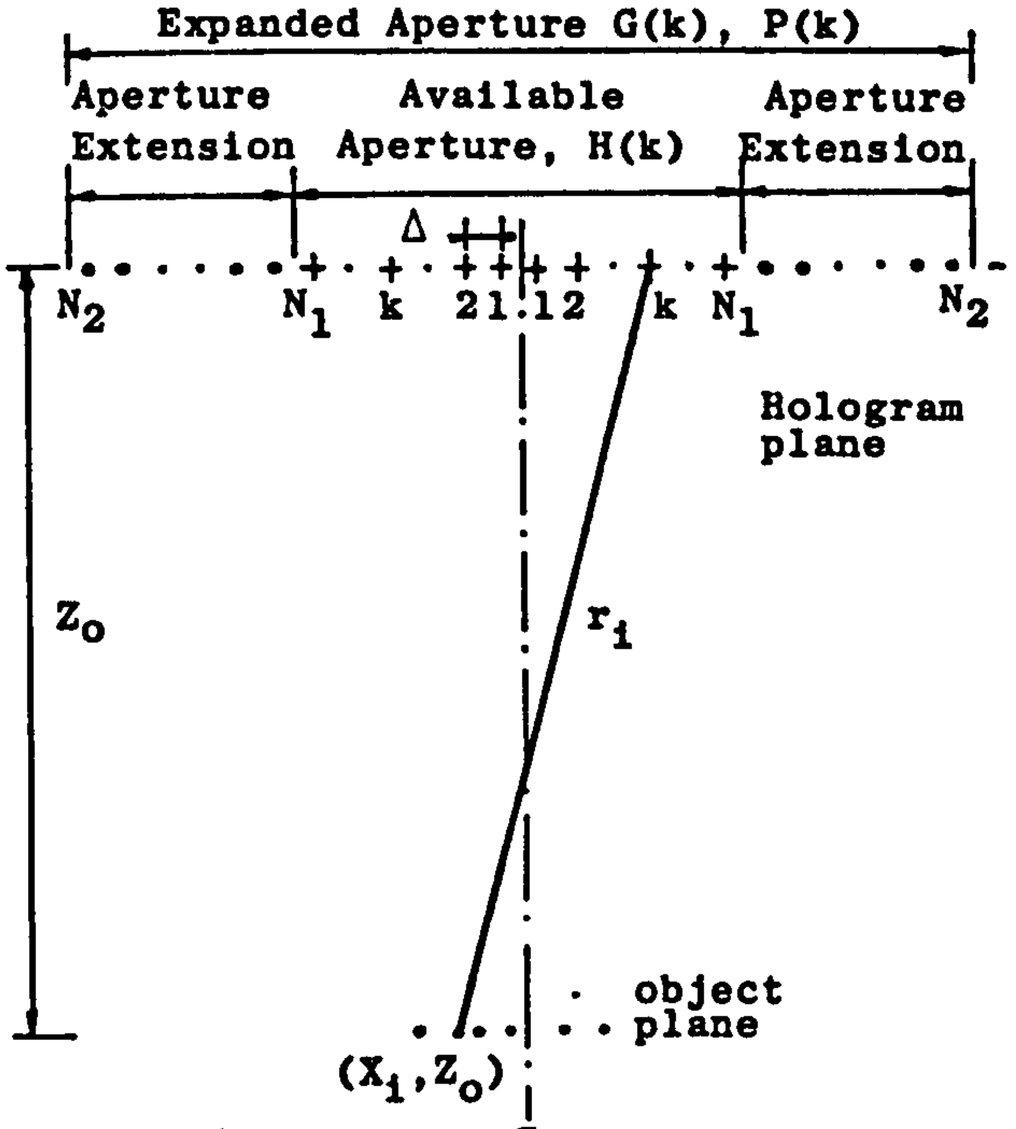


Fig 1. Geometry of the imaging system

Consider the holographic imaging system shown schematically in Fig 1. For simplicity the object is assumed to consist of a finite number of point sources which radiate acoustic energy coherently. The hologram is sampled at $2N_1$ uniformly distributed points in the available aperture, spaced at distance $\Delta$ wavelengths. The object lies in a plane parallel to the hologram at distance $Z_o$ from it, $Z_o$ is assumed to be known beforehand.

The complex hologram signal at sampling point k in the avavilable aperture is given by:

$$H(k) = \sum_{i=1}^{\ell} \frac{A_i}{r_i} \exp K r_i = \alpha_k + j \beta_k$$

where $\ell$ is the number of points in the object, K is the wavenumber, $K = 2\pi/\lambda$, $\lambda$ is the wavelength, $A_i$ is an amplitude factor, and $r_i$ is the length of the vector joining point i on the object to point k on the aperture.

$$\alpha_k = \sum_{i=1}^{\ell} \frac{A_i}{r_i} \cos (K r_i), \quad \beta_k = \sum_{i=1}^{\ell} \frac{A_i}{r_i} \sin (K r_i)$$

We assume in practice that the hologram is obtained by measuring the quantities $\alpha_k$ and $\beta_k$ at the sampling points. The measured quantities, $\alpha'_k$ and $\beta'_k$, will contain random noise which can be simulated by relating $\alpha'_k$ and $\beta'_k$ to $\alpha_k$ and $\beta_k$ as follows:

$$\alpha'_k = \alpha_k + \eta_k$$

$$\beta'_k = \beta_k + \xi_k$$

where $\eta_k$ and $\xi_k$ are white noise processes with zero mean and vari-

ance prescribed by the input signal to noise ratio. The noise level is expressed throughout as the relative peak amplitude of $\eta_k$ wrt the hologram signal $\alpha_k$. This is taken to be equal to that of $\xi_k$ wrt $\beta_k$.

Prediction and the definition of errors

This paper is concerned with expanding the aperture in the space domain by predicting new points. The prediction of signals to the right of the available aperture is based on a model derived from the signals at the RH half of the available aperture. Similarly the LH half is used to predict points to the left. The following definitions are made, (see Fig 1):

- H(k), $k \leqslant N_1$ is the true hologram signal over the small available aperture
- G(k), $k \leqslant N_2$ is the predicted hologram signal over the expanded aperture,

$$G(k) = \begin{cases} H(k) & k \leqslant N_1 \\ \text{Predicted signal at point k} & N_1 < k \leqslant N_2 \end{cases}$$

- P(k), $k \leqslant N_2$ is the true hologram signal over the expanded aperture.

Let $G(k) = g_1(k) + j\, g_2(k)$

$P(k) = p_1(k) + j\, p_2(k)$

The percentage error at point k($k=N_1+1, N_1+2, \ldots N_2$) is defined as:

$$E(k) = 100 \{(g_1(k)-p_1(k))^2+(g_2(k)-p_2(k))^2\}^{\frac{1}{2}} / \{(p_1(k))^2+(p_2(k))^2\}^{\frac{1}{2}} \qquad (1)$$

$$k = N_1+1, N_1+2, \ldots N_2$$

A better expression for the error, which takes into account its effect on the image reconstruction, is obtained by weighting the error in eqn (1) by the ratio between the modulus of the true hologram signal at point k and the modulus of the maximum signal over the whole of the true aperture, $P_{max}$, where:

$$P_{max} \triangleq \max \{|P(k)|\} \quad k = 1, 2, \ldots N_2$$

This leads to:

$$E(k) = 100 \{(g_1(k)-p_1(k))^2+(g_2(k)-p_2(k))^2\}^{\frac{1}{2}} / P_{max} \qquad (2)$$

## THE MOVING AVERAGE (MA) MODEL

Referring to Fig 1, consider a single-point object and assume a total available aperture containing $2N_1$ points and an expanded aperture of $2N_2$ points. Considering the RH side of the aperture, the Moving Average (MA) or space variant model for the hologram signal in the available aperture is obtained by relating the signal at point k to that at point (k-1) by:

$$H(k) = \psi(k)\, H(k-1), \quad k = 2, 3, \ldots N_1 \tag{3}$$

where $\psi(k)$ is a function of the position of point k relative to the centre of the aperture. If $\psi(k)$ is assumed to be a polynomial function in the distance $d_k$ from point k to the centre expressed in wavelengths (see Fig 1), then:

$$\psi(k) = a_1 + a_2(d_k)^1 + a_3(d_k)^2 + \ldots + a_N(d_k)^{N-1} = \sum_{i=1}^{N} a_i(d_k)^{i-1} \tag{4}$$

where $a_i$ is a complex coefficient, and N is the number of terms in the polynomial.

Writing eqn (3) for all values of k and substituting for $\psi(k)$ from eqn (4) we have the following set of equations which are solved for the model coefficients $a_1, a_2, \ldots a_N$:

$$\begin{bmatrix} H(2) \\ H(3) \\ \cdot \\ H(N_1) \end{bmatrix} = \begin{bmatrix} H(1) & H(1)d_1 & H(1)d_1^2 & \cdot & H(1)d_1^{N-1} \\ H(2) & H(2)d_2 & H(2)d_2^2 & \cdot & H(2)d_2^{N-1} \\ \cdot & \cdot & \cdot & \cdot & \cdot \\ H(N_1-1) & H(N_1-1)d_{N_1-1} & H(N_1-1)d_{N_1-1}^2 & \cdot & H(N_1-1)d_{N_1-1}^{N-1} \end{bmatrix} \begin{bmatrix} a_1 \\ a_2 \\ \cdot \\ a_N \end{bmatrix}$$

For an exactly determined system, the number of terms in the polynomial is assumed to be equal to the number of equations, i.e. $N = N_1-1$.

To use the model for prediction we assume that the relationship in eqn (3) holds outside the available aperture, with $\psi(k)$ now defined by the model coefficients $a_1, a_2, \ldots a_N$. Thus the signal at the first predicted point $G(N_1+1)$ is obtained from the signal at the last point in the available aperture $H(N_1)$ by:

$$G(N_1+1) = \psi(N_1+1)\, H(N_1)$$

$$= \{ \sum_{i=1}^{N} a_i (d_{N_1+1})^{i-1} \} H(N_1)$$

Similarly $G(N_1+2)$ is obtained from $G(N_1+1)$, ... and so on. The process of constructing and using the model is repeated for the left half of the aperture with prediction from right to left.

The model has been used to expand a total aperture of 16 points ($N_1=8$), spaced at $1\lambda$, four times ($N_2=32$) to image a 1-point object on the centre at a range of $100\lambda$. Fig 2a shows the percentage prediction error, as defined by eqn (2), over the aperture. The images reconstructed from the small available aperture, the expanded predicted aperture, and the expanded true apertures are shown in Fig 2b normalised to the same peak value. Backward wave propagation has been used throughout to obtain the reconstructed images. The images

(a) Percentage prediction error over the aperture

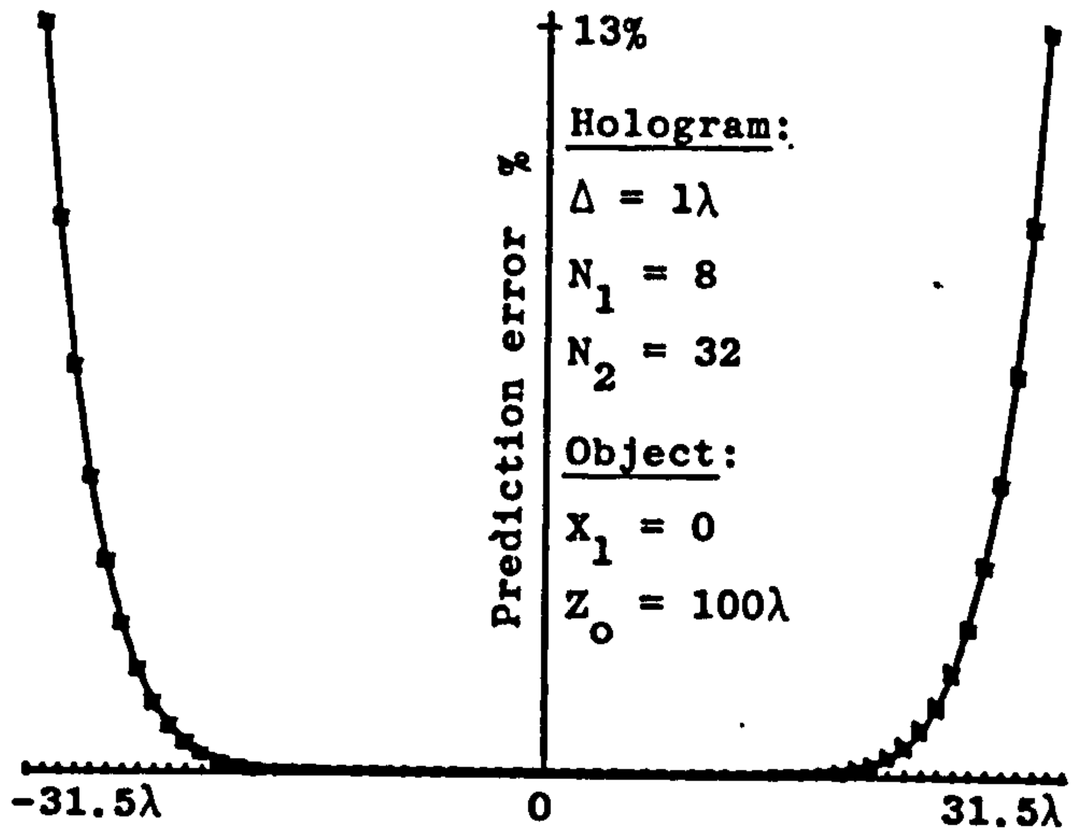


(b) Intensity of reconstructed images normalised to the same peak value

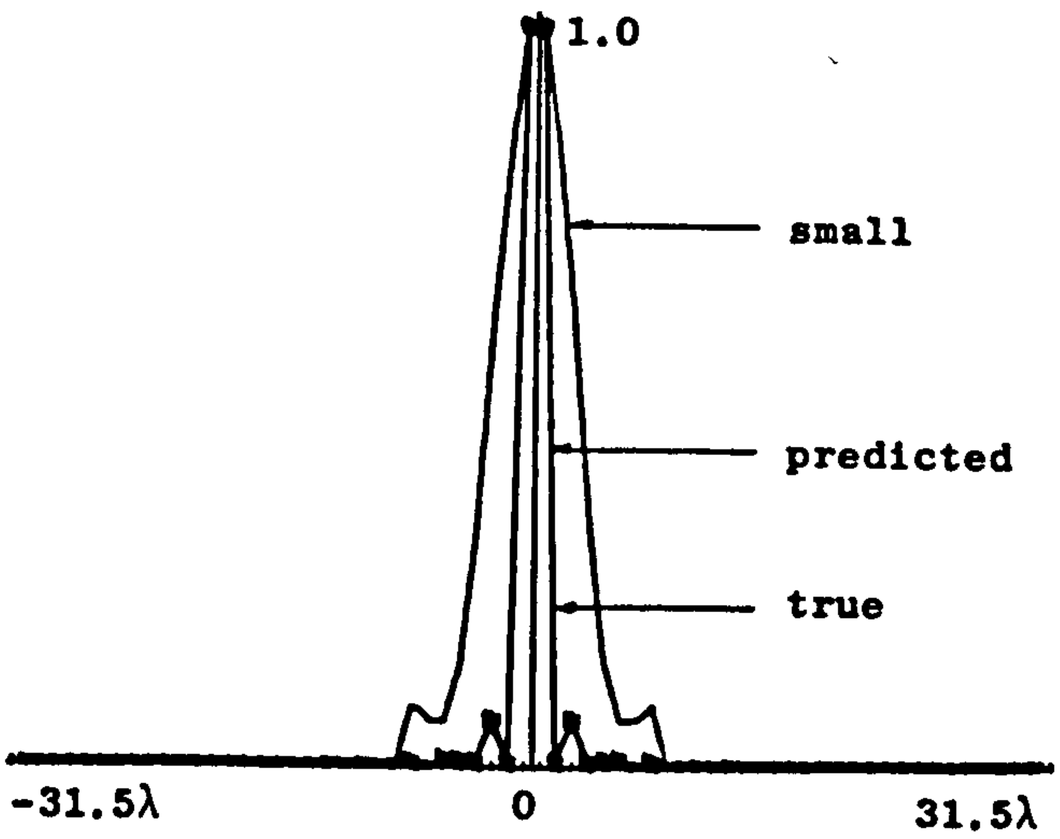


Fig 2. Expanding an aperture four times using an MA predictive model to image a 1-point object

obtained from both the true and predicted holograms are in good agreement with a corresponding improvement in the width of the point image over the case of the small aperture.

For the case of 1-point object at the centre in the Fresnel zone and beyond, it was found that the prediction error is inversely proportional to the object range. It is interesting to note that for this case the spatial frequency over the aperture also varies inversely with range. Obviously, the higher the spatial frequency the greater the errors that would be expected in prediction due to the larger variations in the signal from one point on the aperture to the next.

Several types of polynomials have been tried for the model function $\psi$. Orthogonal Chebyshev, Legendre and Hermite polynomials gave almost identical results to those obtained with ordinary polynomial expressions. In the case of the Fourier series polynomial, it was found that the predication accuracy depends on the choice of the spatial fundamental frequency of the series, which should be optimized for maximum accuracy.

## THE MOVING AVERAGE/AUTOREGRESSIVE (ARMA) MODEL

When attempting to use the MA model for predicting the hologram of a 2-point object the errors were too large to allow for useful expansion ratios. The concept of the ARMA model was then introduced. In this model, the signal at one point is related not only to the signal at the previous point by a space variant function but is also linearly related to the signals at a number of the preceding points. Assuming an ordinary polynomial expansion for the space variant function we have:

$$H(k) = \{\sum_{i=1}^{p} a_i (d_k)^{i-1}\} H(k-1) + \sum_{j=1}^{q} c_j H(k-q+j-1) \qquad (7)$$

$$k = 2, 3, \ldots N_1$$

with

$$H(k-q+j-1) = 0 \quad \text{for} \quad j \leqslant q-k+1$$

where:

p is the number of MA (space variant) terms, q is the number of AR (space invariant) terms, $a_i (i=1, \ldots, p)$ are the MA coefficients, $c_j (j=1, \ldots, q)$ are the AR coefficients.

As both the MA and the AR parts of the model have to share the number of degrees freedom, and assuming an exactly determined system, then:

$$p+q = N = N_1-1$$

Writing eqn (7) for all values of k over the available aperture we

have N equations which can be solved for the model coefficients $a_1$, $a_2$, ... $a_p$, $c_1$, $c_2$, ... $c_q$. The model is then used to predict points outside the available aperture. First, $G(N_1+1)$ is obtained from $H(N_1)$ together with signals at the preceding q-1 points. In general, $G(N_1+\ell)$ is obtained as follows:

$$G(N_1+\ell) = \{\sum_{i=1}^{p} a_1 (d_{N_1+\ell})^{i-1}\} G(N_1+\ell-1) + \sum_{j=1}^{q} c_j\, G(N_1+\ell-q+j-1)$$

It was found that for the case of 1-point objects the optimum model is an MA model (no AR terms). For 2-point objects, however, an ARMA model gives better results. Fig 3 shows the reconstructed images obtained when doubling the size of a 16 point total aperture, spacing 1λ, to image 2 points separated by a distance of 6λ, range

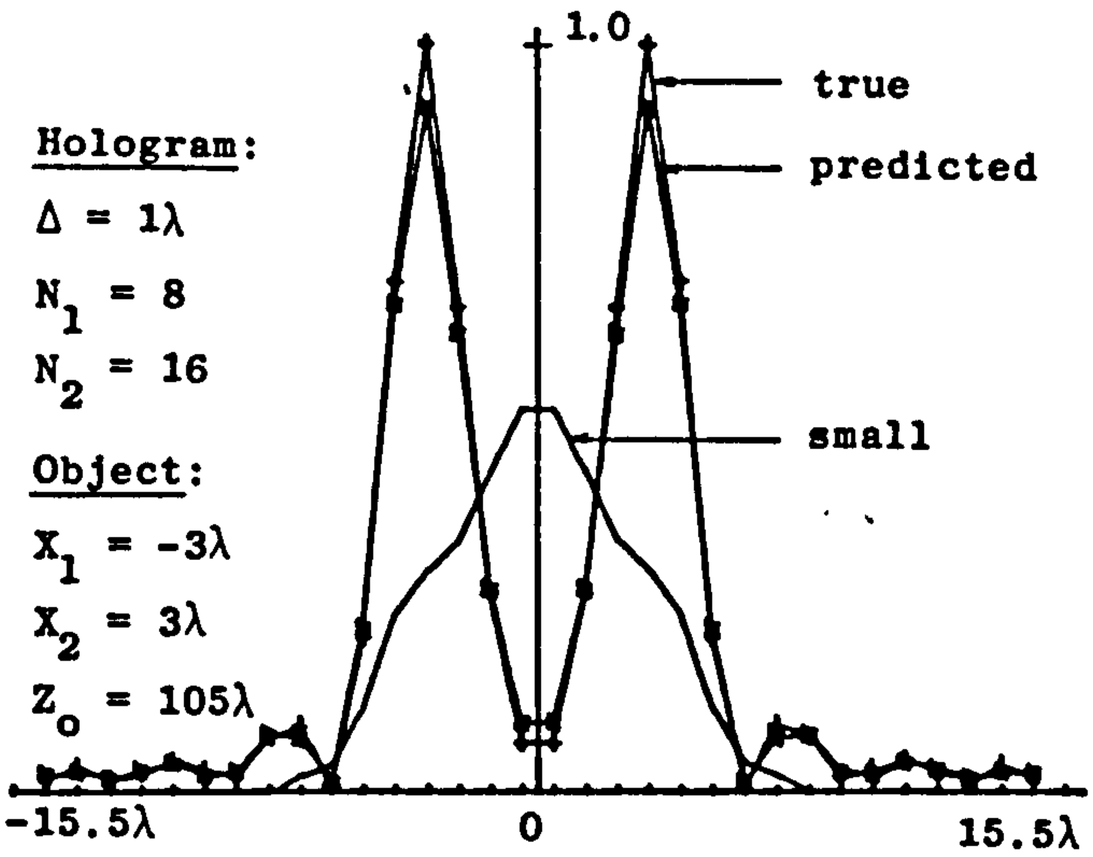


Fig 3. Intensity of reconstructed images obtained when expanding an aperture twice using a 5-2 ARMA predictive model to image a 2-point object

105λ. The prediction is performed using the optimum ARMA model with 5 MA terms and 2 AR terms. The figure shows that while the small available aperture fails to resolve the two points, they are clearly resolved with the expanded predicted aperture which gives an image similar to that obtained from the expanded true aperture.

## THE CORRECTIVE MODEL

An attempt has been made to improve the prediction accuracy by correcting the predicted signals using a corrective model based on comparing the predicted data with corresponding data which are known to be true. To construct such a model the known data over one half of the available aperture is related to the data at the same points obtained by prediction using a predictive model based on the other half. The corrective model is then used to correct predicted data outside the available aperture. The performance of the corrective model depends upon the structure of both the predictive and corrective models employed and a search for the optimum model is often required.

## THE EFFECT OF DISTURBING NOISE

When random perturbations were used to simulate noise in measured hologram signals, the prediction errors were too large and no satisfactory images were obtained even for relative noise amplitudes as low as 1%. The increased errors are due to the sensitivity of the matrix solution to perturbations in the data vector and it was observed that this sensitivity increases as the matrix size increases. It was also noticed that the larger the number of AR terms in an ARMA model the less the sensitivity of the matrix colution to noise. Referring to eqn 7, for a totally AR model (p=0, q=N), the system matrix reduces to a triangular form. It was found that the solution of this form of matrix exhibits better stability with noise than in the case of a square matrix.

Fig 4. Intensity of reconstructed images obtained when expanding an aperture twice to image a 2-point object. Relative noise amplitude: 10%. Predictive model: AR.

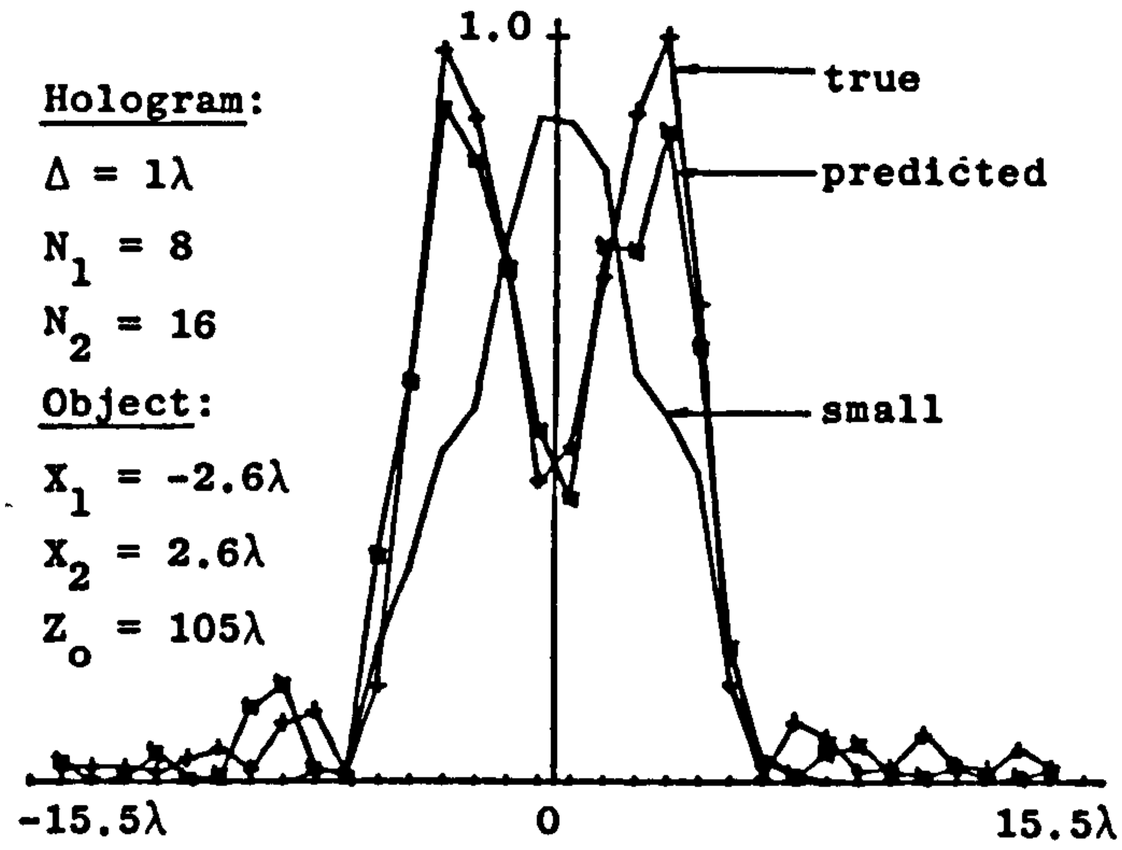


Fig 4 shows the image reconstructions obtained when using an AR predictive model to double the size of a 16 point aperture, spacing 1λ, in the presence of noise with relative amplitude of 10%. The object consists of two points spaced at 5.2λ, range 105λ. Although the AR model is not the optimum model without noise, it gives better results in the presence of noise and the two points in the object are clearly resolved.

To image 1-point objects in the presence of noise the MA model had to be modified such that the system matrix takes a triangular form. Although this achieves better stability with noise, it also reduces the prediction accuracy of the model and a corrective model of a triangular matrix form had to be employed. Fig 5 shows the image reconstructions obtained when doubling the size of a 16 point apertures, spacing 1λ, to image a 1-point object at the centre, range = 100λ with the hologram signals perturbed by noise having 10% relative amplitude. It is clear from the figure that in this case

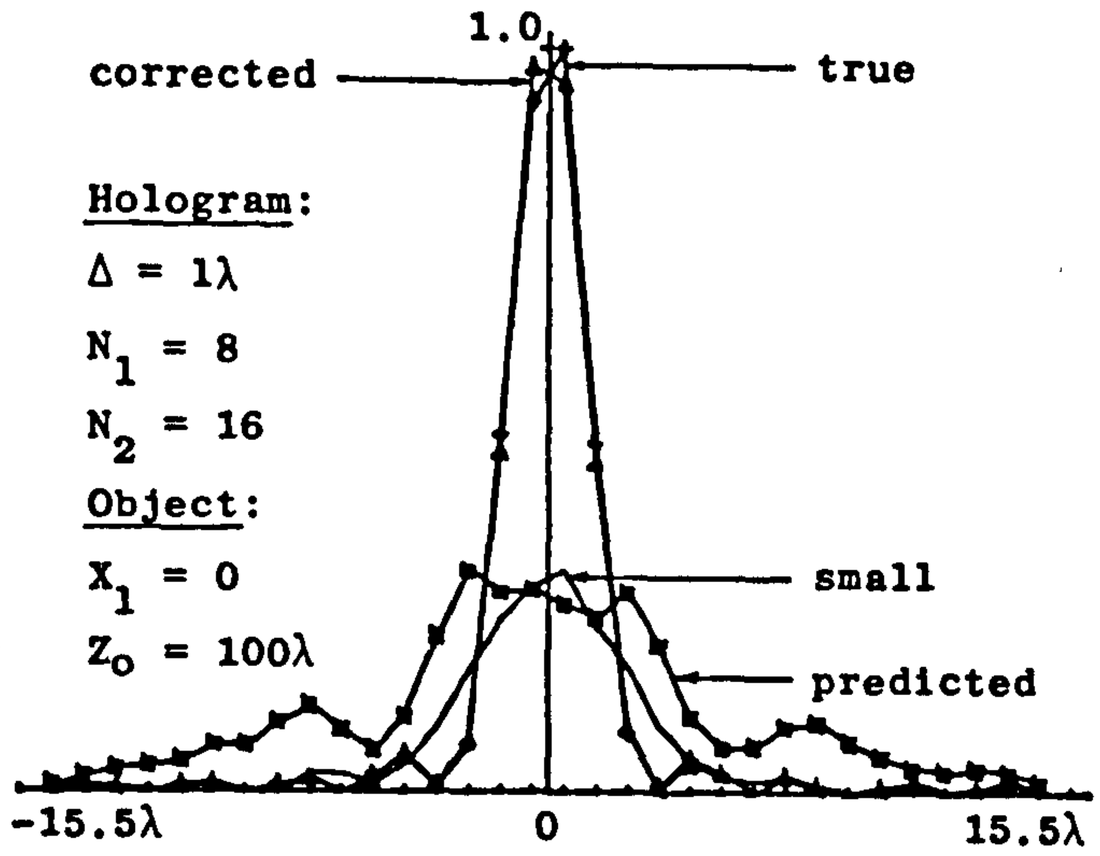


Fig 5. Intensity of reconstructed images obtained when expanding an aperture twice to image a 1-point object. Relative noise amplitude: 10%. Predictive and corrective model: MA type, triangular matrix.

the use of a corrective model is essential for achieving the improvement expected from expanding the small aperture.

## COMMENTS

In this paper a method for increasing the lateral resolution in acoustic holography is described. The approach is essentially based on modelling the hologram signal at the available aperture and this aperture is then expanded in the space domain by using the model to predict the hologram signal at new points outside the aperture. An MA model gives optimum prediction in the case of 1-point objects while for multiple-point objects an ARMA model gives better results in general. The accuracy of determining the estimated signals can be increased by employing a corrective model based on the knowledge of both predicted and true data in part of the available aperture.

The effect of noise in the hologram signals is also discussed and it was found that a triangular model matrix has better stability with noise than a square matrix. This, however, is at the expense of some deterioration in the prediction accuracy. Typical results obtained by computer simulation show the effectiveness of the technique described for improving the resolution with and without noise for both single and multiple-point objects.

## ACKNOWLEDGEMENT

The work described is supported by a research grant, Grant No. GR/B/88686, from the UK SERC. This support is gratefully acknowledged.

## REFERENCES


1. J.W. Goodman, Introduction to Fourier optics, McGraw Hill, New York, 1968.

2. P.N. Keating, T. Sawatari, and G. Zilinskas, "Signal processing in acoustic imaging". Proc. IEEE, Vol 67, 1979, pp 496-510.

3. J.L. Harris, "Diffraction and resolving power". J. Opt. Soc. Am., Vol 54, 1964, pp 931-936.

4. C.W. Barnes, "Object restoration in a diffraction-limited imaging system". J. Opt. Soc. Am., Vol 56, 1966, pp 575-578.

5. R.W. Gerchberg, "Super resolution through error energy reduction". Opt. Acta., Vol 21, 1974, pp 709-720.

6. B.R. Frieden, "Restoring with maximum likelihood and maximum entropy". J. Opt. Soc. Am., Vol 62, 1972, pp 511-518.

7. T. Sato, K. Sasaki, and K. Uemura, "Super-resolution imaging using a sequential estimation of a hologram in an extended area from data obtained in a limited area". J. Acoust. Soc. Am., Vol 65, 1979, pp 976-984.

8. E.G. Williams, J.D. Maynard, and E. Skudrzyk, "Sound source reconstructions using a microphone array". J. Acoust. Soc. Am., Vol 68, 1980, pp 340-344.

9. E.G. Williams and J.D. Maynard, "Holographic imaging without the wavelength resolution limit". Physical Review Letters, Vol 45, 1980, p 554-557.

10. O. Ikeda and T. Sato, "On method of superresolution of a limited number of point targets using ultrasonic scanning". J. Acoust. Soc. Am., Vol 57, 1975, pp 334-337.

# Digital phase meter updates measurement each cycle

by R. E. S. Abdel-Aal
*Department of Electronic Science, University of Strathclyde, Glasgow, Scotland*

Because this meter measures the phase delay between two low-frequency square waves once every cycle, it is useful in applications where instantaneous readings of this delay are continuously required. The circuit resolution is within 1% for signal frequencies of up to 250 kilohertz.

Generally, the meter counts the number of pulses of a 25-megahertz clock for a time equal to the phase delay between the two incoming waveforms. Then it strobes the measured value into output latches once a cycle. The result is a continuously updated value expressed as a 15-bit binary number plus a sign bit.

To achieve this, the cycle is viewed as one that varies from plus to minus 180°. By using only one half of the cycle for measurement, the circuit is free during the other half to store the results in the output latches and to clear the phase counters for the next measurement.

The circuit automatically determines which of the signals is to be the reference, with the phase delay measured from the rising edge of the leading signal to the rising edge of the lagging waveform. The falling edge of the reference serves as the latching signal and to set up the counters for the next cycle.

In operation, the two incoming signals, A and B, are applied to two gates of $A_1$. Here, the complemented signals $\overline{A}$ and $\overline{B}$ are obtained with negligible differential delay. The other two gates in the chip generate gating signals corresponding to $A\overline{B}$ and $\overline{A}B$. Flip-flop $A_2$ determines which input signal is the reference.

If A leads B, then the Q output of $A_2$ goes low and gating signal $A\overline{B}$, together with input signal A, drives the 74LS157 selector chip, $A_3$. Otherwise, gating signal $\overline{A}B$ together with input signal B will be selected.

The selected phase-gating signal is used to enable a chain of synchronous counters, $A_4$–$A_7$, which are driven

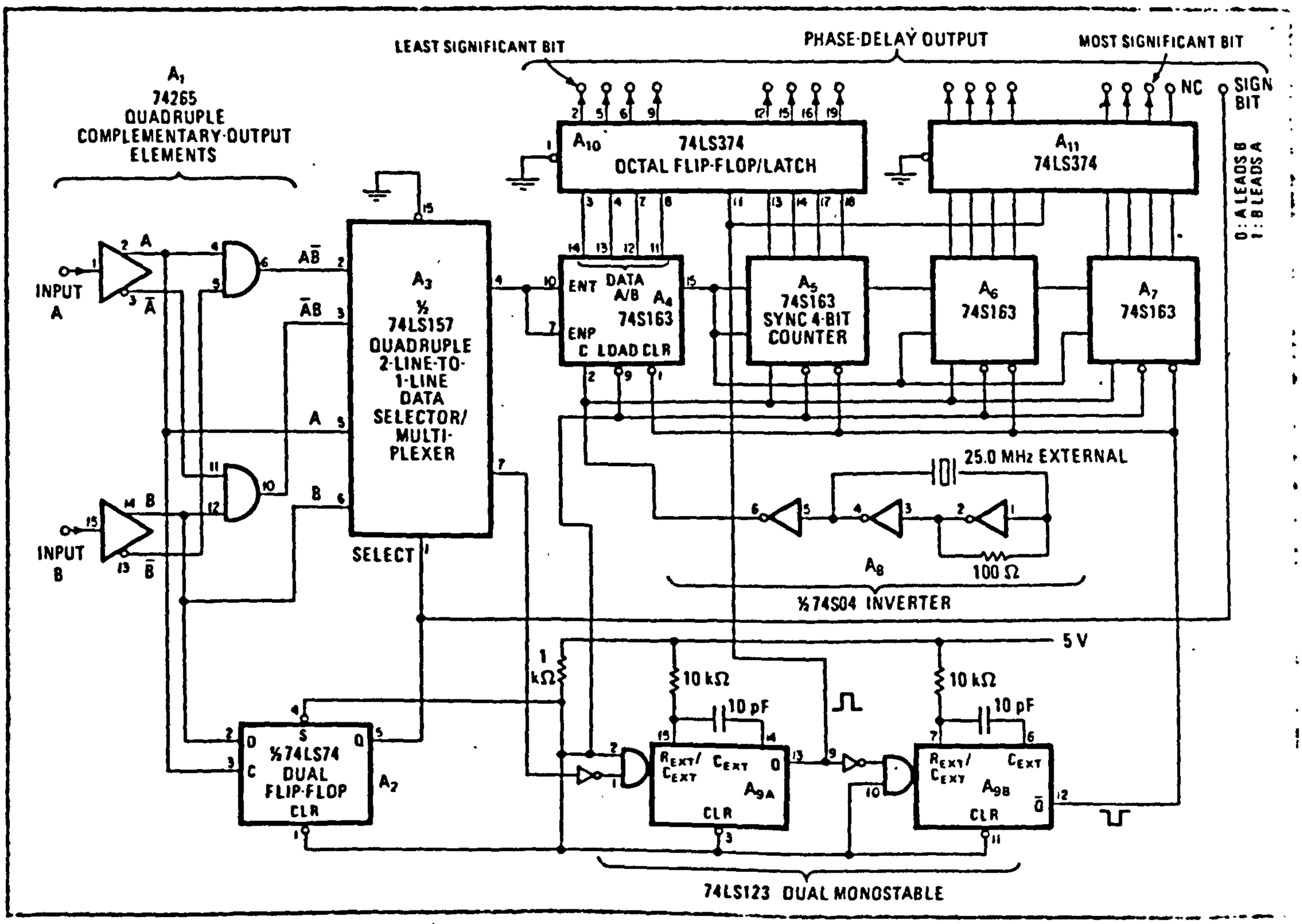


**Instantaneous.** Circuit continuously compares phases of two incoming square waves, providing a 15-bit and plus-sign output that has a resolution of $(f_{in}/250)\%$. With a 25-MHz clock, the practical upper frequency limits that can be handled for incoming signals is 250 kHz, with lowest-frequency boundaries being about 400 Hz. Lower limits can be reduced further by decreasing the clock frequency.

from a crystal-controlled 25-MHz clock built around three inverters in $A_8$. When the phase-gating signal drops, $A_4$–$A_7$ stop counting, holding their final result, which indicates the phase delay, at their parallel outputs. Following this, a short pulse from one-shot $A_{9A}$ latches the results of the count in $A_{10}$ and $A_{11}$. Then the pulse-counter chain is cleared by a second pulse from $A_{9B}$. To ensure a proper count and store cycle, the sum of the widths of the two short pulses should be less than half the period of the highest-frequency input signal. Also, the short pulse used to clear the counters should be greater than the clock period.

The upper limit on the frequency of the input signals is set by the resolution of the phase measurement that can be tolerated. With this circuit, the resolution is given by (f/250)%, where f is the frequency in kilohertz.

The lower limit of the signal frequency is set by the overflow of the phase counters before the end of half a cycle of the input signal (that is, the maximum phase delay measured). With a 25-MHz clock and a 15-bit binary number representing the magnitude of the phase (excluding the sign bit), the minimum input frequency will be $25(10^6)/(2(2^{15}-1)) = 381$ hertz. At low input frequencies, however, a lower-frequency clock can be used while maintaining good resolution, and thus the frequency limit can be brought down even further. □

# Pocket computer tackles classical queuing problems

by Cass R. Lewart
*System Development Corp., Eatontown, N. J.*

This program, written in Basic, permits pocket computers such as the Radio Shack and the Sharp PC-1211 to tackle problems in classical waiting-line (queuing) theory that has proved so useful in solving the tradeoffs that have to be made between utilization and capacity in telecommunications systems. The program can easily be translated to work on other machines.

The classical queuing considerations assume an expo-

```
10 "Z" CLEAR: USING "##.##^"
15 PAUSE "QUEUING PROG. C.R.LEWART"
20 INPUT "ARRIVAL RATE?";L: IF L <= 0 GOTO 45
25 INPUT "SERVICE RATE?";M: IF M <= 0 GOTO 45
30 INPUT "# SERVERS?";S: IF (S <> INT S)+(S <= 0) GOTO 45
40 X=L/M: U=X/S: V=1-U: IF (V > 0)*((S-1)*LOGX < 100)*
   (S < 70) GOTO 50
45 BEEP2: GOTO20
50 Y=S: GOSUB 200
55 T=Z: FOR I=0 TO S-1: Y=I: GOSUB 200
60 P=P+X^I/Z: NEXT I
65 Y=S: GOSUB 200
70 P=1/(P+X^S/T/V): B=X^S*P/T/V
75 W=B/SMV: R=W+1/M: BEEP 1: PRINT "READY"
80 "B" PRINT "P(ALL BUSY)=";B
85 "X" PRINT "UTILIZATION=";U
90 "A" PRINT "P(0)=";P
95 "S" PRINT "AV. WAIT=";W
100 "V" PRINT "AV. RESP.=";R: D=√(2B-B^2)*SVV)*W/B
105 PRINT "ST.DEV.(TR)=";D
110 "N" D=LR: PRINT "AV. IN SYS.=";D
115 "D" D=LW: PRINT "AV. IN QUEUE=";D
120 "F" INPUT "# ITEMS IN SYSTEM?";N: D=P*X^N:
    IF N < S GOTO 130
125 E=D/TS^(N-S): GOTO 140
130 Y=N: GOSUB 200
135 E=D/Z
140 PRINT "P(N=";N;")=";E
145 "C" INPUT "TIME?";H
150 F=B*EXP -SMVH: A$="W"
155 PRINT USING "##.#^";"P(T";A$;">";H;")=";
    USING "##.##^";F
160 G=V-1/S: A$="R": D=EXP  MH: IF G=0 GOTO 170
165 F= D*(1+B/S*(1-EXP -MSGH)/G): GOTO 155
170 F=D*(1+BMH): GOTO 155
200 Z=1: FOR J=1 TO Y: Z=JZ: NEXT J: RETURN
```